A study of volumetric behaviour of compacted clayey soils in the void ratio, moisture ratio and net stress space

A Thesis submitted to Monash University in fulfilment of the requirements for the
Degree of Doctor of Philosophy

By

Md. Tanvirul Islam
BSc/Eng (Honours)

Department of Civil Engineering
Monash University
Australia

January 2015

MONASH University

COPYRIGHT NOTICES

1. Under the Copyright Act 1968, this thesis must be used only under the normal conditions of scholarly fair dealing. In particular no results or conclusions should be extracted from it, nor should it be copied or closely paraphrased in whole or in part without the written consent of the author. Proper written acknowledgement should be made for any assistance obtained from this thesis.

2. I certify that I have made all reasonable efforts to secure copyright permissions for third-party content included in this thesis and have not knowingly added copyright content to my work without the owner's permission.

DECLERATION

I hereby declare that this thesis contains no material which has been accepted for the award of any other degree or diploma at any university or equivalent institution and that, to the best of my knowledge and belief, this thesis contains no material previously published or written by another person, except where due reference is made in the text of the thesis. Where sections of this thesis include the results of joint research or scholarly publication clear acknowledgement of the relative contributions of the respective authors is made.

Md. Tanvirul Islam

Department of Civil Engineering

Monash University

Clayton, Australia

January 2015

ABSTRACT

The volumetric behaviour of unsaturated soils is complicated than saturated soils. Depending on the state paths involving loading/wetting/unloading, compacted unsaturated soils can exhibit swelling, collapse, collapse followed by swelling, swelling followed by collapse and swelling pressure development. While significant advances have been made in modelling of the hydromechanical behaviour of unsaturated soils, it is still difficult to predict these behaviours using most methods that use suction as a constitutive variable, since the required testing effort is overwhelming on one hand and it is difficult to take into account field soil variability on the other. In contrast, the Monash – Peradeniya – Kodikara (MPK) framework proposed by Kodikara (2012) uses void ratio (e) – moisture ratio (e_w) – net stress (p) space accompanied with the Loading Wetting State Boundary Surface (LWSBS) to explain/predict these paths and is relatively simple and has the potential to be applied to practical problems with relative ease. The current research project mainly focuses on a comprehensive validation and extension of the MPK framework and demonstration of its application to practical problems.

A comprehensive series of tests are performed on statically compacted soils for the validation of the MPK framework. Two soil types, namely lightly reactive kaolin and more reactive clay referred to as Merri Creek soil, are used in the testing. The soils were prepared with different moisture contents from dry state and were statically compacted at constant water contents to obtain the $e - e_w - p$ constitutive surfaces as well as soil specimens for the state path tests. The state path test results of yielding under loading, collapse under wetting, swelling pressure development and change in yield pressure due to wetting are explained with the MPK framework. Despite the difference in the degree of reactivity, both soils followed the concepts of the MPK framework reasonably closely. In addition, some published data from the literature were also analysed within the framework, highlighting that the framework is valid, regardless of the degree of reactivity of the soil. No suction was measured in these experiments, as it is not essential to explain most volumetric behaviour as per the MPK framework.

Dynamic compaction is commonly used to construct structural fills for various geo-infrastructures. The current practice is to specify a minimum dry density and moisture

content criterion to be used in the field on the basis of Proctor compaction carried out in the laboratory. Nonetheless, we still do not have practical methods for predicting the behaviour of compacted clay under the expected mechanical and environmental loadings. Current theories are difficult to apply in practice due to difficulty in determining the necessary parameters. In this thesis, the MPK framework is extended to analyse the dynamically compacted soils. Similar to statically compacted soils, a significant number of experiments were performed on the dynamically compacted lightly reactive kaolin and reactive Merri Creek soils at constant moisture contents. Since the compaction stresses were unknown for the dynamic compaction, recompression of the soil specimens from compacted soil was used to establish the relevant LWSBSs. Subsequently, independent tests were undertaken highlighting that the MPK framework could predict well the behaviour of dynamically compacted soils under loading/unloading and yielding, collapse during wetting, change of loading yield stress after wetting, and swelling pressure development during constrained wetting. The value of the approach is that the testing methods are straight-forward, do not require specialised equipment and the testing times are much shorter. In addition, the uncertainty that laboratory dynamic compaction may not relate directly to the field roller compaction can be addressed with the developed framework. Soil specimens obtained from field soil pads compacted by the actual rollers can be used to establish the corresponding LWSBS. This information will allow the direct prediction of the likely behaviour of field compacted fills under the expected environmental and mechanical loadings.

Another addition to the MPK framework is achieved by incorporating loading/wetting suction within the $e - e_w - p$ space. Initially, two hypotheses are proposed to present the suction contours on and inside the LWSBS by analysing several datasets from the literature. Subsequently, a mathematical representation is provided to establish full suction profile within the $e - e_w - p$ space for both kaolin and Merri Creek soils. Although suction is not essential for the application of the MPK framework in many practical problems as demonstrated, yet knowing the suction profile within the $e - e_w - p$ space is essential to complete the hydro-mechanical picture in the volumetric space. This extension will allow the development of constitutive models as well as soil water characteristic curves more rationally in future.

Finally, the MPK framework is applied to analyse the performance of a conceptual compacted clayey fill. The heave/settlement results from the MPK framework and the results available from literature are compared qualitatively for both laboratory behaviour and field scale behaviour of compacted soils. It is found that the complex volumetric behaviour due to major wetting events are easily explainable using the extended MPK framework. It is observed that the initial operational void ratio (or the initial operational density) and the operational stress are the two most important parameters that govern the volumetric behaviour of compacted unsaturated soils.

ACKNOWLEDGEMENTS

LIST OF PUBLICATIONS

List of journal papers

- Islam, T., and Kodikara, J., (2015). Interpretation of the loading/wetting behaviour of compacted soils within the MPK framework: Part I Static compaction. *Submitted to Canadian Geotechnical Journal*.
- Kodikara, J., Islam, T., and Rajeev, P., (2015). Interpretation of the loading/wetting behaviour of compacted soils within the MPK framework: Part II Dynamic compaction. *Submitted to Canadian Geotechnical Journal*.
- Interpretation of the suction within $e - e_w - p$ space. *In progress.*
- Prediction of the volumetric behaviour of compacted fills under environmental loading using the MPK framework. *In progress.*

List of conference papers

- Kodikara, J., Islam, T., and Rajeev, P., (2012). New practical framework for predicting compacted soil behaviour. Proceedings of the International Conference on Ground Improvement and Ground Control, Transport Infrastructure Development and Natural Hazard Mitigation. *Edited by* B. Indraratna, C. Rujikiatkamjorn and J.S. Vinod. Research Publishing Services, University of Wollongong, Australia.
- Kodikara, J., Islam, T., Wijesooriya, S., Bui, H., and Burman, B.C., (2014). On controlling influence of the line of optimums on the compacted clayey soil behaviour. Proceedings of the Sixth International Conference on Unsaturated Soils, UNSAT2014. *Edited by* N. Khalili, A.R. Russell and A. Khoshghalb, Sydney, Australia. pp. 219-225.
- Kodikara, J., and Islam, T., (2015). An Analysis of Compacted Pavement Subgrade Behaviour Due to Climatic Effects. *Accepted In* Sri Lankan Geotechnical Society International Conferences. Colombo, Sri Lanka.

TABLE OF CONTENTS

LIST OF FIGURES

LIST OF TABLES

NOMENCLATURE

a, b, c	constants of the exponential relationship of average hydric coefficient with operational net stress and void ratio
α	hydric coefficient $\left(\frac{\partial e}{\partial e_w}\right)_p$ at constant net stress
α_{av}	average hydric coefficient at constant net stress
β	constant parameter that controls the rate of increase of soil stiffness with suction
c_c	compression Index
c_r	recompression Index
c_v	coefficient of consolidation
c_α	secondary compression
$D_a{}^*$	coefficient of transmission
λ	gradient of v–ln(p) curve at constant moisture content
$\lambda(s)$	gradient of v–ln(p) curve at constant suction
λ_1, λ_2	compression index for saturated and dry soil, respectively
$\lambda_{vp}, \lambda_{vs}$	compressibility coefficients with respect to mean net pressure and suction, respectively
ϕ	model parameter in compaction curve equation
ξ	positive variable representing bonding effects due to suction
e	void ratio
e_s	void ratio at saturation under net stress p
e_{s0}	void ratio at saturation under nominal stress
$e_0{}^*$	void ratio under nominal stress for dry soil
e_0 (chapter 2)	void ratio for dry soil
e_0 (chapter 4 & 5)	initial void ratio
e_0 (chapter 7)	operational void ratio
e_c	compaction void ratio
Δe	change of void ratio
Δe_a	change of air void
$\Delta e_{aggregare}$	increase of void ratio due to soil aggregate expansion
$\Delta e_{slippage}$	decrease of void ratio due to slippage between soil aggregates

e_w	moisture ratio ($= wG_s$, where G_s is specific gravity and w gravimetric moisture content)
Δe_w	change of water void
e_{wc}	optimum moisture ratio for net stress p
e_{w0} (chapter 4 & 5)	initial moisture ratio
e_{w0} (chapter 7)	initial/operational moisture ratio
ε	strain
ε_v	volumetric strain
ε_{sh}	shear strain
g	gravitational acceleration
K	bulk modulus at constant moisture content
κ	gradient of v–$\ln(p)$ curve in unload–reload line
κ_s	elastic stiffness parameter for changes in suction
k	permeability
k_a	coefficient of air compressibility
K_0	one dimensional
m, n, o	gradient of initial, central and final portion of the SWCC, respectively
m_v	coefficient of volume change
$N(s)$	specific volume at an initial/reference stress state
n (chapter 2)	porosity
n (chapter 6)	linearly converted logarithmic net stress axis ($= \log(p)$)
θ	angle created by the constant suction contours from nominal stress line on the LWSBS with horizontal axis
σ	applied stress
p	net stress
p^c	reference net stress
p_n	nominal net stress
p'	effective stress
p_c	compaction net stress
p_o	operational net stress
p_{atm}	atmospheric pressure
Δp	change of net stress

P_0, P_1, P_2, P_3	points control the cubic Bézier curve
$P_0, P_1, P_2, P_3, P_4, P_5$	points control the fifth order Bézier curve
q	deviatoric stress
r	constant parameter related to the maximum stiffness of the soil
S_r	degree of saturation
$S_{r_{LOO}}$	degree of saturation on the LOO
S_{ro}	degree of saturation at operational condition
s	suction
s^*	modified suction $(= ns)$
t	dummy variable of the Bézier curve which varies between 0 to 1
u_a	pore air pressure
u_w	pour water pressure
v	specific volume
Δv	change of specific volume
v_w	specific water volume
W	rate of work input per unit volume of soil
dW	rate of work input per unit volume of unsaturated soil
w	gravimetric moisture content
w_L, w_p	liquid and plastic limits, respectively
χ	Bishop's effective stress parameter
γ	bulk soil unit weight
γ_d	dry soil unit weight

ABBREVIATION

AS	Australian Standards
ASCE	American Society of Civil Engineers
ASTM	American Society for Testing and Materials
BBM	Barcelona Basic Model
BK	mixture of Bentonite and Speswhite kaolin soil
BS	British Standards
CH	clay of high plasticity
CPT	Collapse Potential test
DC	Dynamic compaction
EK	Ecalite kaolin soil
LC	Loading/wetting collapse
LL	Liquid Limit
LOO	line of optimum
LUL	Loading – Unloading – Loading
LUW	Loading – Unloading – Wetting
LUWL	Loading – Unloading – Wetting – Loading
LUWUW	Loading – Unloading – Wetting – Unloading – Wetting
LUWUWUWUW	Loading – Unloading – Wetting – Unloading – Wetting– Unloading – Wetting – Unloading – Wetting
LW	Loading – Wetting
LWL	Loading – Wetting – Loading
LWSBS	Loading Wetting State Boundary Surface
MC	Merri Creek soil
MP	Modified Proctor
MPK	Monash-Peradeniya-Kodikara
NCL	normal compression line
OMC	optimum moisture content
PI	Plasticity Index
PL	Plastic Limit
SBS	State Boundary Surface
SC	Static compaction

SFG	Sheng-Fredlund-Gens
SP	Standard Proctor
SPT	Swelling Pressure test
SWCC	Soil Water Characteristics Curve
US I	unloading stress Isotropic
US	unloading stress
USCS	Unified Soil Classification Systems
USDA	United States Department of Agriculture

INTRODUCTION

1.1 Background

Soil mechanics has often been divided into saturated soil mechanics and unsaturated soil mechanics due to differences in natural and engineering behaviour (Fredlund and Rahardjo, 1993). Much geotechnical work is associated with unsaturated soil, either as compacted fill or natural soil above the water table (Kodikara, 2012). The behaviour of unsaturated soils is more complicated than that of saturated soils. Our understanding of and ability to model their behaviour are still developing. Expansive soils cause $9 billion damage each year in the United States alone, a total which exceeds the combined damage from natural disasters, such as floods, hurricanes, earthquakes, and tornadoes (Jones and Holtz, 1973; Krohn and Slosson, 1980). Most of these damages are triggered by the response of post compaction wetting/drying of unsaturated soils. Therefore, it is not surprising that for almost over half a century, modelling of the hydromechanical behaviour of unsaturated soils has been a frontier in soil mechanics research, with many significant advances having been made (e.g., Bishop, 1959; Matyas and Radhakrishna, 1968; Fredlund and Morgenstern, 1976; Alonso et al., 1990; Wheeler and Sivakumar, 1995; Alonso et al., 1999; Khalili et al., 2000; Sivakumar and Wheeler, 2000; Gallipoli et al., 2003a; Gallipoli et al., 2003b; Lloret et al., 2003; Wheeler et al., 2003b; Sivakumar et al., 2006; Sheng et al., 2008; Tarantino and De Col, 2008; Fityus and Buzzi, 2009; Sivakumar et al., 2010; Boyd and Sivakumar, 2011; Sheng and Zhou, 2011). All these advancements have utilised suction, either as an independent stress variable or in combination, to define the effective stress that controls the soil behaviour. It is well accepted that 'matric' suction, defined as the pressure deficit between air and water pressure at the water meniscus, has a direct stress-like influence on soil's behaviour. Therefore, it is appropriate that it is incorporated as either an independent or component stress variable in unsaturated soil constitutive modelling. However, a major practical difficulty of using suction is its accurate measurement, both in the laboratory and in the field. This difficulty has been the main contributor to the significant gap that currently exists between theoretical models and practical applications. In addition, it has been recently recognised that to explain unsaturated soil behaviour, suction alone is not

generally sufficient, but the soil water content or its surrogates, such as the soil's degree of saturation, needs to be incorporated in the constitutive modelling, commonly referred to as hydromechanical coupling. It therefore follows that there is merit in pursuing alternative ways of incorporating hydromechanical coupling that will make unsaturated models more practical (Kodikara, 2012; Islam and Kodikara, 2015*).

Kodikara (2012) presented a novel framework (referred to as the Monash-Peradeniya-Kodikara (MPK) framework) for explaining the volumetric behaviour of unsaturated compacted soils using void ratio (e), net stress (p) and soil moisture ratio ($e_w = wG_s$, where w is the soil gravimetric moisture content and G_s is the specific gravity of soil particles). A novel feature of this framework is the establishment of a direct relationship between the traditional compaction curve and the soil's constitutive behaviour. In this framework, soil suction is presented as the fourth variable explaining volumetric soil constitutive behaviour, and it has been shown that suction is not essential for explaining most state paths that are relevant to practice, such as soil deformation under: (a) loading/unloading; (b) wetting under constant (net) stress; (c) evaluation of collapse potential; (d) swelling pressure development under constrained volume; (e) shrinkage cracking during drying and; (f) likely soil 'environmental' stabilisation behaviour under wet-dry cycling. For instance, in a compacted fill situation, knowledge of suction is required if a question related to a field situation involving suction is raised, such as what will the soil collapse strain be if the suction is reduced from 2000 kPa to 100 kPa? However, such field-related questions are more likely to be based on gravimetric water content, which geotechnical engineers commonly use in practice (Islam and Kodikara, 2015*). Therefore, there is merit in pursuing research that develops practical approaches to field design and analysis without direct reference to suction. Nonetheless, it is acknowledged that suction is the thermodynamic potential that controls the behaviour of unsaturated soils and cannot be entirely ignored. This is particularly true for unsaturated water flow conditions and dealing with multiple layers of soil. Furthermore, in some applications such as slope stability, suction may be more relevant than the water content. In general, suction and moisture ratio are considered energy conjugate state parameters, and therefore both are important in constitutive behaviour. In this thesis, the validation and enhancement of the MPK framework is considered, and the incorporation of suction's role within the MPK framework is also addressed.

1.2 Research objectives

As Kodikara (2012) provided a qualitative validation of the MPK framework on the basis of typical experimental data and the behaviour of compacted soils reported in the research literature, the present research program mainly focuses on: (a) the complete validation of the MPK framework from experimental evidence; and (b) the extension of the MPK framework by achieving (i) an expansion of the MPK framework into dynamically compacted soils, (ii) incorporation of suction and the average hydric coefficient within $e - e_w - p$ space, and (iii) comparison of MPK-predicted heave/settlement results and experimental results obtained from the research literature for field-scale compacted fills.

These specific objectives of the current research program are further explained below.

Validation of the MPK framework using statically compacted soils: A complete set of experimental data is generated for two types of soils: slightly reactive (shrinking/swelling) commercially available kaolin and reactive (natural) Merri Creek soil from Melbourne, Australia. At the beginning, the Loading Wetting State Boundary Surfaces (LWSBSs) are developed for both of the soils using the compression curves obtained from 1-D compression. Subsequently, various state path tests are performed, including loading/unloading, wetting under constant (net) stress, collapse potential evaluation, swelling pressure development under constrained volume. In addition, the datasets of Jotisankasa (2005), Sharma (1998) and Romero (1999) are used to validate the MPK framework.

An expansion of the MPK framework into dynamically compacted soils: Initially, the MPK framework was proposed for statically compacted soils only. Therefore, as part of the extension of the MPK framework, an expansion is performed into dynamically compacted soils. An experimental method is developed to construct the LWSBSs for dynamically compacted soils. In addition, different state path validation tests are performed to examine whether volumetric behaviour proves the validity of the MPK framework. Similar to the validation of the MPK framework by statically compacted soils, two types of soils are used in the experimentation, namely kaolin, and Merri Creek soil.

Incorporation of suction within the MPK framework: First, two hypotheses are developed regarding the shape of the suction contours on and inside the LWSBS in the $e - e_w - p$ space, based on the research literature. Later, a mathematical representation of suction contours is presented for both the kaolin and Merri Creek soils within the $e - e_w - p$ space.

Prediction of heave/settlement for field-scale compacted fills using the MPK framework: Initially, the average hydric coefficient is incorporated within the $e - e_w - p$ space for both the kaolin and Merri Creek soils. Subsequently, validation is performed to discover whether the MPK framework is capable of correctly predicting volumetric behaviour for major wetting events. The volumetric behaviour of a 30 meter high hypothetical embankment problem with different initial conditions, such as degrees of saturation and compaction levels is modelled for major wetting events, using the concept of the enhanced MPK framework for both kaolin and Merri Creek soils.

1.3 Overview of the thesis

The thesis contains eight chapters and a list of references. In each chapter, a brief introduction is followed by methodology/results/mathematical representation/modelling and discussion and conclusions. Each chapter is intended to be self-explanatory. However, the previous chapters may contain information necessary to understand the data and their details. The chapters are summarised below.

Chapter 1 – Introduction

This chapter provides the background to research on unsaturated soil, the recent advance made by Kodikara (2012) and the aims of the current research program.

Chapter 2 – Literature review

This chapter describes compaction, including the different curves, theories and methods of compaction and the behaviour of compacted soil under external and environmental loadings; net stress and suction-based unsaturated soil models: the Barcelona Basic Model (BBM), the effective stress model and the Sheng-Fredlund-Gens (SFG) model; new volumetric frameworks; different aspects of the MPK framework and the explanation of the volumetric behaviour of compacted/virgin unsaturated soils using the

MPK framework; the shape of the suction contours on the compaction curves and different features of the Soil Water Characteristics Curve (SWCC); and heave and compression behaviour of compacted fills under environmental loading.

Chapter 3 – Preliminary soil tests, soil preparation and experimental apparatus

This chapter presents the results of preliminary soil tests, soil preparation and the experimental apparatus. Two soils are used in the current research program: slightly reactive (shrinking/swelling) commercially available kaolin, and reactive (natural) Merri Creek soil from Melbourne, Australia. The first part of the chapter describes various physical and geotechnical property tests (e.g., soil classification, specific gravity, particle size distribution, Atterberg limits, proctor compaction and consolidation tests) on the soils, while the final part presents the soil preparation technique and the experimental procedure and apparatus for statically and dynamically compacted validation testing.

Chapter 4 – Validation of the MPK framework using statically compacted soils

This chapter provides the validation of the MPK framework presented by Kodikara (2012). Two types of soils are used in the experimentation, namely kaolin and Merri Creek soils. Initially, the LWSBSs are developed for both soils using the compression curves obtained from 1-D compression. Subsequently, experiments are reported on the following state paths: (a) loading/unloading; (b) wetting under constant (net) stress; (c) collapse potential evaluation and (d) swelling pressure development under constrained volume. In addition, this chapter presents the validation of the MPK framework using the following datasets (a) Jotisankasa (2005), (b) Sharma (1998) and (c) Romero (1999).

Chapter 5 – Volume change behaviour of dynamically compacted unsaturated soils within the MPK framework

An experimental method is developed in this chapter to construct the LWSBSs for dynamically compacted soils. Different validation tests are then performed in various state paths to examine the validity of the MPK framework for dynamically compacted soils. Two types of soils are used in the experimentation, namely kaolin and Merri Creek soils.

Chapter 6 – Incorporation of suction within the MPK framework

This chapter presents two hypotheses to interpret the shape of the loading/wetting suction contours on and inside the LWSBS using the datasets of Tarantino and De Col (2008), Jotisankasa (2005), Sharma (1998) and Romero (1999). In addition, a mathematical representation of suction contours is presented, based on the hypotheses developed for both kaolin and Merri Creek soils within $e - e_w - p$ space.

Chapter 7 – Field application of the MPK framework

This chapter presents the predicted volumetric behaviour of a hypothetical 30 meter high embankment problem with different initial conditions, such as, degrees of saturation and compaction levels for major wetting events using the concept of the enhanced MPK framework for both kaolin and Merri Creek soils. Before that, incorporation of the average hydric coefficient within $e - e_w - p$ space and the validation of the capability of the MPK framework in predicting volumetric behaviour for major wetting events are conducted.

Chapter 8 – Conclusions and directions for future research

This chapter presents the conclusions of the current research program and directions for future research.

LITERATURE REVIEW

2.1 Introduction

As the present research mainly focuses on the validation and extension of the new volumetric framework for compacted unsaturated soils, namely the Monash-Peradeniya-Kodikara (MPK) framework developed by Kodikara (2012). Therefore, in this chapter, special attention is paid to the explanation of the MPK framework. First, different curves, theories and methods of compaction and the behaviour of compacted soil under external and environmental loadings are provided under soil compaction section. Next, the constitutive models for unsaturated soils available to date, including the Barcelona Basic Model (BBM), the effective stress model and the Sheng-Fredlund-Gens (SFG) model are presented. In the next section, the main topic of this chapter, different features of the MPK framework and the volumetric behaviour of compacted unsaturated soils based on the MPK framework are outlined. The theoretical basis for using moisture ratio over suction in unsaturated soil modelling, the experimental basis of the MPK framework, the relationship of the MPK framework with the compaction curve and the Loading Wetting State Boundary Surface (LWSBS), which is the basic building block of the MPK framework, are summarized at the beginning of this section. Subsequently, an explanation of various volumetric behaviours of compacted unsaturated soils, such as compression, unloading and recompression, swelling and/or collapse due to wetting, the dependence of collapse potentiality on the operational stress, swelling pressure and cracking of compacted/virgin unsaturated soils, are provided on the basis of the MPK framework. At the end of this chapter, the shapes of the loading/wetting suction contours on the compaction curves, different features of the Soil Water Characteristics Curve (SWCC) and the heave and compression behaviour of compacted fills under environmental loading are presented. Finally, a summary of the literature review and the scope of the research are provided.

2.2 Compaction

Compaction is the densification of soil by putting mechanical energy into it. Compaction of soil primarily occurs by the reduction of air voids. Compacted soil is commonly used

as a construction material in different engineering structures, such as retaining walls, highways, embankments, ramps, airport landing strips and dams. The basic theoretical background of the compaction of soil was developed by Proctor (1933) with the introduction of the compaction curve, which is taught at undergraduate level all over the world. In this section, different curves, theories and methods of compaction are presented. In addition, the behaviour of compacted soil under external and environmental loadings is discussed.

2.2.1 Compaction curves

The relationship between the moisture content and dry density for a given energy level is presented by the compaction curve. Typically, the field compaction is specified on the basis of the laboratory Proctor test, which characterises the compaction curve. This test was originally developed by Proctor in (1933) to simulate field compaction in the laboratory. As stated earlier, both the Proctor test and the compaction curve are taught at the undergraduate level all over the world. There are two types of Proctor tests: the Standard Proctor test and the Modified Proctor test. The Standard Proctor, which imparts a gross energy density of 560 kJ/m^3 (AS1289.5.1.1), is commonly used when moderately heavy machinery is used for compaction. In situations where heavier machinery is used, the Modified Proctor energy of 2550 kJ/m^3 (AS1289.5.2.1) is used. To cater for other situations, varied forms of gross energy are used, including reduced compaction energy to simulate hand-operated machinery (Daniel and Benson, 1990). Figure 2-1 presents the typical soil compaction curves obtained from laboratory Standard and Modified Proctor tests. A compaction specification typically involves a minimum dry density (on the basis of a Proctor's maximum dry density) to be achieved and a range of moisture contents that could be used. More elaborate criteria have been developed for special applications such as clay liners, where the primary intention is to achieve a minimum hydraulic conductivity (see, Daniel and Benson, 1990). However, it remains unclear how these compaction energy levels relate to field compaction, where rollers are commonly used. More importantly, it is still difficult at the compaction design stage to examine the likely behaviour of compacted fills under mechanical and environmental loadings that may be imposed during their field operation.

2.2.2 Compaction theories

As stated earlier, the first explanation of the mechanism of compaction was presented by Proctor (1933). Many researchers have since attempted to explain the mechanism in the compaction stages. These studies have provided the qualitative explanation of the shape of the compaction curve. The various theories of compaction are summarized below.

2.2.2.1 Proctor's theory (1933)

Proctor (1933) stated that water has both capillary and lubrication effects on soil. If a small amount of water is added to soil, it makes a thin film around the soil particles, due to surface tension. When these films come together, binding effects occur among the soil particles. Therefore, compaction force is insufficient to overcome these inter-particular forces, which, in turn, reduces the dry density that could be achieved with low moisture content. If sufficient amount of water is added to the soil, the inter-particular forces between the soil particles may be reduced. Therefore, the compacted dry density of soil may increase with the reduction of air voids. Proctor explained this based more on the concept of lubrication than the concept of capillarity. Horn (1960) explained that water does not act as a lubricant for all soils because it was found that water reduces friction by approximately two times for sheet silicates, but for three-dimensional network silicates (i.e., quartz and feldspar), water increases the frictional coefficient by almost five times. Therefore, if the lubrication theory is valid, sand should have its maximum dry density in the dry stage. However, sand typically has a similar bell-shaped compaction curve like other soils, although towards the very dry side, it may show signs of increasing density.

2.2.2.2 Hogentogler's theory (1936)

Hogentogler (1936) explained the shape of compaction curve with the help of viscous water theory. According to Hogentogler (1936), at the time of compaction, soil goes through four stages of wetting: hydration, lubrication, swelling and saturation. When a small amount of water is added to soil, it makes a thin film around the soil particles. At that time, the shearing strength of the soil is very high because of the high viscosity of water. Therefore, at low moisture content, the compacted dry density of soil is also low. If a sufficient amount of water is added, the viscosity and shearing strength of the soil reduces. This stage is called the lubrication stage, and the compacted dry density of the soil increases at this stage. The maximum amount of lubrication occurs at the optimum

moisture content (OMC). Hogentogler (1936) also stated that if more water is added to soil after OMC, the soil particles start to be displaced. Consequently, the compacted dry density of the soil reduces. This stage is called the swelling stage. Through this stage, the soil swells without any change in air volume. During the saturation stage, all the air is displaced and the saturation line joins with the zero air voids line. At present, it is known that the compaction of soils does not result in complete saturation, therefore, the compaction curve never intersects zero air void line.

2.2.2.3 Hilf's theory (1956)

Hilf (1956) explained the compaction curve using pore air and pore water pressure theory. A relationship based on the void ratio (e) versus soil moisture ratio $(e_w = wG_s,$ where, w is the soil gravimetric moisture content and G_s is the specific gravity of soil particles) was used by Hilf (1956) instead of the common moisture content (w) versus dry density (γ_d) curve. The minimum void ratio corresponds to the maximum dry density in the curve, and the shape of the compaction curve is similar to the usual Proctor's curve. According to Hilf (1956), the capillary bridges in dry soils resist the compaction stress. Therefore, with low moisture content, the compacted dry density of the soil is also low. When the moisture content increases, the menisci become flatter and cannot resist the compaction stress. As a result, the compacted dry density of the soil increases with the increase of moisture content. When the soil reaches the OMC, the air is trapped and the air phase becomes discontinuous. The trapped air builds up high air pressure, and therefore reduces the effectiveness of the compaction. The research conducted by Gilbert (1959) and Langfelder et al. (1968) support Hilf's (1956) pore pressure explanation for the shape of the compaction curve that the air permeability is zero close to the OMC. Hilf (1956) believed that negative pressures in the moisture films are interconnected for the moisture content used in field compaction and these pressures result in an all-round effective compressive stress on the soil skeleton which is equal in magnitude to the negative pressure. However, Bishop (1959) and Bishop et al. (1960) explained that capillary pressure acts as an effective stress by a factor of χ. However, it is very difficult to determine the value of χ and direct measurements are difficult to perform.

2.2.2.4 Lambe's theory (1958)

Lambe (1958) explained the shape of the compaction curve using surface chemical theory. When the moisture content is low, the electrolyte concentration of pore water is high. Therefore, the inter-particular repulsion force between the soil particles reduces, which allows flocculation to occur at low moisture content and results in low compacted dry density of the soil. If more water is added to the soil, the electrolyte concentration in pore water becomes low. As a result, the inter-particular repulsion force and the compacted dry density of the soil increase. Olson (1963) noted that Lambe's (1958) theory is based on the double layer theory, which can be used to predict the shape of the swelling curve of sodium illite. However, this is not applicable for calcium illite, which has a similar compaction curve to other soils. Olson (1963) therefore concluded that Lambe's (1958) theory lacks general acceptability.

2.2.2.5 Olson's theory (1963)

Olson (1963) explained the compaction curve using effective stress theory. At the dry side of the OMC, the degree of saturation and pore pressure increase with the increase of moisture content, resulting in reduction of the effective stress and limiting the shearing stress of the soil. Therefore, the compacted dry density of the soil increases. Olson (1963) noted that Proctor's lubrication theory (1933) and Hogentogler's viscous water theory (1936) are applicable for low moisture content compaction curves. With very low moisture content, the electrical forces which attract the first layer of the water to the mineral surfaces are stronger than the forces between the water molecules. Water acts as a lubricant between the soil particles at this stage. The addition of more water results in the formation of menisci and creates the peak of the compaction curve. If more water is added to the soil, the compacted dry density of the soil starts to decrease. Low OMC compaction curves can be seen if the soil has a high percentage of plate-shaped particles (Olson, 1963).

2.2.2.6 Barden and Sides's theory (1970)

Barden and Sides (1970) undertook an experimental project to investigate the compaction processes of unsaturated clay and related their results to microscopic observations. It was found that initially the water is absorbed by the micro pores of the clay particles. The macro pores which are filled with air have high strength and are able

to resist high compaction stresses. Consequently, clay gives a low compacted dry density at low moisture content. If sufficient water is mixed with clay prior to compaction, the macro pores become wetter and weaker and due to compaction, these macro pores are broken down. Therefore, the compacted dry density of the soil increases. If more water is added to clay beyond OMC, the water layers in the clay become thicker. Consequently, the compacted dry density of the soil decreases.

In general Proctor's (1933), Hogentogler's (1936) and Lambe's (1958) theories are reasonably consistent with the existing knowledge at the time when these theories were developed. However, none of these theories were subjected to diagnostic laboratory experiments. Therefore, according to Kurucuk (2011), these theories are rather speculative. Hilf (1975) stated that the effective stress explanation of the shape of compaction curve carried out by Hilf (1956), Olson (1963) and Barden and Sides (1970) appears to be more reasonable than the lubrication, viscous water and physio-chemical theories.

2.2.3 Compaction methods

The compaction efforts on soil can be divided into four types: vibration, impact, kneading and pressure. These different types of efforts are found in the two principal modes of compaction: static and vibratory. Static force is simply the dead weight of the machine, applying downward force on the soil surface, compressing the soil particles. The addition or subtraction of the weight of the machine is the only way to change the effective compactive force on the soil. Static compaction is confined to the upper layers of soils and its effect is limited to a certain depth. Kneading and pressure are examples of static compaction. Vibratory force uses engine-driven mechanisms to create a downward force in addition to the static weight of the machine. The vibrating mechanism is usually a rotating eccentric weight or piston/spring combination in rammers. The compactors deliver a rapid sequence of blows (impacts) to the surface, thereby affecting the top layers as well as deeper layers. Vibration moves through the material, setting particles in motion and moving them closer together to achieve the highest density possible. Depending on the material being compacted, a certain amount of force must be used to overcome the cohesive nature of the particular particles. Different types of rollers are used in the field to compact soils. The three most common types of rollers are: sheeps

foot rollers, used mainly for clayey and silty soils; smooth-drum rollers and vibratory rollers, used primarily for granular soils.

2.2.4 Compacted soil under environmental loading

As stated earlier, field compaction is typically specified on the basis of the laboratory Proctor test, which characterises the compaction curves. It is not yet clear how the laboratory Proctor test relates to field compaction. In addition, it is impossible at the compaction design stage to predict the likely volumetric behaviour of compacted fills under environmental loading that may be imposed during their field operation. Compacted soils can exhibit complex volumetric behaviours under environmental loading, such as deformation under compressive loading, swelling during wetting, collapse during wetting, swelling pressure development under constrained conditions, cracking during drying, tensile loading, and change in behaviour during wet/dry cycles. During compressive loading, compacted soil usually deforms elastically. However, if the compacted soil is subjected to wetting before the compressive loading, it may also deform plastically. On the other hand, if the compacted soil is subjected to wetting, it may show a wide range of swelling or collapse behaviours. In addition, compacted soil may be subjected to constrained wetting, when swelling pressure develops which can be detrimental to shallow foundations and other rigid structures such as buried pipes. Moreover, during drying, tensile loading and cracking may develop in compacted soils. In addition, the volumetric behaviour of compacted soil may change completely during wet/dry cycles, which can lead to the failure of a structure a long time after construction. Therefore, the current practice of compacted filling requires to be improved to cater for these field scenarios.

2.3 Net stress and suction based constitutive models for unsaturated soils

Most constitutive models for unsaturated soils developed to date use net stress and suction as constitutive variables, either independently (e.g., Fredlund and Morgenstern, 1976; Alonso et al., 1990; Wheeler and Sivakumar, 1995; Sivakumar and Wheeler, 2000) or in combination (e.g., Loret and Khalili, 2002; Sheng et al., 2008). According to Sheng (2010) and Kodikara (2012), past research on the modelling of the volumetric behaviour of unsaturated soils can be divided into three types: the Barcelona Basic

Model (BBM), the effective stress model and the Sheng-Fredlund-Gens (SFG) model. In the following section, brief explanations of these unsaturated soil models are presented.

2.3.1 Barcelona Basic Model (BBM)

Alonso et al. (1990) proposed the first elasto-plastic model for unsaturated soils, which is known as the Barcelona Basic Model (BBM). The net stress $(p = \sigma - u_a)$ and suction $(s = u_a - u_w)$ are used as independent stress state variables in this model. The normal or virgin compression behaviour is presented as:

$$v = N(s) - \lambda(s)ln\frac{p}{p^c} \ldots\ldots\ldots\ldots\ldots\ldots\ldots\ldots\ldots\ldots\ldots\ldots\ldots\ldots\ldots..\ldots..\textbf{Equation 2-1}$$

where, $v(= 1 + e)$ is the specific volume, $\lambda(s)$ is the slope of normal compression line (NCL) and p^c is a reference stress state for which $v = N(s)$.

In Equation 2-1, $\lambda(s)$ is defined as:

$$\lambda(s) = \lambda(0)[(1 - r)e^{-\beta s} + r \ldots\ldots\ldots\ldots\ldots\ldots\ldots\ldots\ldots\ldots..\ldots\ldots.\textbf{Equation 2-2}$$

where, $\lambda(0)$ is the slope of the NCL for saturated soil, r is a constant parameter related to the maximum stiffness of the soil and β is also a constant parameter which controls the rate of increase of soil stiffness with suction.

In the BBM, $N(s)$ is defined as:

$$N(s) = N(0) - \left(\lambda(0) - \lambda(s)\right)lnp^c - \kappa_s ln(\frac{s + p_{atm}}{p_{atm}}) \ldots\ldots\ldots\ldots\ldots\ldots.\textbf{Equation 2-3}$$

where, $N(0)$ is the specific volume, at a reference stress state p^c for saturated soil.

From the above discussion, it can be stated that $N(s)$ and $\lambda(s)$ are functions of suction. Therefore, it is possible to plot multiple lines defined by different suctions to form a state boundary surface (SBS) in $v - s - p$ space for normal compression of soil (Zhang and

Lytton, 2009; Kodikara, 2012). The unloading due to reduction of p and reloading are handled by a slope given by κ in $v - \ln(p)$ plane (Kodikara, 2012).

Wheeler and Sivakumar (1995) made some modifications to the BBM. For example, they abandoned the use of a reference stress (p^c) at which the change of suction only produces elastic volume deformations (a yield curve is a straight vertical line in suction and stress relationship), and began the use of atmospheric pressure as a reference pressure in the volume change equation. Wheeler and Sivakumar (1995) also started to use empirical values for $\lambda(s)$ and $N(s)$, rather than introducing an equation. In addition, Wheeler and Sivakumar (1995) and Sivakumar et al. (2010) noticed in the experimental results that $\lambda(s)$ increases with increasing suction. This is completely opposite to the observation from the BBM. As hydro-mechanical coupling, Vaunat et al. (2000) and Thu et al. (2007) incorporated the SWCC into the BBM. However, the same assumption for the slope of the NCLs $(\lambda(s))$ as that proposed in the BBM was retained.

Chiu and Ng (2003) also incorporated the SWCC into the BBM. For the variation of the slope of the NCLs $(\lambda(s))$, a similar approach to that proposed in the BBM was used. Nevertheless, to fit the experimental data, the parameter "r" was considered to be bigger than unity, which gives a situation similar to that proposed by Wheeler and Sivakumar (1995). Wheeler et al. (2002) also proposed a similar modification in order to capture the increase in compressibility with the increase in suction. This is a reasonable modification and captures the behaviour of tested soil in their studies well because soil compressibility increases with the increase in suction, particularly for compacted soils.

In conclusion, the BBM is the first and most widely accepted elasto-plastic model for unsaturated soils, and the other models based on two stress state variables approach are mainly derived in a similar manner or have been further improved by the addition of other important behaviours of unsaturated soils not covered in the BBM (e.g., incorporation of the SWCC).

2.3.2 Effective stress model

In the effective stress model, a combination of net stress $(p = \sigma - u_a)$ and suction $(s = u_a - u_w)$ is used for model formulation. This approach was proposed by Bolzon et

al. (1996). Following Bishop's (1959) approach, an effective or skeleton stress ($\sigma - u_a + S_r(u_a - u_w)$) is used in this approach as a combination of net stress ($p = \sigma - u_a$) and suction ($s = u_a - u_w$) (Loret and Khalili, 2002). This modification gives an advantage over the BBM when the transition zone between unsaturated and saturated soils is considered. The virgin compression equation of this model is similar to the BBM with the net stress replaced with the effective or skeleton stress. The available experimental evidence indicates that, even with the definition of effective stress, there exists a SBS for virgin compression, since both N and λ can still be functions of suction (Kodikara, 2012). Therefore, this dilutes the effectiveness of the effective stress concept. Among others, Santagiuliana and Schreer (2006) included hydraulic hysteresis in the model. However, this modification did not improve compaction prediction because only the wetting path is followed during compaction. Again, as required for hydro-mechanical coupling, Gallipoli et al. (2003a) argued that both N and λ are functions of not only suction but also of the degree of saturation (S_r). These researchers provided the following relationship that produced acceptable results for volume change as well as for the critical state of shearing for certain datasets:

$$v = (N - \lambda \ln(p'))(1 - a(1 - e^{b\xi})) \dots\dots\dots\dots\dots\dots\dots\dots\dots\dots\dots\dots\text{Equation 2-4}$$

where, N and λ are the two parameters of the NCL for saturated states, the effective stress p' is defined as ($\sigma - u_a + S_r(u_a - u_w)$) and ξ is a positive variable representing bonding effects due to suction and may be given as $f(s)(1 - S_r)$.

With the effective stress model, Loret and Khalili (2002) were able to uniquely represent critical state shearing with the effective stress but not the volume change. Houlsby (1997) suggested to use different work conjugates than those which were used in the BBM. Tarantino and De Col (2008) explained the static soil compaction results where they used the average skeleton stress ($\sigma - u_a + S_r(u_a - u_w)$) and modified suction ($s^* = ns$) as work conjugates. In addition, Tarantino and De Col (2008) considered the change in suction with loading by incorporating the model proposed by Gallipoli et al. (2003b). Their model is similar to that developed by Gallipoli et al. (2003a), but uses different stress state variables (Kurucuk, 2011).

2.3.3 Sheng-Fredlund-Gens (SFG) model

This model was proposed by Sheng et al. (2008), and is known as the Sheng-Fredlund-Gens (SFG) model. This model was developed in a different way than the other models, because an incremental form of the basic volumetric deformation was considered. The mathematical formulations of this volumetric model were developed by extending the incremental volumetric equation for saturated soil to unsaturated soil by adding a suction parameter. The rate of volumetric strain $(d\varepsilon_v)$ of the SFG model is suggested in the following form:

$$d\varepsilon_v = \lambda_{vp}\frac{dp}{p+f(s)} + \lambda_{vs}\frac{ds}{p+f(s)} \quad\text{..Equation 2-5}$$

where, dp is the change in vertical net stress, ds is the change in suction, λ_{vp} is the slope of the NCL for saturated soil defined in double logarithmic relationship and λ_{vs} is the slope of the volume change vs. suction curve defined in double logarithmic graph. Sheng et al. (2008) noted that these coefficients are functions of suction up to the air entry value. This also indicates that λ_{vp} and λ_{vs} will have values corresponding to saturated soil and then they would decrease as suction increases with desaturation. The function $f(s)$ is taken as $'s'$ by Sheng et al. (2008), but could have other functions. Equation 2-5 is integrable for vertical net stress (p), which changes under a constant suction, or for suction (s), which changes under a constant vertical net stress, which leads to:

$$ln(v) = lnN(s) - \lambda_{vp}ln\frac{p+s_0}{p_0+s_0} \quad\text{...Equation 2-6}$$

where, $ds = 0$ and $N(s)$ is the specific volume at an initial stress state (p_0, s_0). If $dp = 0$ and suction $(s) < s_{sa}$, where, s_{sa} is the saturation suction. Then:

$$ln(v) = lnN(s) - \lambda_{vp}ln\frac{p_0+s}{p_0+s_0} \quad\text{...Equation 2-7}$$

and, when $dp = 0$, p_0 equals unity and $(s) > s_{sa}$. Then:

$$ln(v) = lnN(s) - \lambda_{vp}ln\frac{p_0+s_{sa}}{p_0+s_0} - \lambda_{vp}(1 - \frac{s_{sa}+1}{s+1}) \quad\text{...........................Equation 2-8}$$

According to Sheng and Zhou (2011), with the SFG approach, the SBS will depend on the stress path. This means that if a soil specimen is dried to a particular suction (s) from the slurry state and then loaded to a stress (p), it will have different specific volume to another soil specimen if that is loaded to stress (p) at saturation and then dried to the same suction (s). Zhang and Lytton (2008) stated that with the SFG model, there can be path dependency even in the elastic space. One of the major hindrances in its application to compacted soil is that according to Equation 2-5, the void ratio decreases with increasing suction (at a constant stress, say such as nominal stress) according to the second term of the equation. However, it is well established that in virgin states of compacted soils (c.f., Wheeler and Sivakumar, 1995; Kodikara, 2012), the void ratio increases with increasing suction or decreasing moisture content due to the introduction of macro structures during the soil preparation process.

2.4 New volumetric framework for compacted unsaturated soils

Kodikara (2012) proposed a new framework, namely the MPK, for the volumetric constitutive behaviour of unsaturated soils, with particular emphasis on compacted soils. In this framework, void ratio (e), net stress (p) and moisture ratio (e_w) are used as constitutive variables, while suction (s) is treated as the fourth (dependent) variable.

2.4.1 Features of the MPK framework

In this section, different features of the MPK framework, including the theoretical basis of giving prominence to moisture ratio over suction in unsaturated soil modelling, the experimental basis of the framework, the relationship of the MPK framework with the compaction curve and the LWSBS, the basic building block of the MPK framework, are presented.

2.4.1.1 Justification of using moisture ratio over suction

Kodikara, his students and co-workers at Monash University have been working for over a decade on cracking of unsaturated soils, soil compaction and hydraulic behaviour with atmospheric coupling in unsaturated soil mechanics research. In many instances, moisture content has been given prominence over suction. For instance, Kodikara and

Choi (2006), Costa (2009) and Kodikara (2012) used a hydric coefficient $(\alpha = \left(\frac{\partial e}{\partial e_w}\right)_p)$
in soil cracking research to predict the tensile stresses developed during soil shrinkage. Also, Rajeev and Kodikara (2011) used (α) in soil-structure interaction in soil swelling problems. Gould et al. (2011) presented the swelling and shrinkage behaviour of environmentally stabilised soils (soils that have undergone a sufficient number of wet/dry cycles to reach a stabilised state) under loading as a surface in $e - w - p$ space. All these achievements suggested that the moisture ratio can be used in place of suction in many field applications. In an environmentally stabilised state, unlike suction, the moisture ratio does not show hydraulic hysteresis with void ratios during wetting and drying (Fleureau et al., 2002; Gould et al., 2011). Kodikara (2012) stated that this may happen because both moisture ratio and void ratio display significant hysteresis with suction and the effect appears to cancel out when these two are considered together. Kodikara (2012) also explained that from a pore interaction point of view, this may happen because both drying and wetting the water-filled pores lead to void ratio changes, thereby producing a direct correspondence of the void and moisture ratio. In the MPK framework paper, Kodikara (2012) developed a theoretical backing for the use of moisture ratio (or equivalent moisture content or specific moisture volume) over suction. However, prior to environmental stabilisation, it is expected that soil undergoes irreversible changes which reflect the non-unique behaviour in the $e - e_w$ plane.

Ignoring the mechanical dissipation associated with fluid flow and air compressibility, and following Houlsby (1997), the rate of work input per unit volume of unsaturated soil during volumetric compression can be written as:

$$W = (p + S_r s)d\varepsilon_v - ns S_r \ \dots\dots\dots\dots\dots\dots\dots\dots\dots\dots\dots\dots\dots\dots\dots\text{.}\textbf{Equation 2-9}$$

where, $d\varepsilon_v$ is volumetric strain, n is porosity and s is suction. For isotropic loading, p is the mean net stress and for K_0 (or 1-D) loading, p should be the net (vertical) stress. Taking differentials of the phase equation $S_r e = e_w$ gives:

$$nd S_r = -S_r \frac{de}{(1+e)} + \frac{1}{(1+e)}de_w = S_r d\varepsilon_v + \frac{1}{(1+e)}de_w \ \dots\dots\dots\dots\dots\text{..}\textbf{Equation 2-10}$$

Substituting Equation 2-10 into Equation 2-9 gives:

$$W = pd\varepsilon_v - \frac{s}{(1+e)} \, de_w = -p\frac{de}{(1+e)} - \frac{s}{(1+e)} \, de_w \quad \ldots\ldots\ldots\ldots\ldots..\ldots\ldots..\textbf{Equation 2-11}$$

Therefore, based on Equation 2-11, during volumetric changes under isotropic or K_0 conditions, the constitutive behaviour can be expressed by the state variables of p, e, e_w and s. As a result, Kodikara (2012) suggested that it is possible to develop state boundary surfaces using $e - e_w - p$ or $v - v_w - p$ space, where $dv = de$ and $dv_w = de_w$ and the suction will be related to the void ratio and moisture ratio through the soil's water characteristics curve or water retention curve. Groenevelt and Bolt (1972) stated that a deforming (swelling) system is characterized by void ratio, water ratio, net vertical stress (in the case of K_0 conditions) and suction. Therefore, for a certain value of net stress, there exists a single value of void ratio and moisture ratio which fully defines the suction. Gould et al. (2011) developed an environmentally stabilized state surface in $e - w - p$ space on this basis.

2.4.1.2 Experimental basis of the MPK framework presented in Kodikara (2012)

Most research studies undertaken on compacted soils have been based on experiments carried out on unloaded soils after compaction. However, Kodikara (2012) suggested that it would be enlightening to study the behaviour of soil during compaction to establish evaluation of the initial state. Kurucuk (2011) stated that the shape of the compaction curve is qualitatively predictable using soil mechanics principles. Kurucuk (2011) also showed that the shape of the compaction curve could be predicted using Equation 2-5, even neglecting the suction change and with the compressibility coefficient associated with dp significantly changing with suction. In the MPK framework paper, Kodikara (2012) used Tarantino and De Col (2008) data set for the experimental basis of the MPK framework. Tarantino and De Col (2008) reported $e - e_w - s - p$ data for static compaction of Speswhite kaolin using an oedometer which was instrumented with a high performance tensiometer. All of these tests fell on the dry side of optimum. Kodikara (2012) reproduced a consistent set of $e - e_w - s - p$ data by fitting regression curves to the measured data. Figure 2-2 shows the graphical representation of these data in $e - e_w - p$ space. It is clear that the void ratio increases with decreased moisture ratio at

a certain net stress. This is typical behaviour of compacted soils, particularly at the dry side of optimum (Wheeler and Sivakumar, 1995). Kodikara (2012) stated that this behaviour is inherent to the mixing of dry soils with water to the various moisture contents which lead to particle aggregation. The constant stress contours form a surface in $e - e_w - p$ space, which is identified as the LWSBS by Kodikara (2012), and this applies only to virgin wetting/loading of compacted soils. The existence of the state boundary surface in $e - s - p$ space has been suggested by a number of researchers (Lloret and Alonso, 1985; Fredlund and Rahardjo, 1993; Zhang and Lytton, 2009). Nevertheless, the uniqueness of such a surface for highly expansive soils has been questioned in the $e - s - p$ space (Justo et al., 1984; Lloret et al., 2003). Kodikara (2012) noted that wetting collapse occurs along a constant stress contour in $e - e_w$ relationship when a swelling path at a constant stress intersects this contour. An example is presented in Figure 2-2. A loose soil specimen with a constant moisture ratio $e_w = 0.63$ is loaded from nominal stress at Point O to 700 kPa net stress at Point A. Now, if this specimen is wetted subsequently, it would follow a path AC on the LWSBS. On the other hand, if the specimen is unloaded to 275 kPa at Point B and then wetted, the state path would swell first and follow a path like BD. Now, path BD would hit the LWSBS at Point D and then undergo plastic collapse down to a Point E on the saturation line, following the LWSBS. This simple example highlights the basis of the MPK framework. However, as will be explained in Chapter 6, the swelling gradient BD is a combination of swelling of aggregates and slipping at the aggregate contacts.

2.4.1.3 Relationship to the compaction curve

Kodikara (2012) examined the direct relationship of LWSBS to the well-known compaction curve. Figure 2-3a presents a set of compaction curves in the $e - e_w - p$ framework. A typical line of optimums (LOO) is also shown, which generally falls at around 80 to 90% saturation, particularly for clayey soils. Kodikara (2012) noted that if the compaction curves are generated during the compaction process (as in Tarantino and De Col (2008) dataset), they will contain both elastic and plastic deformations, while the traditional compaction curves generated from unloaded soil specimens will have only the plastic component of deformation. In the MPK framework paper, Kodikara (2012) explained the significance of the LOO. When the compaction moisture content is increased from the dry side of optimum, on the LOO, the air is trapped and, therefore,

the air phase becomes discontinuous at the wet side of optimum (Hilf, 1956; Gilbert, 1959; Langfelder et al., 1968; Kodikara, 2012). This state may be considered to be close to a wetting saturation from a drier state (Kurucuk, 2011). Kodikara (2012) stated that this situation happens all along the LOO. Therefore, both water and air pressure build up when the soil wetter than an optimum is compressed. In Figure 2-3, this behaviour may be explained by considering two initial loose states of soil at the beginning of compaction given by Points A_0 and B_0. The soil from A_0 reaches the LOO at A when the net stress reaches p_A. At this point, the air has just been trapped but is still close to the atmospheric conditions. Therefore, the externally applied stress $p_A{}^e$ is equal to p_A. Now, if the soil from B_0 is also compressed, it would reach the LOO at B at a smaller net stress than p_A (i.e., $p_B < p_A$). If the applied stress (p_B) is increased further to the same applied stress as $p_A{}^e (= p_A)$, the air and water pressure would build up and the net stress p would increase only slightly, which will give rise to a further small reduction in void ratio, a small increase in dry density and a small increase in saturation, as given by Point B_1. Similarly, compaction of soil to the same applied stress from a higher moisture content like at C_0 will lead to a state like C_1, with even less net stress. Now, if the excess water pressures that built up at states B_1 and C_1 are allowed to dissipate completely, then new drained states will be reached, as shown at B_2 and C_2 respectively. These drained states can be joined up as a curve AB_2C_2 representing the drained part of the $e - e_w$ curve corresponding to the net stress p_A, as shown in Figure 2-3. At Point C_2, the soil is fully saturated, and the water pressure will therefore be zero (or atmospheric). The corresponding effective stress will be p_A and the void ratio e (which is equal to the moisture ratio e_w) will be that which corresponds to the normally consolidated line for fully saturated soil at the effective stress p_A. From C_2, B_2 to A, the soil suction will increase and the effective stress will therefore be maximum at A. Figure 2-3 also shows the conceptual suction contours on the LWSBS. The suction values will increase from the NCL as e_w decreases.

2.4.1.4 The Loading Wetting State Boundary Surface (LWSBS)

In the MPK framework, the LWSBS is defined as the surface depicting the loosest states compacted soil can attain under loading or wetting or a combination of these paths. According to Kodikara (2012), the basic building block of the LWSBS is the family of compaction curves with a drained section between the LOO and the NCL.

The $e - e_w$ curve corresponding to $p = 1$ kPa (i.e., loosely compacted soil) represents the upper boundary of the LWSBS, where, $e_{s0} = e_w$ on the NCL for the saturated soil and $e = e_0^*$ when $e_w = 0$. Kodikara (2012) assumed that the variation of e with e_w is a cosine function given by:

$$\frac{e}{e_s} = [\left(\frac{e_0}{e_s} - 1\right) \cos\left(\frac{\phi e_w}{e_s}\right) + \left(1 - \frac{e_0}{e_s} \cos(\phi)\right)] \frac{1}{1-\cos(\phi)} \quad \text{............................Equation 2-12}$$

here, $\phi = \frac{\pi}{e_{wc}/e_s}$, where, e_{wc} is the optimum moisture ratio and e_s is the void ratio at saturation for stress p. For simplicity, Kodikara (2012) modelled the variation of $e(= e_w)$ along the NCL by the traditional linear relationship in semi-log graph:

$$e_s = e_{s0} - \lambda_1 \ln(p) \quad \text{...Equation 2-13}$$

where, λ_1 is the compression index for saturated soil and e_{s0} is the saturated void ratio at $p = 1$ kPa. Kodikara (2012) assumed that the variation of e_0 is a similar form with a compression index λ_2:

$$e_0 = e_0^* - \lambda_2 \ln(p) \quad \text{...Equation 2-14}$$

where, e_0^* is the void ratio at $e_w = 0$ and $p = 1$ kPa. Kodikara (2012) noted that although this linear relationship is unlikely to be valid for the entire stress range, particularly at very low stresses, it can serve the purpose of the explanation in this framework. Figure 2-4 shows the general topographic features of the LWSBS. Kodikara (2012) used the following parameters in this example: $\lambda_1 = 0.07$; $\lambda_2 = 0.1$; $\frac{e_{wc}}{e_s} = 0.75$; $e_{s0} = 1$ and $e_0^* = 1.4$. Kodikara (2012) mentioned that in $e - e_w - p$ space, the LWSBS tapers down to the point depicting $e = e_w = 0$ at infinite stress, which represents a mathematical singularity. As stated earlier in the definition of the LWSBS, the LWSBS provides the upper surface for the volumetric behaviour of soil. Kodikara (2012) noted that the LWSBS is applicable for the loading and wetting pathways only. There is another surface for drying state paths which is located slightly below the LWSBS.

2.4.2 Explanation of the volumetric behaviour of compacted/virgin unsaturated soils using the MPK framework

In the MPK framework paper, Kodikara (2012) explained various volumetric behaviours, such as compression, unloading and recompression, swelling and/or collapse due to wetting, dependence of collapse potentiality on operational stress, swelling pressure and cracking of compacted/virgin unsaturated soils using the MPK framework. In this section, these volumetric behaviours are described on the basis of the MPK framework.

2.4.2.1 Compression, unloading and recompression

Kodikara (2012) explained the volumetric behaviour of unsaturated soils due to compression, unloading and recompression phenomena. According to the MPK framework, when a loose soil specimen with a particular moisture content is compacted to a certain high stress, the state path will follow the LWSBS along the constant moisture content path from nominal stress to the compaction stress. These constant moisture content paths are presented in Figure 2-5. These paths can be called normal/virgin compression curves for these constant moisture contents. It can be seen from Figure 2-5 that each constant moisture content path touches the LOO, and with further loading, reaches the NCL without significant reduction in the void ratio from those achieved at the LOO. Now, if the soil specimen is unloaded to a lower stress from the compaction stress, the state path will follow an unloading-reloading line, with a gradient of κ in the $e - \log(p)$ relationship. In Figure 2-2, state path OA is on the LWSBS for virgin compression of the soil specimen, while state path AB is the unloading pathway inside the LWSBS. According to Kodikara (2012), if the soil specimen is loaded again, it will behave elastically until it reaches the previous compaction stress and then start to follow the LWSBS again.

2.4.2.2 Swelling and/or collapse during wetting

Kodikara (2012) stated that if a compacted soil is wetted under a certain stress, it can undergo some swelling (depending on the soil shrink/swell potential) and, in many cases, can collapse, leading to potentially significant compression strains and settlement. In the MPK framework paper, clear indications are provided when the soil specimen will swell and/or collapse during wetting using the LWSBS. If a loose soil specimen is loaded to a certain high stress and then wetted, the soil will follow the constant e_w line on the

LWSBS to reach the compaction stress and then during wetting, it will collapse until the LOO following that specific stress line. After the LOO, the soil will swell and reach the saturation line. In Figure 2-6, state path GHIJ is the graphical presentation of the above explanation. Now, what will happen to the state path if a soil specimen is compressed to a high stress from loose state and then unloaded to a certain lower stress and then wetted? This type of scenario is presented in Figure 2-6. A soil specimen is compacted to a stress of 403 kPa and then unloaded to 1 kPa stress. In the figure, Point O is the location of that unloaded point. Point O is on the 403 kPa stress line because the elastic expansion due to unloading is almost zero. According to Kodikara (2012), if the soil specimen is wetted subsequently, it will swell following a wetting path OA′ or OA and then after the interception of the LWSBS, it will start to follow the 1 kPa stress line on the LWSBS and finally, move to the saturation line at A′′′. The gradient of the OA′ or OA line is called the average hydric coefficient α_{av} , which is also used by Rajeev and Kodikara (2011). Sivakumar and Wheeler (2000) examined the experimental data obtained from compacted Speswhite kaolin, which indicated that the value of α can vary in a range of 0.14 to 0.25. For an expansive soil, the α value is higher than the normal value. The value of α usually increases as the LOO is approached. Again, in Figure 2-6, if the soil specimen is unloaded to 55 kPa stress now, and then wetted, the state path will swell following a wetting path OB and subsequently, start following 55 kPa constant net stress contour on the LWSBS until saturation. It is clear that whether soil specimen will swell or collapse totally depend on the unloading position of the state path inside the LWSBS. If the unloading position is close the LWSBS, overall deformation of the soil specimen will probably be collapse, while the soil specimen with unloading position far away from the LWSBS will probably swell during wetting. Sivakumar and Wheeler (2000) also reported overall swelling of densely compacted soil specimen, while collapse behaviour was observed for loosely compacted soil specimen.

2.4.2.3 Compression after partial wetting/drying

There are different scenarios where compression can take place after partial wetting/drying. If a loose soil specimen with a particular moisture content is compacted to a certain high stress, the state path will follow the LWSBS along that constant moisture content path from nominal stress to the compaction stress. Subsequently, during partial wetting, it will collapse on the LWSBS until the final moisture content. Then, if

the soil specimen is compressed again, the state path will follow the LWSBS that final moisture content path up to the final compression stress. Other scenarios are possible. For instance, if a soil specimen is compacted to a certain stress level and then unloaded to a lower stress level, the state path follows the LWSBS and then moves inside the LWSBS due to unloading. Now, if the soil specimen is partially wetted, the state path will swell and, depending on the moisture input and the difference between compaction stress and unloading stress, the state path may intercept the LWSBS. During further compression, if the state path intercepts the LWSBS, it will follow the LWSBS at that final moisture content path up to the final compression stress. However, if the location of the state path is still inside the LWSBS after the wetting stage, during further compression, the state path will move along the unloading/reloading path inside the LWSBS, then intercept the LWSBS, and finally follow the LWSBS. Now the question is what will the value of the yield stress be if the soil specimen is loaded again at the as-compacted moisture content or after wetting or drying? The answer depends on the shape of the LWSBS. If compression is performed with the as-compacted moisture content, the state path will intercept the LWSBS at the same stress as the compaction stress, while if loading is applied after wetting or drying, the state path will intercept the LWSBS at a lower or higher stress than the compaction stress, respectively. Figure 2-7 shows the of the interception of the LWSBS of a compacted unloaded soil specimen during loading at as-compacted moisture content or after wetting or drying. The soil specimen is prepared at 700 kPa initially and then unloaded to 100 kPa. If the soil specimen is loaded at as-compacted moisture content, the state path will intercept the LWSBS at 700 kPa, while if the soil specimen is loaded after wetting or drying, the state path will intercept the LWSBS at 300 and 1300 kPa, respectively. As stated earlier, yield stress depends on the shape of the LWSBS. During drying, the state path moves away from the LWSBS, while during wetting, the state path comes close to the LWSBS. That is why soil specimens yield at lower stress during wetting and higher stress during drying. It should be noted that, although the drying scenario was also presented, the original work of Kodikara (2012) discussed the wetting/loading scenarios only. A conceptually similar argument may be made for the drying case, but it is possible that the LSWSB will change with drying, and this may need further investigation in future.

2.4.2.4 Dependence of collapse potentiality on the operational stress

Kodikara (2012) stated that the collapse potentiality, given as a reduction of void ratio or a compressive strain during collapse, depends on a number of state variables. However, if the initial compaction remains the same, it is possible to create a relationship between collapse potentiality and operational stress. Figure 2-6 shows a soil specimen compacted to the stress of 403 kPa from loose state and then unloaded to 1 kPa and subsequently wetted. Point O will be the unloaded position of the state path. During wetting, it will follow path OAA‴, and the collapse potential will drop to zero or even negative when wetting is applied at the nominal stress (p_1) (1 kPa in this example). For any other wetting events under stresses higher than p_1, the collapse potential will increase. For example, for wetting at a stress of 55 kPa, the swelling will happen between Point O and A and the collapse will occur from Point B to C. The amount of swelling and collapse are 'a'. Therefore, the overall collapse potential is zero for this particular example. The collapse potential will be maximum when the soil specimen is wetted at the compaction stress (403 kPa in this example). In Figure 2-6, for this particular example, 'b' is that maximum collapse potential. If the stress is increased further along path OD, the collapse potential will decrease and reach zero as the LOO is approached at D as shown. Figure 2-8 presents the computed collapse potential with operational stress for three initial positions. It is clear that in all three cases, maximum collapse occurs when the soil specimens are wetted at the compaction stress. The collapse potential will be lower than maximum if the operational stress is lower or higher than the compaction stress.

2.4.2.5 Constrained volume wetting and swelling pressure

When an unsaturated soil specimen is constrained against swelling during wetting, pressure develops against the constrained surface (Boyd and Sivakumar, 2011; Kodikara, 2012). This pressure is called swelling pressure. For various geotechnical engineering problems, such as foundations and buried pipes, this pressure needs to be considered. Alonso et al. (1987) and Kodikara (2012) state that there are three common methods to determine swelling pressure: (a) soaking the soil specimen to swell under some stress and loading it subsequently until the specimen reaches the original void ratio at the initial moisture content; (b) finding the swell and collapse under-load curve by testing a series of identical specimens at different loads and then finding the stress that gives zero

swelling (in soaking under load curve); and (c) the soil specimen is wetted when the swelling is fully constrained and the maximum stress that develops is measured using a load cell. Alonso et al. (1987) also state that, on the basis of experimental evidence, method (a) gives the highest and method (b) the lowest value for swelling pressure. These observations have led to the conclusion that swelling is path-dependent and not a fundamental property of soil. Kodikara (2012) examined these methods using the MPK framework. Figure 2-6 shows the soil specimen is at point O initially (in unloaded state below the LWSBS with ($e_0 = 0.63$)). Under method (a), the soil specimen is wetted under a stress (for example 1 kPa), and will therefore swell/collapse to A and then swell back to A´´´ on the saturated line. When it is subjected to drained compression (loading after soaking), it will follow a path close to the NCL and reach the initial void ratio at a stress somewhat higher than 148 kPa (at Point E), which can be considered the swelling pressure for method (a). In method (b), swelling and collapse will take place at various stresses, and it appears that a stress of 55 kPa will give the same void ratio when the specimen collapses, giving a swelling pressure of 55 kPa. Therefore, it can be seen that method (a) gives the highest and method (b) gives the lowest value of swelling pressure. Kodikara (2012) noted that method (c) involves wetting under fully constrained conditions or at a constant void ratio and monitoring the pressure development to detect the maximum swelling pressure that develops. This means that the hydromechanical path of this method takes place on the constant void ratio plane through the initial void ratio. In $e - e_w - p$ space, the void ratio is usually located along the z-axis, which means that the constant void ratio plane means the horizontal $x - y \equiv e_w - p$ plane. Therefore, this hydromechanical path can be better viewed on the $e_w - \log(p)$ plane passing through that void ratio. Figure 2-9 shows constrained volume swelling paths during wetting using the MPK framework. Usually the state path of the constrained volume swelling starts from inside the LWSBS. During wetting at a constant void ratio, net stress increases up to the interception point on the LWSBS and then the state path starts to follow the LWSBS by maintaining the constant initial void ratio. During the following of the LWSBS, net stress reduces initially until the LOO and then net stress increases with the increase of moisture ratio up to the saturation line. An experimental result is presented in Figure 2-9b from Imbert and Villar (2006). It is evident that the constrained swelling state path of this test during wetting is qualitatively the same as that predicted by the MPK framework.

2.4.2.6 Cracking

When a compacted soil is dried under restrained conditions, tensile stresses can develop, which eventually lead to tensile fracture or cracking. Kodikara (2012) explains tensile fracture using the following equation:

$$dp = K[d\varepsilon_v - d\varepsilon_{sh}]$$ ………………………..…………………..……**Equation 2-15**

where, $d\varepsilon_v = -\dfrac{de}{1+e_0}$; $K = -\dfrac{1}{1+e_0}\left(\dfrac{\partial p}{\partial e})_{e_w}\right)$ and $d\varepsilon_{sh} = -\dfrac{\alpha_p}{1+e_0}de_w$. It should be noted that K is the bulk modulus at constant moisture content and the sign convention for positive compression stresses/strains is followed. If $d\varepsilon_v$ is zero (the fully constrained condition), the full free shrinkage strain (more precisely, the shrinkage under constant stress) will give rise to the development of the maximum tensile stress possible. When the constraints are partial (some actual compressive strains occur (i.e., $d\varepsilon_v > 0$), lower tensile stress would develop. At the other extreme, when no restraints are provided or under free shrinkage conditions, no tensile stresses will develop (i.e., $dp = 0$).

2.5 Suction contours on the compaction curves and the Soil Water Characteristics Curve (SWCC)

Kodikara (2012) states that most compaction-related research has been performed on unloaded soil under nominal or small amounts of stress. Therefore, all the results obtained from these tests usually lie in the unloading space. Even if the well-known compaction curves are also plotted in the unloading condition which contain only the plastic deformation of the soil as the elastic deformation is regained during unloading process. Tarantino and De Col (2008) is the only study where load, deformation and suction data were captured during the compaction process and also in the unloading condition. Numerous studies have been performed where the value of suction was measured on the compaction curves (c.f., Gens et al., 1995; Ridley and Perez-Romero, 1998; Dineen et al., 1999; Romero, 1999). However, as these studies were performed on unloaded soil, the obtained constant suction contours lie in the unloading space. Figure 2-10 presents the observed typical constant suction contours on the compaction curves in the unloading space. Tarantino and De Col (2008) also observed a similar type

of constant suction contours on the compaction curves in the unloading space. All the experiments that have been discussed so far were performed on clayey or silty soil. Montanez (2002) found similar types of constant suction contours on the compaction curves in the unloading space using a mixture of bentonite and sand. As a result, in the unloading space, the constant suction contours which are presented here are very common in the compaction curves for most clayey soil types.

The Soil Water Characteristics Curve (SWCC) is the relationship between the moisture content and the soil suction when other variables, such as temperature and net stress, remain the same. According to Gould (2011), the SWCC is measured in the laboratory, commonly as a series of discrete points which for modelling purposes are represented as a continuous curve by fitting some form of mathematical function. The SWCC tends to move downward with the increase of net stress. The characteristic features of the SWCC are presented in Figure 2-11. According to Fredlund and Xing (1994), the air entry value of the soil is the suction where air starts to enter the largest pores in the soil, while the residual moisture content is the moisture content where a large suction change is required to remove additional moisture from the soil. However, Fredlund and Xing (1994) also noted that these definitions are vague and empirical procedures for their quantification would be useful. The value of minimum suction value (S_{min}) is usually close to zero near saturation, while oven-dried soil gives the maximum value of suction ($S_{max} = 10^6$ kPa). The SWCC can be divided into three segments: initial, central and final. In Figure 2-11, the slopes of the initial, central and final portions of the curves are shown as m, n and o respectively. It is apparent that the central portion is steeper than the other two portions of the SWCC curve. Usually, the air entry value, which occurs at the end of the initial portion and at the beginning of the central portion, takes place close to the LOO. On the other hand, as the SWCC tends to move downward with the increase of net stress, the value of residual moisture content decreases with the increase of net stress. The SWCCs are called main wetting/drying curves if they are developed over the full wetting/drying range. The main wetting/drying and in-between curves (or scanning curves) can be found in studies such as those of Mancuso et al. (2012), Pham et al. (2003), and Pham et al. (2005). The main wetting curve can be used to determine the suction contours on the LWSBS of the MPK framework. However, there is some

confusion about the influence of these curves on changes to the void ratio and on virgin states to non-virgin states.

2.6 Behaviour of compacted fills under environmental loading

Compacted fills which are mainly unsaturated soils commonly suffer tress due to environmental loading (wetting/drying). Volume change behaviour is the biggest challenge in unsaturated soils, where collapse and swelling of the Compacted fills can lead to excessive settlements and heave respectively (e.g., Sitharam et al., 1995; Skinner, 2001; Boyd and Sivakumar, 2011); combining them together may results differential settlements (e.g., Charles et al., 1993; Skinner et al., 1999; Blanchfield and Anderson, 2000; Boyd and Sivakumar, 2011). Uneven distribution of moisture is the main contributor of differential settlements of the Compacted fills underneath the structure. During rain or watering, the soil near the edge of the structure absorbs more water than the soil at the central part underneath the structure. Therefore, at different areas underneath the structure, the heave and settlement will be different. In the case of side slopes, the soil can also move laterally near the slope. A number of researchers have worked on the detrimental effects of environmental loading on structures, especially on houses built on compacted fills (c.f., DiMillio, 1982; Noorany, 1987; Noorany and Stanley, 1990; Lawton et al., 1992; Meehan and Karp, 1994; Noorany and Stanley, 1994; Day, 1995; Houston and Houston, 1995; Ferber et al., 2008). Anywhere on the compacted fill, if the soil is wetted equally along the depth of the compacted fill, the top soil may undergo swelling, while the bottom soil may experience compression. Figure 2-12 presents the typical relationship between the strain and the operational stress anywhere on compacted fill along the depth of the fill. Most researchers have found a similar type of relationship between the strain and the operational stress. Operational stress increases from the top to the bottom of compacted fills. It is evident that for the same amount of moisture change, soil experiences heave if the operational stress is low, while soil with high operational stress undergoes collapse. Kodikara (2012) explained this behaviour with the help of the MPK framework. According to the framework, during wetting, unloaded soil swells first and then collapses after the interception of the LWSBS. The MPK framework also states that the collapse potential decreases during wetting with the increase of the difference between compacted and unloaded stresses. Therefore, as the difference between compacted and unloaded stresses is high for the top

soil, it experiences heave. On the other hand, the lower layer soil compresses more because of the small difference between the compacted and unloaded stresses. Kodikara (2012) also noted that the maximum collapse will occur at the compacted stress and after that, with the increase of stress, collapse potential reduces. However, in engineered fills, since it is not common for operational stresses to be higher than the compaction hence research into such high stresses is not readily available. However, it is possible to encounter such conditions, especially in unengineerd fills or fills made with less compaction (e.g., hand-held equipment or light rollers). Since the compaction stress is low, the operational load does not need to be very large to exceed the compaction stress. Under such conditions, during wetting, the state path would be along the LWSBS, mainly featuring collapse strains. Similarly, it is possible for construction delays to generate such scenarios. For instance, let us say that a compacted fill is made under relatively dry conditions but prior to the construction of the building significant wetting of the fill took place causing it to swell substantially. Under such conditions, the state points would be brought closer to the LWSBS and during subsequent loading it is possible for LWSBS to be intercepted. This can lead to reduction in yield stress and therefore, increased settlement under structural loading. There is therefore merit in applying the MPK framework to examine fill performance due to wetting, and this will be undertaken in Chapter 7.

2.7 Summary

At the beginning of this chapter, different theories, curves and methods of compaction and the behaviour of compacted soil under external and environmental loadings were presented. The compaction process of soil has not been well examined, particularly in a quantitative sense. Moreover, most researchers have been interested in the dry side of optimum. Therefore, it is difficult to explain the wet side of optimum using the existing compaction theories.

Past research on the constitutive models for unsaturated soils have been discussed in the second section of this chapter. All of these models use net stress and suction as constitutive variables, either independently (i.e., BBM and its variations) or in combination (i.e., the effective stress model and the SFG model). It is well accepted that 'matric' suction, defined as the pressure deficit between air and water pressure at the

water meniscus, has a direct stress-like influence on soil behaviour. Therefore, it is quite fitting that it is incorporated as either an independent or component stress variable in unsaturated soil constitutive modelling. However, a major practical difficulty of using suction is its accurate measurement, both in the laboratory and in the field. This difficulty has been the main contributor to the significant gap that currently exists between theoretical models and practical applications. In addition, it has been recognised recently that to explain unsaturated soil behaviour, suction alone is not generally adequate, but soil moisture content or its surrogates, such as the soil's degree of saturation, needs to be incorporated in the constitutive modelling, commonly referred to as hydromechanical coupling. Therefore, there is merit in pursuing alternative ways of incorporating hydromechanical coupling that will make unsaturated models more practical.

Kodikara (2012) has presented a novel framework (referred to as the MPK framework) for explaining the volumetric behaviour of compacted unsaturated soils using void ratio (e), net stress (p) and moisture ratio (e_w) as constitutive variables, while suction (s) is treated as a fourth (dependent) variable. The MPK framework, its features and the volumetric behaviour of compacted unsaturated soils have been discussed in the next section of this chapter. A novel feature of the MPK framework is the establishment of a direct relationship between the traditional compaction curve and soil's constitutive behaviour. In the framework, soil suction is presented as the fourth variable explaining volumetric soil constitutive behaviour, and it has been shown that suction is not essential for explaining most state paths that are relevant to practice, such as soil deformation under loading/unloading, wetting under constant (net) stress, collapse potential evaluation, swelling pressure development under constrained volume, shrinkage cracking during drying, and likely soil 'environmental' stabilisation behaviour under wet-dry cycling.

The shape of the loading/wetting suction contours on the compaction curves and different features of the SWCC have been presented in the later part of this chapter. The compaction curves are usually plotted in the unloading condition. Therefore, the suction contours provided on the compaction curves are laid in the unloading space. The suction contours on the LWSBS of the MPK framework can be obtained from the main wetting curves which are actually the SWCCs developed from virgin compression data. Finally,

the heave and the compression behaviour of compacted fills under environmental loading have been presented as the last topic of this chapter. The typical relationship between the strain and the operational stress anywhere on the compacted fill along the depth of the fill can be explained with the help of the MPK framework. Structural failure due to plastic compression during construction loading on the compacted fills has also been discussed in the light of the MPK framework.

2.8 Scope of the research

On the basis of the literature review undertaken, the following scope of research was developed to be undertaken in the research detailed in this thesis. When the MPK framework (Kodikara, 2012) was first published, a qualitative validation of the MPK framework was provided on the basis of typical experimental data and the behaviour of compacted soils in the research literature. Therefore, the complete validation and extension of the MPK framework are the two main objectives of the current research program. The following goals were set to achieve the first objective:

➢ To provide a complete set of experimental evidence in support of the MPK framework for two types of soils, namely kaolin, which is commercially available lightly reactive clay, and Merri Creek soil, which is a reactive natural soil.

➢ To validate the MPK framework using different datasets available in the research literature.

The second and final objective of this research is the extension of the MPK framework. The following goals were set for this purpose:

➢ An expansion of the MPK framework to dynamically compacted soils. To do this, an experimental method is needed to develop the LWSBS for dynamically compacted soils. In addition, different state path validation tests are required for the examination of the validity of the MPK framework. Two types of soils were used in the experimentation, namely lightly expansive kaolin, and expansive Merri Creek soil.

➢ Incorporation of the loading/wetting suction within $e - e_w - p$ space. In order to achieve this, it is necessary to develop hypotheses regarding the shape of the suction contours on and inside the LWSBS in $e - e_w - p$ space. This may be achieved by considering data available in the research literature and generating new data using kaolin and Merri Creek soil. Moreover, a mathematical representation of suction contours is also required in the 3-D space of $e - e_w - p$.

➢ Incorporation of the average hydric coefficient within $e - e_w - p$ space for both kaolin and Merri Creek soils.

➢ Comparison between the MPK framework-predicted heave/settlement results and the experimental results obtained from the research literature for field-scale compacted fills. For this purpose, a hypothetical 30-meter high embankment with different initial conditions, such as degree of saturation and compaction level is needed to model major wetting events using the concept of the MPK framework for both kaolin and Merri Creek soils.
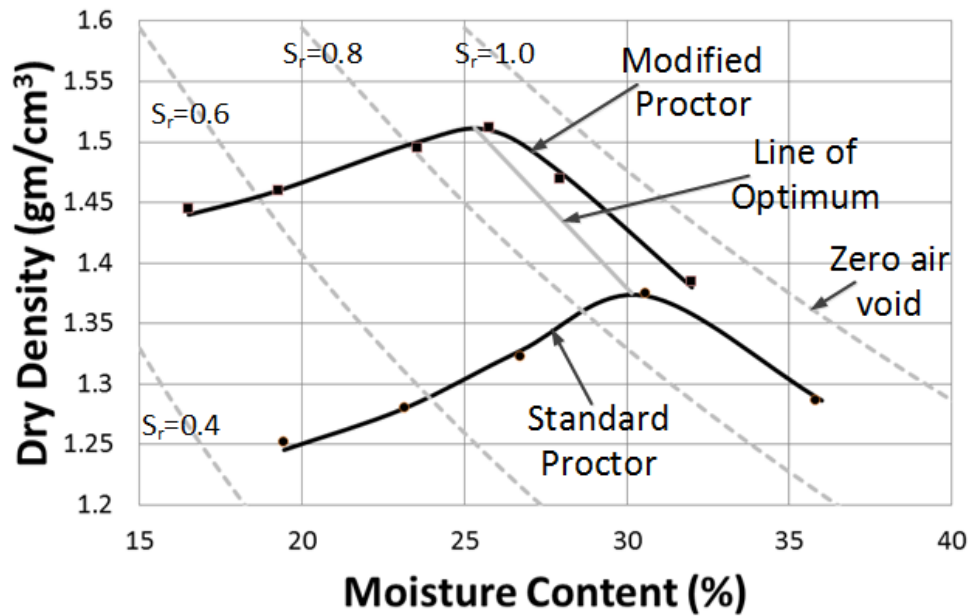
Figure 2-1: Typical soil compaction curves obtained from laboratory Standard and Modified Proctor tests
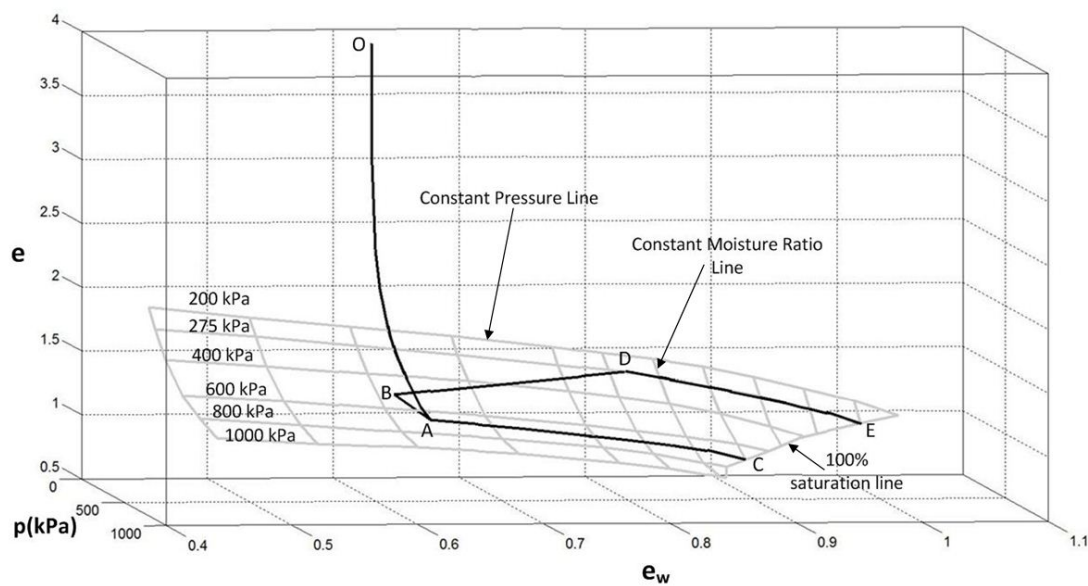
Figure 2-2: Tarantino and De Col (2008) test data in $e - e_w - p$ space (obtained from Kodikara (2012) with permission from Canadian Science Publishing)

(a) Family of $e - e_w$ at constant applied stress (or energy)
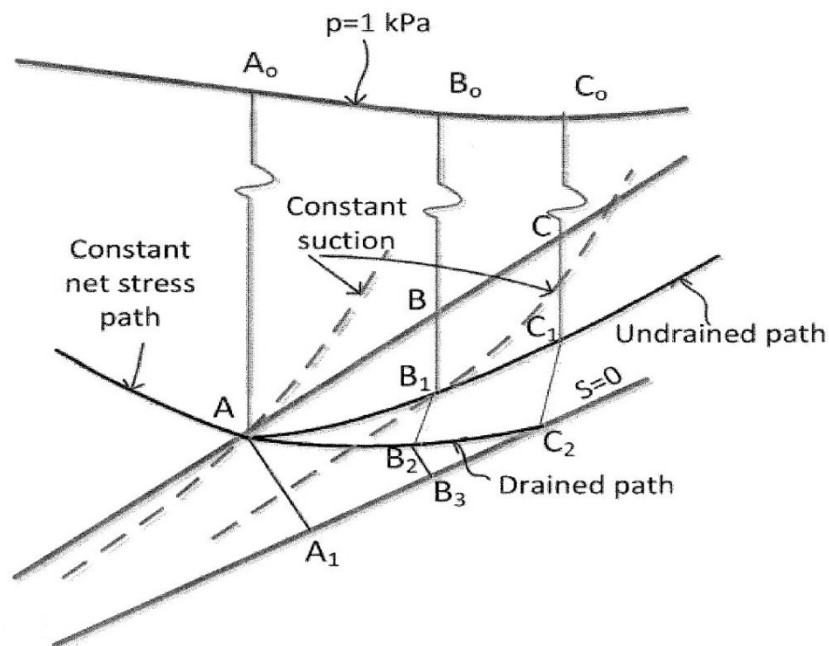
(b) Expanded view of a constant net stress line crossing the LOO towards the normally consolidated line (NCL)

Figure 2-3: Family of $e - e_w$ at constant applied stress (or energy) (obtained from Kodikara (2012) with permission from Canadian Science Publishing)

(a) In compaction space
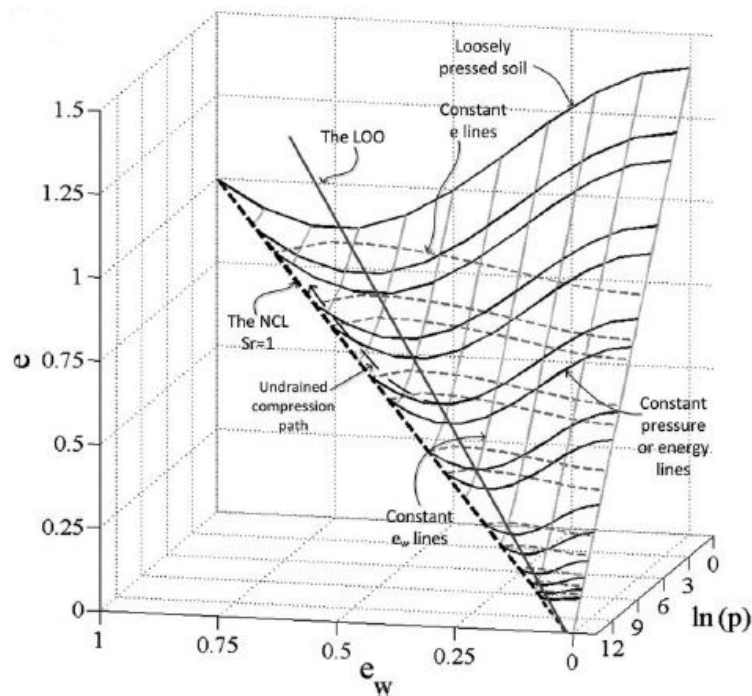
(b) In $e - e_w - p$ space

Figure 2-4: Three-dimensional view of the LWSBS (obtained from Kodikara (2012) with permission from Canadian Science Publishing)

Figure 2-5: Constant moisture content NCLs in $e - \log(p)$ plane (obtained from Kodikara (2012) with permission from Canadian Science Publishing

Figure 2-6: Demonstration of swelling and/or collapse during wetting of compacted/ virgin unsaturated soils (obtained from Kodikara (2012) with permission from Canadian Science Publishing)

(a) In $e - e_w$ plane
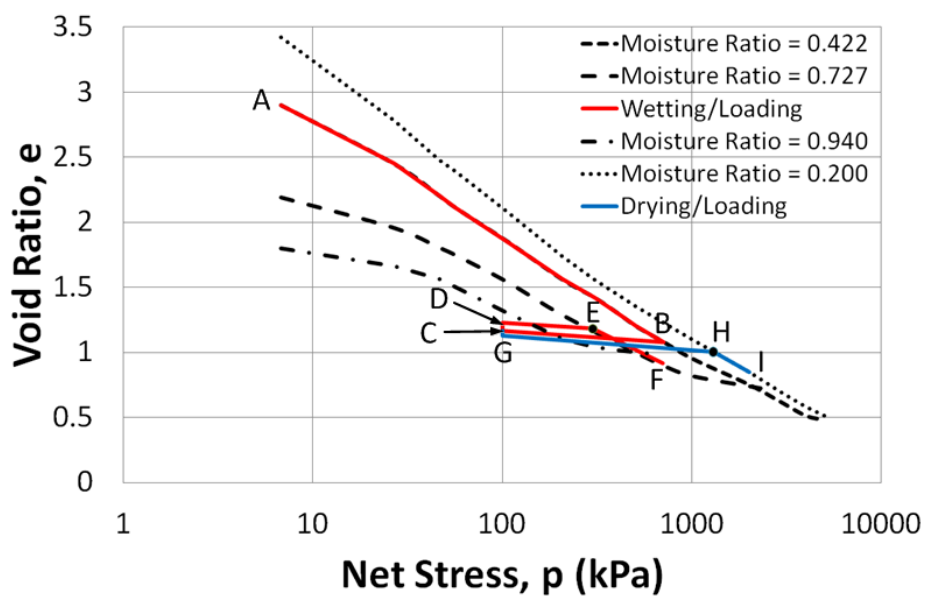
(b) In $e - \log(p)$ plane

Figure 2-7: Yielding of compacted unloaded soil specimens during loading at as-compacted moisture content or after wetting or after drying
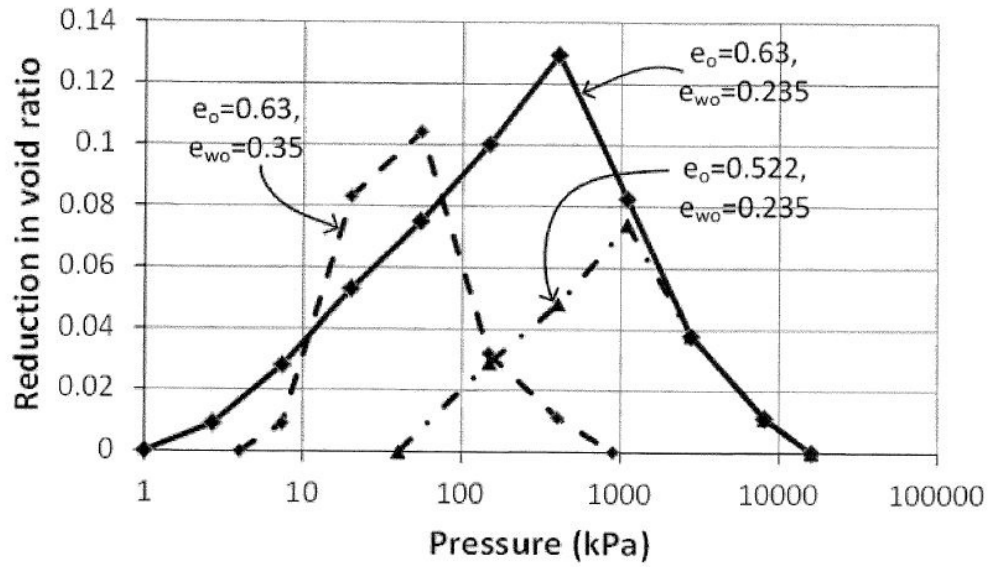
Figure 2-8: Relationship between the collapse potentiality given as reduction of void ratio with operational stress (obtained from Kodikara (2012) with permission from Canadian Science Publishing)

* This material may be downloaded for personal use only. Any other use requires prior permission of Canadian Science Publishing.
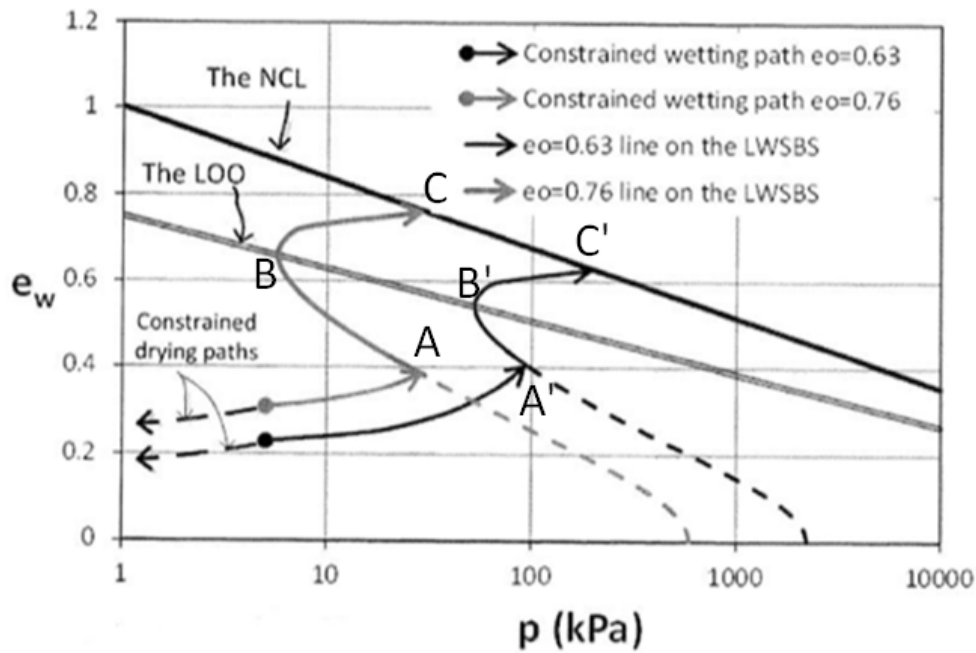
(a) Hydromechanical behaviour during constrained swelling predicted using the MPK framework
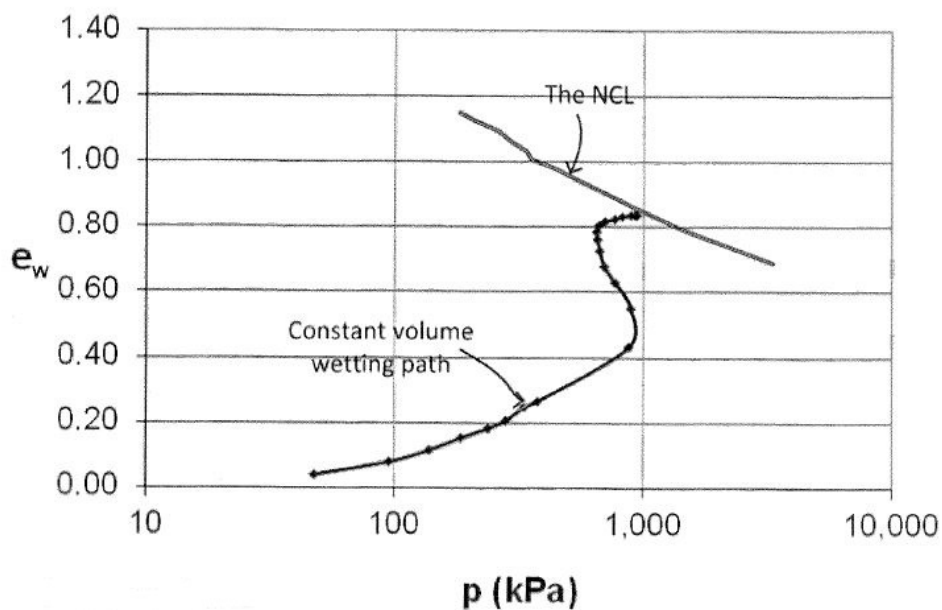
(b) Experimental result of constrained swelling by Imbert and Villar (2006)

Figure 2-9: Hydromechanical behaviour during constrained swelling (obtained from Kodikara (2012) with permission from Canadian Science Publishing)
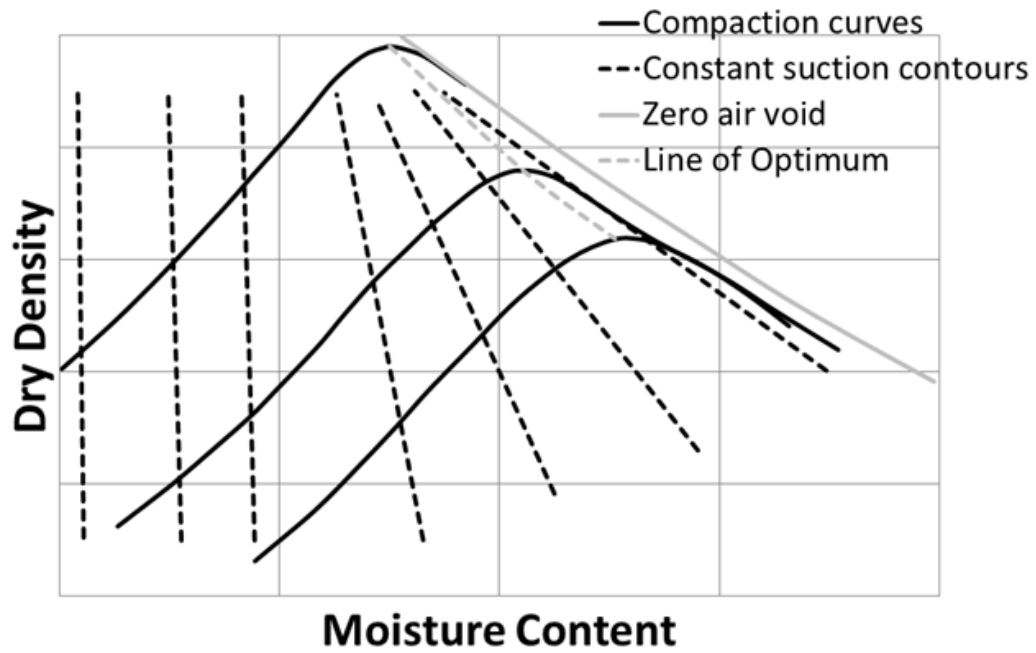
Figure 2-10: Typical constant suction contours on the compaction curves in the unloading condition observed from literature
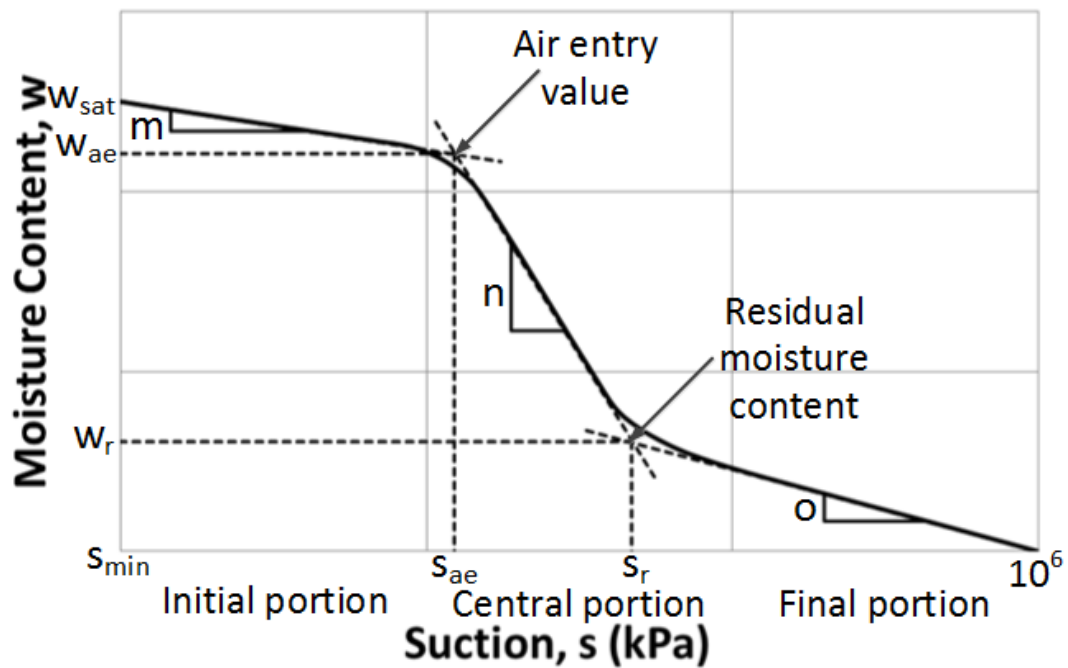
Figure 2-11: Idealised SWCC with labelled features (x-axis in log scale)
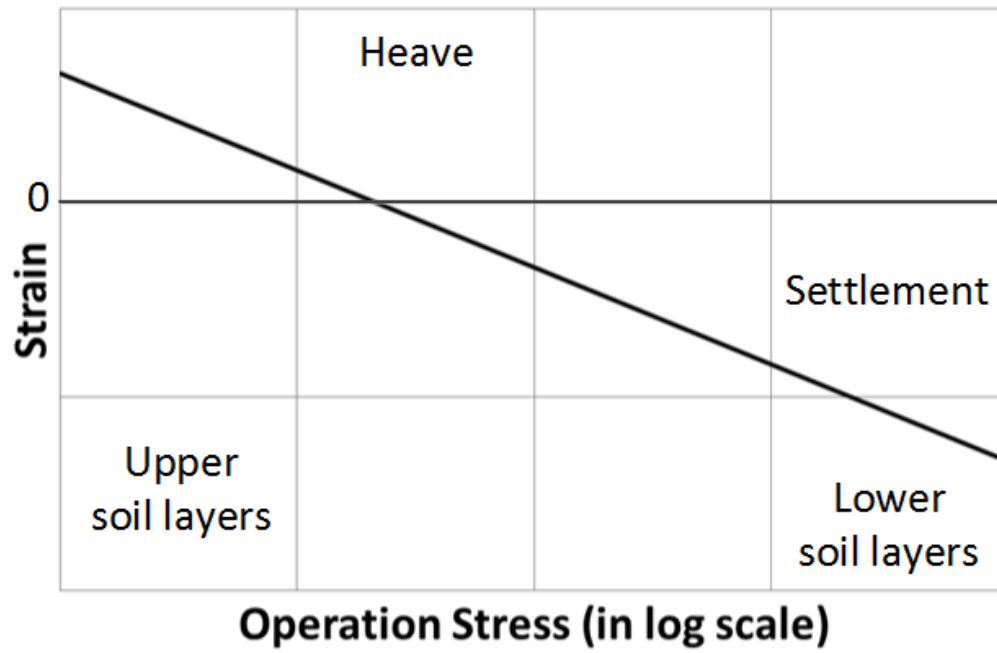
Figure 2-12: Typical relationship between strain and operational stress anywhere on the compacted fill along the depth of the fill due to equal wetting

Chapter 3

PRELIMINARY SOIL TESTS, SOIL PREPARATION AND EXPERIMENTAL APPARATUS

3.1 Introduction

Details of the preliminary soil tests, soil preparation and experimental apparatus are presented in this chapter. In this research, two types of soils were used, kaolin, known by the trade name Ecalite, and Merri Creek soil. Kaolin is a commercially available white (china) lightly reactive clay; on the other hand, Merri Creek soil is a grey/black reactive natural soil sourced from Merri Creek in north-east Melbourne. While the kaolin is available in dry form in bags, the preparation of Merri Creek soil involved drying, grinding, and subsequently sieving to remove any deleterious material. Both soils were used in the experiments reported in Chapters 4 & 5. Chapter 4 presents the validation of the Monash-Peradeniya-Kodikara (MPK) framework using statically compacted soils, while Chapter 5 extends the MPK framework into dynamically compacted soils. The first part of this chapter presents basic geotechnical property tests for soil classification, specific gravity, particle size distribution, Atterberg limits, Proctor compaction and consolidation. The final part of this chapter presents soil preparation technique and experimental procedure and apparatus used for different tests, such as validation of the MPK framework using statically compacted soils and extension of the MPK framework into dynamically compacted soils.

3.2 Soil property tests

As stated earlier, two types of soils were used in the experimentation: kaolin, known by the trade name Ecalite, and Merri Creek soil. Kaolin is manufactured at Granville, New South Wales, Australia. Merri Creek soil is a residual soil weathered from basalt, which has subsequently mixed with alluvium from the creek (Joyce, 1992b). Because of its sticky nature, it is commonly used for the preparation of cricket pitches around Melbourne. The basic geotechnical property tests of the soils are presented below. All tests were performed following Australian Standards.

3.2.1 Particle size distribution

First, both soils were wet-sieved following Australian Standards AS1289.3.6.3 (2003). All of the kaolin soil particles passed through a 75μm wet-sieve, while 6% of the Merri Creek soil particles were retained on the sieve. Hydrometer testing was performed for both soils because most of the soil particles were sized less than 75μm. Figure 3-1 shows the particle size distributions of the two soils. It is clear that 75% of the particles of the kaolin soil and 50% of the Merri Creek soil are clay-sized. It is also evident that the kaolin soil does not have any sand-sized particle, while 6% of the particles of the Merri Creek soil are sand-sized.

3.2.2 Atterberg limits

The objectives of the Atterberg limit tests are to find the liquid limit, plastic limit and shrinkage limit of the soil. The Australian Standards (AS1289.3.4.1, 2008; AS1289.3.1.1, 2009; AS1289.3.2.1, 2009) were followed for these tests. Before the tests, the Merri Creek soil was sieved using 425μm sieve and the portion of the soil that passed through the sieve was used for the tests. On the other hand, kaolin soil was used from the bag because the particles were finer than 425μm. Water was added to the dry soil which was left for 24 hours before the tests. This allowed uniform water penetration into the soil.

3.2.2.1 Liquid limit

The four-point Casagrande method was used to determine the liquid limit of the soils (AS1289.3.1.1, 2009). The liquid limit was found to be 61% for the kaolin soil and 72% for the Merri Creek soil.

3.2.2.2 Plastic limit

The plastic limit of the soils was determined according to Australian Standards AS1289.3.2.1 (2009). Following the standard, a 0.125 inch or 3 mm diameter soil thread was rolled from 8-10 gm of soil which was crumbled under the pressure of rolling. The plastic limits were found to be 28% for the kaolin soil and 33% for the Merri Creek soil. Therefore, the plasticity indices of the kaolin and the Merri Creek soil were 33% and 39% respectively.

3.2.2.3 Linear shrinkage test and shrinkage limit

Following Australian Standards AS1289.3.4.1 (2008), water was mixed with the soil up to the liquid limit, and grease was then applied inside the test mould and the slurry was placed in the mould. The specimen was then dried at a constant room temperature. Linear shrinkage was found to be 9.3% for the kaolin soil and 13.5% for the Merri Creek soil. It can be inferred that the shrinkage/swelling reactivity of Merri Creek soil is higher than that of kaolin soil. The shrinkage limit was found to be 24.2% and 11.9% for the kaolin and the Merri Creek soil respectively. It can be inferred that because of its higher linear shrinkage, Merri Creek soil has a low shrinkage limit.

3.2.3 Soil classification

To classify the soils, the Unified Soil Classification System (USCS) was used according to Australian Standards AS1726 (1993). Figure 3-2 shows USCS classification of fine-grained soils adopted from AS1726 (1993). It is clear that kaolin soil falls in the clay of high plasticity (CH) region, while Merri Creek soil falls on the A-line, which means that it has some organic clay properties.

Another soil classification system, the United States Department of Agriculture (USDA) was also used to classify the soils. USDA classifies the soil based on the sand, silt and clay proportions. According to the USDA classification, kaolin is a clayey soil, while Merri Creek soil is a silty clay.

3.2.4 Specific gravity

A fully automatic density analyser, Multipycnometer, produced by Quantachrome Instruments, was used to determine the specific gravity of the soils. At the beginning of the test, an oven-dried soil sample was weighed and put into a sample cup. The gas displacement technique is used by the Multipycnometer to determine the soil volume in the sample cup. Because of its research-grade purity and non-reactive nature, helium is preferred for use. The specific gravity results obtained from this instrument are usually very precise because it reports data from five consecutive runs. The specific gravity was found to be 2.65 for the kaolin soil and 2.62 for the Merri Creek soil.

3.2.5 Proctor compaction test

Soil compaction by applying stress is a common practice in geotechnical engineering. Increment of density and improvement of the engineering properties of soil are the main objectives of soil compaction. Soil compaction is usually assessed using Standard and Modified Proctor (SP and MP) compaction tests. Australian standards AS1289.5.1.1 (2003) and AS1289.5.2.1 (2003) were used for the SP and MP tests respectively. For each soil type, compaction tests were performed for different moisture contents. An automatic compaction machine shown in Figure 3-4 was used for all SP and MP compaction tests.

Figure 3-5 and Figure 3-6 show the compaction curves for the kaolin and the Merri Creek soil respectively. It is clear that for kaolin soil, the SP and MP optimum moisture contents (OMCs) are 30.2% and 25.3% respectively, while the SP and MP OMCs of Merri Creek soil are 27.3% and 19.2% respectively. For the SP tests, the maximum dry densities are 1.374 gm/cm^3 for the kaolin soil and 1.4 gm/cm^3 for the Merri Creek soil, and for MP tests, the maximum dry densities are 1.51 gm/cm^3 and 1.65 gm/cm^3 respectively. In addition, the peaks of the compaction curves occur around 90% degree of saturation (S_r) for the kaolin soil and 85% for the Merri Creek soil. As the Merri Creek soil is very sticky and dense in nature, it gives a higher density than the kaolin soil under the same amount of energy. For this reason, the compaction curves of the Merri Creek soil are positioned above the kaolin soil.

3.2.6 Consolidation test

A one-dimensional automatic consolidation testing machine, Loadtrac II, produced by Geocomp Corporation was used for the consolidation tests. First, a slurry was prepared by mixing approximately twice the liquid limit amount of water with the soil. Water was mixed with the soil using a mechanical soil mixer to minimize air bubbles and increase workability. The slurry was then put into a 63 mm diameter and 18.2 mm high oedometer ring. During the consolidation tests, pressure was increased step-by-step and each step lasted 2 to 24 hours, depending on the approximate end of deformation under that pressure.

Taylor's method (Taylor, 1948) was used to calculate the coefficient of consolidation (c_v) for all the soils, which was found to be $1.3*10^{-7}$ m^2/sec for the kaolin soil and $3.2*10^{-8}$ m^2/sec for the Merri Creek soil. The coefficient of volume change (m_v) was determined for 50 to 100 kPa steps. The values of m_v were 0.0016 kPa^{-1} and 0.0014 kPa^{-1} for the kaolin and the Merri Creek soil respectively. Permeability (k) was found to be $2*10^{-9}$ m/sec for the kaolin soil and $4.4*10^{-10}$ m/sec for the Merri Creek soil. Figure 3-7 shows the consolidation curves (e vs log p) of kaolin and Merri Creek soil. By analysing Figure 3-7, the slopes of the compression curves (λ) are found to be 0.251 for the kaolin soil and 0.289 for the Merri Creek soil, and the slopes of the recompression curves (κ) are 0.045 and 0.045 for the kaolin and the Merri Creek soil respectively. A summary of the basic geotechnical properties of the kaolin and the Merri Creek soil is presented in Table 3-1.

3.3 Soil sample preparation

Samples with (gravimetric) moisture content of 0 to 50% were prepared for both soils. In order to prepare homogenously wetted soil from the dry state, soil was sieved onto a tray to make a layer of uniform thickness of around 5 mm and the tray of soil was then placed in a high humidity room (100% humidity) to achieve the targeted moisture content. Subsequently, the soil was thoroughly mixed and placed in sealed plastic bags until further testing, within not less than 48 hours. Soil sample preparation using this process is very time consuming. However, to ensure uniform moisture distribution in the soil, this procedure was followed to prepare the soil samples for all tests.

3.4 Experimental procedure and apparatus

Different experimental procedures and apparatus were used for different types of tests. However, to reduce any friction, for all tests lubricating grease was applied to the walls of the soil compression moulds prior to adding the soil. An experiment was performed to observe the effect of grease on the height of soil specimens. Kaolin soil was used in this experiment. It was found that the void ratio *(e)* does not depend on the height of the soil specimen if grease is applied to the wall of the soil compression mould. Three compression tests were performed on 0% moisture content (oven-dry) kaolin soil specimens. Table 3-2 presents the summary of these compression tests.

Figure 3-8 shows the compression behaviour (e vs log p) in these tests. It is clear that the compression lines of both of the greased specimens are very close to each other, whereas the compression line of the ungreased specimen shows a significant effect. As a result, it can be concluded that greased test results would always be identical, irrespective of the initial height of the soil specimen. Hence, grease was always applied to the walls of the soil compression moulds prior to testing. The experimental procedures and apparatus used for different tests are described below.

3.4.1 Experimental procedure and apparatus for the validation of the MPK framework using statically compacted soil

The first step in the validation of the MPK framework was the development of the Loading Wetting State Boundary Surface (LWSBS). The compression curves of the soil specimens at different (gravimetric) moisture contents (0 to 50%) were used to develop the LWSBS for both soils. The soil was statically compacted into a steel mould of 63 mm internal diameter and 50 mm high, using a 1-D compression set-up, Loadtrac II. Figure 3-9 and Figure 3-10 show the steel mould which was used for the soil compression and the 1-D compression set-up, respectively. As explained earlier, lubricating grease was applied to the walls of the moulds prior to adding the soil to reduce any friction. The initial condition was that the loading cap (weighing 2.12 kg) was loosely placed providing 7 kPa initial stress. A filter medium between the soil and the loading cap was provided for any possible drainage from the top, but the bottom was sealed. For tests dry of the line of optimums (LOO), a higher loading rate of 20 kPa per minute was used up to about 2000 kPa, and a higher loading rate of 100 kPa per minute above 2000 kPa. Once the soil approached the LOO during loading, a much lower loading rate (i.e., 0.1 kPa/min) was used.

After establishing the LWSBS, a series of state path tests was undertaken to examine the validity of the concepts proposed by the MPK framework. To facilitate wetting tests, the top loading cap was modified to allow injection of water into the soil specimen under loading. Figure 3-11 and Figure 3-12 show the loading assembly and the top and bottom configurations of the top loading cap. As these figures show, in order to supply water to the soil specimen, four 3 mm diameter holes were provided in the top cap. A controlled amount of moisture was added through these holes equally using a syringe to increase

the moisture content of the soil specimen to a targeted value. This simple testing mechanism, which was used to wet the soil specimens under stress, was developed based on the confidence obtained from the trial tests. It was found from the trial tests that if the initial heights of the soil specimens under nominal stress are kept at approximately 15 mm for kaolin soil and 10 mm for Merri Creek soil, after each 2% to 5% moisture increment, the soil specimens would take 6 to12 hours to reach equilibrium at the dry side of the LOO. After reaching equilibrium, stress was removed and the soil specimens were tested for moisture contents from at least five different locations of the 63 mm diameter test mould. It was found that these moisture contents ranged around average $\pm$ 0.50% in all cases. Moreover, moisture contents were measured from different locations of the 63 mm diameter test mould at the end of the original tests, and the results also showed that the deviation of moisture contents for any specific test was less than $\pm$ 0.50%. Therefore, it was concluded that this experimental procedure would provide water consistently into the soil and moisture uniformity could be achieved throughout the entire soil specimen. Usually, one single wetting event took place in 4 to 6 steps, depending on the requirement of the number of points to draw the state path in $e - e_w$ plane. Moisture contents could not be measured after every step of moisture injection in these tests. However, the moisture contents of the soil specimens after each step of water application were calculated from the known initial moisture content and the amount of moisture input into the soil during that step. This is how a single wetting event was performed during different state path validation tests. Apart from the modification to the top cap, the other test set-up features were the same as for the compression tests. The constant volume swelling pressure tests were also performed using Loadtrac II. This is a versatile compression machine. Both load control and strain control tests are possible using this machine. One single test can be programed by the combination of load control and strain control manner. Usually loading of soil specimen was performed by load control manner. Then constant volume wetting tests were performed by strain control manner where the strain was programed to zero and the increase of stress was recorded due to wetting.

3.4.2 Experimental procedure and apparatus for the extension of the MPK framework into dynamically compacted soil

Samples with (gravimetric) moisture contents of 12 to 45% were prepared in a fog room for both soils. The soil was then dynamically compacted in a Standard Proctor compaction mould, which has a 105 mm internal diameter and is 115 mm in height. An automated compaction machine shown in Figure 3-4 was used to prepare high and intermediate compaction soil cylinders, while moderate, low and very low compaction soil cylinders were prepared manually. This is because the falling height of the hammer of the automated compaction machine could only be fixed to 300 and 450 mm. The falling height was kept at 150mm during manual compaction. After compaction, soil cylinders were extruded carefully from the mould and wrapped with several layers of plastic and aluminium foil. Finally, the cylinders were placed in plastic bags and stored in a high humidity room.

For subsequent static loading tests, soil specimens were cut from the dynamically compacted soil cylinders after removing them from the fog room. A bottomless steel mould with 63 mm internal diameter and 50 mm in height was used to cut the soil specimens from the dynamically compacted soil cylinders. Figure 3-13 shows the preparation procedure for soil specimens for the static compaction tests. First, the generously-greased steel mould was put upside down on top of a dynamically compacted soil cylinder and then a steel plate was put on the bottom of the steel mould. Next, load was applied on the steel plate manually using a Loadtrac II compression set-up until the soil specimen was inside the steel mould. Subsequently, the soil specimen was separated carefully from the dynamically compacted soil cylinder with the help of a knife and the top surface was made smooth. Finally, as shown in Figure 3-13, the soil specimen was pushed down slowly to the bottom of the test mould and a steel base was attached to the bottom of the mould using duct tape. Following the procedure for static compaction, the soil specimens were compressed using the Loadtrac II compression set-up. A filter medium between the soil and the loading cap was provided for any possible drainage from the top, but the bottom was sealed. For tests dry of the LOO, a higher loading rate of 20 kPa per minute was used up to about 2000 kPa and a higher loading rate of 100 kPa per minute above 2000 kPa vertical stress. Once the soil approached the LOO, a much lower loading rate (i.e., 0.1 kPa/min) was used to provide adequate drained conditions.

After establishing the LWSBS, a series of state path tests was undertaken to examine the validity of the concepts proposed by the MPK framework. The soil specimen preparation technique was similar to that used for the compression tests presented earlier. As the soil specimens needed to be wetted during loading, a similar top loading cap as shown in the validation by static compaction in Figure 3-11 and Figure 3-12 was used to facilitate water ingress. The same process that explained in the statically compacted soil section was used for moisture increment in the soil specimens. Compared with the compression tests, the test set-up features remained the same, with the exception of the load cap. The constant volume swelling pressure tests were also performed using Loadtrac II by following the same procedure explained in the statically compacted soil section.

3.5 Discussion

In the experiments, both light to medium reactive kaolin soil and medium to high reactive Merri Creek soil were used to check the validity of the MPK framework for a wide range of reactivity. Kaolin soil contains more clay particles than Merri Creek soil. For this reason, kaolin soil is classified as clay, while Merri Creek soil is classified as silty clay. Merri Creek soil is very sticky in nature and gives a higher density than kaolin soil under the same energy application.

The application of grease on the wall of the compaction mould is a good way of producing uniform soil specimens at nominal stress. Without grease, the deformation and the strain of the soil specimen become height-dependent. As a result, the chances of obtaining misleading results from experiments increase.

It is very difficult to produce low moisture content (unsaturated) soil samples by mixing water directly in the dry soil, since as soon as the water droplets fall into the dry soil, clods start to form. However, production of low moisture content soil samples becomes very easy if a thin layer ($\approx$ 5 mm) of dry soil is put into the fog room (100% saturation room). As a result, water distribution into the dry soil becomes uniform.

A simple but effective experimental procedure was used to develop the LWSBS for statically compacted soils. Only load and deformation were recorded in these tests. During validation tests on the statically compacted soils, it is very important to produce

soil specimens as uniform as possible at the nominal stress. The application of grease to the wall of the test moulds becomes very useful at that time. Measures must be taken during water application into the soil specimen so that the air can drain out without any interruption. Moreover, sufficient time must be provided for wetting-induced deformation of the soil specimens.

The dynamically compacted soil specimens needed to yield at different stress levels to develop the LWSBS. Soil cylinders were prepared using different compaction efforts. The process used to prepare the soil specimens for static compaction tests from soil cylinders can also be used for large-scale field compaction pads. Similar precautions to those for statically compacted soil specimens must be taken during wetting events to facilitate uninterrupted air drainage.

3.6 Conclusion

All the basic activities related to the experimentation, including the determination of physical properties of the soils, soil sample preparation, experimental procedures and apparatus for the validation and extension of the MPK framework have been presented in this chapter. Kaolin and Merri Creek soil were chosen for the validation experiments to cover a wide range of reactivity. It has been found that the application of grease to the wall of the test moulds is necessary to prepare uniform soil specimens at nominal stress and reduce the frictional effects at the sidewalls. It has also been established that using a fog room to uniformly wet the soil is effective for preparing unsaturated soil samples. A very simple but effective experimental procedure has been developed for the preparation of the LWSBS and for the validation tests for both statically and dynamically compacted soil specimens.

Table 3-1: A summary of geotechnical properties of kaolin and Merri Creek soil

Soil Properties	Kaolin Soil	Merri Creek Soil
Colour	White	Grey / Black
Swelling / Non-swelling	Non-swelling	Swelling
Liquid Limit, LL (%)	61	72
Plastic Limit, PL (%)	28	33
Plasticity Index, PI (%)	33	39
Linear Shrinkage (%)	9.3	13.5
Shrinkage Limit (%)	24.2	11.9
Specific Gravity, G_s	2.65	2.62
Clay Proportion (%)	75	50
Silt Proportion (%)	25	44
Sand Proportion (%)	0	6
Soil Classification		
Unified Soil Classification System	CH	CH / OH
United States Department of Agriculture	Clay	Silty Clay
Standard Proctor Compaction		
Maximum Dry Density (gm/cm^3)	1.374	1.4
Optimum Moisture Content (OMC) (%)	30.2	27.3
Modified Proctor Compaction		
Maximum Dry Density (gm/cm^3)	1.51	1.65
Optimum Moisture Content (OMC) (%)	25.3	19.2
Consolidation Parameters		
Initial Moisture Content (%)	118	113
Compression Index, $(c_c = \frac{\Delta e}{log(\frac{p_2}{p_1})})$	0.58	0.66
Compressibility Parameter, $(\lambda = \frac{\Delta e}{ln(\frac{p_2}{p_1})})$	0.2513	0.289
Unloading-reloading parameter, κ	0.045	0.0454
Coefficient of consolidation, c_v (m^2/sec)	$1.3*10^{-7}$	$3.2*10^{-8}$
Permeability, k (m/s)	$2*10^{-9}$	$4.4*10^{-10}$
Coefficient of volume change, m_v (kPa^{-1}) (at 50 – 100 kPa step)	0.0016	0.0014
Secondary compression, c_α	0.0058	0.056

Table 3-2: A summary of compression tests to observe the effect of grease on soil specimen height

Number of Test	Whether or not Grease applied on the wall of test mould	Specimen Height
1st Test	Not Used	50 mm
2nd Test	Used	50 mm
3rd Test	Used	25 mm
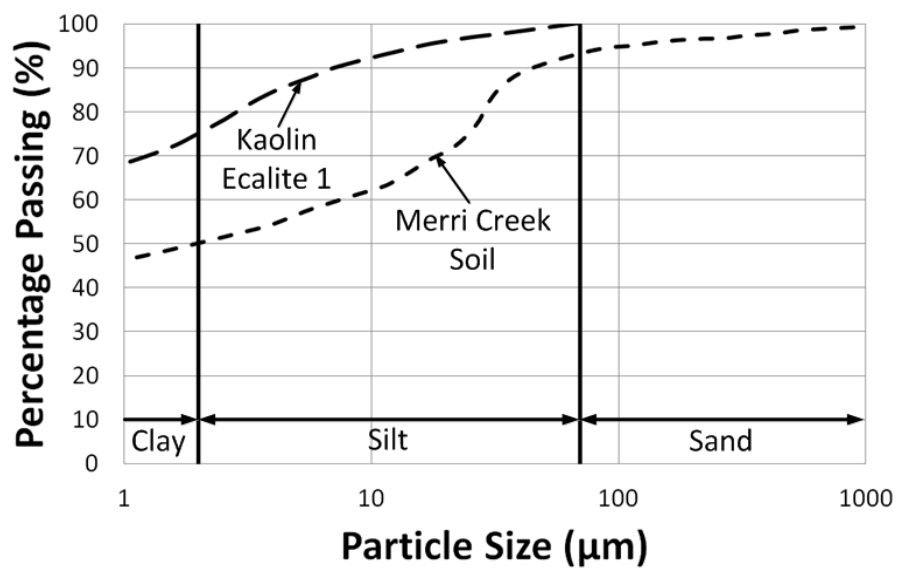
Figure 3-1: Particle size distribution of kaolin and Merri Creek soil
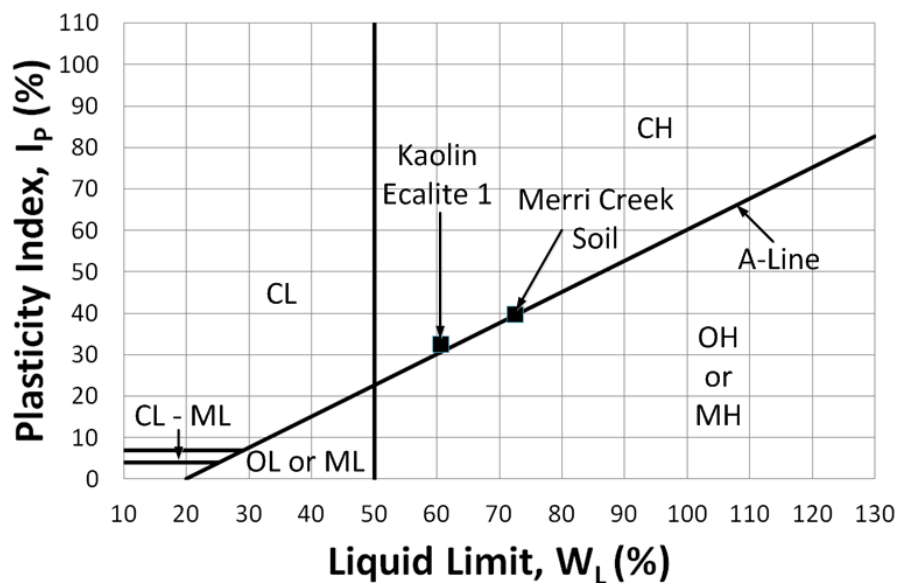
Figure 3-2: USCS classification of fine-grained soils (AS1726, 1993)

Figure 3-3: Multipycnometer. An automatic soil specific gravity testing instrument

Figure 3-4: An automatic compaction machine
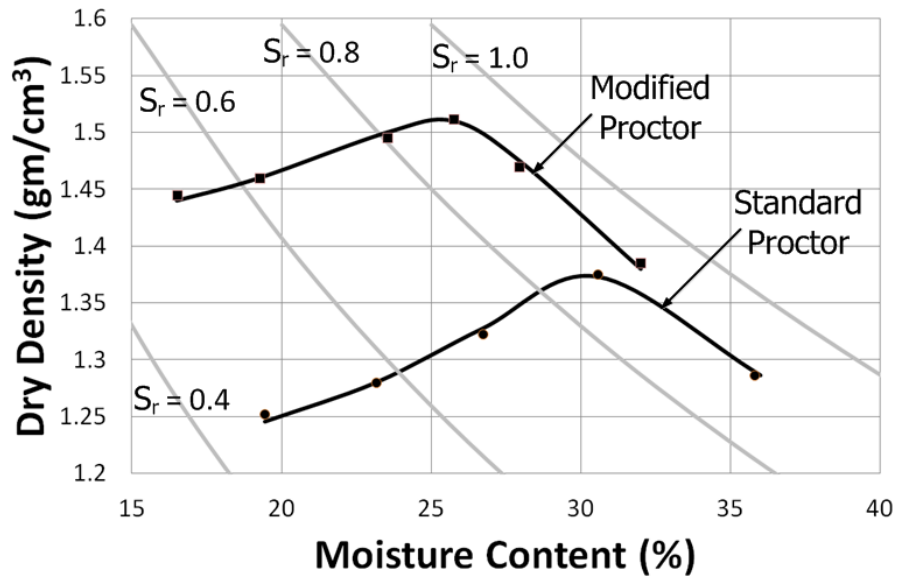
Figure 3-5: Standard Proctor and Modified Proctor compaction curves of kaolin soil
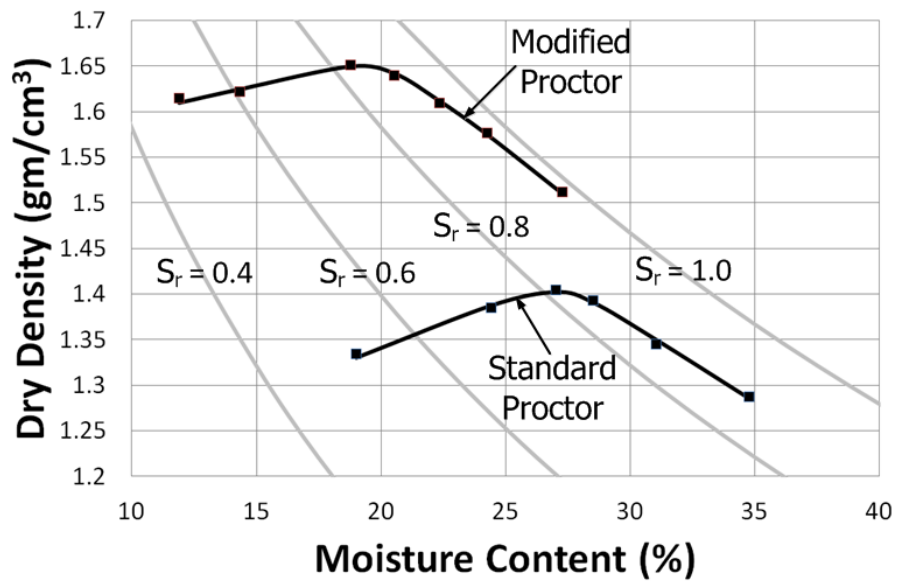
Figure 3-6: Standard Proctor and Modified Proctor compaction curves of the Merri Creek soil
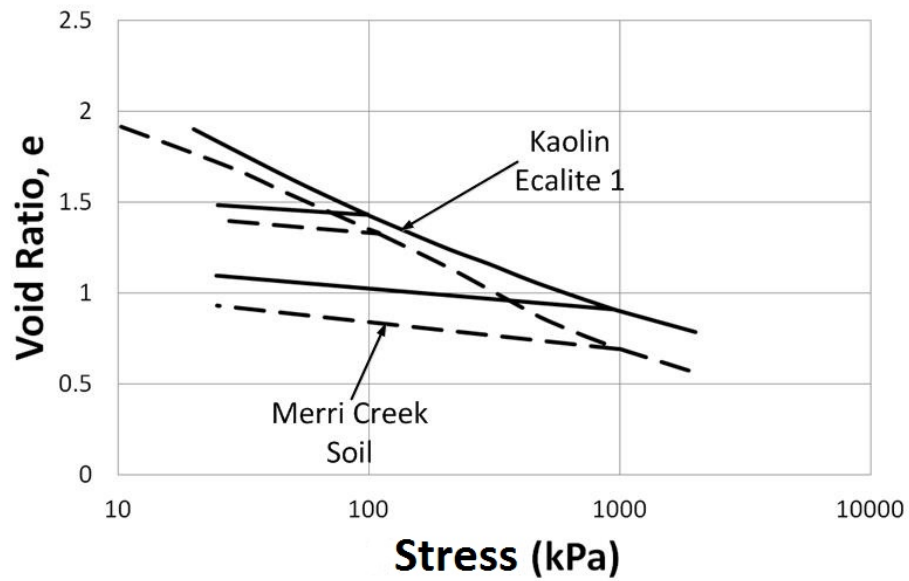
Figure 3-7: Consolidation curves of the kaolin and the Merri Creek soil
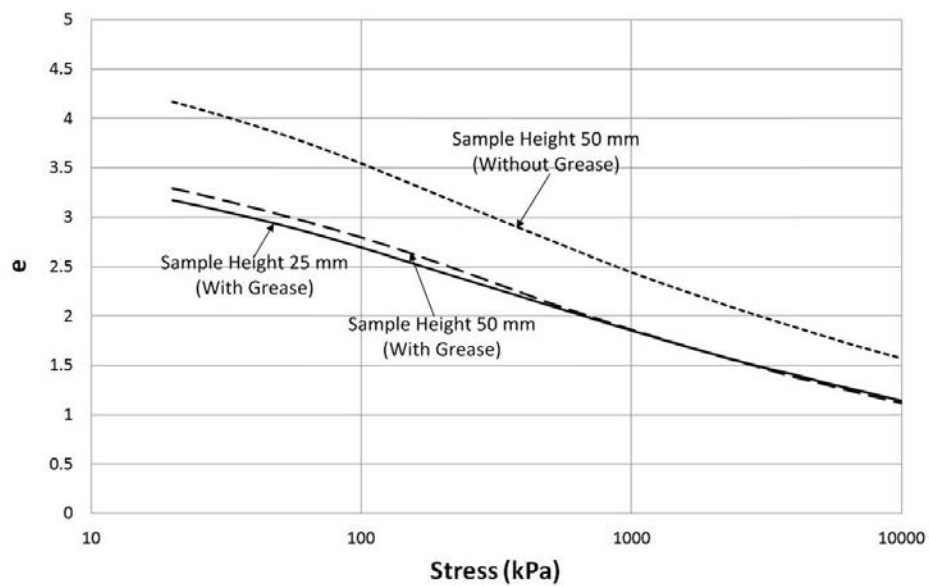
Figure 3-8: Compression curves of kaolin soil to observe the effect of grease on soil specimen height
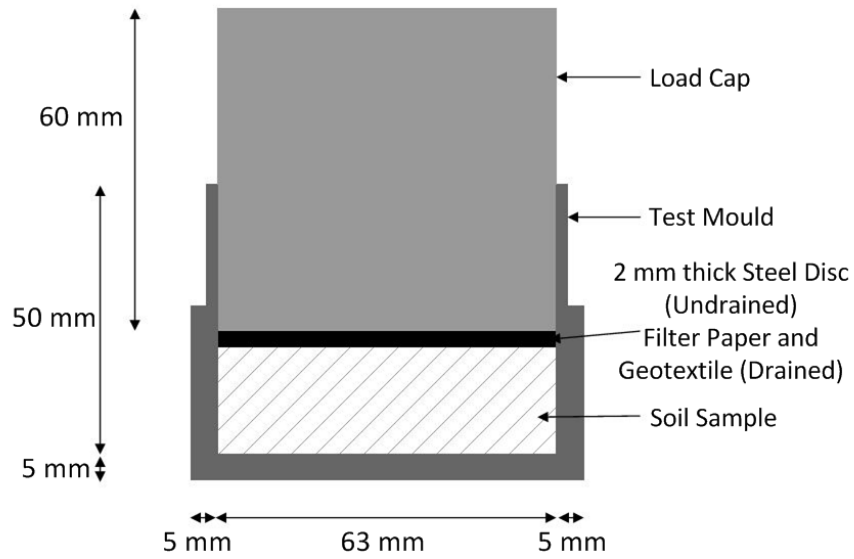
Figure 3-9: Steel mould used for soil compression to develop the LWSBS

Figure 3-10: 1-D compression set-up, Loadtrac II
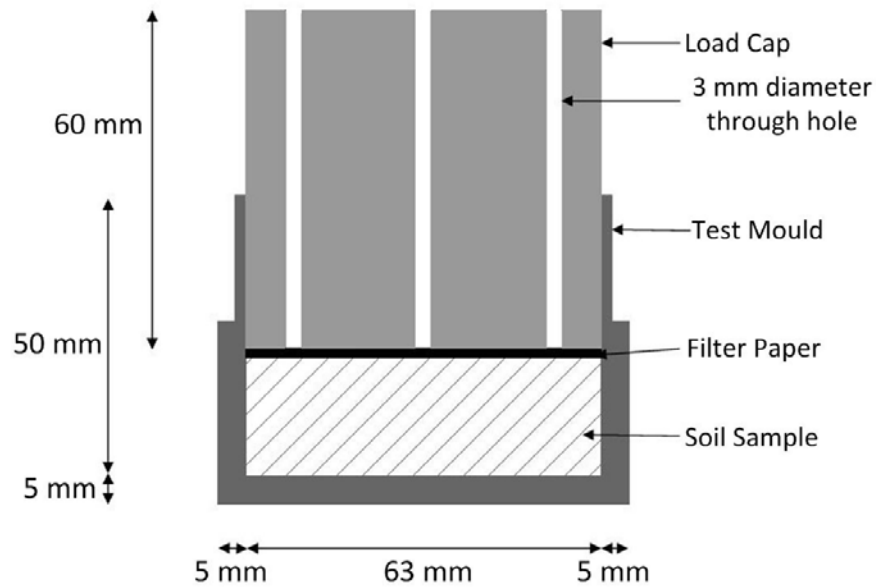
Figure 3-11: Experimental apparatus for state path tests
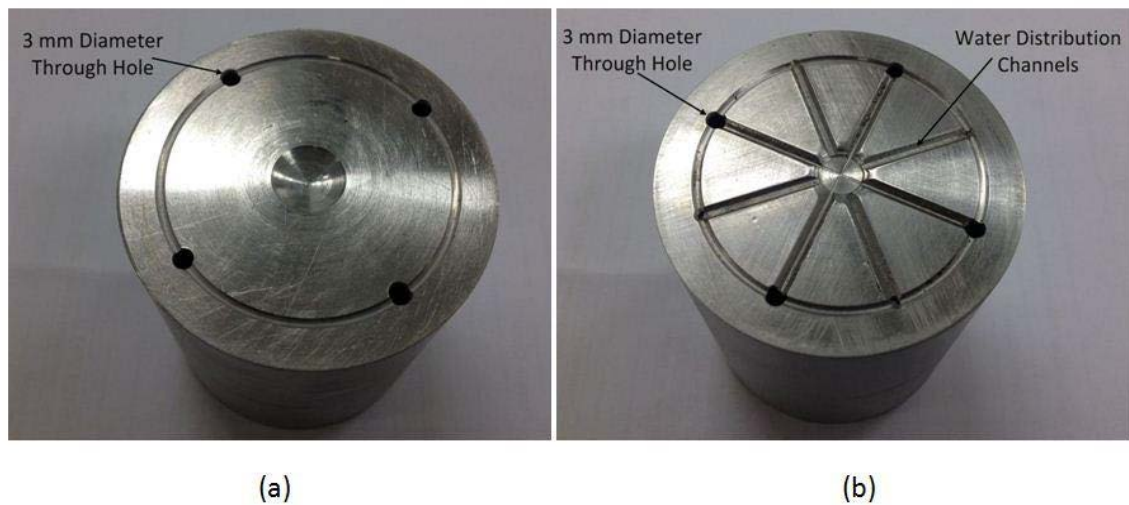
Figure 3-12: (a) Top view; **(b)** Bottom view of the loading cap used for state path tests
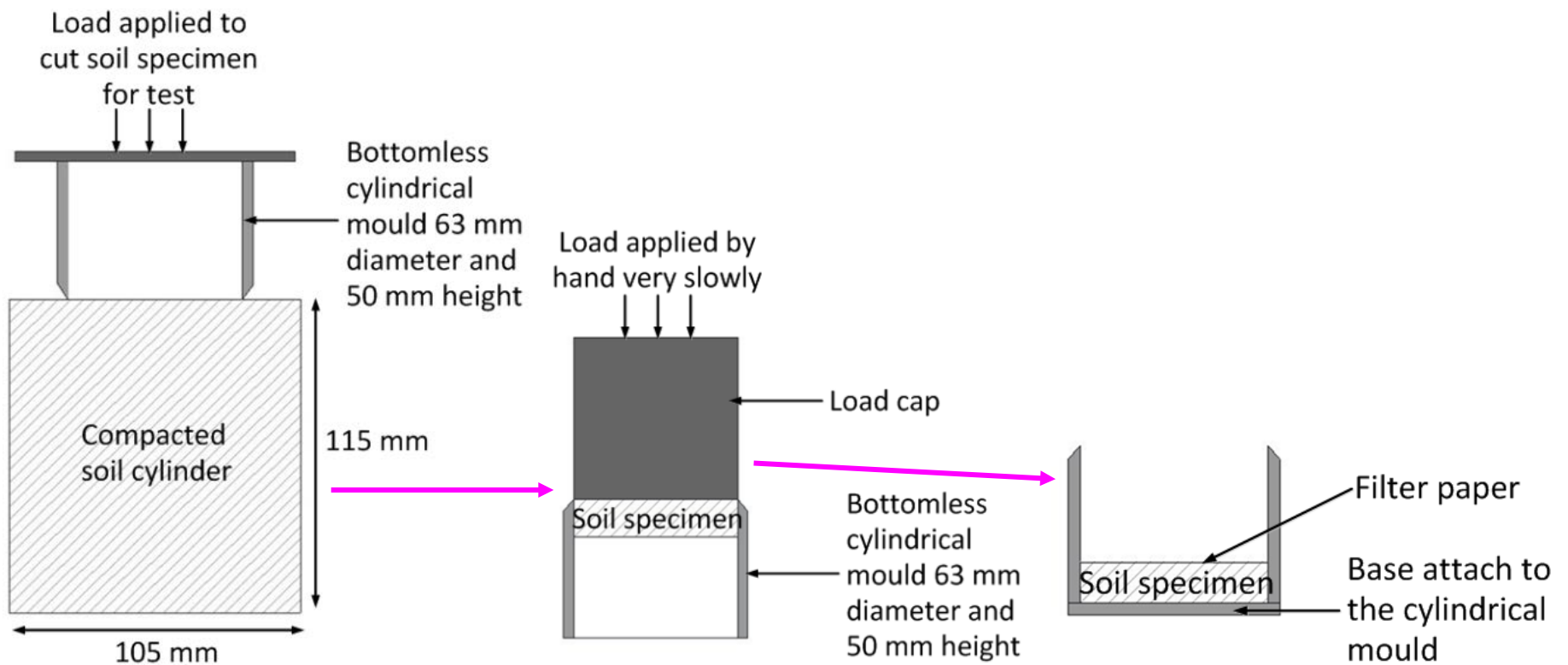
Figure 3-13: Preparation of dynamically compacted soil specimen for static compaction tests

VALIDATION OF THE MPK FRAMEWORK

USING STATICALLY COMPACTED SOILS

4.1 Introduction

This chapter presents the validation of the Monash-Peradeniya-Kodikara (MPK) framework using statically compacted soils. A number of loading/unloading/wetting experiments were performed to see whether experimental points fall along the MPK framework-predicted state paths with respect to the Loading Wetting State Boundary Surface (LWSBS). As indicated in Chapter 3, two types of soils were used in the experimentation: kaolin, known by the trade name Ecalite, and Merri Creek soil. While the kaolin is available in dry form in bags, the preparation of the Merri Creek soil involved drying, grinding, and subsequently sieving to remove any deleterious material. The basic geotechnical property tests of the soils were presented in Chapter 3. In addition, the datasets reported by Jotisankasa (2005), Jotisankasa et al. (2007a), Sharma (1998) and Romero (1999) as compiled by Wijesooriya (2012) were used to examine the validity of the MPK framework. Jotisankasa (2005) used soil A, a mixture of 70% HPF4 silt, 20% Speswhite kaolin and 10% London clay. Sharma (1998) used 10% Wyoming sodium bentonite with Speswhite kaolin (BK) in his study, and finally, Romero (1999) used Boom clay. All of these soils are fine-grained and some (Merri Creek, Soil A, Soil BK) are expansive in nature.

4.2 Validation of the MPK framework using experimental data

The initial step of the validation process was the development of the LWSBS using the compression curves of the soil specimens with different (gravimetric) moisture contents (0 to 50%) produced under 1-D static compression. After that, various state path tests, namely loading/wetting, loading/wetting/loading, loading/unloading/wetting, loading/unloading/wetting/loading, loading/unloading/wetting/unloading/wetting, and loading/unloading/loading, collapse potential tests and swelling pressure tests were performed on the soil specimens to examine the validity of the MPK framework.

4.2.1 Development of the LWSBS

In the MPK framework, the LWSBS is defined as the surface depicting the loosest state compacted soil can attain under loading or wetting or a combination of these paths. Kodikara (2012) developed the LWSBS combining compaction curves produced at different net stresses, starting from that corresponding to a nominal stress, such as 10 kPa, which represents the loosest state that soil would take when water is mixed from the soil's dry state. In the static compaction test program reported here, the LWSBSs for the two soils were developed using the compression curves produced under 1-D static compression, as described in the previous chapter.

4.2.1.1 The LWSBS of kaolin soil

The LWSBS of kaolin soil was developed using the compression curves of the soil specimens with different moisture contents (0 to 50%). Loadtrac II, a 1-D compression apparatus shown in the previous chapter, was used for this purpose. The static compression stress applied on the soil specimens ranged between nominal stress (7 kPa) to a high stress (5000 kPa). The test procedures and the experimental set-up used for these 1-D compression tests were described in the previous chapter. Typical load-deformation curves obtained for the kaolin soil are shown in Figure 4-1, which shows the characteristic strain hardening behaviour of 1-D compression. Figure 4-2 shows the compression curves presented in traditional e versus log (p) relationships. A number of tests repeated at identical conditions indicated that the results are well reproducible. As the grease was applied on the wall of the test mould prior to the test, the initial height did not affect the compression results of the soil specimens.

4.2.1.1.1 Undrained LWSBS

When a kaolin soil specimen with a certain moisture content was compressed from nominal stress (7 kPa) to a certain high stress (5000 kPa) using Loadtrac II, the loading rate was maintained at 20 kPa/min between 7 to 2000 kPa stress and 100 kPa/min over 2000 kPa stress. For the dry states of the Line of Optimum (LOO), air is generally free to drain even under these faster rates of loading. However, as soil goes past the LOO, the air is trapped and, therefore, the air phase becomes discontinuous (Hilf, 1956; Gilbert, 1959; Langfelder et al., 1968; Kodikara, 2012). Kodikara (2012) stated that this situation occurs all along the LOO. As a result, when a soil specimen wetter than the optimum is

compressed, it will hardly reach the 100% saturation ($S_r = 1.0$) line, especially if it is compressed too fast. Figure 4-3a shows the LWSBS presented in the form of compaction contours corresponding to actual stress values generated from the undrained compression data. Figure 4-3b shows a 3-D view of the LWSBS generated.

4.2.1.1.2 Drained LWSBS

As explained earlier, for the dry states of the LOO, air is generally free to drain even under the faster rates of loading. Therefore, it can be assumed that air pressure did not build up from the atmospheric level during compression. As a result, undrained and drained LWSBS are the same at the dry states of the LOO. On the other hand, when soil goes past the LOO, a slow loading rate (0.1 kPa/min) was used to establish the drained states without allowing the air pressure to build up. Therefore, it is assumed that air pressure did not build up from the atmospheric level during compression, meaning that the applied total stress is equal to the net stress. Figure 4-4 shows the development of several drained constant net stress contours for the kaolin soil. It is apparent that to develop each drained constant net stress contour, two identical soil specimens with the same moisture contents were compressed. Once the soil specimens approached close to the LOO, a much slower loading rate was used, as explained earlier. Figure 4-5a shows the drained LWSBS presented in the form of compaction contours corresponding to the net stress values. Figure 4-5b shows a 3-D view of the LWSBS generated.

4.2.1.2 The LWSBS of Merri Creek soil

The LWSBS of Merri Creek soil was developed using the compression curves of the soil specimens at different moisture contents (0 to 50%). Following the previous approach, Loadtrac II was used for this purpose and the static compression stress applied on the soil specimens ranged between nominal stress (7 kPa) to a certain high stress (5000 kPa). Typical load-deformation curves obtained for the Merri Creek soil are shown in Figure 4-6, which shows the characteristic strain hardening behaviour of 1-D compression. Figure 4-7 shows the compression curves presented in traditional e versus log (p) relationships.

4.2.1.2.1 Undrained LWSBS

Figure 4-8 shows the LWSBS of the Merri Creek soil presented in the form of compaction contours corresponding to the actual stress values generated from the undrained compression data. This development was made by following the same procedure under faster loading rates, as described earlier.

4.2.1.2.2 Drained LWSBS

Figure 4-9 shows the development of different drained constant net stress contours for the Merri Creek soil. This was also performed by following the same approach as for kaolin, such that once the soil specimens went close to the LOO, a much slower loading rate was applied. Figure 4-10a shows the drained LWSBS presented in the form of compaction contours corresponding to the net stress values. Figure 4-10b shows a 3-D view of the LWSBS generated.

4.2.2 State path tests performed on kaolin soil

Once the LWSBS was established using compression tests, a series of state path tests was undertaken to examine the validity of the concepts proposed by the MPK framework. To facilitate wetting tests, the top loading cap was modified to allow injection of water into the soil specimen under loading. The loading assembly and the top and bottom configurations of the top loading cap were presented in the previous chapter. In order to supply water to the soil specimen, four 3 mm diameter holes were provided in the top cap. A controlled amount of moisture was added through these holes equally using a syringe to increase the moisture content of the soil specimen to a targeted value. Apart from these modifications to the top cap, the other test set-up features were the same as for the compression tests. The state path tests performed on the kaolin soil are listed in Table 4-1.

4.2.2.1 State paths involving a combination of loading and wetting

A series of tests was undertaken where the soil was mixed to a certain water content from the dry state as for the compression tests, compressed to a certain stress level and then wetted at that stress level. During wetting under constant net stress (p), sufficient time (i.e., 6 to 12 hours for the dry side of the LOO and 24 to 48 hours for the wet side of the LOO) was provided for equilibrium. These test results are shown in Figure 4-11a,

4-11b, 4-11c; 4-11d, 4-11e, 4-11f and 4-11g, 4-11h and 4-11i. Figure 4-11a, 4-11b and 4-11c show a dry soil specimen loaded to 50 kPa and then wetted to 41.62% moisture content ($e_w = 1.103$). It is apparent that the state path followed the LWSBS during loading. Subsequently, during wetting, it moved inside the LWSBS initially, and then followed the 50 kPa constant net stress contour of the LWSBS, staying below the LWSBS. On the LWSBS, the void ratio increases with decreasing moisture ratio due to the macroscopic structure build-up (this is not drying), but for very low moisture contents, the void ratio can decrease again. As a result, when dry soil specimens are wetted under low stress levels, the wetting path may not follow the exact shape of the LWSBS. Repetition of this test also showed the similar behaviour. Figure 4-11d, 4-11e and 4-11f show a dry soil specimen loaded to 100 kPa and then wetted to 29.66% moisture content ($e_w = 0.787$). It is clear that the state path generally followed the stress contour for 100 kPa of the LWSBS. Figure 4-11g, 4-11h and 4-11i show a soil specimen at 11.69% moisture content ($e_w = 0.310$) loaded to 20 kPa stress and then wetted to 31.25% moisture content ($e_w = 0.828$). It is apparent that the state path followed the LWSBS up to 20 kPa stress and then followed that contour to the final moisture content. It is also apparent that when the soils were wetted at a particular stress level, they underwent collapse (or compression) as depicted by the LWSBS.

A series of tests was undertaken where the soil specimens were loaded to a particular stress level, wetted to certain moisture content and then loaded again to a higher stress level. These test results are shown in Figure 4-12a, 4-12b, 4-12c; 4-12d, 4-12e, 4-12f; 4-12g, 4-12h, 4-12i and 4-12j, 4-12k, 4-12l. Figure 4-12a, 4-12b and 4-12c show a dry soil specimen loaded to 1000 KPa stress and then wetted to 21.52% moisture content ($e_w = 0.570$) and then loaded to 2000 kPa stress. It is clear that the state path followed the LWSBS up to 1000 kPa stress during loading. Subsequently, during wetting, it followed the stress contour for 1000 kPa of the LWSBS. Finally, during the last stage loading at 21.52% moisture content ($e_w = 0.570$), it followed the LWSBS up to 2000 kPa stress. Figure 4-12d, 4-12e and 4-12f show a soil specimen at 8.96% moisture content ($e_w = 0.237$) loaded to 50 kPa stress and then wetted to 27.35% moisture content ($e_w = 0.725$) and then loaded to 2000 kPa stress. It is evident that the state path followed the path dictated by the LWSBS, consistent with the MPK framework. It also should be noted that in these two tests, the soil was initially totally on the LWSBS during

loading and wetting. Figure 4-12g, 4-12h, 4-12i and 4-12j, 4-12k, 4-12l show dry soil specimens loaded to 50 kPa and 20 kPa respectively and then wetted to moisture content of 19.69% ($e_w = 0.522$) and 21.60% ($e_w = 0.572$), and then loaded to 2000 KPa stress. It is apparent that during wetting, the state paths initially moved inside the LWSBS, and then followed the LWSBS, staying below the LWSBS. As the void ratio decreases with the decrease of moisture ratio with very low moisture contents and net stresses on the LWSBS, when dry soil specimens were wetted from this position of the LWSBS, the wetting path appeared not to follow the exact shape of the LWSBS.

4.2.2.2 State paths involving a combination of loading, unloading and wetting

A series of tests was undertaken where the soil was mixed to certain water content from the dry state and then subjected to a combination of loading, unloading and wetting. These test results are shown in Figure 4-13a, 4-13b, 4-13c and 4-13d, 4-13e, 4-13f. Figure 4-13a, 4-13b and 4-13c show a soil specimen at 4.04% moisture content ($e_w = 0.107$) loaded to 1000 kPa, unloaded to 20 kPa, then wetted to 23.67% moisture content ($e_w = 0.628$), and finally loaded to 2000 kPa. It is clear that the state path followed the LWSBS up to 1000 kPa stress and then moved inside the LWSBS due to unloading. After that, during wetting, it swelled towards the stress contour for 20 kPa of the LWSBS. The position of the stress path is still inside the LWSBS at the end of the wetting stage. Finally, during loading at 23.67% moisture content ($e_w = 0.628$), it moved towards the LWSBS and followed the LWSBS up to 2000 kPa stress after intercepting the LWSBS. Figure 4-13d, 4-13e and 4-13f show a soil specimen at 8.96% moisture content ($e_w = 0.237$) loaded to 1000 kPa stress, unloaded to 100 kPa, and then wetted to 28.30% moisture content ($e_w = 0.750$), and finally loaded to 2000 kPa. It is apparent that the state path followed the LWSBS up to 1000 kPa stress and then moved inside the LWSBS due to unloading. During subsequent wetting, it swelled towards the stress contour for 100 kPa of the LWSBS. The position of the state path is still inside the LWSBS at the end of the wetting stage. Finally, during loading at 28.30% moisture content ($e_w = 0.750$), it moved towards the LWSBS and followed the LWSBS up to 2000 kPa stress after intercepting the LWSBS. It is apparent from both tests that due to wetting, the yield (i.e., the LWSBS interception) stress of the soil specimens decreases during loading. This phenomenon happens because during wetting, the state path

approaches close to the LWSBS and as a result, the state path intercepts the LWSBS at lower stress. Furthermore, it is also evident that the two state paths presented followed the path dictated by the LWSBS, consistent with the MPK framework.

A series of tests was undertaken where the soil specimens were loaded to a particular stress level, unloaded to a lower stress level and then wetted to certain moisture content. These test results are shown in Figure 4-14a, 4-14b, 4-14c; 4-14d, 4-14e, 4-14f; 4-14g, 4-14h, 4-14i and 4-14j, 4-14k, 4-14l. Figure 4-14a, 4-14b, 4-14c and 4-14g, 4-14h, 4-14i show soil specimens with 11.88% moisture content ($e_w = 0.315$) and 15.85% moisture content ($e_w = 0.420$) loaded to 1000 kPa stress and then unloaded to 700 kPa stress and then wetted to 34.14% moisture content ($e_w = 0.905$) and 32.77% moisture content ($e_w = 0.868$) respectively. It is clear that the state paths followed the LWSBS up to 1000 kPa stress and then moved inside the LWSBS due to unloading. Finally, during wetting, they swelled and intercepted the LWSBS around 14.72% moisture content ($e_w = 0.390$) and 19.25% moisture content ($e_w = 0.510$) respectively, and then followed the 700 kPa constant net stress contour on the LWSBS to the final moisture contents. Figure 4-14d, 4-14e, 4-14f and 4-14j, 4-14k, 4-14l show soil specimens with 11.88% moisture content ($e_w = 0.315$) and 15.85% moisture content ($e_w = 0.420$) loaded to 500 kPa stress, unloaded to 300 kPa stress and then wetted to 34.95% moisture content ($e_w = 0.926$) and 32.80% moisture content ($e_w = 0.869$) respectively. It is apparent that the state paths followed the LWSBS up to 500 kPa stress and then moved inside the LWSBS due to unloading. Finally, during wetting, they swelled and intercepted the LWSBS around 26.04% moisture content ($e_w = 0.690$) and 23.77% moisture content ($e_w = 0.630$) respectively, and then followed the 300 kPa constant net stress contour on the LWSBS to the final moisture contents. An interesting feature of these results is that the state paths intercepted the LWSBS (at point D) and were subsequently controlled by the LSWBS, where they underwent collapse.

A series of tests was undertaken where the soil specimens were loaded to a certain stress level and then unloaded and wetted twice at particular stress levels. These test results are shown in Figure 4-15a, 4-15b, 4-15c; 4-15d, 4-15e, 4-15f; 4-15g, 4-15h, 4-15i and 4-15j, 4-15k, 4-15l. Figure 4-15a, 4-15b and 4-15c show soil specimens with 15.85% moisture content ($e_w = 0.420$) loaded to 500 kPa stress, unloaded to 400 kPa stress, then wetted

to 26.29% moisture content ($e_w = 0.697$), unloaded to 300 kPa stress and then wetted to 34.14% moisture content ($e_w = 0.905$). It is clear that the state path followed the LWSBS up to 500 kPa stress and then moved inside the LWSBS due to unloading. Subsequently, during wetting, it swelled and intercepted the LWSBS around 19.43% moisture content ($e_w = 0.515$) and then followed the 400 kPa constant net stress contour on the LWSBS. After that, during unloading, it moved inside the LWSBS, and finally, during wetting, it swelled and intercepted the LWSBS around 32.38% moisture content ($e_w = 0.858$) and then followed the 300 kPa constant net stress contour on the LWSBS. Figure 4-15d, 4-15e and 4-15f show soil specimens with 11.88% moisture content ($e_w = 0.315$) loaded to 1000 kPa stress, unloaded to 700 kPa stress, then wetted to 22.23% moisture content ($e_w = 0.589$), unloaded to 500 kPa stress and then wetted to 30.98% moisture content ($e_w = 0.821$). It is apparent that the soil specimen behaved the same way as shown in the previous test, following the LWSBS up to 1000 kPa stress and then moving inside the LWSBS due to unloading. Subsequently, during wetting, it swelled and intercepted the LWSBS around 19.43% moisture content ($e_w = 0.515$) and then followed 700 kPa constant net stress contour on the LWSBS. After that, during unloading, it moved inside the LWSBS, and finally, during wetting, it hswelled and intercepted the LWSBS around 29.36% moisture content ($e_w = 0.778$) and then followed the 500 kPa constant net stress contour on the LWSBS. Figure 4-15g, 4-15h, 4-15i and 4-15j, 4-15k, 4-15l show soil specimens with 15.85% moisture content ($e_w = 0.420$) and 11.69% moisture content ($e_w = 0.310$) loaded to 300 kPa stress, unloaded to 200 kPa stress, then wetted to 28.60% moisture content ($e_w = 0.758$) and 25.80% moisture content ($e_w = 0.684$) respectively, unloaded to 100 kPa stress and then wetted to 39.26% moisture content ($e_w = 1.040$) and 38.56% moisture content ($e_w = 1.022$) respectively. It is evident that the soil specimens behaved in the same way as shown in the previous two tests, moving inside the LWSBS during unloading stages, intercepting the LWSBS during wetting stages and then following the LWSBS to the final moisture contents. In all the tests presented here, the unloaded stress levels for wetting paths were chosen strategically to examine the control of the LWSBS when the wetting paths intercepted it. The test results show that the state paths followed the paths dictated by the LWSBS during two interceptions.

4.2.2.3 State paths involving a combination of loading and unloading

A series of tests was undertaken to examine the loading-unloading-reloading behaviour of kaolin soil with different moisture contents (0% – 30%). These test results are shown in Figure 4-16. Figure 4-16a shows the normal compression (black) line and the loading-unloading-reloading (grey) line for a 0% moisture content ($e_w = 0$) soil specimen. It can be seen that the soil specimen was unloaded at 50, 100, 500, 1000, 2000 and 5000 kPa stresses. It is clear that the state path followed the LWSBS at the beginning of the test. Subsequently, during unloading, it moved inside the LWSBS. After that, during reloading, it behaved predominantly elastically before intercepting the LWSBS. Finally, it followed the LWSBS after intercepting the LWSBS. Figure 4-16b, 4-16c, 4-16d, 4-16e and 4-16f show similar behaviour for five more state paths for initial moisture contents of 8.3% ($e_w = 0.22$), 15.8% ($e_w = 0.419$), 20.4% ($e_w = 0.541$), 23.8% ($e_w = 0.632$) and 30.2% ($e_w = 0.80$) respectively. By analysing the loading-unloading-reloading curves presented earlier, the slope of normal compression curve (λ) and the slope of unloading-reloading curve (κ) were determined for various moisture contents and stresses. Figure 4-17a and 4-17b show the relationship of λ and κ with moisture ratio (e_w) respectively. It is apparent from Figure 4-17a that the value of λ decreases with increasing moisture ratio. This means that dry kaolin soil is more compressible than wet kaolin soil. λ is actually proportional to the void ratio at the nominal stress level. If the void ratio at the nominal stress for a certain moisture content soil is high, it will be more compressible. This is because of the compression of the large macro voids. Drier/powder kaolin soil is not stiff at all, therefore, it has higher void ratio. As a result, it compresses more during loading and provides higher value of λ. In the Barcelona Basic Model (BBM), Alonso et al. (1990) proposed that λ decreases with increasing soil suction. However, Wheeler and Sivakumar (1995) found the opposite results in their experiments. It was observed that λ showed small variation between 100 kPa to 300 kPa soil suction, while a significant drop was noticed when soil suction was reduced to zero. Sivakumar et al. (2010) also observed a similar trend of λ with soil suction to that of Wheeler and Sivakumar (1995). The result obtained here are consistent with the findings of Wheeler and Sivakumar (1995) and Sivakumar et al. (2010). On the other hand, it is clear from Figure 4-17b that κ can be considered as constant over moisture contents and stress levels, which is consistent with the assumptions of both Alonso et al. (1990) and Wheeler and Sivakumar (1995). Although this works relate to λ obtain from constant

suction testing as can be seen from Chapter 6, the λ obtain from the constant water content test should also show the similar behaviour.

4.2.2.4 Collapse test

While the test results presented earlier in this chapter show the collapse behaviour of compacted kaolin soil, a series of tests was undertaken to examine the variation of collapse potential with stress level. Soil specimens were prepared with 15.77% moisture content ($e_w = 0.420$), compressed to 500 kPa stress and then wetted to saturation in controlled steps of moisture ingress at stress levels of 50, 100, 500, 1000, 2000 and 4000 kPa. These test results are shown in Figure 4-18a, 4-18b, 4-18c; 4-18d, 4-18e, 4-18f; 4-18g, 4-18h, 4-18i; 4-18j, 4-18k, 4-18l; 4-18m, 4-18n, 4-18o and 4-18p, 4-18q, 4-18r. Figure 4-18a, 4-18b, 4-18c and 4-18d, 4-18e, 4-18f show soil specimens with 15.77% moisture content ($e_w = 0.420$) loaded to 500 kPa stress and then unloaded to 50 kPa and 100 kPa stress respectively and then wetted to saturation. It is clear that the state paths followed the LWSBS up to 500 kPa stress and then moved inside the LWSBS due to unloading. Subsequently, during wetting, they swelled towards the LWSBS. The stress paths are still inside but very close to the LWSBS at the end of the wetting stage. As kaolin is a non-reactive soil, it is evident that the unloaded soil specimens did not swell much during wetting. Figure 4-18g, 4-18h, 4-18i; 4-18j, 4-18k, 4-18l; 4-18m, 4-18n, 4-18o and 4-18p, 4-18q, 4-18r show soil specimens with 15.77% moisture content ($e_w = 0.420$) loaded to 500, 1000, 2000 and 4000 kPa stress respectively and then wetted to saturation. It is apparent that the state paths followed the LWSBS during loading and subsequently during wetting. Figure 4-19 presents the collapse potential (given as the reduction in void ratio) with operational stress. It is clear that the collapse potential increases with increasing operational stress up to the compaction stress, and then decreases for higher stress levels, as explained by the MPK framework. This behaviour is consistent with the typical behaviour reported for the collapse potential of soils (c.f., Sun et al., 2004).

4.2.2.5 Swelling pressure tests

While the tests presented in Figure 4-13, Figure 4-14, Figure 4-15and Figure 4-18 show the swelling behaviour of unloaded kaolin soil during wetting, a series of tests was undertaken to examine the swelling pressure development for constant volume

(constrained) wetting of kaolin soil specimens. The tests were undertaken by locking the soil specimen against volumetric deformation but measuring the applied stress variation when the specimen was wetted. The same mould and set-up used for the other validation tests was used in this test program. Figure 4-20 shows the results of the tests undertaken. Figure 4-20a and 4-20b show the state path of a soil specimen prepared at 10.69% moisture content ($e_w = 0.283$), loaded to 500 kPa (path AB), unloaded to 100 kPa (path BC) and then wetted at constant volume (i.e., e constant) to saturation (path CDEF). It is clear that the unloaded position at 100 kPa is below the LWSBS (point C), and during wetting the swelling pressure builds up to D (around 180 kPa), at which the state reached the LWSBS. Subsequently, the path DE is on the LWSBS (at constant initial void ratio = 1.366), reducing the swelling pressure until the LOO is intercepted at point E. Further wetting causes the soil to increase swelling pressure again towards saturation, as shown by path EF. This behaviour is consistent with the MPK framework and with test results reported in the past (Kodikara, 2012). Figure 4-20c, 4-20d and 4-20g, 4-20h show similar behaviours for two more state paths for initial moisture contents of 10.69% ($e_w = 0.283$) and 19.88% ($e_w = 0.527$) respectively. In comparison to Figure 4-20a, 4-20b; 4-20c, 4-20d and 4-20g, 4-20h, Figure 4-20e and 4-20f show the soil specimen loaded to 2000 kPa (path AB), then unloaded to 100 kPa (path BC) at the 10.69% moisture content and then wetted (path CD). It is evident that this soil specimen did not reach the LWSBS, and swelling pressure continued to increase with wetting. It appears that it was too far below the LWSBS initially at 100 kPa stress (due to increased compaction stress of 2000 kPa), and this led to the observed result. At point D, S_r is equal to 0.973, but the position of D is well away from the normal compression line (NCL). This is because it has reached close to the saturation plane corresponding to the constant void ratio of 0.925 well below the NCL. The projected $S_r = 1$ line is shown in Figure 4-20e. Another test result presented in Figure 4-20i and 4-20j indicates that similar behaviour can occur for lower compaction stress (i.e., 1000 kPa) if the initial moisture content is higher (i.e., 19.88% ($e_w = 0.527$)) due to changes in the relative positions of the LWSBS. Figure 4-20k and 4-20l also show similar behaviours for a state path for initial moisture content of 19.88% ($e_w = 0.527$). Figure 4-20m, 4-20n; 4-20o, 4-20p; and 4-20q, 4-20r show comparisons of the state paths presented earlier. Figure 4-20m and 4-20n show the state paths of three soil specimens prepared with 10.69% moisture content ($e_w = 0.283$) individually loaded to 500, 1000 and 2000 kPa, unloaded to 100 kPa and then wetted at

constant volume (i.e., e constant) to saturation (paths $C_{1,2,3}D_{1,2,3}E_{1,2}F_{1,2}$). It is clear that, as the compaction stress increases (or initial void ratio decreases or initial density increases), the maximum swelling pressure increases. Similar behaviour has been reported previously (c.f., Kassiff and Shalom, 1971; Imbert and Villar, 2006). Figure 4-20q and 4-20r also show the effect of compaction stress (500, 1000 and 2000 kPa) on the swelling state paths for soil specimens prepared with the higher moisture content of 19.88% ($e_w = 0.527$). It is apparent that, as reported previously (c.f., Kassiff and Shalom, 1971; Imbert and Villar, 2006) and the state paths for soil specimens with 10.69% moisture content ($e_w = 0.283$), the maximum swelling pressure increases with the increase of compaction stress. Figure 4-20o and 4-20p show two test results demonstrating the influence of initial moisture contents of 10.69% and 19.88%. The soil specimens were prepared by loading to 500 kPa, unloading to 100 kPa and then wetting at constant void ratio. It is evident that the swelling pressure decreases with increasing initial moisture content, in agreement with published results (c.f., Kassiff and Shalom, 1971; Lee et al., 1999). As per the MPK framework, the intersection with the LWSBS is also evident from the shape of the state paths and 3-D relationships.

4.2.3 State path tests performed on Merri Creek soil

A series of state path tests was undertaken on the Merri Creek soil to examine the validity of the concepts proposed by the MPK framework. The soil sample preparation technique and the test procedures were similar to those for kaolin soil presented earlier. The state path tests which were performed on the Merri Creek soil are listed in Table 4-2.

4.2.3.1 State paths involving a combination of loading and wetting

After developing the LWSBS for Merri Creek soil, a series of tests was undertaken where the soil was mixed to a certain water content from the dry state as for the compression tests, compressed to a certain stress level and then wetted at that stress level. During wetting under constant net stress (p), sufficient time (i.e., 6 to 12 hours for the dry side of the LOO and 24 to 48 hours for the wet side of the LOO) was provided to facilitate adequate drainage conditions. These test results are shown in Figure 4-21a, 4-21b, 4-21c and 4-21d, 4-21e, 4-21f. Figure 4-21a, 4-21b and 4-21c show a soil specimen with 10.35% moisture content ($e_w = 0.271$) loaded to 500 kPa stress and then wetted to 28.38% moisture content ($e_w = 0.743$). It is clear that the state path followed

the LWSBS during loading and subsequently during wetting. Figure 4-21d, 4-21e and 4-21f show a soil specimen with 10.35% moisture content ($e_w = 0.271$) loaded to 200 kPa stress and then wetted to 27.95% moisture content ($e_w = 0.732$). It is apparent that the state path followed the LWSBS during loading. Subsequently, during wetting, it initially moved inside the LWSBS, and then intercepted and followed the LWSBS to the final moisture content. It is evident from the LWSBS that, similar to the kaolin soil, the void ratio of the constant net stress contours increases with increasing moisture ratio for dry soil (i.e., degree of saturation, Sr < 40%). However, this phenomenon disappears for wet soil. The LWSBSs were usually developed by compressing constant moisture content soil specimens from nominal to a certain high pressure. As a result, when the dry soil specimens were wetted under low stress levels, the wetting path may not have followed the exact shape of the LWSBS. Repetition of this test also showed the same behaviour. Similar behaviour was also observed during the validation tests for the kaolin soil. Figure 4-22a, 4-22b and 4-22c show a test where a soil specimen was loaded to a particular stress level, wetted to a certain moisture content and then loaded again to a higher stress level. It is apparent that the state path followed the path dictated by the LWSBS, in agreement with the MPK framework.

4.2.3.2 State paths involving a combination of loading, unloading and wetting

A series of tests was undertaken where the soil was mixed to certain water content from the dry state and then subjected to a combination of loading, unloading and wetting. These test results are shown in Figure 4-23a, 4-23b, 4-23c; Figure 4-24a, 4-24b, 4-24c and 4-24d, 4-24e, 4-24f. Figure 4-23a, 4-23b and 4-23c show a soil specimen with 15.0% moisture content ($e_w = 0.393$) loaded to 1000 kPa stress, unloaded to 100 kPa stress, then wetted to 27.52% moisture content ($e_w = 0.721$), and finally loaded to 1000 kPa stress. It is clear that the state path followed the LWSBS up to 1000 kPa stress and then moved inside the LWSBS due to unloading. After that, during wetting, it swelled towards the stress contour for 100 kPa of the LWSBS. The position of the state path was still inside the LWSBS at the end of wetting stage. Finally, during loading at 27.52% moisture content ($e_w = 0.721$), it moved towards the LWSBS and followed the LWSBS up to 1000 kPa stress after intercepting the LWSBS. As the state path reached 100% saturation around 800 kPa stress during the second stage loading and the test was

performed under drained conditions, the moisture content of the soil specimen at the end of the test was measured lower than 27.52% moisture content ($e_w = 0.721$). This means that during the second stage loading, the moisture was drained out when the state path moved from 800 kPa to 1000 kPa stress on the 100% saturation line. Figure 4-24a, 4-24b and 4-24c show a soil specimen with 10.35% moisture content ($e_w = 0.271$) loaded to 2000 kPa stress, and unloaded to 100 kPa stress, and finally wetted to 26.0% moisture content ($e_w = 0.681$). It is apparent that the state path followed the LWSBS up to 2000 kPa stress and then moved inside the LWSBS due to unloading. Finally, during wetting, it swelled up to the final moisture content 26.0% ($e_w = 0.681$). The position of the state path was still inside the LWSBS at the end of the test. Figure 4-24d, 4-24e and 4-24f show a soil specimen with 10.35% moisture content ($e_w = 0.271$) loaded to 1000 kPa stress, unloaded to 400 kPa stress, and finally wetted to 17.42% moisture content ($e_w = 0.456$). It is clear that the soil specimen behaved the same way as shown in the previous test. The state path followed the LWSBS up to 1000 kPa and then moved inside the LWSBS due to unloading. Finally, during wetting, it swelled up to the final moisture content and ended inside the LWSBS. It is evident that the three state paths presented followed the path, in agreement with the MPK framework.

A series of tests was undertaken where the soil specimens were loaded to a certain stress level and then unloaded and wetted twice at particular stress levels. These test results are shown in Figure 4-25a, 4-25b, 4-25c; 4-25d, 4-25e, 4-25f; 4-25g, 4-25h, 4-25i and 4-25j, 4-25k, 4-25l. Figure 4-25a, 4-25b, 4-25c and 4-25d, 4-25e, 4-25f show soil specimens with 10.35% ($e_w = 0.271$) and 15.0% ($e_w = 0.393$) moisture content respectively, loaded to 2000 kPa stress, and subsequently unloaded and wetted twice. The unloaded stress levels were 1000 kPa and 100 kPa in both of the cases. It is clear that the state paths followed the LWSBS up to 2000 kPa stress and then moved inside the LWSBS during the first unloading. Subsequently, during wetting, they swelled, then intercepted and then followed the LWSBS. After that, during the second unloading, they moved inside the LWSBS. Finally, during wetting, they swelled and ended inside the LWSBS without intercepting it. In both cases, the second unloaded position was far below the LWSBS and the amount of swelling during wetting was not sufficient to bring them on to the LWSBS. However, both of the soil specimens ended on the saturation plane (i.e., $Sr = 1.0$) and if any further unloading and wetting took place on the specimens, the

movement of the state paths would be noticeable on the saturation plane. Figure 4-25g, 4-25h, 4-25i and 4-25j, 4-25k, 4-25l show soil specimens with 15.0 % moisture content ($e_w = 0.393$) loaded to 400 kPa and 1000 kPa stress respectively and then unloaded and wetted twice under particular stress levels. The unloaded stress levels for wetting paths were chosen strategically, being 300 kPa and 200 kPa for the first test and 700 kPa and 500 kPa for the second test, to examine the control of the LWSBS when the wetting paths intercepted twice. The test results show that the state paths follow the paths dictated by the LWSBS during the two interceptions. Figure 4-26a, 4-26b and 4-26c show a soil specimen with 10.35% moisture content ($e_w = 0.271$) loaded to 2000 kPa stress and subsequently, unloaded and wetted four times. Despite this complex test, it is evident that the state path followed the path, in agreement with the MPK framework.

4.2.3.3 State paths involving a combination of loading and unloading

A series of tests was undertaken to examine the loading-unloading-reloading behaviour of Merri Creek soil with different moisture contents (0% – 23%). These test results are shown in Figure 4-27. Figure 4-27a shows the loading-unloading-reloading (gray line) behaviour of a soil specimen with 0% moisture content ($e_w = 0$) that was unloaded at 50, 100, 500, 1000, 2000 and 5000 kPa stresses. It is clear that the state path followed the LWSBS at the beginning. Subsequently, during unloading, it moved inside the LWSBS. Finally, during reloading, it behaved predominantly elastically, intercepted the LWSBS, and then followed the LWSBS. Figure 4-27b, 4-27c, 4-27d and 4-27e show similar behaviour for four more state paths for initial moisture contents of 7.83% ($e_w = 0.205$), 13.19% ($e_w = 0.346$), 16.06% ($e_w = 0.421$) and 22.68% ($e_w = 0.594$) respectively. By analysing the loading-unloading-reloading curves presented earlier, the slope of the normal compression curve (λ) and the slope of the unloading-reloading curve (κ) were determined for various moisture contents and stresses. Figure 4-28a and 4-28b show the relationship of λ and κ with moisture content, respectively. It is apparent from Figure 4-28a that the value of λ increases with increasing moisture content. This means that dry Merri Creek soil is less compressible than wet Merri Creek soil. λ is actually proportional to the void ratio at the nominal stress level. If the void ratio at the nominal stress for a certain moisture content soil is high, it will be more compressible. This is because of the compression of the large macro voids. Drier/powder Merri Creek soil is very stiff, therefore, it has lower void ratio. As a result, it compresses less during loading

and provides lower value of λ. In the Barcelona Basic Model (BBM), Alonso et al. (1990) proposed that λ decreases with increasing soil suction. However, Wheeler and Sivakumar (1995) and Sivakumar et al. (2010) found the opposite results from their experiments. The result obtained here is consistent with the BBM (1990) findings. On the other hand, it is clear from Figure 4-17b that κ can be considered as constant over moisture contents and stress levels, which is consistent with the assumptions of both Alonso et al. (1990) and Wheeler and Sivakumar (1995). Although this works relate to λ obtain from constant suction testing as can be seen from Chapter 6, the λ obtain from the constant water content test should also show the similar behaviour.

4.2.3.4 Collapse tests

While the test results presented previously show the collapse behaviour of compacted Merri Creek soil, a series of tests was undertaken to examine the variation of collapse potential with stress level. Soil specimens were prepared with 16.06% moisture content ($e_w = 0.421$), compressed to 500 kPa stress and then wetted almost to saturation in controlled steps of moisture ingress at stress levels of 40, 100, 500, 700, 1000 and 2000 kPa. These test results are shown in Figure 4-29a, 4-29b, 4-29c; 4-29d, 4-29e, 4-29f; 4-29g, 4-29h, 4-29i; 4-29j, 4-29k, 4-29l; 4-29m, 4-29n, 4-29o and 4-29p, 4-29q, 4-29r. Figure 4-29a, 4-29b, 4-29c and 4-29d, 4-29e, 4-29f show soil specimens with 16.06% moisture content ($e_w = 0.421$) loaded to 500 kPa stress and then unloaded to 40 kPa and 100 kPa stress respectively, and then wetted almost to saturation. It is clear that the state paths followed the LWSBS up to 500 kPa stress and then moved inside the LWSBS due to unloading. Subsequently, during wetting, they swelled towards the LWSBS. The stress paths are still inside the LWSBS at the end of the wetting stage. The Merri Creek soil is reactive in nature. However, in both cases, the unloaded position was far below the LWSBS and the amount of swelling during wetting was not sufficient to bring them on to the LWSBS. Figure 4-29g, 4-29h, 4-29i; 4-29j, 4-29k, 4-29l; 4-29m, 4-29n, 4-29o and 4-29p, 4-29q, 4-29r show soil specimens with 16.06% moisture content ($e_w = 0.421$) loaded to 500, 700, 1000 and 2000 kPa stress respectively, and then wetted close to saturation. It is apparent that the state paths followed the LWSBS during loading, and subsequently during wetting. Figure 4-30 presents the collapse potential (given as the reduction in void ratio) with operational stress. It is clear that collapse potential increases with increasing operational stress up to the compaction stress and then decreases for

higher stress levels, as explained in the MPK framework. This behaviour matches the typical behaviour observed by Sun et al. (2004) on the collapse potential of soils.

4.2.3.5 Swelling pressure tests

A series of tests was undertaken to examine the swelling pressure development for constant volume (constrained) wetting of Merri Creek soil specimens. As for the kaolin soil, the tests were performed by locking the soil specimen against volumetric deformation but measuring the applied stress variation when the specimen was wetted. The same mould and set-up used for the other validation tests was used in this test program. Figure 4-31 shows the results of the tests undertaken. Figure 4-31a and 4-31b show the state path of a soil specimen prepared with 8.69% moisture content ($e_w =$ 0.228) loaded to 500 kPa (path AB), unloaded to 200 kPa (path BC) and then wetted at constant volume (i.e., e constant) to saturation (path CDEF). It is clear that the unloaded position at 200 kPa is below the LWSBS (point C), and during wetting the swelling pressure builds up to D (around 270 kPa), at which the state reached the LWSBS. Subsequently, the path DE is on the LWSBS (at constant initial void ratio = 0.977) reducing the swelling pressure until the LOO is intercepted at point E. Further wetting causes the soil to increase swelling pressure again towards saturation, as shown by path EF. This behaviour is consistent with the MPK framework and with the test results reported by Kodikara (2012). Figure 4-31c, 4-31d and 4-31e, 4-31f show identical behaviour for two more state paths for the initial moisture content of 8.69% ($e_w =$ 0.228). In the same way, Figure 4-31g and 4-31h show similar behaviour for higher moisture content of 14.87% ($e_w = 0.390$). In comparison to Figure 4-31a, 4-31b; 4-31c, 4-31d; 4-31e, 4-31f and 4-31g, 4-31h, Figure 4-31i and 4-31j show a soil specimen loaded to 1000 kPa (path AB), then unloaded to 200 kPa (path BC) with 14.87% moisture content and then wetted (path CD). It is apparent that this soil specimen did not reach the LWSBS and swelling pressure continued to increase with wetting. It appears that it was too far below the LWSBS initially at 200 kPa stress (due to increased compaction stress of 1000 kPa), and this led to the observed result. At point D, S_r is equal to 0.968, but the position of D is away from the NCL. This is because it has reached close to the saturation plane corresponding to the constant void ratio of 0.775 well below the NCL. The projected $S_r = 1$ line is shown in Figure 4-31i. Figure 4-31k and 4-31l show the indistinguishable behaviour for another state path for initial moisture

content of 14.87% ($e_w = 0.390$). Figure 4-31m, 4-31n; 4-31o, 4-31p and 4-31q, 4-31r show the comparison of the state paths presented earlier. Figure 4-31m and 4-31n show the state paths of three soil specimens prepared with 8.69% moisture content ($e_w = 0.228$) individually loaded to 500, 1000 and 2000 kPa, unloaded to 200 kPa and then wetted at constant volume (i.e., e constant) to saturation (paths $C_{1,2,3}D_{1,2,3}E_{1,2,3}F_{1,2,3}$). Similar to the behaviour of kaolin soil, these results indicate that the swelling pressure increases with the compaction stress (with initial density) when all other variables are kept constant. Identical behaviour has been reported in the research literature (c.f., Kassiff and Shalom, 1971; Imbert and Villar, 2006). Figure 4-31q and 4-31r also show the effect of compaction stress (500 and 1000 kPa) on the swelling state paths for soil specimens prepared with the higher moisture content of 14.87% ($e_w = 0.39$). It is apparent that, similar to the finding reported in the literature (c.f., Kassiff and Shalom, 1971; Imbert and Villar, 2006) and the state paths for soil specimens with 8.69% moisture content ($e_w = 0.228$), the maximum swelling pressure increases with the increase of the compaction stress. Figure 4-31o and 4-31p show two test results demonstrating the influence of initial moisture contents of 8.69% and 14.87%. The soil specimens were prepared by loading to 500 kPa, unloading to 200 kPa and then wetting at constant void ratio. It is evident that the swelling pressure decreases with increasing initial moisture content, consistent with published results (c.f., Kassiff and Shalom, 1971; Lee et al., 1999).

4.3 Validation of the MPK framework using data from the research literature

Data published in the research literature were also examined for analysis. Unfortunately, most test results were not directly usable since the tests were not carried out with the MPK framework in mind. Notwithstanding this, here it is attempted to examine the data presented by Jotisankasa (2005), Jotisankasa et al. (2007a), Sharma (1998) and Romero (1999) within this framework.

4.3.1 Interpretation of data reported by Jotisankasa (2005) and Jotisankasa et al. (2007a)

Jotisankasa (2005) and Jotisankasa et al. (2007a) reported a large number of suction-monitored oedometer tests results by using specific volume verses net stress, degree of saturation verses net stress and suction verses net stress relationships. This is the most complete data-set available in the literature to check the validation of the MPK framework. The following section presents the examination of this data within the MPK framework.

4.3.1.1 Materials and methods

Jotisankasa (2005) and Jotisankasa et al. (2007a) used Soil A, a mixture of 70% silt, 20% kaolin and 10% London clay, for these suction-monitored oedometer tests. The soil preparation technique is described by Jotisankasa et al. (2007a) and Jotisankasa (2009), who also noted that the final soil mixture was of low plasticity (LL = 28%, PL = 18%) and contained a large proportion of silt (clay content = 26%, silt content = 52%, and sand content = 22%) with a specific gravity of 2.64. All test specimens were prepared by static compaction. Three series of test specimens were prepared, namely 7-10 (void ratio ≈ 0.7 and moisture content ≈ 10%), 5-10 (void ratio ≈ 0.5 and moisture content ≈ 10%) and 7-13 (void ratio ≈ 0.7 and moisture content ≈ 13%). Different types of suction-monitored oedometer tests were performed on these soil specimens, including: (1) wetting at first and then loading and finally unloading; (2) drying at first and then loading and finally unloading; and (3) loading at first and then wetting and then loading again and finally unloading. Results of all of these different tests are presented in the following sections.

4.3.1.2 The LWSBS

The compaction characteristics of Soil A presented by Jotisankasa (2005) are shown in Figure 4-32. Four compaction curves, viz., static compaction curves at 400 kPa and 800 kPa stress levels and those corresponding to heavy and light compactions according to BS1377 – Part 4 (1990), are shown in the figure. Also shown in this figure are the initial positions of the three test series undertaken. Figure 4-33 shows the approximate development of the LWSBS from these compaction curves. The black lines show the void ratio vs moisture ratio relationship of the compaction curves shown in Figure 4-32. The other parts of the LWSBS are developed by considering a linear relationship

between the void ratio and logarithmic stress along the LOO and yield and post-yield data available from different oedometer tests. The light and heavy compactions approximately represent 1000 and 7000 kPa constant stress lines. The dashed lines are inferred extrapolations of the test results. Figure 4-34a shows the LWSBS of Soil A presented in the form of the compaction contours corresponding to net stress values generated from the compression data. Figure 4-34b shows a 3-D view of the LWSBS generated.

4.3.1.3 Interpretation of state path tests

Once the LWSBS was established, a series of test results involving state paths of wetting and loading, drying and loading and loading, wetting and loading presented by Jotisankasa (2005) and Jotisankasa et al. (2007a) were examined. Table 4-3 shows the list of the state path tests which were examined.

4.3.1.3.1 Interpretation of state path tests involving Wetting and Loading

Test results are presented by Jotisankasa (2005) and Jotisankasa et al. (2007a), who wetted statically compacted soil specimens to certain water content at the beginning of the test, compressed the specimens to a certain stress level and then unloaded to a certain lower stress level. Selected test results are shown in Figure 4-35a, 4-35b, 4-35c; 4-35d, 4-35e, 4-35f; 4-35g, 4-35h, 4-35i; 4-35j, 4-35k, 4-35l; 4-35m, 4-35n, 4-35o and 4-35p, 4-35q, 4-35r. Figure 4-35a, 4-35b and 4-35c show a soil specimen with 0.51 initial void ratio and 9.80% moisture content ($e_w = 0.260$), wetted to 13.50% moisture content ($e_w = 0.360$) at 0 kPa stress, loaded to 3220 kPa stress, and finally unloaded to 54 kPa stress with constant moisture content. It is clear that the initial position of the soil is inside the LWSBS (point A). During wetting, it swells towards the stress contour for 0 kPa (1 kPa is used here) of the LWSBS. The position of the stress path is still inside the LWSBS at the end of the wetting stage (path AB). Next, during loading at 13.50% moisture content ($e_w = 0.360$), it moves toward the LWSBS and follows the LWSBS up to 3220 kPa stress (point C) after intercepting the LWSBS around 1150 kPa (point H). Finally, it moves inside the LWSBS during unloading to the 54 kPa stage. Figure 4-35d, 4-35e, 4-35f; 4-35g, 4-35h, 4-35i; 4-35j, 4-35k, 4-35l and 4-35m, 4-35n, 4-35o show the test results of four soil specimens with different initial conditions (i.e., moisture content ≈ 10.0% and void ratio (e) ≈ 0.5 and 0.7) (point A), wetted at 0 kPa stress (point B) and

then loaded to certain high stresses (point C) and finally unloaded to 54 kPa stress (point D). It is apparent that in all of the tests, point H (around 1500, 2000, 650 and 380 kPa respectively) shows the interception of the LWSBS and the path HC is on the LWSBS. Figure 4-35p, 4-35q and 4-35r show another soil specimen with 0.72 initial void ratio (point A) and 10.60% moisture content ($e_w = 0.280$), loaded to 3220 kPa stress (point B) and finally unloaded to 54 kPa stress (point C). Again, point H (around 750 kPa) shows the interception of the LWSBS and the path HB is on the LWSBS. It is evident that in all of the tests, the soil specimens respond in a similar way, as expected according to the MPK framework.

4.3.1.3.2 Interpretation of state path tests involving Drying and Loading

Jotisankasa (2005) and Jotisankasa et al. (2007a) also present a series of test results in which statically compacted soil specimens were dried to certain lower moisture content at the beginning of the test, compressed to a certain stress level and then unloaded to a certain lower stress level. Selected test results are shown in Figure 4-36a, 4-36b, 4-36c; 4-36d, 4-36e, 4-36f; 4-36g, 4-36h, 4-36i; 4-36j, 4-36k, 4-36l; 4-36m, 4-36n, 4-36o and 4-36p, 4-36q, 4-36r. Figure 4-36a, 4-36b and 4-36c show a soil specimen with 0.49 initial void ratio and 10.10% moisture content ($e_w = 0.267$), dried to 2.20% moisture content ($e_w = 0.058$) at 0 kPa stress, then loaded to 13400 kPa stress and finally unloaded to 224 kPa stress with constant moisture content. It is clear that the initial position of the soil specimen is inside the LWSBS (point A). During drying, it moves to 2.20% moisture content level (path AB) without any deformation. The position of the state path is still inside the LWSBS at the end of the drying stage. Next, during loading, it moves toward the LWSBS and follows the LWSBS up to 13400 kPa stress (point C) after intercepting the LWSBS around 9000 kPa (point H). Finally, it moves inside the LWSBS during unloading to the 224 kPa stress stage. Figure 4-36d, 4-36e and 4-36f show a soil specimen with 0.69 initial void ratio and 10.0% moisture content ($e_w = 0.264$), dried to 9.20% moisture content ($e_w = 0.243$) at 0 kPa stress, then loaded to 3220 kPa stress and finally unloaded to 54 kPa stress with constant moisture content. It is apparent that the initial position of the soil specimen is inside the LWSBS (point A). During drying, it moves to 9.20% moisture content level (path AB) without changing volume. The position of the state path is still inside the LWSBS at the end of the drying stage. Next, during loading, it moves toward the LWSBS and follows the LWSBS up to

3220 kPa stress (point C) after intercepting the LWSBS around 1000 kPa (point H). Finally, it moves inside the LWSBS during unloading to the 54 kPa stress stage. Figure 4-36g, 4-36h, 4-36i; 4-36j, 4-36k, 4-36l and 4-36p, 4-36q, 4-36r show the test results of three soil specimens with different initial conditions (i.e., moisture content ≈ 10.0% and 13.0% and void ratio (e) ≈ 0.7) (point A), dried at 0 kPa stress to point B and then loaded to certain high stresses (point C) and finally unloaded to certain low stresses (point D). It is evident that in all of the tests, the specimens shrink during drying and the amount of shrinkage, Δv (= Δe), between point A and B is 0.008, 0.024 and 0.004 respectively. The state paths intercept the LWSBS at point H (around 1800, 3300 and 700 kPa respectively) during loading and then follow the path HC on the LWSBS. Figure 4-36m, 4-36n and 4-36o show another soil specimen with 0.71 initial void ratio and 13.50% moisture content (e_w = 0.356), loaded to 3235 kPa stress with as-compacted water content and then unloaded to 54 kPa stress. It is clear that the initial position of the soil specimen is inside the LWSBS (point A or B). During loading, it moves toward the LWSBS and follows the LWSBS up to 3235 kPa stress (point C) after intercepting the LWSBS around 450 kPa (point H). Finally, it moves inside the LWSBS during unloading to 54 kPa stress.

4.3.1.3.3 Interpretation of state path tests involving Loading, Wetting and Loading

Jotisankasa (2005) and Jotisankasa et al. (2007a) also present a series of test results in which statically compacted soil specimens were compressed to certain stress levels with as-compacted moisture content and then wetted to a certain suction level and finally either loaded to a certain stress level or not. Selected test results are shown in Figure 4-37a, 4-37b, 4-37c; 4-37d, 4-37e, 4-37f; 4-37g, 4-37h, 4-37i; 4-37j, 4-37k, 4-37l; 4-37m, 4-37n, 4-37o and 4-37p, 4-37q, 4-37r. Figure 4-37a, 4-37b and 4-37c show a soil specimen with 0.5 initial void ratio and 10.0% moisture content (e_w = 0.264), loaded to 1184 kPa stress with as-compacted moisture content (path AB) and then wetted to suction of 0 kPa at 1184 kPa stress (path BD). It was found from the specific volume, v versus $log\ p$ graph presented in Jotisankasa (2005) and Jotisankasa et al. (2007a) that Δv (= Δe) between point B and D is 0.036 (collapse). Point D is located on the saturation line (S_r = 1.0) as the value of suction is zero. According to the MPK framework, during wetting, the state path swells from point B towards the stress contour for 1184 kPa of the

LWSBS, intercepts the LWSBS at point C and then follows the 1184 kPa constant net stress contour on the LWSBS to the saturation line at point D. Figure 4-37d, 4-37e and 4-37f show a soil specimen with 0.5 initial void ratio and 10.0% moisture content ($e_w = 0.264$), loaded to 1619 kPa stress with as-compacted moisture content (path AB) and then wetted to suction of 0 kPa at 1619 kPa stress (path BD). Analysing the v versus $log\ p$ graph presented in Jotisankasa (2005) and Jotisankasa et al. (2007a), it was found that $\Delta v\ (= \Delta e)$ between point B and D is 0.033 (collapse). Point D is located on the saturation line ($S_r = 1.0$) as the value of suction is zero. According to the MPK framework, during wetting, the state path swells from point B towards the stress contour for 1619 kPa of the LWSBS, intercepts the LWSBS at point C, and then follows the 1619 kPa constant net stress contour on the LWSBS to the saturation line at point D. Figure 4-37g, 4-37h and 4-37i show a soil specimen with 0.71 initial void ratio and 10.30% moisture content ($e_w = 0.270$), loaded to 430 kPa stress at as-compacted moisture content (path AB), then wetted to a suction of 130 kPa at 430 kPa stress (path BCD), and finally loaded to 3220 kPa stress (path DE) at constant moisture content. From the v versus $log\ p$ graph presented in Jotisankasa (2005) and Jotisankasa et al. (2007a), it was found that $\Delta v\ (= \Delta e)$ between point B and D is 0.059 (collapse). As the moisture content data during wetting are not presented in Jotisankasa (2005) and Jotisankasa et al. (2007a), the value of the moisture ratio ($e_w = 0.37$) at point D was found by plotting D point on the LWSBS, as the net stress (p) and the void ratio (e) are known. Finally, during loading at constant moisture content, the state path follows the LWSBS up to 3220 kPa stress. Figure 4-37j, 4-37k and 4-37l show a soil specimen with 0.73 initial void ratio and 10.10% moisture content ($e_w = 0.270$) loaded to 215 kPa stress with as-compacted moisture content (path AB), then wetted to the suction of 140 kPa at 215 kPa stress (path BC), and finally loaded to 3220 kPa stress (path CD) with constant moisture content. Analysing the v versus $log\ p$ graph presented in Jotisankasa (2005) and Jotisankasa et al. (2007a), it was found that $\Delta v\ (= \Delta e)$ between point B and C is ≈ 0, which means the position of the state path is still inside the LWSBS at the end of the wetting stage. Finally, during loading with constant moisture content, the state path intercepts the LWSBS around 400 kPa stress (point H) and follows the LWSBS up to 3220 kPa stress. Figure 4-37m, 4-37n and 4-37o show a soil specimen with 0.71 initial void ratio and 10.0% moisture content ($e_w = 0.264$), loaded to 108 kPa stress at as-compacted moisture content (path AB), and then wetted to the suction of 10 kPa at 108

kPa stress (path BCD). From the v versus $log\ p$ graph presented in Jotisankasa (2005) and Jotisankasa et al. (2007a), it was found that Δv ($= \Delta e$) between point B and D is 0.039 (collapse). As the moisture content data during wetting are not presented in Jotisankasa (2005) and Jotisankasa et al. (2007a), the value of moisture ratio ($e_w = 0.37$) at point D was found by plotting D point on the LWSBS, as the net stress (p) and the void ratio (e) are known. Figure 4-37p, 4-37q and 4-37r show a soil specimen with 0.71 initial void ratio and 13.50% moisture content ($e_w = 0.356$), loaded to 303 kPa stress with as-compacted moisture content (path AB) and then wetted to the suction of 0 kPa at 303 kPa stress (path BC). Analysis of the v versus $log\ p$ graph presented in Jotisankasa (2005) and Jotisankasa et al. (2007a), revealed that Δv ($= \Delta e$) between point B and C is 0.13 (collapse). Point C is located on the saturation line ($S_r = 1.0$) because the value of suction at that point is zero. As point B is located on the stress contour for 303 kPa of the LWSBS, according to the MPK framework, during wetting, the state path follows the 303 kPa constant net stress contour on the LWSBS from point B to the saturation line at point C. It is apparent that in all of the tests, the state paths follow the paths consistent with the MPK framework.

4.3.1.4 Further validation of the MPK framework based on Jotisankasa (2005) and Jotisankasa et al. (2007a)

According to the MPK framework, when a soil specimen is compacted to a certain stress level and then unloaded to a lower stress level, the state path follows the LWSBS and then moves inside the LWSBS. Now the question is, what will happen to the state path if the soil specimen is loaded again at as-compacted moisture content or wetted and then loaded or dried and then loaded? The answer lies in the shape of the LWSBS. If loading is performed at as-compacted moisture content, the state path will intercept the LWSBS at the same stress as the compacted stress, while if loading is applied after wetting or drying, the state path will intercept the LWSBS at a lower or higher stress than the compacted stress, respectively. Figure 4-38 shows the demonstration of the interception of the LWSBS of an compacted unloaded soil specimen during loading at as-compacted moisture content, or after wetting or drying. The soil specimen is prepared at 700 kPa initially and then unloaded to 100 kPa. Now, if the soil specimen is loaded at as-compacted moisture content, the state path will intercept the LWSBS at 700 kPa, while if the soil specimen is loaded after wetting or drying, the state path will intercept the

LWSBS at 300 and 1300 kPa respectively. As stated earlier, yield stress depends on the shape of the LWSBS. During drying, the state path moves away from the LWSBS, while during wetting, the state path comes close to the LWSBS. That is the reason why the soil specimen yields at lower stress during wetting and higher stress during drying. Similar behaviour of yield stress is found in the experimental results of Jotisankasa (2005) and Jotisankasa et al. (2007a), which are presented in Table 4-4. It is evident that all the soil specimens which are wetted yield at lower stress than the initial compaction stress, while the soil specimens which are dried yield at higher stress than the initial compaction stress. These experimental results are consistent with the prediction of the MPK framework. However, it should be noted that drying paths were not part of the original definition of the MPK framework by Kodikara (2012). In the present thesis, most emphasis has been placed on loading/wetting paths, although some drying paths were examined, as outlined above. While the data are not conclusive, it appears that conceptually at least, state paths involving drying appear to be consistent with the same LWSBS developed for loading/wetting state paths. However, examination of state paths involving drying would be a subject for future research.

4.3.2 Interpretation of other datasets

Wijesooriya (2012) analysed wetting and drying experimental data reported by Sharma (1998) and Romero (1999). In this section, first or major wetting events from these experimental data are examined within the MPK framework.

4.3.2.1 Analysis of experimental data from Sharma (1998)

Sharma (1998) conducted suction control tri-axial tests to measure the swell-shrink behaviour of an expansive soil. A mixture of 10% Wyoming sodium bentonite with Speswhite kaolin was used as the expansive soil, which is represented by 'BK' here. The properties of the soil are presented in Table 4-5, while Table 4-6 lists the state path tests (first wetting) examined.

The first or major wetting events from various swell-shrink tests performed by Sharma (1998) on Soil 'BK' are presented in Figure 4-39. The soil specimens were loaded to 400 kPa and then unloaded to 10 kPa and then wetted in Tests 1, 8 and 16. It is clear that the state paths swelled towards the 10 kPa stress contour of the LWSBS during wetting and

eventually the state paths of Tests 8 and 16 intercepted the LWSBS. Test 2 involved a soil specimen which was loaded to 400 kPa, then unloaded to 50 kPa and then wetted. It is apparent that during wetting, the state path swelled towards, intercepted and followed 50 kPa stress contour of the LWSBS. In Tests 2, 3 and 4, soil specimens were loaded to 800 kPa and then unloaded to 50, 10 and 20 kPa respectively and then wetted. It is evident that during wetting, the soil specimen of Test 2 swelled and the state path intercepted the LWSBS, whereas the state paths of Tests 3 and 4 did not intercept the LWSBS because the amount of wetting was not sufficient. Tests 19 and 20 were of soil specimens which were loaded to 3200 kPa, then unloaded to 10 kPa and then wetted. It is clear that the state paths swelled massively during wetting. In all of the tests, the soil specimens responded in a similar way, as expected according to the MPK framework.

4.3.2.2 Analysis of experimental data from Romero (1999)

The research of Romero (1999) was focused on the volumetric behaviour of unsaturated clays (swelling, collapse, and shrinkage) under suction, stress and temperature changes. Various isothermal wetting and drying tests were performed using both oedometers and isotropic methods. The material tested is known as Boom Clay. Initially, the soil was air-dried to 15.4% moisture content and then the soil specimens were compacted statically to achieve 16.7 or 13.7 kN/m^3 dry unit weight. Subsequently, wetting and drying cycles were carried out on the soil specimens under certain stress levels. The properties of Boom Clay are presented in Table 4-7, while Table 4-8 lists the state path tests (first wetting) which have been examined from Romero (1999).

The first or major wetting events from various wetting and drying tests performed by Romero (1999) on Boom Clay are presented in Figure 4-40. It is clear that the state paths of the US 0.026, US 0.085, US 0.3 and US 0.55 MPa tests swelled towards the LWSBS during wetting. The statically compacted dry unit weight of these soil specimens was 16.7 kN/m^3 and the first or major wetting events were performed at 0.026, 0.085, 0.3 and 0.55 MPa stress respectively. On the other hand, the statically compacted dry unit weight of the US 0.6 and US 1.2 MPa tests was 13.7 kN/m^3 and the first or major wetting events were carried out at 0.6 and 1.2 MPa stress, respectively. It is evident that the state paths of these tests followed the LWSBS during wetting. Finally, US I0.085 and US I0.6 MPa are isotropic tests, where the first or major wetting events were performed at 0.085 and

0.6 MPa stresses respectively. The statically compacted dry unit weights of these soil specimens were 16.7 and 13.7 kN/m^3 respectively. It is apparent that the state path of US I0.085 swelled during wetting, whereas for the US I0.6 MPa test, it collapsed. As the wetting was performed at lower stress in the US I0.085 test, the position of the state path was inside the LWSBS before wetting. For this reaon, it swelled during wetting. In contrast, the position of the state path was on the LWSBS before wetting in the US I0.6 MPa test. As a result, it collapsed during wetting. However, the state path of the US I0.6 MPa test did not follow the 0.6 MPa stress contour of the LWSBS because the LWSBS presented here was actually obtained from oedometer tests, and it is inevitable that the LWSBSs developed using oedometers and isotropic methods are not identical. Although the LWSBS contours were developed approximately, it is evident that in all of the tests, the state paths appear to follow the paths consistent with the MPK framework.

4.4 Discussion

A large number of experiments were performed on statically compacted lightly reactive kaolin and reactive Merri Creek clay under constant water content testing. Despite the difference in their degree of reactivity, both soils closely followed the concepts of the MPK framework. This highlights that the macroscopic behaviour of compacted soil in general can be presented within this framework. In the following discussion, some of the specific features observed are examined.

Kodikara (2012) shows that one major difference between slurry soils and compacted clay may be that the void ratio for virgin compaction states (i.e., on the LWSBS) increases with decreasing moisture ratio (the strictly dry side of the LOO). For slurry clay, these states may be derived by drying from the slurry state and this would lead to reduction in void ratio as the moisture ratio is decreased. Experimental results obtained for both kaolin (Figure 4-3a) and the Merri Creek soil (Figure 4-10a) show that due to the macroscopic structure build-up, the void ratio increases with decreasing moisture ratio, but with very low moisture contents, the void ratio can decrease again. This feature is more prominent for the Merri Creek soil. However, the effect appears to decrease and eventually vanishes at higher net stress levels. The occurrence of this feature is similar to having compaction curves with multiple peaks, and appears to be related to the weakening of the effect of suction to form stronger contacts among aggregates that give

larger macro void space. The limited tests undertaken indicate that when wetted from a position on such LWSBS located at a very low moisture ratio, the wetting path may not follow the exact shape of the LWSBS, but the soil may swell until the LWSBS is intercepted, after which it may undergo collapse (c.f., Figure 4-22d). This aspect may need further examination in future, but practically, it is not very significant since operational moisture contents may not be as low.

Another feature worth observing is the cross-validity and uniqueness of the compression curves at constant moisture ratio to represent the LWSBS across moisture ratios, as embedded in the MPK framework. This is highlighted by the validated ability of the LWSBS to predict the behaviour of soil state paths during wetting and loading (or a combination) when the LWSBS is intercepted (c.f., Figure 4-13e, Figure 4-15j). Alonso et al. (1987) also noted that if a state path does not decrease the degree of saturation, the resulting volumetric deformation is mostly path-independent. The existence of such a unique surface in the non-decreasing degree of saturation paths was also noted by Tarantino and Tombolato (2005) with respect to the void ratio-suction-degree of saturation space.

An important feature of the MPK framework is the introduction of the influence of the LOO on soil behaviour, which demarcates the boundary between dry and wet of optimum. The LOO is defined as the boundary where the air phase moves from a continuous phase in the dry side to a discontinuous phase in the wet side. Along with this, the all-round influence of suction becomes prominent in the wet side and this gives rise to the increase of void ratio with increasing moisture ratio (or vice versa). This behaviour gives the canyon-like feature in the LWSBS with the LOO at its bottom associated with the minimum void ratio (or maximum dry density). The wetting tests that followed the LWSBS showed the existence of this feature (c.f., Figure 4-22a). Similarly, constrained swelling tests also clearly demonstrated the influence of the LOO on the LWSBS. For instance, the swelling pressure increased to a peak until the state path intercepted the LWSBS and then followed it, subsequently the swelling pressure decreased to the LOO and then increased again towards full saturation (c.f., Figure 4-31o). Another important validation is the confirmation of the characteristic

behaviour of collapse potential, where the peak collapse occurred at the compaction stress.

Although this thesis places emphasis on loading/wetting state paths as introduced in the MPK framework, some state paths that involved initial drying were examined. It appears that for the test results examined, the LWSBS concept is still valid to explain these paths. However, more experimental results would be required to examine the influence of paths involving initial drying. In any event, the change of yield point with respect to both wetting (conceptually and quantitatively) and drying (at least conceptually) can be explained using the LWSBS concept in the MPK framework. This is inherently related to change in the loading/collapse curve as in the Barcelona Basic Model (BBM) with wetting or drying, as also expounded by Wheeler et al. (2003a).

4.5 Conclusion

This chapter has presented experimental results for statically compacted lightly reactive kaolin soil and reactive Merri Creek clay under combinations of loading, wetting and unloading state paths subject to different boundary and initial conditions. The results were consistent with the MPK framework proposed by Kodikara (2012). Some tests undertaken by Jotisankasa (2005), Jotisankasa et al. (2007a), Sharma (1998) and Romero (1999) were also successfully interpreted within the framework. The results indicate that void ratio-moisture ratio-net stress space along with the Loading Wetting State Boundary Surface (LWSBS) can be used to explain/predict the behaviour of statically compacted soil under hydro-mechanical state paths with non-decreasing degrees of saturation. The LWSBS can be established by constant moisture content compression tests and assuming cross-validity (the applicability of the LWSBS in wetting in a constant net stress plane when the LWSBS has been developed using compression lines developed at constant water content) in the increasing direction of moisture content. Since constant moisture content tests do not require the specialised test equipment necessary for suction control tests, this approach remarkably simplifies the test method and reduces testing time.

Suction was not measured in the experiments presented in this chapter, as it was not essential to explain most volumetric behaviour as per the MPK framework. However, the role of suction within the MPK framework is explained fully with some experimental

results in Chapter 6. In particular, the dependency of water retention characteristics on the state position within and on the LWSBS is studied. Furthermore, no experiment has been performed to examine the influence of drying and, in general, the influence of wet/dry cycles and the possible environmental stabilisation of soils in this research. However, some state paths involving initial drying were considered. It was found that, at least conceptually, the LWSBS concept can explain the resulting behaviour, especially in relation to the change in yield stress as found in the loading/collapse curve in models based on BBM. However, further research is needed to examine this aspect in future. In the following chapter, the application of the MPK framework to dynamically compacted soils is presented.

Table 4-1: A summary of state path tests performed on the kaolin soil

Test Identity	Description of the Test
Loading – Wetting Tests	
SC – EK – LW – 1	0% moisture content ($e_w = 0$) loaded to 50 KPa and then wetted to 41.62% moisture content ($e_w = 1.103$)
SC – EK – LW – 2	0% moisture content ($e_w = 0$) loaded to 100 KPa and then wetted to 29.66% moisture content ($e_w = 0.786$)
SC – EK – LW – 3	11.69% moisture content ($e_w = 0.310$) loaded to 20 KPa and then wetted to 31.25% moisture content ($e_w = 0.828$)
Loading – Wetting – Loading Tests	
SC – EK – LWL – 1	0% moisture content ($e_w = 0$) loaded to 1000 KPa and then wetted to 21.52% moisture content ($e_w = 0.570$) and then loaded to 2000 KPa
SC – EK – LWL – 2	8.96% moisture content ($e_w = 0.237$) loaded to 50 KPa and then wetted to 27.35% moisture content ($e_w = 0.725$) and then loaded to 2000 KPa
SC – EK – LWL – 3	0% moisture content ($e_w = 0$) loaded to 50 KPa and then wetted to 19.69% moisture content ($e_w = 0.522$) and then loaded to 2000 KPa
SC – EK – LWL – 4	0% moisture content ($e_w = 0$) loaded to 20 KPa and then wetted to 21.60% moisture content ($e_w = 0.572$) and then loaded to 2000 KPa
Loading – Unloading – Wetting – Loading Tests	
SC – EK – LUWL – 1	4.04% moisture content ($e_w = 0.107$) loaded to 1000 KPa and then unloaded to 20 KPa and then wetted to 23.67% moisture content ($e_w = 0.627$) and then loaded to 2000 KPa
SC – EK – LUWL – 2	8.96% moisture content ($e_w = 0.237$) loaded to 1000 KPa and then unloaded to 100 KPa and then wetted to 28.30% moisture content ($e_w = 0.750$) and then loaded to 2000 KPa
Loading – Unloading – Wetting Tests	
SC – EK – LUW – 1	11.88% moisture content ($e_w = 0.315$) loaded to 1000 KPa and then unloaded to 700 KPa and then wetted to 34.14% moisture content ($e_w = 0.905$)
SC – EK – LUW – 2	11.88% moisture content ($e_w = 0.315$) loaded to 500 KPa and then unloaded to 300 KPa and then wetted to 34.95% moisture content ($e_w = 0.926$)
SC – EK – LUW – 3	15.85% moisture content ($e_w = 0.420$) loaded to 1000 KPa and then unloaded to 700 KPa and then wetted to 32.77% moisture content ($e_w = 0.868$)
SC – EK – LUW – 4	15.85% moisture content ($e_w = 0.420$) loaded to 500 KPa and then unloaded to 300 KPa and then wetted to 32.80% moisture content ($e_w = 0.869$)
Loading – Unloading – Wetting – Unloading – Wetting Tests	
SC – EK – LUWUW – 1	15.85% moisture content ($e_w = 0.420$) loaded to 500 KPa and then unloaded to 400 KPa and then wetted to 26.29% moisture content ($e_w = 0.697$) and then unloaded to 300 KPa and then wetted to 34.14% moisture content ($e_w = 0.905$)

SC – EK – LUWUW – 2	11.88% moisture content ($e_w = 0.315$) loaded to 1000 KPa and then unloaded to 700 KPa and then wetted to 22.23% moisture content ($e_w = 0.589$) and then unloaded to 500 KPa and then wetted to 30.98% moisture content ($e_w = 0.821$)
SC – EK – LUWUW – 3	15.85% moisture content ($e_w = 0.420$) loaded to 300 KPa and then unloaded to 200 KPa and then wetted to 28.60% moisture content ($e_w = 0.758$) and then unloaded to 100 KPa and then wetted to 39.26% moisture content ($e_w = 1.040$)
SC – EK – LUWUW – 4	11.69% moisture content ($e_w = 0.310$) loaded to 300 KPa and then unloaded to 200 KPa and then wetted to 25.80% moisture content ($e_w = 0.684$) and then unloaded to 100 KPa and then wetted to 38.56% moisture content ($e_w = 1.022$)
Collapse Potential Tests	
SC – EK – CPT – 1 or SC – EK – LUW – 5	15.77% moisture content ($e_w = 0.420$) loaded to 500 kPa and then unloaded to 50 kPa and then wetted to 45.43% moisture content ($e_w = 1.204$)
SC – EK – CPT – 2 or SC – EK – LUW – 6	15.77% moisture content ($e_w = 0.420$) loaded to 500 kPa and then unloaded to 100 kPa and then wetted to 43.16% moisture content ($e_w = 1.144$)
SC – EK – CPT – 3 or SC – EK – LW – 4	15.77% moisture content ($e_w = 0.420$) loaded to 500 kPa and then wetted to 38.10% moisture content ($e_w = 1.010$)
SC – EK – CPT – 4 or SC – EK – LW – 5	15.77% moisture content ($e_w = 0.420$) loaded to 1000 kPa and then wetted to 33.0% moisture content ($e_w = 0.875$)
SC – EK – CPT – 5 or SC – EK – LW – 6	15.77% moisture content ($e_w = 0.420$) loaded to 2000 kPa and then wetted to 28.30% moisture content ($e_w = 0.750$)
SC – EK – CPT – 6 or SC – EK – LW – 7	15.77% moisture content ($e_w = 0.420$) loaded to 4000 kPa and then wetted to 20.75% moisture content ($e_w = 0.550$)
Combination of SC – EK – CPT – 1 to 6	A "Reduction of Void Ratio – Net Stress" graph shows the results obtained from Collapse Potential Tests (1 – 6)
Loading – Unloading – Loading Tests	
SC – EK – LUL – 1	0% moisture content ($e_w = 0$) loaded to 50 kPa and then unloaded to 20 kPa and then loaded to 100 kPa and then unloaded to 20 kPa and then loaded to 500 kPa and then unloaded to 50 kPa and then loaded to 1000 kPa and then unloaded to 100 kPa and then loaded to 2000 kPa and then unloaded to 100 kPa and then loaded to 5000 kPa and then unloaded to 100 kPa

SC – EK – LUL – 2	8.30% moisture content ($e_w = 0.220$) loaded to 50 kPa and then unloaded to 20 kPa and then loaded to 100 kPa and then unloaded to 20 kPa and then loaded to 500 kPa and then unloaded to 50 kPa and then loaded to 1000 kPa and then unloaded to 100 kPa and then loaded to 2000 kPa and then unloaded to 100 kPa and then loaded to 5000 kPa and then unloaded to 100 kPa
SC – EK – LUL – 3	16.05% moisture content ($e_w = 0.425$) loaded to 50 kPa and then unloaded to 20 kPa and then loaded to 100 kPa and then unloaded to 20 kPa and then loaded to 500 kPa and then unloaded to 50 kPa and then loaded to 1000 kPa and then unloaded to 100 kPa and then loaded to 2000 kPa and then unloaded to 100 kPa and then loaded to 5000 kPa and then unloaded to 100 kPa
SC – EK – LUL – 4	20.67% moisture content ($e_w = 0.548$) loaded to 50 kPa and then unloaded to 20 kPa and then loaded to 100 kPa and then unloaded to 20 kPa and then loaded to 500 kPa and then unloaded to 50 kPa and then loaded to 1000 kPa and then unloaded to 100 kPa and then loaded to 2000 kPa and then unloaded to 100 kPa and then loaded to 3000 kPa and then unloaded to 100 kPa
SC – EK – LUL – 5	22.73% moisture content ($e_w = 0.602$) loaded to 50 kPa and then unloaded to 20 kPa and then loaded to 100 kPa and then unloaded to 20 kPa and then loaded to 500 kPa and then unloaded to 50 kPa and then loaded to 1000 kPa and then unloaded to 100 kPa and then loaded to 2000 kPa and then unloaded to 100 kPa
SC – EK – LUL – 6	23.84% moisture content ($e_w = 0.632$) loaded to 50 kPa and then unloaded to 20 kPa and then loaded to 100 kPa and then unloaded to 20 kPa and then loaded to 500 kPa and then unloaded to 50 kPa and then loaded to 1000 kPa and then unloaded to 100 kPa and then loaded to 2000 kPa and then unloaded to 100 kPa
SC – EK – LUL – 7	30.20% moisture content ($e_w = 0.800$) loaded to 50 kPa and then unloaded to 20 kPa and then loaded to 100 kPa and then unloaded to 20 kPa and then loaded to 500 kPa and then unloaded to 50 kPa and then loaded to 1000 kPa and then unloaded to 100 kPa
Swelling Pressure Tests	
SC – EK – SPT – 1	10.69% moisture content ($e_w = 0.283$) loaded to 500 kPa and then unloaded to 100 kPa and then wetted to 50.90% moisture content ($e_w = 1.350$) ($S_r = 0.988$ and $e_0 = 1.366$) in constant volume
SC – EK – SPT – 2	10.69% moisture content ($e_w = 0.283$) loaded to 1000 kPa and then unloaded to 100 kPa and then wetted to 43.40% moisture content ($e_w = 1.150$) ($S_r = 0.975$ and $e_0 = 1.179$) in constant volume
SC – EK – SPT – 3	10.69% moisture content ($e_w = 0.283$) loaded to 2000 kPa and then unloaded to 100 kPa and then wetted to 34.0% moisture content ($e_w = 0.900$) ($S_r = 0.973$ and $e_0 = 0.925$) in constant volume

SC – EK – SPT – 4	19.88% moisture content (e_w = 0.527) loaded to 500 kPa and then unloaded to 100 kPa and then wetted to 42.30% moisture content (e_w = 1.120) (S_r = 0.968 and e_0 = 1.156) in constant volume
SC – EK – SPT – 5	19.88% moisture content (e_w = 0.527) loaded to 1000 kPa and then unloaded to 100 kPa and then wetted to 35.10% moisture content (e_w = 0.930) (S_r = 0.974 and e_0 = 0.955) in constant volume
SC – EK – SPT – 6	19.88% moisture content (e_w = 0.527) loaded to 2000 kPa and then unloaded to 100 kPa and then wetted to 30.20% moisture content (e_w = 0.800) (S_r = 0.976 and e_0 = 0.82) in constant volume

SC => Static Compaction, EK => Ecalite Kaolin, LW => Loading – Wetting, LWL => Loading – Wetting – Loading, LUWL => Loading – Unloading – Wetting – Loading, LUW => Loading – Unloading – Wetting, LUWUW => Loading – Unloading – Wetting – Unloading – Wetting, CPT => Collapse Potential Test, LUL => Loading – Unloading – Loading, SPT => Swelling Pressure Test.

Table 4-2: A summary of state path tests performed on the Merri Creek soil

Test Identity	Description of the Test
Loading – Wetting Tests	
SC – MC – LW – 1	10.35% moisture content ($e_w = 0.271$) loaded to 500 kPa and then wetted to 28.38% moisture content ($e_w = 0.743$)
SC – MC – LW – 2	10.35% moisture content ($e_w = 0.271$) loaded to 200 and then wetted to 27.95% moisture content ($e_w = 0.732$)
Loading – Wetting – Loading Tests	
SC – MC – LWL – 1	15.0% moisture content ($e_w = 0.393$) loaded to 1000 kPa and then wetted to 20.24% moisture content ($e_w = 0.530$) and then loaded to 2000 kPa
Loading – Unloading – Wetting – Loading Tests	
SC – MC – LUWL – 1	15.0% moisture content ($e_w = 0.393$) loaded to 1000 kPa and then unloaded to 100 kPa and then wetted to 27.52% moisture content ($e_w = 0.721$) and then loaded to 1000 kPa
Loading – Unloading – Wetting Tests	
SC – MC – LUW – 1	10.35% moisture content ($e_w = 0.271$) loaded to 2000 kPa and then unloaded to 100 kPa and then wetted to 26.0% moisture content ($e_w = 0.681$)
SC – MC – LUW – 2	10.35% moisture content ($e_w = 0.271$) loaded to 1000 kPa and then unloaded to 400 kPa and then wetted to 17.42% moisture content ($e_w = 0.456$)
Loading – Unloading – Wetting – Unloading – Wetting Tests	
SC – MC – LUWUW – 1	10.35% moisture content ($e_w = 0.271$) loaded to 2000 kPa and then unloaded to 1000 kPa and then wetted to 18.37% moisture content ($e_w = 0.481$) and then unloaded to 100 kPa and then wetted to 27.10% moisture content ($e_w = 0.710$)
SC – MC – LUWUW – 2	15.0% moisture content ($e_w = 0.393$) loaded to 2000 kPa and then unloaded to 1000 kPa and then wetted to 20.0% moisture content ($e_w = 0.524$) and then unloaded to 100 kPa and then wetted to 27.0% moisture content ($e_w = 0.707$)
SC – MC – LUWUW – 3	15.0 % moisture content ($e_w = 0.393$) loaded to 400 kPa and then unloaded to 300 kPa and then wetted to 20.78% moisture content ($e_w = 0.544$) and then unloaded to 200 kPa and then wetted to 27.35% moisture content ($e_w = 0.717$)
SC – MC – LUWUW – 4	15.0 % moisture content ($e_w = 0.393$) loaded to 1000 kPa and then unloaded to 700 kPa and then wetted to 19.82% moisture content ($e_w = 0.519$) and then unloaded to 500 kPa and then wetted to 23.92% moisture content ($e_w = 0.627$)
Loading – Unloading – Wetting – Unloading –Wetting – Unloading – Wetting – Unloading – Wetting	

Tests	
SC – MC – LUWUWUWUW – 1	10.35% moisture content ($e_w = 0.271$) loaded to 2000 kPa and then unloaded to 700 kPa and then wetted to 14.83% moisture content ($e_w = 0.388$) and then unloaded to 500 kPa and then wetted to 19.32% moisture content ($e_w = 0.506$) and then unloaded to 300 kPa and then wetted to 23.80% moisture content ($e_w = 0.624$) and then unloaded to 200 kPa and then wetted to 28.28% moisture content ($e_w = 0.741$)
Collapse Potential Tests	
SC – MC – CPT – 1 or SC – MC – LUW – 3	16.06% moisture content ($e_w = 0.421$) loaded to 500 kPa and then unloaded to 40 kPa and then wetted to 38.06% moisture content ($e_w = 0.997$)
SC – MC – CPT – 2 or SC – MC – LUW – 4	16.06% moisture content ($e_w = 0.421$) loaded to 500 kPa and then unloaded to 100 kPa and then wetted to 34.14% moisture content ($e_w = 0.894$)
SC – MC – CPT – 3 or SC – MC – LW – 3	16.06% moisture content ($e_w = 0.421$) loaded to 500 kPa and then wetted to 23.80% moisture content ($e_w = 0.624$)
SC – MC – CPT – 4 or SC – MC – LW – 4	16.06% moisture content ($e_w = 0.421$) loaded to 700 kPa and then wetted to 21.0% moisture content ($e_w = 0.550$)
SC – MC – CPT – 5 or SC – MC – LW – 5	16.06% moisture content ($e_w = 0.421$) loaded to 1000 kPa and then wetted to 19.0% moisture content ($e_w = 0.500$)
SC – MC – CPT – 6 or SC – MC – LW – 6	16.06% moisture content ($e_w = 0.421$) loaded to 2000 kPa and then wetted to 17.0% moisture content ($e_w = 0.445$)
Combination of SC – MC – CPT – 1 to 6	A "Reduction of Void Ratio – Net Stress" graph shows the results obtained from Collapse Potential Tests (1 – 6)
Loading – Unloading – Loading Tests	
SC – MC – LUL – 1	0% moisture content ($e_w = 0$) loaded to 50 kPa and then unloaded to 20 kPa and then loaded to 100 kPa and then unloaded to 20 kPa and then loaded to 500 kPa and then unloaded to 50 kPa and then loaded to 1000 kPa and then unloaded to 100 kPa and then loaded to 2000 kPa and then unloaded to 100 kPa and then loaded to 5000 kPa and then unloaded to 2500 kPa
SC – MC – LUL – 2	7.83% moisture content ($e_w = 0.205$) loaded to 50 kPa and then unloaded to 20 kPa and then loaded to 100 kPa and then unloaded to 20 kPa and then loaded to 500 kPa and then unloaded to 50 kPa and then loaded to 1000 kPa and then unloaded to 100 kPa and then loaded to 2000 kPa and then unloaded to 100 kPa and then loaded to 5000 kPa and then unloaded to 2500 kPa

SC – MC – LUL – 3	13.19% moisture content ($e_w = 0.346$) loaded to 50 kPa and then unloaded to 20 kPa and then loaded to 100 kPa and then unloaded to 20 kPa and then loaded to 500 kPa and then unloaded to 50 kPa and then loaded to 1000 kPa and then unloaded to 100 kPa and then loaded to 2000 kPa and then unloaded to 100 kPa and then loaded to 5000 kPa and then unloaded to 2500 kPa
SC – MC – LUL – 4	16.06% moisture content ($e_w = 0.421$) loaded to 50 kPa and then unloaded to 20 kPa and then loaded to 100 kPa and then unloaded to 20 kPa and then loaded to 500 kPa and then unloaded to 50 kPa and then loaded to 1000 kPa and then unloaded to 100 kPa and then loaded to 2000 kPa and then unloaded to 100 kPa
SC – MC – LUL – 5	22.68% moisture content ($e_w = 0.594$) loaded to 50 kPa and then unloaded to 20 kPa and then loaded to 100 kPa and then unloaded to 20 kPa and then loaded to 500 kPa and then unloaded to 50 kPa and then loaded to 1000 kPa and then unloaded to 100 kPa
Swelling Pressure Tests	
SC – MC – SPT – 1	8.69% moisture content ($e_w = 0.228$) loaded to 500 kPa and then unloaded to 200 kPa and then wetted to 36.26% moisture content ($e_w = 0.950$) ($S_r = 0.972$ and $e_0 = 0.977$)in constant volume
SC – MC – SPT – 2	8.69% moisture content ($e_w = 0.228$) loaded to 1000 kPa and then unloaded to 200 kPa and then wetted to 32.06% moisture content ($e_w = 0.840$) ($S_r = 0.966$ and $e_0 = 0.87$)in constant volume
SC – MC – SPT – 3	8.69% moisture content ($e_w = 0.228$) loaded to 2000 kPa and then unloaded to 200 kPa and then wetted to 27.48% moisture content ($e_w = 0.720$) ($S_r = 0.968$ and $e_0 = 0.744$)in constant volume
SC – MC – SPT – 4	14.87% moisture content ($e_w = 0.390$) loaded to 500 kPa and then unloaded to 200 kPa and then wetted to 35.50% moisture content ($e_w = 0.930$) ($S_r = 0.969$ and $e_0 = 0.96$)in constant volume
SC – MC – SPT – 5	14.87% moisture content ($e_w = 0.390$) loaded to 1000 kPa and then unloaded to 200 kPa and then wetted to 28.63% moisture content ($e_w = 0.750$) ($S_r = 0.968$ and $e_0 = 0.775$)in constant volume
SC – MC – SPT – 6	14.87% moisture content ($e_w = 0.390$) loaded to 2000 kPa and then unloaded to 200 kPa and then wetted to 21.37% moisture content ($e_w = 0.560$) ($S_r = 0.981$ and $e_0 = 0.571$)in constant volume

SC => Static Compaction, MC => Merri Creek Soil, LW => Loading – Wetting, LWL => Loading – Wetting – Loading, LUWL => Loading – Unloading – Wetting – Loading, LUW => Loading – Unloading – Wetting, LUWUW => Loading – Unloading – Wetting – Unloading – Wetting, LUWUWUWUW => Loading – Unloading – Wetting – Unloading – Wetting– Unloading – Wetting – Unloading – Wetting, CPT => Collapse Potential Test, LUL => Loading – Unloading – Loading, SPT => Swelling Pressure Test.

Table 4-3: A summary of state path tests examined from Jotisankasa (2005) and Jotisankasa et al. (2007a)

Test Identity	Description of the Test
Wetting – Loading Tests	
5 – 10 – B	Test 5 – 10 – B (initial void ratio = 0.51 and moisture content = 9.80% (e_w = 0.260)) – firstly, soil specimen was wetted to 13.50% moisture content (e_w = 0.360) at 0 kPa stress and then loaded to 3220 kPa stress and then unloaded to 54 kPa stress
5 – 10 – E	Test 5 – 10 – E (initial void ratio = 0.51 and moisture content = 10.0% (e_w = 0.264)) – firstly, soil specimen was wetted to 11.80% moisture content (e_w = 0.312) at 0 kPa stress and then loaded to 3232 kPa stress and then unloaded to 54 kPa stress
5 – 10 – F	Test 5 – 10 – F (initial void ratio = 0.49 and moisture content = 9.90% (e_w = 0.260)) – firstly, soil specimen was wetted to 10.90% moisture content (e_w = 0.290) at 0 kPa stress and then loaded to 3238 kPa stress and then unloaded to 54 kPa stress
7 – 10 – D	Test 7 – 10 – D (initial void ratio = 0.71 and moisture content = 10.20% (e_w = 0.270)) – firstly, soil specimen was wetted to 10.60% moisture content (e_w = 0.280) at 0 kPa stress and then loaded to 3220 kPa stress and then unloaded to 54 kPa stress
7 – 10 – H	Test 7 – 10 – H (initial void ratio = 0.69 and moisture content = 10.20% (e_w = 0.270)) – firstly, soil specimen was wetted to 13.50% moisture content (e_w = 0.360) at 0 kPa stress and then loaded to 3220 kPa stress and then unloaded to 54 kPa stress
7 – 10 – K	Test 7 – 10 – K (initial void ratio = 0.72 and moisture content = 10.60% (e_w = 0.280)) – firstly, soil specimen was loaded to 3220 kPa stress at as-compacted water content and then unloaded to 54 kPa stress
Drying – Loading Tests	
5 – 10 – L	Test 5 – 10 – L (initial void ratio = 0.49 and moisture content = 10.10% (e_w = 0.267)) – firstly, soil specimen was dried to 2.20% moisture content (e_w = 0.058) at 0 kPa stress and then loaded to 13400 kPa stress and then unloaded to 224 kPa stress
7 – 10 – T	Test 7 – 10 – T (initial void ratio = 0.69 and moisture content = 10.0% (e_w = 0.264)) – firstly, soil specimen was dried to 9.20% moisture content (e_w = 0.243) at 0 kPa stress and then loaded to 3220 kPa stress and then unloaded to 54 kPa stress
7 – 10 – U	Test 7 – 10 – U (initial void ratio = 0.7 and moisture content = 10.10% (e_w = 0.267)) – firstly, soil specimen was dried to 3.90% moisture content (e_w =

	0.103) at 0 kPa stress and then loaded to 7526 kPa stress and then unloaded to 125 kPa stress
7 – 13 – D	Test 7 – 13 – D (initial void ratio = 0.71 and moisture content = 13.90% (e_w = 0.367)) – firstly, soil specimen was dried to 1.30% moisture content (e_w = 0.034) at 0 kPa stress and then loaded to 7500 kPa stress
7 – 13 – I	Test 7 – 13 – I (initial void ratio = 0.71 and moisture content = 13.50% (e_w = 0.356)) – firstly, soil specimen was loaded to 3235 kPa stress at as-compacted water content and then unloaded to 54 kPa stress
7 – 13 – J	Test 7 – 13 – J (initial void ratio = 0.7 and moisture content = 13.60% (e_w = 0.359)) – firstly, soil specimen was dried to 12.60% moisture content (e_w = 0.333) at 0 kPa stress and then loaded to 3214 kPa stress and then unloaded to 54 kPa stress
Loading – Wetting – Loading Tests	
5 – 10 – D	Test 5 – 10 – D (initial void ratio = 0.5 and moisture content = 10.0% (e_w = 0.260)) – firstly, soil specimen was loaded to 1184 kPa stress at as-compacted moisture content and then wetted to suction of 0 kPa at 1184 kPa stress
5 – 10 – G	Test 5 – 10 – G (initial void ratio = 0.5 and moisture content = 10.0% (e_w = 0.264)) – firstly, soil specimen was loaded to 1619 kPa stress at as-compacted moisture content and then wetted to suction of 0 kPa at 1619 kPa stress
7 – 10 – I	Test 7 – 10 – I (initial void ratio = 0.71 and moisture content = 10.30% (e_w = 0.270)) – firstly, soil specimen was loaded to 430 kPa stress at as-compacted moisture content and then wetted to suction of 130 kPa at 430 kPa stress and then loaded to 3220 kPa stress
7 – 10 – L	Test 7 – 10 – L (initial void ratio = 0.73 and moisture content = 10.10% (e_w = 0.270)) – firstly, soil specimen was loaded to 215 kPa stress at as-compacted moisture content and then wetted to suction of 140 kPa at 215 kPa stress and then loaded to 3220 kPa stress
7 – 10 – N	Test 7 – 10 – N (initial void ratio = 0.71 and moisture content = 10.0% (e_w = 0.264)) – firstly, soil specimen was loaded to 108 kPa stress at as-compacted moisture content and then wetted to suction of 10 kPa at 108 kPa stress
7 – 13 – M	Test 7 – 13 – M (initial void ratio = 0.71 and moisture content = 13.50% (e_w = 0.356)) – firstly, soil specimen was loaded to 303 kPa stress at as-compacted moisture content and then wetted to suction of 0 kPa at 303 kPa stress

Table 4-4: Yield stress of compacted unloaded soil specimens during loading at as-compacted moisture content or after wetting or after drying from Jotisankasa (2005) and Jotisankasa et al. (2007a)

Specimen No.	Initial Moisture Content	Initial Compaction Stress	Final Moisture Content	Comment on Final Moisture Content	Yield Stress	Final Comment
5 – 10 – B	9.8 %	≈ 2400 kPa	13.5 %	Wetting	1156 kPa	All experimental results agree with the MPK framework
5 – 10 – E	10.0 %	≈ 2400 kPa	11.8 %	Wetting	1152 kPa	
5 – 10 – F	9.9 %	≈ 2400 kPa	10.9 %	Wetting	2004 kPa	
5 – 10 – H	10.1 %	≈ 2400 kPa	9.7 %	Drying	2600 kPa	
5 – 10 – I	10.1 %	≈ 2400 kPa	1.2 %	Drying	5603 kPa	
5 – 10 – K	10.1 %	≈ 2400 kPa	4.0 %	Drying	4702 kPa	
5 – 10 – L	10.1 %	≈ 2400 kPa	2.2 %	Drying	5389 kPa	
7 – 10 – D	10.2 %	≈ 750 kPa	10.6 %	Wetting	629 kPa	
7 – 10 – G	10.1 %	≈ 750 kPa	14.8 %	Wetting	245 kPa	
7 – 10 – H	10.2 %	≈ 750 kPa	13.5 %	Wetting	374 kPa	
7 – 10 – K	10.6 %	≈ 750 kPa	10.6 %	As it is	730 kPa	
7 – 10 – P	10.1 %	≈ 750 kPa	0.81 %	Drying	3773 kPa	
7 – 10 – T	10.0 %	≈ 750 kPa	9.2 %	Drying	1060 kPa	
7 – 10 – U	10.1 %	≈ 750 kPa	3.9 %	Drying	1862 kPa	
7 – 10 – V	10.2 %	≈ 750 kPa	4.3 %	Drying	2435 kPa	
7 – 10 –W	10.1 %	≈ 750 kPa	2.0 %	Drying	2206 kPa	
7 – 13 – D	13.9 %	≈ 400 kPa	1.3 %	Drying	3592 kPa	
7 – 13 – G	13.7 %	≈ 400 kPa	2.89 %	Drying	2578 kPa	
7 – 13 – I	13.5 %	≈ 400 kPa	13.5 %	As it is	432 kPa	
7 – 13 – J	13.6 %	≈ 400 kPa	12.6 %	Drying	672 kPa	
7 – 13 – K	13.7 %	≈ 400 kPa	9.9 %	Drying	1310 kPa	
7 – 13 – L	13.6 %	≈ 400 kPa	15.1 %	Wetting	303 kPa	

Table 4-5: Properties of the soil 'BK'

Parameter	Value
Specific Gravity (G_s)	2.65
Liquid Limit	93%
Plasticity Index	60%
Optimum Moisture Content	29%
Optimum Dry Density	14.13 kN/m^3

Table 4-6: A summary of state path tests (first wetting) examined from Sharma (1998)

Test No.	Materials	Initial Static Stress	Unloaded Stress
Test 1	BK	400 kPa	10 kPa
Test 2	BK	400 kPa	50 kPa
Test 3	BK	800 kPa	50 kPa
Test 4	BK	800 kPa	10 kPa
Test 5	BK	800 kPa	20 kPa
Test 8	BK	400 kPa	10 kPa
Test 16	BK	400 kPa	10 kPa
Test 19	BK	3200 kPa	10 kPa
Test 20	BK	3200 kPa	10 kPa

Table 4-7: Properties of Boom Clay

Parameter	Value
Specific Gravity (G_s)	2.7
Liquid Limit	55.7±0.9%
Plasticity Index	26.9±1.0%
Soil Class (USCS, ASTM D2487)	CH
De-structured dry unit weight	10.8 kN/m^3
De-structured void ratio	1.46
Compressibility parameter for saturated conditions [$\lambda(0)$]	0.150 (γd = 13.7 kN/m3) 0.136 (γd = 16.7 kN/m3)
Compressibility parameter for unload/reload conditions [κ]	0.01

Table 4-8: A summary of state path tests (first wetting) examined from Romero (1999)

Tests	Materials	Initial Dry Density	Unloaded Stress
US 0.026 MPa	Boom Clay	16.7 kN/m^3	0.026 MPa
US 0.085 MPa	Boom Clay	16.7 kN/m^3	0.085 MPa
US 0.3 MPa	Boom Clay	16.7 kN/m^3	0.3 MPa
US 0.55 MPa	Boom Clay	16.7 kN/m^3	0.55 MPa
US 0.6 MPa	Boom Clay	13.7 kN/m^3	0.6 MPa
US 1.2 MPa	Boom Clay	13.7 kN/m^3	1.2 MPa
US I0.085 MPa	Boom Clay	16.7 kN/m^3	0.085 MPa
US I0.6 MPa	Boom Clay	13.7 kN/m^3	0.6 MPa

US => Unloading Stress, US I => Unloading Stress Isotropic.
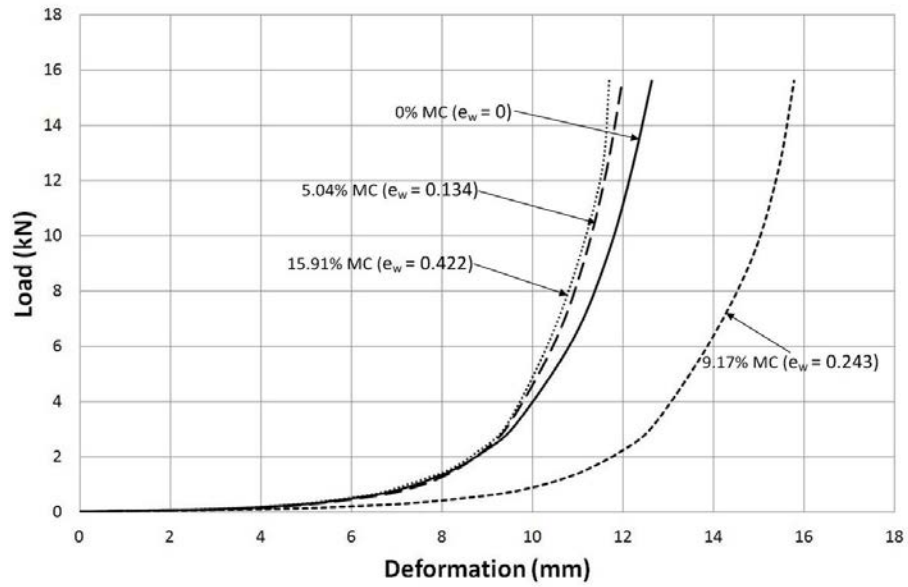
Figure 4-1: Typical Load vs Deformation curves for the kaolin soil with different moisture contents
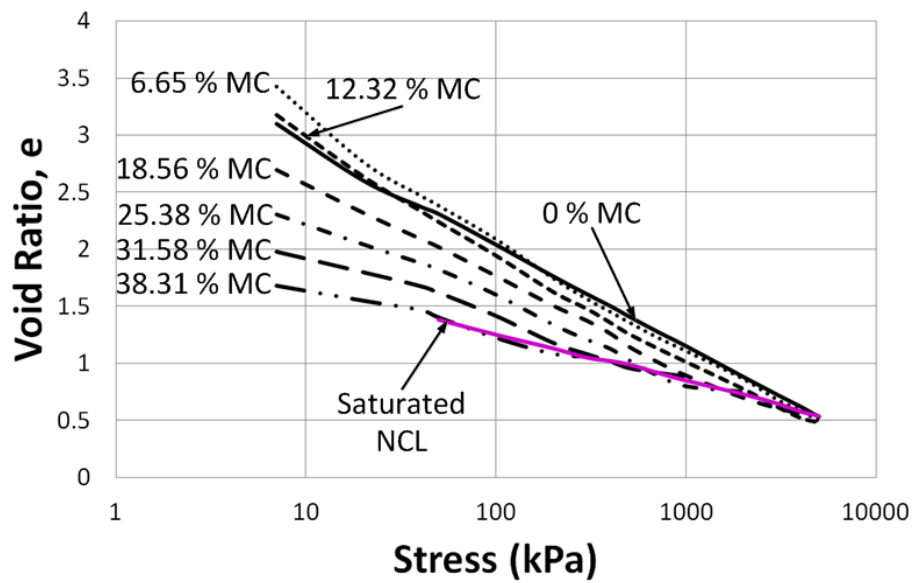
Figure 4-2: Void Ratio vs Stress compression for the kaolin soil with different moisture contents
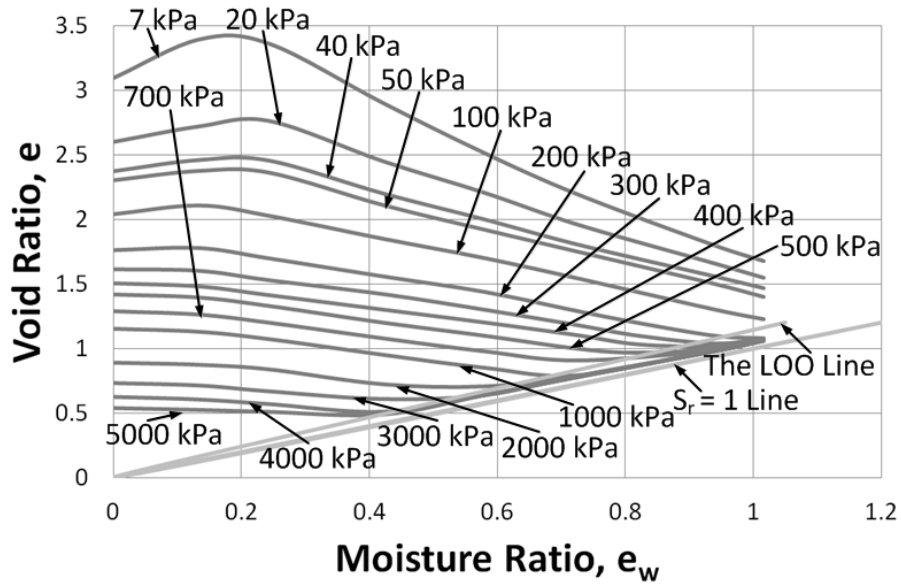
(a) In $e - e_w$ plane
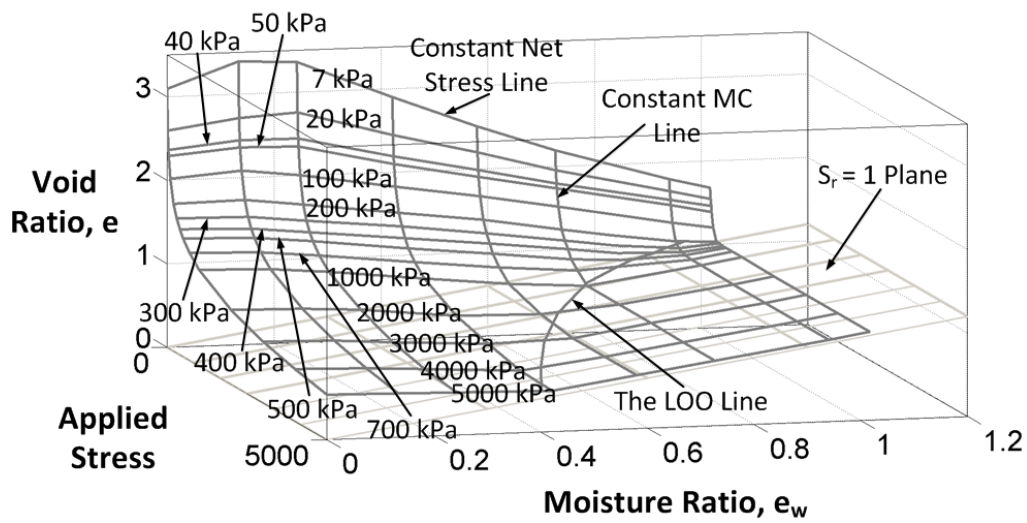
(b) In $e - e_w - p$ space

Figure 4-3: Undrained LWSBS for the kaolin soil
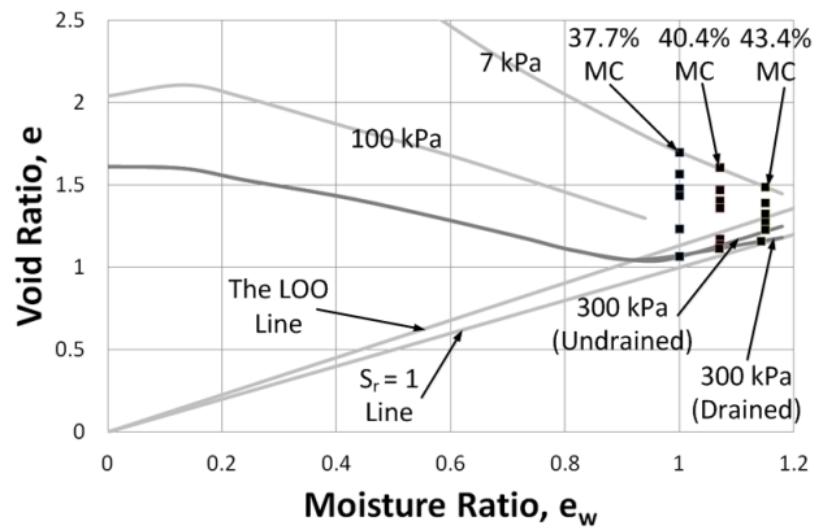
(a) 300 kPa drained constant net stress contour
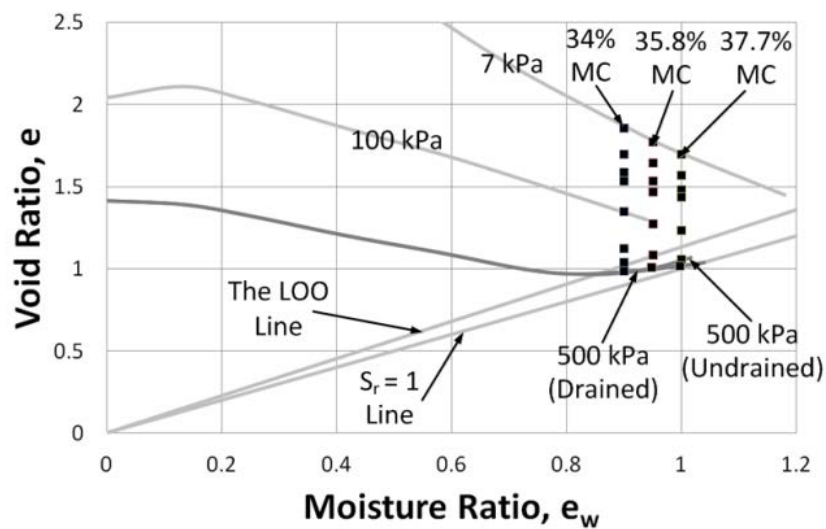
(b) 500 kPa drained constant net stress contour
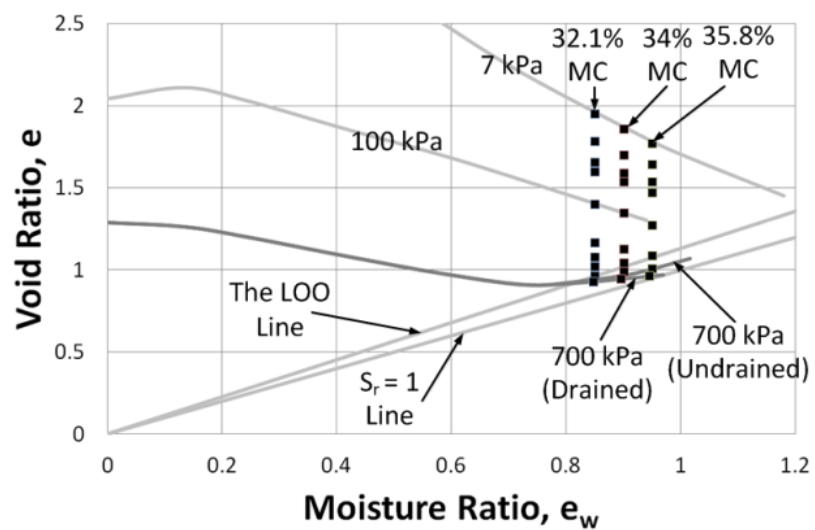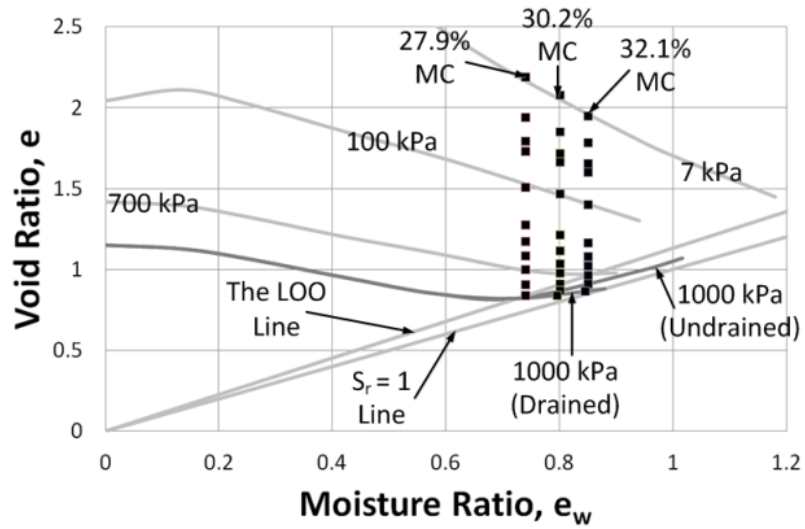
(c) 700 kPa drained constant net stress contour

(d) 1000 kPa drained constant net stress contour
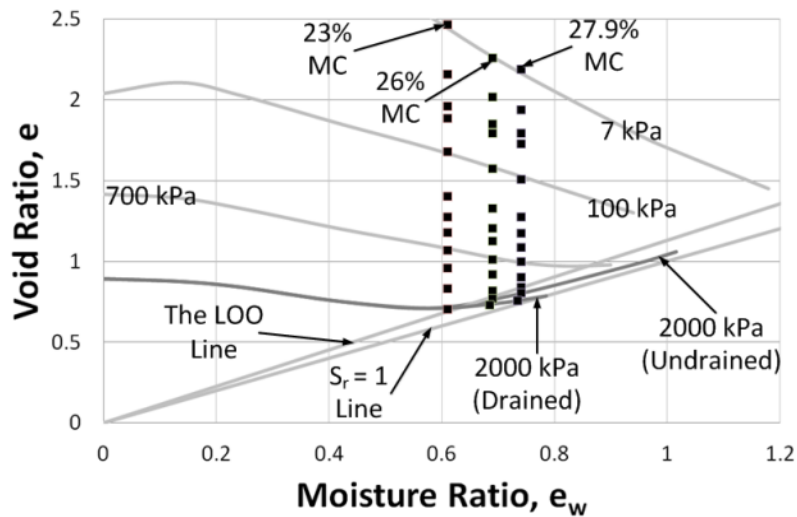
(e) 2000 kPa drained constant net stress contour
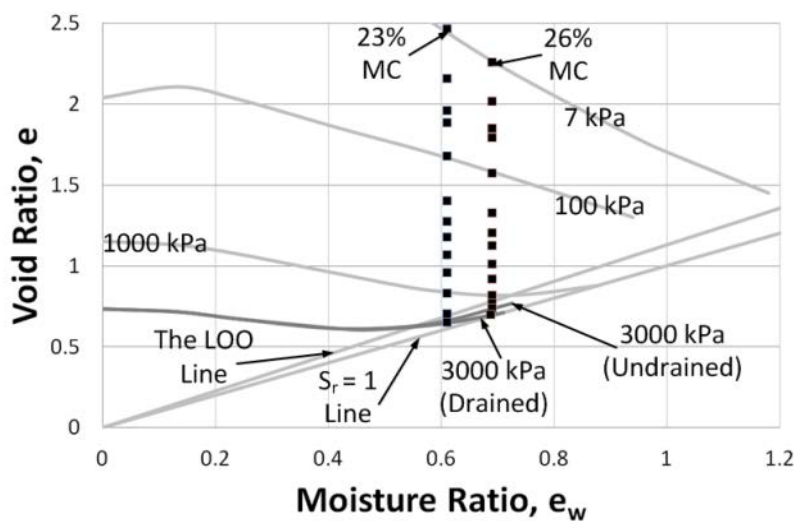
(f) 3000 kPa drained constant net stress contour
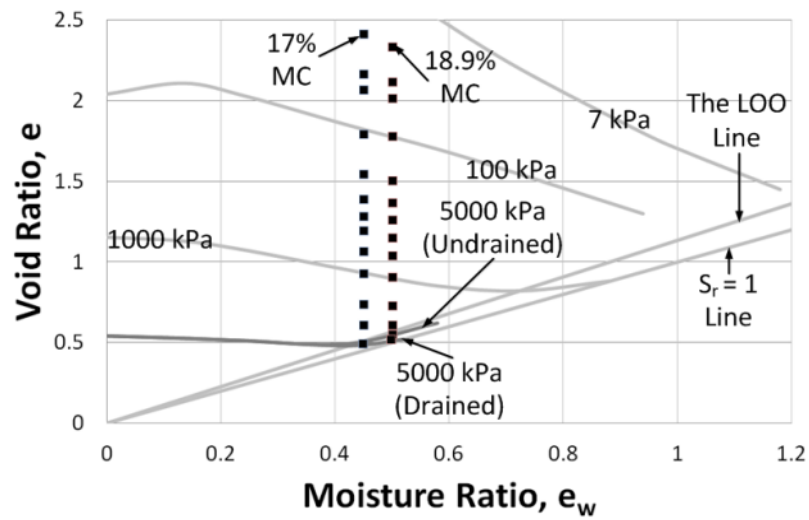
(g) 5000 kPa drained constant net stress contour

Figure 4-4: Development of different drained constant net stress contours for the kaolin soil
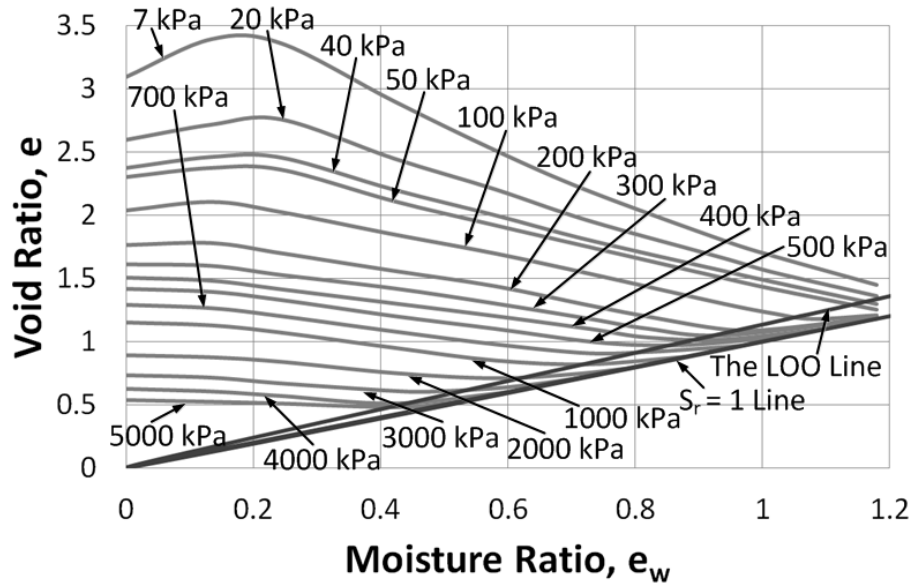
(a) In $e - e_w$ plane
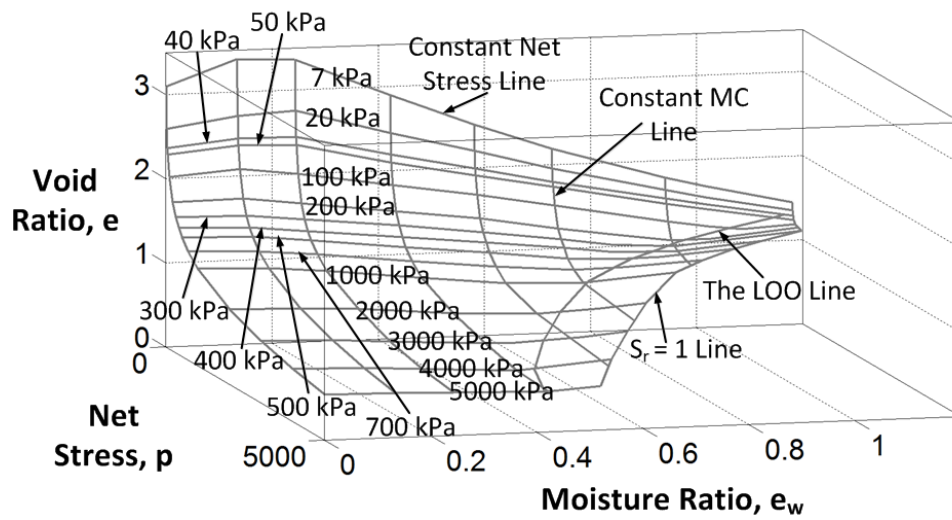
(b) In $e - e_w - p$ space

Figure 4-5: Drained LWSBS for the kaolin soil
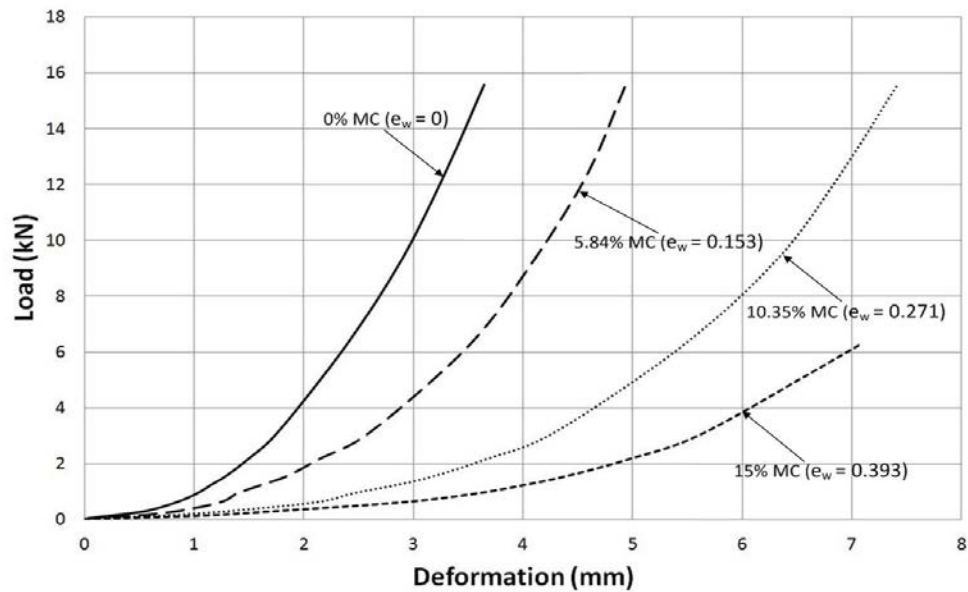
Figure 4-6: Typical Load vs Deformation curves for the Merri Creek soil with different moisture contents
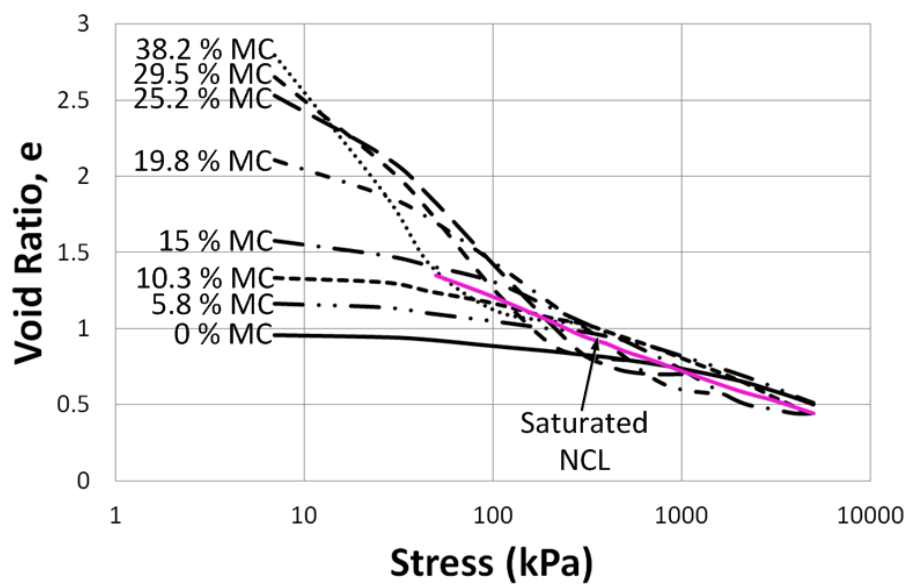
Figure 4-7: Void Ratio vs Stress compression for the Merri Creek soil with different moisture contents
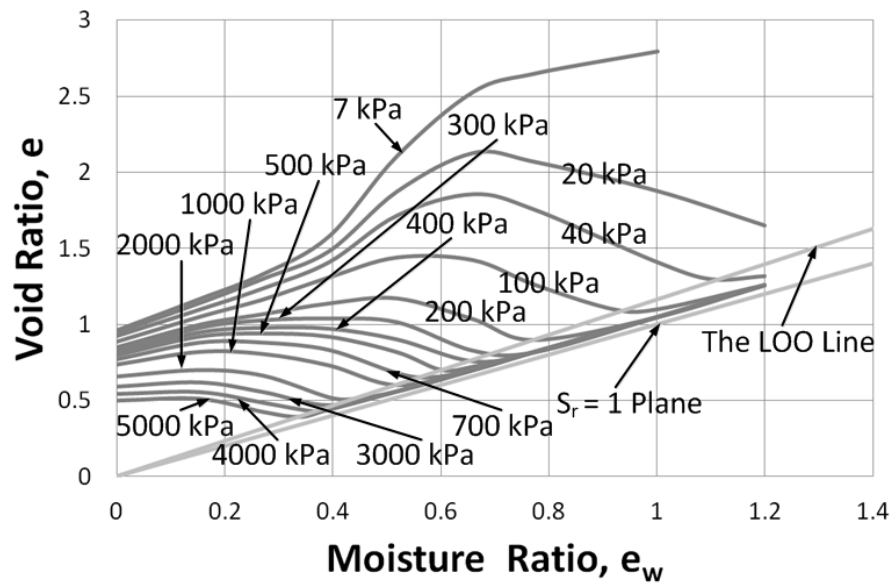
Figure 4-8: Undrained LWSBS for the Merri Creek soil in the form of compaction contours
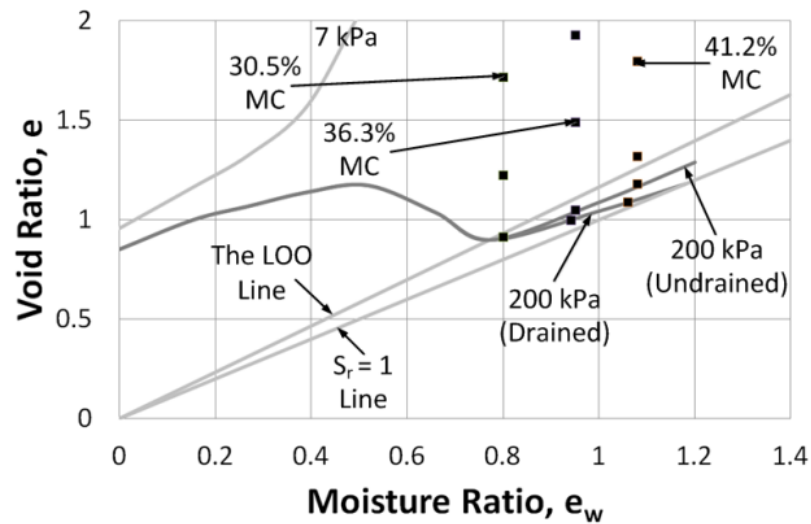
(a) 200 kPa drained constant net stress contour
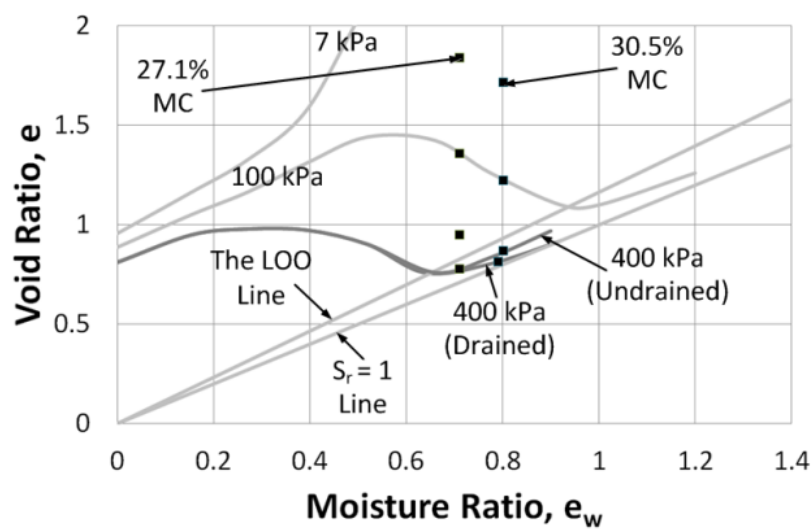
(b) 400 kPa drained constant net stress contour
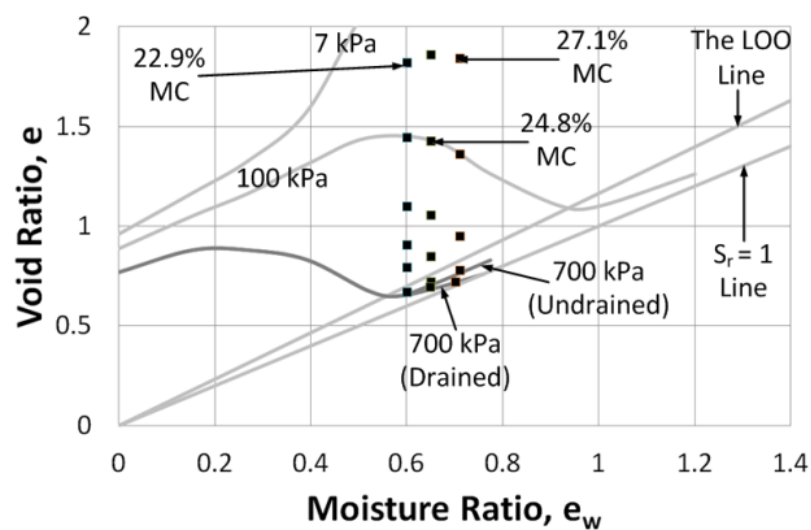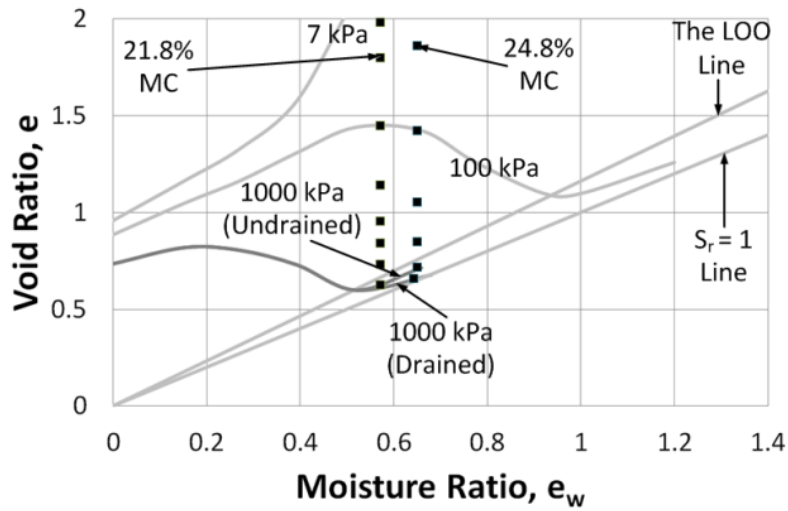
(c) 700 kPa drained constant net stress contour

(d) 1000 kPa drained constant net stress contour
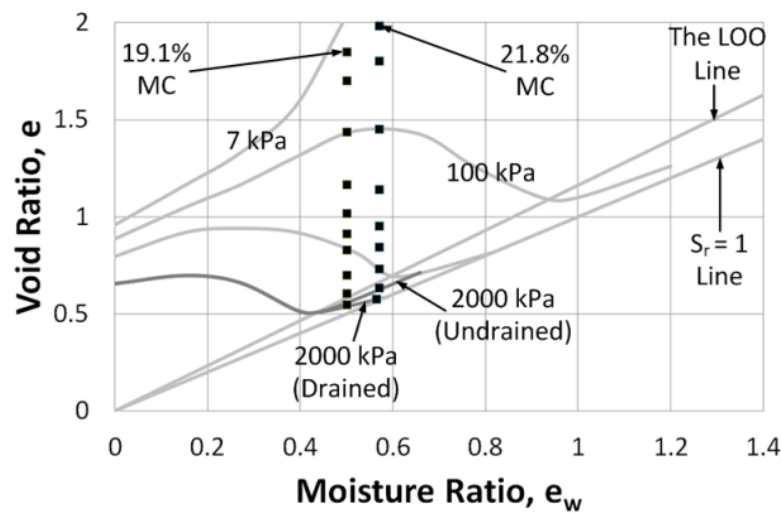
(e) 2000 kPa drained constant net stress contour
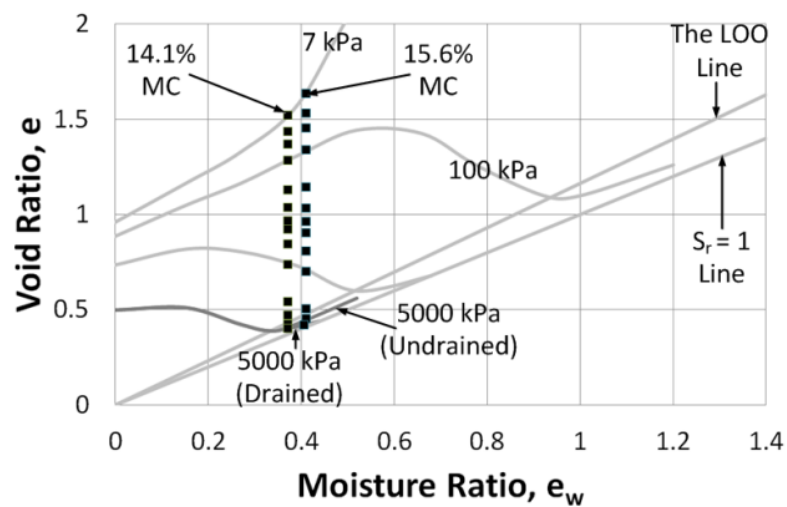
(f) 5000 kPa drained constant net stress contour

Figure 4-9: Development of different drained constant net stress contours for the Merri Creek soil
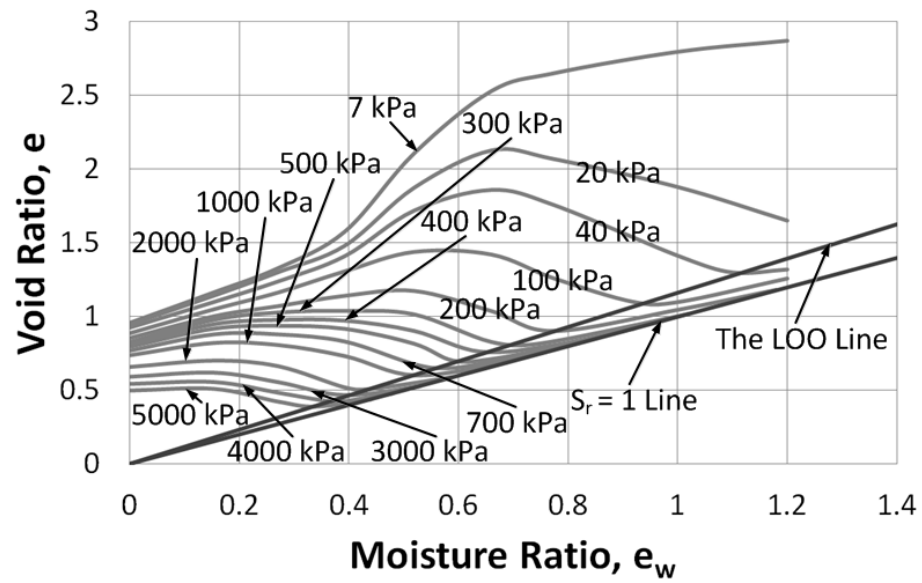
(a) In $e - e_w$ plane
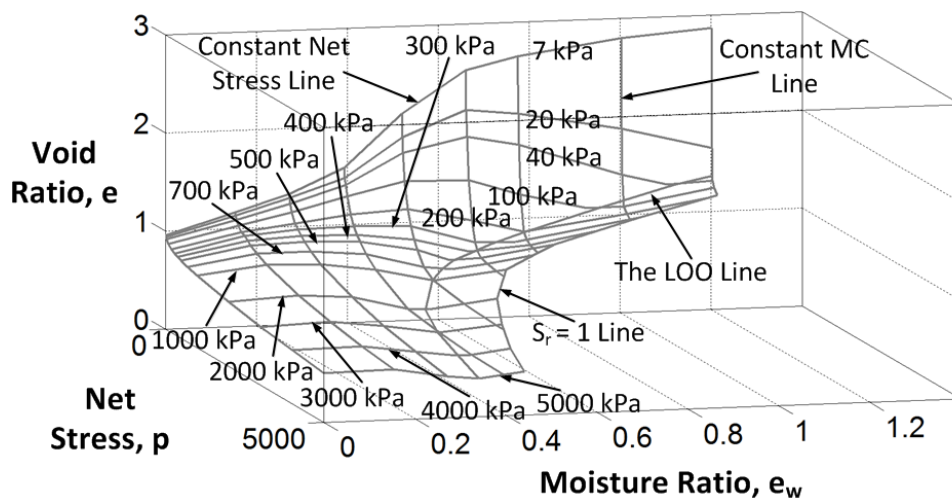
(b) In $e - e_w - p$ space

Figure 4-10: Drained LWSBS for the Merri Creek soil
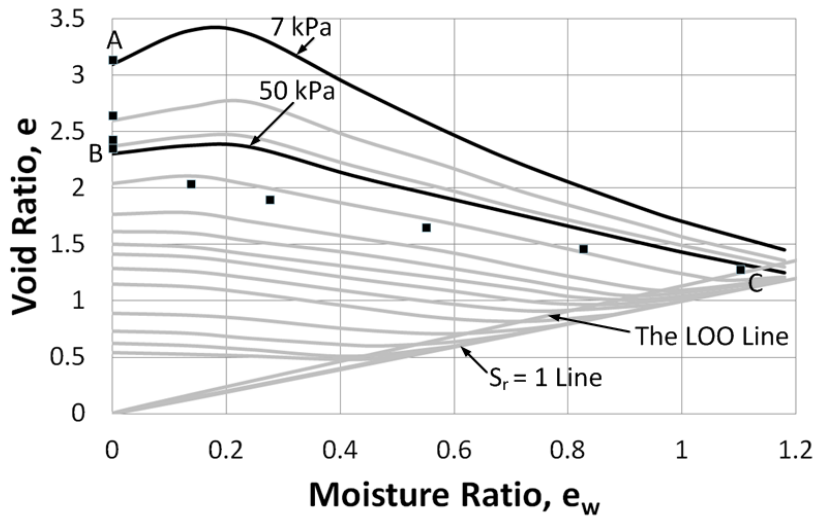
(a) Loading at 0% moisture content ($e_w = 0$) to 50 kPa stress and then wetted to 41.62% moisture content ($e_w = 1.103$) [Test Identity => SC – EK – LW – 1]
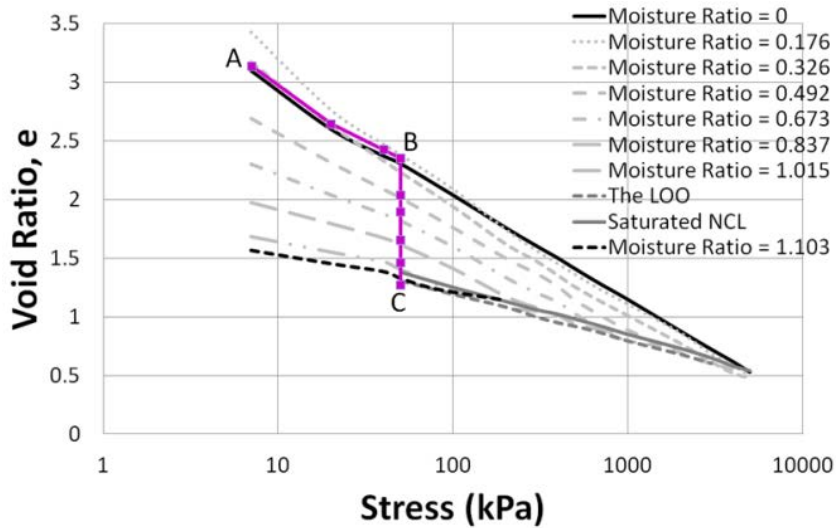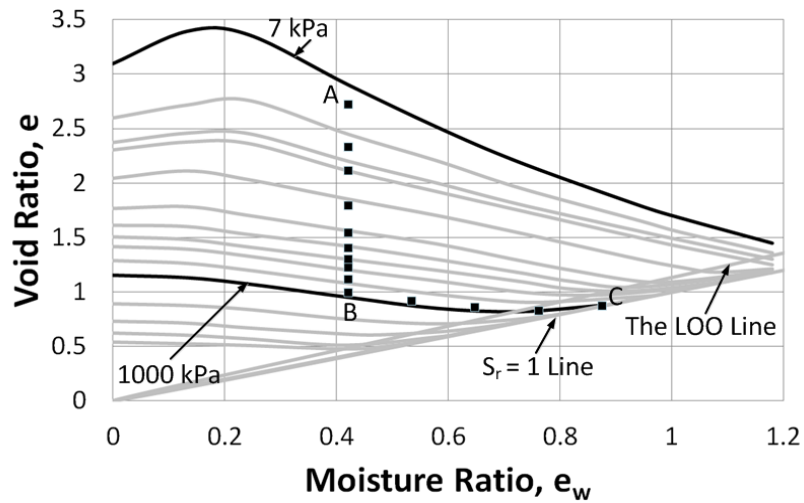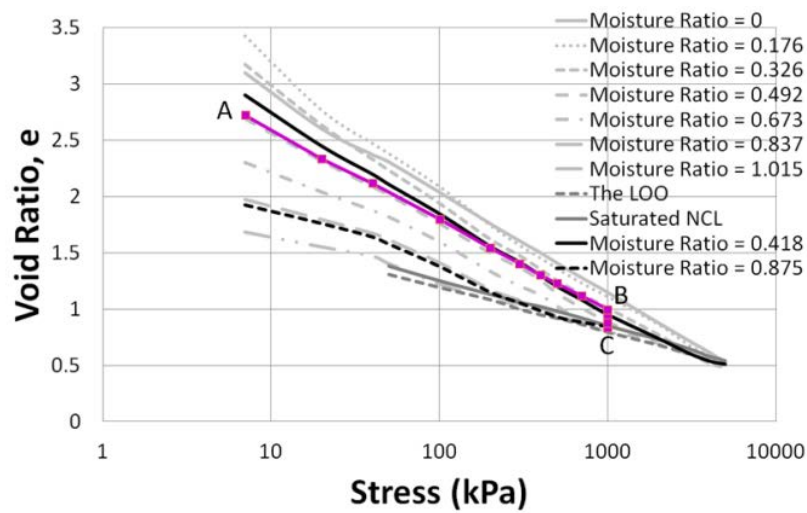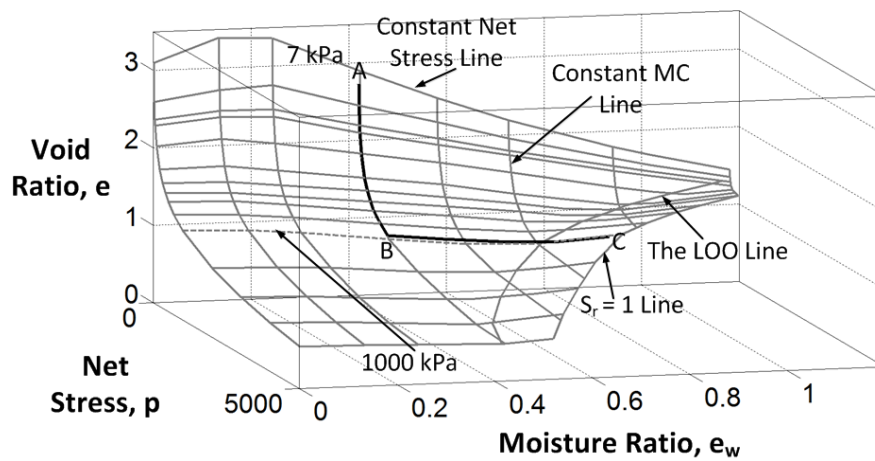

(b) $e - \log p$ relationship of state path test (a)
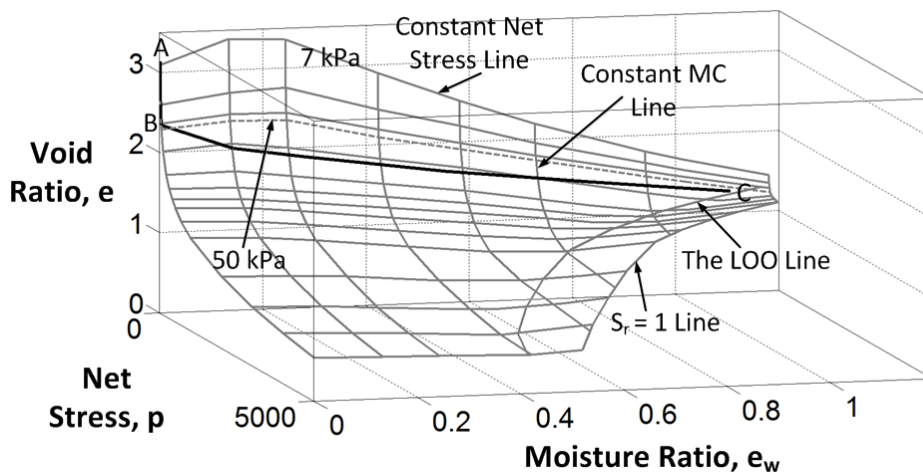
(c) 3-D view of state path test (a)
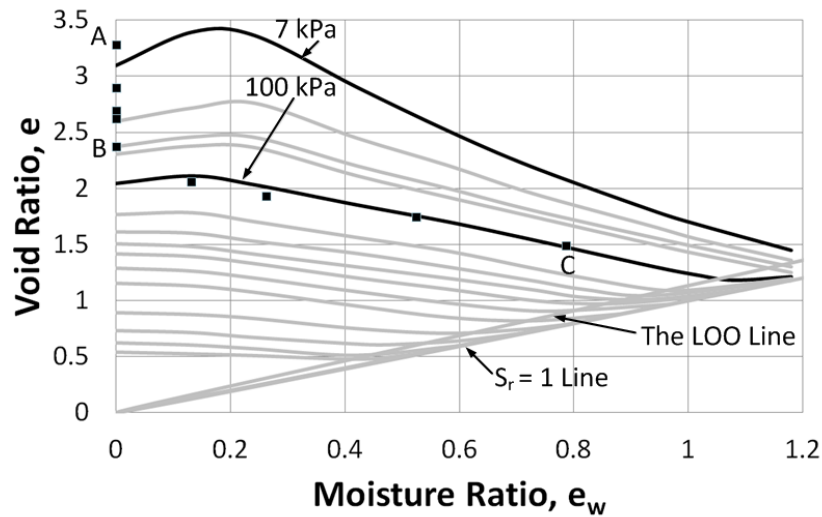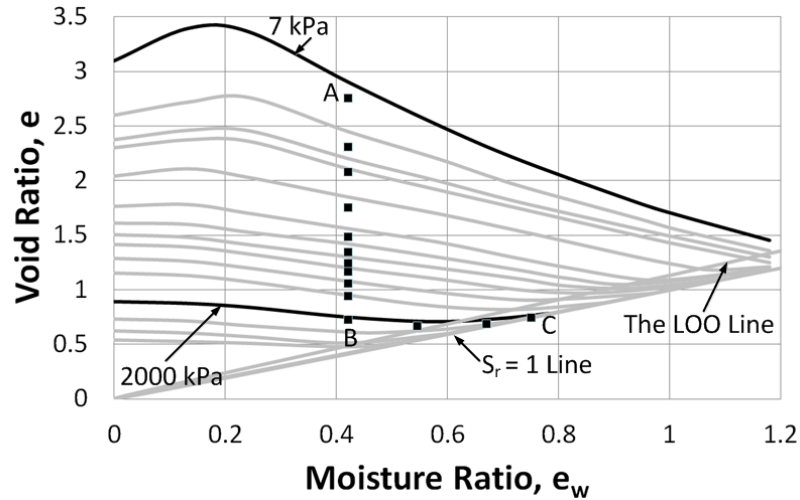
(d) Loading at 0% moisture content ($e_w = 0$) to 100 kPa stress and then wetted to 29.66% moisture content ($e_w = 0.786$) [Test Identity => SC – EK – LW – 2]
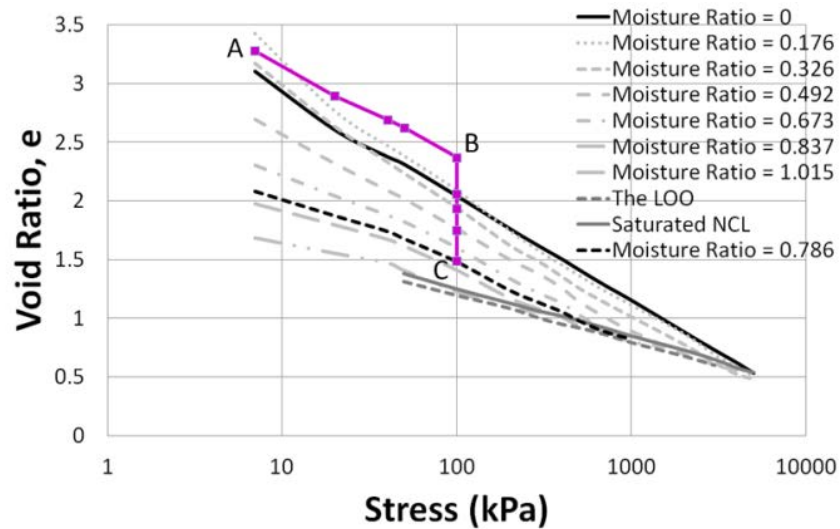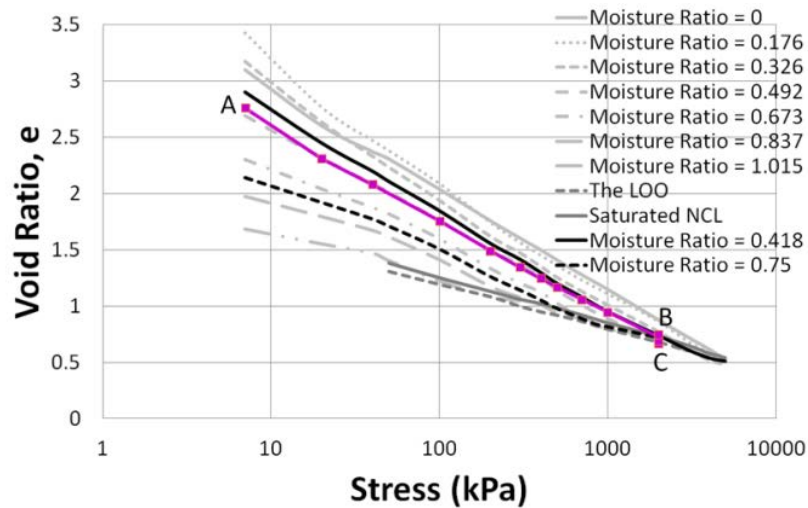

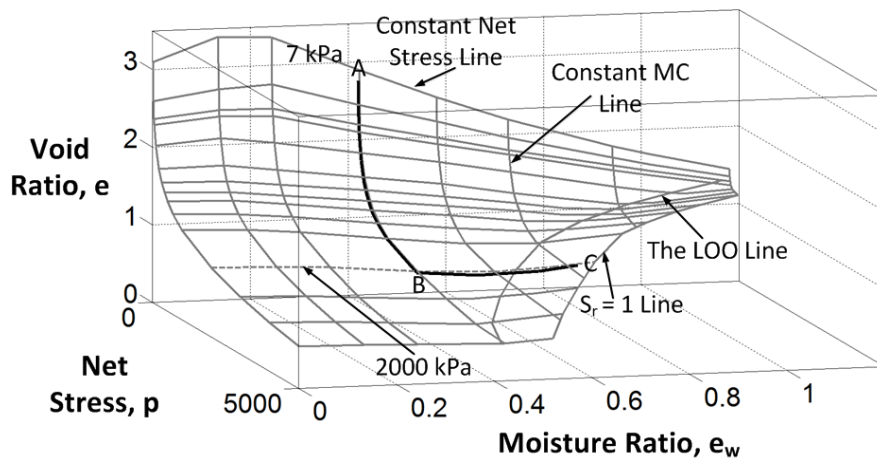**(e)** $e - \log p$ relationship of state path test (d)
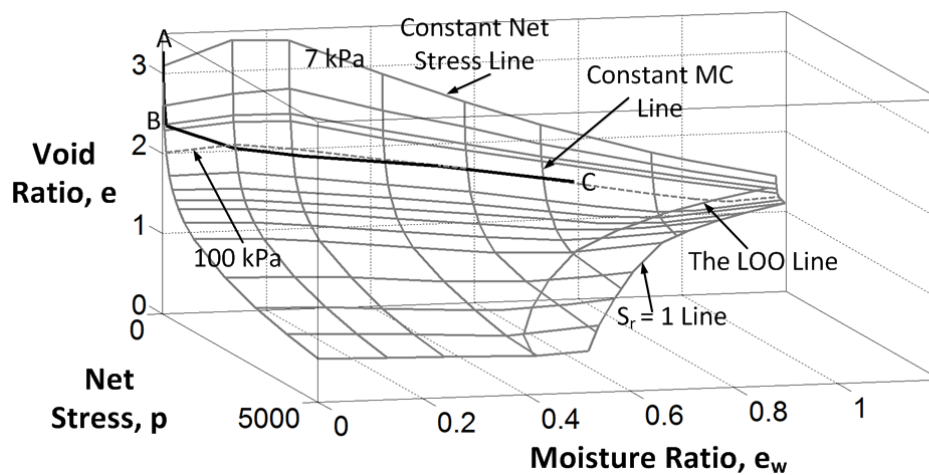
(f) 3-D view of state path test (d)
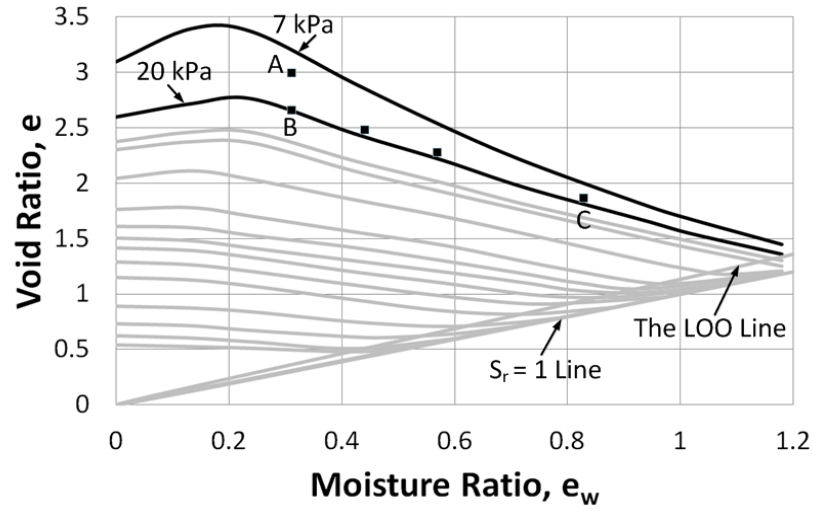
(g) Loading at 11.69% moisture content ($e_w = 0.310$) to 20 kPa stress and then wetted to 31.25% moisture content ($e_w = 0.828$) [Test Identity => SC – EK – LW – 3]
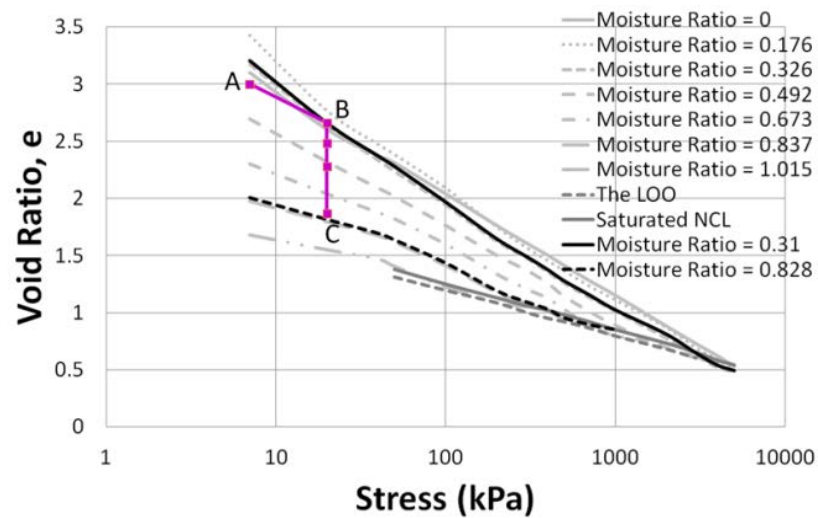
(h) $e - \log p$ relationship of state path test (g)
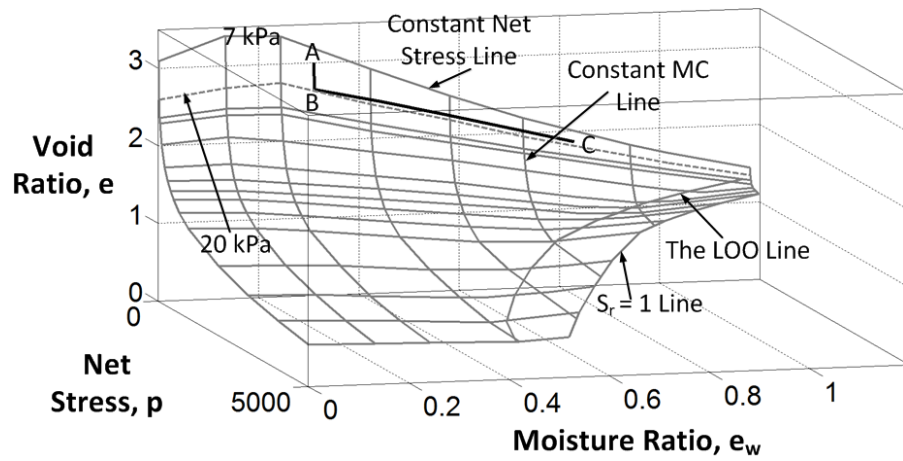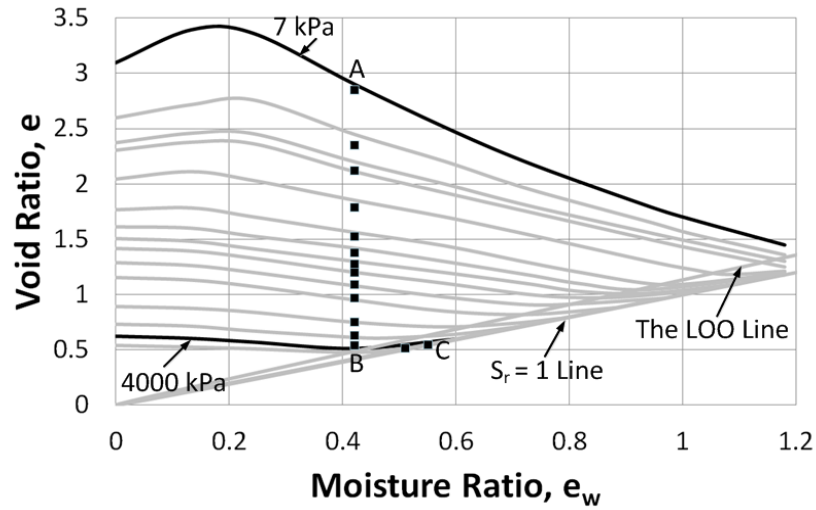
(i) 3-D view of state path test (g)

Figure 4-11: Loading/wetting state path tests for the kaolin soil
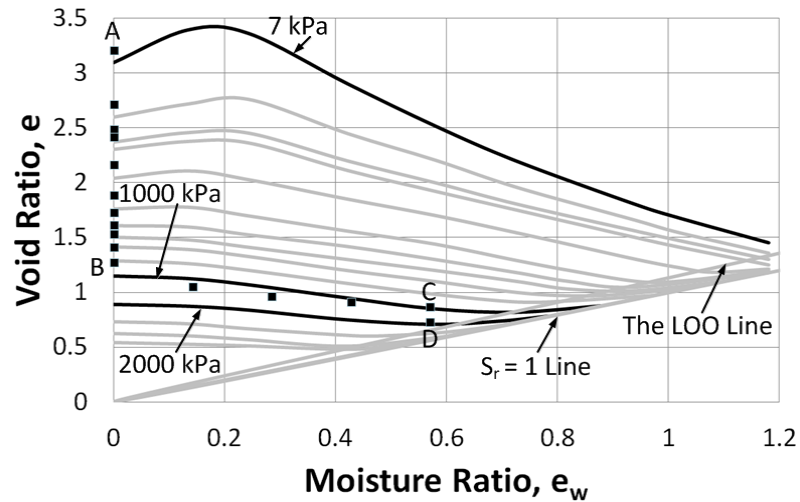
(a) Loading at 0% moisture content ($e_w = 0$) to 1000 kPa stress and then wetted to 21.52% moisture content ($e_w = 0.570$) and then loaded to 2000 kPa stress [Test Identity => SC – EK – LWL – 1]
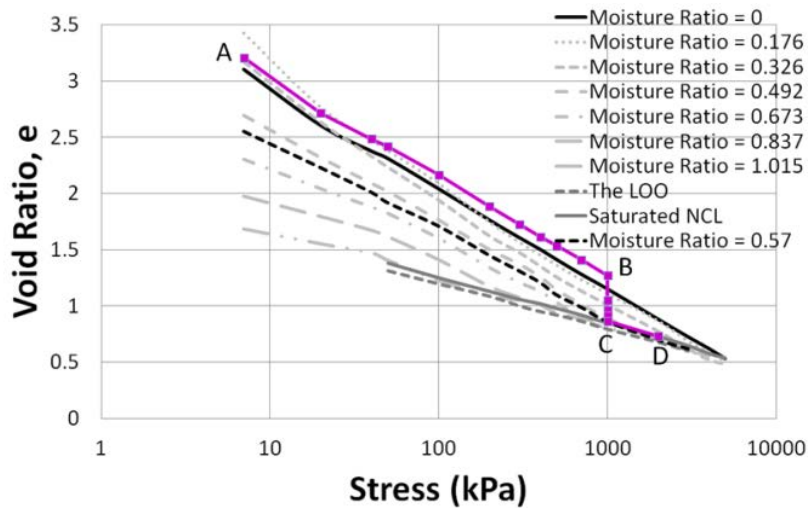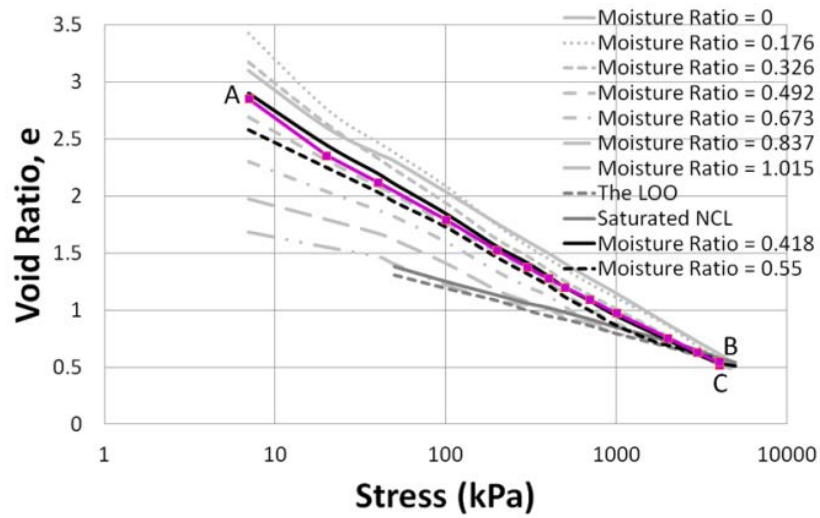

**(b)** $e – \log p$ relationship of state path test (a)
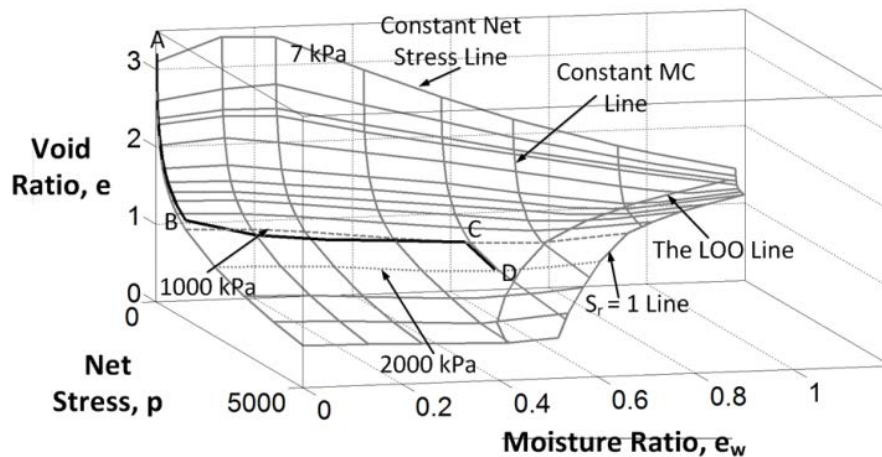
(c) 3-D view of state path test (a)
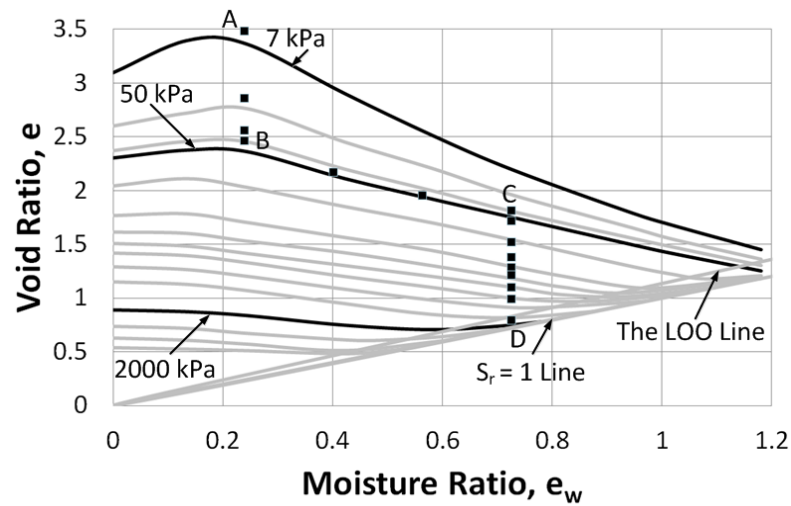
(**d**) Loading at 8.96% moisture content ($e_w = 0.237$) to 50 kPa stress and then wetted to 27.35% moisture content ($e_w = 0.725$) and then loaded to 2000 kPa stress [Test Identity => SC – EK – LWL – 2]
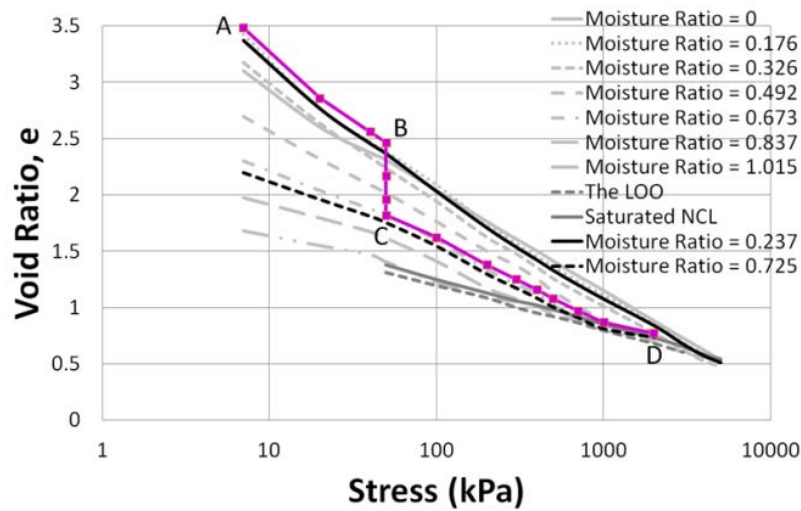
(**e**) $e - \log p$ relationship of state path test (d)
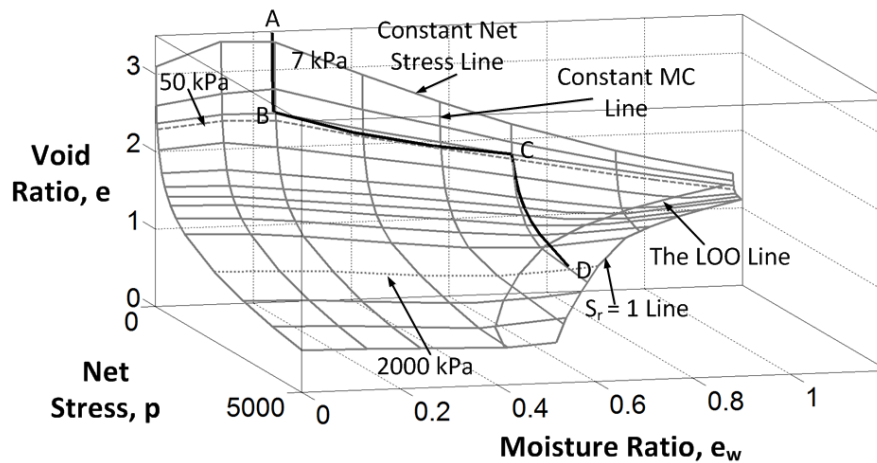
(**f**) 3-D view of state path test (d)
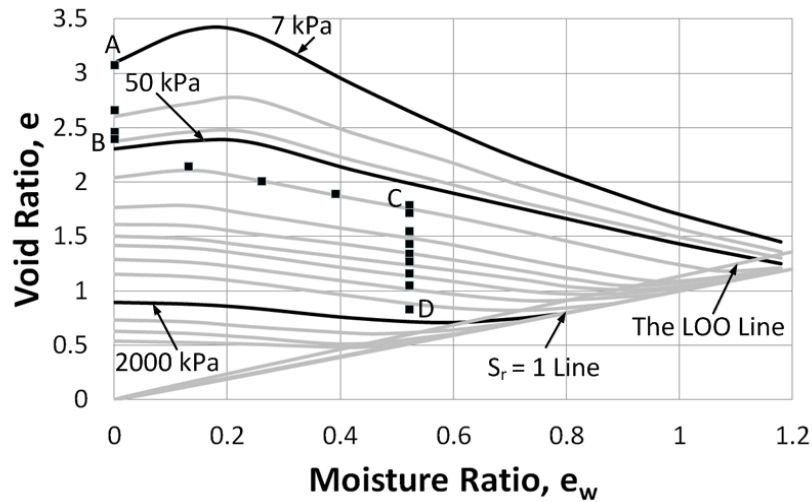
(g) Loading at 0% moisture content ($e_w = 0$) to 50 kPa stress and then wetted to 19.69% moisture content ($e_w = 0.522$) and then loaded to 2000 kPa stress [Test Identity => SC – EK – LWL – 3]
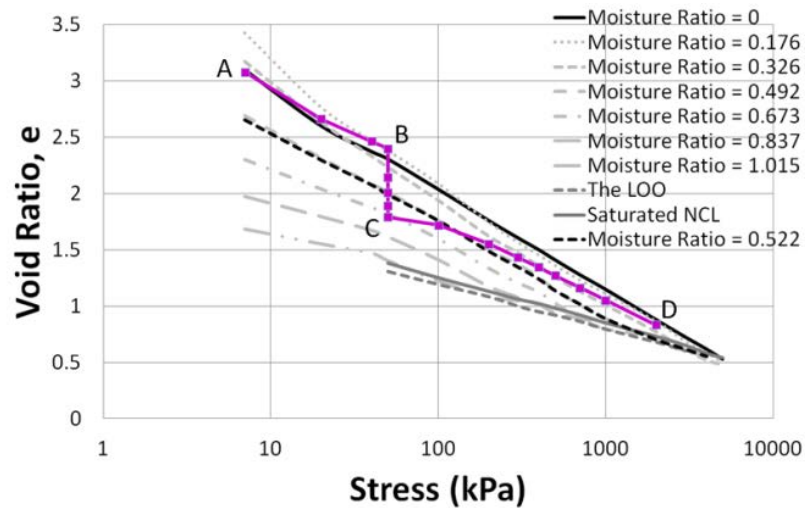
(h) e – log p relationship of state path test (g)
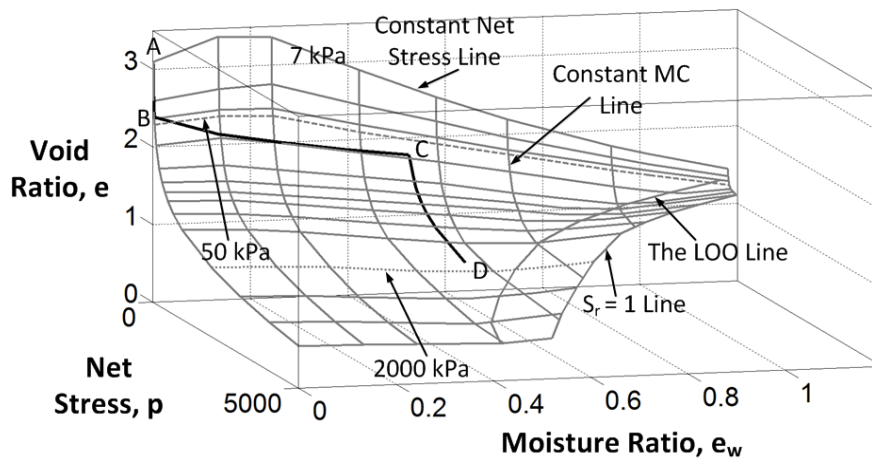
(i) 3-D view of state path test (g)
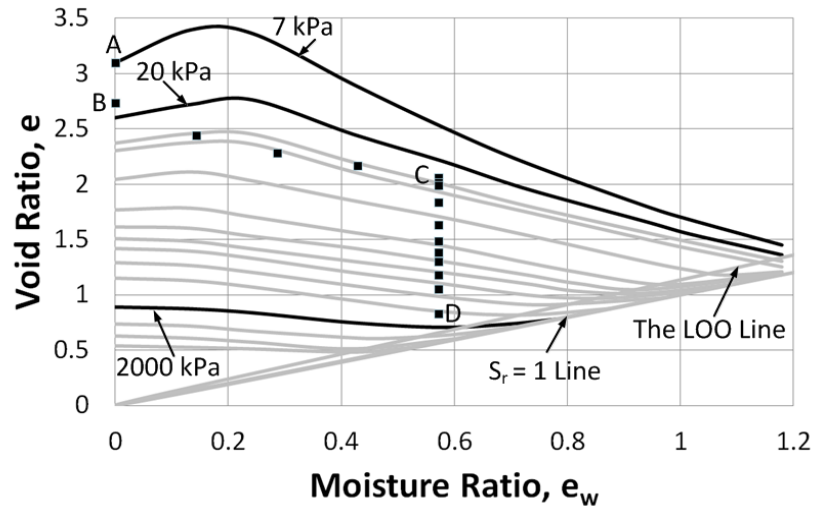
(j) Loading at 0% moisture content ($e_w = 0$) to 20 kPa stress and then wetted to 21.60% moisture content ($e_w = 0.572$) and then loaded to 2000 kPa stress [Test Identity => SC – EK – LWL – 4]
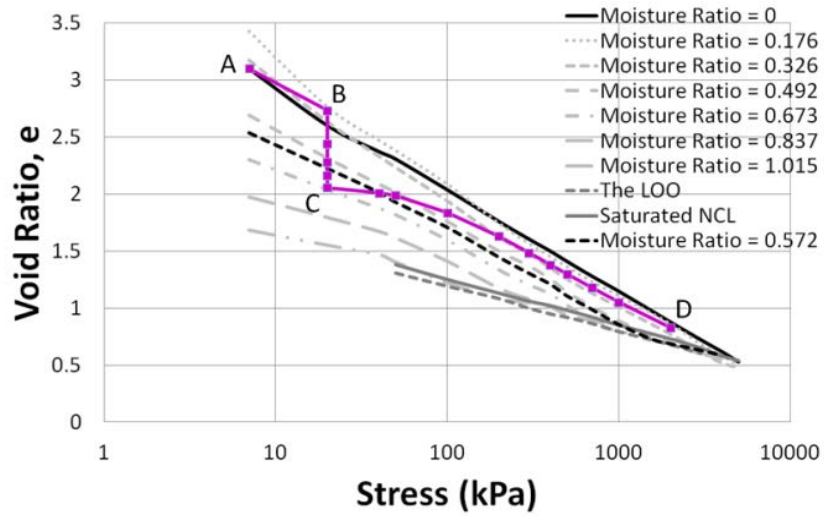
(k) $e – \log p$ relationship of state path test (j)
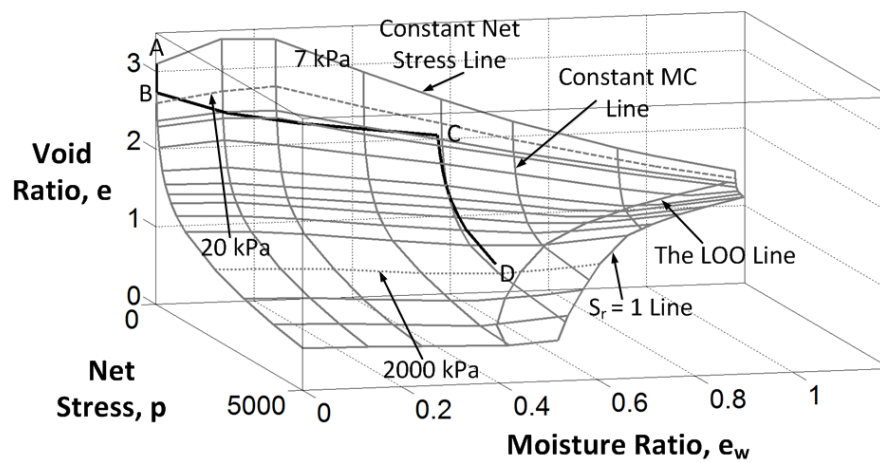
(l) 3-D view of state path test (j)

Figure 4-12: Loading/wetting/loading state path tests for the kaolin soil
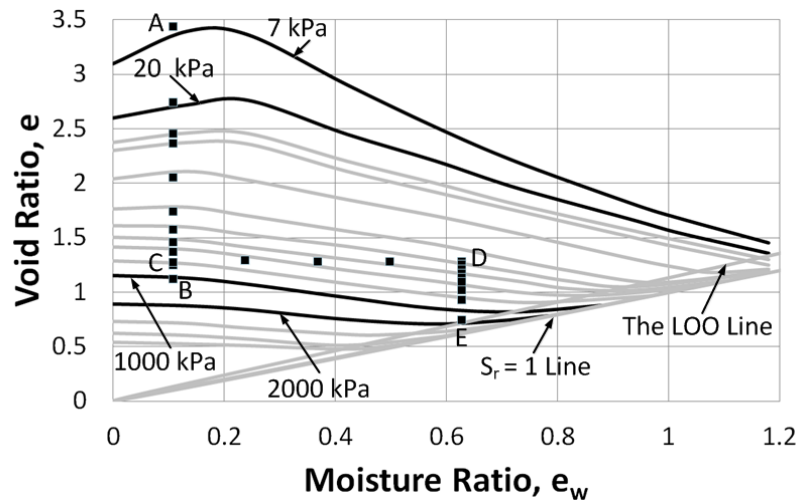
(a) Loading at 4.04% moisture content ($e_w = 0.107$) to 1000 kPa stress and then unloaded to 20 kPa stress and then wetted to 23.67% moisture content ($e_w = 0.627$) and then loaded to 2000 kPa stress [Test Identity => SC – EK – LUWL – 1]
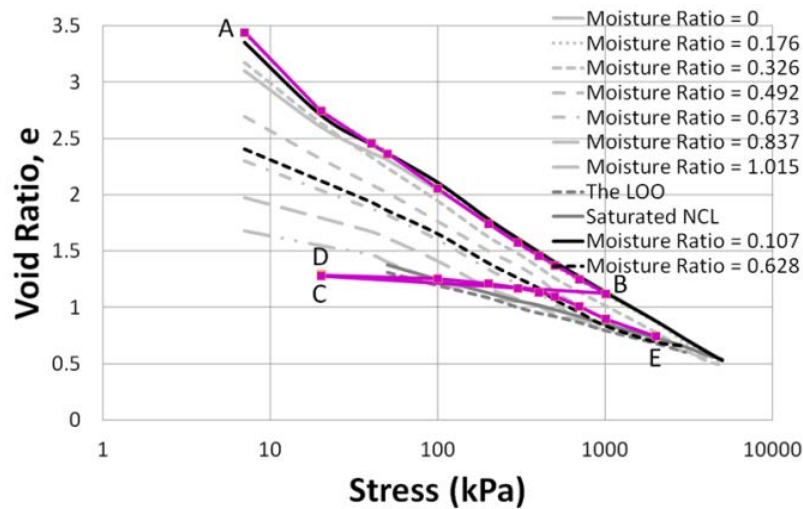
(b) $e – \log p$ relationship of state path test (a)
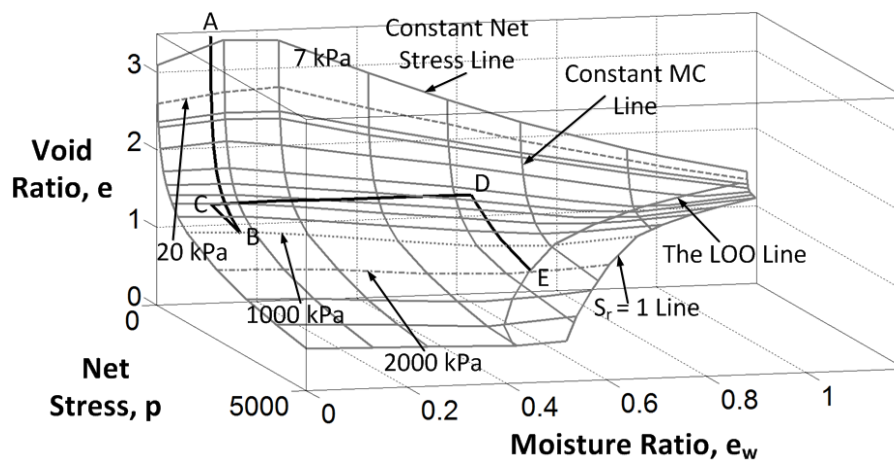
(c) 3-D view of state path test (a)
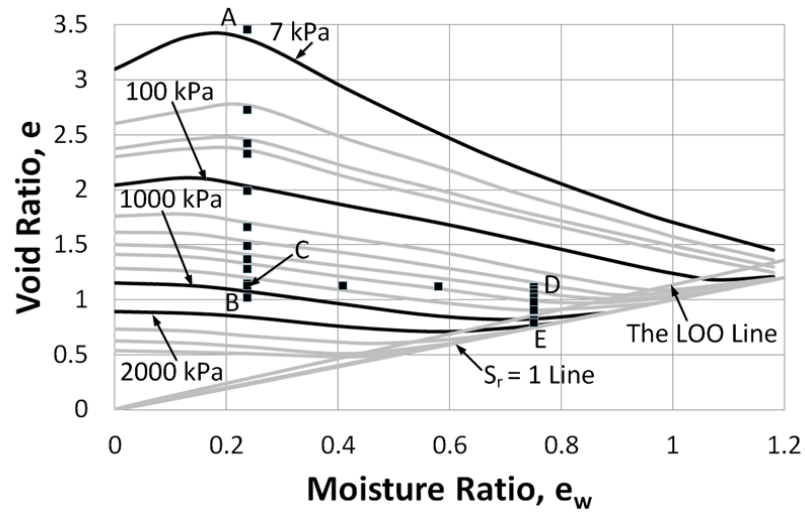
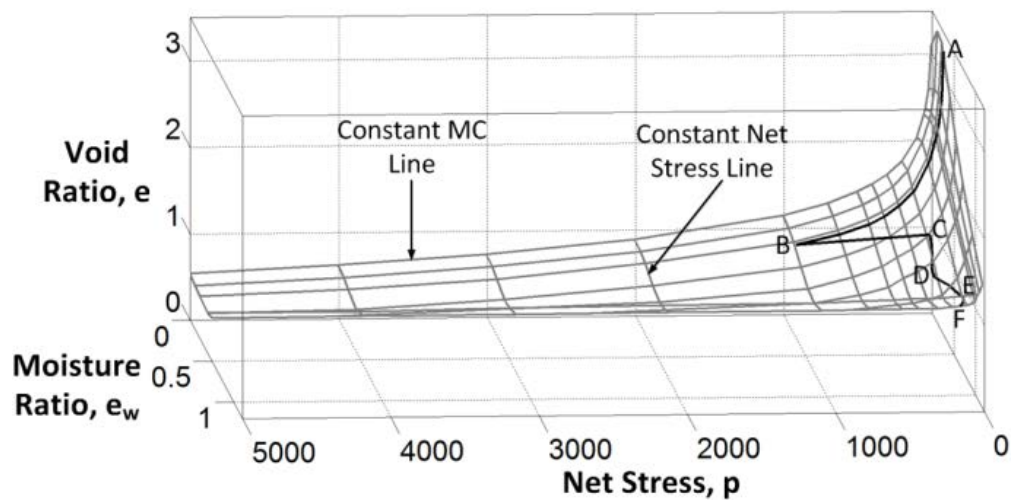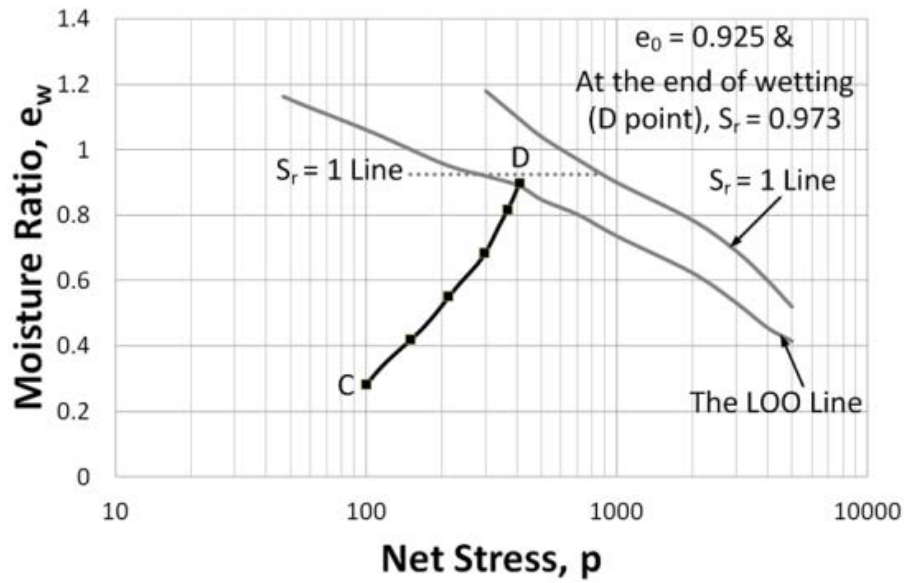**(d)** Loading at 8.96% moisture content ($e_w = 0.237$) to 1000 kPa stress and then unloaded to 100 kPa stress and then wetted to 28.30% moisture content ($e_w = 0.750$) and then loaded to 2000 kPa stress [Test Identity => SC – EK – LUWL – 2]
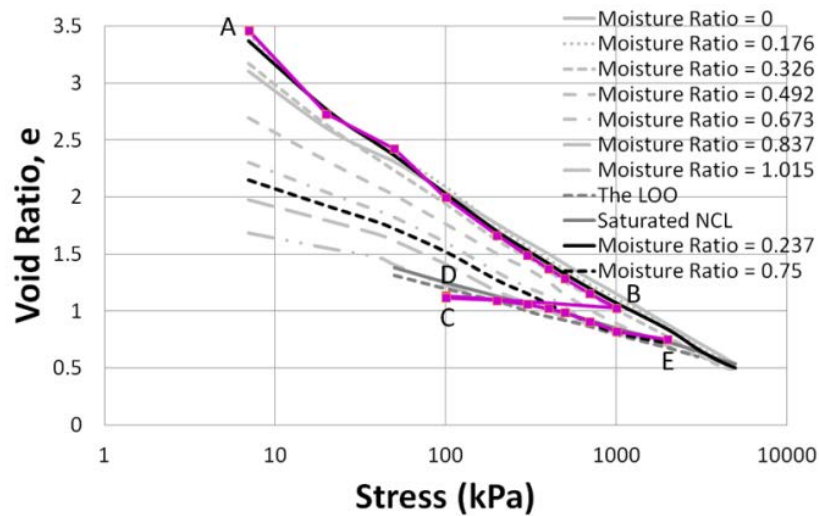
(e) $e - \log p$ relationship of state path test (d)
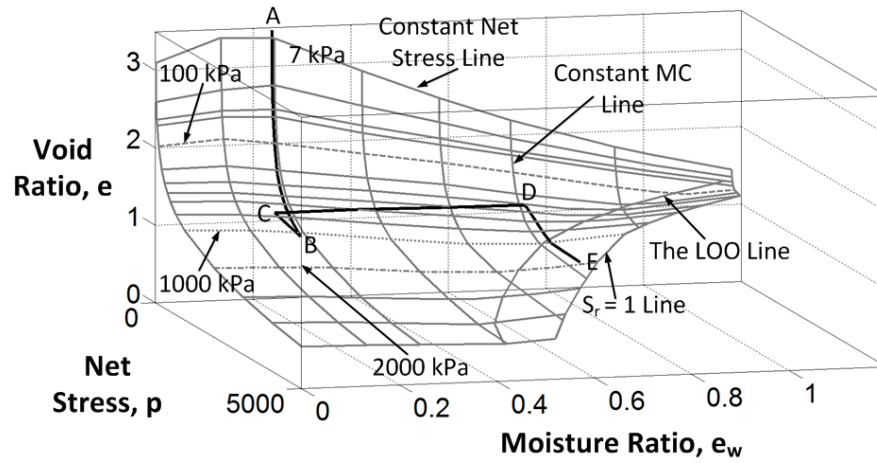
(f) 3-D view of state path test (d)

Figure 4-13: Loading/unloading/wetting/loading state path tests for the kaolin soil
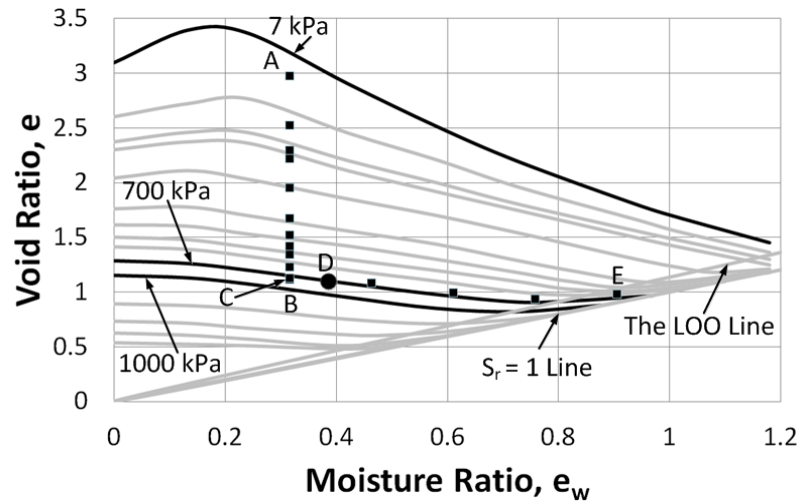
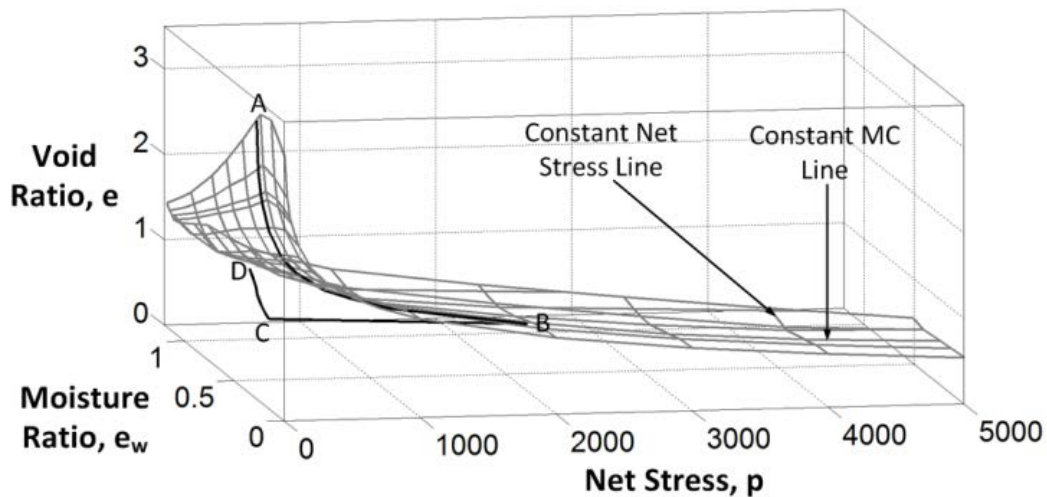**(a)** Loading at 11.88% moisture content (e_w = 0.315) to 1000 kPa stress and then unloaded to 700 kPa stress and then wetted to 34.14% moisture content (e_w = 0.905) [Test Identity => SC – EK – LUW – 1]
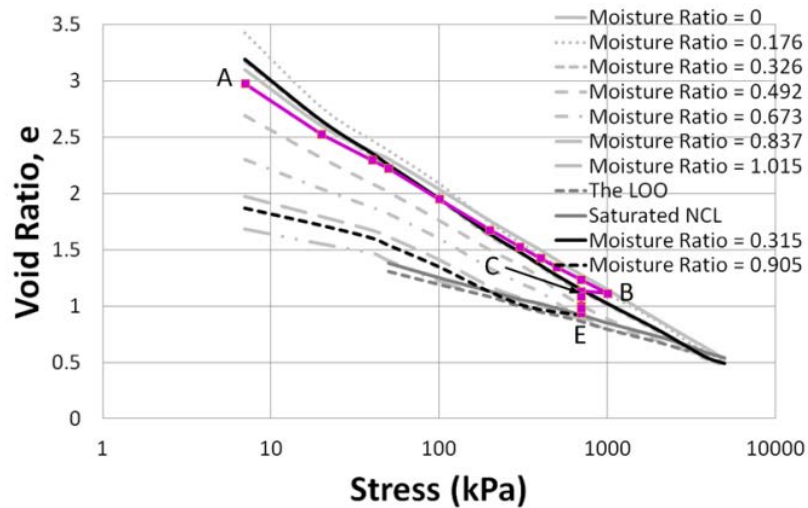
(b) e – log p relationship of state path test (a)
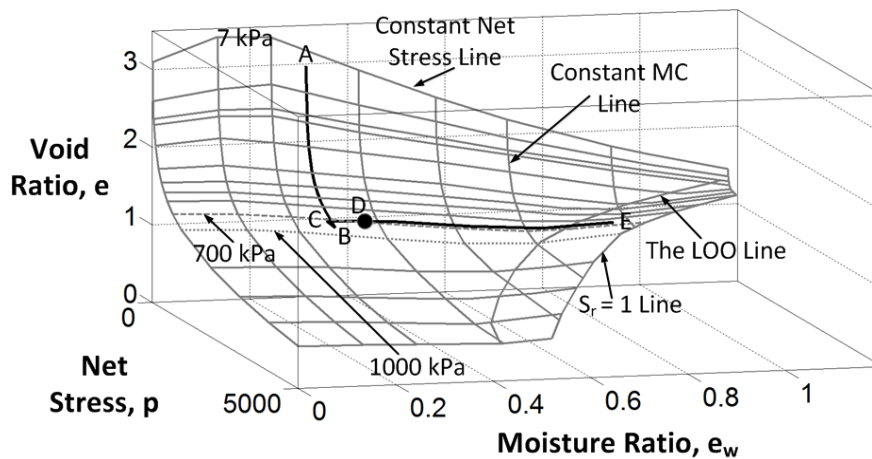
(c) 3-D view of state path test (a)
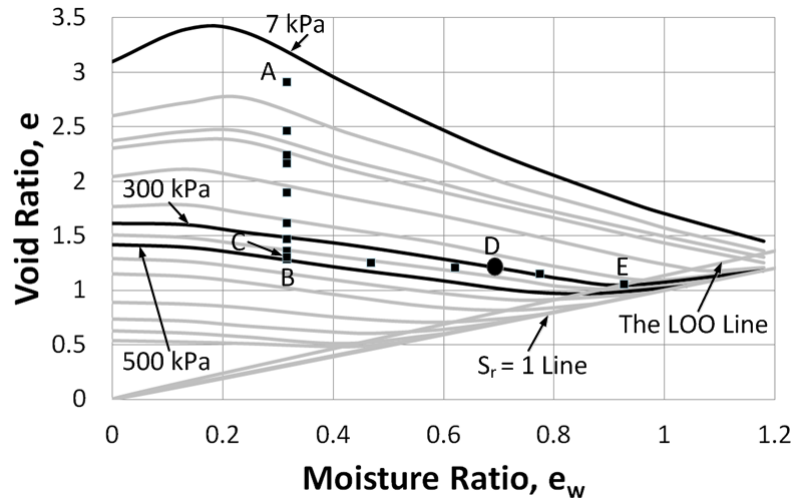
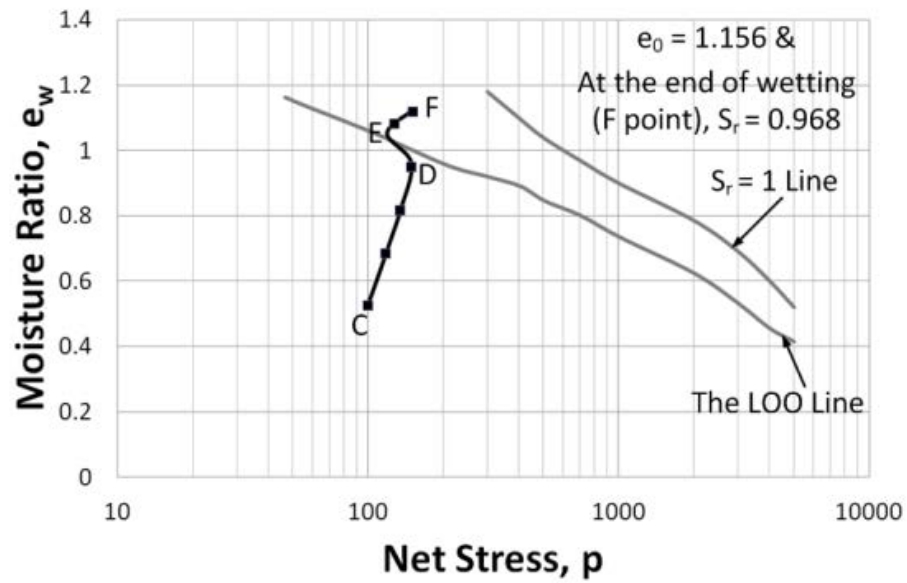**(d)** Loading at 11.88% moisture content ($e_w = 0.315$) to 500 kPa stress and then unloaded to 300 kPa stress and then wetted to 34.95% moisture content ($e_w = 0.926$) [Test Identity => SC – EK – LUW – 2]
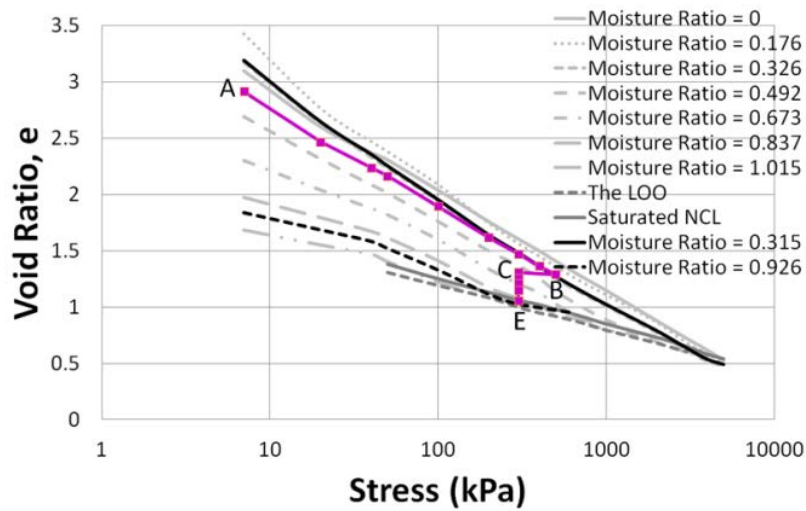
(e) $e - \log p$ relationship of state path test (d)
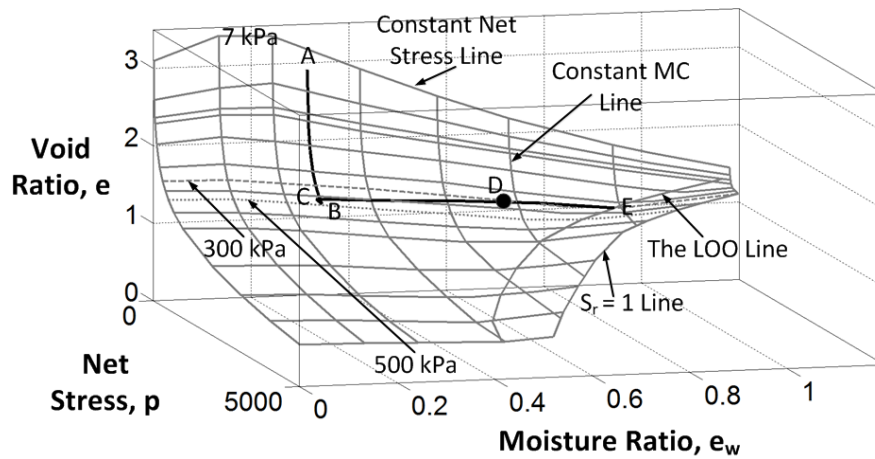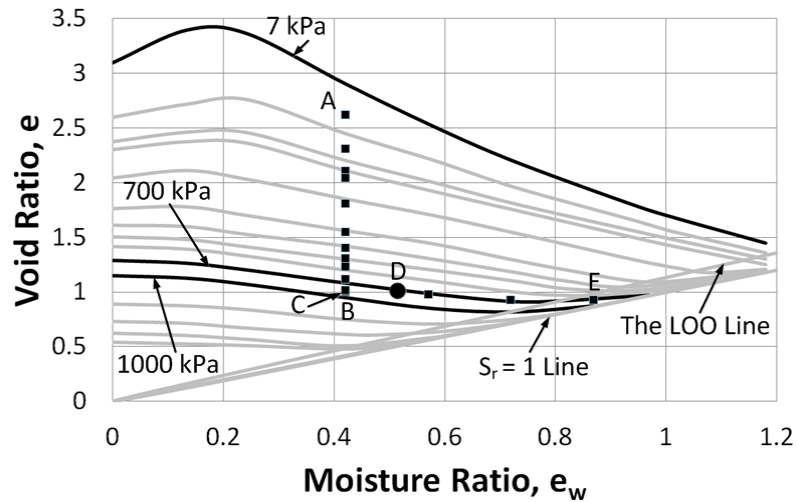
(f) 3-D view of state path test (d)

(g) Loading at 15.85% moisture content ($e_w = 0.420$) to 1000 kPa stress and then unloaded to 700 kPa stress and then wetted to 32.77% moisture content ($e_w = 0.868$) [Test Identity => SC – EK – LUW – 3]
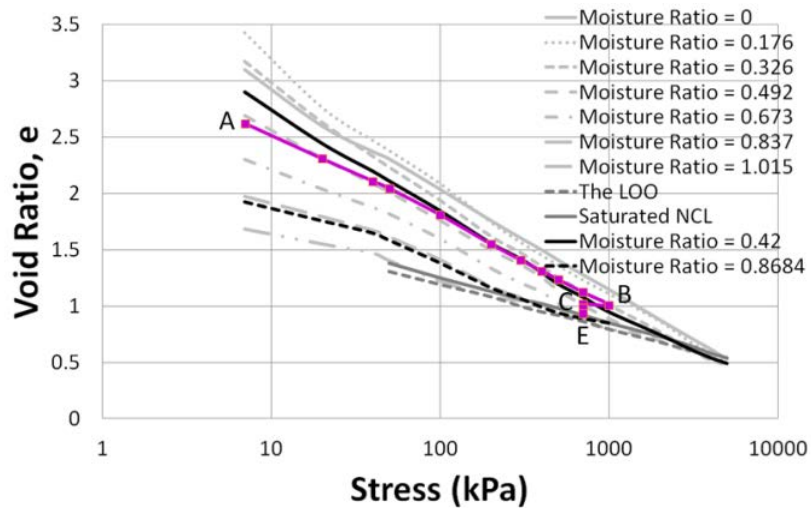
(h) $e - \log p$ relationship of state path test (g)
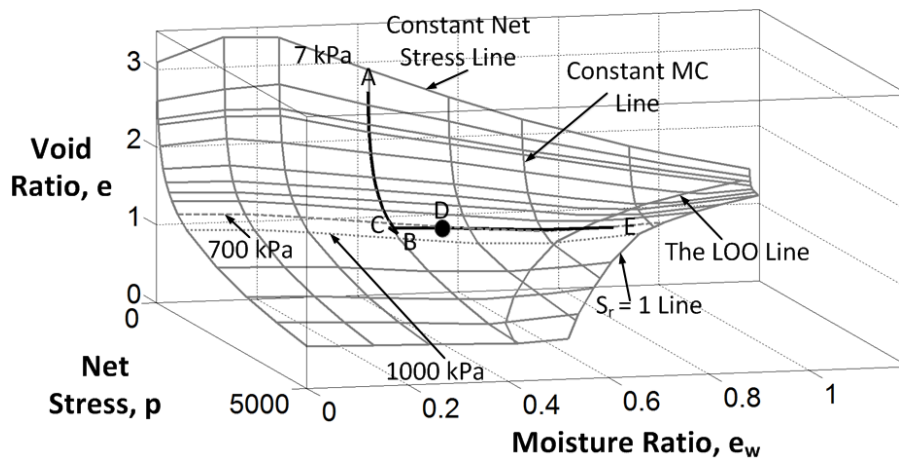
(i) 3-D view of state path test (g)
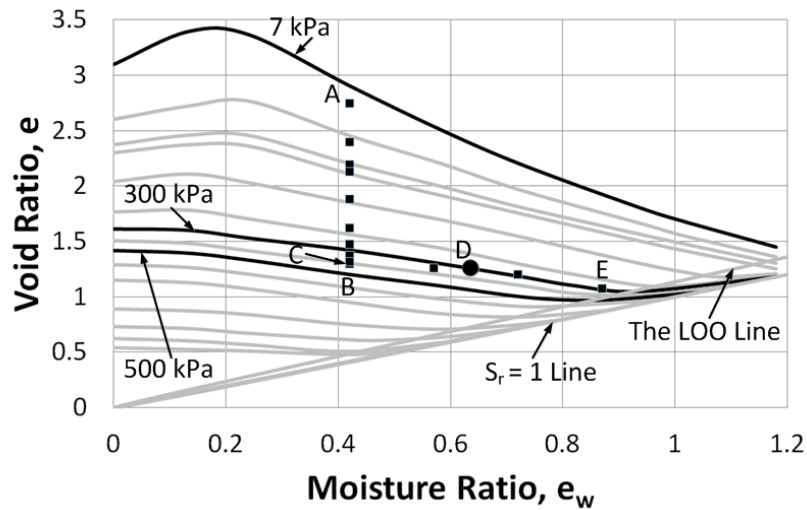
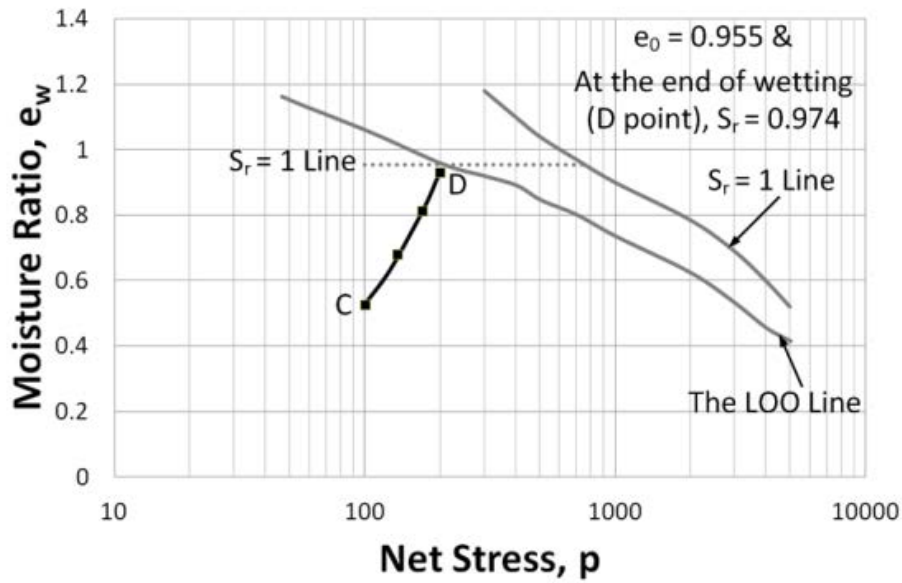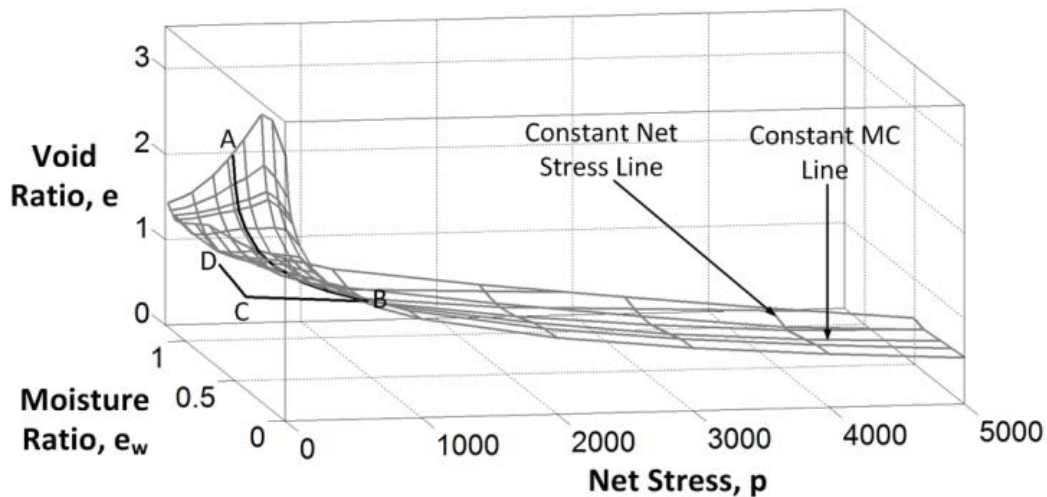**(j)** Loading at 15.85% moisture content ($e_w = 0.420$) to 500 kPa stress and then unloaded to 300 kPa stress and then wetted to 32.80% moisture content ($e_w = 0.869$) [Test Identity => SC – EK – LUW – 4]
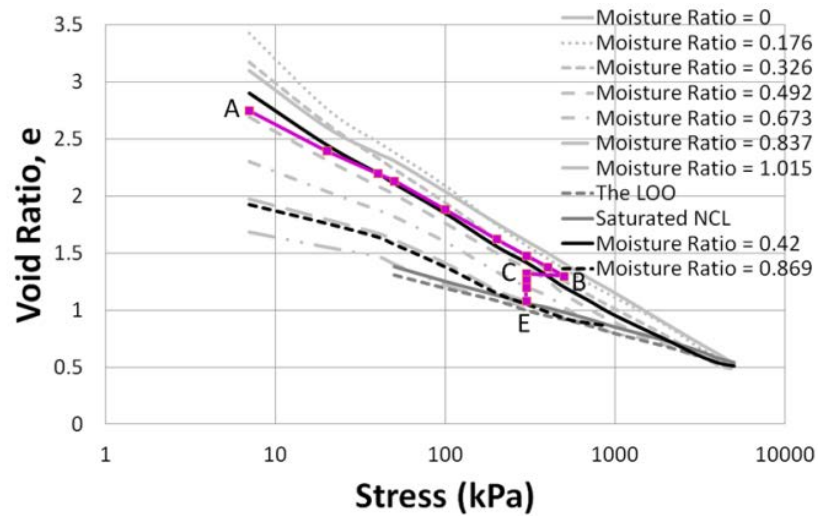
(k) e – log p relationship of state path test (j)
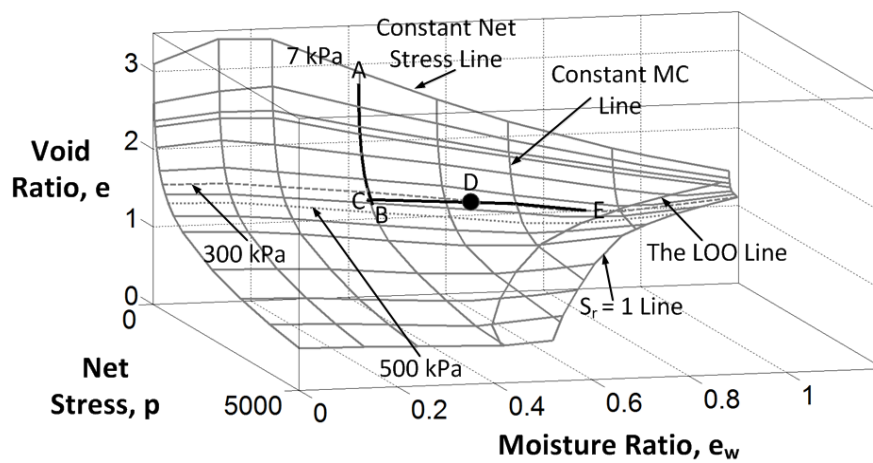
(l) 3-D view of state path test (j)

Figure 4-14: Loading/unloading/wetting state path tests for the kaolin soil
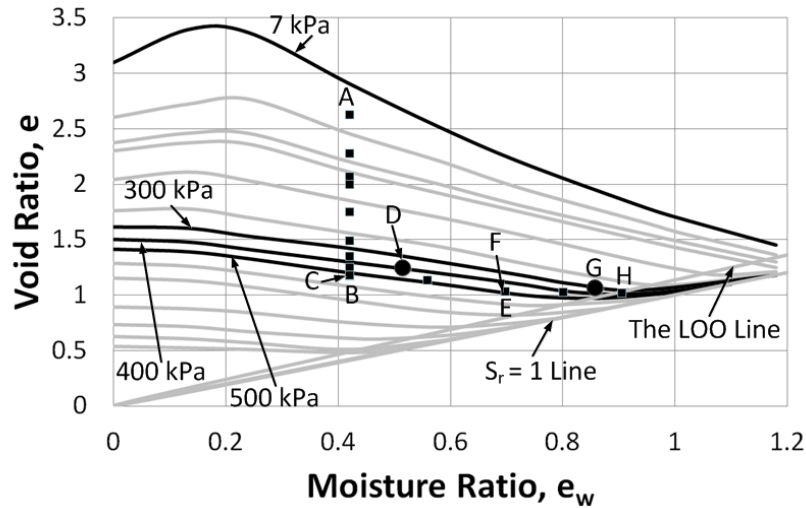
(a) Loading at 15.85% moisture content ($e_w = 0.420$) to 500 kPa stress and then unloaded to 400 kPa stress and then wetted to 26.29% moisture content ($e_w = 0.697$) and then unloaded to 300 kPa stress and then wetted to 34.14% moisture content ($e_w = 0.905$) [Test Identity => SC – EK – LUWUW – 1]
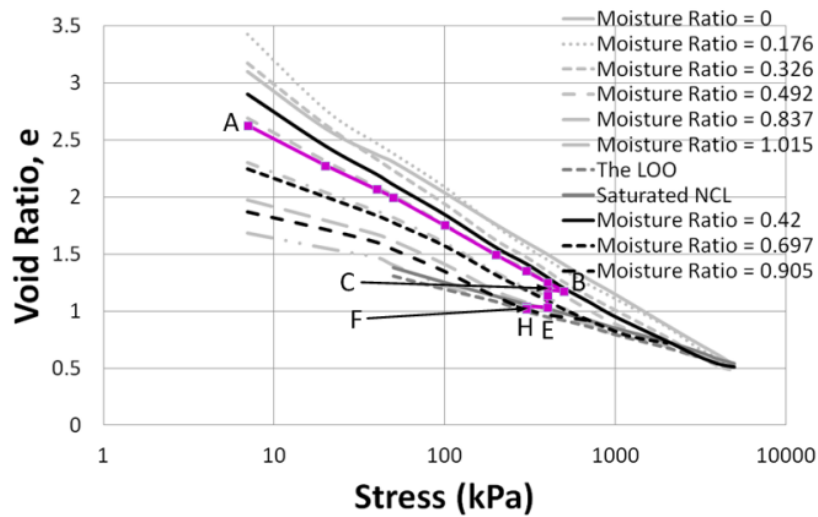
(b) $e - \log p$ relationship of state path test (a)
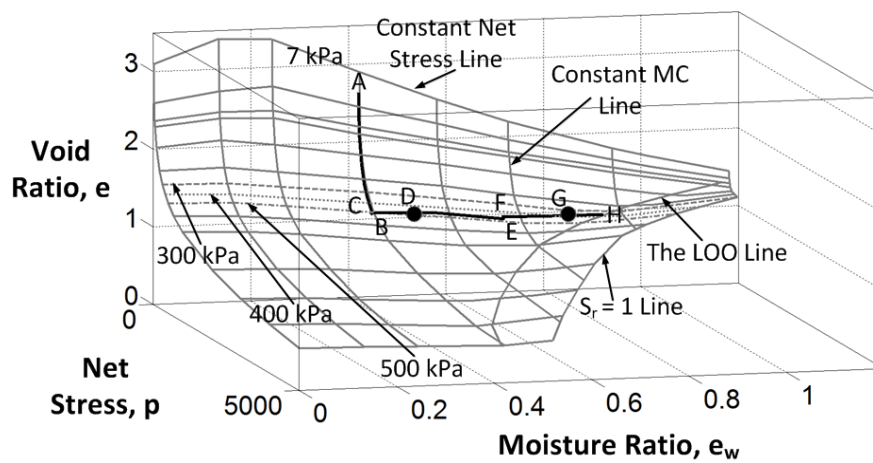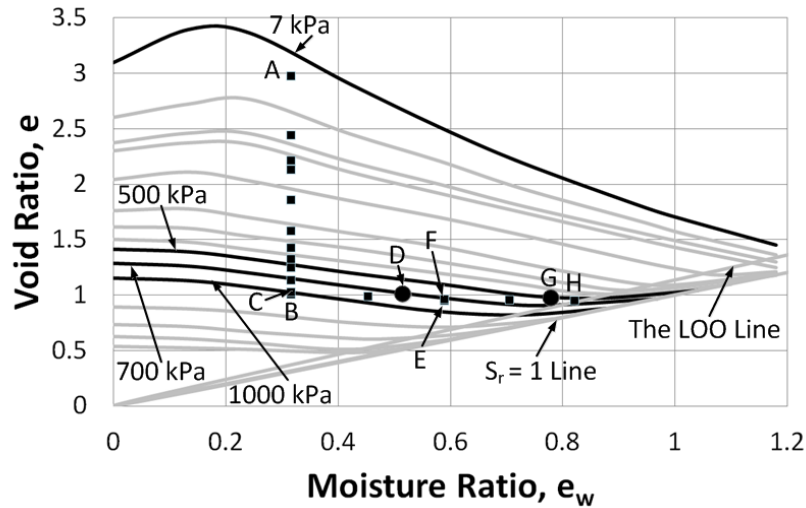
(c) 3-D view of state path test (a)

(d) Loading at 11.88% moisture content ($e_w = 0.315$) to 1000 kPa stress and then unloaded to 700 kPa stress and then wetted to 22.23% moisture content ($e_w = 0.589$) and then unloaded to 500 kPa stress and then wetted to 30.98% moisture content ($e_w = 0.821$) [Test Identity => SC – EK – LUWUW – 2]
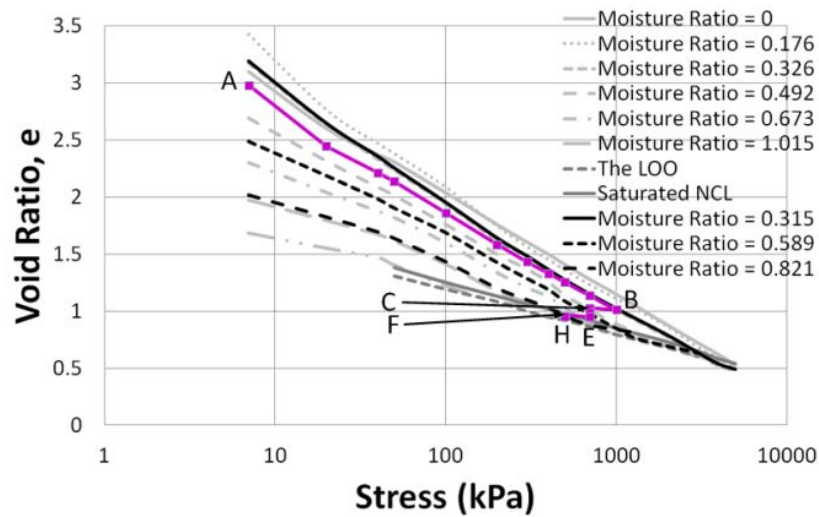
(e) $e – \log p$ relationship of state path test (d)
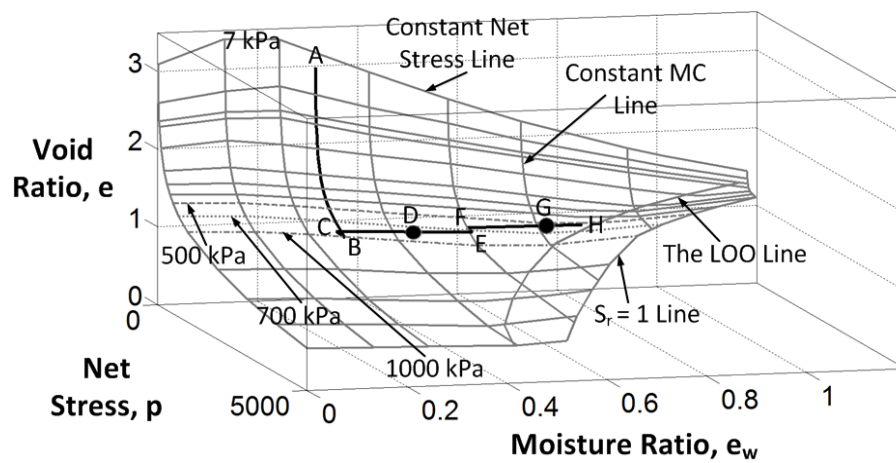
(f) 3-D view of state path test (d)
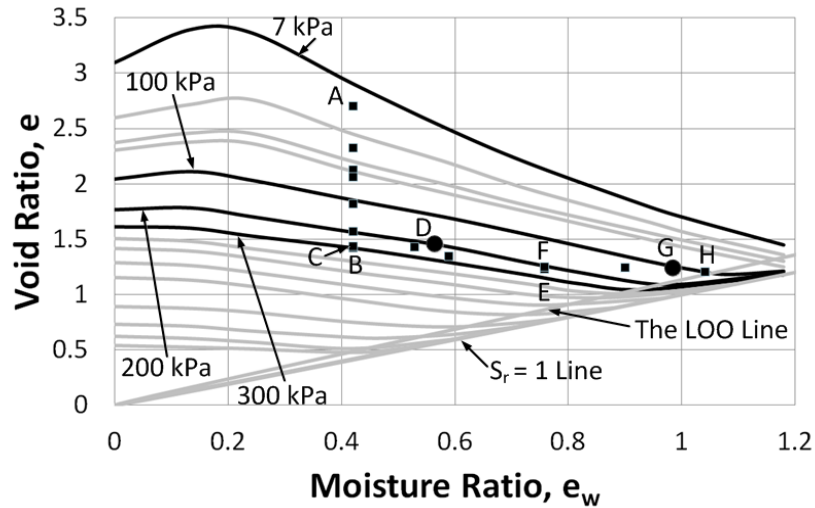
(g) Loading at 15.85% moisture content ($e_w = 0.420$) to 300 kPa stress and then unloaded to 200 kPa stress and then wetted to 28.60% moisture content ($e_w = 0.758$) and then unloaded to 100 kPa stress and then wetted to 39.26% moisture content ($e_w = 1.040$) [Test Identity => SC – EK – LUWUW – 3]
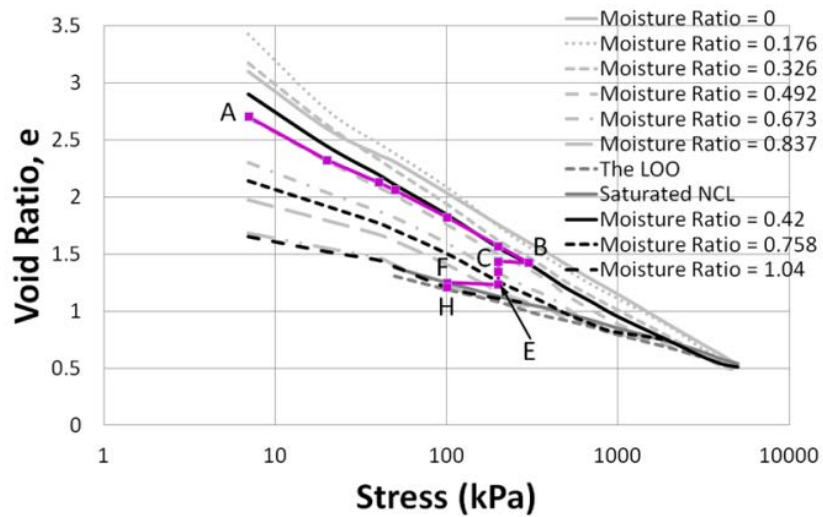
(h) $e – \log p$ relationship of state path test (g)
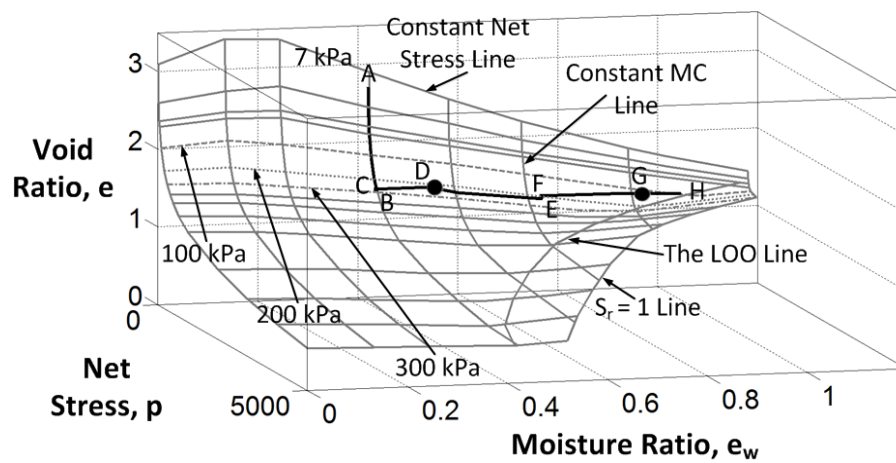
(i) 3-D view of state path test (g)
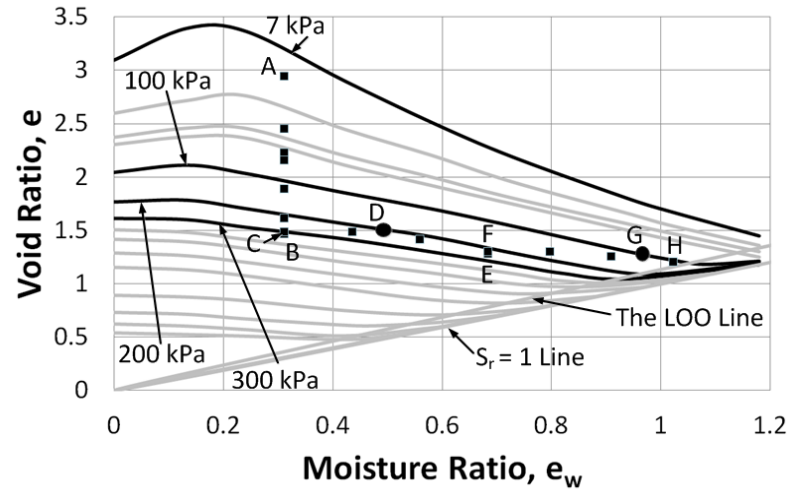
(j) Loading at 11.69% moisture content ($e_w = 0.310$) to 300 kPa stress and then unloaded to 200 kPa stress and then wetted to 25.80% moisture content ($e_w = 0.684$) and then unloaded to 100 kPa stress and then wetted to 38.56% moisture content ($e_w = 1.022$) [Test Identity => SC – EK – LUWUW – 4]
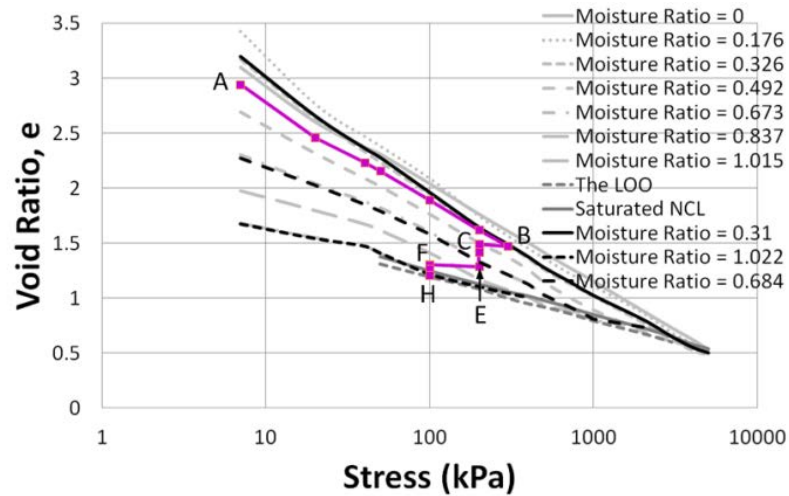
(k) $e – \log p$ relationship of state path test (j)
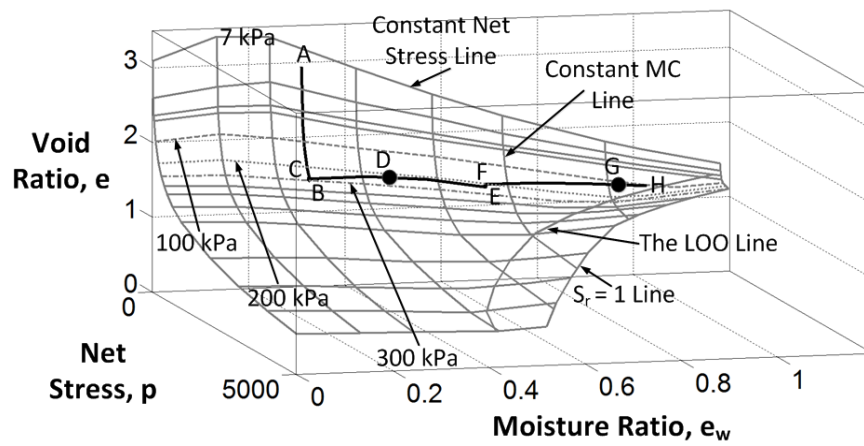
(l) 3-D view of state path test (j)

Figure 4-15: Loading/unloading/wetting/unloading/wetting state path tests for the kaolin soil
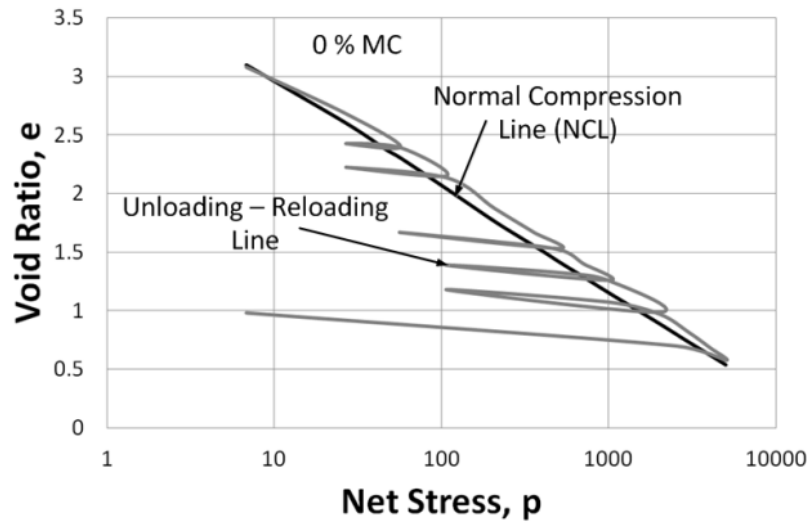
(a) 0% moisture content ($e_w = 0$) soil specimen
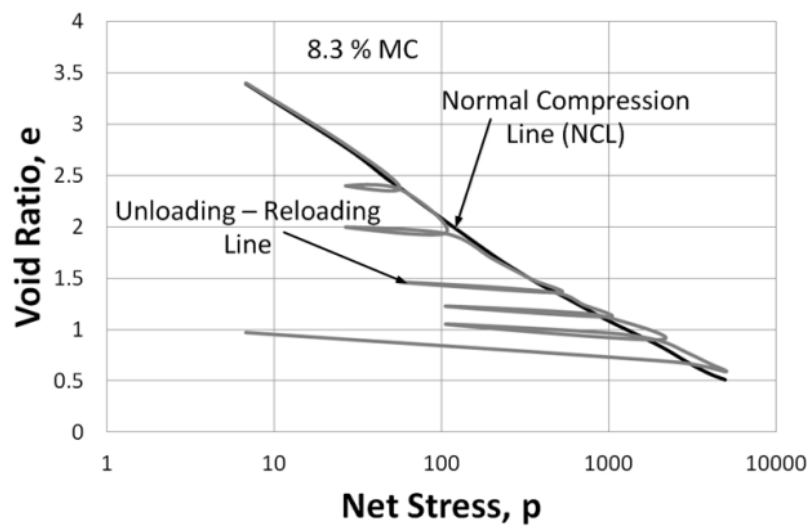
(b) 8.3% moisture content ($e_w = 0.22$) soil specimen
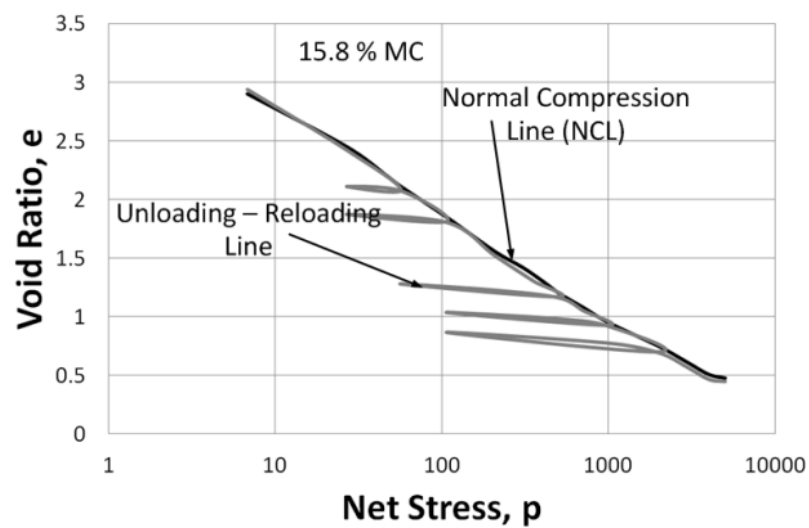
(c) 15.8% moisture content ($e_w = 0.419$) soil specimen
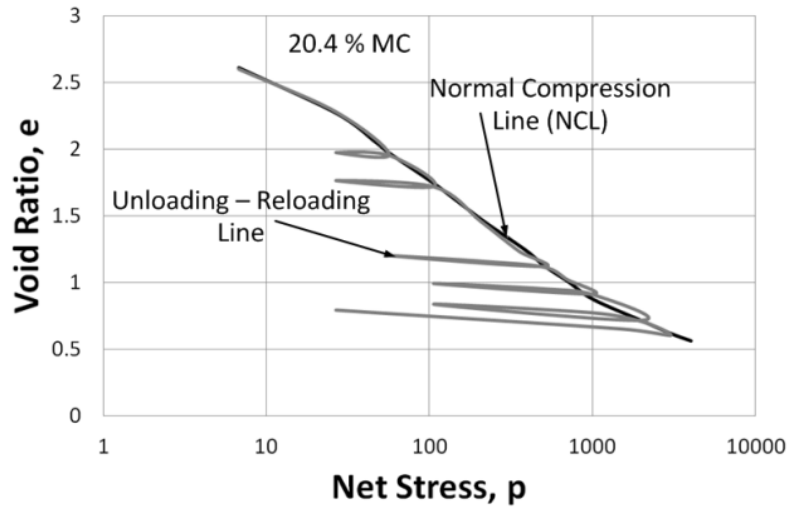
(d) 20.4% moisture content ($e_w = 0.541$) soil specimen
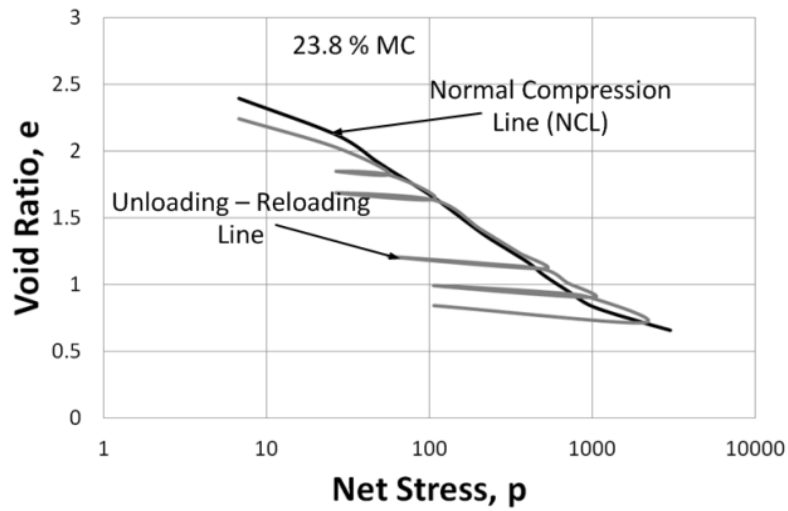
(e) 23.8% moisture content ($e_w = 0.632$) soil specimen
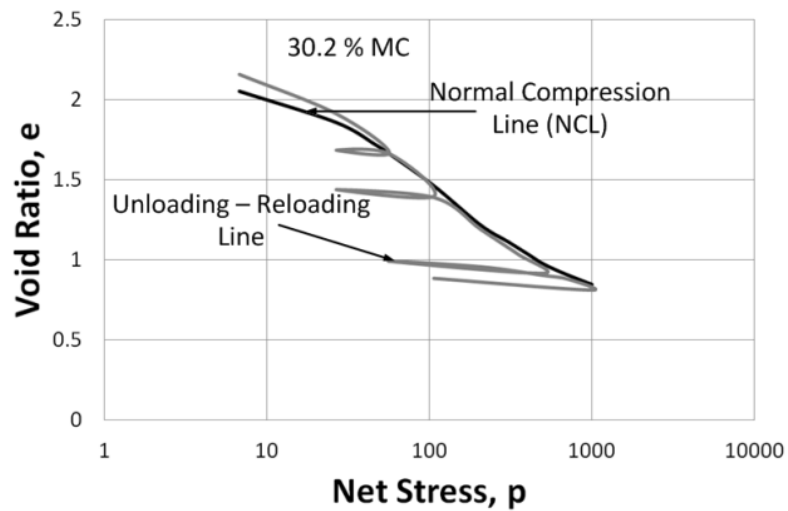
(f) 30.2% moisture content ($e_w = 0.80$) soil specimen

Figure 4-16: Loading/unloading/reloading state path tests for the kaolin soil
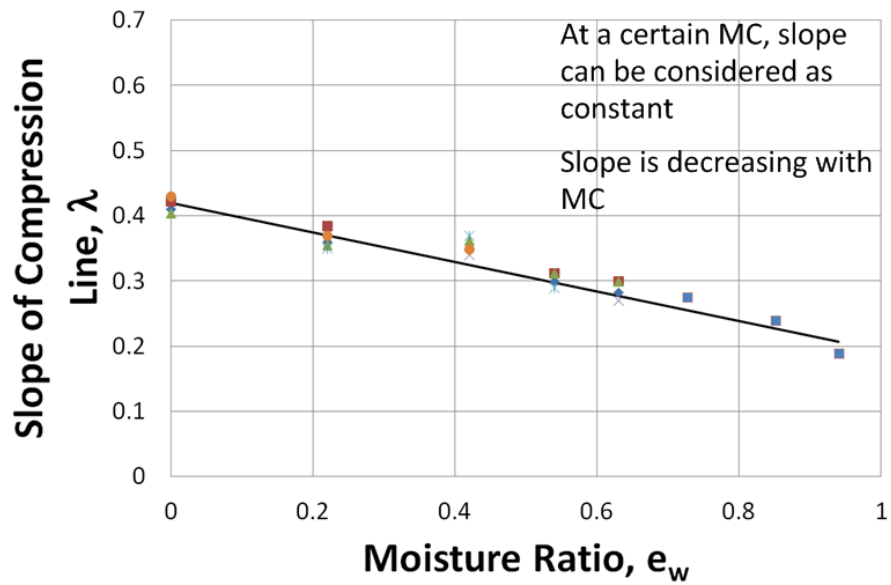
(a) Gradient of compression line (λ) versus moisture ratio (e_w)
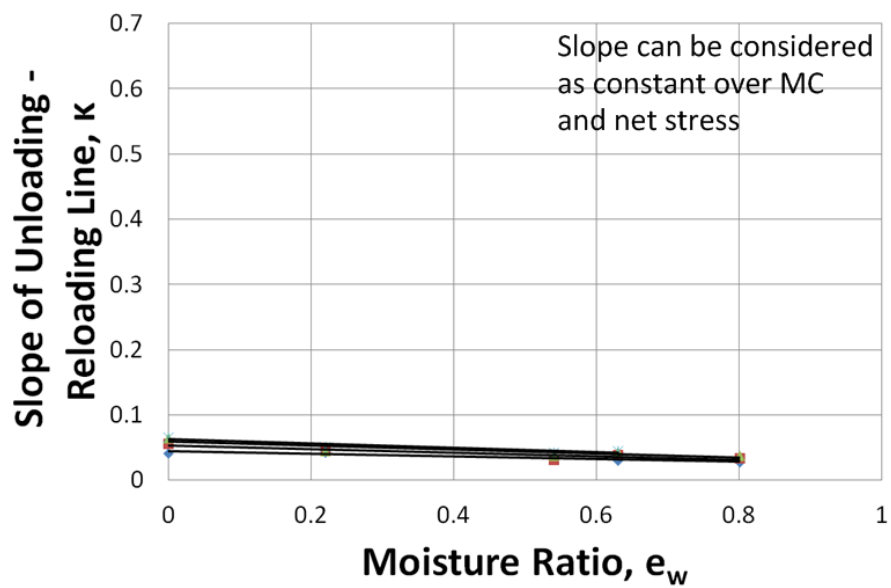
(b) Gradient of recompression line (κ) versus moisture ratio (e_w)

Figure 4-17: Relationship of the gradient of compression and recompression line with moisture ratio for the kaolin soil
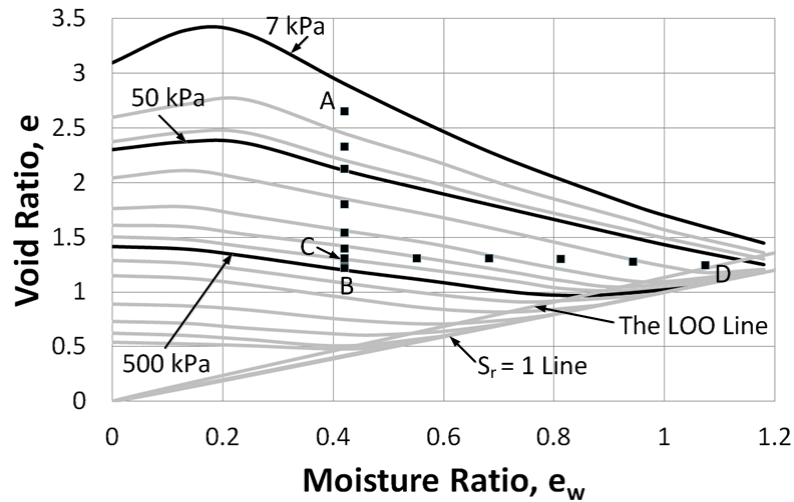
(a) Loading at 15.77% moisture content ($e_w = 0.420$) to 500 kPa stress and then unloaded to 50 kPa stress and then wetted to 45.43% moisture content ($e_w = 1.204$) [Test Identity => SC – EK – CPT – 1 or SC – EK – LUW – 5]
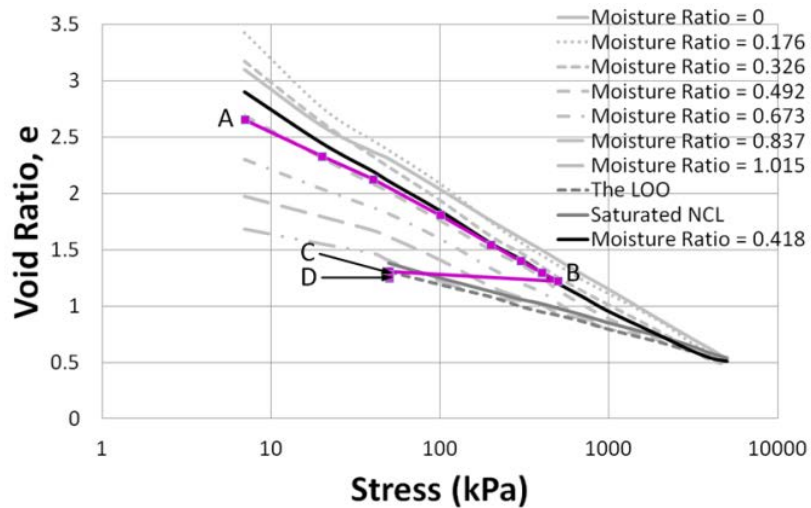
(b) $e – \log p$ relationship of state path test (a)
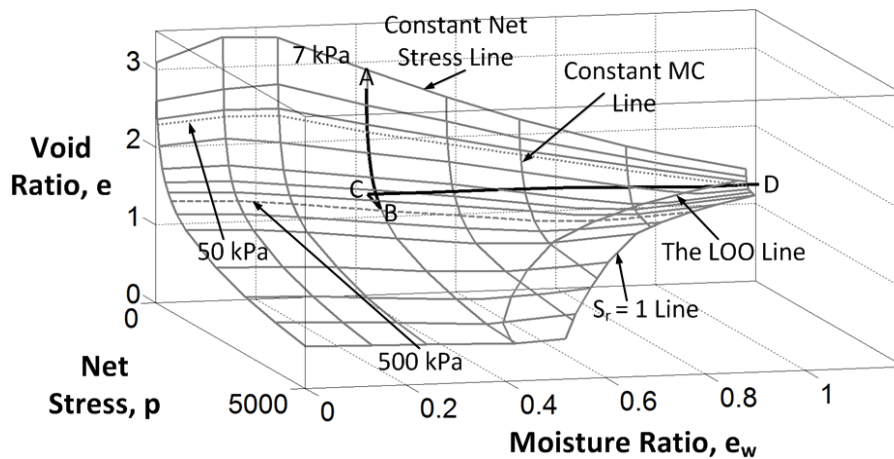
(c) 3-D view of state path test (a)
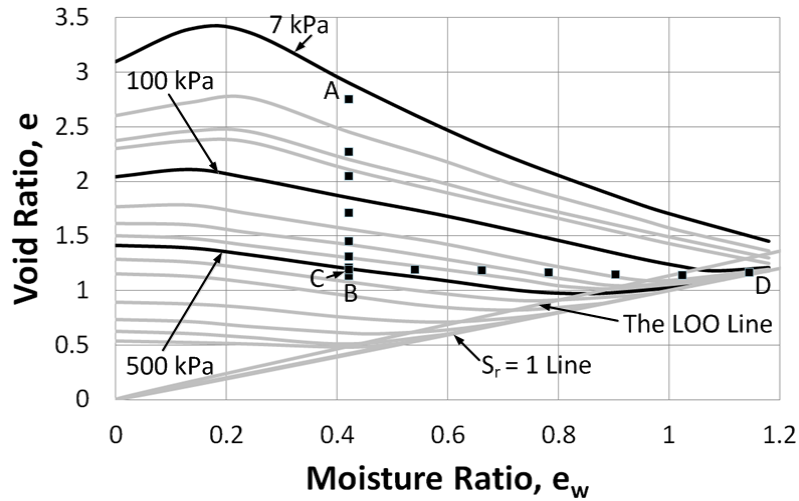
(d) Loading at 15.77% moisture content ($e_w = 0.420$) to 500 kPa stress and then unloaded to 100 kPa stress and then wetted to 43.16% moisture content ($e_w = 1.144$) [Test Identity => SC – EK – CPT – 2 or SC – EK – LUW – 6]
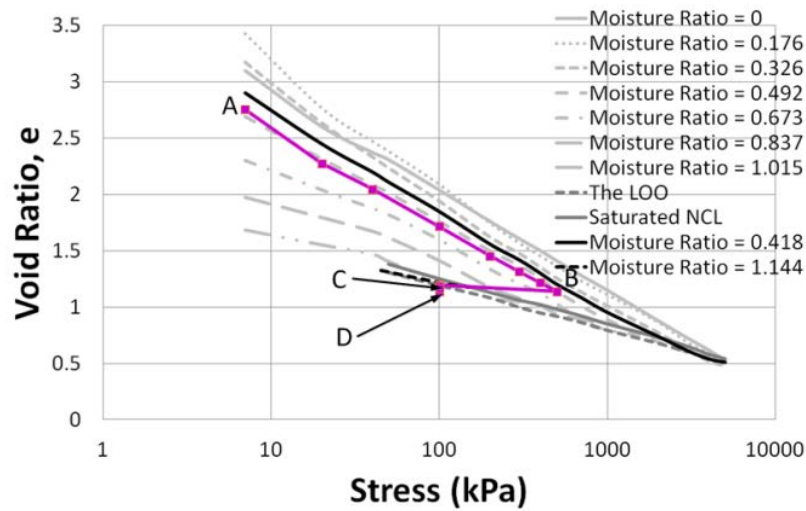
(e) $e - \log p$ relationship of state path test (d)
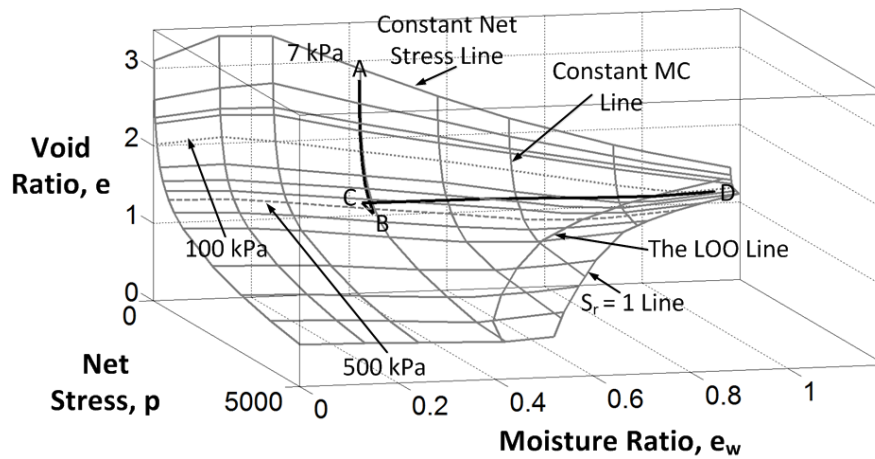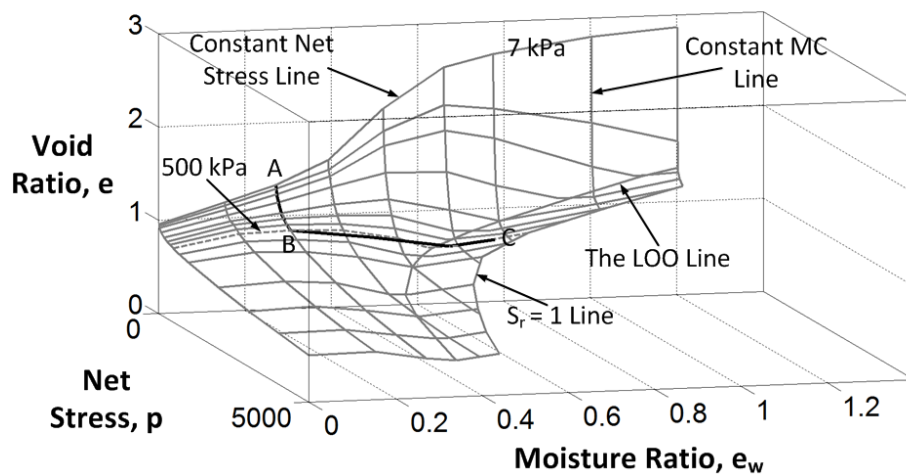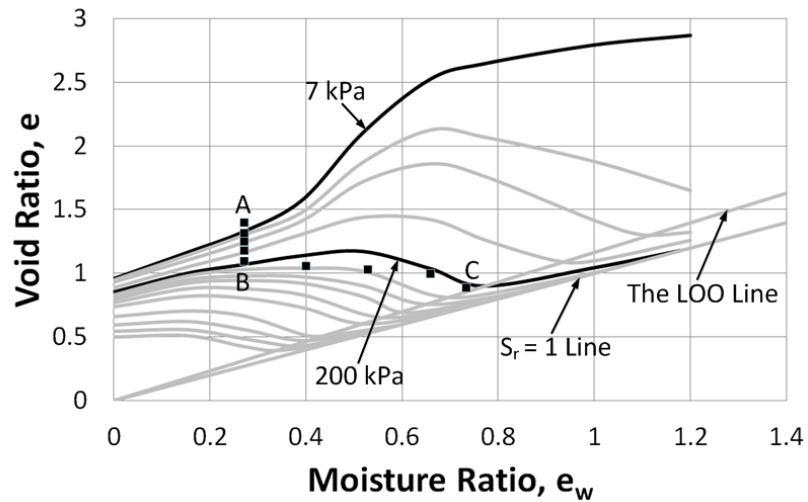

(f) 3-D view of state path test (d)
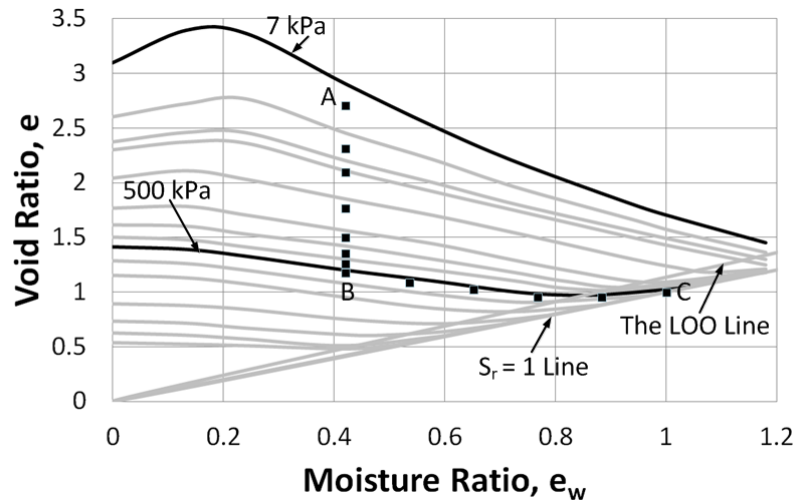
(g) Loading at 15.77% moisture content ($e_w = 0.420$) to 500 kPa stress and then wetted to 38.10% moisture content ($e_w = 1.010$) [Test Identity => SC – EK – CPT – 3 or SC – EK – LW – 4]
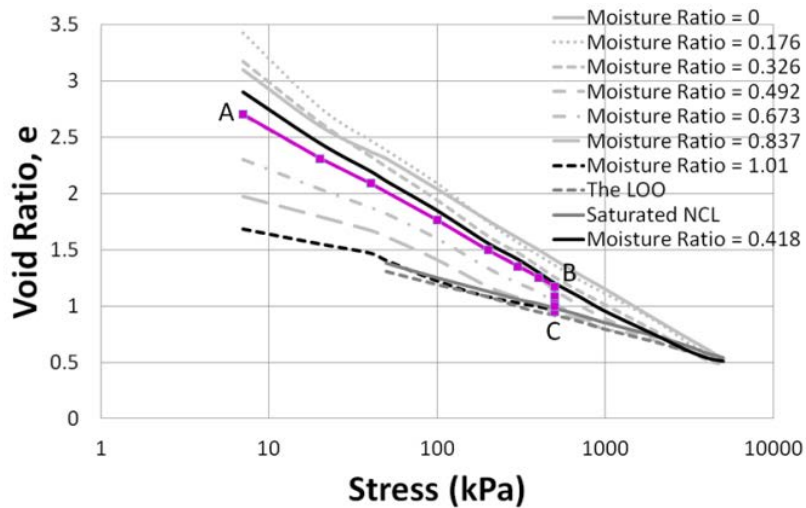
(h) $e – \log p$ relationship of state path test (g)
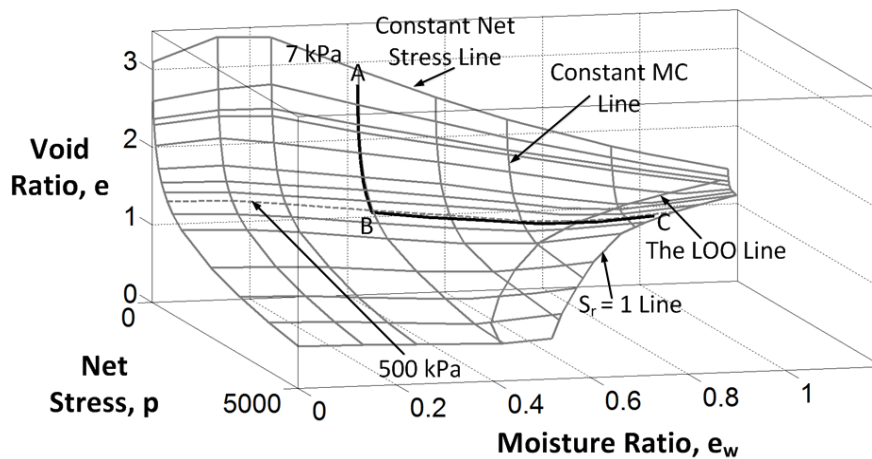
(i) 3-D view of state path test (g)

(j) Loading at 15.77% moisture content ($e_w = 0.420$) to 1000 kPa stress and then wetted to 33.0% moisture content ($e_w = 0.875$) [Test Identity => SC – EK – CPT – 4 or SC – EK – LW – 5]
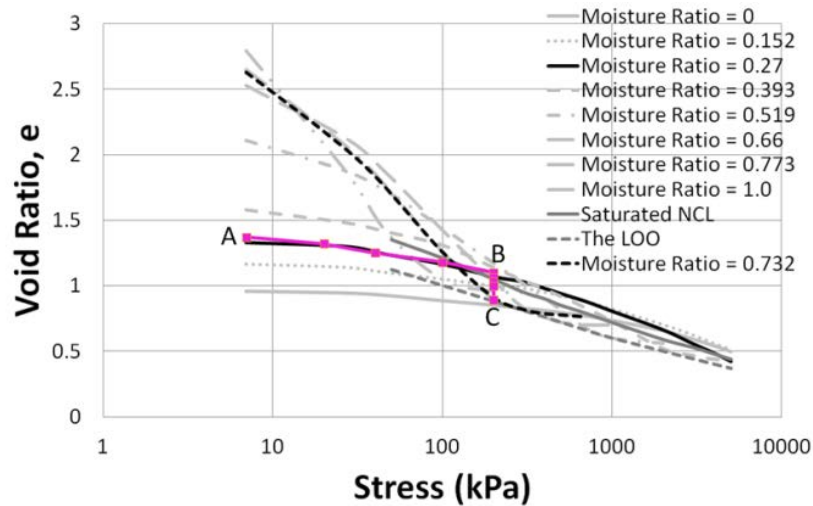

(k) e – log p relationship of state path test (j)
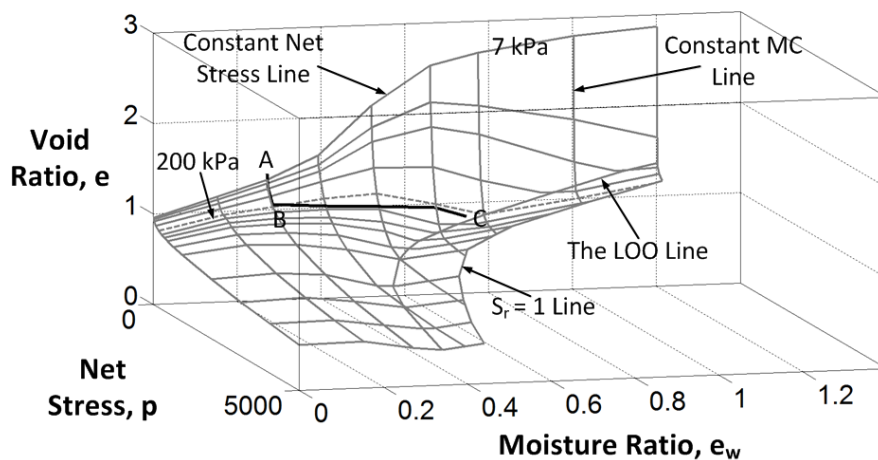

(l) 3-D view of state path test (j)

(m) Loading at 15.77% moisture content ($e_w = 0.420$) to 2000 kPa stress and then wetted to 28.30% moisture content ($e_w = 0.750$) [Test Identity => SC – EK – CPT – 5 or SC – EK – LW – 6]

(n) $e - \log p$ relationship of state path test (m)

(o) 3-D view of state path test (m)

(p) Loading at 15.77% moisture content ($e_w = 0.420$) to 4000 kPa stress and then wetted to 20.75% moisture content ($e_w = 0.550$) [Test Identity => SC – EK – CPT – 6 or SC – EK – LW – 7]
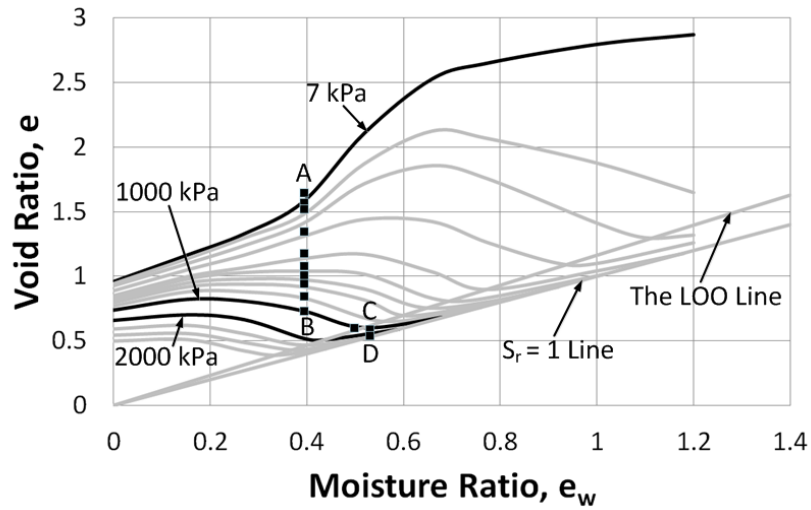

(q) $e – \log p$ relationship of state path test (p)
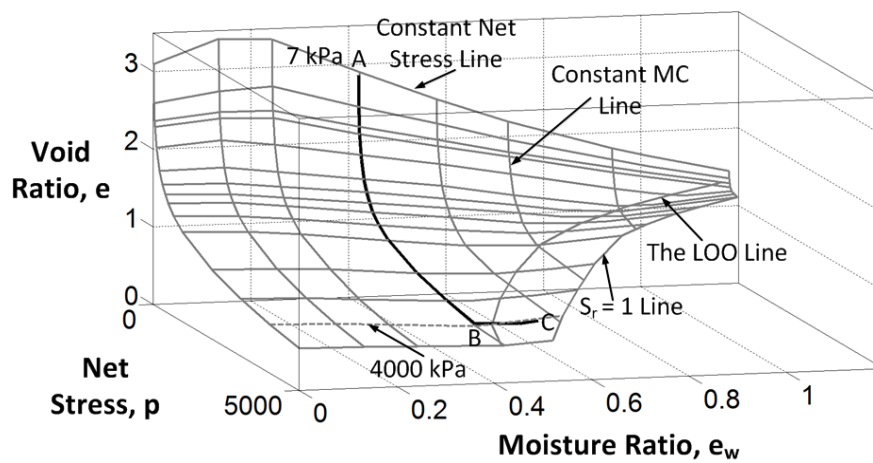
(r) 3-D view of state path test (p)

Figure 4-18: Various state path tests to examine collapse potentiality for compacted kaolin soil
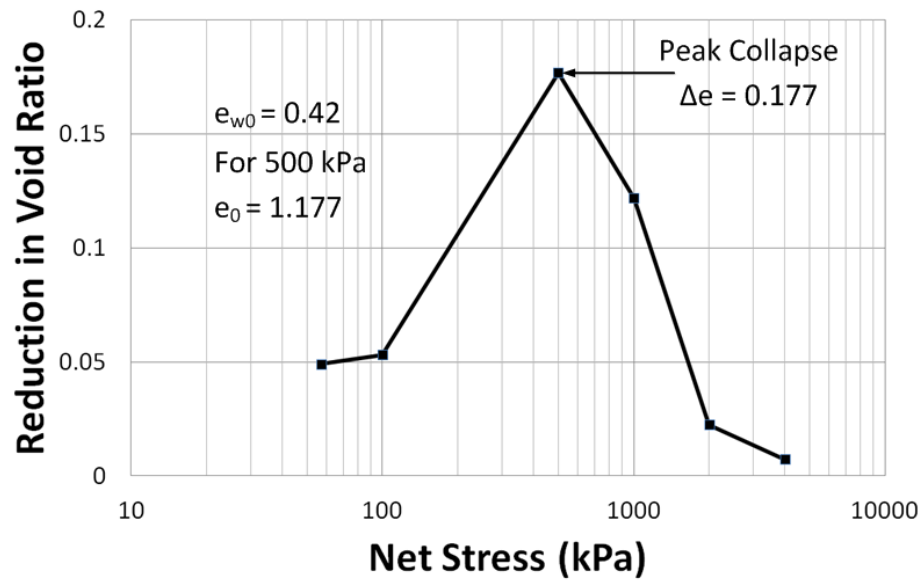
Figure 4-19: Collapse potential given as reduction of void ratio for the kaolin soil specimens with initial $e_{wo} = 0.420$ and $e_o = 1.177$ and a compaction stress of 500 kPa
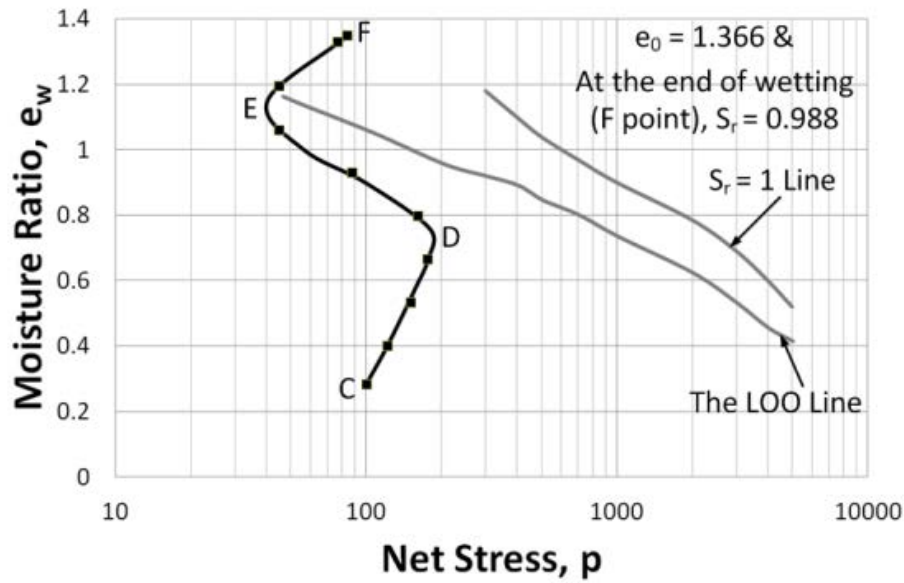
(a) Specimen of 10.69% moisture content (e_w = 0.283) loaded to 500 kPa stress and then unloaded to 100 kPa stress and then wetted to 50.90% moisture content (e_w = 1.350) (S_r = 0.988 and e_0 = 1.366) at constant volume [Test Identity => SC – EK – SPT –1]

(b) 3-D view of state path test (a)

The chart shows:
- y-axis: Moisture Ratio, e_w (0 to 1.4)
- x-axis: Net Stress, p (10 to 10000)
- $e_0 = 1.179$ &
- At the end of wetting (F point), $S_r = 0.975$
- $S_r = 1$ Line
- The LOO Line
- Points labeled C, D, E, F
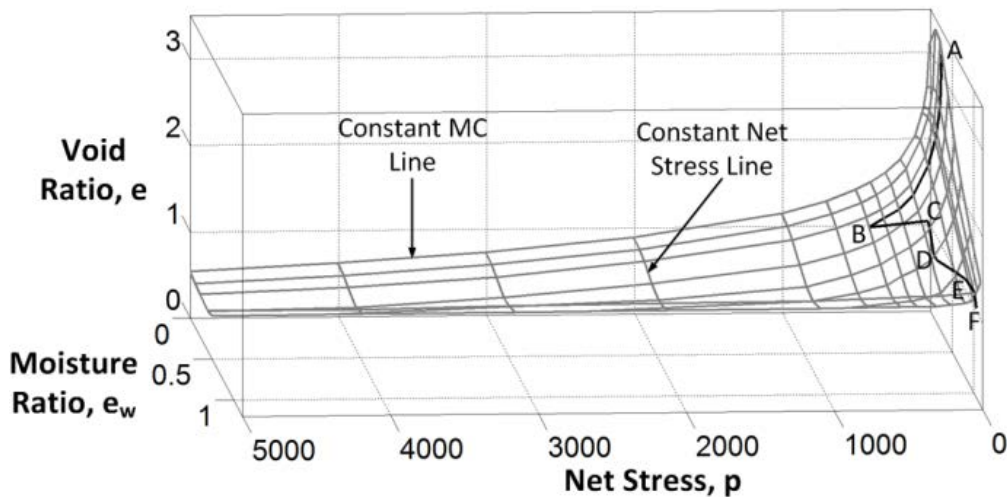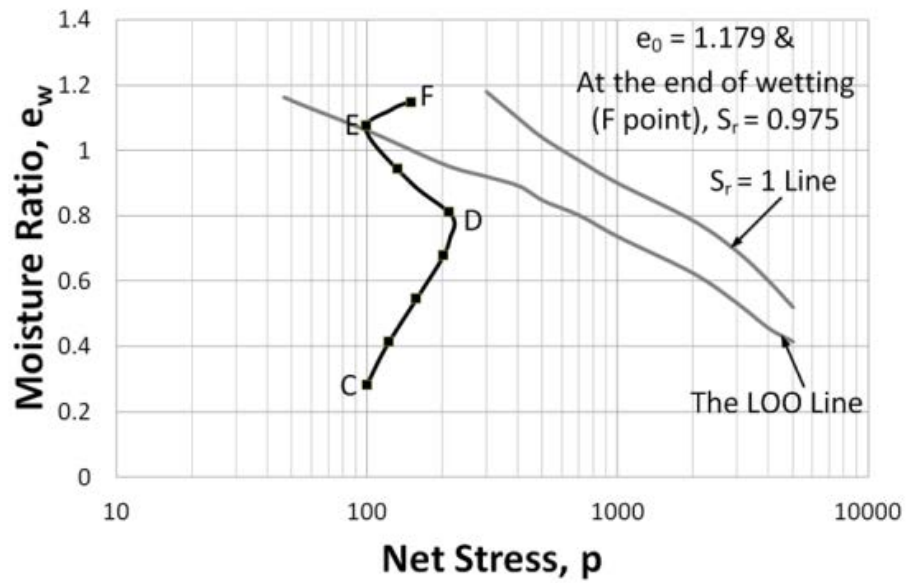
(c) Specimen of 10.69% moisture content ($e_w = 0.283$) loaded to 1000 kPa stress and then unloaded to 100 kPa stress and then wetted to 43.40% moisture content ($e_w = 1.150$) ($S_r = 0.975$ and $e_0 = 1.179$) at constant volume [Test Identity => SC – EK – SPT –2]

(d) 3-D view of state path test (c)

(e) Specimen of 10.69% moisture content (e_w = 0.283) loaded to 2000 kPa stress and then unloaded to 100 kPa stress and then wetted to 34.0% moisture content (e_w = 0.900) (S_r = 0.973 and e_0 = 0.925) at constant volume [Test Identity => SC – EK – SPT –3]

(f) 3-D view of state path test (e)

(g) Specimen of 19.88% moisture content ($e_w = 0.527$) loaded to 500 kPa stress and then unloaded to 100 kPa stress and then wetted to 42.30% moisture content ($e_w = 1.120$) ($S_r = 0.968$ and $e_0 = 1.156$) at constant volume [Test Identity => SC – EK – SPT –4]
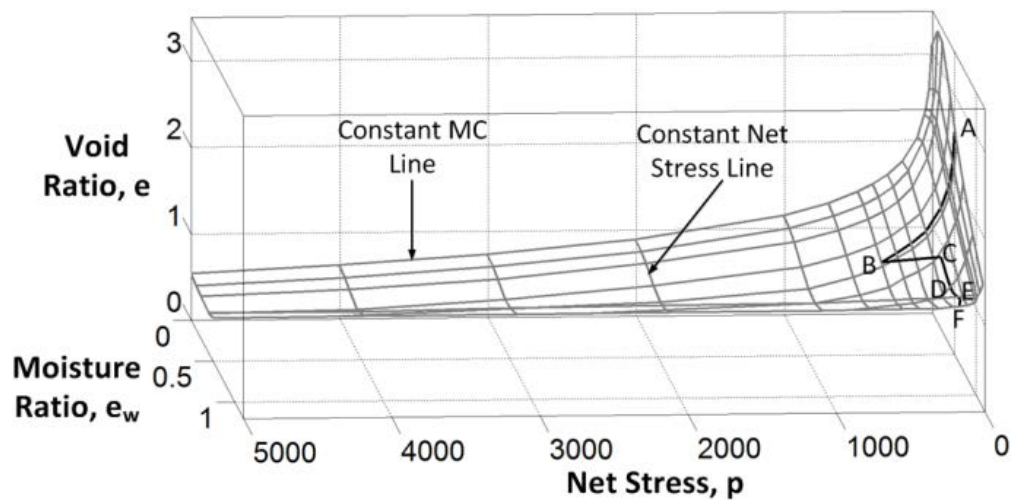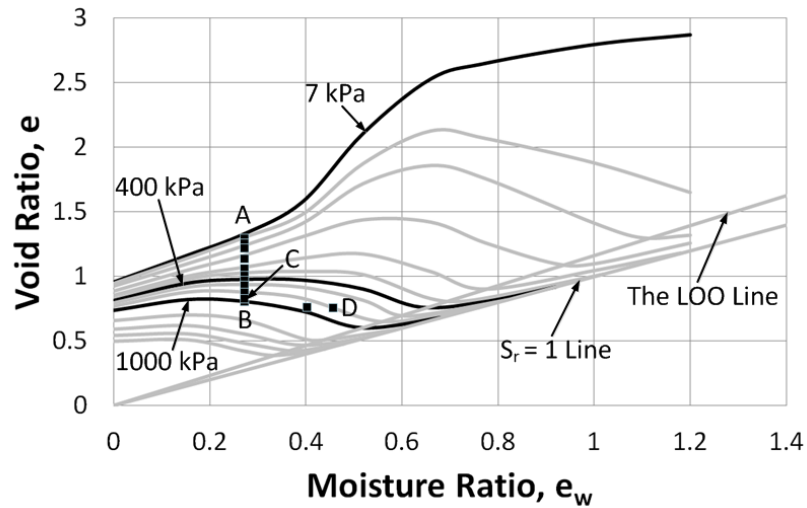

(h) 3-D view of state path test (g)

(i) Specimen of 19.88% moisture content ($e_w = 0.527$) loaded to 1000 kPa stress and then unloaded to 100 kPa stress and then wetted to 35.10% moisture content ($e_w = 0.930$) ($S_r = 0.974$ and $e_0 = 0.955$) at constant volume [Test Identity => SC – EK – SPT –5]

(j) 3-D view of state path test (i)
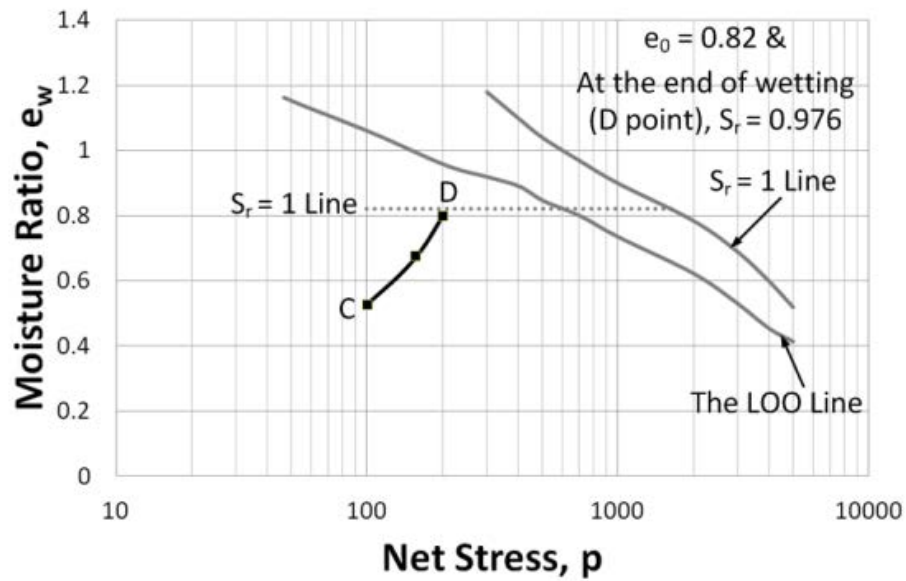
(k) Specimen of 19.88% moisture content ($e_w = 0.527$) loaded to 2000 kPa stress and then unloaded to 100 kPa stress and then wetted to 30.20% moisture content ($e_w = 0.800$) ($S_r = 0.976$ and $e_0 = 0.82$) at constant volume [Test Identity => SC – EK – SPT – 6]
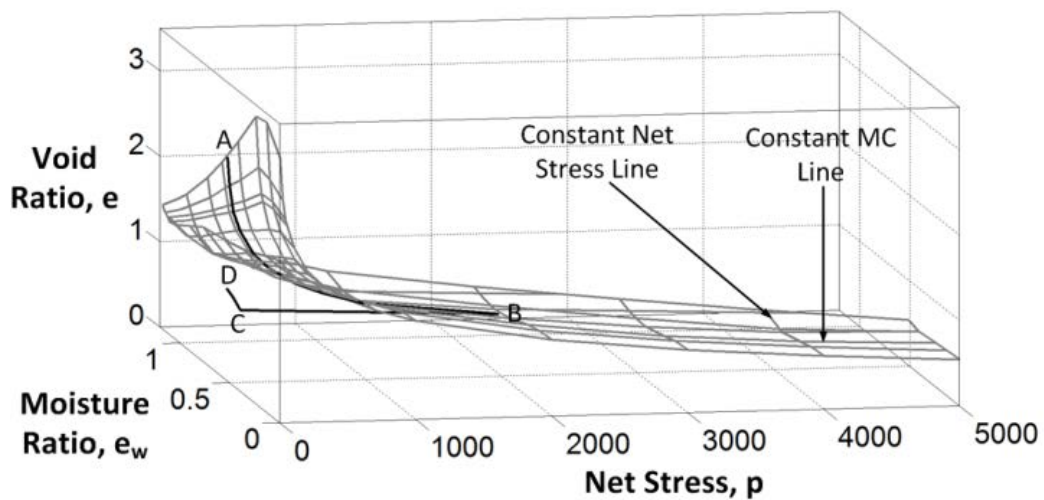
(l) 3-D view of state path test (k)
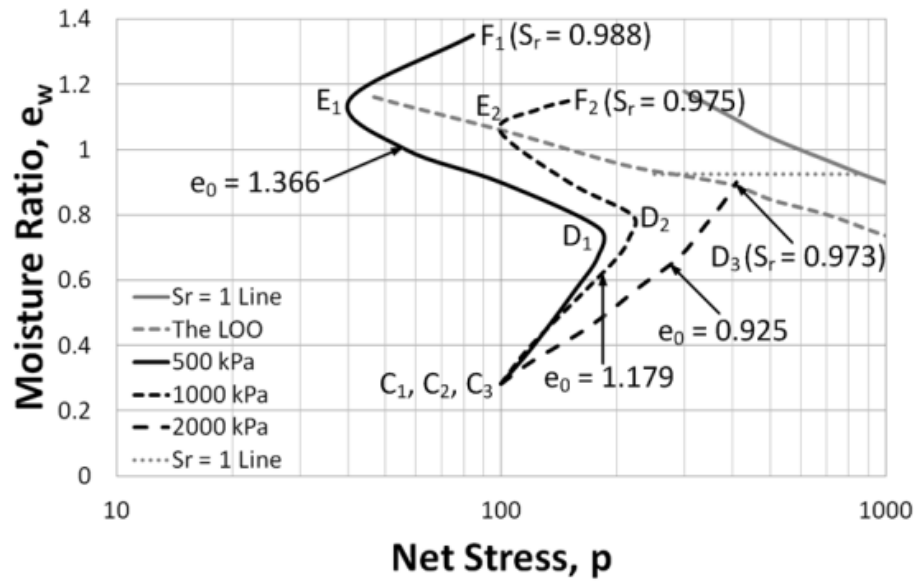
(m) Specimen of 10.69% moisture content ($e_w = 0.283$) loaded to 500, 1000 and 2000 kPa and then unloaded to 100 kPa and then wetted to 50.90% moisture content ($e_w = 1.350$) ($S_r = 0.988$ and $e_0 = 1.366$), 43.40% moisture content ($e_w = 1.150$) ($S_r = 0.975$ and $e_0 = 1.179$) and 34.0% moisture content ($e_w = 0.900$) ($S_r = 0.973$ and $e_0 = 0.925$) respectively at constant volume [Test Identity => SC – EK – SPT – 1, 2 & 3]
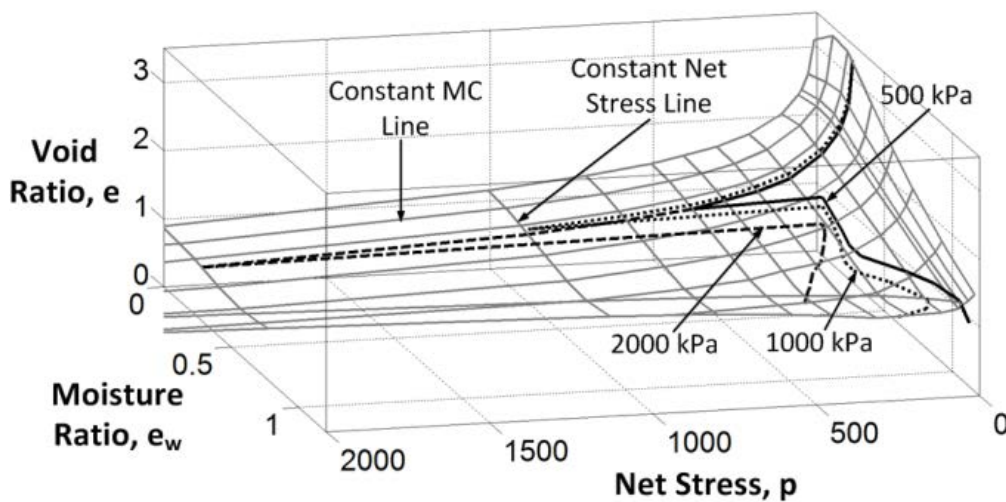
(n) 3-D view of state path test (m)
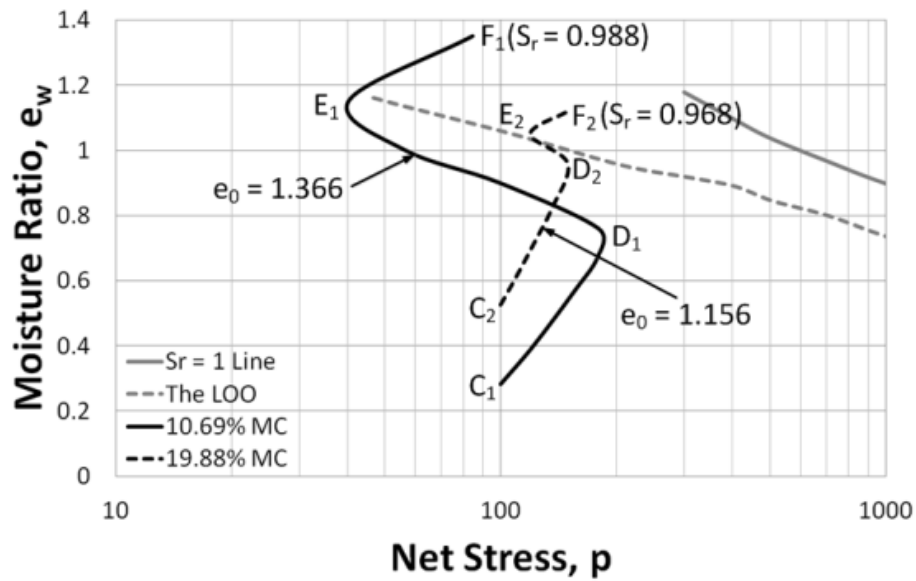
(o) Specimen of 10.69% moisture content ($e_w = 0.283$) and 19.88% moisture content ($e_w = 0.527$) loaded to 500 kPa and then unloaded to 100 kPa and then wetted to 50.90% moisture content ($e_w = 1.350$) ($S_r = 0.988$ and $e_0 = 1.366$) and 42.30% moisture content ($e_w = 1.120$) ($S_r = 0.968$ and $e_0 = 1.156$) respectively at constant volume [Test Identity => SC – EK – SPT – 1 & 4]
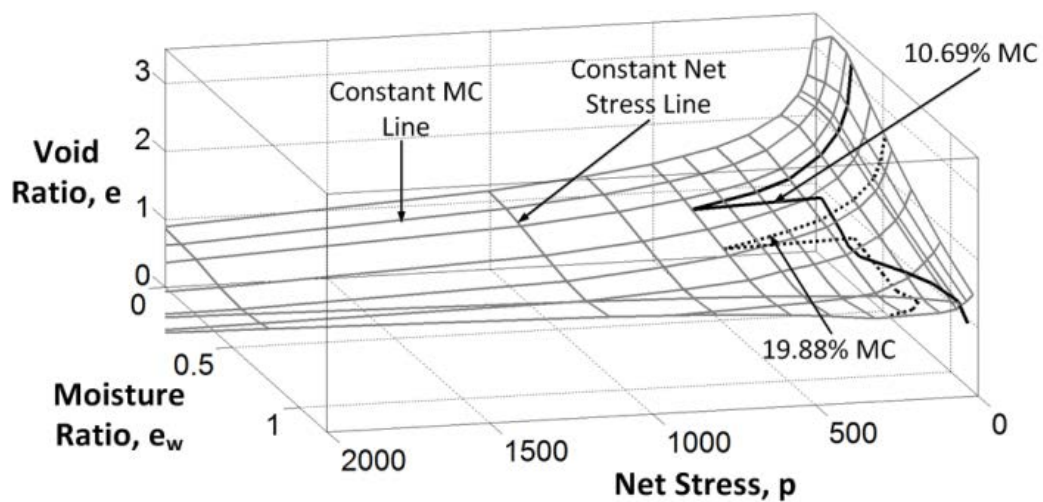
(p) 3-D view of state path test (o)
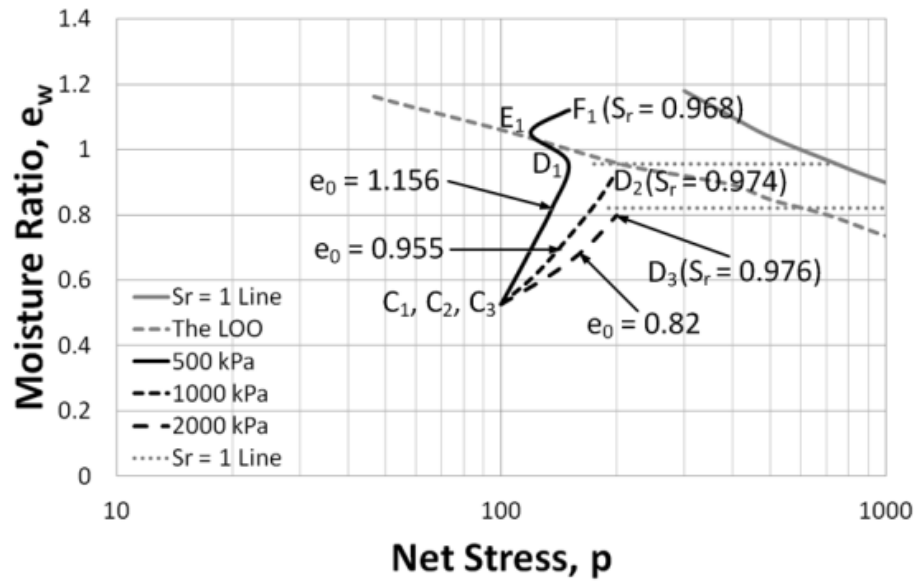
(q) Specimen of 19.88% moisture content ($e_w = 0.527$) loaded to 500, 1000 and 2000 kPa and then unloaded to 100 kPa and then wetted to 42.30% moisture content ($e_w = 1.120$) ($S_r = 0.968$ and $e_0 = 1.156$), 35.10% moisture content ($e_w = 0.930$) ($S_r = 0.974$ and $e_0 = 0.955$) and 30.20% moisture content ($e_w = 0.800$) ($S_r = 0.976$ and $e_0 = 0.82$) respectively at constant volume [Test Identity => SC – EK – SPT – 4, 5 & 6]
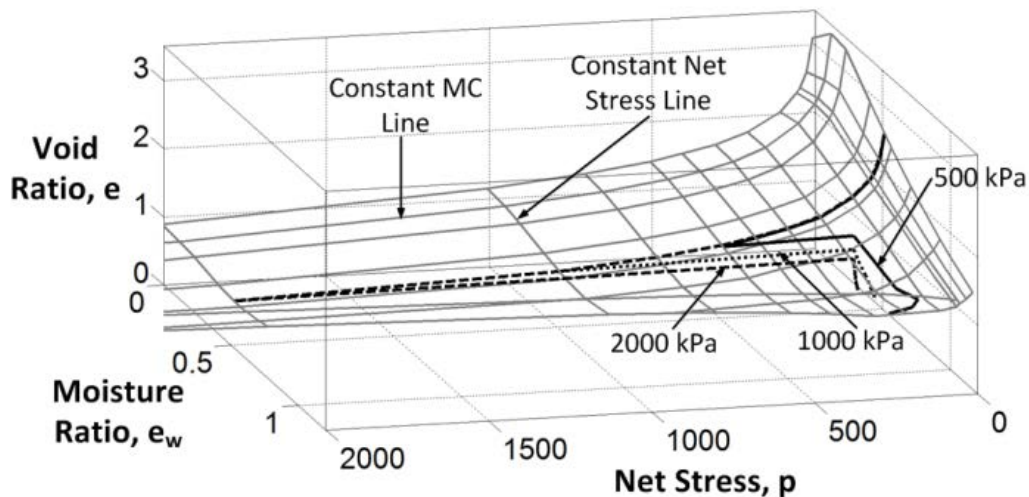
(r) 3-D view of state path test (q)

Figure 4-20: Constant volume wetting state path tests for the kaolin soil
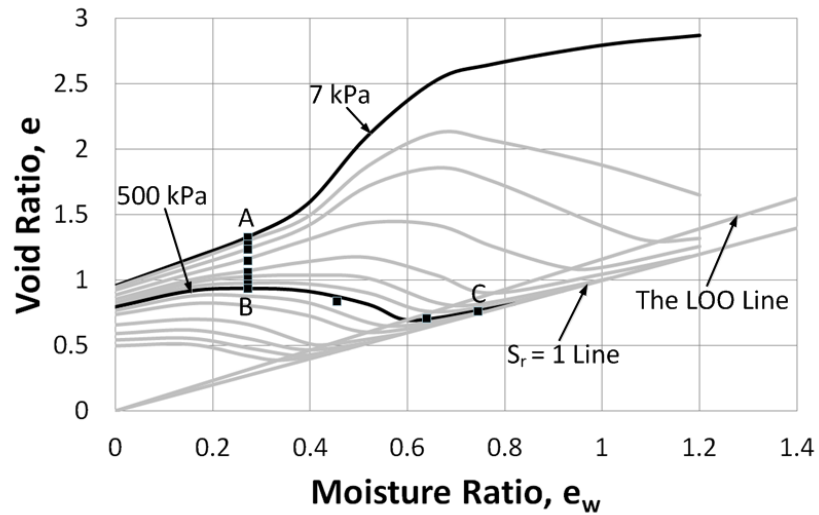
(a) Loading at 10.35% moisture content ($e_w = 0.271$) to 500 kPa stress and then wetted to 28.38% moisture content ($e_w = 0.743$) [Test Identity => SC – MC – LW – 1]
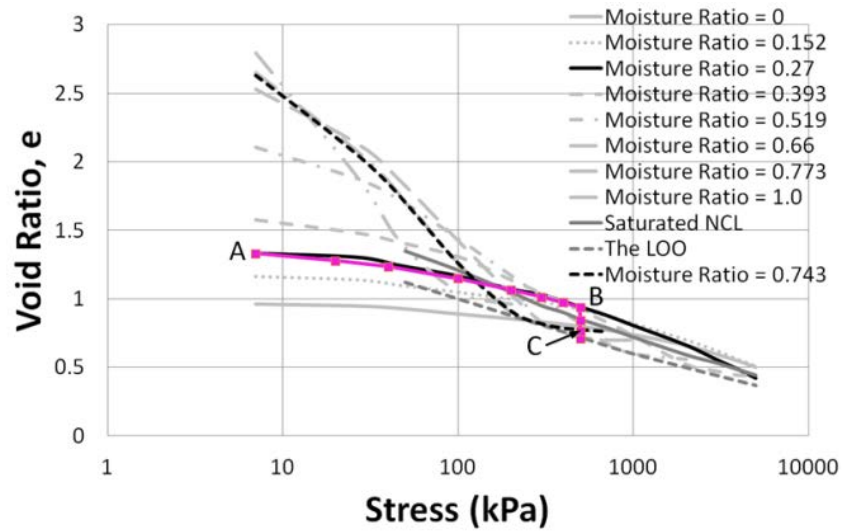
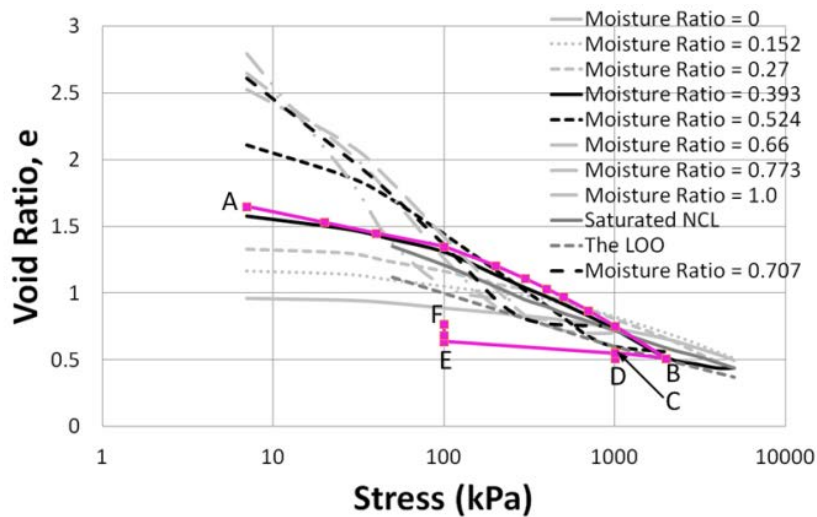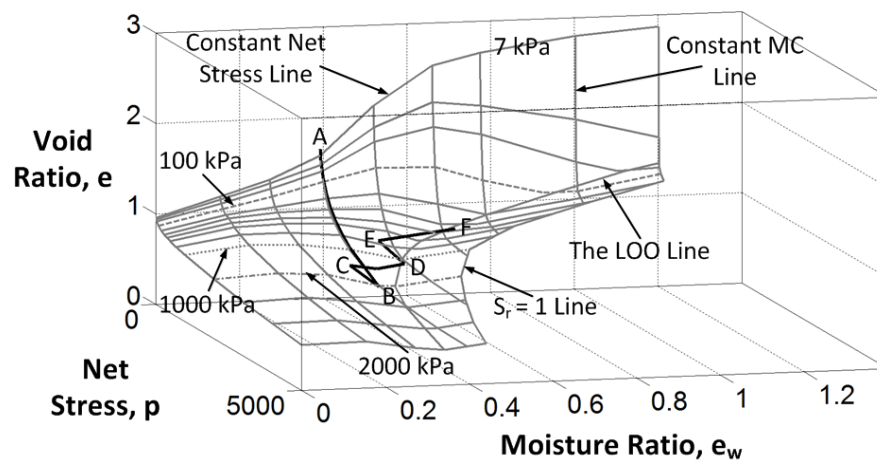**(b)** $e - \log p$ relationship of state path test (a)
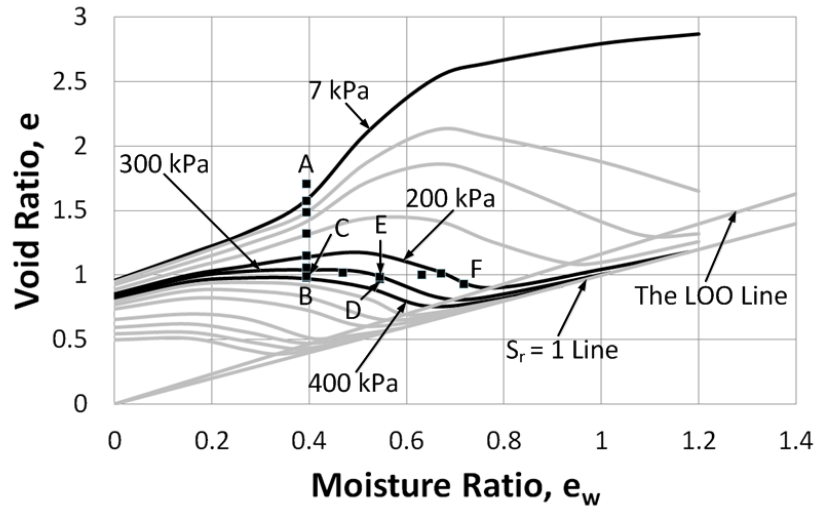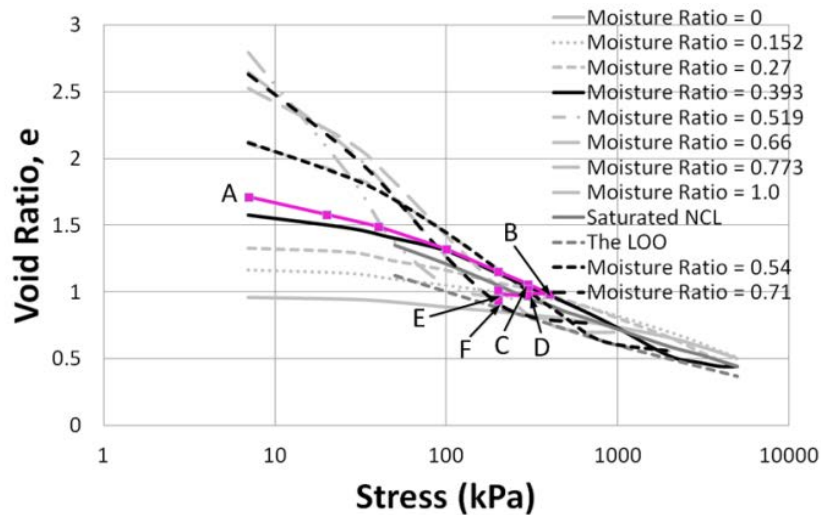

(c) 3-D view of state path test (a)

(d) Loading at 10.35% moisture content ($e_w = 0.271$) to 200 kPa stress and then wetted to 27.95% moisture content ($e_w = 0.732$) [Test Identity => SC – MC – LW – 2]

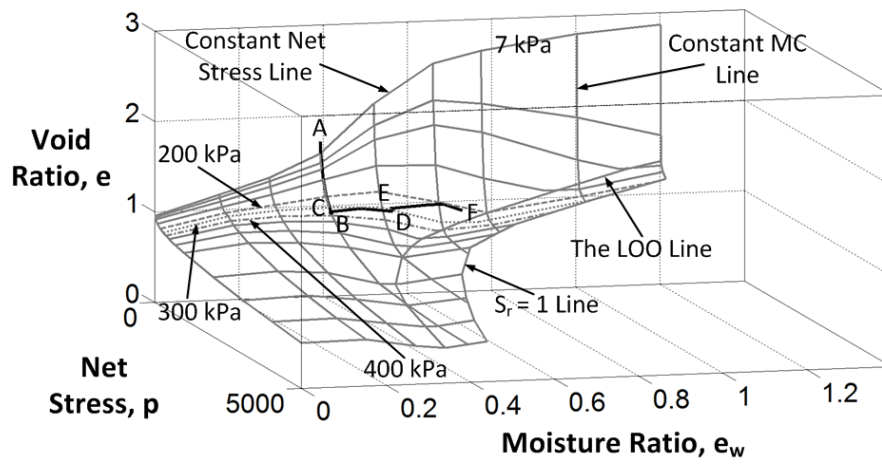**(e)** $e – \log p$ relationship of state path test (d)
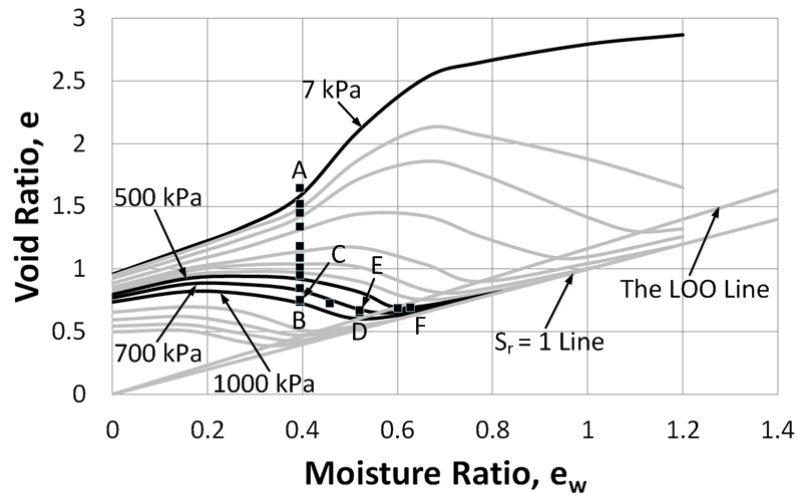

(f) 3-D view of state path test (d)

Figure 4-21: Loading/wetting state path tests for the Merri Creek soil

(a) Loading at 15.0% moisture content ($e_w = 0.393$) to 1000 kPa stress and then wetted to 20.24% moisture content ($e_w = 0.530$) and then loaded to 2000 kPa stress [Test Identity => SC – MC – LWL – 1]
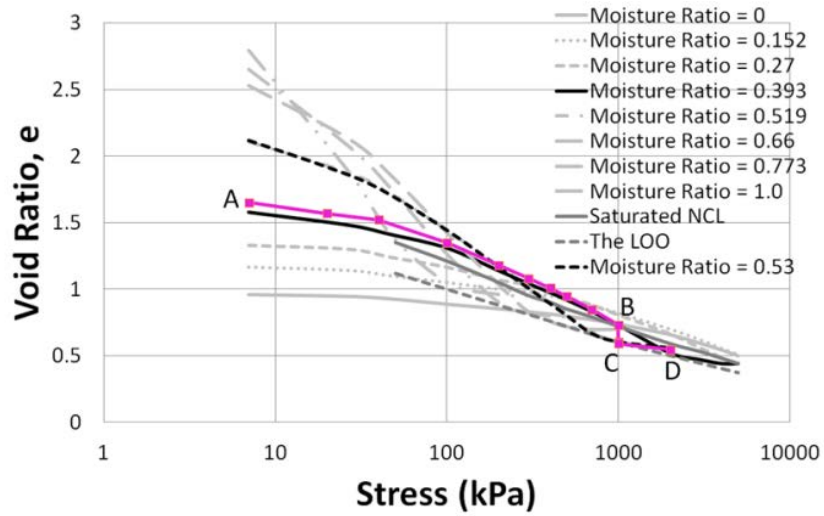
(b) $e – \log p$ relationship of state path test (a)
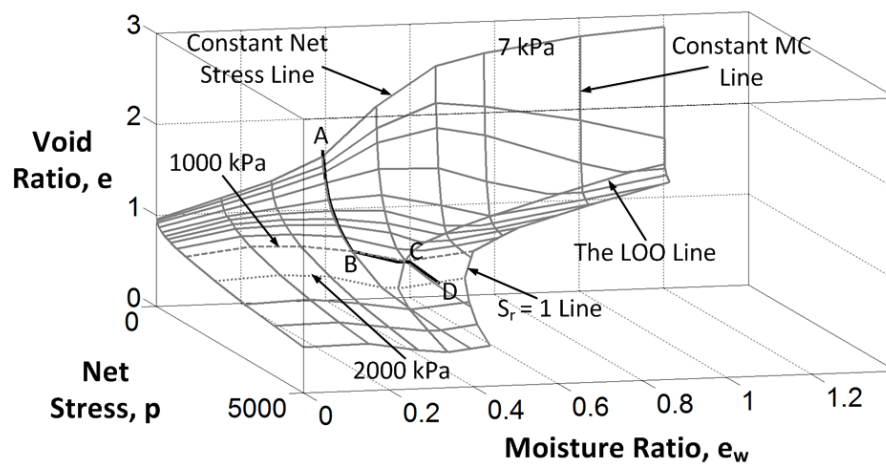
(c) 3-D view of state path test (a)

Figure 4-22: Loading/wetting/loading state path tests for the Merri Creek soil
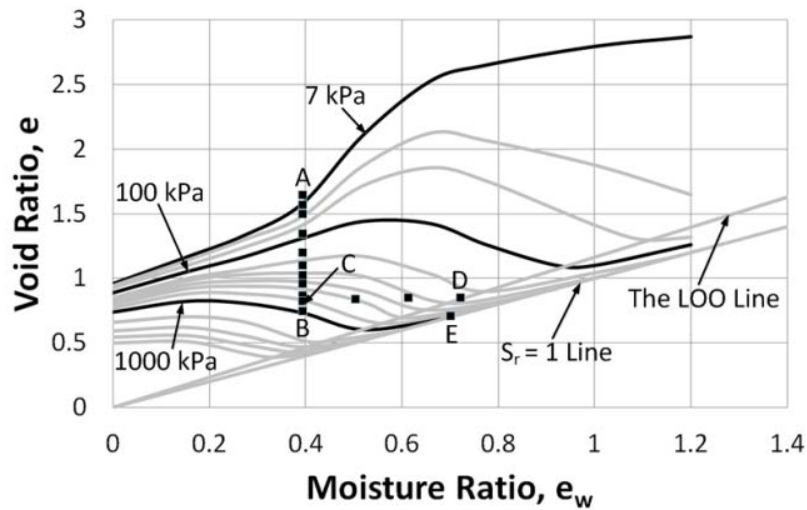
(a) Loading at 15.0% moisture content ($e_w = 0.393$) to 1000 kPa stress and then unloaded to 100 kPa stress and then wetted to 27.52% moisture content ($e_w = 0.721$) and then loaded to 1000 kPa stress [Test Identity => SC – MC – LUWL – 1]
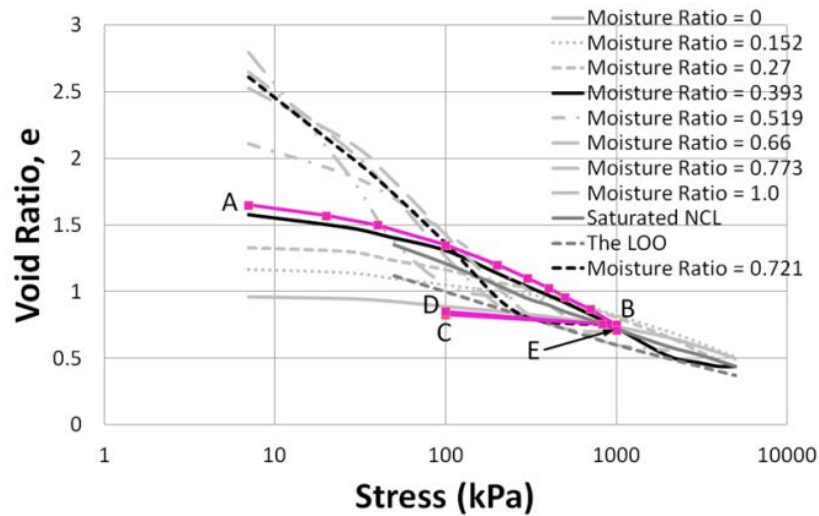
(b) $e - \log p$ relationship of state path test (a)
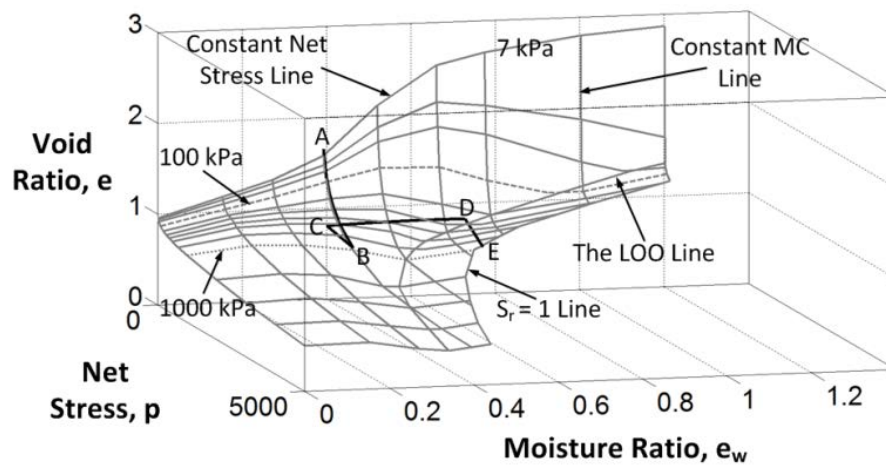
(c) 3-D view of state path test (a)

Figure 4-23: Loading/unloading/wetting/loading state path tests for the Merri Creek soil
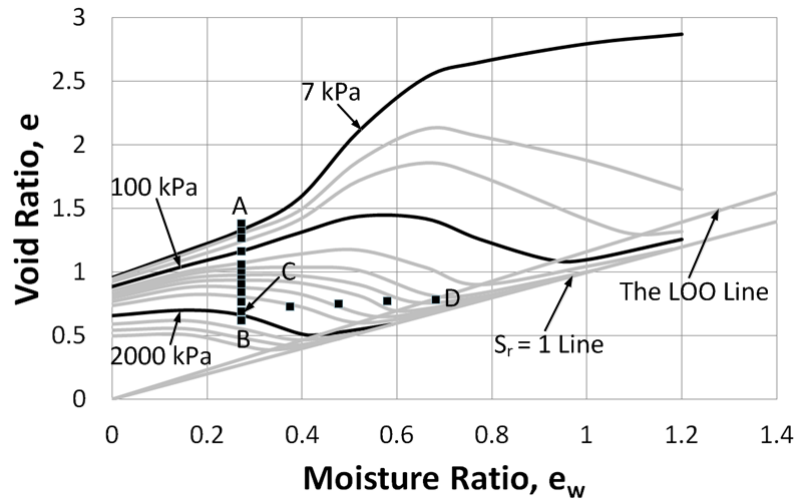
(a) Loading at 10.35% moisture content ($e_w = 0.271$) to 2000 kPa stress and then unloaded to 100 kPa stress and then wetted to 26.0% moisture content ($e_w = 0.681$) [Test Identity => SC – MC – LUW – 1]
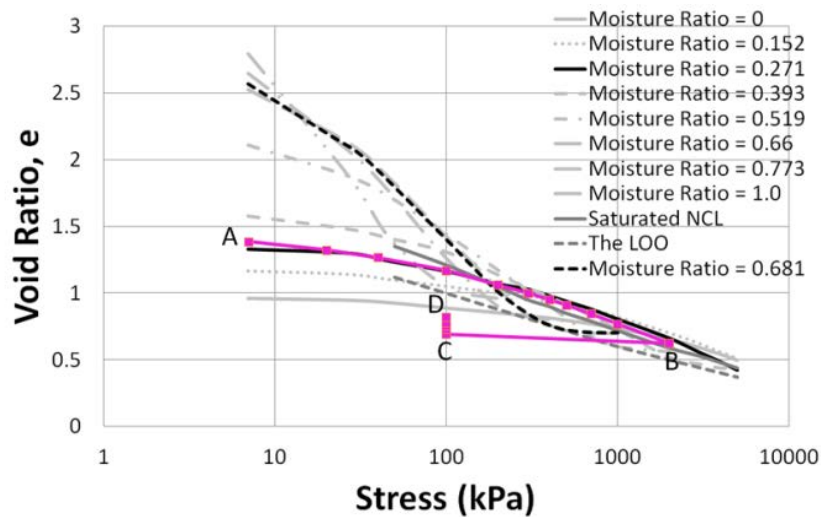
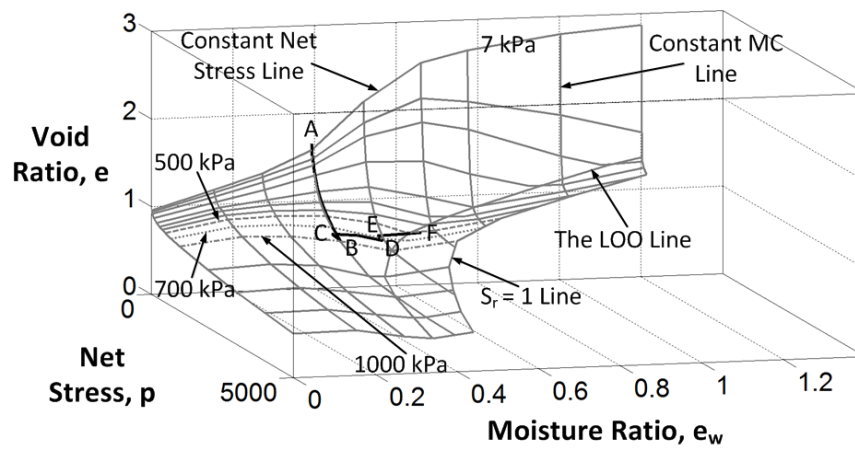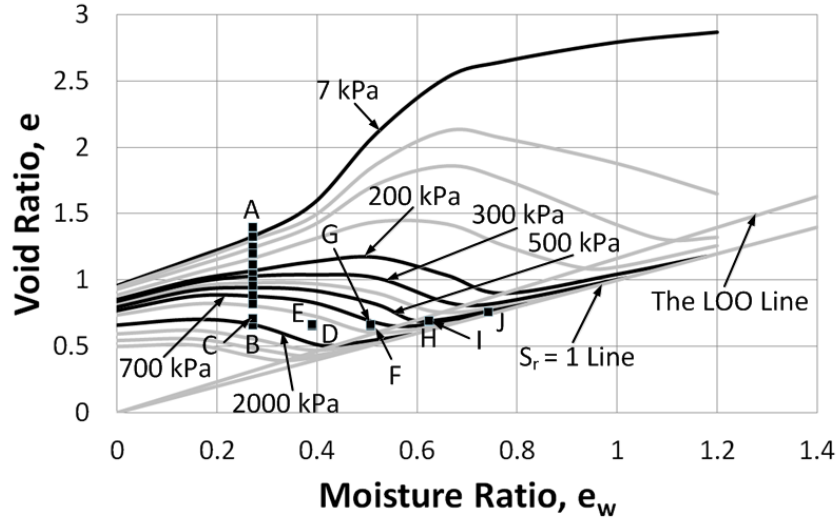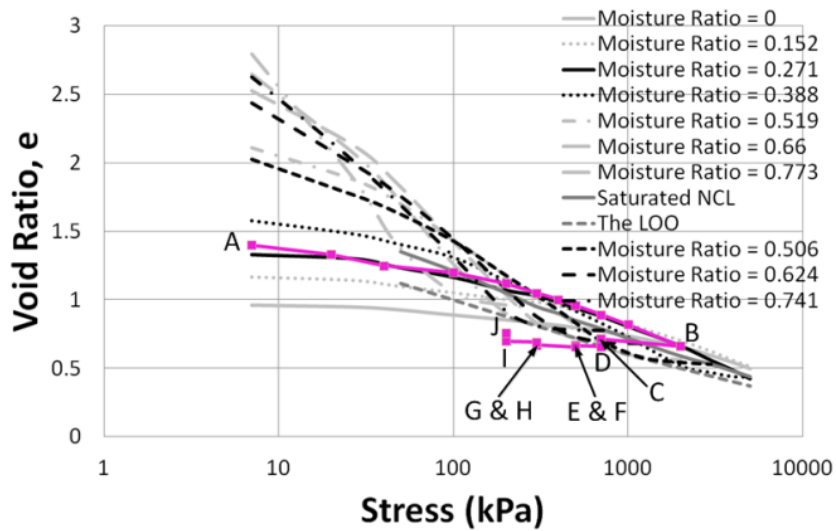

(b) $e - \log p$ relationship of state path test (a)
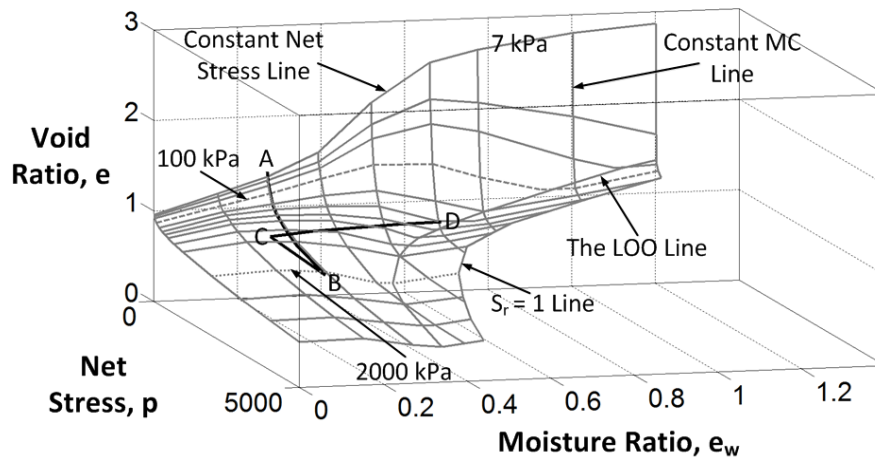
(c) 3-D view of state path test (a)

(d) Loading at 10.35% moisture content ($e_w = 0.271$) to 1000 kPa stress and then unloaded to 400 kPa stress and then wetted to 17.42% moisture content ($e_w = 0.456$) [Test Identity => SC – MC – LUW – 2]
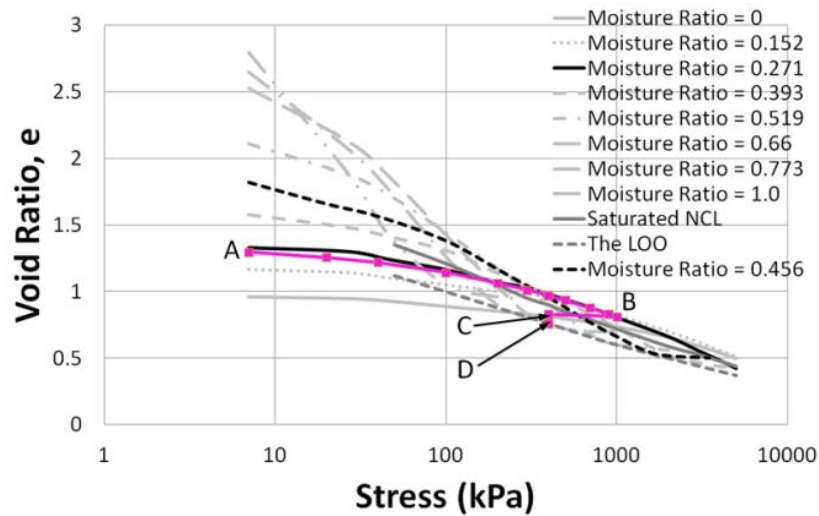
(e) e – log p relationship of state path test (d)
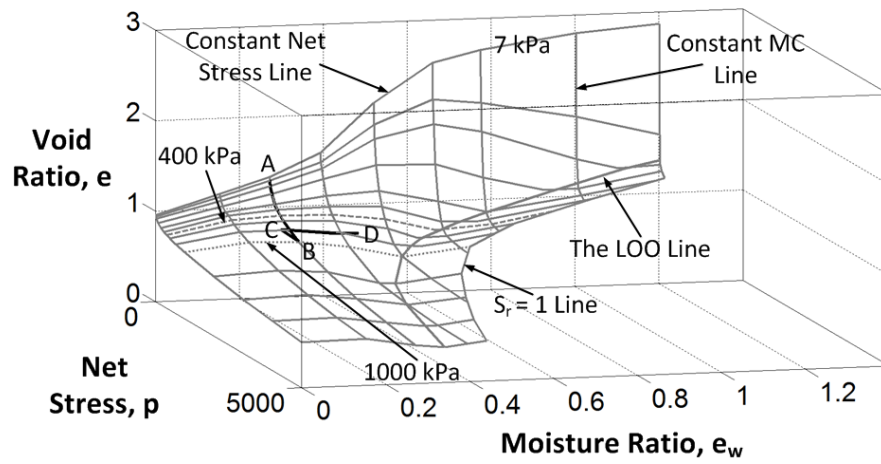
(f) 3-D view of state path test (d)

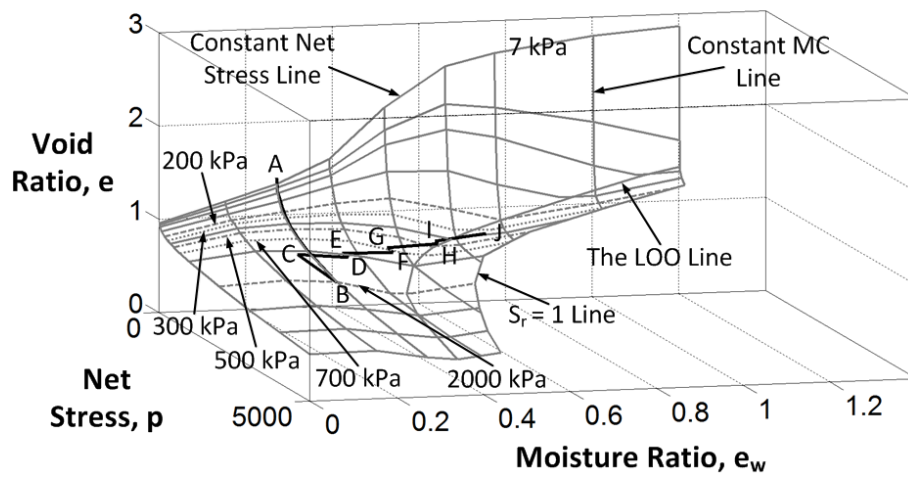**Figure 4-24:** Loading/unloading/wetting state path tests for the Merri Creek soil
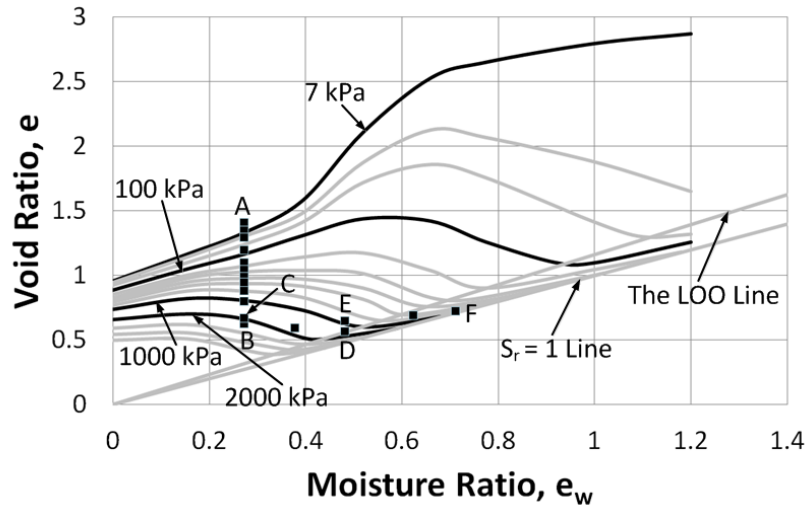
(a) Loading at 10.35% moisture content ($e_w = 0.271$) to 2000 kPa stress and then unloaded to 1000 kPa stress and then wetted to 18.37% moisture content ($e_w = 0.481$) and then unloaded to 100 kPa stress and then wetted to 27.10% moisture content ($e_w = 0.710$) [Test Identity => SC – MC – LUWUW – 1]
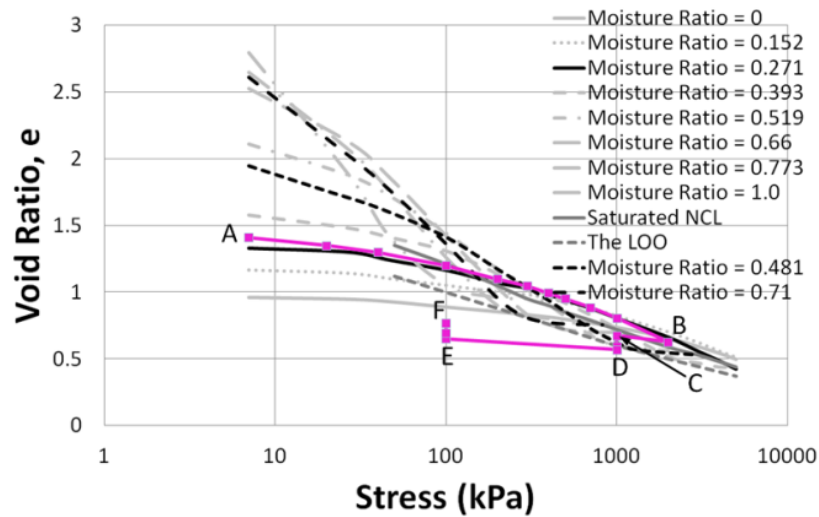
**(b)** $e - \log p$ relationship of state path test (a)
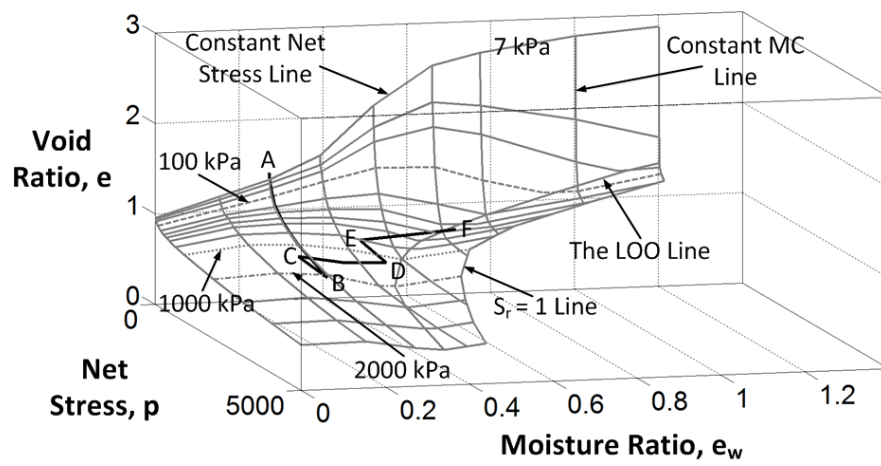
(c) 3-D view of state path test (a)
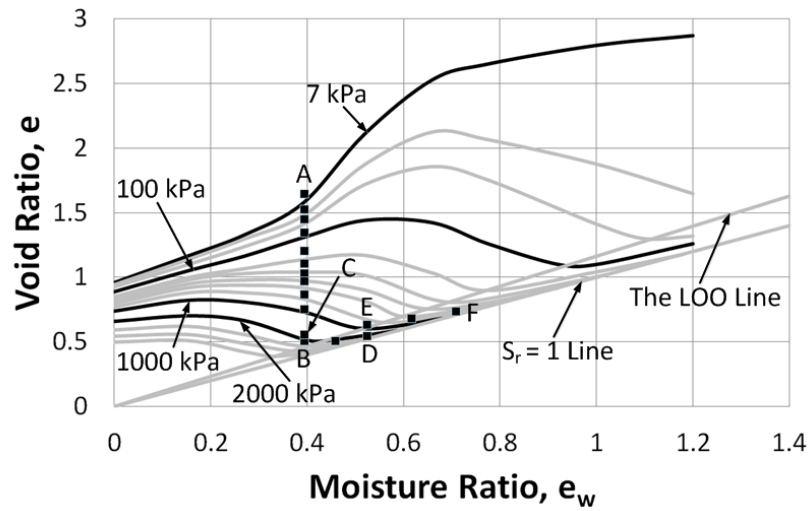
(d) Loading at 15.0% moisture content ($e_w = 0.393$) to 2000 kPa stress and then unloaded to 1000 kPa stress and then wetted to 20.0% moisture content ($e_w = 0.524$) and then unloaded to 100 kPa stress and then wetted to 27.0% moisture content ($e_w = 0.707$) [Test Identity => SC – MC – LUWUW – 2]


(e) $e - \log p$ relationship of state path test (d)
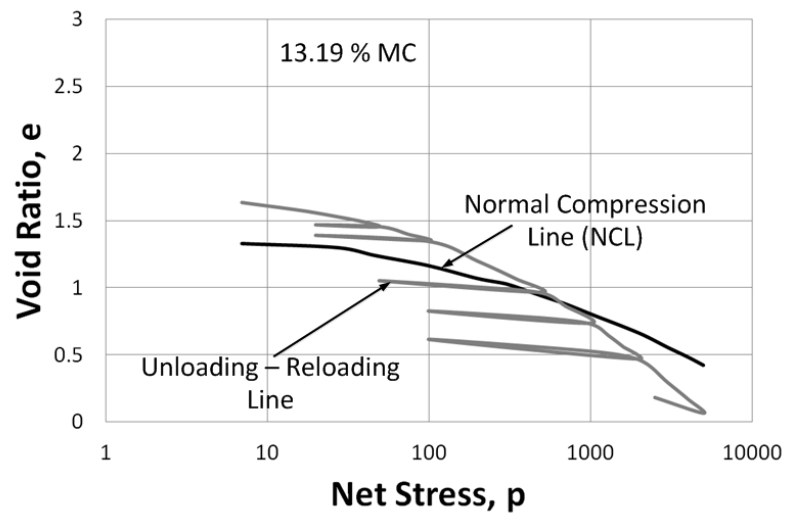
(f) 3-D view of state path test (d)

(g) Loading at 15.0 % moisture content ($e_w = 0.393$) to 400 kPa stress and then unloaded to 300 kPa stress and then wetted to 20.78% moisture content ($e_w = 0.544$) and then unloaded to 200 kPa stress and then wetted to 27.35% moisture content ($e_w = 0.717$) [Test Identity => SC – MC – LUWUW – 3]

(h) $e - \log p$ relationship of state path test (g)

(i) 3-D view of state path test (g)

(j) Loading at 15.0 % moisture content ($e_w = 0.393$) to 1000 kPa stress and then unloaded to 700 kPa stress and then wetted to 19.82% moisture content ($e_w = 0.519$) and then unloaded to 500 kPa stress and then wetted to 23.92% moisture content ($e_w = 0.627$) [Test Identity => SC – MC – LUWUW – 4]
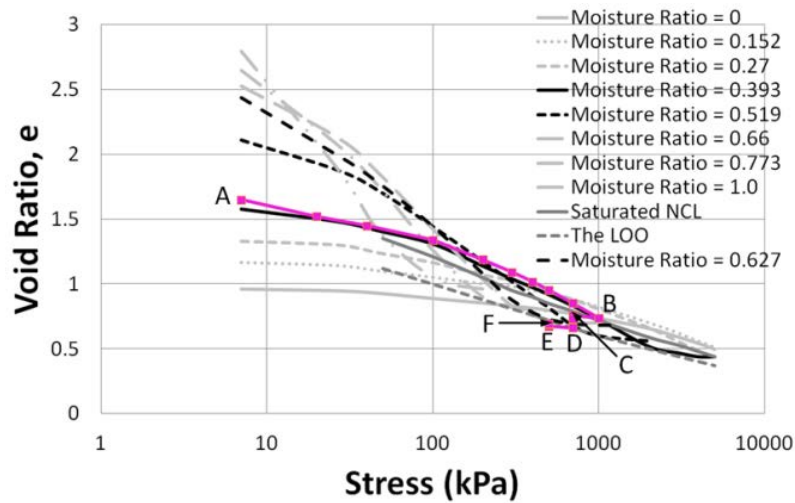
(k) $e - \log p$ relationship of state path test (j)

(l) 3-D view of state path test (j)

Figure 4-25: Loading/unloading/wetting/unloading/wetting state path tests for the Merri Creek soil

(a) Loading at 10.35% moisture content ($e_w = 0.271$) to 2000 kPa stress and then unloaded to 700 kPa stress and then wetted to 14.83% moisture content ($e_w = 0.388$) and then unloaded to 500 kPa stress and then wetted to 19.32% moisture content ($e_w = 0.506$) and then unloaded to 300 kPa stress and then wetted to 23.80% moisture content ($e_w = 0.624$) and then unloaded to 200 kPa stress and then wetted to 28.28% moisture content ($e_w = 0.741$) [Test Identity => SC – MC – LUWUWUWUW – 1]

(b) $e – \log p$ relationship of state path test (a)

(c) 3-D view of state path test (a)

Figure 4-26: Loading/unloading/wetting/unloading/wetting/unloading/wetting/unloading /wetting state path tests for the Merri Creek soil
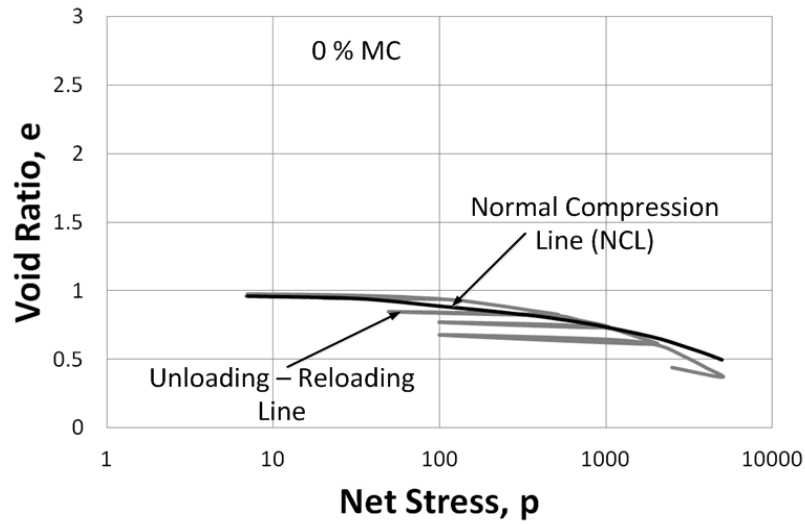
(a) 0% moisture content ($e_w = 0$) soil specimen
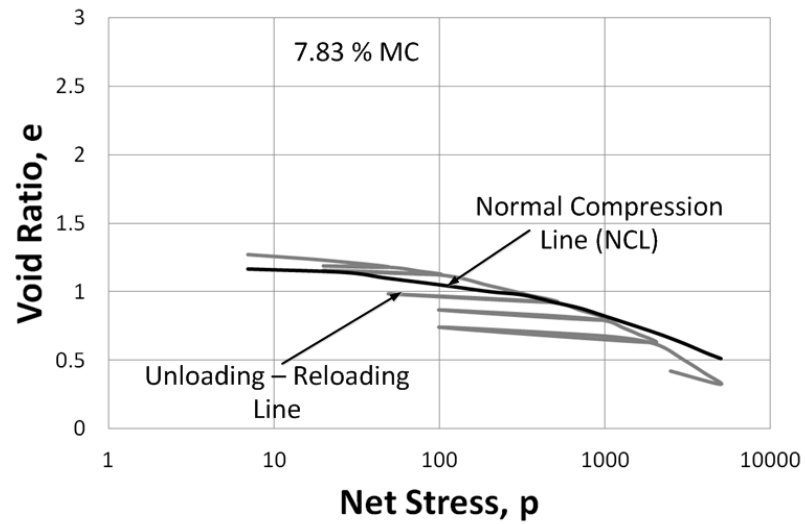
(b) 7.83% moisture content ($e_w = 0.205$) soil specimen

(c) 13.19% moisture content ($e_w = 0.346$) soil specimen
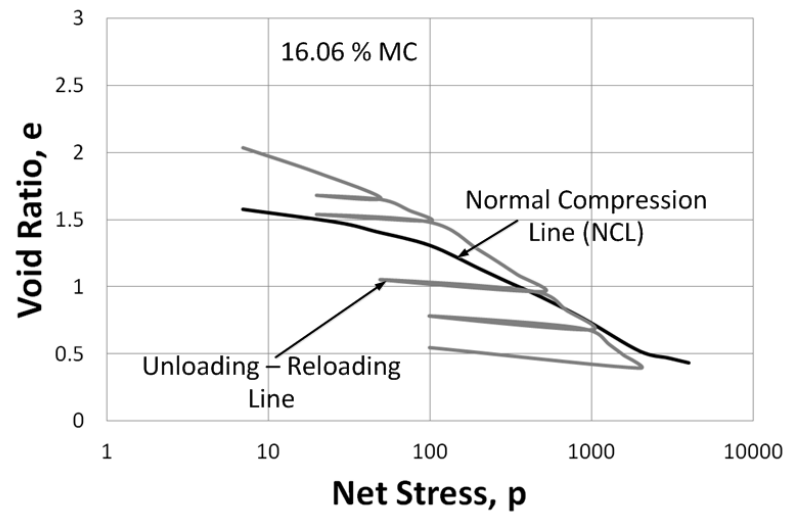
(d) 16.06% moisture content ($e_w = 0.421$) soil specimen
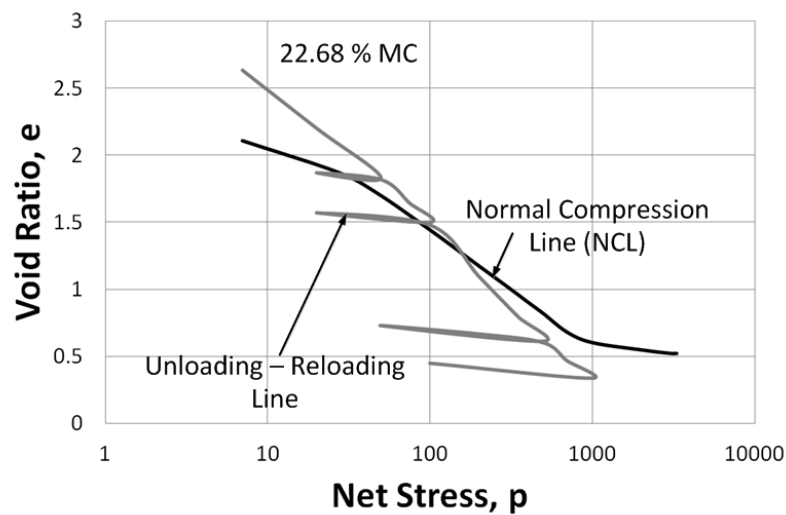
(e) 22.68% moisture content ($e_w = 0.594$) soil specimen

Figure 4-27: Loading/unloading/reloading state path tests for the Merri Creek soil
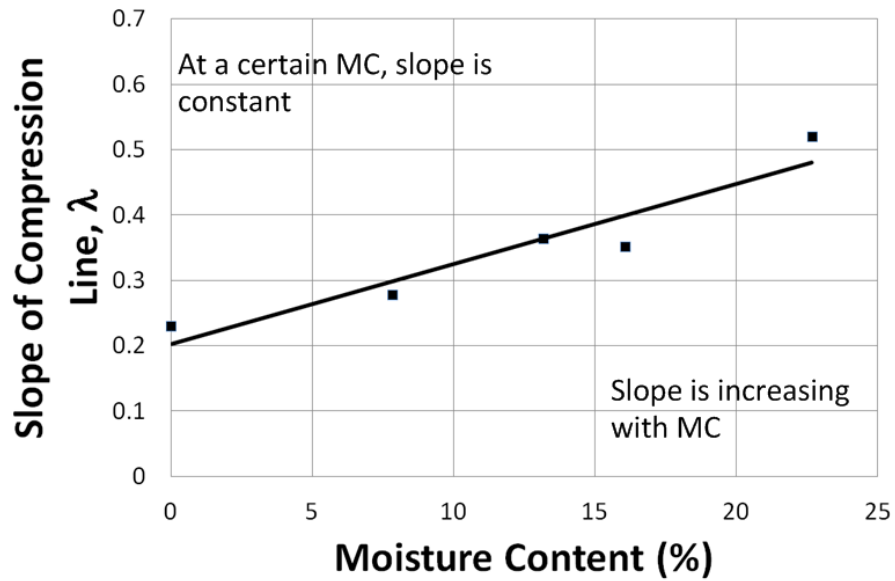
(a) Gradient of compression line (λ) versus moisture content
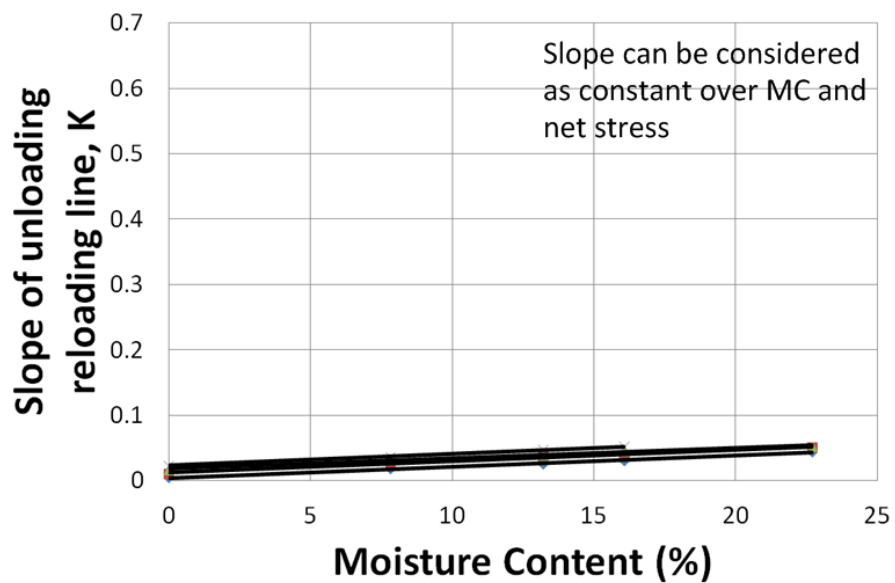
(b) Gradient of recompression line (κ) versus moisture content

Figure 4-28: Relationship of slope of: **(a)** compression line (λ); **(b)** recompression line (κ) with moisture content for the Merri Creek soil
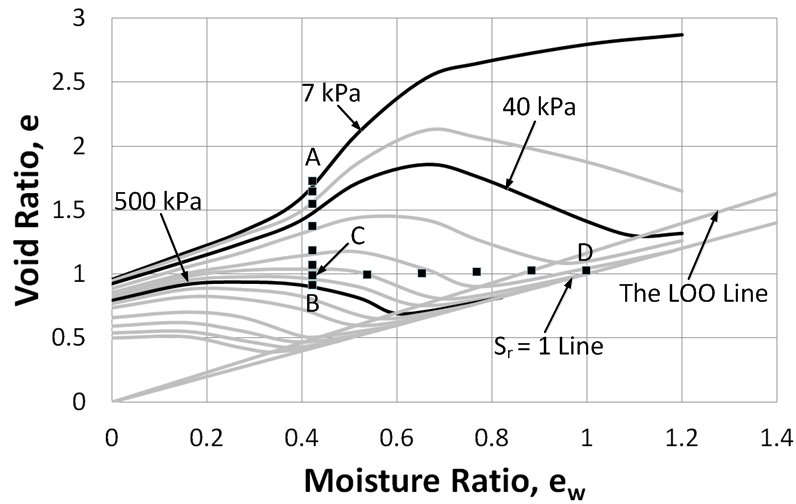
(a) Loading at 16.06% moisture content ($e_w = 0.421$) to 500 kPa stress and then unloaded to 40 kPa stress and then wetted to 38.06% moisture content ($e_w = 0.997$) [Test Identity => SC – MC – CPT – 1 or SC – MC – LUW – 3]
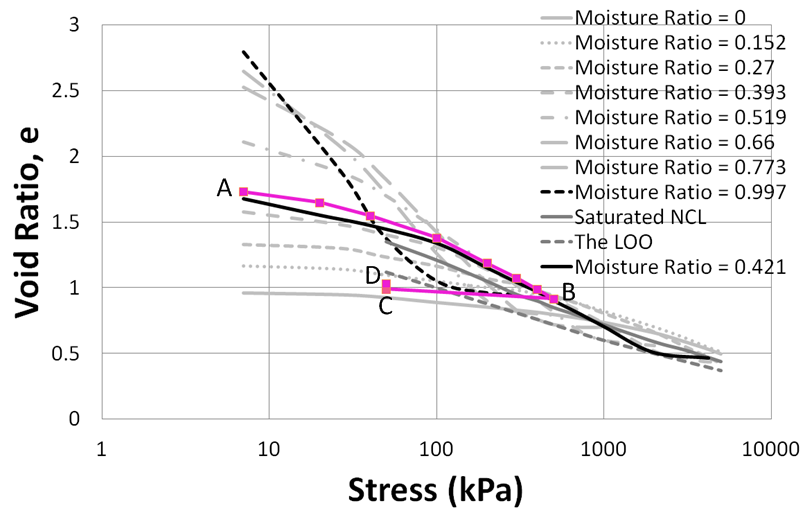
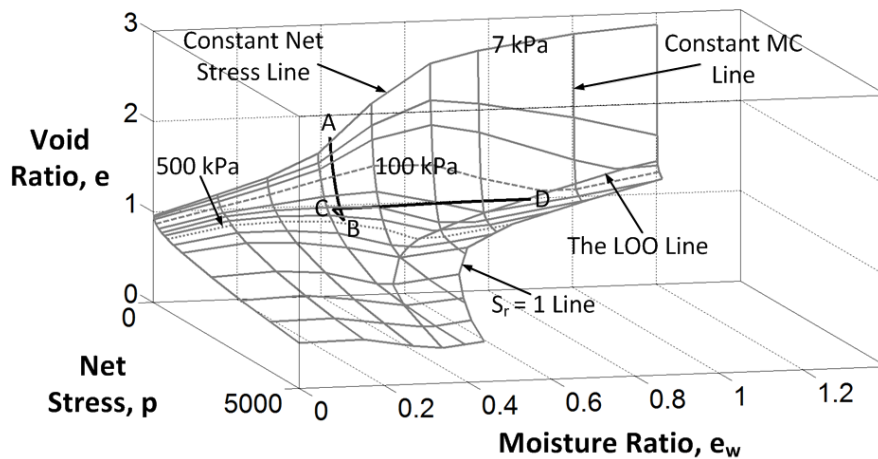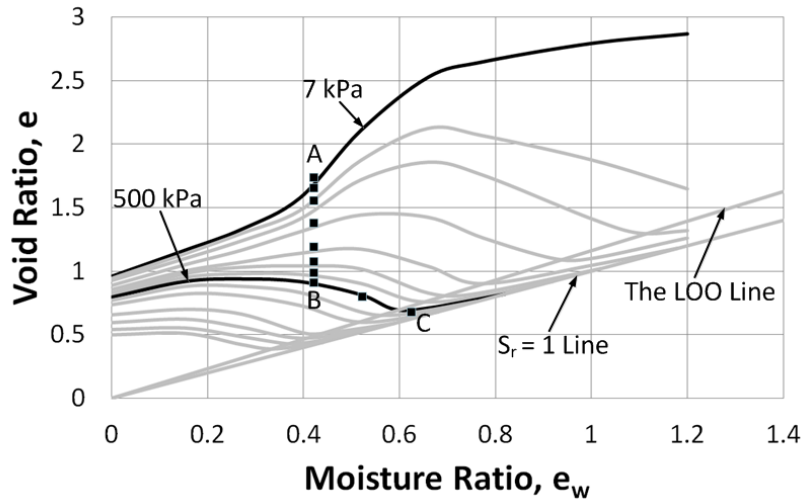**(b)** $e – \log p$ relationship of state path test (a)
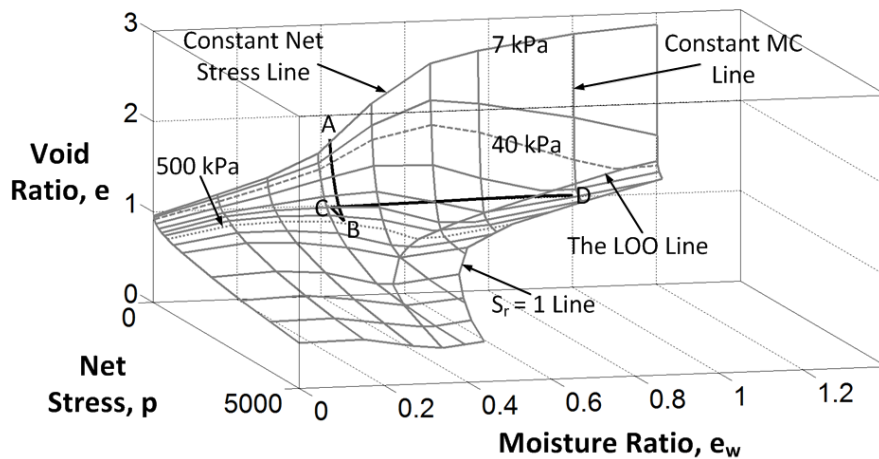
(c) 3-D view of state path test (a)
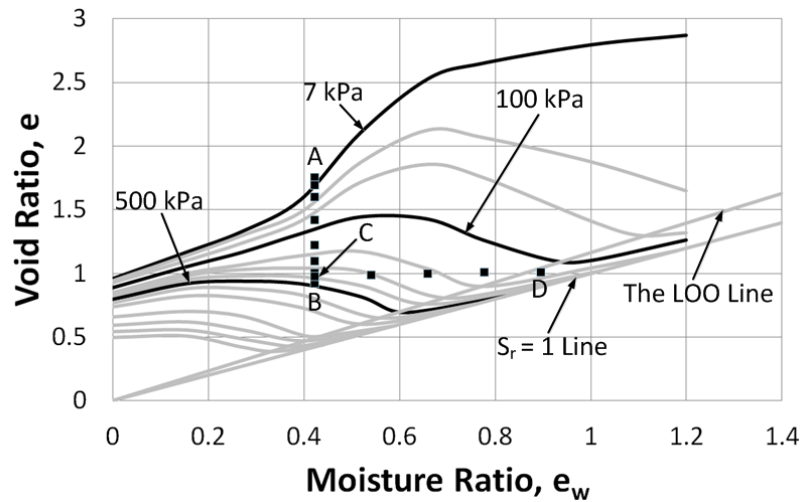
(d) Loading at 16.06% moisture content ($e_w = 0.421$) to 500 kPa stress and then unloaded to 100 kPa stress and then wetted to 34.14% moisture content ($e_w = 0.894$) [Test Identity => SC – MC – CPT – 2 or SC – MC – LUW – 4]
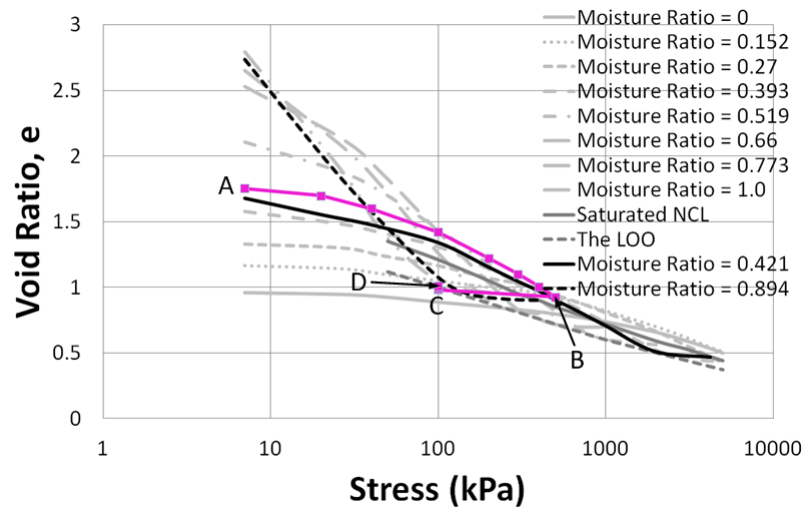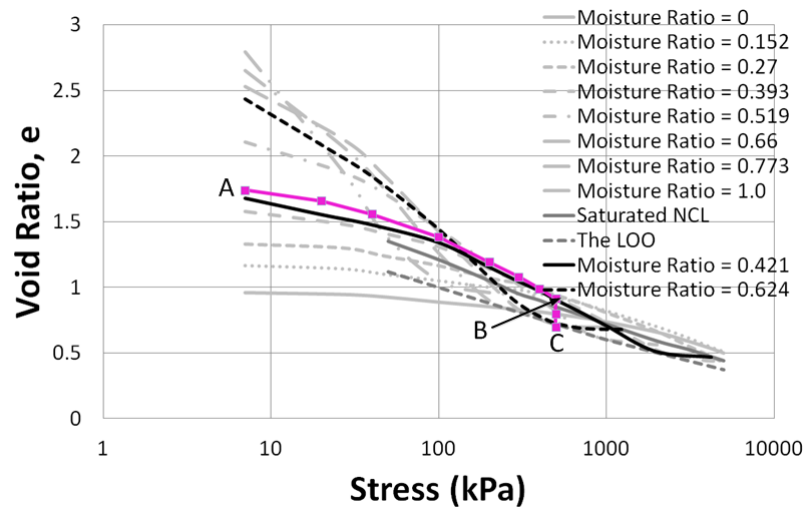

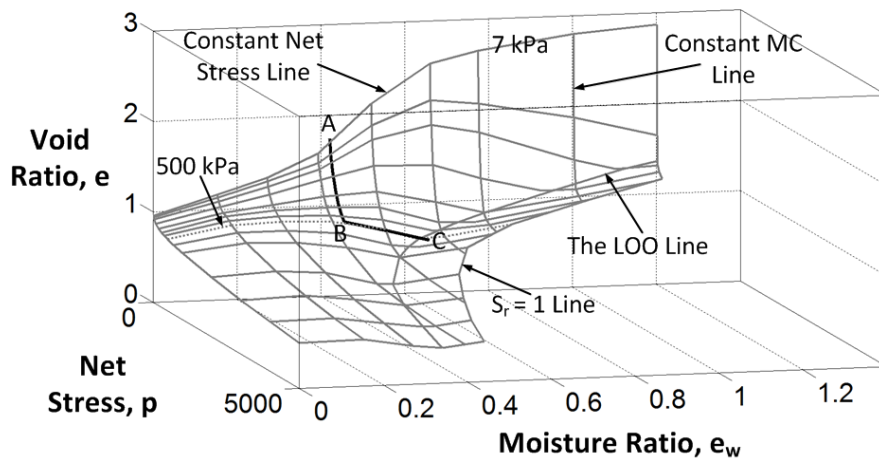**(e)** $e – \log p$ relationship of state path test (d)
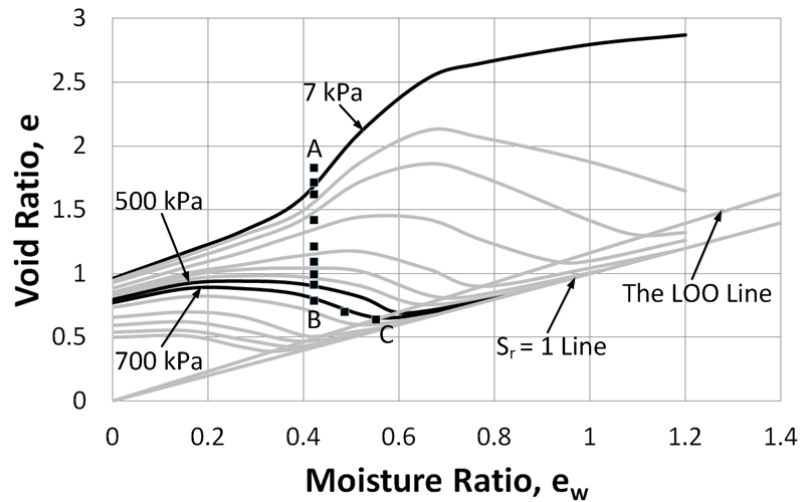

(f) 3-D view of state path test (d)

(g) Loading at 16.06% moisture content ($e_w = 0.421$) to 500 kPa stress and then wetted to 23.80% moisture content ($e_w = 0.624$) [Test Identity => SC – MC – CPT – 3 or SC – MC – LW – 3]
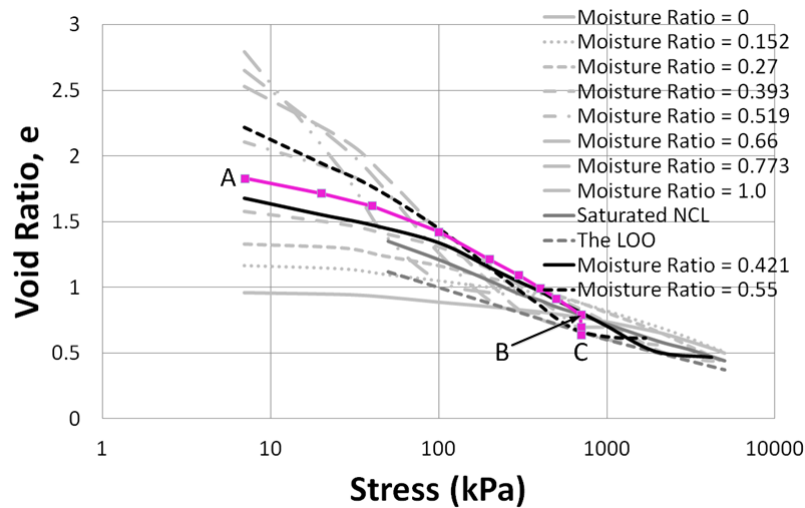

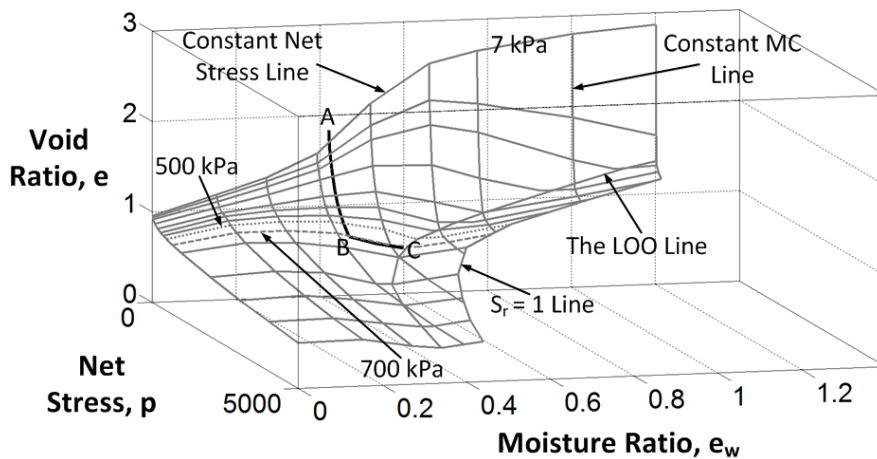**(h)** $e – \log p$ relationship of state path test (g)

(i) 3-D view of state path test (g)

(j) Loading at 16.06% moisture content ($e_w = 0.421$) to 700 kPa stress and then wetted to 21.0% moisture content ($e_w = 0.550$) [Test Identity => SC – MC – CPT – 4 or SC – MC – LW – 4]

(k) $e – \log p$ relationship of state path test (j)

(l) 3-D view of state path test (j)

(m) Loading at 16.06% moisture content ($e_w = 0.421$) to 1000 kPa stress and then wetted to 19.0% moisture content ($e_w = 0.500$) [Test Identity => SC – MC – CPT – 5 or SC – MC – LW – 5]
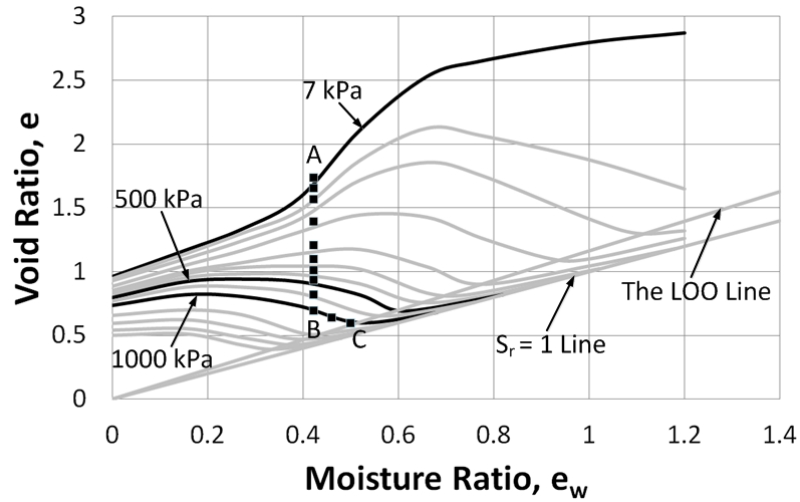

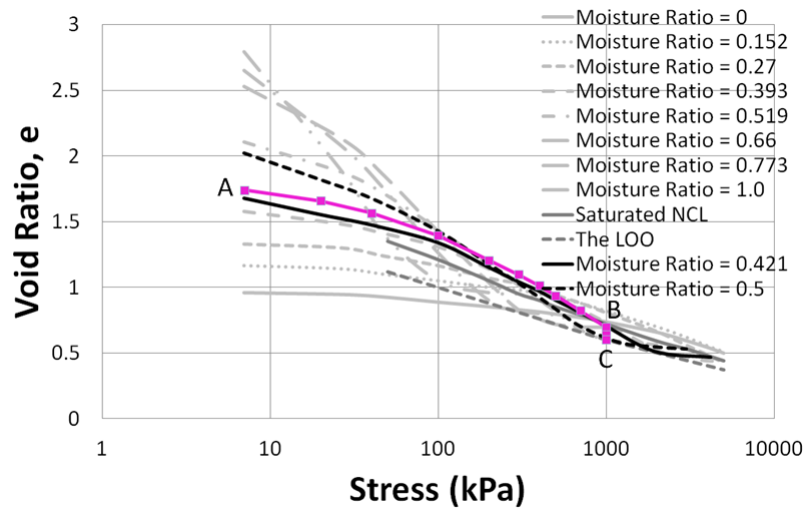(n) $e – \log p$ relationship of state path test (m)
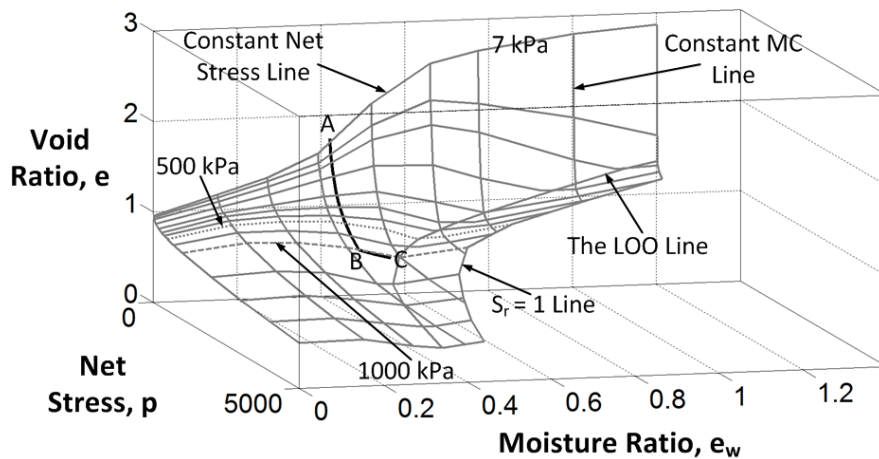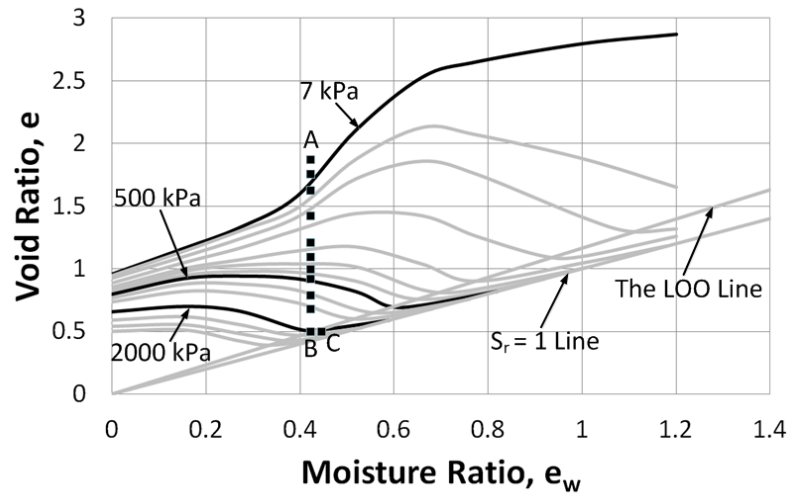

(o) 3-D view of state path test (m)

(p) Loading at 16.06% moisture content ($e_w = 0.421$) to 2000 kPa stress and then wetted to 17.0% moisture content ($e_w = 0.445$) [Test Identity => SC – MC – CPT – 6 or SC – MC – LW – 6]
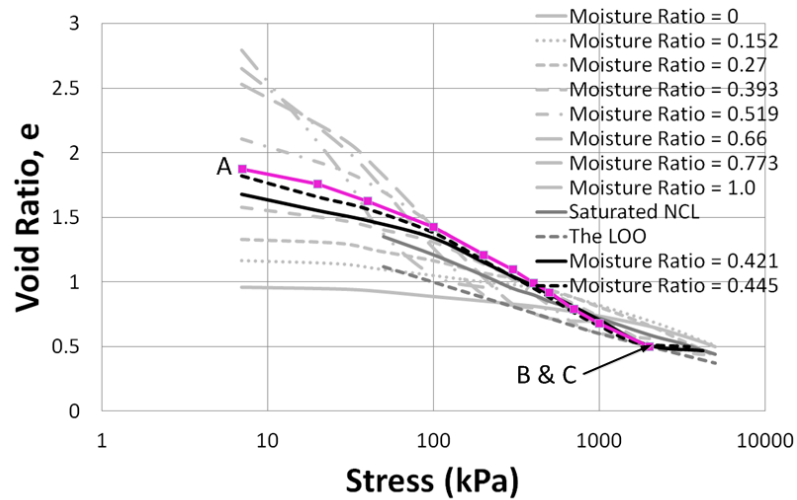

(q) e – $\log p$ relationship of state path test (p)
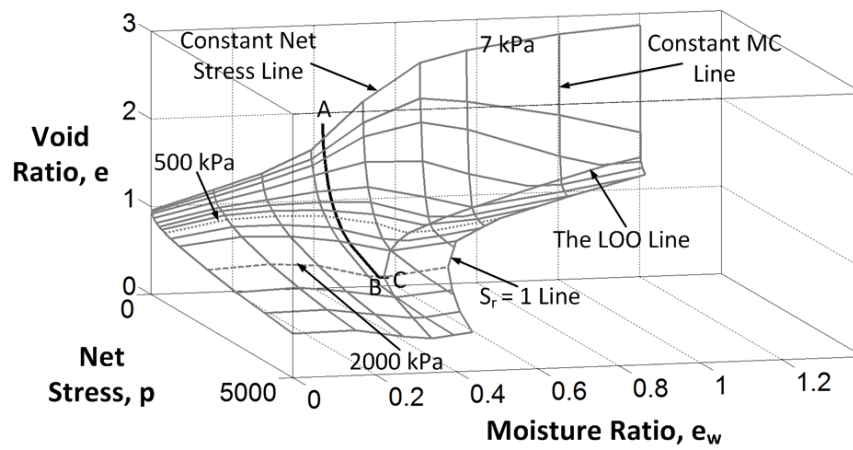
(r) 3-D view of state path test (p)

Figure 4-29: Various state path tests to examine collapse potentiality for the compacted Merri Creek soil
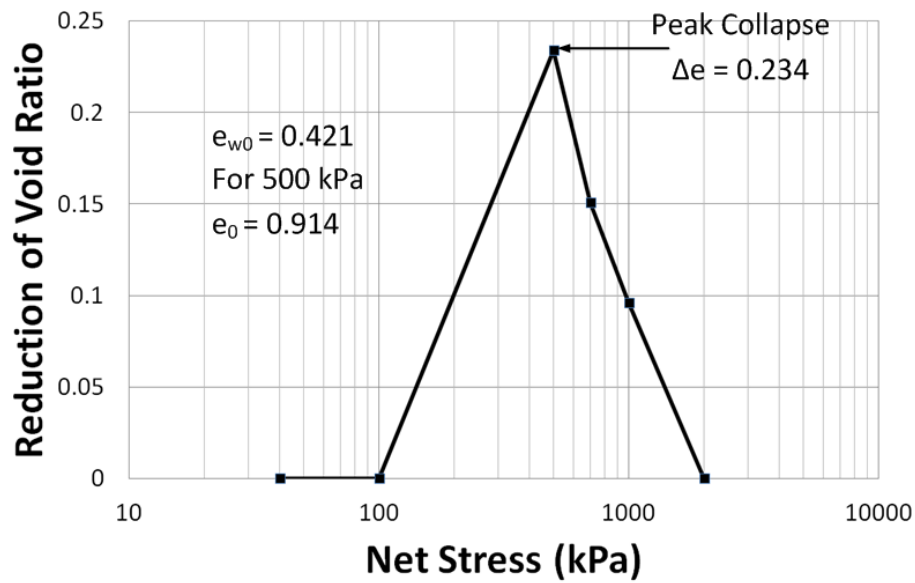
Figure 4-30: Collapse potential given as reduction of void ratio for the Merri Creek soil specimen with initial $e_{wo} = 0.421$ and $e_o = 0.914$ and a compaction stress of 500 kPa
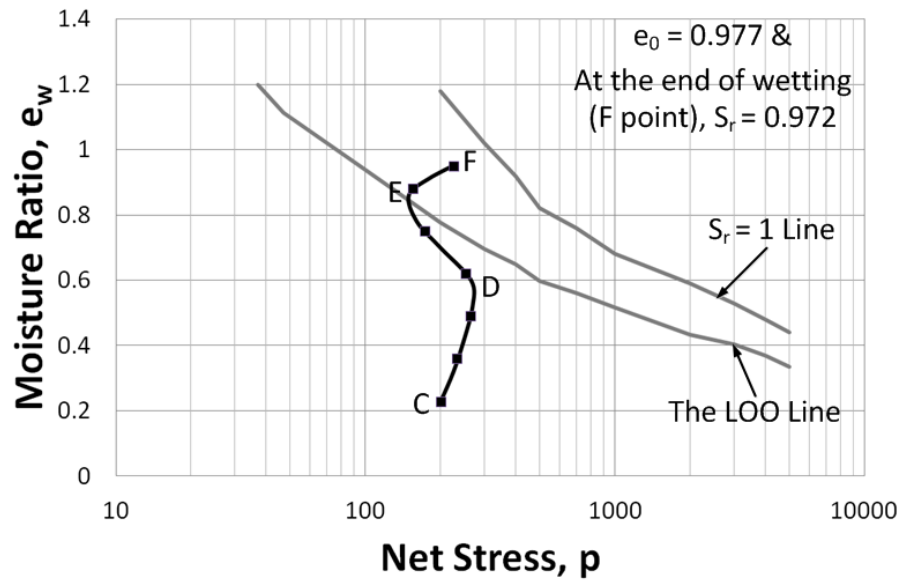
(a) Specimen of 8.69% moisture content ($e_w = 0.228$) loaded to 500 kPa stress and then unloaded to 200 kPa stress and then wetted to 36.26% moisture content ($e_w = 0.950$) ($S_r = 0.972$ and $e_0 = 0.977$) at constant volume [Test Identity => SC – MC – SPT – 1]
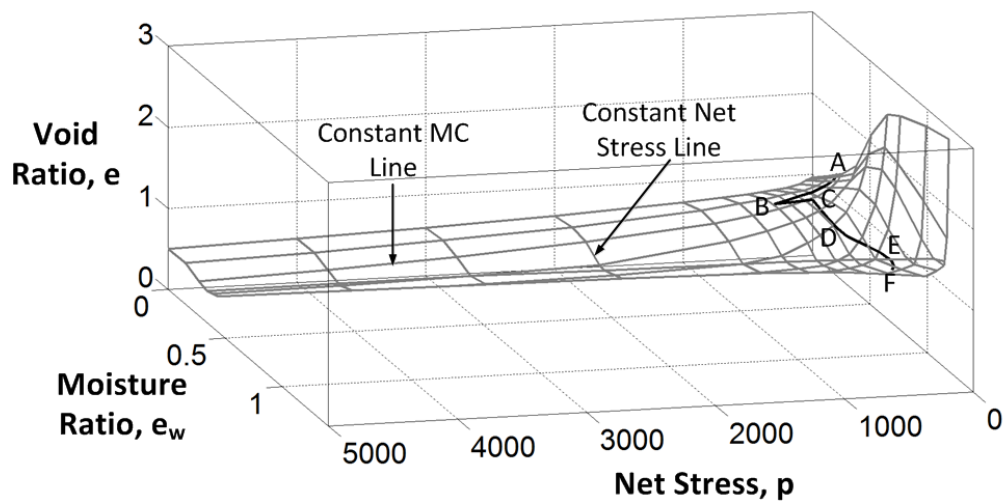
(b) 3-D view of state path test (a)
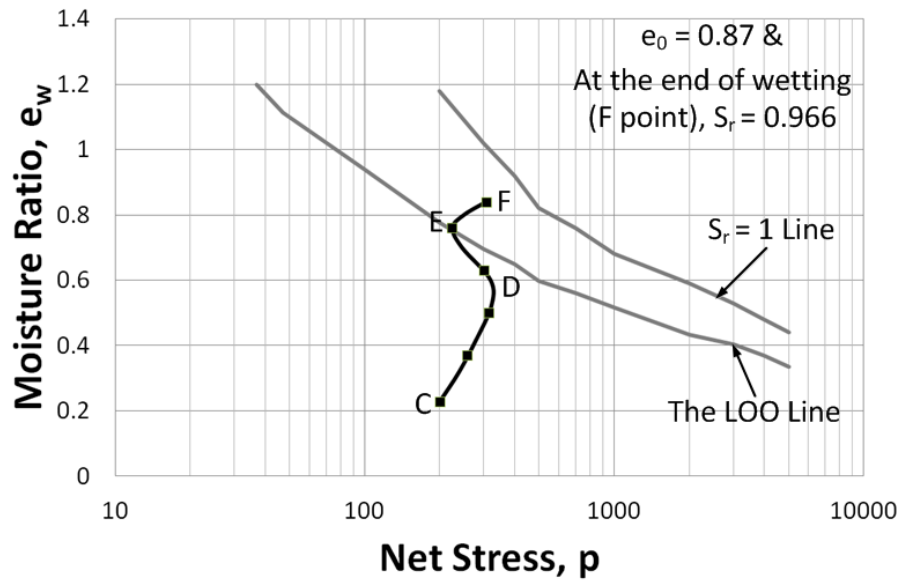
(c) Specimen of 8.69% moisture content ($e_w = 0.228$) loaded to 1000 kPa stress and then unloaded to 200 kPa stress and then wetted to 32.06% moisture content ($e_w = 0.840$) ($S_r = 0.966$ and $e_0 = 0.87$) at constant volume [Test Identity => SC – MC – SPT – 2]

(d) 3-D view of state path test (c)

(e) Specimen of 8.69% moisture content ($e_w = 0.228$) loaded to 2000 kPa stress and then unloaded to 200 kPa stress and then wetted to 27.48% moisture content ($e_w = 0.720$) ($S_r = 0.968$ and $e_0 = 0.744$) at constant volume [Test Identity => SC – MC – SPT – 3]

(f) 3-D view of state path test (e)

(g) Specimen of 14.87% moisture content ($e_w = 0.390$) loaded to 500 kPa stress and then unloaded to 200 kPa stress and then wetted to 35.50% moisture content ($e_w = 0.930$) ($S_r = 0.969$ and $e_0 = 0.96$) at constant volume [Test Identity => SC – MC – SPT – 4]

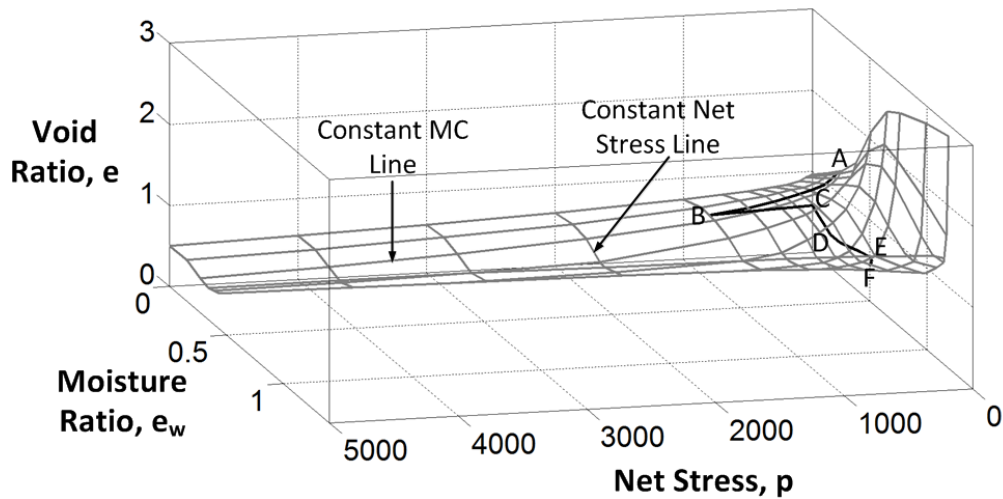**(h)** 3-D view of state path test (g)

(i) Specimen of 14.87% moisture content ($e_w = 0.390$) loaded to 1000 kPa stress and then unloaded to 200 kPa stress and then wetted to 28.63% moisture content ($e_w = 0.750$) ($S_r = 0.968$ and $e_0 = 0.775$) at constant volume [Test Identity => SC – MC – SPT – 5]
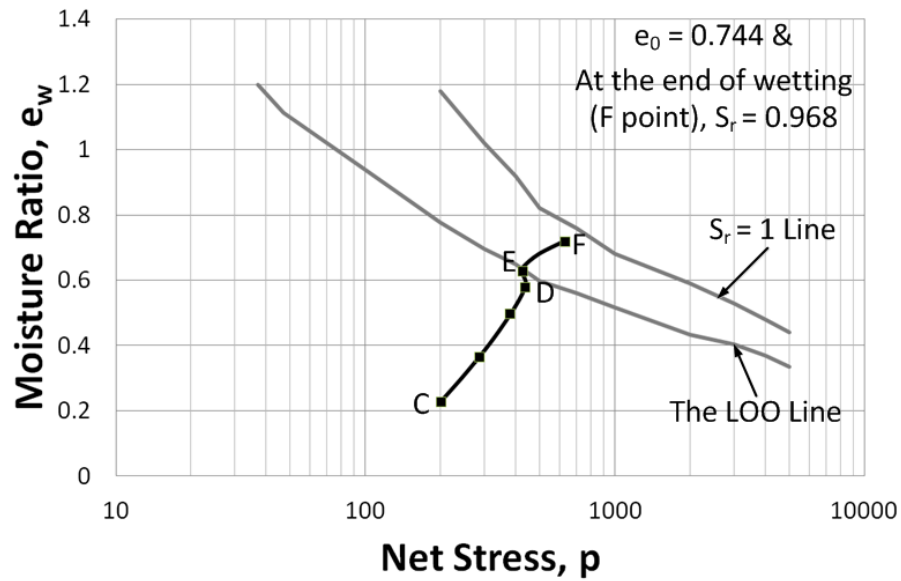

(j) 3-D view of state path test (i)

(k) Specimen of 14.87% moisture content (e_w = 0.390) loaded to 2000 kPa stress and then unloaded to 200 kPa stress and then wetted to 21.37% moisture content (e_w = 0.560) (S_r = 0.981 and e_0 = 0.571) at constant volume [Test Identity => SC – MC – SPT – 6]
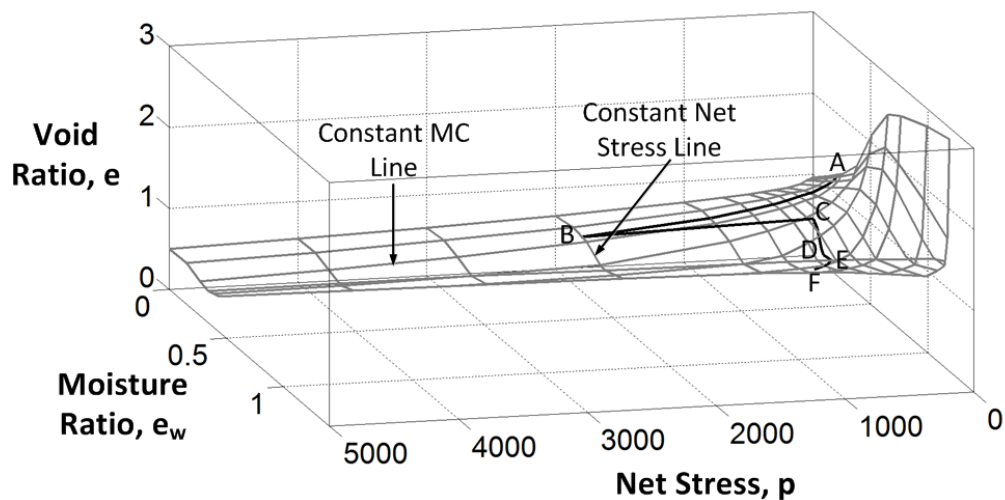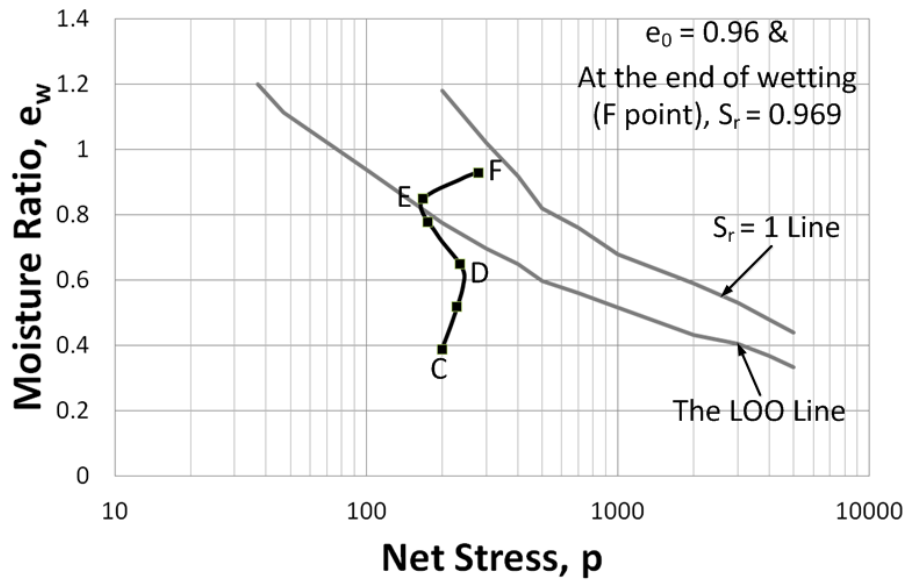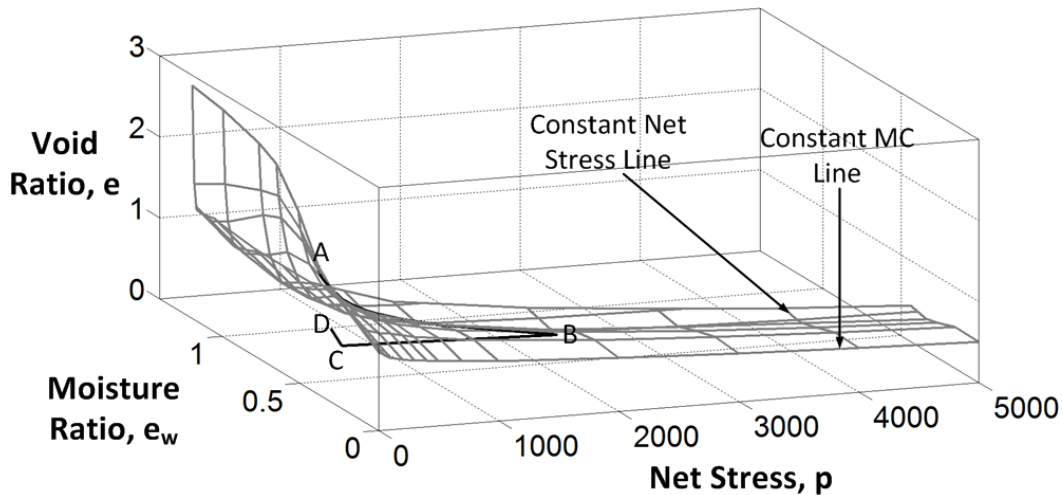

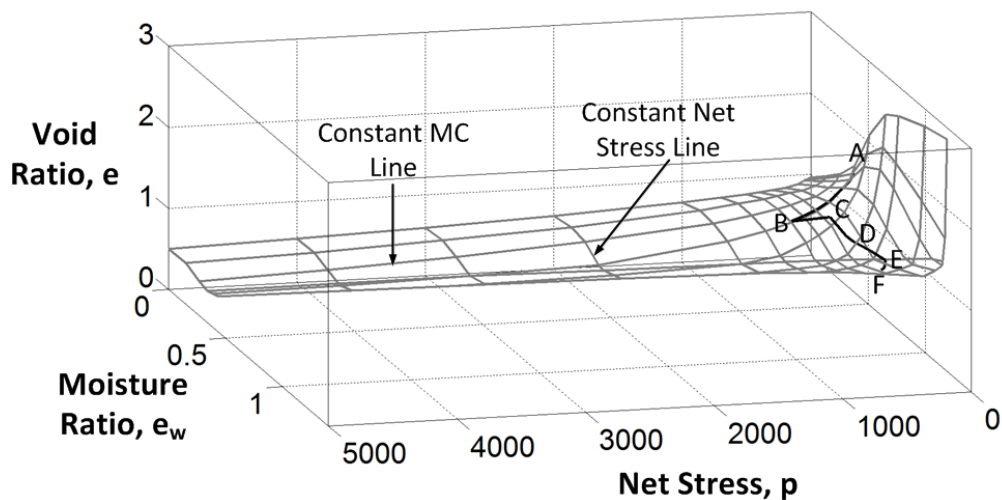**(l)** 3-D view of state path test (k)
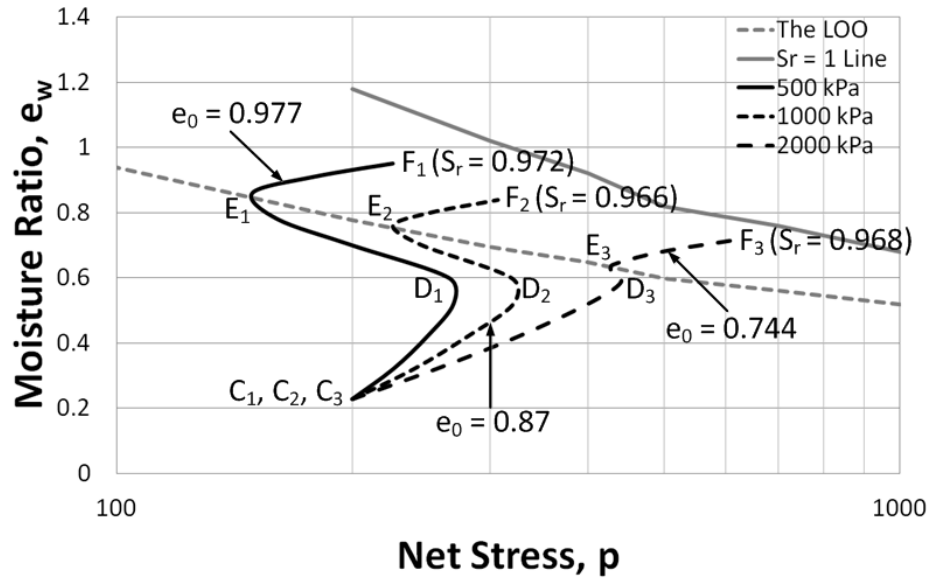
(m) Specimen of 8.69% moisture content ($e_w = 0.228$) loaded to 500, 1000 and 2000 kPa stress and then unloaded to 200 kPa stress and then wetted to 36.26% moisture content ($e_w = 0.950$) ($S_r = 0.972$ and $e_0 = 0.977$), 32.06% moisture content ($e_w = 0.840$) ($S_r = 0.966$ and $e_0 = 0.87$) and 27.48% moisture content ($e_w = 0.720$) ($S_r = 0.968$ and $e_0 = 0.744$) respectively at constant volume [Test Identity => SC – MC – SPT – 1, 2 & 3]
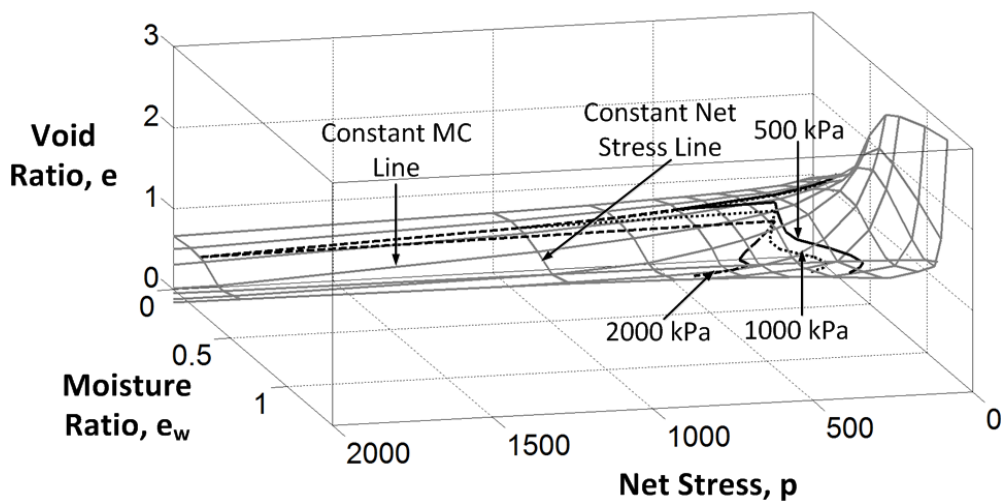
(n) 3-D view of state path test (m)
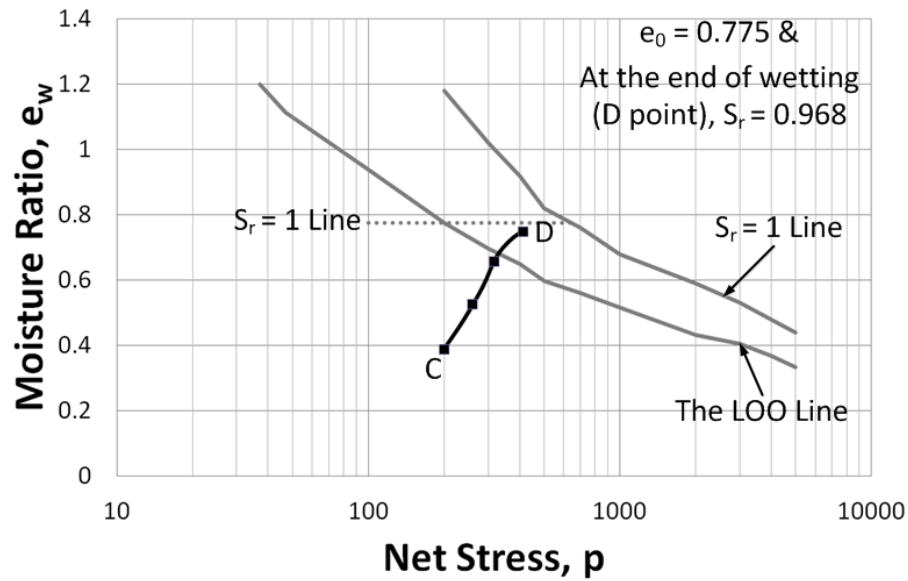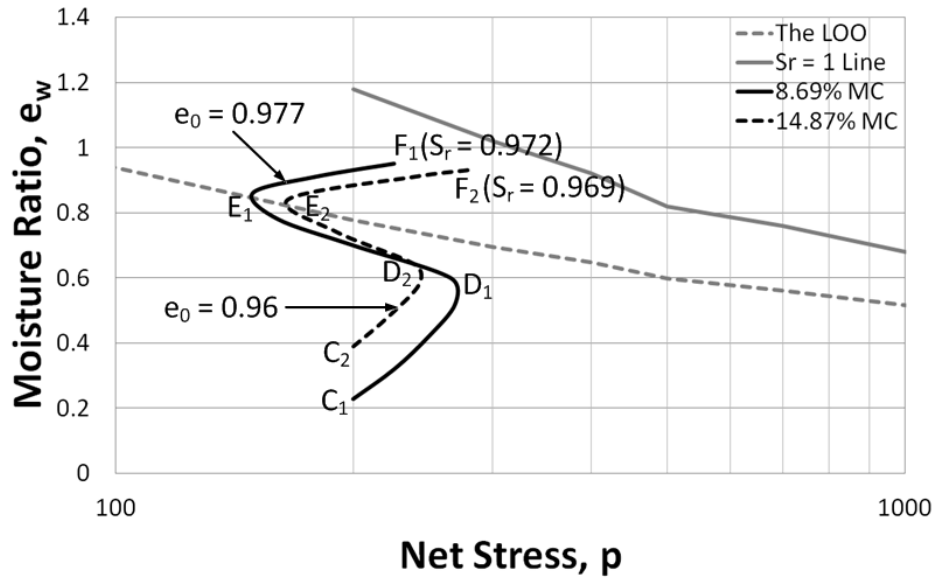
(o) Specimen of 8.69% moisture content ($e_w = 0.228$) and 14.87% moisture content ($e_w = 0.39$) loaded to 500 kPa stress and then unloaded to 200 kPa stress and then wetted to 36.26% moisture content ($e_w = 0.950$) ($S_r = 0.972$ and $e_0 = 0.977$) and 35.50% moisture content ($e_w = 0.930$) ($S_r = 0.969$ and $e_0 = 0.96$) respectively at constant volume [Test Identity => SC – MC – SPT – 1 & 4]
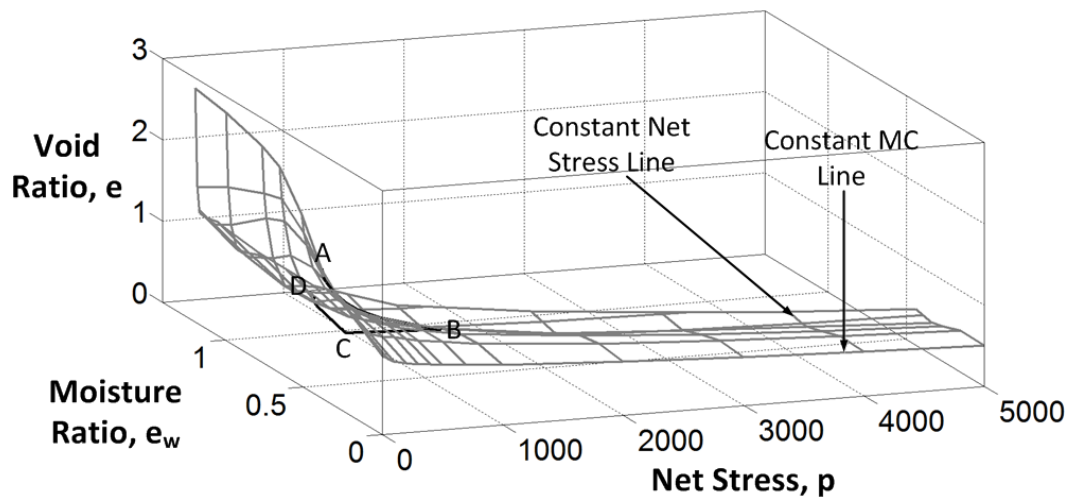

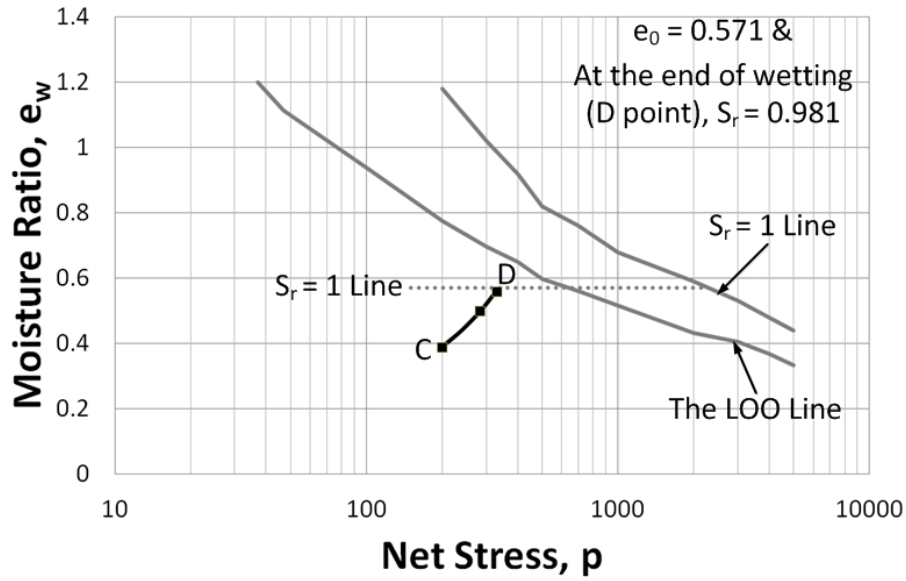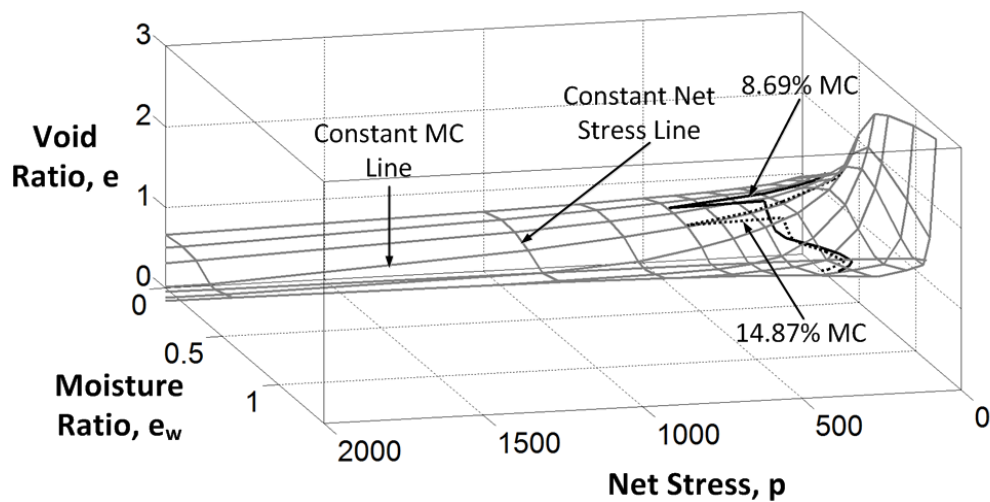**(p)** 3-D view of state path test (o)
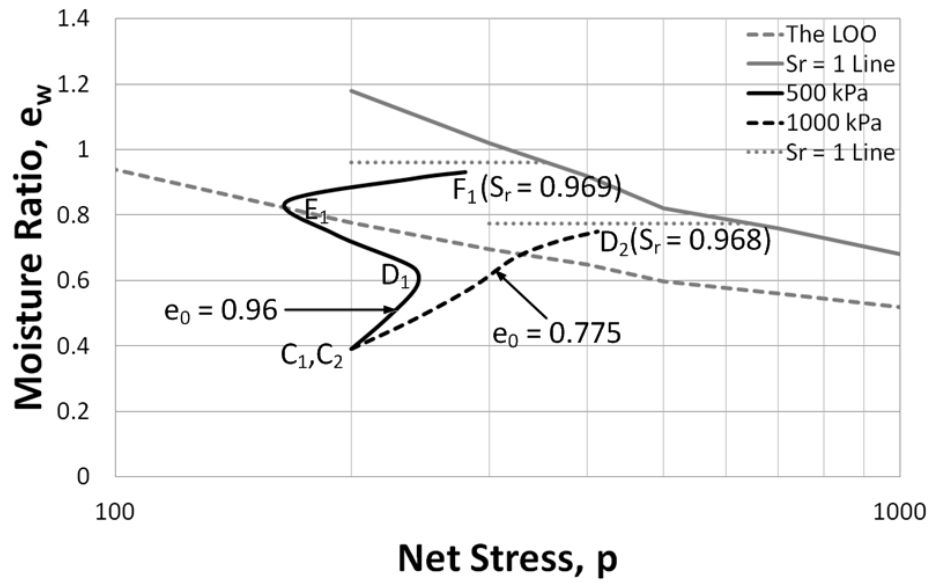
(q) Specimen of 14.87% moisture content (e_w = 0.39) loaded to 500 kPa stress and 1000 kPa stress and then unloaded to 200 kPa stress and then wetted to 35.50% moisture content (e_w = 0.930) (S_r = 0.969 and e_0 = 0.96) and 28.63% moisture content (e_w = 0.750) (S_r = 0.968 and e_0 = 0.775) respectively at constant volume [Test Identity => SC – MC – SPT – 4 & 5]
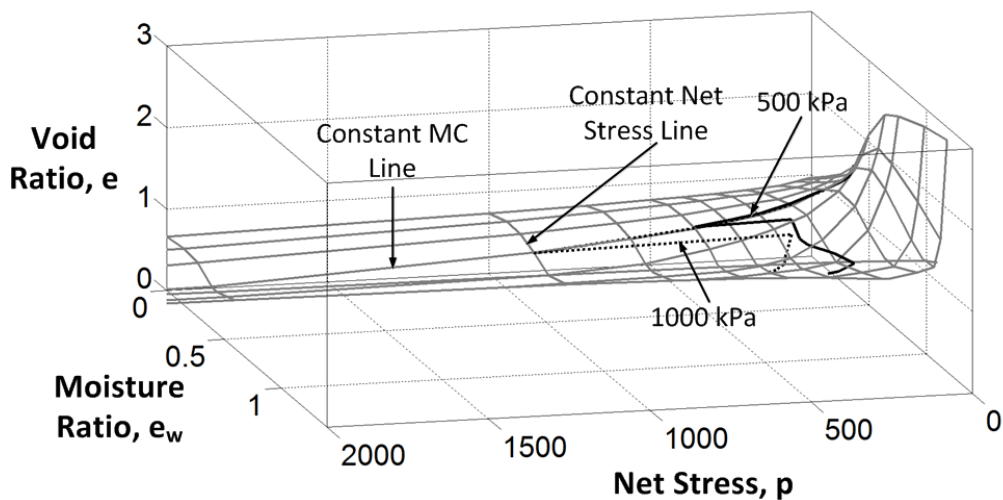
(r) 3-D view of state path test (q)

Figure 4-31: Constant volume wetting state path tests for the Merri Creek soil
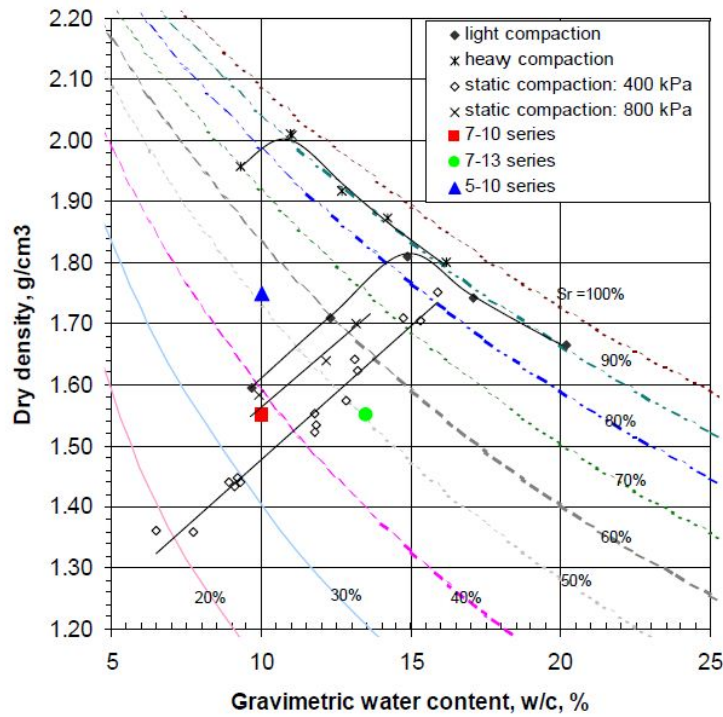
Figure 4-32: Compaction characteristics of Soil 'A' (Jotisankasa, 2005)
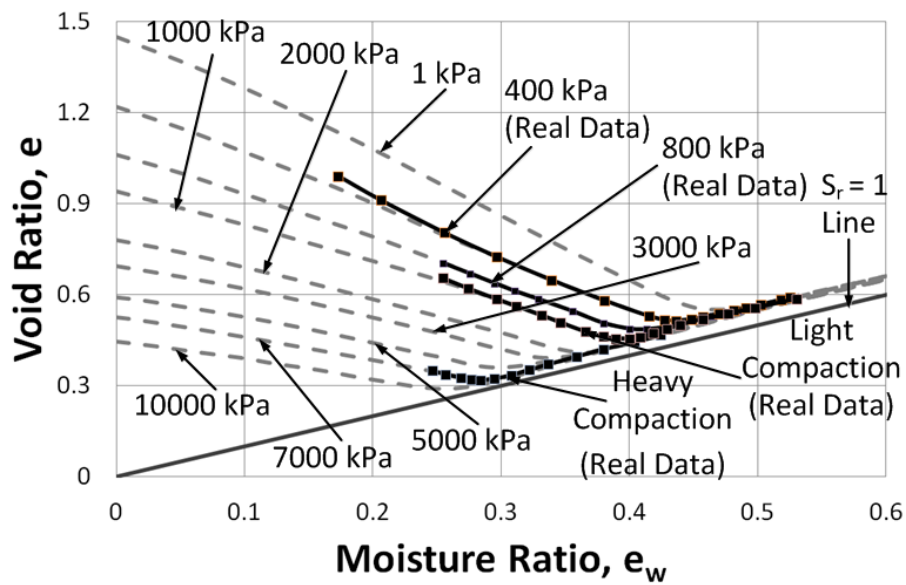
Figure 4-33: Development of the LWSBS for Soil 'A' from the compaction curves
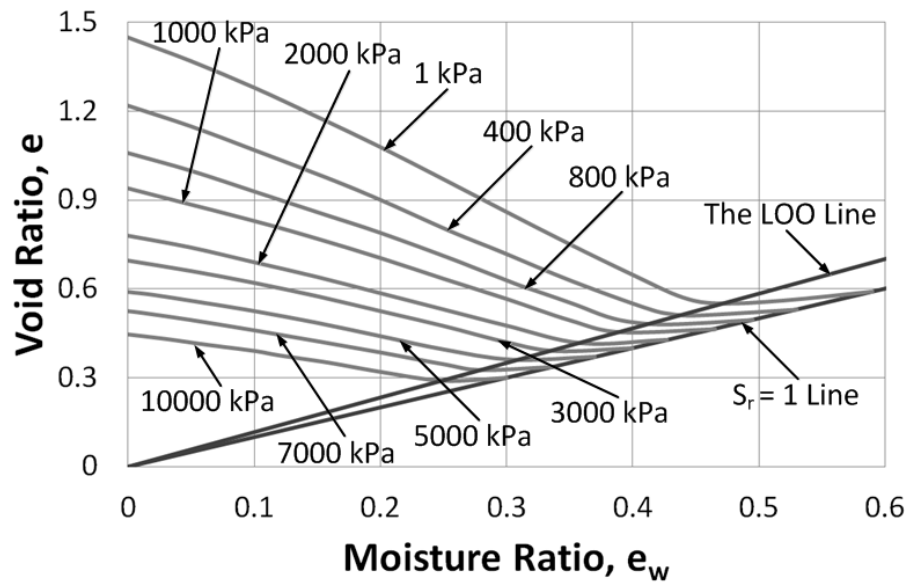
(a) In $e - e_w$ plane
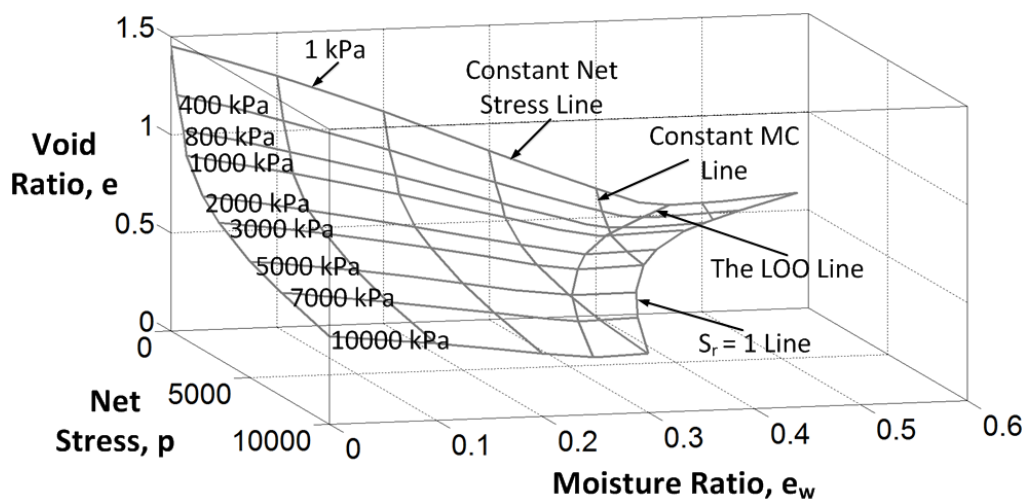
(b) In $e - e_w - p$ space

Figure 4-34: The LWSBS for Soil 'A'
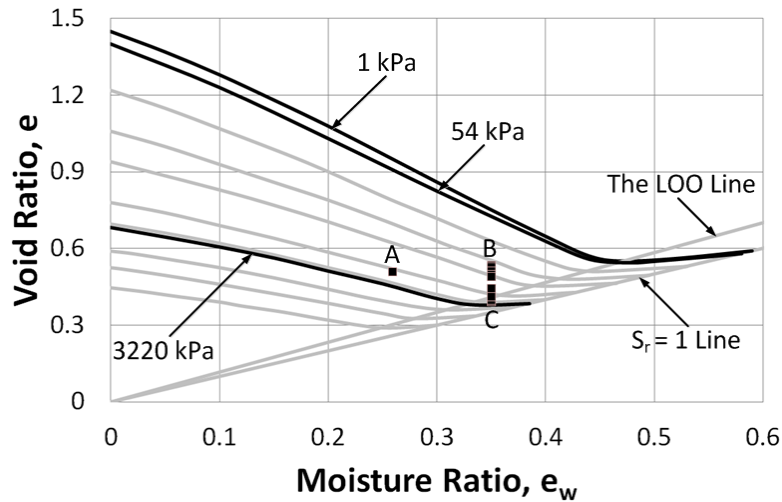
(a) Test 5 – 10 – B (initial void ratio = 0.51 and moisture content = 9.80% (e_w = 0.260)) – firstly, soil specimen was wetted to 13.50% moisture content (e_w = 0.360) at 0 kPa stress and then loaded to 3220 kPa stress and then unloaded to 54 kPa stress
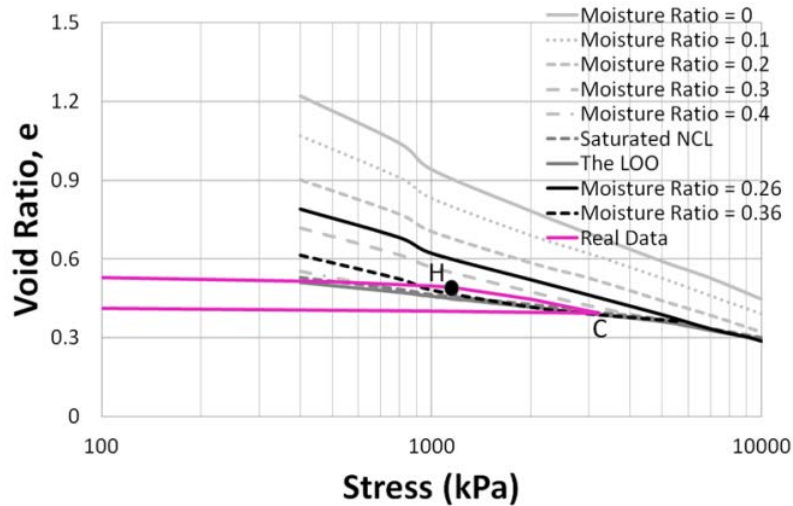
(b) $e - \log p$ relationship of state path test (a)
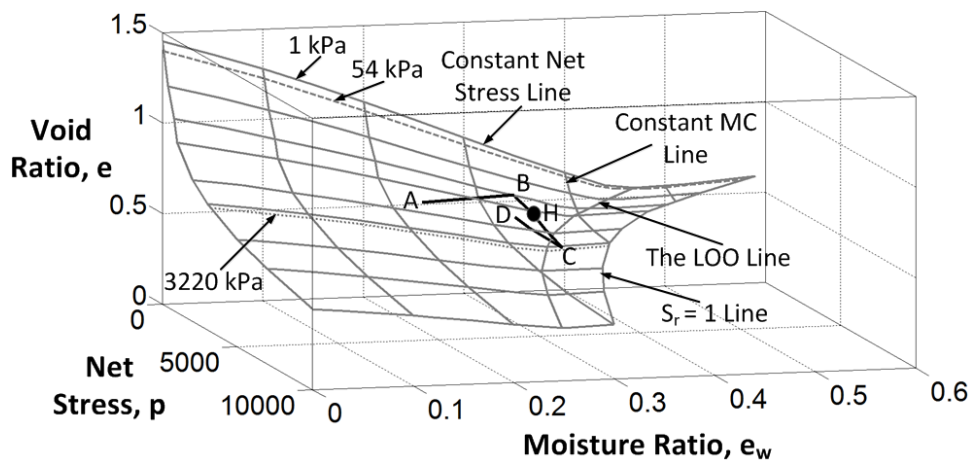
(c) 3-D view of state path test (a)
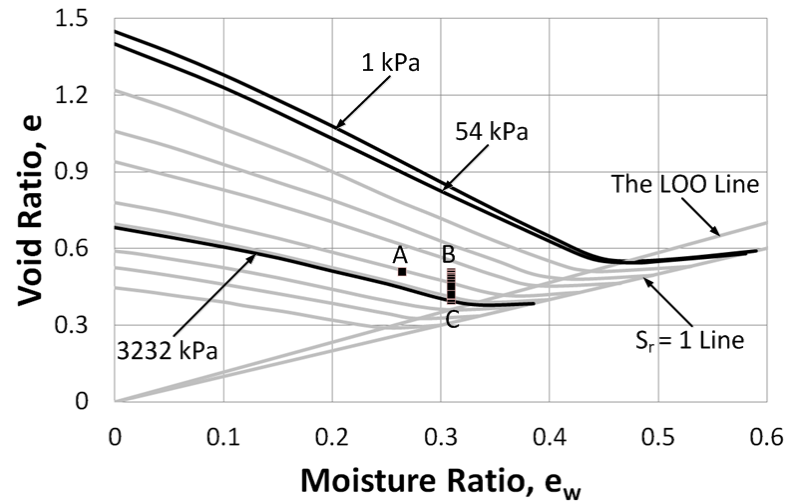
(d) Test 5 – 10 – E (initial void ratio = 0.51 and moisture content = 10.0% (e_w = 0.264)) – firstly, soil specimen was wetted to 11.80% moisture content (e_w = 0.312) at 0 kPa stress and then loaded to 3232 kPa stress and then unloaded to 54 kPa stress

(e) $e - \log p$ relationship of state path test (d)

(f) 3-D view of state path test (d)
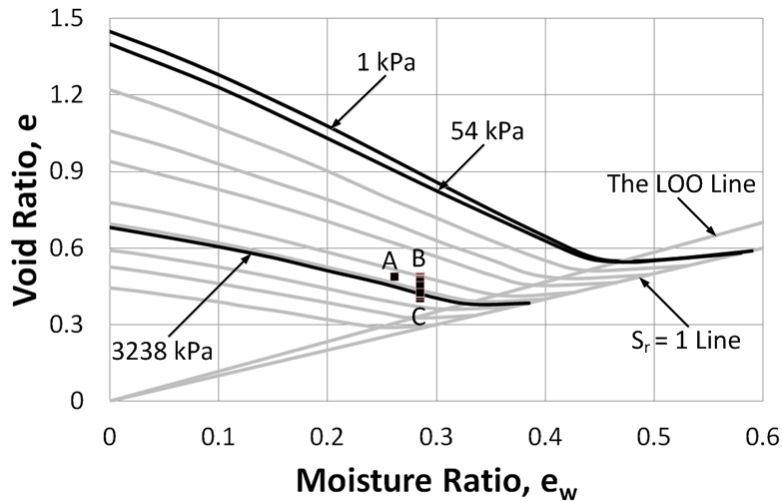
(g) Test 5 – 10 – F (initial void ratio = 0.49 and moisture content = 9.90% ($e_w = 0.260$)) – firstly, soil specimen was wetted to 10.90% moisture content ($e_w = 0.290$) at 0 kPa stress and then loaded to 3238 kPa stress and then unloaded to 54 kPa stress

(h) e – log p relationship of state path test (g)

(i) 3-D view of state path test (g)

(j) Test $7 - 10 - D$ (initial void ratio $= 0.71$ and moisture content $= 10.20\%$ ($e_w = 0.270$)) – firstly, soil specimen was wetted to 10.60% moisture content ($e_w = 0.280$) at 0 kPa stress and then loaded to 3220 kPa stress and then unloaded to 54 kPa stress

(k) $e - \log p$ relationship of state path test (j)

(l) 3-D view of state path test (j)

(m) Test 7 – 10 – H (initial void ratio = 0.69 and moisture content = 10.20% (e_w = 0.270)) – firstly, soil specimen was wetted to 13.50% moisture content (e_w = 0.360) at 0 kPa stress and then loaded to 3220 kPa stress and then unloaded to 54 kPa stress

(n) e – log p relationship of state path test (m)

(o) 3-D view of state path test (m)
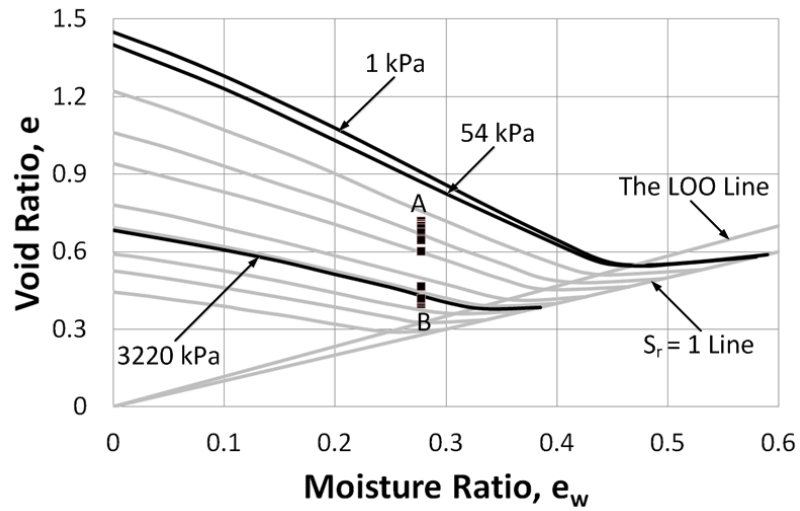
(p) Test 7 – 10 – K (initial void ratio = 0.72 and moisture content = 10.60% (e_w = 0.280)) – firstly, soil specimen was loaded to 3220 kPa stress at as-compacted water content and then unloaded to 54 kPa stress

(q) e – log p relationship of state path test (p)
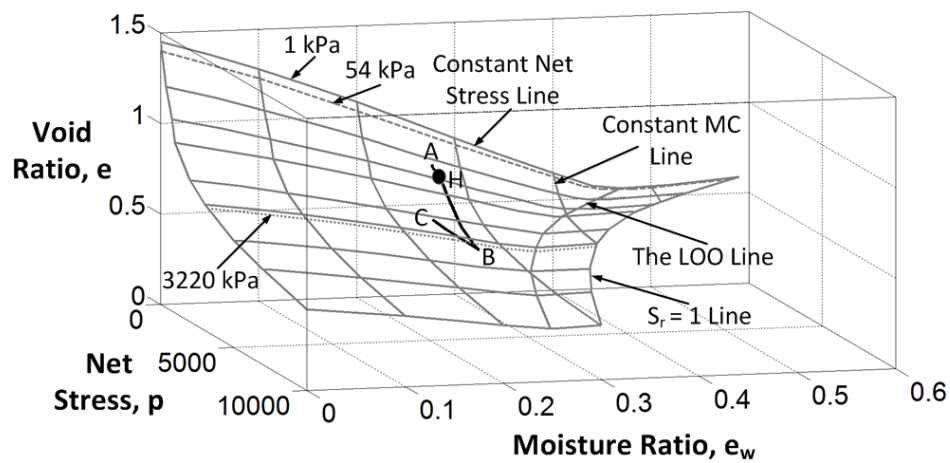
(r) 3-D view of state path test (p)

Figure 4-35: Wetting and loading state path tests for soil 'A'
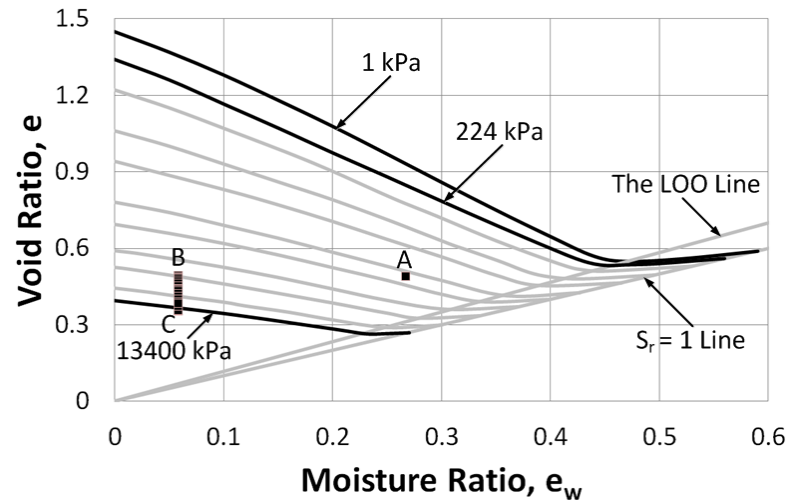
(a) Test 5 – 10 – L (initial void ratio = 0.49 and moisture content = 10.10% (e_w = 0.267)) – firstly, soil specimen was dried to 2.20% moisture content (e_w = 0.058) at 0 kPa stress and then loaded to 13400 kPa stress and then unloaded to 224 kPa stress
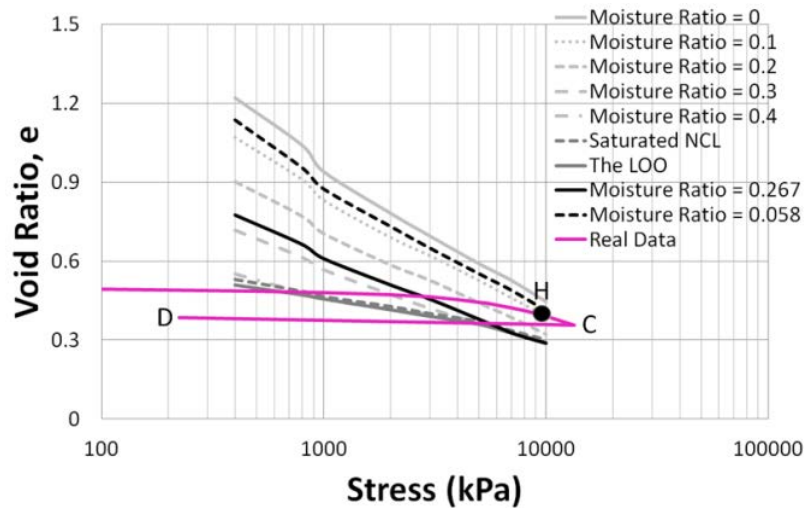
(b) $e - \log p$ relationship of state path test (a)
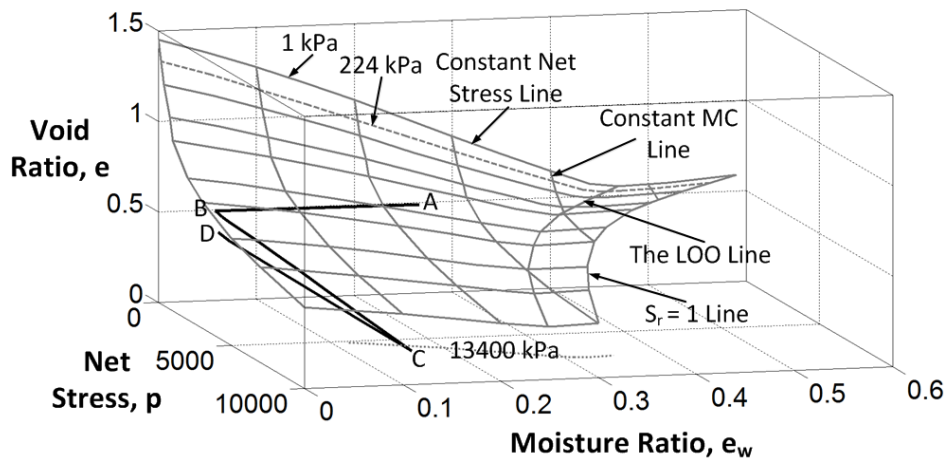
(c) 3-D view of state path test (a)

(d) Test 7 – 10 – T (initial void ratio = 0.69 and moisture content = 10.0% (e_w = 0.264)) – firstly, soil specimen was dried to 9.20% moisture content (e_w = 0.243) at 0 kPa stress and then loaded to 3220 kPa stress and then unloaded to 54 kPa stress
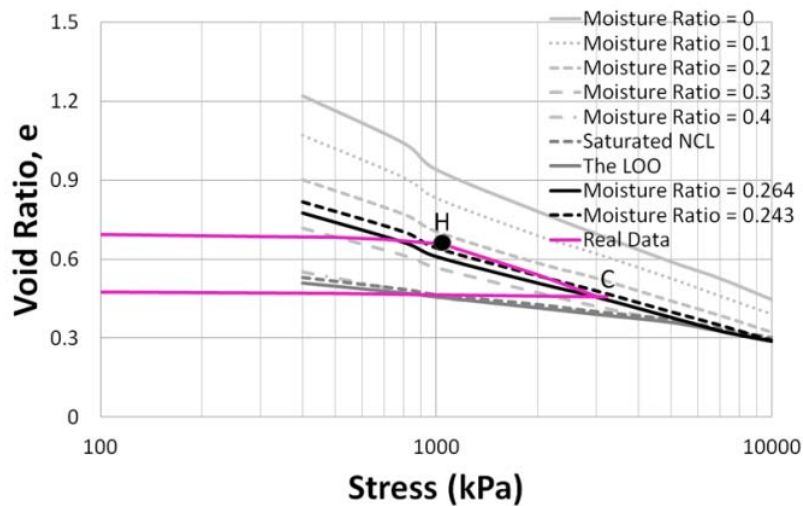
(e) e – log p relationship of state path test (d)
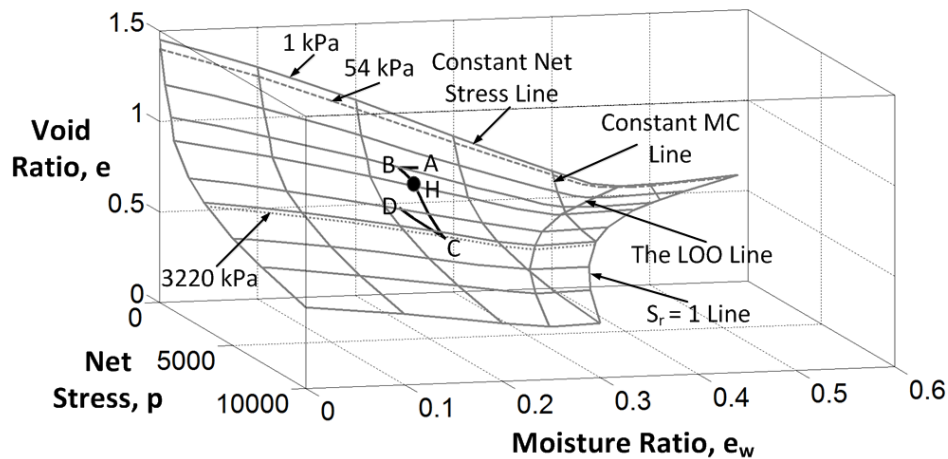
(f) 3-D view of state path test (d)
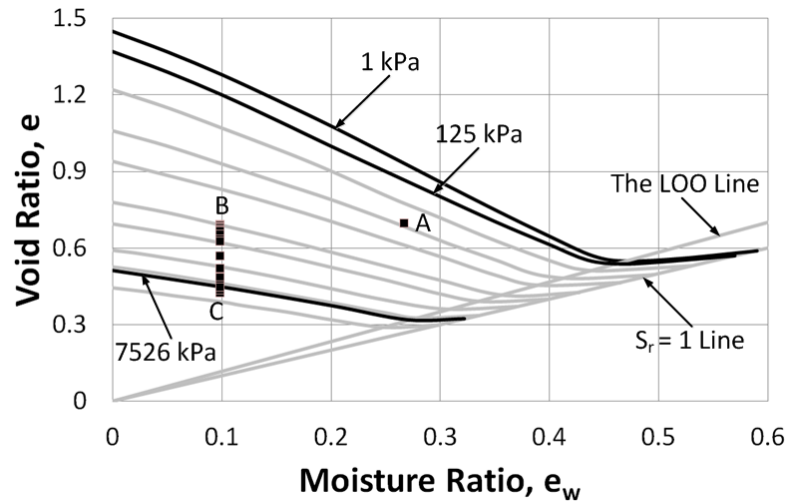
(g) Test 7 – 10 – U (initial void ratio = 0.7 and moisture content = 10.10% (e_w = 0.267)) – firstly, soil specimen was dried to 3.90% moisture content (e_w = 0.103) at 0 kPa stress and then loaded to 7526 kPa stress and then unloaded to 125 kPa stress
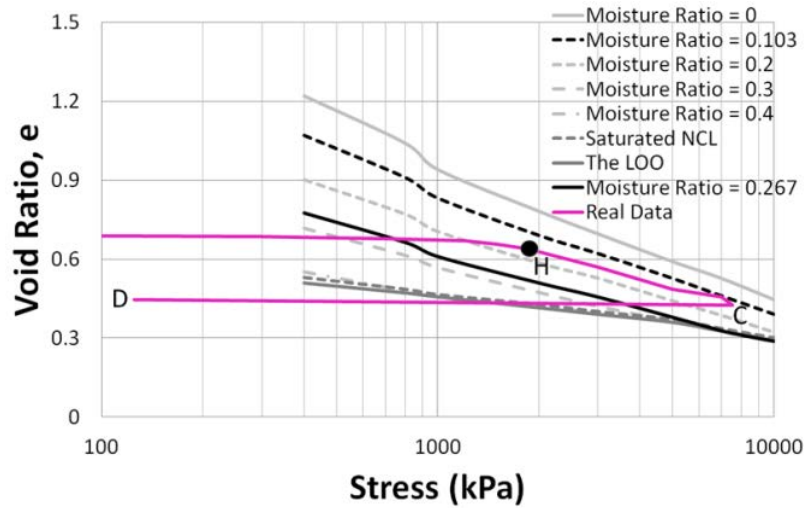
(h) e – log p relationship of state path test (g)

(i) 3-D view of state path test (g)

(j) Test $7 - 13 - D$ (initial void ratio = 0.71 and moisture content = 13.90% (e_w = 0.367)) – firstly, soil specimen was dried to 1.30% moisture content (e_w = 0.034) at 0 kPa stress and then loaded to 7500 kPa stress
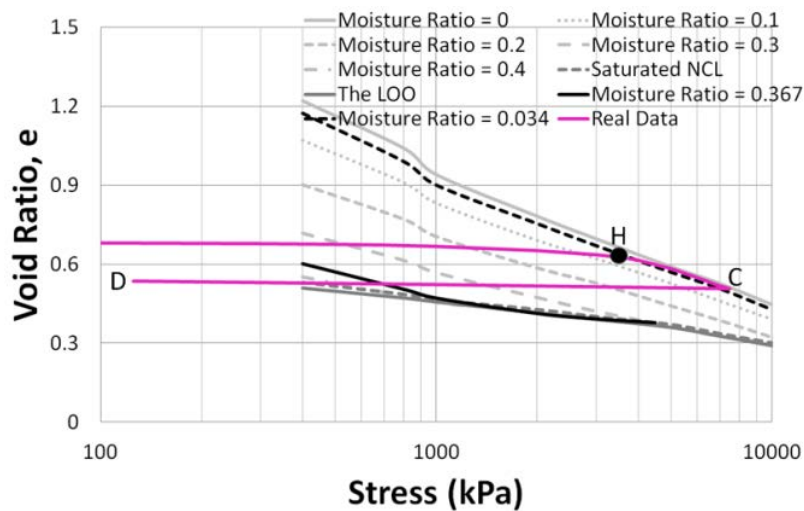
(k) $e - \log p$ relationship of state path test (j)
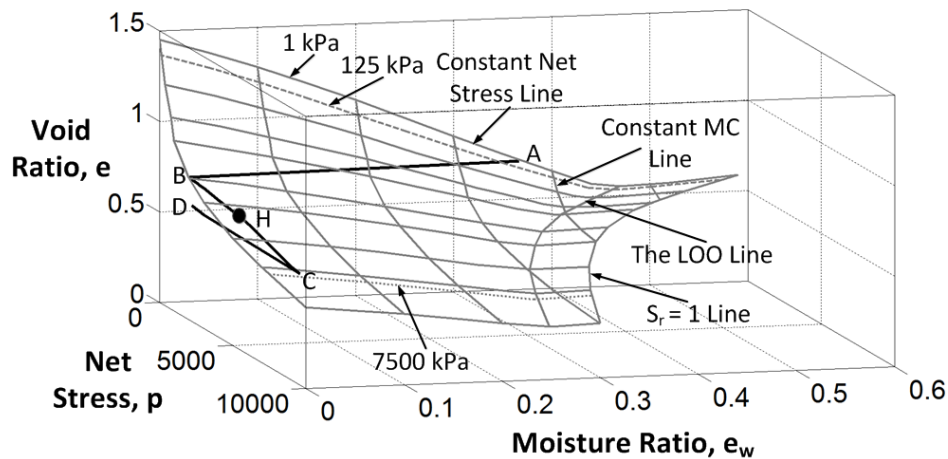
(l) 3-D view of state path test (j)
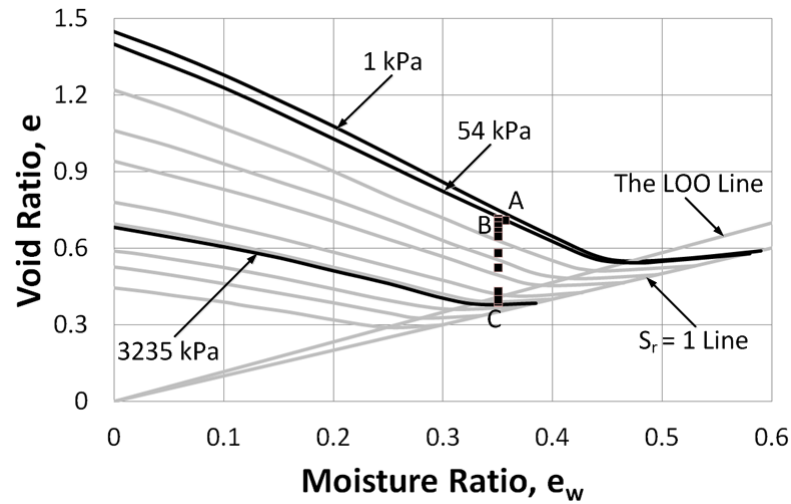
(m) Test 7 – 13 – I (initial void ratio = 0.71 and moisture content = 13.50% (e_w = 0.356)) – firstly, soil specimen was loaded to 3235 kPa stress at as-compacted water content and then unloaded to 54 kPa stress
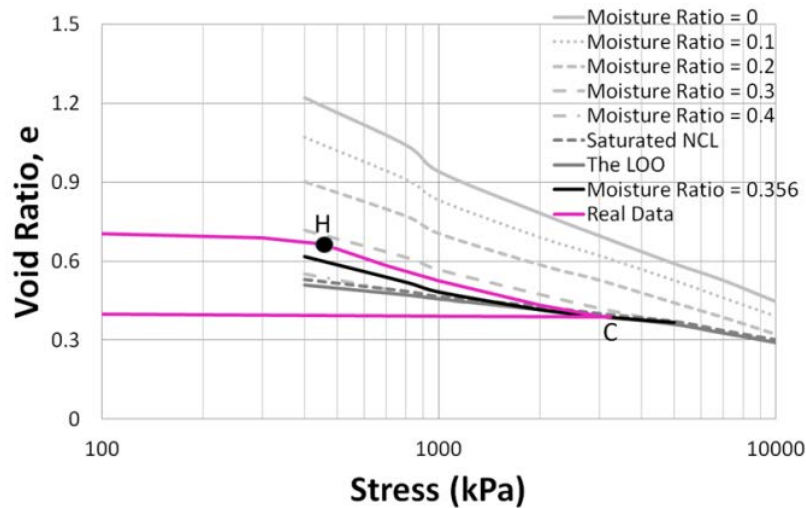
(n) e – log p relationship of state path test (m)
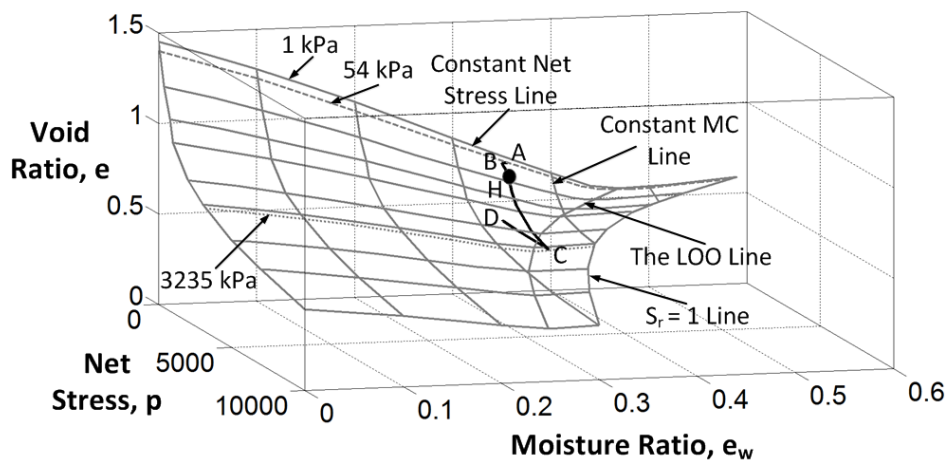
(o) 3-D view of state path test (m)
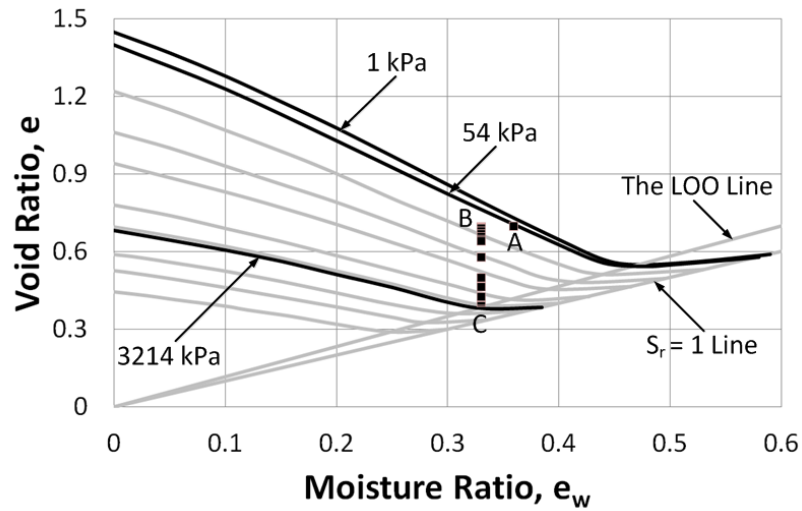
(p) Test 7 – 13 – J (initial void ratio = 0.7 and moisture content = 13.60% ($e_w = 0.359$)) – firstly, soil specimen was dried to 12.60% moisture content ($e_w = 0.333$) at 0 kPa stress and then loaded to 3214 kPa stress and then unloaded to 54 kPa stress
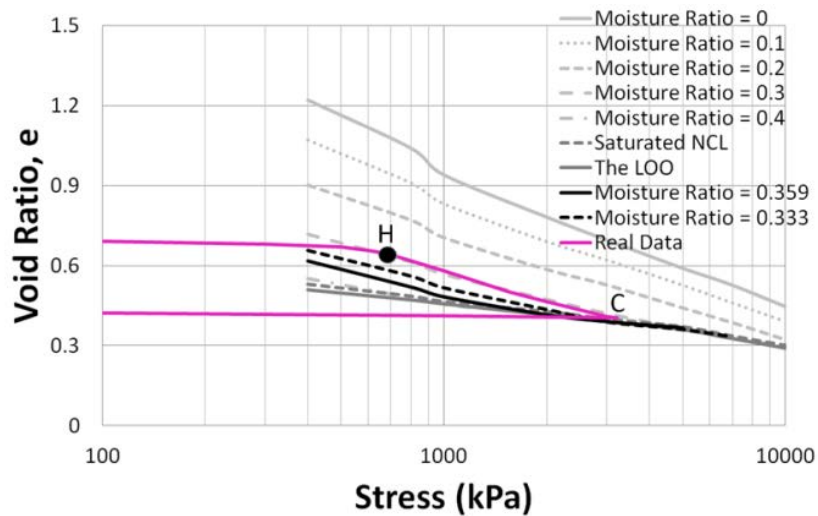

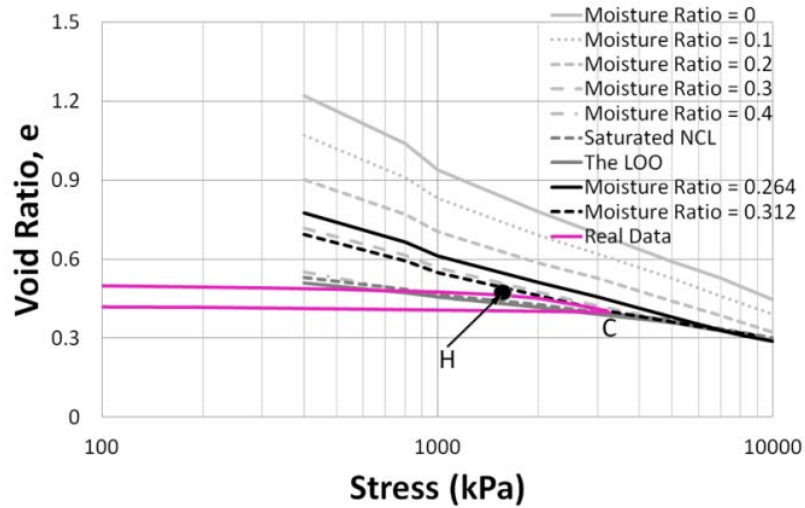**(q)** e – log p relationship of state path test (p)
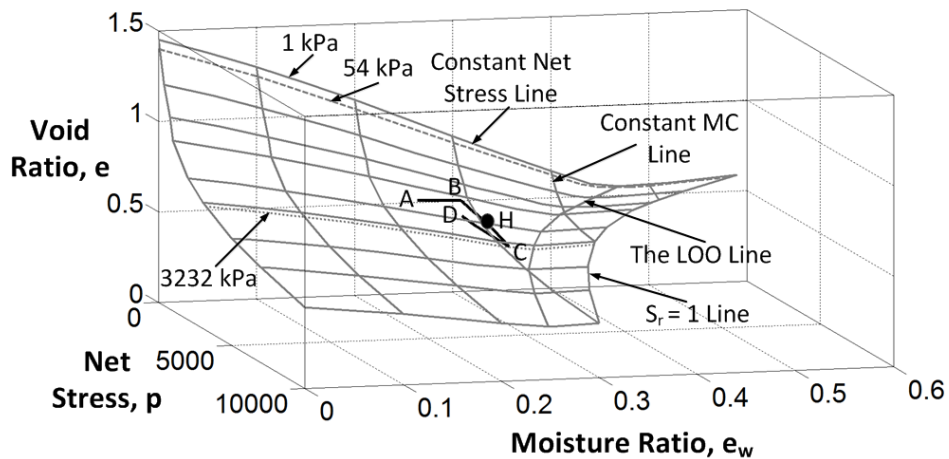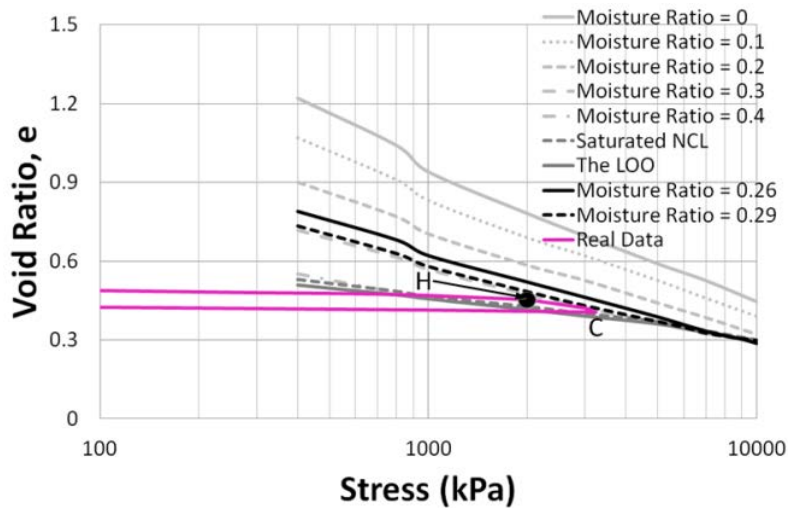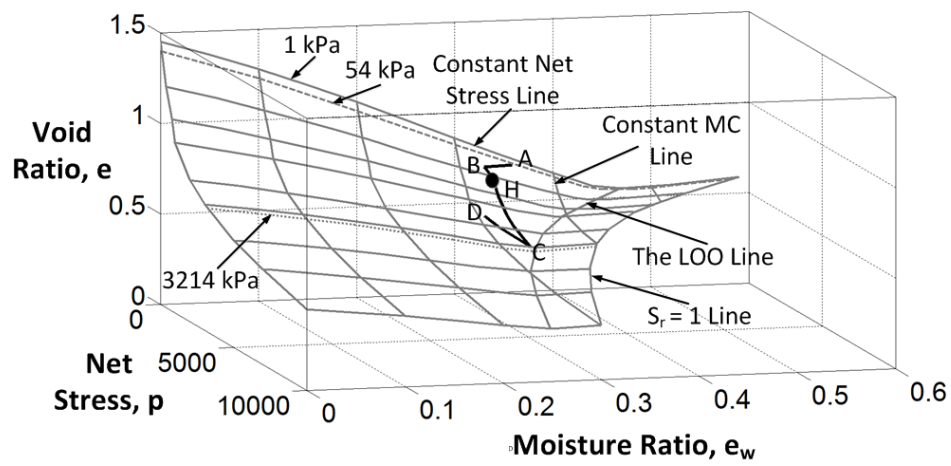
(r) 3-D view of state path test (p)

Figure 4-36: Drying and loading state path tests for soil 'A'
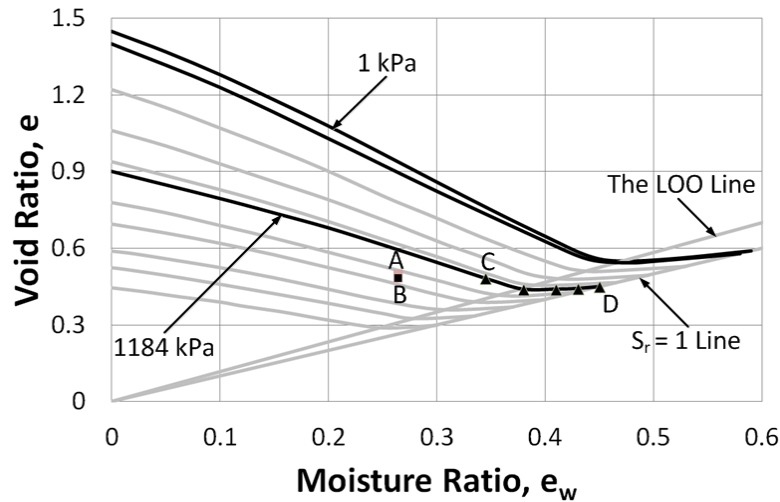
(a) Test 5 – 10 – D (initial void ratio = 0.5 and moisture content = 10.0% ($e_w = 0.264$))
– firstly, soil specimen was loaded to 1184 kPa stress at as-compacted moisture content
and then wetted to suction of 0 kPa at 1184 kPa stress
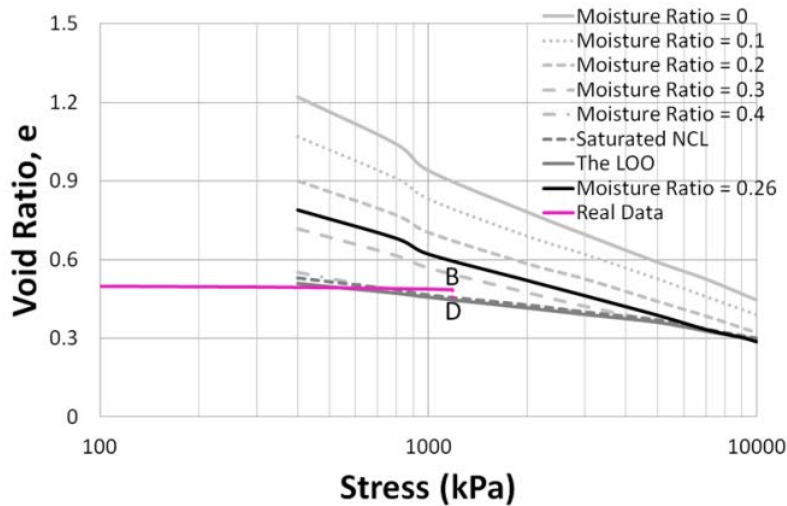
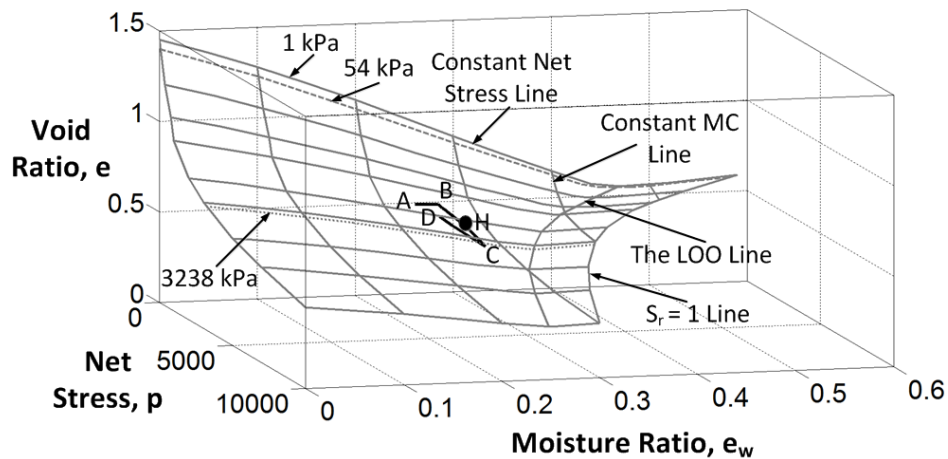**(b)** $e – \log p$ relationship of state path test (a)
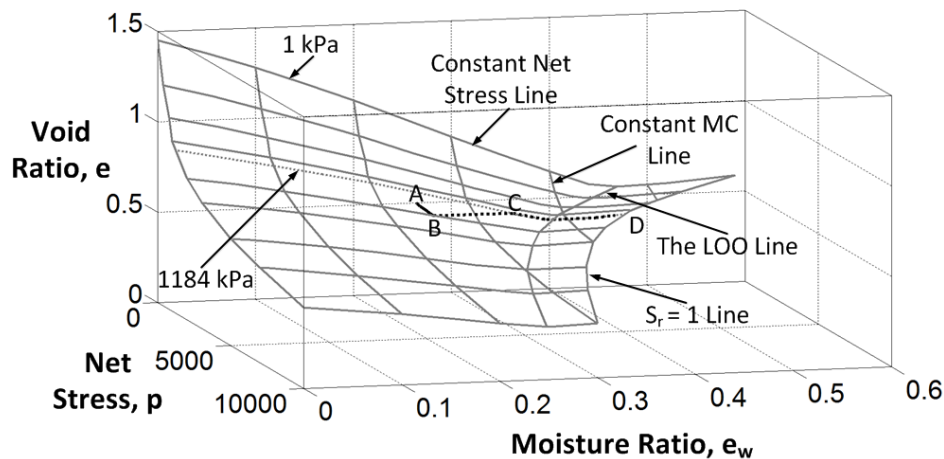
(c) 3-D view of state path test (a)
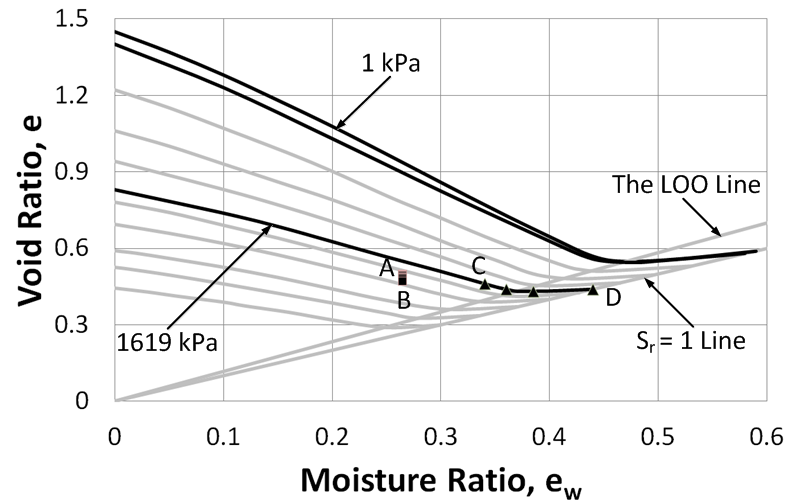
(d) Test 5 – 10 – G (initial void ratio = 0.5 and moisture content = 10.0% ($e_w = 0.264$)) – firstly, soil specimen was loaded to 1619 kPa stress at as-compacted moisture content and then wetted to suction of 0 kPa at 1619 kPa stress
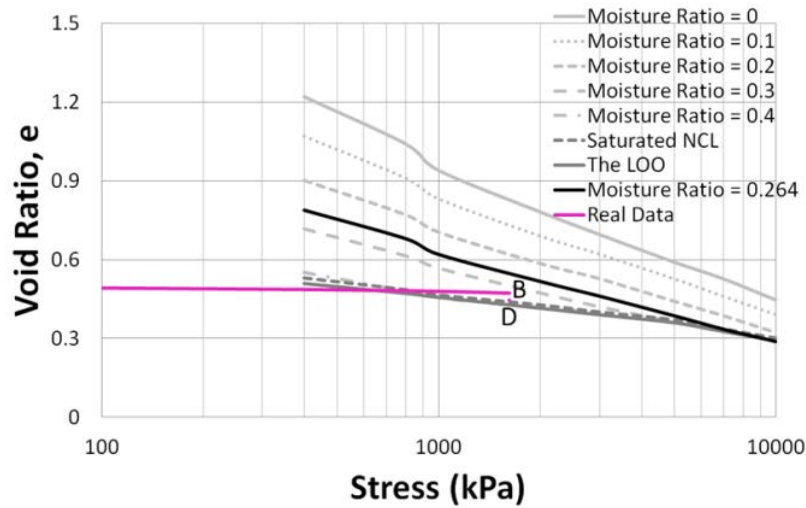
(e) e – log p relationship of state path test (d)
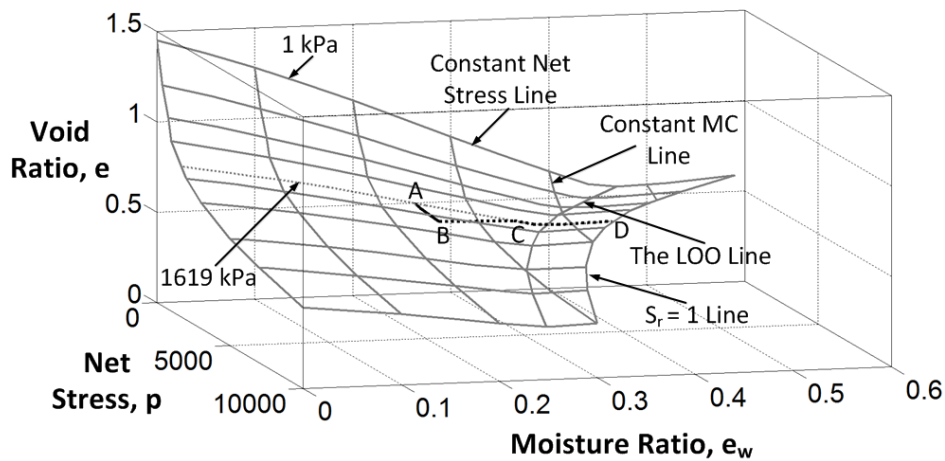
(f) 3-D view of state path test (d)
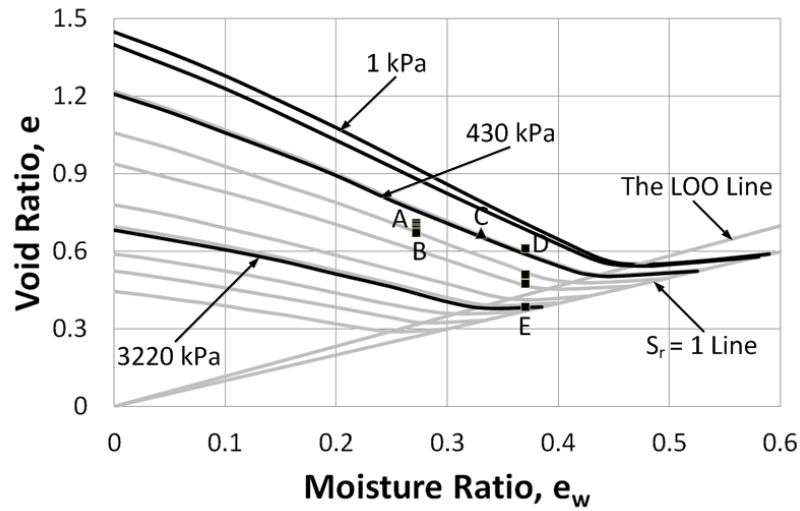
(g) Test 7 – 10 – I (initial void ratio = 0.71 and moisture content = 10.30% (e_w = 0.270)) – firstly, soil specimen was loaded to 430 kPa stress at as-compacted moisture content and then wetted to suction of 130 kPa at 430 kPa stress and then loaded to 3220 kPa stress
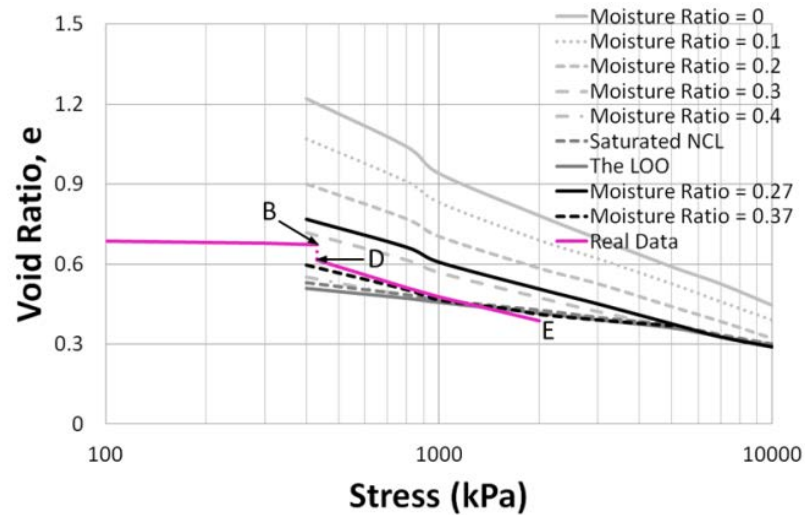
(h) $e – \log p$ relationship of state path test (g)
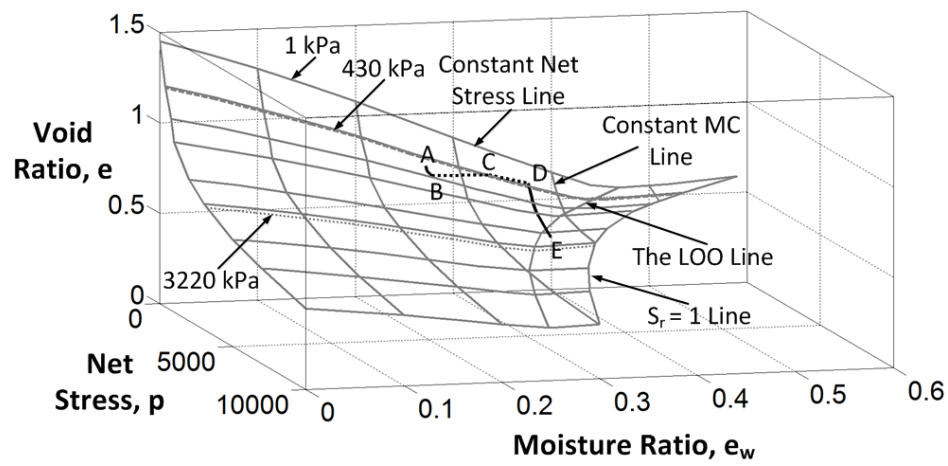
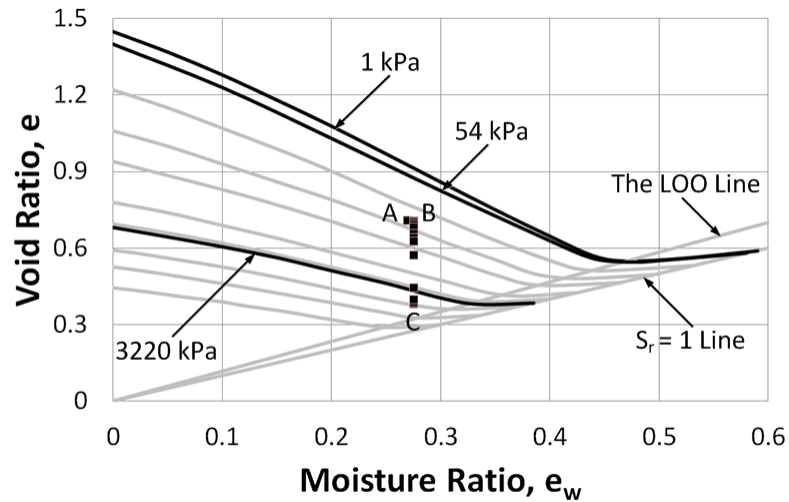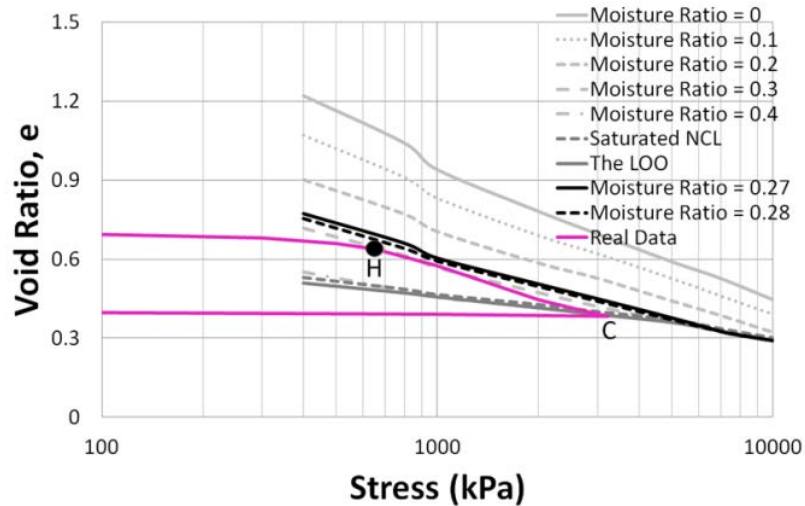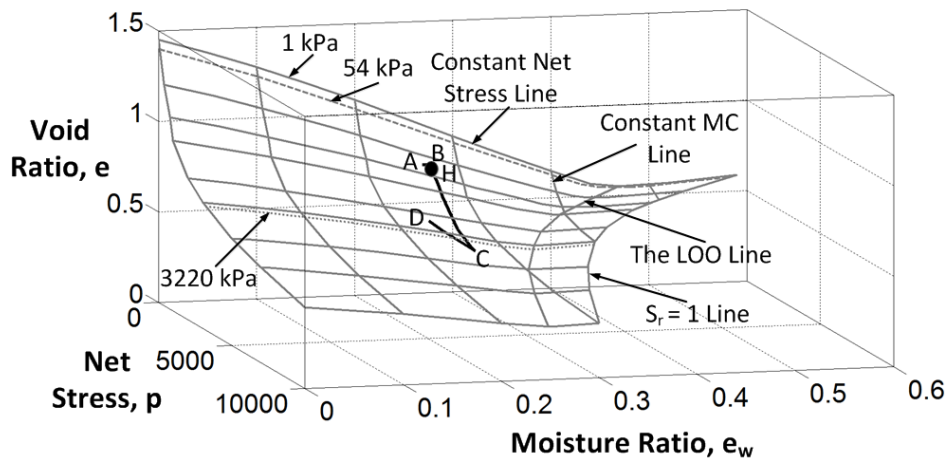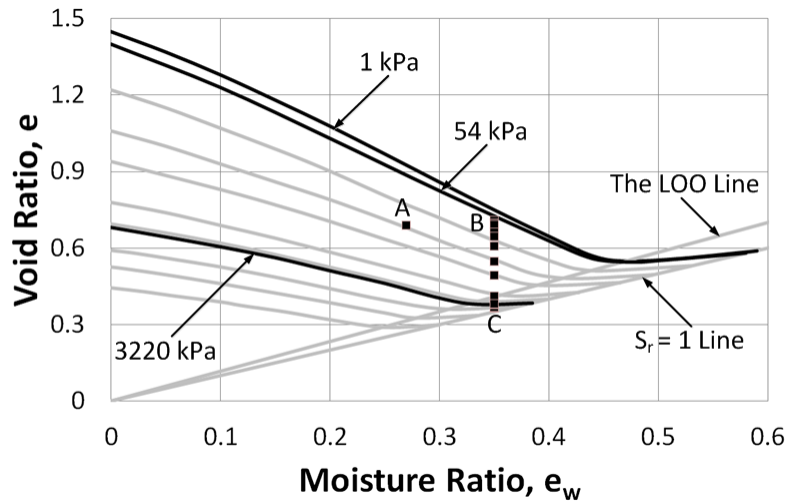**(i)** 3-D view of state path test (g)
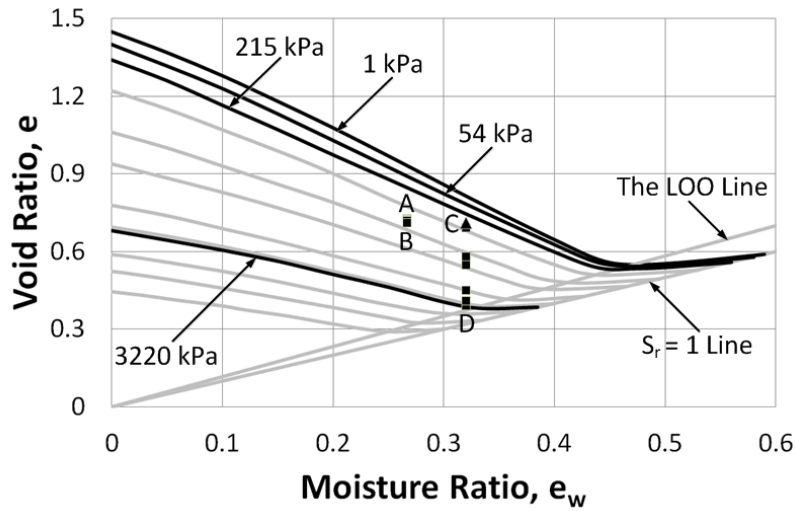
(j) Test 7 – 10 – L (initial void ratio = 0.73 and moisture content = 10.10% (e_w = 0.270)) – firstly, soil specimen was loaded to 215 kPa stress at as-compacted moisture content and then wetted to suction of 140 kPa at 215 kPa stress and then loaded to 3220 kPa stress
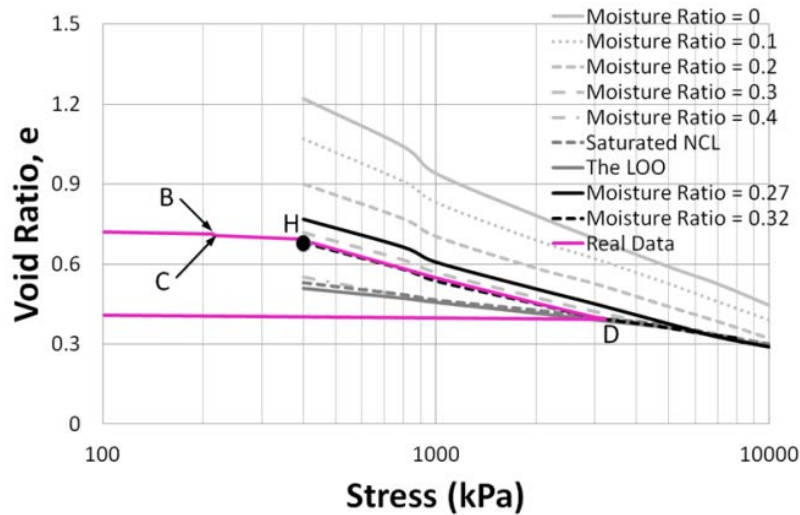
(k) e – log p relationship of state path test (j)
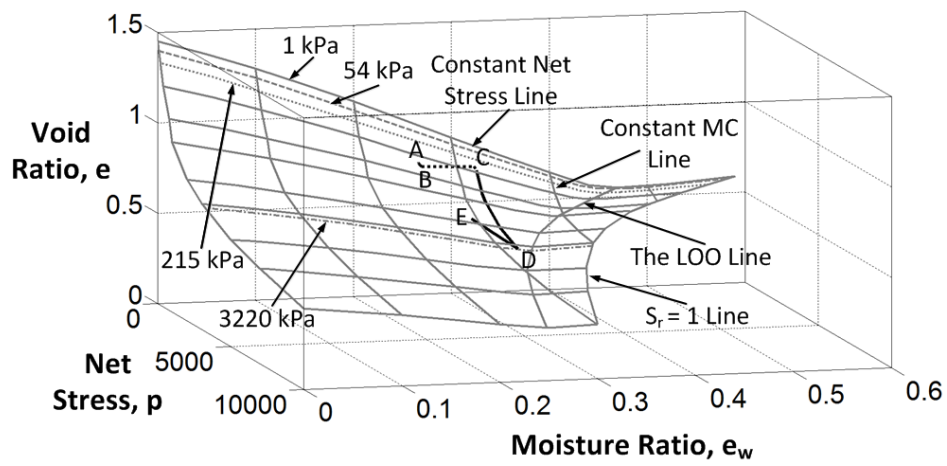
(l) 3-D view of state path test (j)
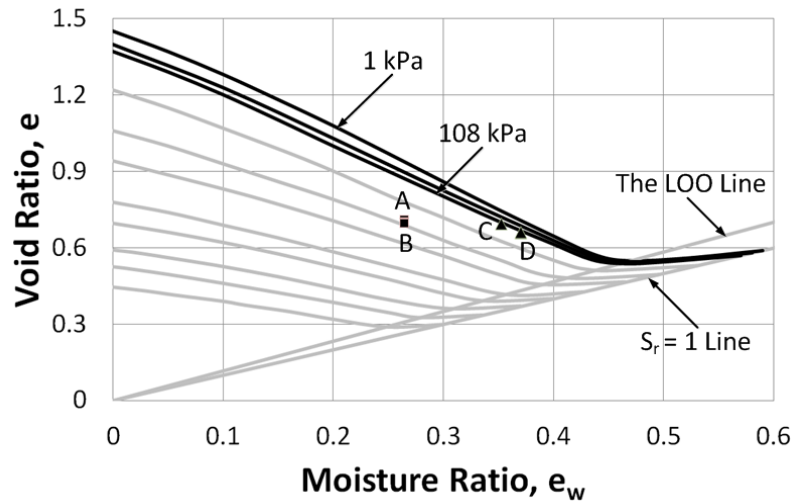
(m) Test $7 - 10 - N$ (initial void ratio $= 0.71$ and moisture content $= 10.0\%$ ($e_w = 0.264$)) – firstly, soil specimen was loaded to 108 kPa stress at as-compacted moisture content and then wetted to suction of 10 kPa at 108 kPa stress
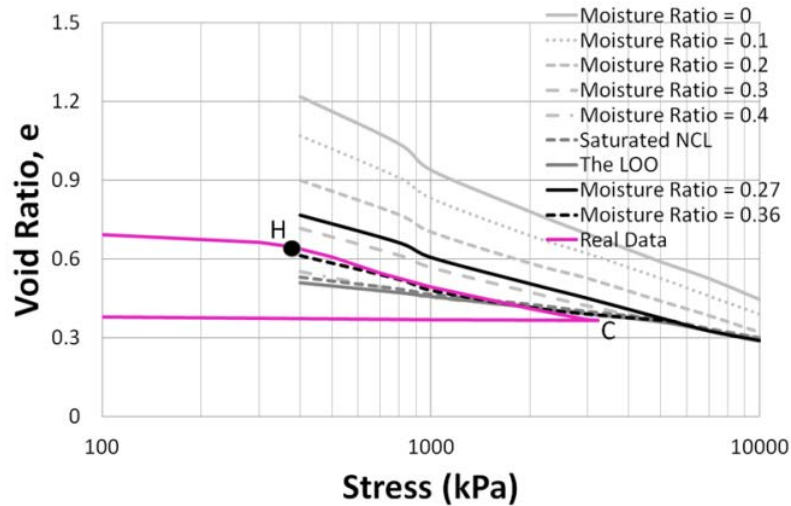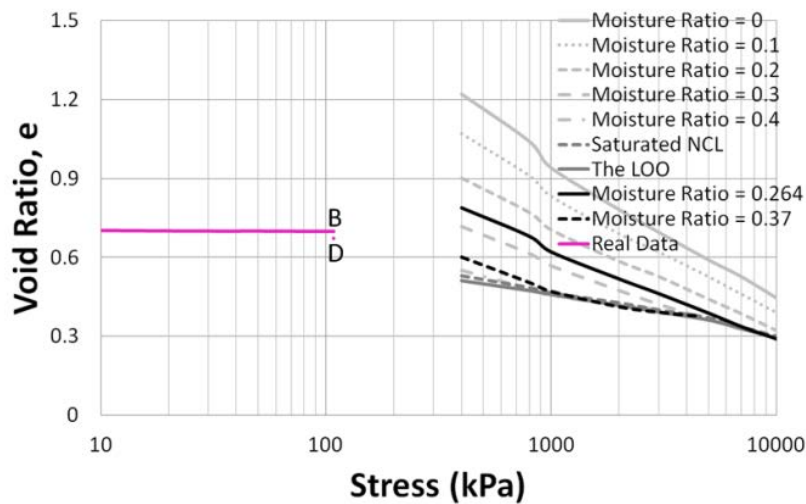

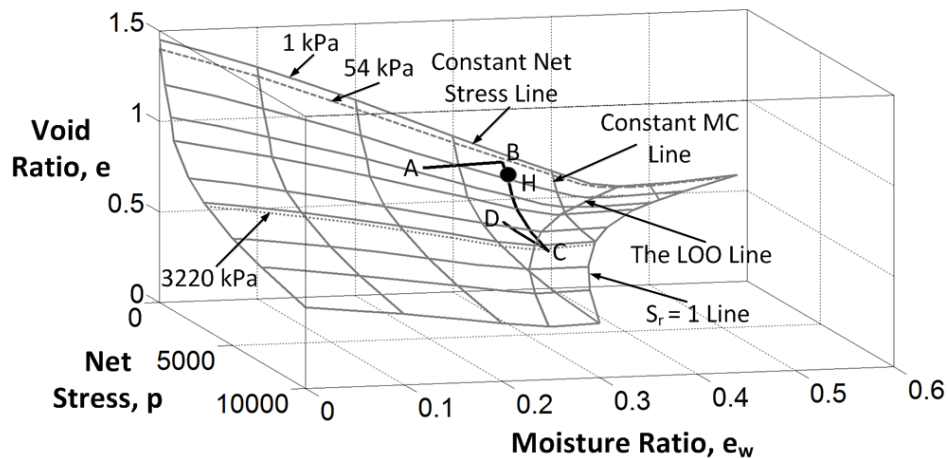**(n)** $e - \log p$ relationship of state path test (m)
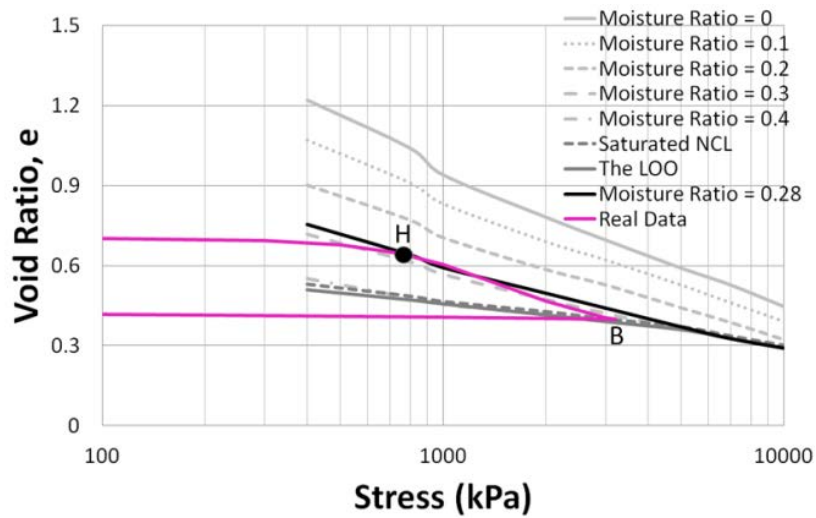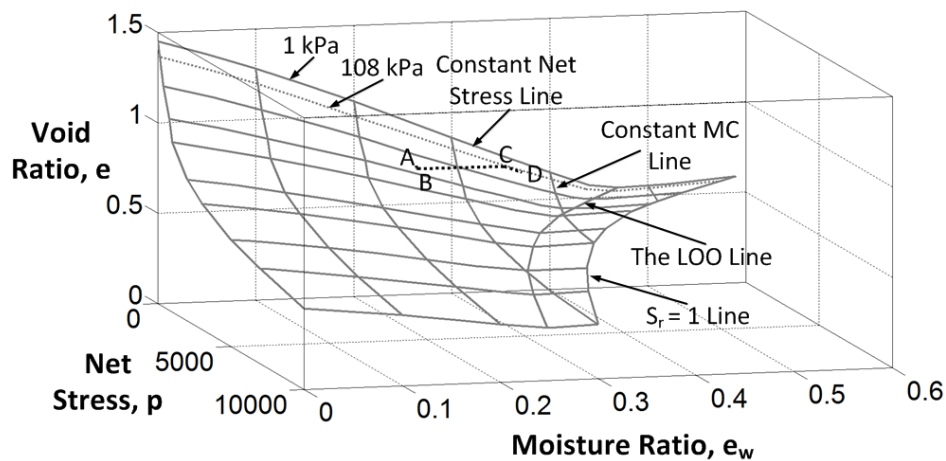

(o) 3-D view of state path test (m)
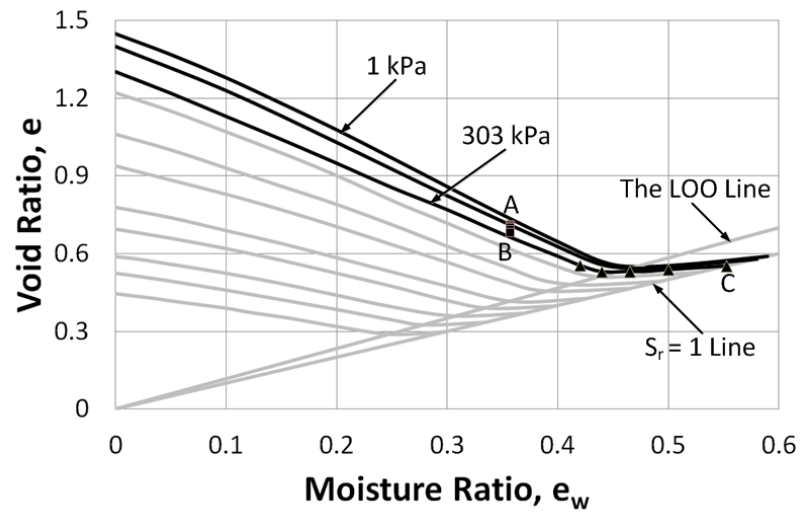
(p) Test 7 – 13 – M (initial void ratio = 0.71 and moisture content = 13.50% (e_w = 0.356)) – firstly, soil specimen was loaded to 303 kPa stress at as-compacted moisture content and then wetted to suction of 0 kPa at 303 kPa stress
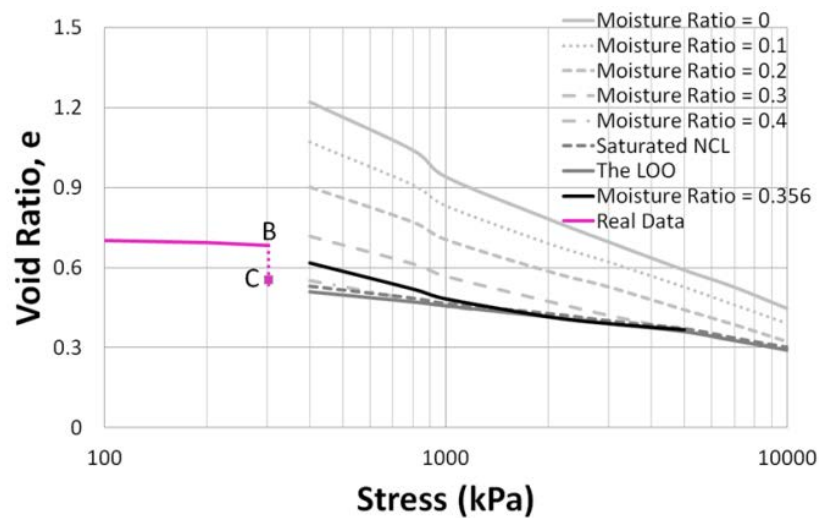
(q) e – log p relationship of state path test (p)
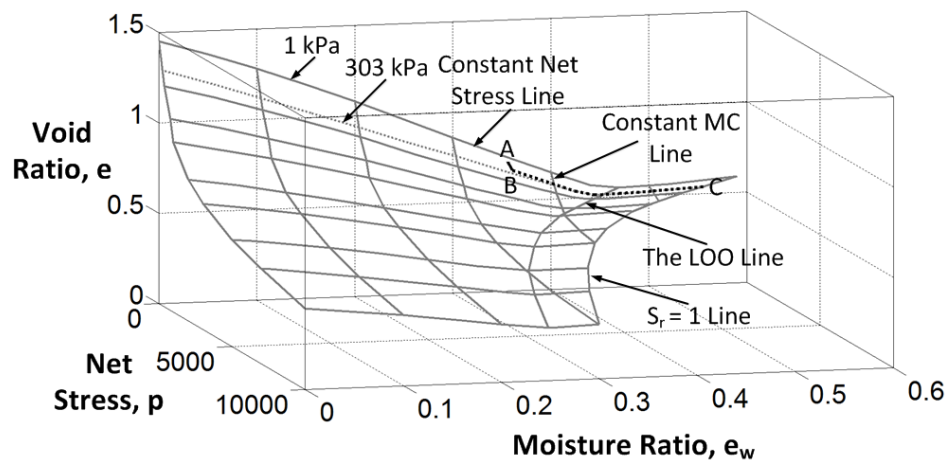
(r) 3-D view of state path test (p)

Figure 4-37: Loading, wetting and loading state path tests for soil 'A'
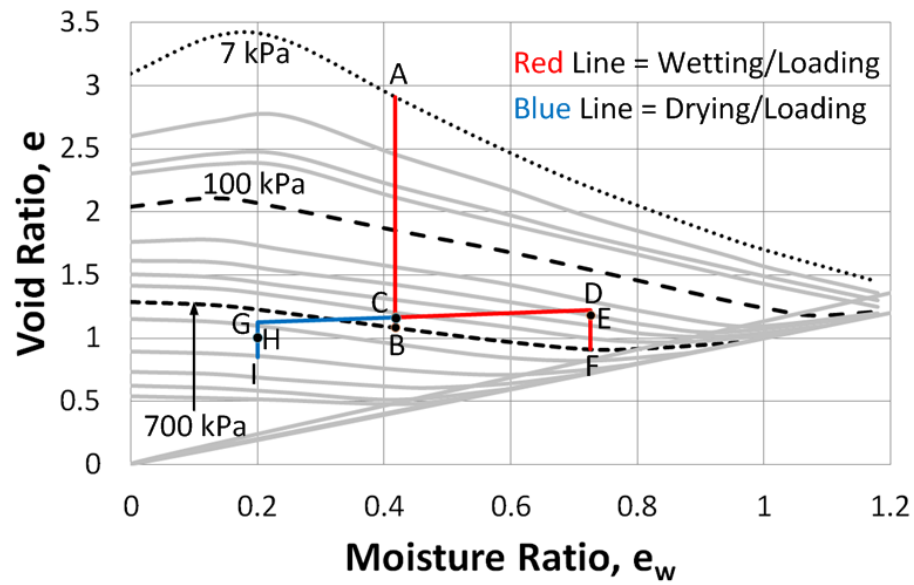
(a) In $e - e_w$ plane
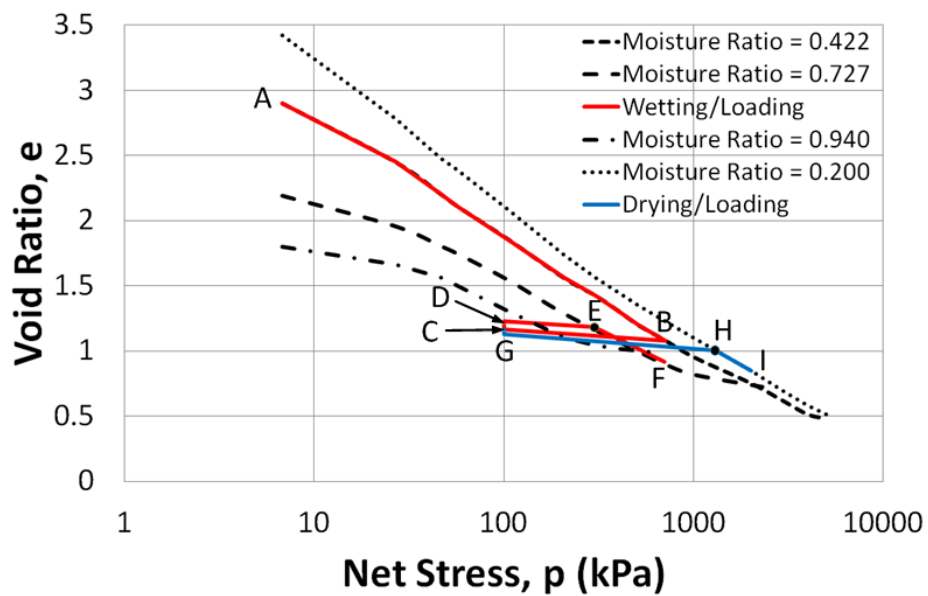
(b) In $e - \log p$ plane

Figure 4-38: Demonstration for yielding of compacted unloaded soil specimen during loading at as-compacted moisture content or after wetting or after drying
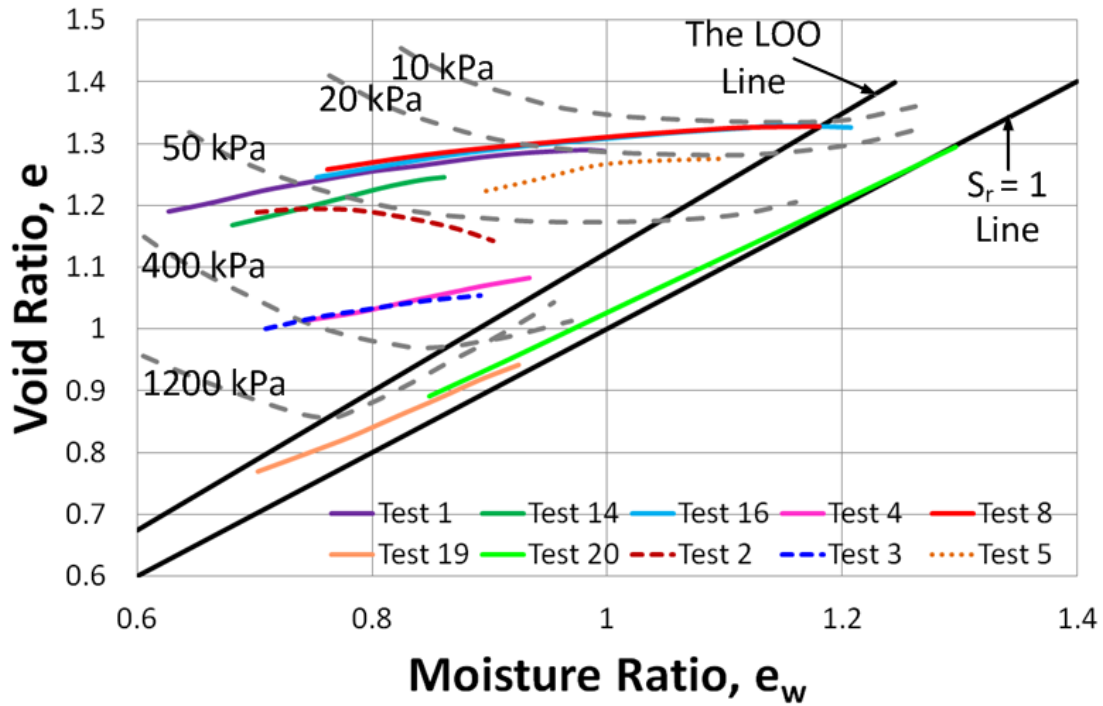
Figure 4-39: First or major wetting state paths of swell-shrink tests for soil 'BK'
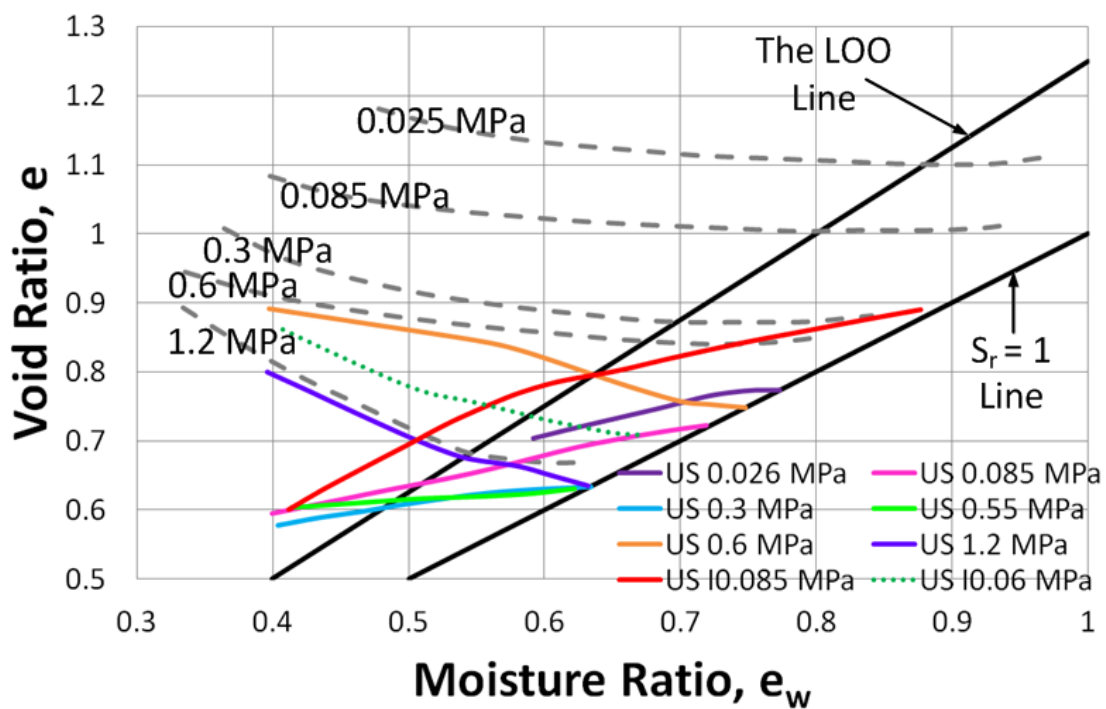
Figure 4-40: First or major wetting state paths of wetting and drying tests for Boom Clay

VOLUME CHANGE BEHAVIOUR OF DYNAMICALLY COMPACTED UNSATURATED SOILS WITHIN THE MPK FRAMEWORK

5.1 Introduction

This chapter is dedicated to the extension of the Monash-Peradeniya-Kodikara (MPK) framework proposed by Kodikara (2012) to dynamically compacted unsaturated soils. An experimental method was developed to construct the Loading Wetting State Boundary Surface (LWSBS) for dynamically compacted soils. In addition, different validation tests were performed to examine whether volume change behaviour can be predicted by the MPK framework. Similar to the validation of MPK framework for statically compacted soils, two types of soils were used in the experimentation, namely kaolin, known by the trade name Ecalite, and Merri Creek soil. While kaolin soil is available in dry form in bags, the preparation of Merri Creek soil involved drying, grinding, and subsequently sieving to remove any deleterious material. The basic geotechnical property tests of the soils were presented in Chapter 3.

5.2 Importance of the extension of the MPK framework into dynamically compacted soils

Dynamic compaction is commonly used to undertake earthworks in civil engineering. It is carried out in the field using various forms of rollers to impart mechanical energy into the soil mass to achieve a competent engineered fill for an intended purpose, such as to support a structural foundation. Typically, the compaction specification is based on the laboratory Proctor test, which characterises the relationship between the water content and dry density for a given energy level. This test was originally developed by Proctor (1933) to simulate field compaction in the laboratory. Standard Proctor, which imparts a gross energy density of 560 kJ/m^3 (AS1289.5.1.1, 2003), is commonly used when moderately heavy machinery is used for compaction. In situations where heavier machinery is used, Modified Proctor energy of 2550 kJ/m^3 (AS1289.5.2.1, 2003) is used.

To cater for other situations, various forms of gross energy are used, including reduced compaction energy to simulate hand-operated machinery (Daniel and Benson, 1990). Compaction specification typically involves a minimum dry density (on the basis of a Proctor's maximum dry density) to be achieved and a range of moisture contents that can be used. More elaborate criteria have been developed for special applications such as clay liners, where the primary intention is to achieve a minimum hydraulic conductivity (e.g., Daniel and Benson, 1990). However, it is still not clear how these compaction energy levels relate to field compaction, where rollers are commonly used. More importantly, it is still difficult at the compaction design stage to examine the likely behaviour of compacted fills under mechanical and environmental loadings that may be imposed during their field operation.

Although static compaction is preferred owing to its simplicity and reproducibility, dynamically compacted clay has also been used by researchers working in the unsaturated soil mechanics field to develop predictive models (e.g., Sivakumar and Wheeler, 2000). However, most of this research has constructed compacted test soil specimens, not using Proctor's compaction methods but using simplified ways of manual compaction, in many cases using miniature compaction hammers. These kinds of simplifications are necessary to construct reproducible specimens for consistency of test results. It is acknowledged that different compaction methods can give rise to different clay structures (Lambe, 1958), and therefore, even when the density and the moisture content are the same, somewhat different behaviours under mechanical and environmental loadings can be expected. While it is possible to extract samples from field compacted cores representing the field compaction procedures and then test them in the laboratory to develop predictive models, it is not very practical, since current suction control test methods are very tedious and time-consuming. It follows therefore that alternative approaches to address these shortcomings are useful. Building on the MPK framework proposed by (Kodikara, 2012), the current chapter presents a series of experimental results and a methodology that may help to address these issues.

5.3 Experimental work

Samples with (gravimetric) moisture contents of 12 to 45% were prepared in a fog room for both soils. The procedure of soil sample preparation in a fog room has been elaborated in Chapter 3. The soil was then dynamically compacted into a Standard Proctor compaction mould, which has a 105 mm internal diameter and is 115 mm in height. Soil cylinders were compacted using different compaction efforts, as listed in Table 5-1. An automated compaction machine was used to prepare High and Intermediate compaction soil cylinders, while Moderate, Low and Very low compaction soil cylinders were prepared manually. This is because the falling height of the hammer of the automated compaction machine could only be fixed to 300 and 450 mm. As can be seen from Table 5-1, the falling height was kept at 150mm during the manual compaction using the Standard Proctor compaction equipment. After compaction, soil cylinders were extruded carefully from the mould and wrapped with several layers of plastic and aluminium foil. Finally, the cylinders were placed in plastic bags and stored in a high humidity room. The dynamic compaction curves for the kaolin and Merri Creek soil are shown in Figure 5-1. For the kaolin soil, the degree of saturation (S_r) at the line of optimum (LOO) varies between 82 to 89% depending on the compaction effort, while for the Merri Creek soil, this value is around 82% for most compaction efforts. For subsequent static loading tests, soil specimens were cut from the dynamically compacted soil cylinders after removing them from the fog room. A bottomless steel mould with dimensions of 63 mm internal diameter and 50 mm height was used to cut the soil specimens from the dynamically compacted soil cylinders. The preparation procedure of soil specimens for the static compaction tests was presented in Chapter 3. Following the procedure for static compaction similar to that explained in the previous chapter, the soil specimens were compressed using the Loadtrac II compression set-up. A filter medium between the soil and the loading cap was provided for any possible drainage from the top, but the bottom was sealed. For tests dry of the LOO, a higher loading rate of 20 kPa per minute was used up to about 2000 kPa and a higher loading rate of 100 kPa per minute above 2000 kPa vertical stress. Once the soil approached the LOO, a much lower loading rate (i.e., 0.1 kPa/min) was used to provide adequate drained conditions.

5.3.1 Development of the LWSBS

The LWSBS in the MPK framework (Kodikara, 2012) is the surface depicting the loosest states compacted soil can attain under loading or wetting or combination of these paths. The LWSBS for statically compacted soil is usually developed by compressing soil specimens with different moisture contents from a nominal pressure to a certain high pressure. In Chapter 4, the LWSBSs of statically compacted kaolin and Merri Creek soil were constructed following this procedure. The nominal pressure on these soils was taken as 7 kPa, which represented the loosest state that the soils take when water is mixed with soil from dry state. In contrast, in the current test program the soil cylinders were compacted dynamically with different compaction efforts during soil preparation. As a result, initially the soil specimens retrieved from compacted cylinders were unloaded and positioned inside the LWSBS applicable to the dynamically compacted soil. Therefore, it was necessary to establish the LWSBS for dynamically compacted soil by retesting soil specimens to undergo yielding. It was expected that soil would deform predominantly elastically up to the LWSBS, where it would undergo yielding (i.e., yield pressure) and, for further loading, would follow the LWSBS. On this basis, the yield point and post-yield loading state paths were used to develop the LWSBS for dynamically compacted soils. To reduce the effort required and to be relevant to typical field conditions, the LWSBS was only targeted above a degree of saturation of 50%. Obtaining test specimens with very low moisture contents could also be difficult using the established procedure, especially for sandy materials.

5.3.1.1 The LWSBS of the kaolin soil

The kaolin soil specimens obtained with different moisture contents and different initial dynamic compaction efforts were compressed statically from zero to a certain high pressure to obtain deformation versus load graphs, and then void ratio versus stress graphs were generated using this data. Figure 5-2(a-g) show measured compression curves presented in traditional e versus log (p) relationships. As explained previously, the soil specimens travelled along the elastic space initially and then followed the normal compression lines (NCL) after yielding. In the figures, solid black lines represent the NCLs at those moisture contents. It is important to note that the moisture contents which are shown in the figures are actually applicable for the dry side of the LOO and as the compression tests were drained, the final moisture contents, which are lower than the

mentioned moisture contents, were measured at the end of the tests. The air pressure was zero at the dry side of the LOO and as the tests were drained, also at the wet side. After developing NCLs at different moisture contents, the void ratio (e) versus moisture ratio (e_w) lines at different stress levels were generated. Figure 5-3a and 5-3b show how the LWSBS of dynamically compacted kaolin soil was constructed. Figure 5-3a shows the LWSBS that was constructed from the NCLs at different moisture contents obtained from Figure 5-2, while the dotted lines in Figure 5-3b show the complete LWSBS. Figure 5-4a shows the LWSBS presented in the form of compaction contours and Figure 5-4b shows a 3-D view of the LWSBS generated.

5.3.1.2 The LWSBS of the Merri Creek soil

Figure 5-5(a-g) show the measured compression curves for the Merri Creek soil presented in traditional e versus log (p) relationships. The test procedure was similar to that of kaolin soil presented earlier. Figure 5-6a and 5-6b show how the LWSBS of dynamically compacted Merri Creek soil was constructed. Figure 5-6a shows the LWSBS which was constructed from the NCLs at different moisture contents obtained from Figure 5-5, while the dotted lines in Figure 5-6b show the complete LWSBS. Figure 5-7a shows the LWSBS presented in the form of compaction contours and Figure 5-7b shows a 3-D view of the LWSBS generated.

5.3.2 State path tests performed on the kaolin soil

Once the LWSBS was established using compression tests, a series of state path tests was undertaken to examine the validity of the concepts proposed by the MPK framework. The soil specimen preparation technique was similar to that of the compression tests presented earlier. As the soil specimens needed to be wetted during loading, the load cap was modified by having four 3 mm diameter holes inserted to facilitate water ingress. The description, the loading assembly and the top and bottom configurations of the top loading cap were presented in Chapter 3. Compared with the compression tests, the test set-up remained the same, with the exception of the load cap. The state path tests which were preformed on the dynamically compacted kaolin soil are listed in Table 5-2.

5.3.2.1 State paths involving a combination of loading and wetting

A series of tests was undertaken where the dynamically compacted kaolin soil specimens were compressed to certain stress levels and then wetted at that stress level. These test results are shown in Figure 5-8a, 5-8b, 5-8c and 5-8d, 5-8e, 5-8f. Figure 5-8a, 5-8b and 5-8c show a soil specimen with High compaction and 19.27% moisture content ($e_w = 0.511$) loaded to 500 kPa and then wetted to 27.94% moisture content ($e_w = 0.732$). As the soil specimen was compacted previously, it is clear that the state path started from inside the LWSBS and then moved towards the LWSBS. The position of the state path is still inside the LWSBS at the end of loading stage because the pre-compaction stress of the kaolin soil specimens due to High compaction is around 1500 kPa. Finally, during wetting at 500 kPa, it swelled towards the stress contour for 500 kPa of the LWSBS to final moisture content but ended inside the LWSBS. Figure 5-8d, 5-8e and 5-8f show a soil specimen with Moderate compaction 19.85 % moisture content ($e_w = 0.526$) loaded to 1000 kPa and then wetted to 29.92% moisture content ($e_w = 0.793$). It is apparent that the state path started from inside the LWSBS, then intercepted the LWSBS around 600 kPa stress and then followed the LWSBS up to 1000 kPa stress. The pre-compaction stress of the kaolin soil specimens due to Moderate compaction is around 600 kPa. Finally, during wetting, the state path followed the 1000 kPa constant net stress contour on the LWSBS to the final moisture content. Figure 5-8g, 5-8h and 5-8i show a test where a dynamically compacted Ecalite soil specimen was loaded to a particular stress level, wetted to certain moisture content and then loaded again to higher stress level. It is evident that the state path intercepted the LWSBS during initial loading stage and then followed the LWSBS during wetting. Finally, during the second stage of loading, instead of following, it moved somewhat away from the LWSBS. This slight deviation may have occurred because of measurement errors. It is apparent from the loading/wetting tests that once the soil specimens intercept the LWSBS they undergo collapse (or compression) controlled by the LWSBS due to wetting. It is also evident that the state paths follow the path dictated by the LWSBS, in agreement with the MPK framework. More loading/wetting state path tests on dynamically compacted kaolin soil specimens are presented in Section 5.3.2.3 below.

5.3.2.2 State paths involving a combination of loading, unloading and wetting

Only a small number of loading/unloading/wetting tests were performed for the validation of the MPK framework for dynamically compacted soils, because at the beginning of the validation tests the dynamically compacted soil specimens were at the unloading stage. As a result, the unloading behaviour of the soil specimens was captured during the loading/wetting tests. Two state path tests involving loading, unloading and wetting undertaken on dynamically compacted kaolin soil are shown in Figure 5-9. Figure 5-9a, 5-9b and 5-9c show a soil specimen with Moderate compaction with 19.85 % moisture content ($e_w = 0.526$) loaded to 3000 kPa and then unloaded to 1000 kPa and then wetted to 23.24% moisture content ($e_w = 0.616$). As the soil specimen was compacted to higher stress earlier, the state path started from inside the LWSBS and then moved towards the LWSBS due to the initial loading. Next, it intercepted the LWSBS around 600 kPa, which is the pre-compaction stress of the kaolin soil specimens subjected to Moderate compaction. After that, it followed the LWSBS up to 3000 kPa stress and then moved inside the LWSBS because of unloading. Finally, during wetting at 1000 kPa, it swelled towards the stress contour for 1000 kPa of the LWSBS to the final moisture content but ended inside the LWSBS. Figure 5-9d, 5-9e and 5-9f show soil specimen with Intermediate compaction and 19.94% moisture content ($e_w = 0.528$) loaded to 2000 kPa and then unloaded to 1000 kPa and then wetted to 26.90% moisture content ($e_w = 0.713$). It is clear that the soil specimen behaved very much the same way as shown in the previous test, intercepting the LWSBS around 1000 kPa during the initial loading, moving inside the LWSBS due to unloading and ending inside the LWSBS after the wetting stage. It is apparent from both of the tests that the soil specimens stayed inside the LWSBS during the wetting stage. As a result, they did not undergo any collapse (or compression) during this stage. Once again, it is evident that the state paths followed the path dictated by the LWSBS, in agreement with the MPK framework.

5.3.2.3 Collapse potential tests

Five loading/wetting tests were performed on dynamically compacted kaolin soil specimens to examine the variation of collapse potential with stress level. Specimens were prepared with 16.51% moisture content ($e_w = 0.438$) and then subjected to High compaction. The soil specimens were then loaded to 500, 1000, 1500, 2000 and 3000

kPa and then wetted. The test results are shown in Figure 5-10a, 5-10b, 5-10c; 5-10d, 5-10e, 5-10f; 5-10g, 5-10h, 5-10i; 5-10j, 5-10k, 5-10l and 5-10m, 5-10n, 5-10o. Figure 5-10a, 5-10b and 5-10c show a soil specimen with High compaction and 16.51% moisture content ($e_w = 0.438$) loaded to 500 kPa and then wetted to 29.86% moisture content ($e_w = 0.791$). As the soil specimen was compacted previously, it is clear that the state path started from inside the LWSBS and then moved towards the LWSBS. The position of the state path is still inside the LWSBS at the end of the loading stage because the pre-compaction stress of the kaolin soil specimens due to High compaction is around 1500 kPa. Finally, during the wetting at 500 kPa, it swelled towards the stress contour for 500 kPa of the LWSBS to the final moisture content but ended inside the LWSBS. Figure 5-10d, 5-10e and 5-10f show a soil specimen with High compaction and 16.51% moisture content ($e_w = 0.438$) loaded to 1000 kPa and then wetted to 28.15% moisture content ($e_w = 0.746$). As the pre-compaction stress of the kaolin soil specimens due to High compaction is around 1500 kPa, the position of the state path is still inside the LWSBS at the end of the loading stage. Finally, during wetting, it swelled and intercepted the LWSBS around 24.50% moisture content ($e_w = 0.650$) and then followed the 1000 kPa constant net stress contour on the LWSBS to the final moisture content. Figure 5-10g, 5-10h and 5-10i show a soil specimen with High compaction and 16.51% moisture content ($e_w = 0.438$) loaded to 1500 kPa and then wetted to 27.65% moisture content ($e_w = 0.733$). It is clear that the state path started from inside the LWSBS and then moved towards the LWSBS and intercepted the LWSBS around 1500 kPa. Finally, during wetting, the state paths followed the 1500 kPa constant net stress contours on the LWSBS to the final moisture content. Figure 5-10j, 5-10k, 5-10l and 5-10m, 5-10n and 5-10o show soil specimens with High compaction and 16.51% moisture content ($e_w = 0.438$) loaded to 2000 kPa and 3000 kPa and then wetted to 25.90% moisture content ($e_w = 0.686$) and 22.78% moisture content ($e_w = 0.604$) respectively. As the soil specimens were compacted previously, it is apparent in both cases that the state paths started from inside the LWSBS and then moved towards the LWSBS. Next, they followed the LWSBS up to 2000 kPa and 3000 kPa stress respectively after intersecting the LWSBS around 1500 kPa stress. The pre-compaction stress of the kaolin soil specimens due to High compaction is around 1500 kPa. Finally, during wetting, the state paths followed the 2000 kPa and 3000 kPa constant net stress contours respectively on the LWSBS to the final moisture contents. It is evident from these loading/wetting

tests that once the soil specimens intercepted the LWSBS, they underwent collapse (or compression) as depicted by the LWSBS due to wetting. Figure 5-11a shows the collapse potential (given as the reduction in void ratio) vs stress graphs, while Figure 5-11b shows the compression curve of 16.51% moisture content ($e_w = 0.438$) High compaction presented in traditional e versus log (p) relationships. It is clear from Figure 5-11b that the pre-compaction stress of the kaolin soil specimens subjected to High compaction is 1500 kPa. According to the MPK framework, during wetting, the maximum collapse occurs when the operational stress becomes the same as the compaction stress. This behaviour is also apparent from Figure 5-11a. It is also evident from Figure 5-11a that when the operational stress is higher or lower than the compaction stress, the amount of collapse is lower than the maximum. This behaviour is consistent with the typical behaviour reported for the collapse potential of soils (e.g., Sun et al., 2004).

Another five loading/wetting tests were performed on Low compaction, 25.96% moisture content ($e_w = 0.688$) kaolin soil specimens to examine the variation of collapse potential with the stress level. At the beginning, the dynamically compacted soil specimens were loaded to 100, 250, 300, 700 and 1000 kPa and then wetted. These test results are shown in Figure 5-12a, 5-12b, 5-12c; 5-12d, 5-12e, 5-12f; 5-12g, 5-12h, 5-12i; 5-12j, 5-12k, 5-12l and 5-12m, 5-12n and 5-12o. Figure 5-12a, 5-12b and 5-12c show a soil specimen with Low compaction 25.96% and moisture content ($e_w = 0.688$) loaded to 100 kPa and then wetted to 37.89% moisture content ($e_w = 1.004$). As the pre-compaction stress of the kaolin soil specimens due to Low compaction is around 250 kPa, the position of the state path is still inside the LWSBS at the end of the loading stage. Finally, during wetting, it swelled and intercepted the LWSBS around 28.34% moisture content ($e_w = 0.751$) and then followed 100 kPa constant net stress contour on the LWSBS to the final moisture content. Figure 5-12d, 5-12e and 5-12f show a soil specimen with Low compaction and 25.96% moisture content ($e_w = 0.688$) loaded to 250 kPa and then wetted to 39.92% moisture content ($e_w = 1.058$). As the soil specimen was compacted previously, it is clear that the state path started from inside the LWSBS and then moved towards the LWSBS and intercepted the LWSBS around 250 kPa. Finally, during wetting, the state path followed the 250 kPa constant net stress contours on the LWSBS to the final moisture content. Figure 5-12g, 5-12h, 5-12i; 5-12j, 5-12k, 5-12l and 5-12m, 5-12n, 5-12o show soil specimens with Low compaction and 25.96%

moisture content ($e_w = 0.688$) loaded to 300 kPa, 700 kPa and 1000 kPa and then wetted to 36.87% moisture content ($e_w = 0.977$), 32.96% moisture content ($e_w = 0.873$) and 30.01% moisture content ($e_w = 0.795$) respectively. As the soil specimens were compacted previously, it is apparent that the state paths started from inside the LWSBS and then moved towards the LWSBS. Next, they followed the LWSBS up to 300 kPa, 700 kPa and 1000 kPa stress in accordance after intersecting the LWSBS around 250 kPa stress. Finally, during wetting, the state paths followed the 300 kPa, 700 kPa and 1000 kPa constant net stress contours respectively on the LWSBS to the final moisture content. It is evident from these loading/wetting tests that, once the soil specimens intercept the LWSBS they undergo collapse (or compression) controlled by the LWSBS due to wetting. It is also apparent that the state paths follow the path dictated by the LWSBS, in agreement with the MPK framework. Figure 5-13a shows the collapse potential (given as the reduction in void ratio) vs stress graphs, while Figure 5-13b shows the compression curve of 25.96% moisture content ($e_w = 0.688$) Low compaction presented in traditional e versus log (p) relationships. It is clear from Figure 5-13b that the pre-compaction stress of the kaolin soil specimens subjected to Low compaction is 250 kPa. According to the MPK framework, during wetting, the maximum collapse occurs when the operational stress becomes the same as the compaction stress. This behaviour is also apparent from Figure 5-13a. It is also evident from Figure 5-13a that when the operational stress is higher or lower than the compaction stress, the amount of collapse is lower than the maximum. This behaviour matches the typical behaviour observed by Sun et al. (2004) for the collapse potential of soils.

5.3.2.4 Swelling pressure tests

While the tests presented in Figure 5-8, Figure 5-9, Figure 5-10 and Figure 5-12 show the swelling behaviour of unloaded kaolin soil during wetting, a series of tests was undertaken to examine the swelling pressure development at constant volume (constrained) wetting for dynamically compacted kaolin soil specimens. The tests were undertaken by locking the specimen against volumetric deformation but measuring the applied stress variation when the specimen is wetted. The same mould and set-up used for the other validation tests was used in this phase of testing. Figure 5-14 shows the results of the tests. Figure 5-14a and 5-14b show the state path of a Moderate compaction 19.85% moisture content ($e_w = 0.526$) soil specimen that was loaded to 200 kPa (path

AB) and then wetted at constant volume (i.e., e constant) to saturation (path BCDE). As the pre-compaction stress of kaolin soil specimens subjected to Moderate compaction is around 600 kPa, it is clear that the position of the soil specimen after 200 kPa stress application is below the LWSBS (point B), and during wetting, the swelling pressure builds up to C (around 250 kPa), at which the state reaches the LWSBS. Subsequently, the path CD is on the LWSBS (at constant initial void ratio = 1.16), reducing the swelling pressure until the LOO is intercepted at point D. Further wetting makes the soil increase swelling pressure again towards saturation, as shown by path DE. This behaviour is consistent with the MPK framework and with the test results reported in Chapter 4 on statically compacted soils and in the past (Kodikara, 2012). Figure 5-14c, 5-14d and Figure 5-14e, 5-14f also show similar behaviour for the state paths of soil specimens with Moderate compaction and 19.85% moisture content ($e_w = 0.526$), and Intermediate compaction and 19.94% moisture content ($e_w = 0.528$) loaded to 200 kPa (path AB) and 300 kPa (path AB) respectively, and then wetted at constant volume to saturation (path BCDE). It is evident that as the compaction stress increases (or the initial void ratio decreases or the initial density increases), the maximum swelling pressure increases. In comparison to Figure 5-14a, 5-14b, Figure 5-14c, 5-14d and Figure 5-14e, 5-14f; Figure 5-14g, 5-14h, Figure 5-14i, 5-14j and Figure 5-14k, 5-14l show Intermediate compaction with 27.71% moisture content ($e_w = 0.734$), high compaction with 19.27% moisture content ($e_w = 0.511$) and High compaction with 23.54% moisture content ($e_w = 0.624$) soil specimens loaded to 500 kPa (path AB), 500 kPa (path AB) and 1000 kPa (path AB) respectively, and then wetted at constant volume to saturation (path BC). It is evident that these specimens did not reach the LWSBS and the swelling pressure continued to increase with wetting. It appears that at the beginning of wetting, all were well below the LWSBS. It should be noted that this behaviour is common at higher compaction stresses. In addition, similar behaviour can arise for lower compaction stresses if the initial moisture content is higher due to changes in the relative positions of the LWSBS.

5.3.3 State path tests performed on the Merri Creek soil

The state path tests that were performed on the dynamically compacted Merri Creek soil are listed in Table 5-3.

5.3.3.1 State paths involving a combination of loading and wetting

A series of tests was undertaken where the dynamically compacted Merri Creek soil specimens were compressed to a certain stress level and then wetted at that stress level. These test results are shown in Figure 5-15a, 5-15b, 5-15c and 5-15d, 5-15e, 5-15f. Figure 5-15a, 5-15b and 5-15c show a soil specimen with High compaction and 15.70% moisture content ($e_w = 0.411$) loaded to 1000 kPa and then wetted to 22.33% moisture content ($e_w = 0.585$). As the soil specimen was compacted previously, it is clear that the state path started from inside the LWSBS and then moved towards the LWSBS during the loading stage. At the end of this stage, the position of the state path is still inside the LWSBS because the pre-compaction stress of the Merri Creek soil specimens due to High compaction (around 1700 kPa) is higher than the applied stress. Finally, during wetting, it swelled and intercepted the LWSBS around 19.10% moisture content ($e_w = 0.500$) and then followed 1000 kPa constant net stress contour on the LWSBS to the final moisture content. Figure 5-15d, 5-15e and 5-15f show a soil specimen with Low compaction and 23.38% moisture content ($e_w = 0.613$) loaded to 400 kPa and then wetted to 28.62% moisture content ($e_w = 0.750$). It is apparent that the state path intercepted the LWSBS around 300 kPa, which is the pre-compaction stress of the Merri Creek soil specimens subjected to Low compaction. It then followed the LWSBS and during wetting, followed the 400 kPa constant net stress contour on the LWSBS to the final moisture content. Figure 5-15g, 5-15h, 5-15i and 5-15j, 5-15k, 5-15l show tests where the dynamically compacted Merri Creek soil specimens were loaded to a particular stress level, wetted to a certain moisture content and then loaded again to a higher stress level. It is evident from both of the tests that the state paths intercepted the LWSBS during the initial loading stage and then followed the LWSBS during wetting. Finally, during the second stage loading, they followed the corresponding constant moisture ratio contours on the LWSBS to the final stress. It is apparent from the loading/wetting tests that once the soil specimens intercept the LWSBS, they undergo collapse (or compression) as depicted by the LWSBS due to wetting. It is also evident that the LWSBS takes control of the state path when it arrives on the LWSBS. At that time, the volumetric behaviour of a soil specimen can be predicted by the LWSBS, unless the state path leaves the LWSBS again due to unloading. More loading/wetting state path tests on dynamically compacted Merri Creek soil specimens are presented in Section 5.3.3.3 below.

5.3.3.2 State paths involving a combination of loading, unloading and wetting

The results of two state path tests involving loading, unloading and wetting undertaken on the dynamically compacted Merri Creek soil are shown in Figure 5-16. Figure 5-16a, 5-16b and 5-16c show a soil specimen with Intermediate compaction and 15.52% moisture content ($e_w = 0.407$) loaded to 2000 kPa and then unloaded to 1000 kPa and then wetted to 20.52% moisture content ($e_w = 0.538$). As the soil specimen had been compacted earlier, the state path started from inside the LWSBS and then moved towards the LWSBS due to the initial loading. Next, it intercepted the LWSBS around 1000 kPa, which is the pre-compaction stress of Merri Creek soil specimens subjected to Intermediate compaction. It then followed the LWSBS up to 2000 kPa stress and then moved inside the LWSBS because of unloading. Finally, during wetting, it swelled towards the stress contour for 1000 kPa of the LWSBS to the final moisture content but ended inside the LWSBS. Figure 5-16d, 5-16e and 5-16f show a soil specimen with Low compaction and 23.38% moisture content ($e_w = 0.613$) loaded to 500 kPa and then unloaded to 400 kPa and then wetted to 27.86% moisture content ($e_w = 0.730$). It is clear that the soil specimen behaved exactly the same way as shown in the previous test, intercepting the LWSBS around 300 kPa during initial loading, moving inside the LWSBS due to unloading and ending inside the LWSBS after the wetting stage. It is apparent from both tests that the soil specimens stayed inside the LWSBS during the wetting stage. As a result, they did not undergo any collapse (or compression) during this stage. It is also evident that the state paths followed the path dictated by the LWSBS in agreement with the MPK framework.

5.3.3.3 Collapse potential tests

Five loading/wetting tests were performed on dynamically compacted Merri Creek soil specimens to examine the variation of collapse potential with stress level. The specimens were prepared with 15.52% moisture content ($e_w = 0.407$) and then subjected to Intermediate compaction. The soil specimens were then loaded to 100, 500, 1000, 2000 and 3000 kPa and then wetted. These test results are shown in Figure 5-17a, 5-17b, 5-17c; 5-17d, 5-17e, 5-17f; 5-17g, 5-17h, 5-17i; 5-17j, 5-17k, 5-17l and 5-17m, 5-17n, 5-17o. Figure 5-17a, 5-17b and 5-17c show a soil specimen with Intermediate compaction and 15.52% moisture content ($e_w = 0.407$) loaded to 100 kPa and then

wetted to 30.52% moisture content ($e_w = 0.800$). As the soil specimen had been compacted previously, it is clear that the state path started from inside the LWSBS and then moved towards the LWSBS. The position of the state path is still inside the LWSBS at the end of loading stage because the pre-compaction stress of the Merri Creek soil specimens due to Intermediate compaction is around 1000 kPa. Finally, during wetting at 100 kPa, it swelled towards the stress contour for 100 kPa of the LWSBS to the final moisture content but ended inside the LWSBS. Figure 5-17d, 5-17e and 5-17f show a soil specimen with Intermediate compaction and 15.52% moisture content ($e_w = 0.407$) loaded to 500 kPa and then wetted to 27.30% moisture content ($e_w = 0.715$). As the pre-compaction stress of the Merri Creek soil specimens due to Intermediate compaction is around 1000 kPa, the position of the state path is still inside the LWSBS at the end of loading stage. Finally, during wetting, it swelled and intercepted the LWSBS around 21.76% moisture content ($e_w = 0.570$) and then followed the 500 kPa constant net stress contour on the LWSBS to the final moisture content. Figure 5-17g, 5-17h and 5-17i show a soil specimen with Intermediate compaction and 15.52% moisture content ($e_w = 0.407$) loaded to 1000 kPa and then wetted to 22.52% moisture content ($e_w = 0.590$). It is clear that the state path started from inside the LWSBS and then moved towards the LWSBS and intercepted the LWSBS around 1000 kPa. Finally, during wetting, the state path followed 1000 kPa constant net stress contour on the LWSBS to the final moisture content. Figure 5-17j, 5-17k, 5-17l and 5-17m, 5-17n, 5-17o show soil specimens with Intermediate compaction and 15.52% moisture content ($e_w = 0.407$) loaded to 2000 kPa and 3000 kPa and then wetted to 19.46% moisture content ($e_w = 0.510$) and 17.37% moisture content ($e_w = 0.455$) respectively. As the soil specimens had been compacted previously, it is apparent in both cases that the state paths started from inside the LWSBS and then moved towards the LWSBS. Next, they followed the LWSBS up to 2000 kPa and 3000 kPa stress respectively, after intersecting the LWSBS around 1000 kPa stress. Finally, during wetting, the state paths followed 2000 kPa and 3000 kPa constant net stress contours respectively on the LWSBS to the final moisture contents. It is clear from these loading/wetting tests that once the soil specimens intercept the LWSBS, they undergo collapse (or compression), as depicted by the LWSBS due to wetting. It is also evident that the LWSBS takes control of the state path when it arrives on the LWSBS. Figure 5-18a shows the collapse potential (given as the reduction in void ratio) vs stress graphs, while Figure 5-18b shows the compression

curve of a specimen with 15.52% moisture content ($e_w = 0.407$) and Intermediate compaction presented in traditional e versus log (p) relationships. It is clear from Figure 5-18b that pre-compaction stress of the Merri Creek soil specimen subjected to Intermediate compaction is around 1000 kPa. According to the MPK framework, during wetting, maximum collapse occurs when the operational stress becomes the same as the compaction stress. This behaviour is also apparent from Figure 5-18a. It is also evident from Figure 5-18a that when the operational stress is higher or lower than the compaction stress, the amount of collapse is lower than the maximum. This behaviour is consistent with the typical behaviour reported for the collapse potential of soils (e.g., Sun et al., 2004).

Another five loading/wetting tests were performed on Moderate compaction, 20.52% moisture content ($e_w = 0.538$) Merri Creek soil specimens to examine the collapse potential variation with the stress level. First, dynamically compacted soil specimens were loaded to 100, 300, 500, 700 and 1000 kPa and then wetted. These test results are shown in Figure 5-19a, 5-19b, 5-19c; 5-19d, 5-19e, 5-19f; 5-19g, 5-19h, 5-19i; 5-19j, 5-19k, 5-19l and 5-19m, 5-19n, 5-19o. Figure 5-19a, 5-19b and 5-19c show a soil specimen with Moderate compaction and 20.52% moisture content ($e_w = 0.538$) loaded to 100 kPa and then wetted to 33.80% moisture content ($e_w = 0.886$). As the pre-compaction stress of the Merri Creek soil specimens due to Moderate compaction is around 500 kPa, the position of the state path is still inside the LWSBS at the end of the loading stage. Finally, during wetting at 100 kPa, it swelled towards the stress contour for 100 kPa of the LWSBS to final moisture content but ended inside the LWSBS. Figure 5-19d, 5-19e and 5-19f show a soil specimen with Moderate compaction and 20.52% moisture content ($e_w = 0.538$) loaded to 300 kPa and then wetted to 30.52% moisture content ($e_w = 0.800$). As the soil specimen had been compacted previously, it is clear that the state path started from inside the LWSBS and then moved towards the LWSBS during loading. The position of the state path is still inside the LWSBS at the end of the loading stage. Finally, during wetting at 300 kPa, it swelled towards the stress contour for 300 kPa of the LWSBS to the final moisture content but ended inside the LWSBS. Figure 5-19g, 5-19h, 5-19i show a soil specimen with Moderate compaction and 20.52% moisture content ($e_w = 0.538$) loaded to 500 kPa and then wetted to 26.72% moisture content ($e_w = 0.700$). It is clear that the state path started from inside

the LWSBS and then moved towards the LWSBS and intercepted the LWSBS around 500 kPa. Finally, during wetting, the state paths followed the 500 kPa constant net stress contours on the LWSBS to the final moisture content. Figure 5-19j, 5-19k, 5-19l and 5-19m, 5-19n, 5-19o show soil specimens with Moderate compaction and 20.52% moisture content ($e_w = 0.538$) loaded to 700 kPa and 1000 kPa and then wetted to 25.20% moisture content ($e_w = 0.660$) and 22.52% moisture content ($e_w = 0.590$) respectively. As the soil specimens had been compacted previously, it is apparent that the state paths started from inside the LWSBS and then moved towards the LWSBS. Next, they followed the LWSBS up to 700 kPa and 1000 kPa stress respectively, after intercepting the LWSBS around 500 kPa stress. Finally, during wetting, the state paths followed 700 kPa and 1000 kPa constant net stress contours respectively on the LWSBS to the final moisture contents. It is evident from these loading/wetting tests that once the soil specimens intercept the LWSBS, they undergo collapse (or compression) controlled by the LWSBS due to wetting. It is also apparent that the state paths followed the path dictated by the LWSBS in agreement with the MPK framework. Figure 5-20a shows the collapse potential (given as the reduction in void ratio) vs stress graphs, while Figure 5-20b shows the compression curve of a specimen with 20.52% moisture content ($e_w = 0.538$) and Moderate compaction presented in traditional e versus log (p) relationships. It is clear from Figure 5-20b that the pre-compaction stress of the Merri Creek soil specimen subjected to Moderate compaction is around 500 kPa. According to the MPK framework, during wetting, the maximum collapse occurs when the operational stress becomes the same as the compaction stress. This behaviour is also apparent from Figure 5-20a. It is also evident from Figure 5-20a that when the operational stress is higher or lower than the compaction stress, the amount of collapse is lower than the maximum. This behaviour is consistent with the typical behaviour observed by Sun et al. (2004) for the collapse potentiality of soils.

5.3.3.4 Swelling pressure tests

As with the kaolin soil, a series of tests was undertaken to examine the swelling pressure development at constant volume (constrained) wetting of the dynamically compacted Merri Creek soil. Figure 5-21 shows the results of the tests. Figure 5-21c, 5-21d and 5-21i, 5-21j show the state paths of soil specimens with Intermediate compaction 15.52% and moisture content ($e_w = 0.407$) and Moderate compaction and 20.52% moisture

content ($e_w = 0.538$) that were loaded to 500 kPa (path AB) and 400 kPa (path AB) respectively and then wetted at constant volume (i.e., e constant) to saturation (path BCDE). In both cases, the pre-compaction stresses of the soil specimens are higher than the applied stress. As a result, points B are located below the LWSBS, and during wetting, the swelling pressure builds up to points C at which the state paths reach the LWSBS. Subsequently, the paths CD are on the LWSBS, reducing the swelling pressure until the LOO is intercepted at points D. Further wetting makes the soil increase swelling pressure again towards saturation, as shown by paths DE. This behaviour is consistent with the MPK framework, with the test results reported in Chapter 4 on statically compacted soils, those reported earlier in this chapter on dynamically compacted kaolin soil, and in the past (Kodikara, 2012). Figure 5-21a, 5-21b; 5-21e, 5-21f; 5-21g, 5-21h and 5-21k, 5-21l show specimens with High compaction and 15.93% moisture content ($e_w = 0.417$), Intermediate compaction and 18.16% moisture content ($e_w = 0.476$), Intermediate compaction and 19.89% moisture content ($e_w = 0.521$) and Moderate compaction and 23.62% moisture content ($e_w = 0.619$) loaded to 500 kPa (path AB), 500 kPa (path AB), 500 kPa (path AB) and 200 kPa (path AB) respectively and then wetted at constant volume to saturation (path BC). In comparison with the previous two test results, these four soil specimens did not reach the LWSBS and swelling pressure continued to increase with wetting. It appears that at the beginning of wetting, all were well below the LWSBS. It should be noted that this behaviour is common for higher compaction stresses. In addition, similar behaviour can arise for lower compaction stresses if the initial moisture content is higher, due to changes in the relative positions of the LWSBS. Figure 5-21m and 5-21n compare the three test results presented earlier showing the influence of the initial moisture contents of 15.52% ($e_w = 0.407$), 18.16% ($e_w = 0.476$) and 19.89% ($e_w = 0.521$) on the swelling state paths. The specimens were prepared with Intermediate compaction at the beginning and then loaded to 500 kPa and then wetted at constant volume to saturation (paths $B_{1,2,3}C_{1,2,3}D_1E_1$). It is evident that the swelling pressure decreases with increasing initial moisture content, consistent with published results (e.g., Kassiff and Shalom, 1971; Lee et al., 1999). Figure 5-21o and 5-21p show the effect of compaction effort (high and Intermediate compaction) on the swelling state paths for the specimens prepared with initial moisture contents of 15.93% ($e_w = 0.417$) and 15.52% ($e_w = 0.407$) respectively. These test results indicate that the swelling pressure increases with the compaction effort (with initial density) when all

other variables are kept constant. Similar behaviour has been reported in the research literature (e.g., Kassiff and Shalom, 1971; Imbert and Villar, 2006).

5.4 Discussion

A large number of experiments were performed on dynamically compacted lightly reactive kaolin and reactive Merri Creek clay with constant water contents. Despite the difference in their degree of reactivity, both soils closely followed the concepts of the MPK framework. This highlights that the macroscopic behaviour of compacted soil in general can be presented within this framework. It should, however, be recognised that manifestation of the observed macroscopic behaviour is due to the complex interaction between the micro and macro void and associated structural elements, which are inherent in initially compacted soils (Alonso et al., 1999). In the following discussion, some of the specific features observed are examined.

Similar to statically compacted soils, the influence of the LOO is clearly evident from the experimental results. The cross-validity (loading under constant moisture ratio and wetting under constant net stress) and the uniqueness of the LWSBS have been established by a large number of state paths involving a combination of loading, unloading and wetting. The capability of the LWSBS to predict the change in yield point for state paths that undergo wetting at constant stress has also been verified. Similarly, constrained swelling tests also clearly demonstrate the influence of the LOO on the LWSBS. For instance, similar to statically compacted soils, the swelling pressure increases to a peak until the state path intercepts the LWSBS and then follows it, the swelling pressure subsequently decreasing to the LOO, and then increasing again towards full saturation (e.g., Figure 5-14a). Another important validation is the confirmation of the characteristic behaviour of collapse potential, where the peak collapse occurs at the compaction (yield) stress, similar to the behaviour displayed for statically compacted soils.

Figure 5-22 shows 2-D and 3-D comparisons of the LWSBSs of statically and dynamically compacted kaolin and Merri Creek soils. The LWSBS contours and surfaces for the two types of compaction are markedly similar for both soils. This result corroborates the similarity in the observed phenomenological behaviour of the two soil

types under the two types of compaction processes. Nonetheless, for kaolin soil, static compaction appears to produce lower void ratio or higher density at the same compaction stress, especially at lower stress levels. For the more reactive Merri Creek soil, the reverse behaviour seems to be operative, where the lower void ratios are produced for dynamic compaction, especially at lower stress levels. For both soils, at higher stress levels this difference appears to diminish. During the preparation of compacted soil specimens for further testing, Sivakumar and Wheeler (2000) noticed no change in compaction water content or compaction-induced dry density for the Speswhite kaolin soil at the dry of optimum. Ahmed et al. (1974) also reported the same based on the results of pore size distribution of a Grundite clay. However, Sivakumar and Wheeler (2000) noted that this idea may not be conclusive (see, Seed and Chan, 1959). In this case, however, it is unclear why these differences arise, but despite the similar initial state, considering dynamic compaction involves repetitive loading, where soil is progressively compacted, such differences can be expected.

Figure 5-23 shows comparisons of the LWSBSs of the kaolin and Merri Creek soils for statically and dynamically compacted conditions. The LWSBS contours for two types of soils are markedly similar for both compaction states. It is clear that for both types of compaction, the constant stress contours of the kaolin soil are flatter than those for the Merri Creek soil both sides of the LOO. This proves the high sensitivity of Merri Creek soil during loading and wetting. It is alos possible that the influence of suction is higher for the Merri Creek soil, given that it has more reactive clay minerals. This highlights the influence of the shape of the compaction curve or the shape of the LWSBS and its relationship to the behaviour of compacted soils under wetting and loading. It is also apparent that for the same net stress, the Merri Creek soil compresses more than the kaolin soil. As a result, the Merri Creek soil provides higher density than the kaolin soil at the same net stress. Figure 5-24, which presents the consolidation curves (saturated *e vs log p*) of the statically and dynamically compacted kaolin and Merri Creek soils, also show a similar result, as stated earlier.

The most significant application of these findings to practice is that, with the proposed framework, it now appears possible to directly evaluate compacted clay performance at field scale. For instance, it is possible to obtain cores from field pads, where compaction

is conducted using rollers to be used in the field at different energy levels and wide range of moisture contents. These cores can then be used to establish the LWSBS for compacted soils and then analyses can be undertaken to predict the performance under expected field environmental and external loadings. As noted previously, constant moisture content testing is very straightforward and, furthermore, it is only necessary to develop the relevant section of the LWSBS that is considered operative for a given field application.

5.5 Conclusion

Significant experimental results were presented in support of the MPK framework for dynamically compacted soils. Since the compaction stress was unknown for dynamic compaction, recompression of soil specimens from compacted soil was used to establish the LWSBS. Independent tests undertaken showed that the framework can predict well the behaviour of compacted soils under loading/unloading and yielding, collapse during wetting, change of loading yield stress after wetting, and swelling pressure development during constrained wetting. The value of the approach is that the testing methods are straight-forward, do not require specialised equipment and the testing times are short. In addition, the uncertainty that laboratory dynamic compaction may not relate directly to field roller compaction can also be addressed with the developed framework. Soil specimens obtained from field soil pads compacted by actual rollers can be used to establish the LWSBS. Such knowledge will allow the prediction of the likely behaviour of field-compacted fills under expected environmental and external loadings under one-dimensional conditions.

Table 5-1: A summary of compaction efforts used to prepare the dynamically compacted soil cylinders

Compaction Name	Mould volume (cm^3)	No. of layers	No. of blows each layer	Hammer weight (lb/kg)	Hammer falling height (inch/mm)	Total energy input (kN-m/m^3)	Kaolin Soil		Merri Creek Soil	
							Maximum dry density (kN/m^3)	Optimum moisture content (%)	Maximum dry density (kN/m^3)	Optimum moisture content (%)
Modified Proctor	≈1000	5	25	10/4.545	18/450	2548	14.8	25.4	16.2	19.2
High compaction	**≈1000**	**5**	**25**	**10/4.545**	**12/300**	**1669**	**14.4**	**27.1**	**15.4**	**20.5**
Intermediate compaction	**≈1000**	**5**	**25**	**5.5/2.5**	**12/300**	**934**	**13.9**	**29.1**	**14.3**	**24.8**
Standard Proctor	≈1000	3	25	5.5/2.5	12/300	560	13.5	30.4	13.8	27.1
Moderate compaction	**≈1000**	**5**	**25**	**5.5/2.5**	**6/150**	**467**	**13.2**	**31.5**	**13.0**	**30.6**
Low compaction	**≈1000**	**5**	**12**	**5.5/2.5**	**6/150**	**224**	**12.4**	**33.9**	**12.4**	**33.3**
Very low compaction	**≈1000**	**5**	**6**	**5.5/2.5**	**6/150**	**112**	**11.5**	**36.8**	**11.0**	**41.4**

Table 5-2: A summary of the state path tests performed on the dynamically compacted kaolin soil

Test Identity	Description of the Test
Loading – Wetting Tests	
DC – EK – LW – 1	High compaction 19.27% moisture content ($e_w = 0.511$) soil specimen loaded to 500 kPa and then wetted to 27.94% moisture content ($e_w = 0.732$)
DC – EK – LW – 2	Moderate compaction 19.85 % moisture content ($e_w = 0.526$) soil specimen loaded to 1000 kPa and then wetted to 29.92% moisture content ($e_w = 0.793$)
Loading – Unloading – Wetting Tests	
DC – EK – LUW – 1	Moderate compaction 19.85 % moisture content ($e_w = 0.526$) soil specimen loaded to 3000 kPa and then unloaded to 1000 kPa and then wetted to 23.24% moisture content ($e_w = 0.616$)
DC – EK – LUW – 2	Intermediate compaction 19.94% moisture content ($e_w = 0.528$) soil specimen loaded to 2000 kPa and then unloaded to 1000 kPa and then wetted to 26.90% moisture content ($e_w = 0.713$)
Loading – Wetting – Loading Tests	
DC – EK – LWL – 1	Intermediate compaction 19.94% moisture content ($e_w = 0.528$) soil specimen loaded to 1000 kPa and then wetted to 25.66% moisture content ($e_w = 0.680$) and then loaded to 2000 kPa
Collapse Potential Tests	
DC – EK – CPT – 1 or DC – EK – LW – 3	High compaction 16.51% moisture content ($e_w = 0.438$) soil specimen loaded to 2000 kPa and then wetted to 25.90% moisture content ($e_w = 0.686$)
DC – EK – CPT – 2 or DC – EK – LW – 4	High compaction 16.51% moisture content ($e_w = 0.438$) soil specimen loaded to 500 kPa and then wetted to 29.86% moisture content ($e_w = 0.791$)
DC – EK – CPT – 3 or DC – EK – LW – 5	High compaction 16.51% moisture content ($e_w = 0.438$) soil specimen loaded to 1000 kPa and then wetted to 28.15% moisture content ($e_w = 0.746$)
DC – EK – CPT – 4 or DC – EK – LW – 6	High compaction 16.51% moisture content ($e_w = 0.438$) soil specimen loaded to 3000 kPa and then wetted to 22.78% moisture content ($e_w = 0.604$)
DC – EK – CPT – 5 or DC – EK – LW – 7	High compaction 16.51% moisture content ($e_w = 0.438$) soil specimen loaded to 1500 kPa and then wetted to 27.65% moisture content ($e_w = 0.733$)
Combination of DC – EK – CPT – 1 to 5	A "Reduction of Void Ratio – Net Stress" graph shows the results obtained from Collapse Potential Tests (1 – 5)
DC – EK – CPT – 6	Low compaction 25.96% moisture content ($e_w = 0.688$) soil specimen loaded to

or DC – EK – LW – 8	300 kPa and then wetted to 36.87% moisture content ($e_w = 0.977$)
DC – EK – CPT – 7 or DC – EK – LW – 9	Low compaction 25.96% moisture content ($e_w = 0.688$) soil specimen loaded to 1000 kPa and then wetted to 30.01% moisture content ($e_w = 0.795$)
DC – EK – CPT – 8 or DC – EK – LW – 10	Low compaction 25.96% moisture content ($e_w = 0.688$) soil specimen loaded to 700 kPa and then wetted to 32.96% moisture content ($e_w = 0.873$)
DC – EK – CPT – 9 or DC – EK – LW – 11	Low compaction 25.96% moisture content ($e_w = 0.688$) soil specimen loaded to 100 kPa and then wetted to 37.89% moisture content ($e_w = 1.004$)
DC – EK – CPT – 10 or DC – EK – LW – 12	Low compaction 25.96% moisture content ($e_w = 0.688$) soil specimen loaded to 250 kPa and then wetted to 39.92% moisture content ($e_w = 1.058$)
Combination of DC – EK – CPT – 6 to 10	A "Reduction of Void Ratio – Net Stress" graph shows the results obtained from Collapse Potential Tests (6 – 10)
Swelling Pressure Tests	
DC – EK – SPT – 1	Moderate compaction 19.85% moisture content ($e_w = 0.526$) soil specimen loaded to 200 kPa and then wetted to 43.40% moisture content ($e_w = 1.150$) ($S_r = 0.991$ and $e_0 = 1.16$) in constant volume
DC – EK – SPT – 2	Moderate compaction 25.40% moisture content ($e_w = 0.673$) soil specimen loaded to 300 kPa and then wetted to 39.62% moisture content ($e_w = 1.050$) ($S_r = 0.99$ and $e_0 = 1.06$) in constant volume
DC – EK – SPT – 3	Intermediate compaction 19.94% moisture content ($e_w = 0.528$) soil specimen loaded to 300 kPa and then wetted to 36.60% moisture content ($e_w = 0.970$) ($S_r = 0.99$ and $e_0 = 0.98$) in constant volume
DC – EK – SPT – 4	Intermediate compaction 27.71% moisture content ($e_w = 0.734$) soil specimen loaded to 500 kPa and then wetted to 32.08% moisture content ($e_w = 0.850$) ($S_r = 0.975$ and $e_0 = 0.872$) in constant volume
DC – EK – SPT – 5	High compaction 19.27% moisture content ($e_w = 0.511$) soil specimen loaded to 500 kPa and then wetted to 30.20% moisture content ($e_w = 0.800$) ($S_r = 0.96$ and $e_0 = 0.835$) in constant volume
DC – EK – SPT – 6	High compaction 23.54% moisture content ($e_w = 0.624$) soil specimen loaded to 1000 kPa and then wetted to 29.40% moisture content ($e_w = 0.779$) ($S_r = 0.975$ and $e_0 = 0.8$) in constant volume

DC => Dynamic Compaction, EK => Ecalite Kaolin, LW => Loading – Wetting, LUW => Loading – Unloading – Wetting, LWL => Loading – Wetting – Loading, CPT => Collapse Potential Test, SPT => Swelling Pressure Test.

Table 5-3: A summary of the state path tests performed on the dynamically compacted Merri Creek soil

| Test Identity	Description of the Test
Loading – Wetting Tests	
DC – MC – LW – 1	High compaction 15.70% moisture content ($e_w = 0.411$) soil specimen loaded to 1000 kPa and then wetted to 22.33% moisture content ($e_w = 0.585$)
DC – MC – LW – 2	Low compaction 23.38% moisture content ($e_w = 0.613$) soil specimen loaded to 400 kPa and then wetted to 28.62% moisture content ($e_w = 0.750$)
Loading – Unloading – Wetting Tests	
DC – MC – LUW – 1	Intermediate compaction 15.52% moisture content ($e_w = 0.407$) soil specimen loaded to 2000 kPa and then unloaded to 1000 kPa and then wetted to 20.52% moisture content ($e_w = 0.538$)
DC – MC – LUW – 2	Low compaction 23.38% moisture content ($e_w = 0.613$) soil specimen loaded to 500 kPa and then unloaded to 400 kPa and then wetted to 27.86% moisture content ($e_w = 0.730$)
Loading – Wetting – Loading Tests	
DC – MC – LWL – 1	High compaction 15.93% moisture content ($e_w = 0.417$) soil specimen loaded to 2000 kPa and then wetted to 17.27% moisture content ($e_w = 0.452$) and then loaded to 3000 kPa
DC – MC – LWL – 2	Moderate compaction 20.52% moisture content ($e_w = 0.538$) soil specimen loaded to 700 kPa and then wetted to 22.76% moisture content ($e_w = 0.596$) and then loaded to 1000 kPa
Collapse Potential Tests	
DC – MC – CPT – 1 or DC – MC – LW – 3	Intermediate compaction 15.52% moisture content ($e_w = 0.407$) soil specimen loaded to 100 kPa and then wetted to 30.52% moisture content ($e_w = 0.800$)
DC – MC – CPT – 2 or DC – MC – LW – 4	Intermediate compaction 15.52% moisture content ($e_w = 0.407$) soil specimen loaded to 500 kPa and then wetted to 27.30% moisture content ($e_w = 0.715$)
DC – MC – CPT – 3 or DC – MC – LW – 5	Intermediate compaction 15.52% moisture content ($e_w = 0.407$) soil specimen loaded to 1000 kPa and then wetted to 22.52% moisture content ($e_w = 0.590$)
DC – MC – CPT – 4 or DC – MC – LW – 6	Intermediate Compaction 15.52% moisture content ($e_w = 0.407$) soil specimen loaded to 2000 kPa and then wetted to 19.46% moisture content ($e_w = 0.510$)
DC – MC – CPT – 5 or DC – MC – LW – 7	Intermediate compaction 15.52% moisture content ($e_w = 0.407$) soil specimen loaded to 3000 kPa and then wetted to 17.37% moisture content ($e_w = 0.455$)
Combination of	A "Reduction of Void Ratio – Net Stress" graph shows the results obtained from

DC – MC – CPT – 1 to 5	Collapse Potential Tests (1 – 5)
DC – MC – CPT – 6 or DC – MC – LW – 8	Moderate compaction 20.52% moisture content ($e_w = 0.538$) soil specimen loaded to 100 kPa and then wetted to 33.80% moisture content ($e_w = 0.886$)
DC – MC – CPT – 7 or DC – MC – LW – 9	Moderate compaction 20.52% moisture content ($e_w = 0.538$) soil specimen loaded to 300 kPa and then wetted to 30.52% moisture content ($e_w = 0.800$)
DC – MC – CPT – 8 or DC – MC – LW – 10	Moderate Compaction 20.52% moisture content ($e_w = 0.538$) soil specimen loaded to 500 kPa and then wetted to 26.72% moisture content ($e_w = 0.700$)
DC – MC – CPT – 9 or DC – MC – LW – 11	Moderate compaction 20.52% moisture content ($e_w = 0.538$) soil specimen loaded to 700 kPa and then wetted to 25.20% moisture content ($e_w = 0.660$)
DC – MC – CPT – 10 or DC – MC – LW – 12	Moderate compaction 20.52% moisture content ($e_w = 0.538$) soil specimen loaded to 1000 kPa and then wetted to 22.52% moisture content ($e_w = 0.590$)
Combination of DC – MC – CPT – 6 to 10	A "Reduction of Void Ratio – Net Stress" graph shows the results obtained from Collapse Potential Tests (6 – 10)
Swelling Pressure Tests	
DC – MC – SPT – 1	High compaction 15.93% moisture content ($e_w = 0.417$) soil specimen loaded to 500 kPa and then wetted to 21.56% moisture content ($e_w = 0.565$) ($S_r = 0.983$ and $e_0 = 0.575$) in constant volume
DC – MC – SPT – 2	Intermediate compaction 15.52% moisture content ($e_w = 0.407$) soil specimen loaded to 500 kPa and then wetted to 26.27% moisture content ($e_w = 0.688$) ($S_r = 0.983$ and $e_0 = 0.7$) in constant volume
DC – MC – SPT – 3	Intermediate compaction 18.16% moisture content ($e_w = 0.476$) soil specimen loaded to 500 kPa and then wetted to 23.33% moisture content ($e_w = 0.611$) ($S_r = 0.983$ and $e_0 = 0.622$) in constant volume
DC – MC – SPT – 4	Intermediate compaction 19.89% moisture content ($e_w = 0.521$) soil specimen loaded to 500 kPa and then wetted to 22.26% moisture content ($e_w = 0.583$) ($S_r = 0.984$ and $e_0 = 0.593$) in constant volume
DC – MC – SPT – 5	Moderate compaction 20.52% moisture content ($e_w = 0.538$) soil specimen loaded to 400 kPa and then wetted to 28.73% moisture content ($e_w = 0.753$) ($S_r = 0.984$ and $e_0 = 0.765$) in constant volume
DC – MC – SPT – 6	Moderate compaction 23.62% moisture content ($e_w = 0.619$) soil specimen loaded to 200 kPa and then wetted to 28.33% moisture content ($e_w = 0.742$) ($S_r = 0.987$ and $e_0 = 0.7525$) in constant volume

DC => Dynamic Compaction, MC => Merri Creek Soil, LW => Loading – Wetting, LUW => Loading – Unloading – Wetting, LWL => Loading – Wetting – Loading, CPT => Collapse Potential Test, SPT => Swelling Pressure Test.
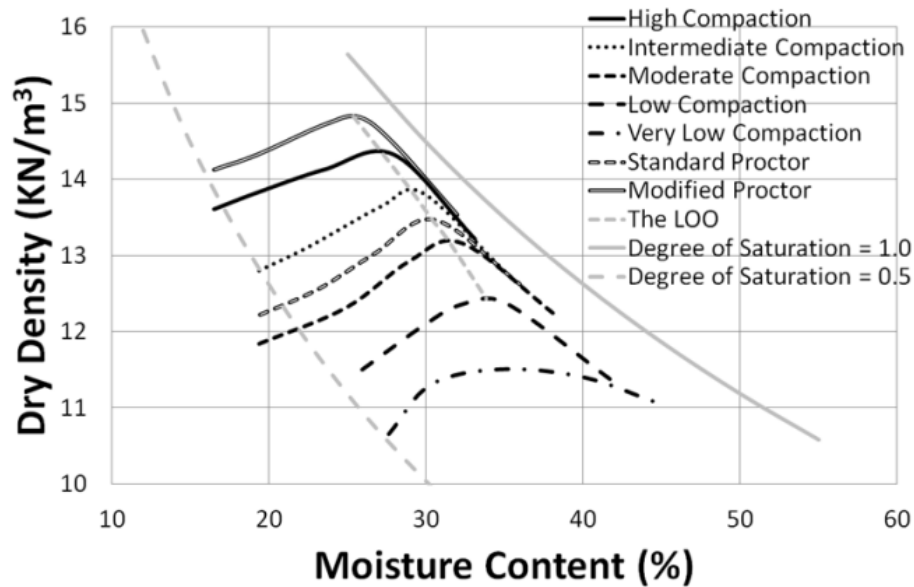
(a) Dynamic compaction curves for the kaolin soil
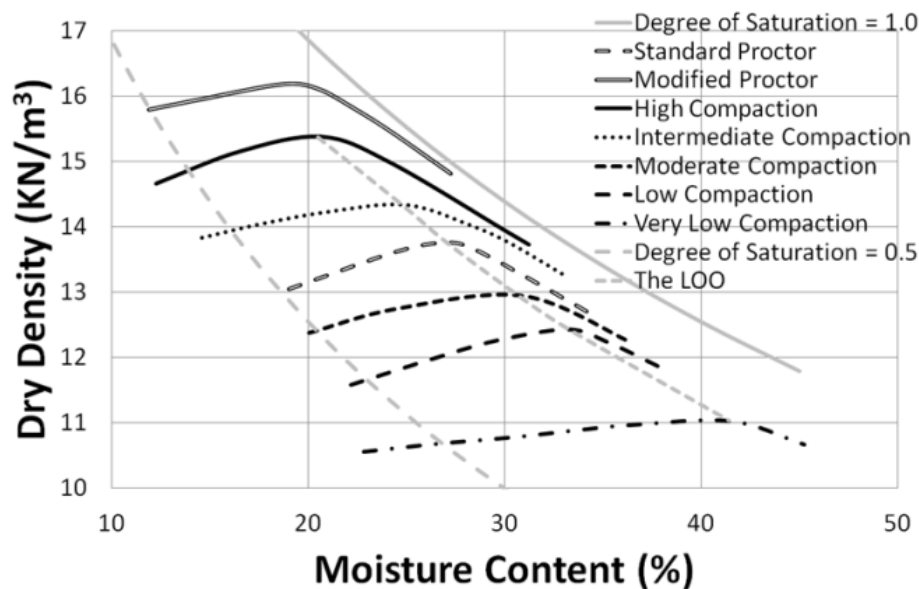
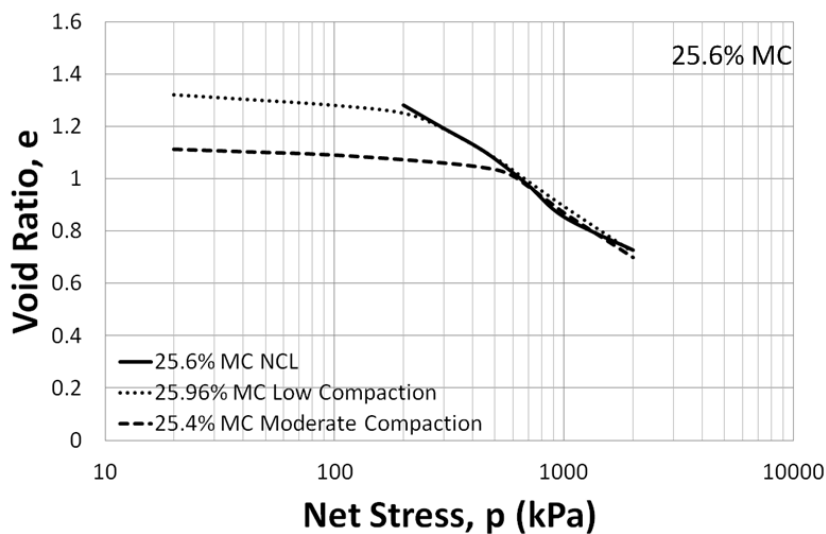
(b) Dynamic compaction curves for the Merri Creek soil

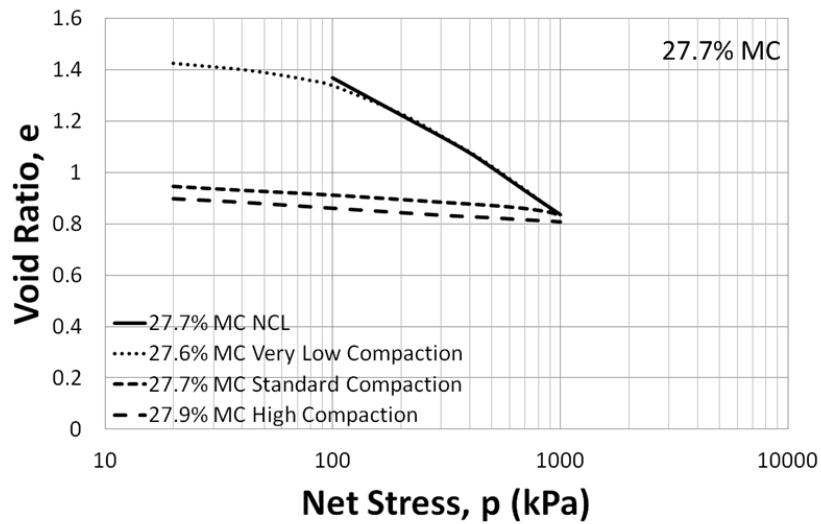**Figure 5-1:** Family of dynamic compaction curves for the kaolin and Merri Creek soil
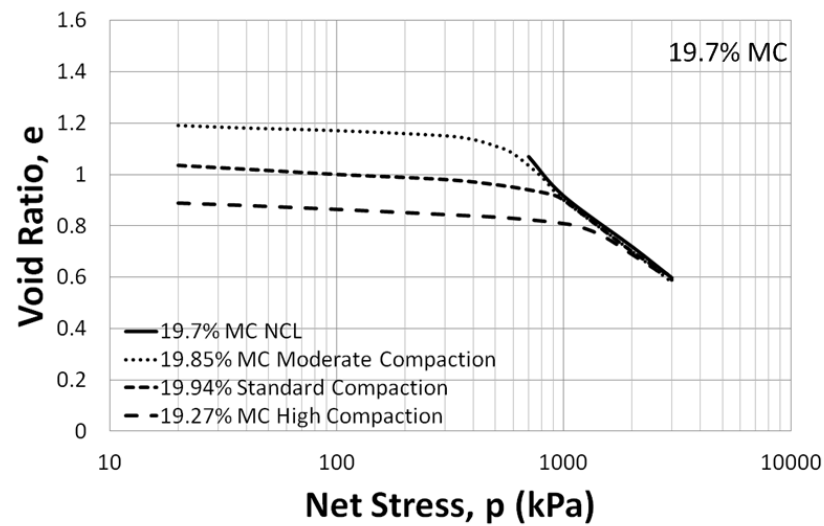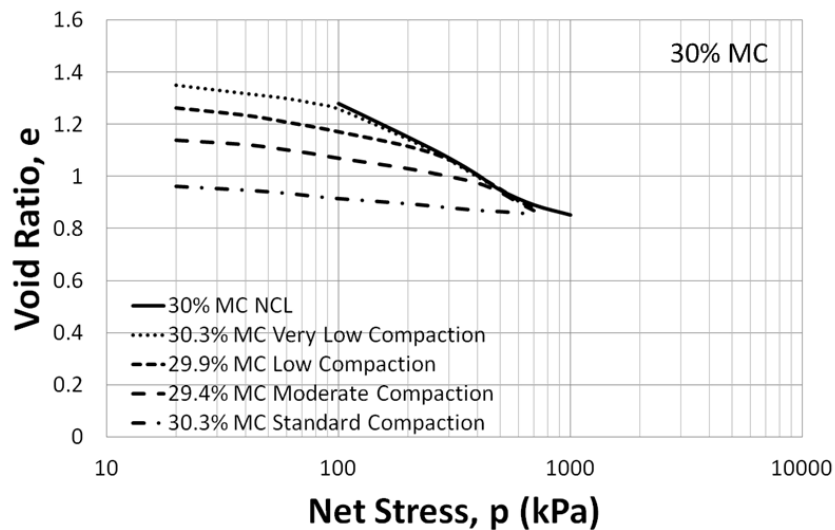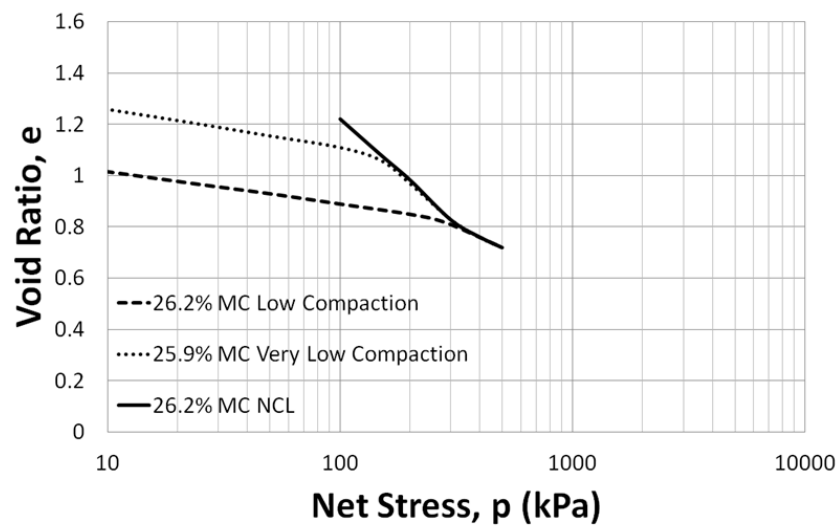
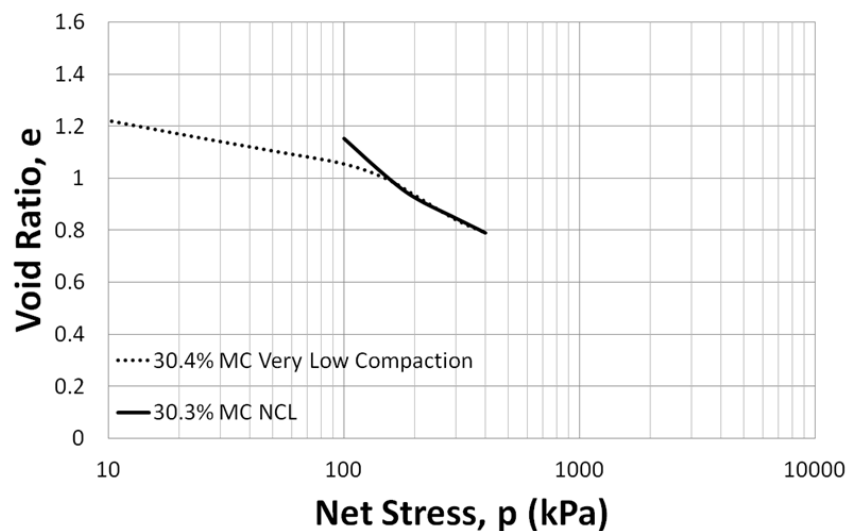**(a)** 19.70% moisture content ($e_w = 0.522$)
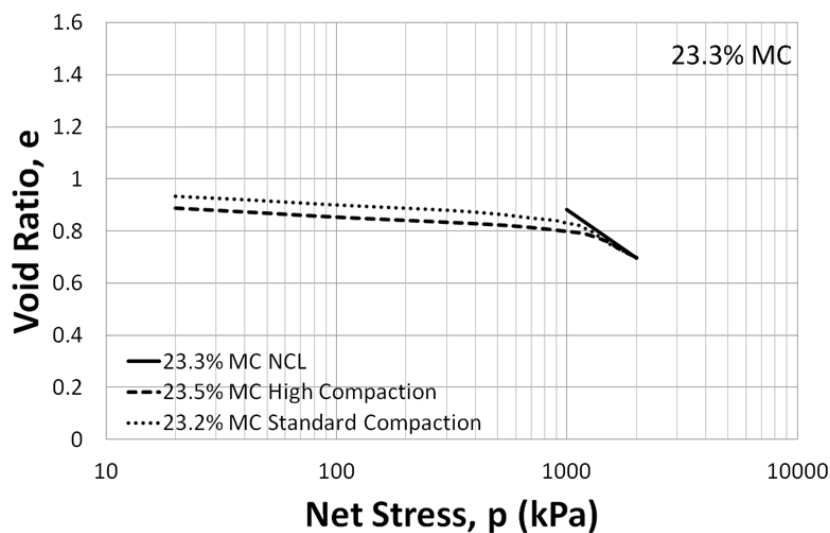
(b) 23.30% moisture content ($e_w = 0.617$)

(c) 25.60% moisture content ($e_w = 0.678$)

(d) 27.70% moisture content ($e_w = 0.734$)


(e) 30.0% moisture content ($e_w = 0.795$)
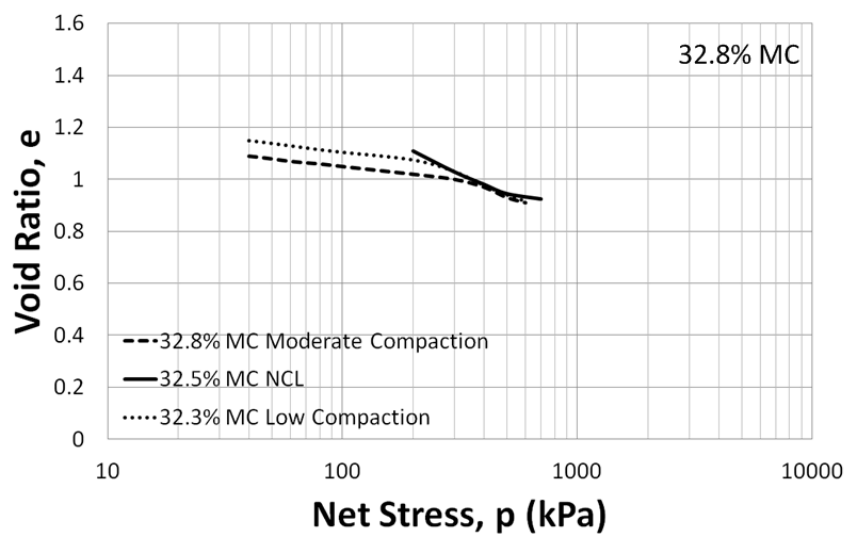

(f) 32.80% moisture content ($e_w = 0.869$)
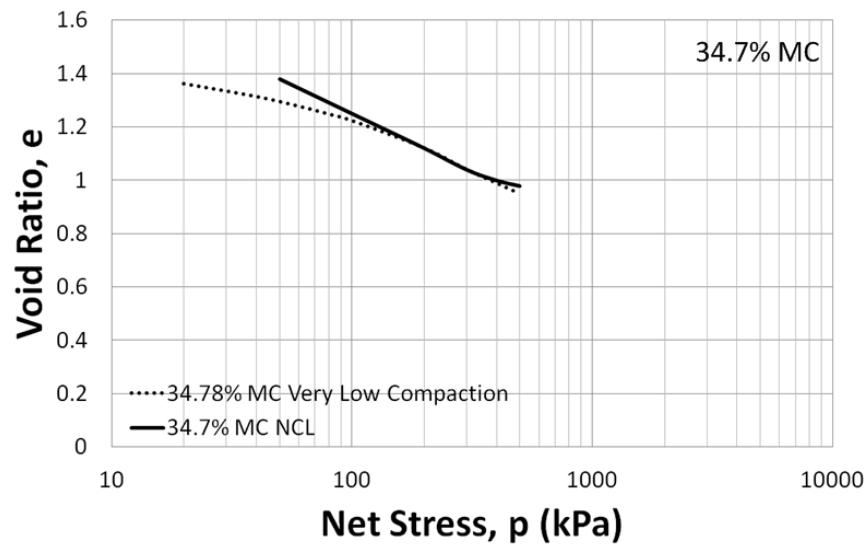
(g) 34.70% moisture content ($e_w = 0.920$)

Figure 5-2: Void Ratio vs Stress curves for the kaolin soil at different moisture contents and different initial dynamic compaction efforts to develop the LWSBS
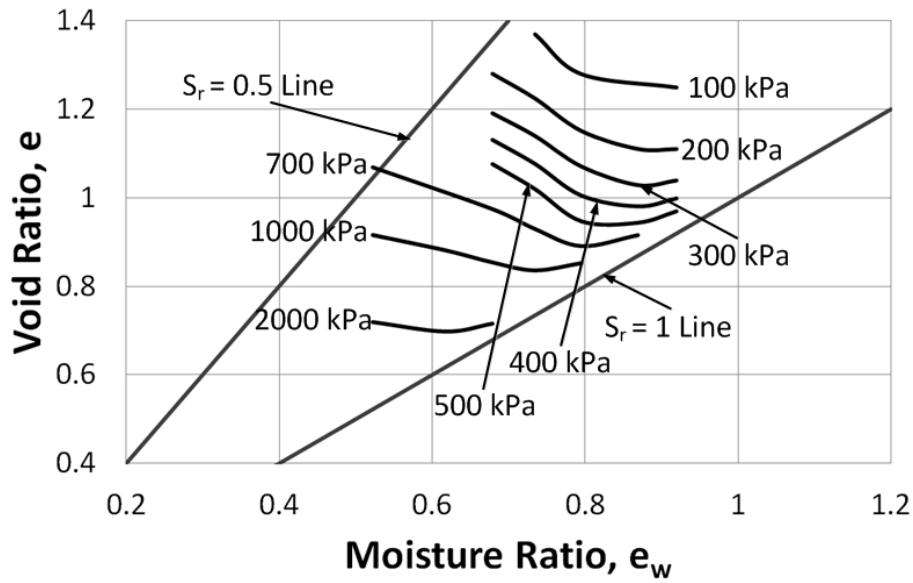
(a) In $e - e_w$ plane (only real data)
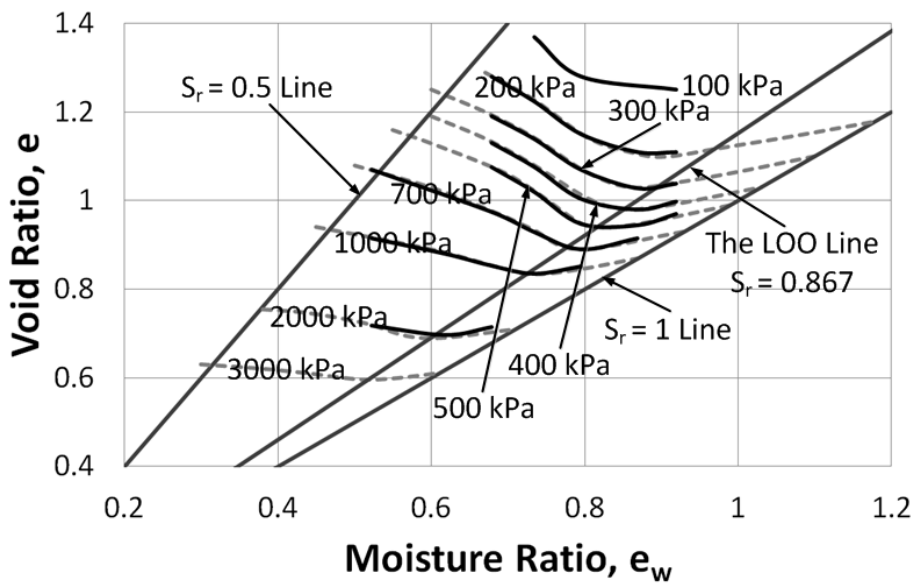
(b) In $e - e_w$ plane (real and extrapolated data)

Figure 5-3: Construction of the LWSBS for the kaolin soil by only real data & real and extrapolated data to complete the surface
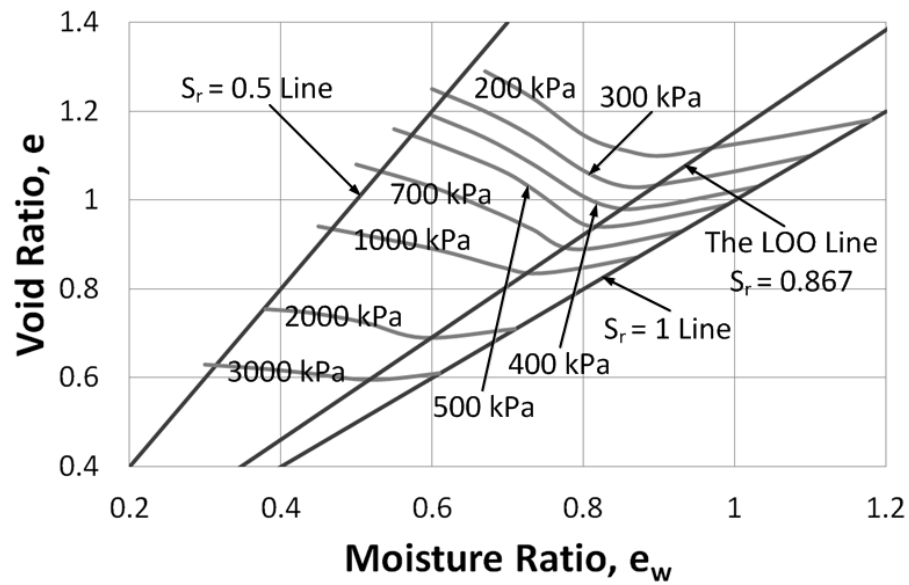
(a) In $e - e_w$ plane
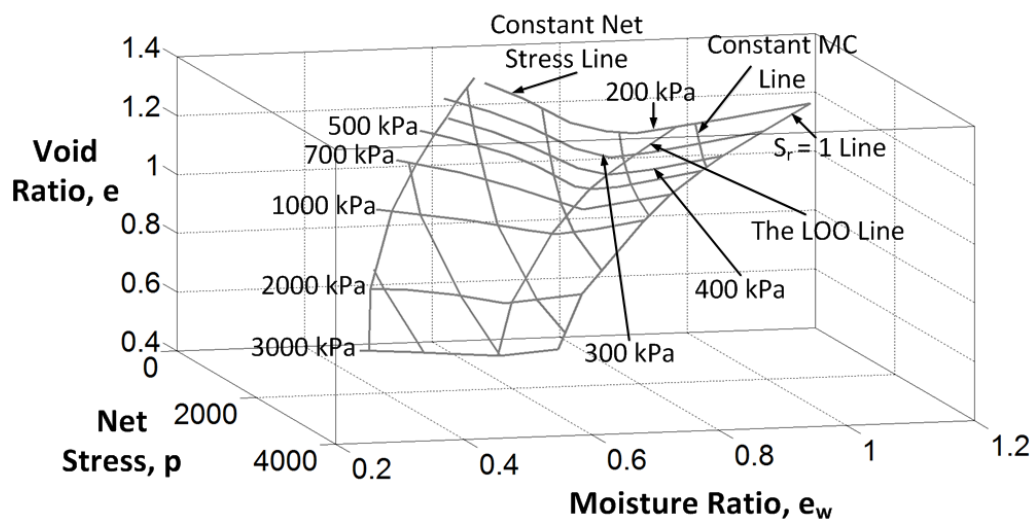
(b) In $e - e_w - p$ space

Figure 5-4: The LWSBS for dynamically compacted kaolin soil
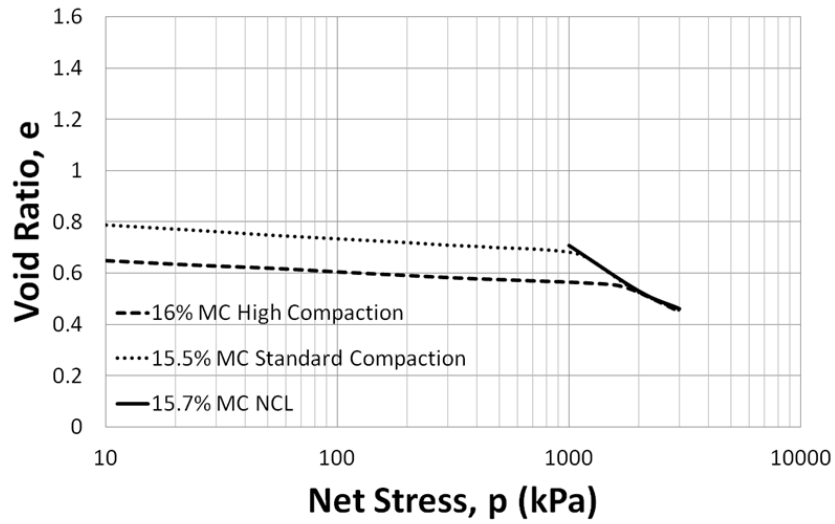
(a) 15.70% moisture content ($e_w = 0.411$)
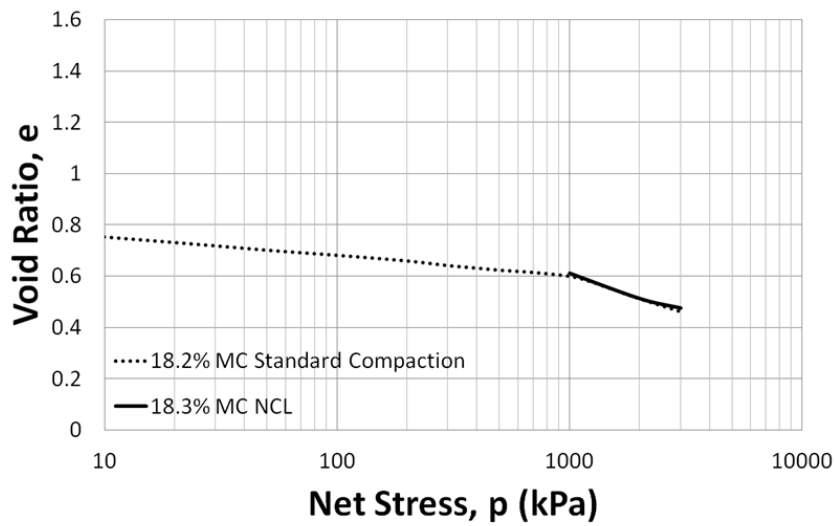
(b) 18.30% moisture content ($e_w = 0.479$)
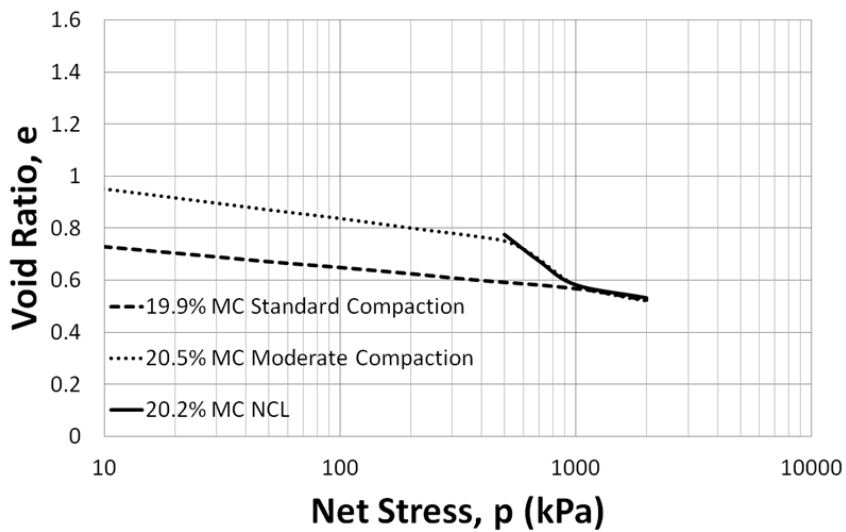
(c) 20.20% moisture content ($e_w = 0.529$)
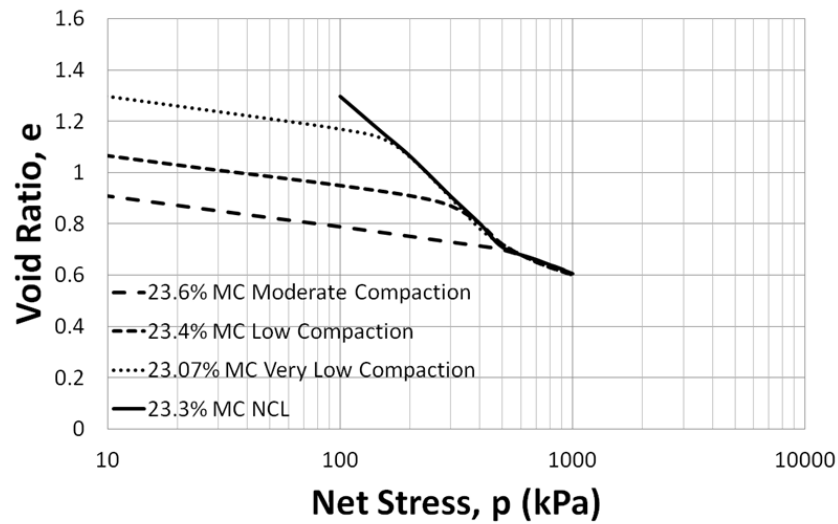
(d) 23.30% moisture content ($e_w = 0.610$)

(e) 26.20% moisture content ($e_w = 0.686$)

(f) 30.30% moisture content ($e_w = 0.794$)
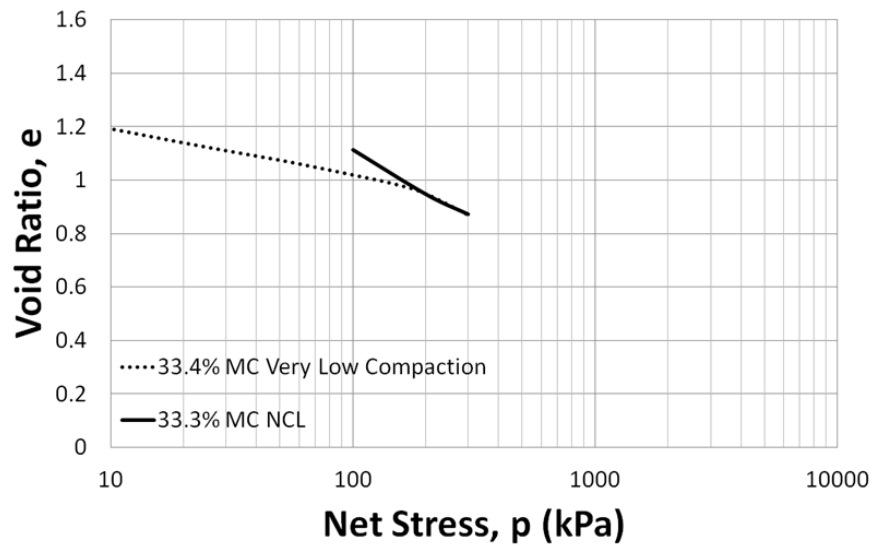
(g) 33.30% moisture content ($e_w = 0.872$)

Figure 5-5: Void Ratio vs Stress curves for the Merri Creek soil at different moisture contents and different initial dynamic compaction efforts to develop the LWSBS
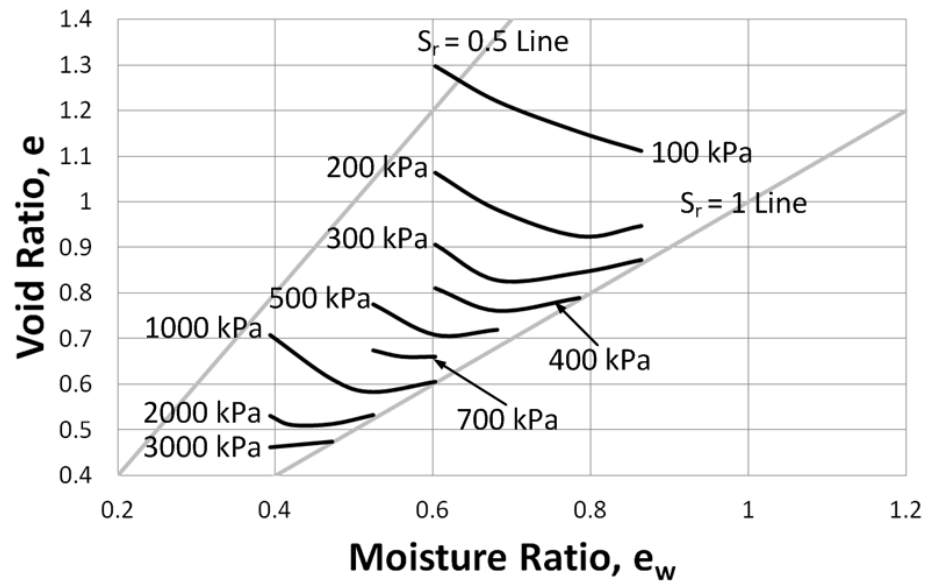
(a) In $e - e_w$ plane (only real data)
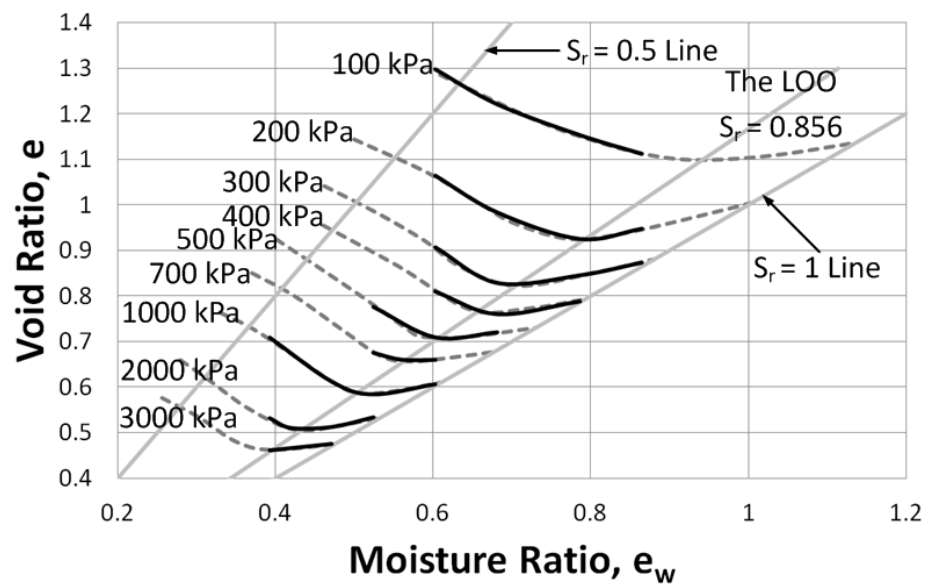
(b) In $e - e_w$ plane (real and extrapolated data)

Figure 5-6: Construction of the LWSBS for the Merri Creek soil by only real data & real and extrapolated data to complete the surface
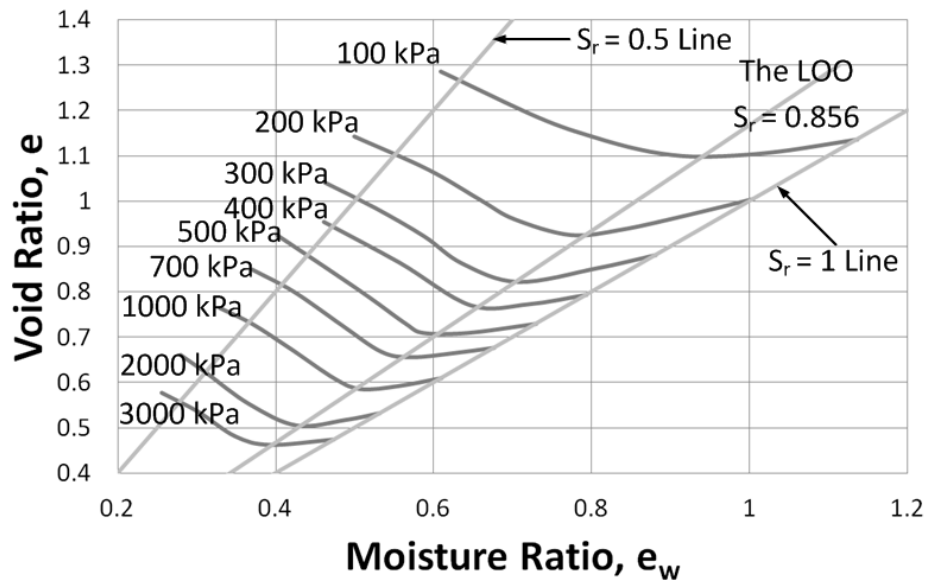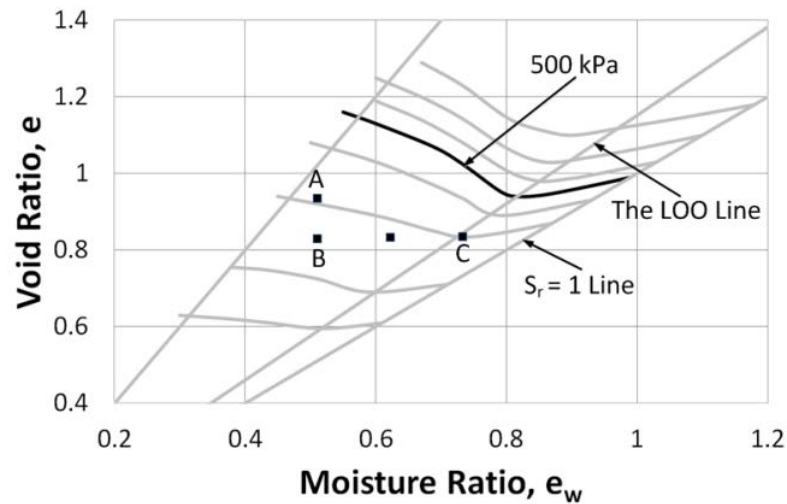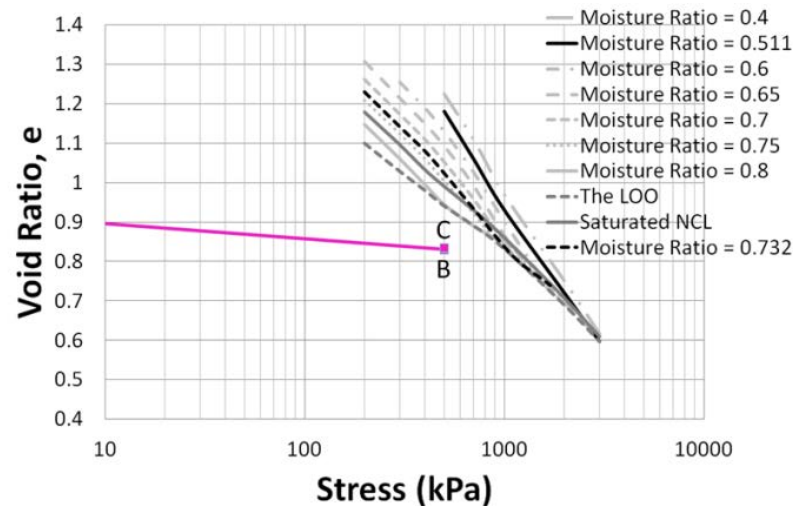
(a) In $e - e_w$ plane
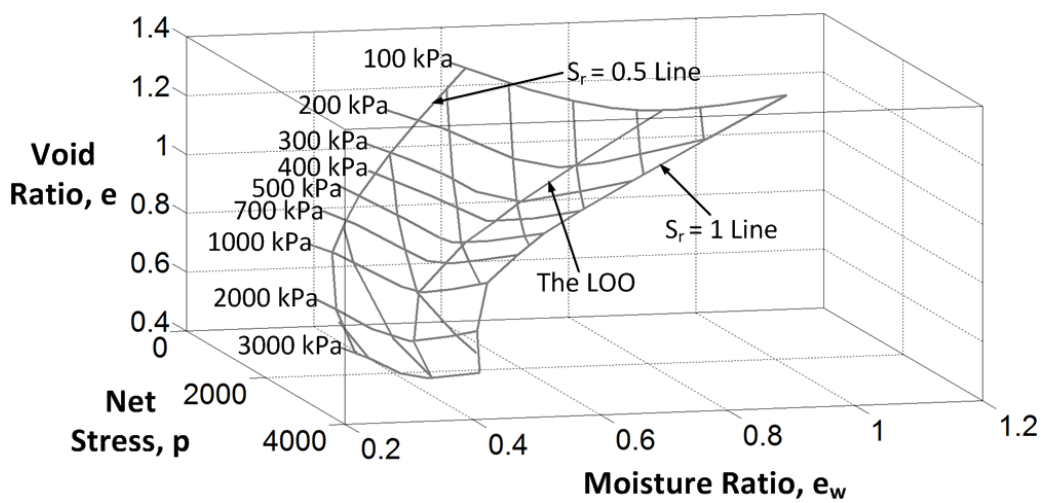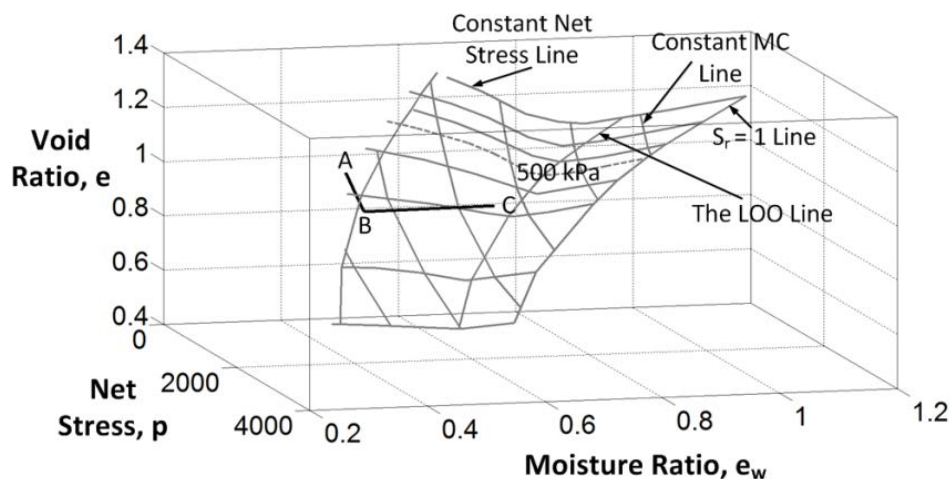

(b) In $e - e_w - p$ space

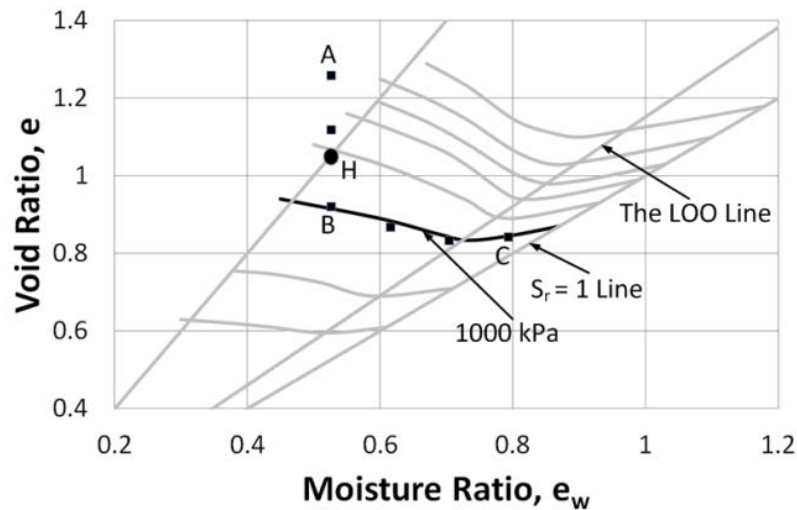**Figure 5-7:** The LWSBS for dynamically compacted Merri Creek soil

(a) High compaction, 19.27% moisture content ($e_w = 0.511$) soil specimen loaded to 500 kPa and then wetted to 27.94% moisture content ($e_w = 0.732$) [Test Identity => DC – EK – LW – 1]
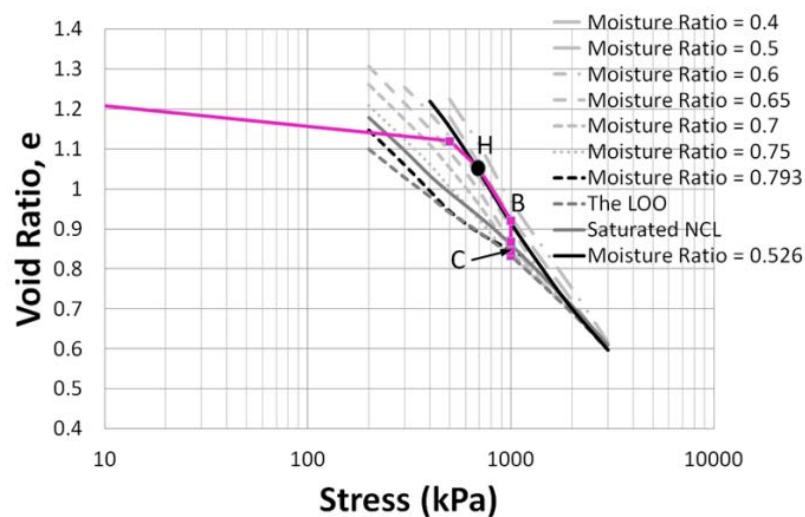

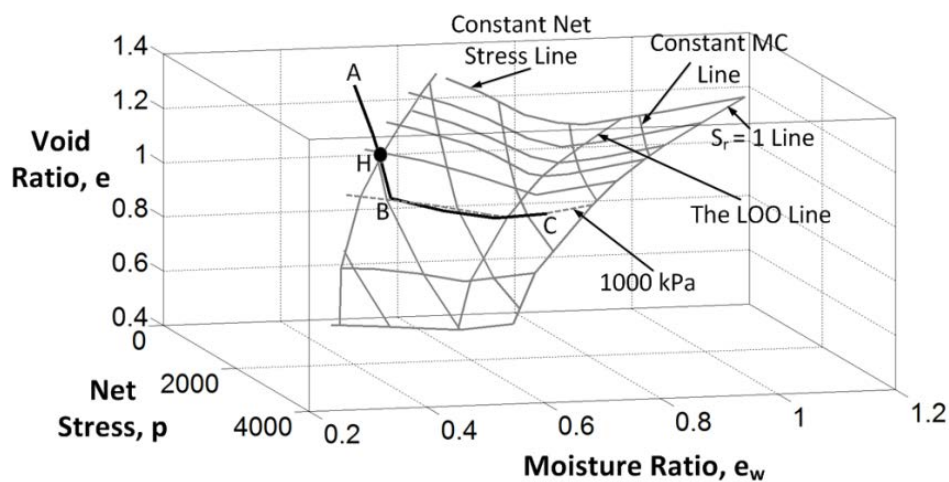**(b)** $e - \log p$ relationship of state path test (a)
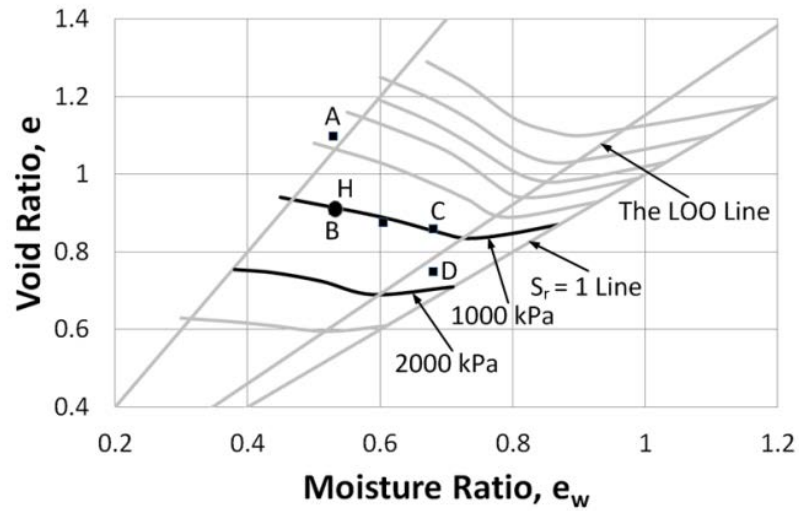

(c) 3-D view of state path test (a)

(d) Moderate compaction, 19.85 % moisture content ($e_w = 0.526$) soil specimen loaded to 1000 kPa and then wetted to 29.92% moisture content ($e_w = 0.793$) [Test Identity => DC – EK – LW – 2]

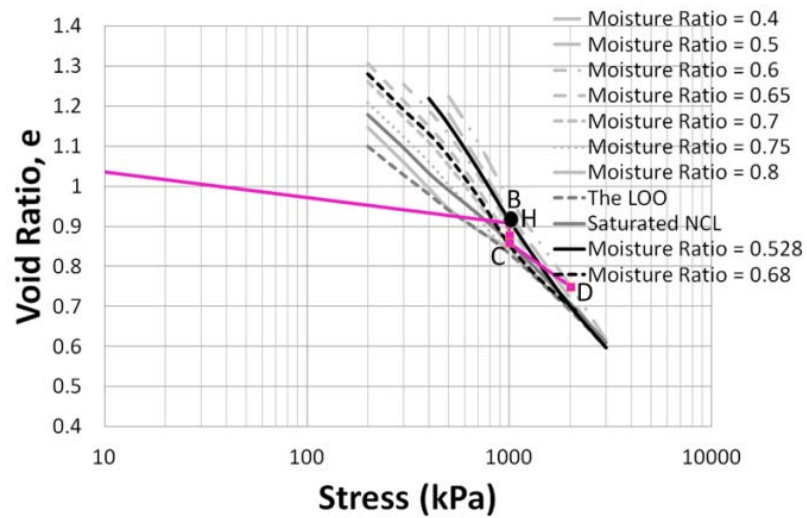**(e)** $e – \log p$ relationship of state path test (d)

(f) 3-D view of state path test (d)

(g) Intermediate compaction, 19.94% moisture content ($e_w = 0.528$) soil specimen loaded to 1000 kPa and then wetted to 25.66% moisture content ($e_w = 0.680$) and then loaded to 2000 kPa [Test Identity => DC – EK – LWL – 1]

(h) $e – \log p$ relationship of state path test (g)

(i) 3-D view of state path test (g)

Figure 5-8: Loading/wetting state path tests for the kaolin soil

(a) Moderate compaction, 19.85 % moisture content ($e_w = 0.526$) soil specimen loaded to 3000 kPa and then unloaded to 1000 kPa and then wetted to 23.24% moisture content ($e_w = 0.616$) [Test Identity => DC – EK – LUW – 1]

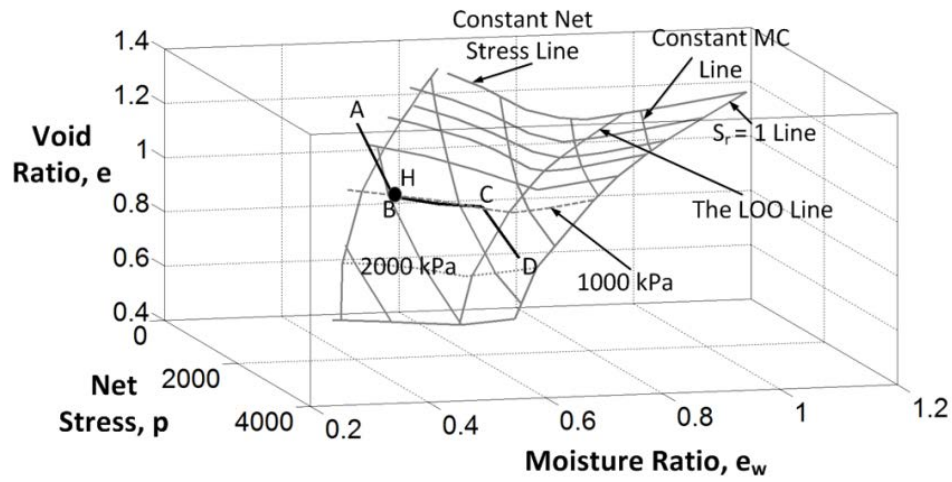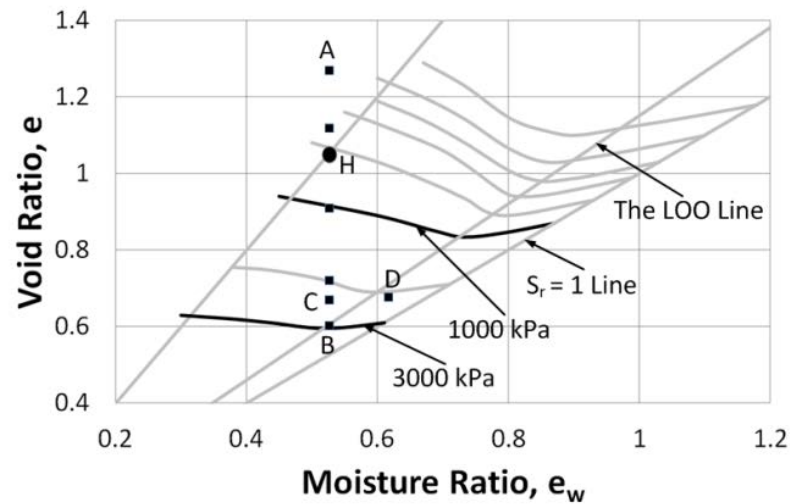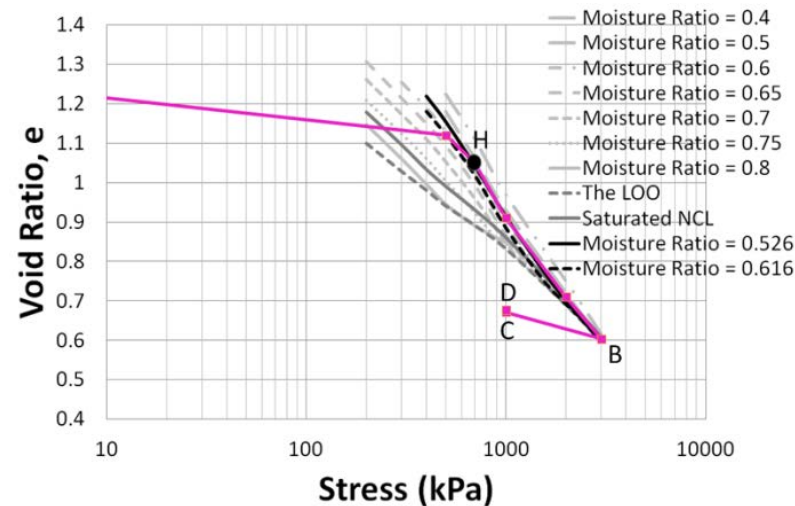(b) $e - \log p$ relationship of state path test (a)

(c) 3-D view of state path test (a)

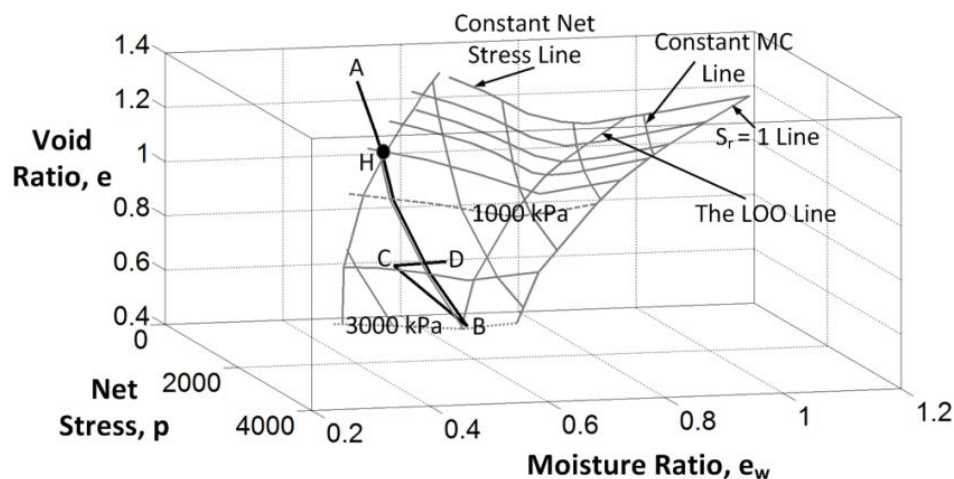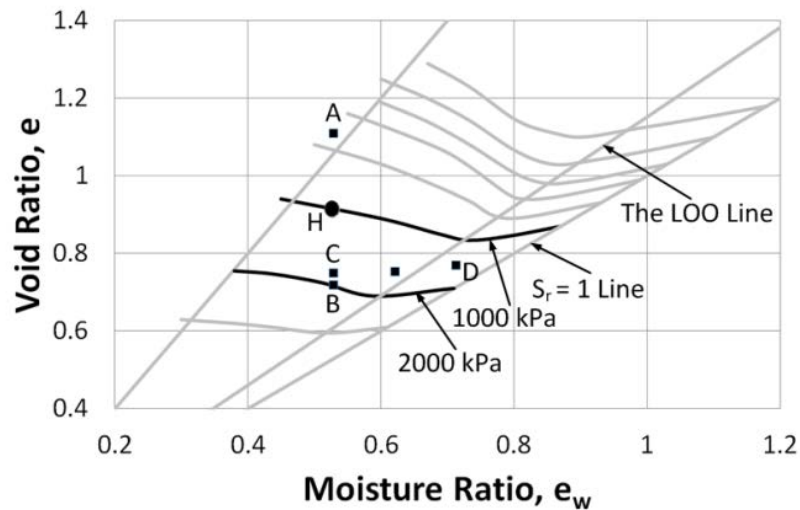**(d)** Intermediate compaction, 19.94% moisture content ($e_w = 0.528$) soil specimen loaded to 2000 kPa and then unloaded to 1000 kPa and then wetted to 26.90% moisture content ($e_w = 0.713$) [Test Identity => DC – EK – LUW – 2]

(e) $e – \log p$ relationship of state path test (d)

(f) 3-D view of state path test (d)

Figure 5-9: Loading/unloading/wetting state path tests for the kaolin soil
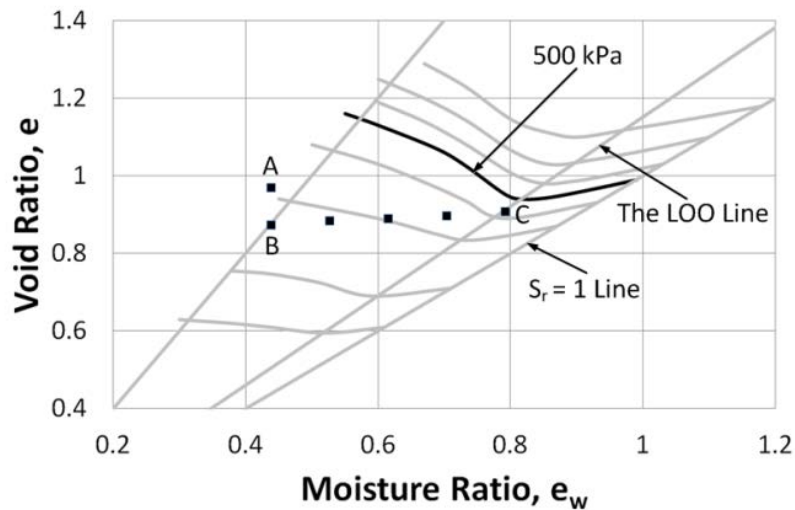
(a) High compaction, 16.51% moisture content ($e_w = 0.438$) soil specimen loaded to 500 kPa and then wetted to 29.86% moisture content ($e_w = 0.791$) [Test Identity => DC – EK – CPT – 2 or DC – EK – LW – 4]
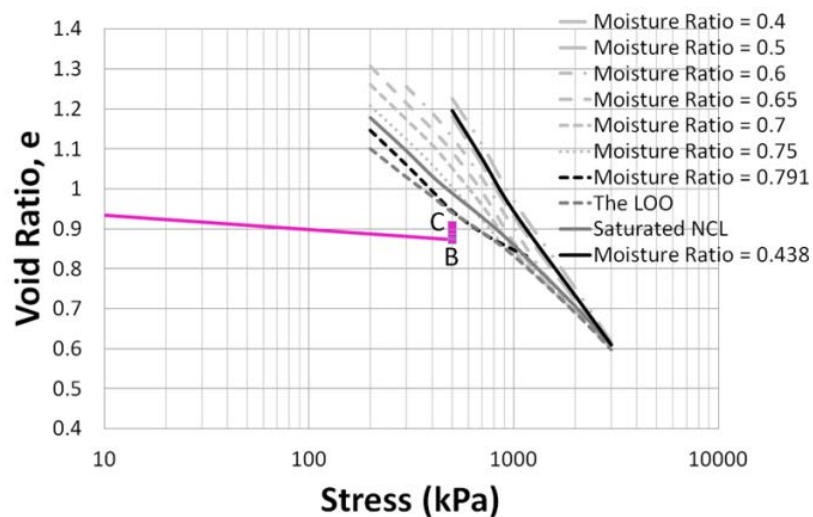
(b) $e – \log p$ relationship of state path test (a)
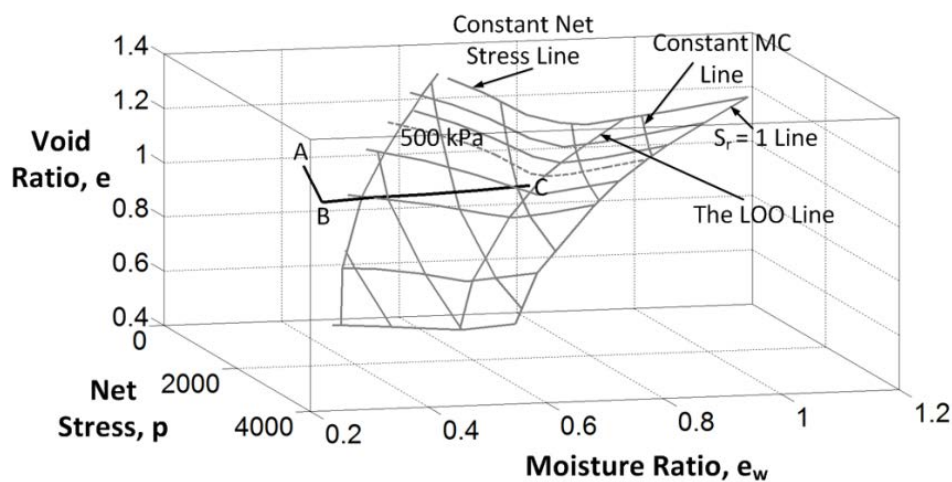
(c) 3-D view of state path test (a)

(**d**) High compaction, 16.51% moisture content ($e_w = 0.438$) soil specimen loaded to 1000 kPa and then wetted to 28.15% moisture content ($e_w = 0.746$) [Test Identity => DC – EK – CPT – 3 or DC – EK – LW – 5]
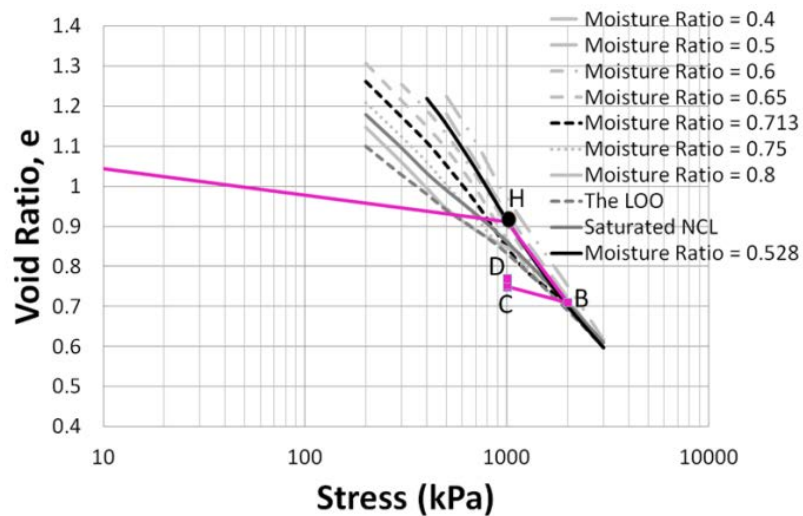

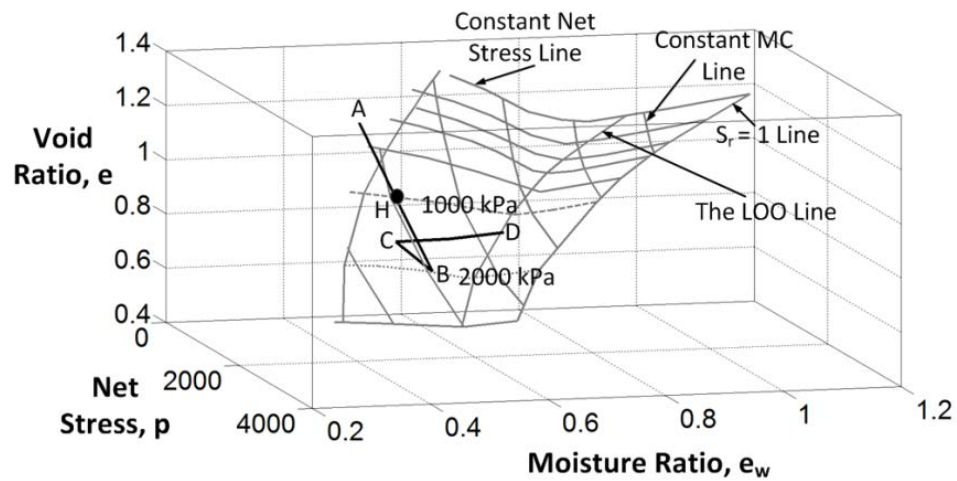(**e**) $e – \log p$ relationship of state path test (d)

(**f**) 3-D view of state path test (d)

(g) High compaction, 16.51% moisture content ($e_w = 0.438$) soil specimen loaded to 1500 kPa and then wetted to 27.65% moisture content ($e_w = 0.733$) [Test Identity => DC – EK – CPT – 5 or DC – EK – LW – 7]

(h) $e - \log p$ relationship of state path test (g)

(i) 3-D view of state path test (g)

(j) High compaction, 16.51% moisture content ($e_w = 0.438$) soil specimen loaded to 2000 kPa and then wetted to 25.90% moisture content ($e_w = 0.686$) [Test Identity => DC – EK – CPT – 1 or DC – EK – LW – 3]

(k) e – log p relationship of state path test (j)

(l) 3-D view of state path test (j)

(m) High compaction, 16.51% moisture content ($e_w = 0.438$) soil specimen loaded to 3000 kPa and then wetted to 22.78% moisture content ($e_w = 0.604$) [Test Identity => DC – EK – CPT – 4 or DC – EK – LW – 6]

(n) e – log p relationship of state path test (m)
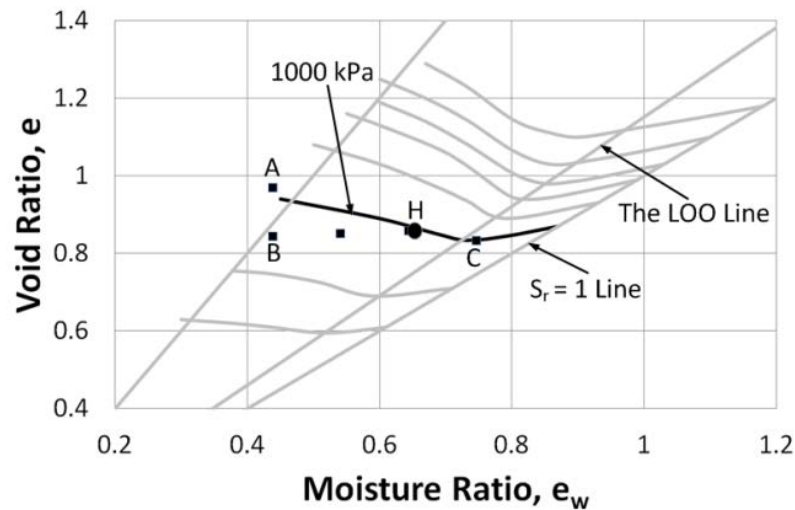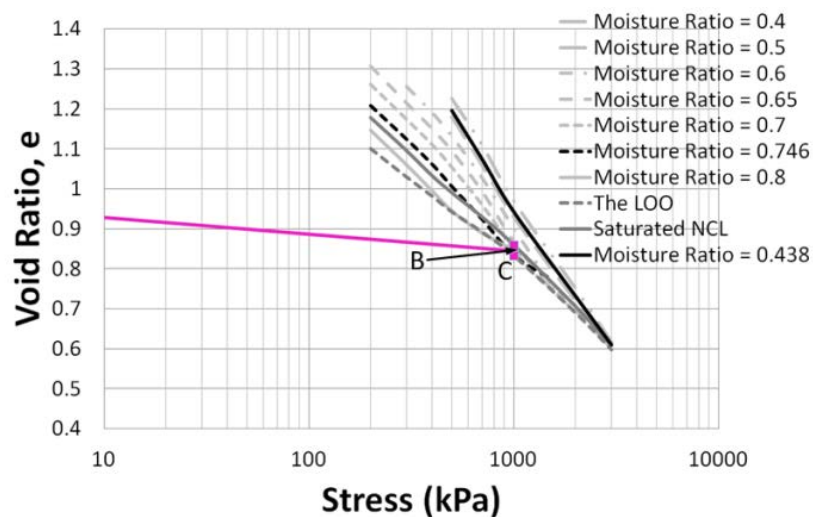
(o) 3-D view of state path test (m)

Figure 5-10: Loading/wetting state path tests on 16.51% moisture content ($e_w = 0.438$), High compaction kaolin soil specimens at different stress levels
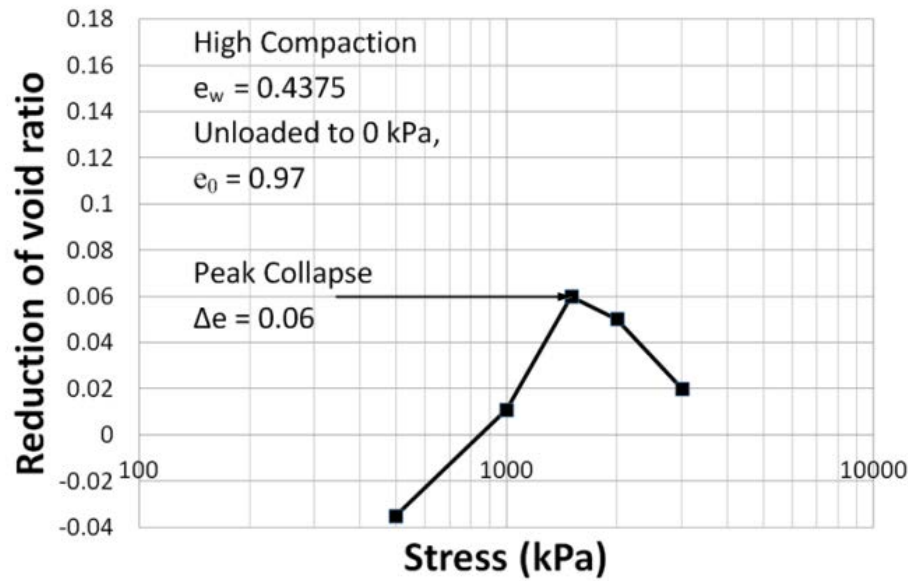
(a) Reduction of void ratio versus Operational Stress
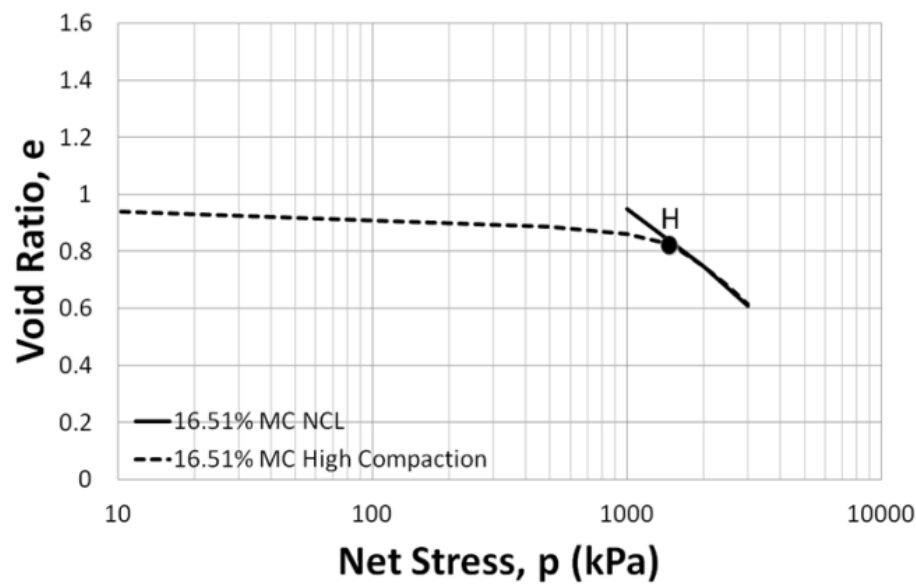
(b) Void Ratio versus Net Stress compression for High compaction kaolin soil specimen with initial $e_{wo} = 0.438$

Figure 5-11: Collapse potential given as a reduction of void ratio with Operational Stress for High compaction (pre-compaction stress ≈ 1500 kPa) kaolin soil specimen with initial $e_{wo} = 0.438$ and unloaded to zero stress $e_o = 0.97$ [Test Identity => Combination of DC – EK – CPT – 1 to 5]
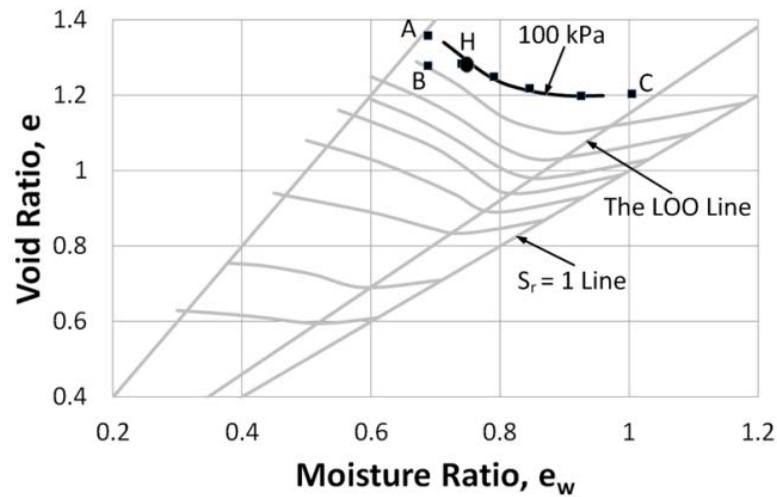
(a) Low compaction, 25.96% moisture content ($e_w = 0.688$) soil specimen loaded to 100 kPa and then wetted to 37.89% moisture content ($e_w = 1.004$) [Test Identity => DC – EK – CPT – 9 or DC – EK – LW – 11]
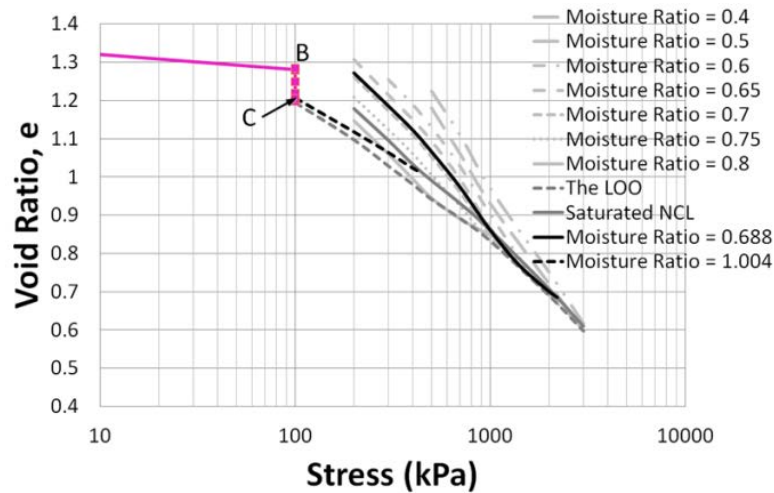
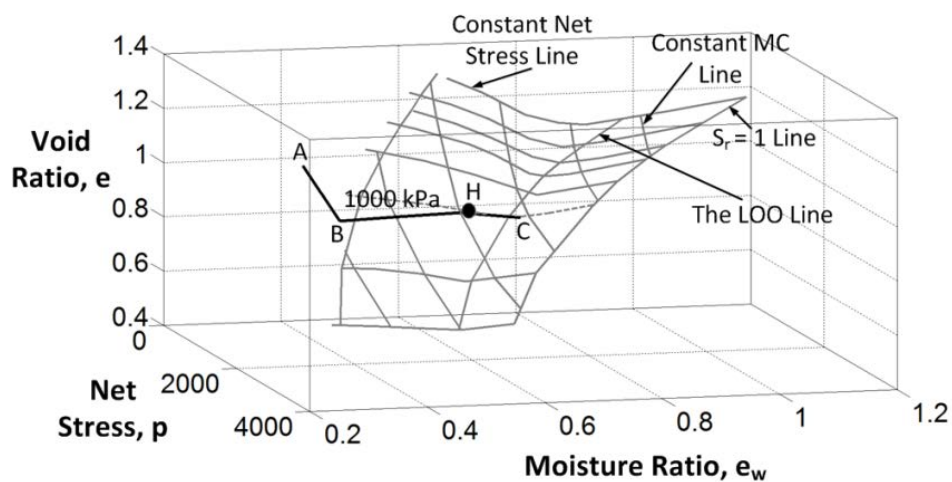**(b)** e – log p relationship of state path test (a)
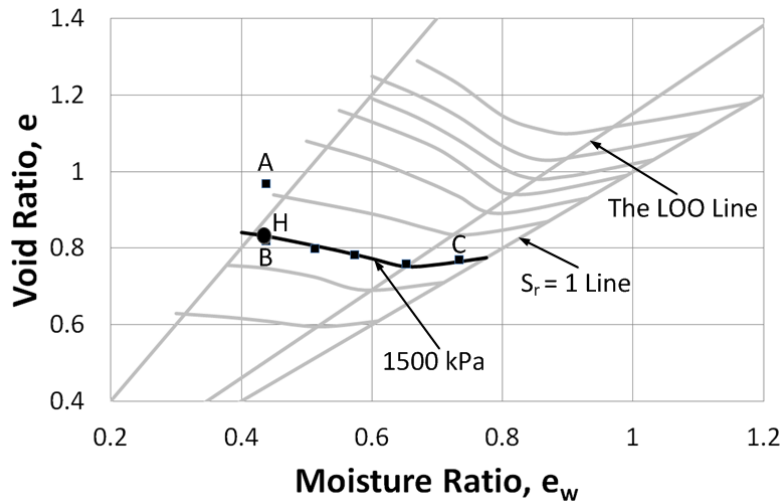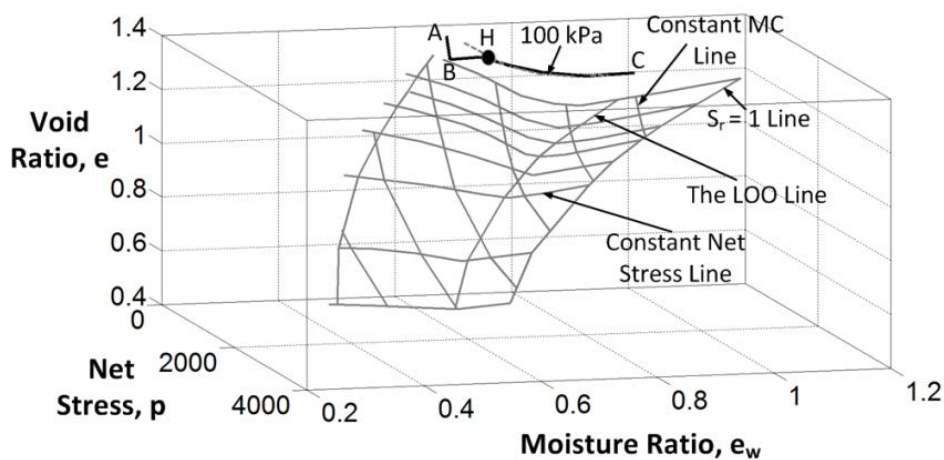

(c) 3-D view of state path test (a)

(d) Low compaction, 25.96% moisture content ($e_w = 0.688$) soil specimen loaded to 250 kPa and then wetted to 39.92% moisture content ($e_w = 1.058$) [Test Identity => DC – EK – CPT – 10 or DC – EK – LW – 12]
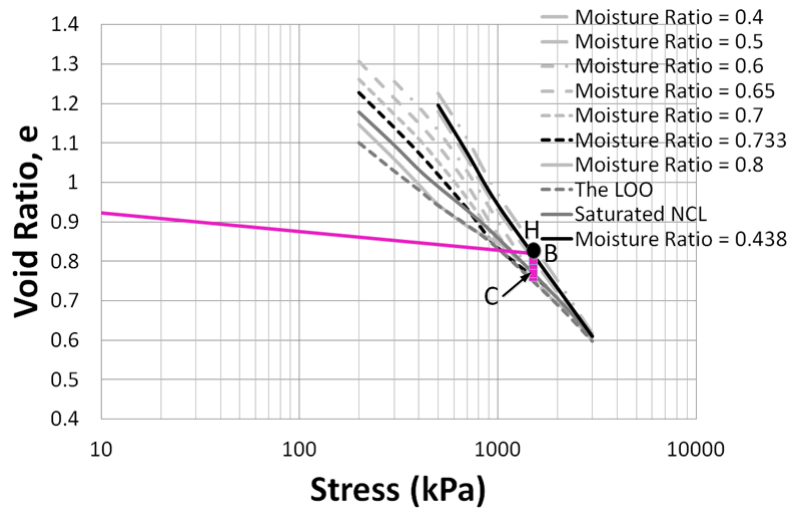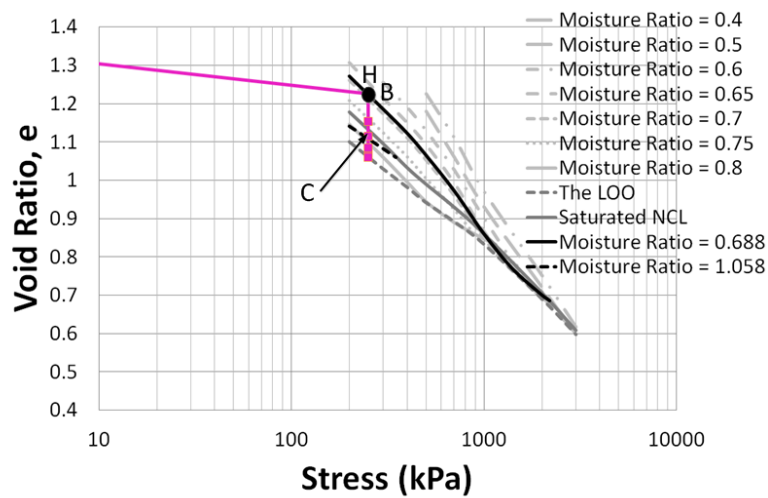

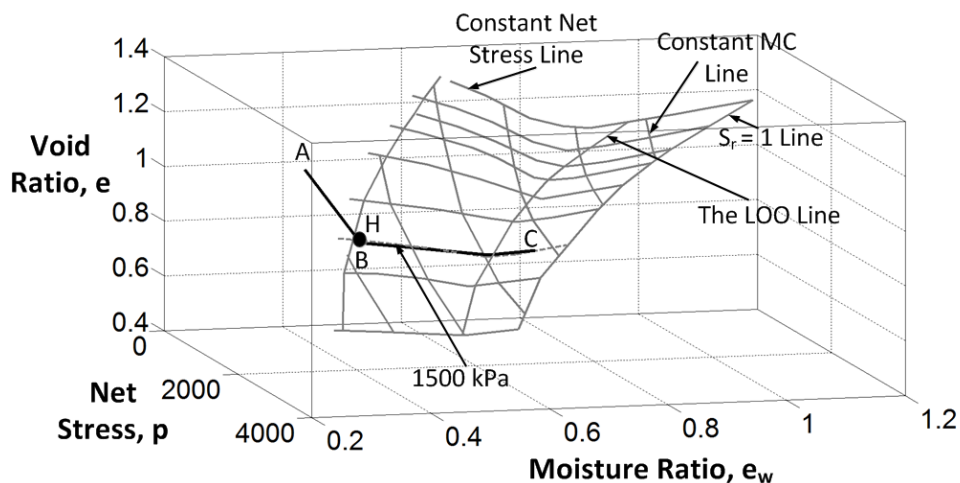**(e)** $e - \log p$ relationship of state path test (d)

(f) 3-D view of state path test (d)

(g) Low compaction, 25.96% moisture content ($e_w = 0.688$) soil specimen loaded to 300 kPa and then wetted to 36.87% moisture content ($e_w = 0.977$) [Test Identity => DC – EK – CPT – 6 or DC – EK – LW – 8]
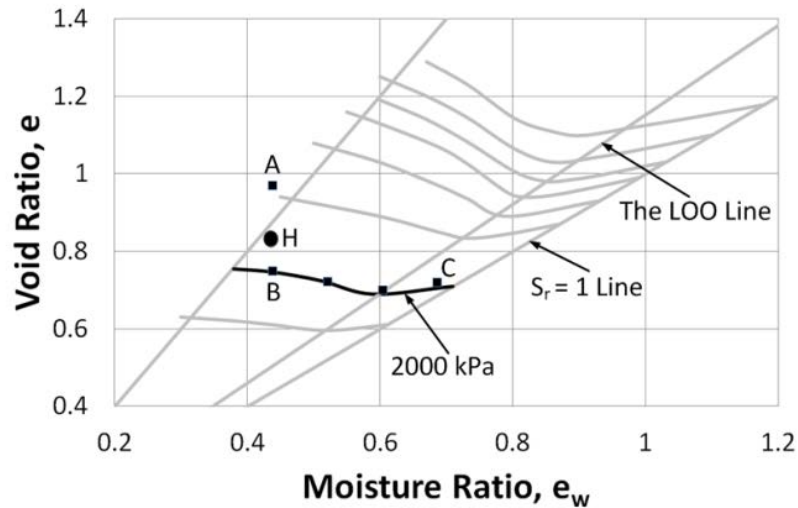

(h) $e – \log p$ relationship of state path test (g)

(i) 3-D view of state path test (g)

(j) Low compaction, 25.96% moisture content ($e_w = 0.688$) soil specimen loaded to 700 kPa and then wetted to 32.96% moisture content ($e_w = 0.873$) [Test Identity => DC – EK – CPT – 8 or DC – EK – LW – 10]

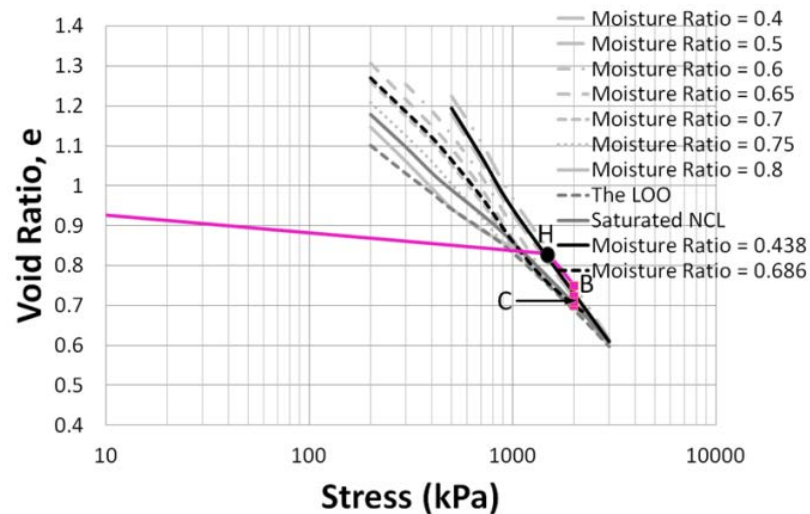
(k) $e – \log p$ relationship of state path test (j)
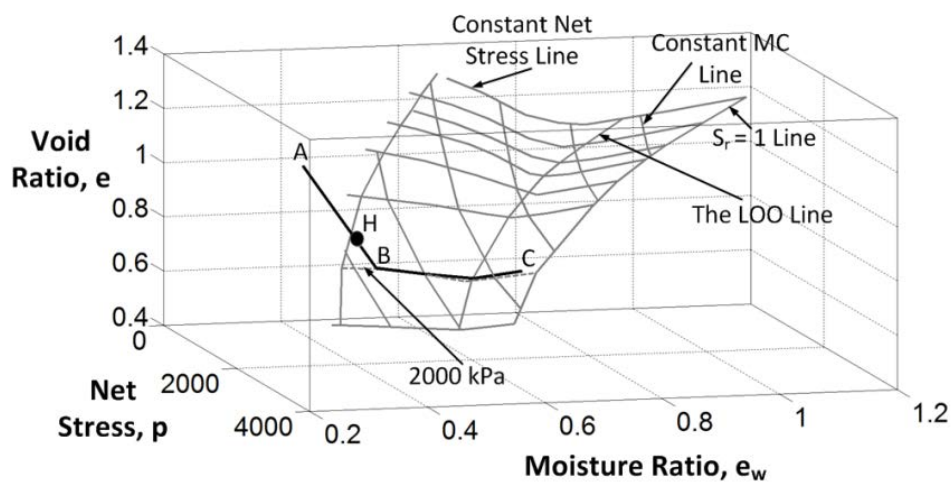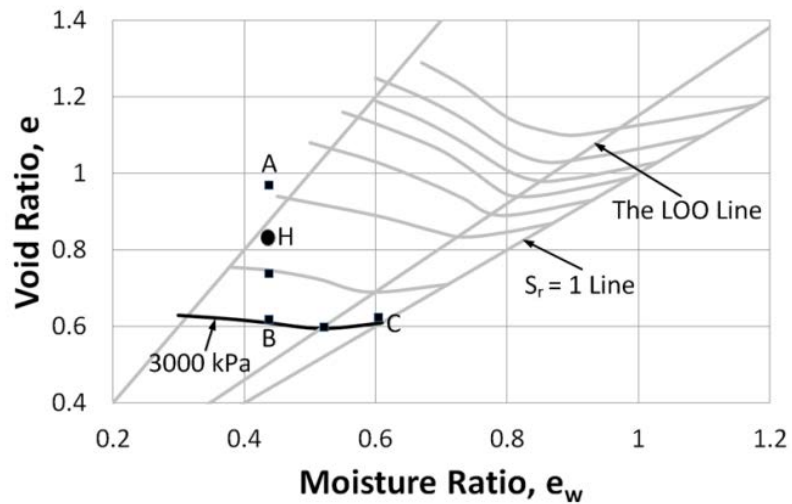

(l) 3-D view of state path test (j)
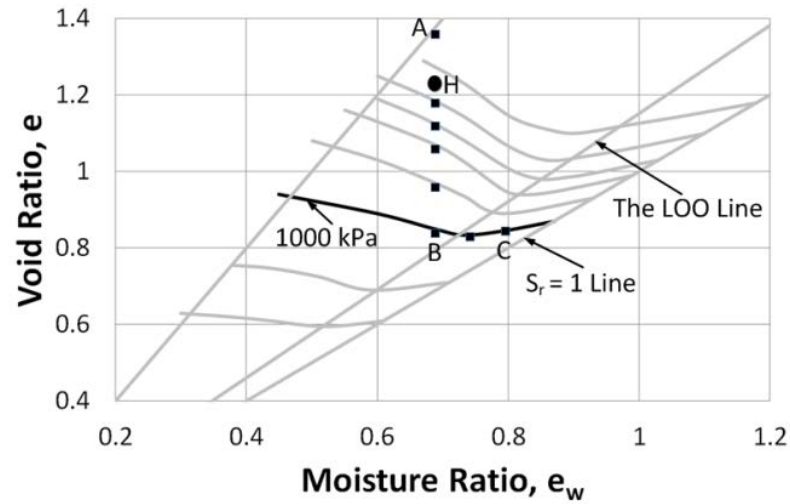
(m) Low compaction, 25.96% moisture content ($e_w = 0.688$) soil specimen loaded to 1000 kPa and then wetted to 30.01% moisture content ($e_w = 0.795$) [Test Identity => DC – EK – CPT – 7 or DC – EK – LW – 9]
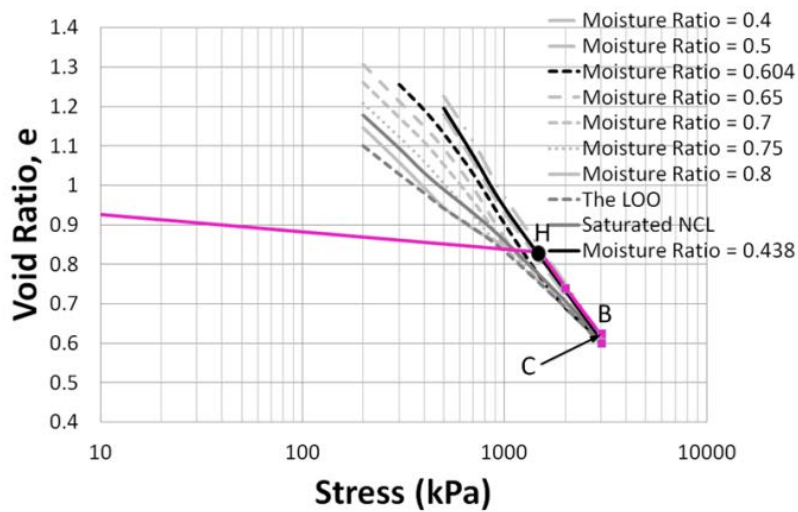

(n) e – log p relationship of state path test (m)
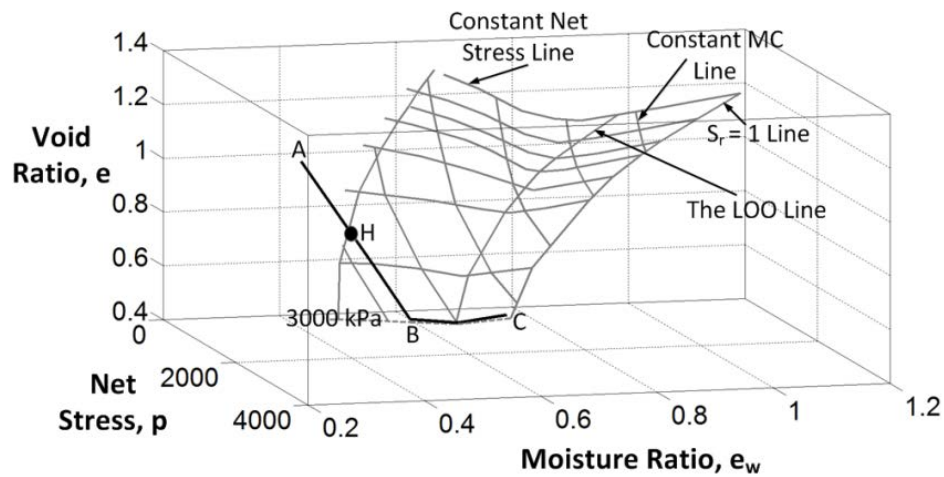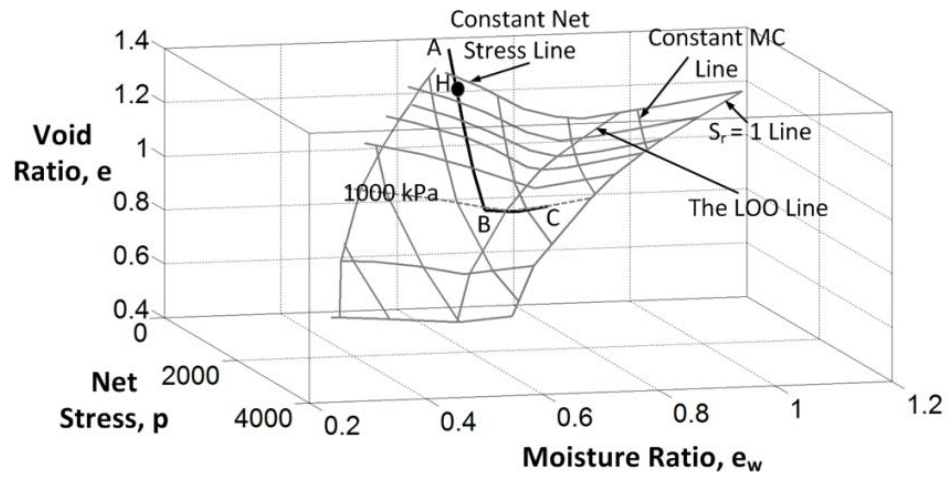
(o) 3-D view of state path test (m)

Figure 5-12: Loading/wetting state path tests on 25.96% moisture content ($e_w = 0.688$), Low compaction kaolin soil specimens at different stress levels
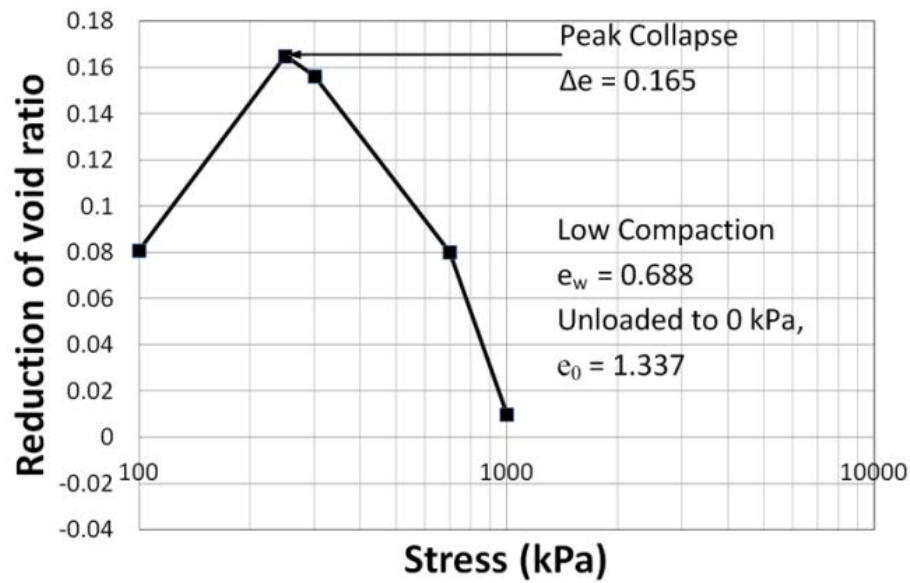
(a) Reduction of void ratio versus Operational Stress
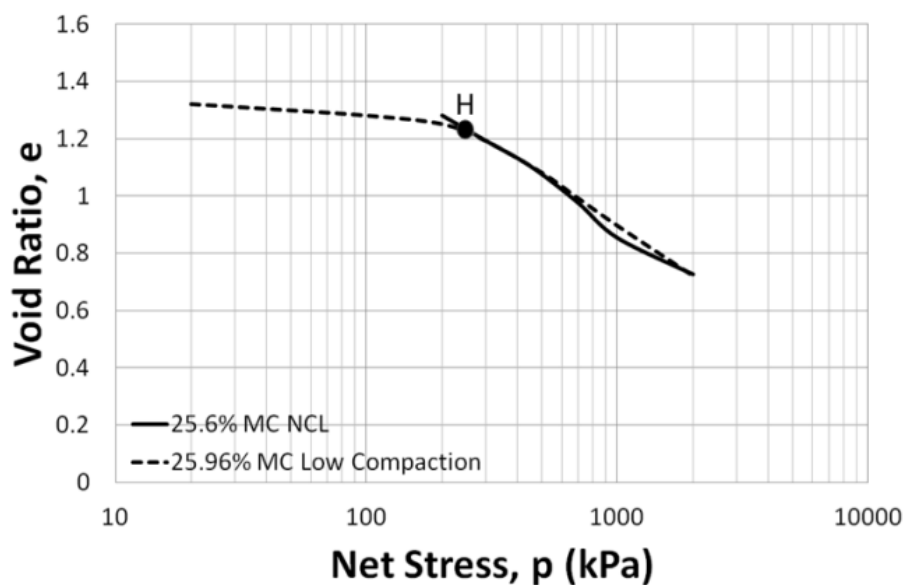
(b) Void Ratio versus Net Stress compression for Low compaction kaolin soil specimen with initial $e_{wo} = 0.688$

Figure 5-13: Collapse potential given as a reduction of void ratio with Operational Stress for Low compaction (pre-compaction stress $\approx$ 250 kPa) kaolin soil specimen with initial $e_{wo} = 0.688$ and unloaded to zero stress $e_o = 1.337$ [Test Identity => Combination of DC – EK – CPT – 6 to 10]
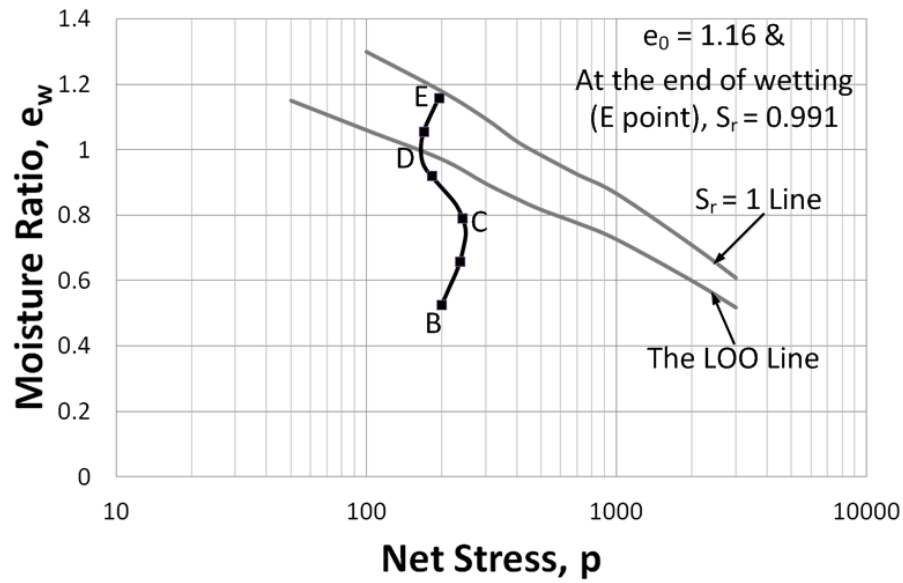
(a) Moderate compaction, 19.85% moisture content (e_w = 0.526) soil specimen loaded to 200 kPa and then wetted to 43.40% moisture content (e_w = 1.150) (S_r = 0.991 and e_0 = 1.16) at constant volume [Test Identity => DC – EK – SPT – 1]
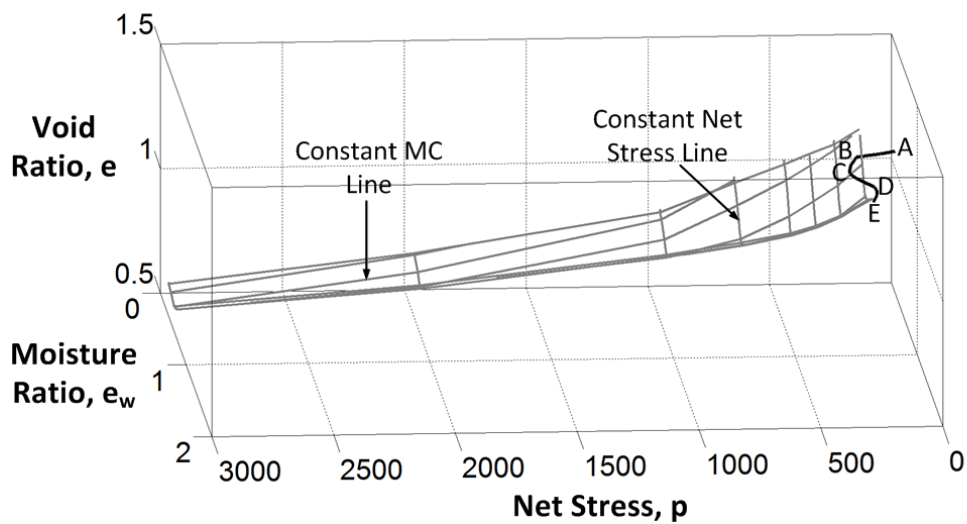
(b) 3-D view of state path test (a)
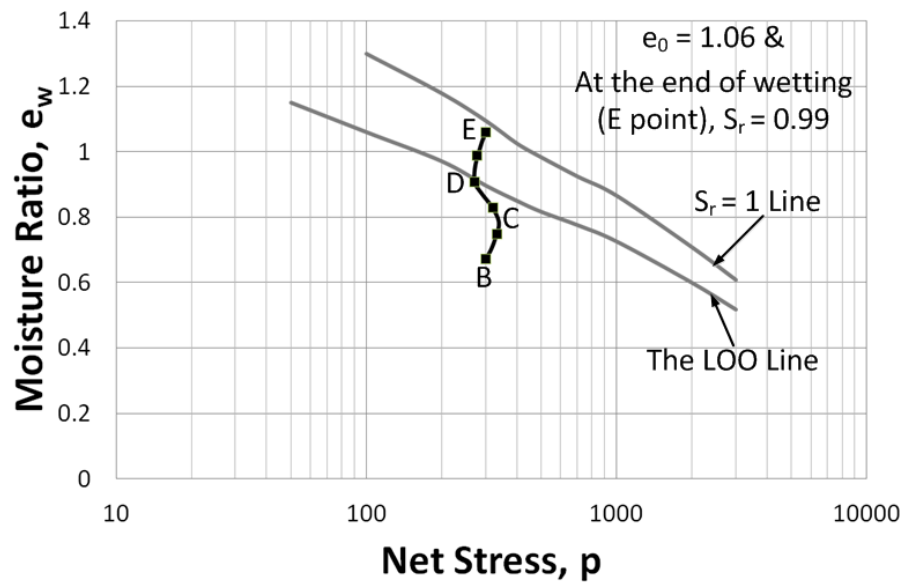
(c) Moderate compaction, 25.40% moisture content ($e_w = 0.673$) soil specimen loaded to 300 kPa and then wetted to 39.62% moisture content ($e_w = 1.050$) ($S_r = 0.99$ and $e_0 = 1.06$) at constant volume [Test Identity => DC – EK – SPT – 2]

(d) 3-D view of state path test (c)

(e) Intermediate compaction, 19.94% moisture content ($e_w = 0.528$) soil specimen loaded to 300 kPa and then wetted to 36.60% moisture content ($e_w = 0.970$) ($S_r = 0.99$ and $e_0 = 0.98$) at constant volume [Test Identity => DC – EK – SPT – 3]

(f) 3-D view of state path test (e)
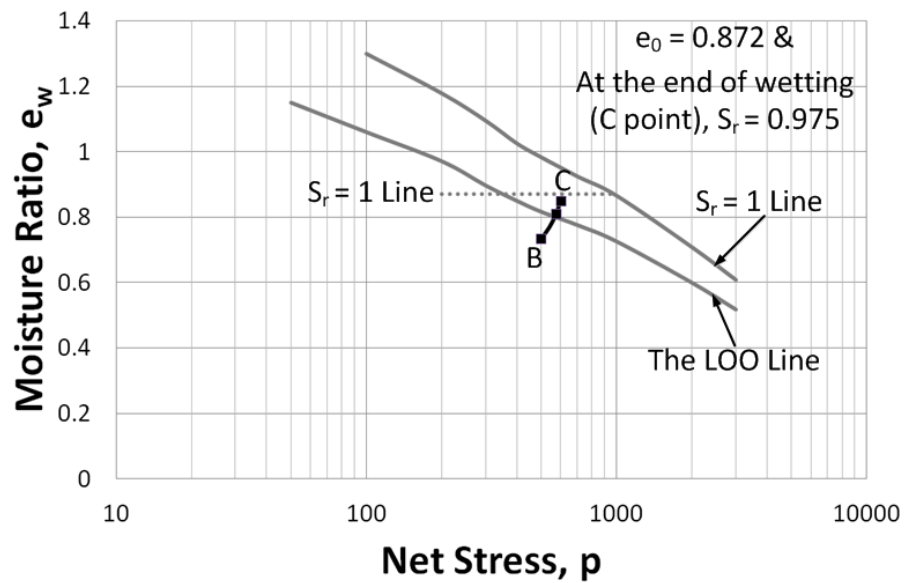
(g) Intermediate compaction, 27.71% moisture content ($e_w = 0.734$) soil specimen loaded to 500 kPa and then wetted to 32.08% moisture content ($e_w = 0.850$) ($S_r = 0.975$ and $e_0 = 0.872$) at constant volume [Test Identity => DC – EK – SPT – 4]
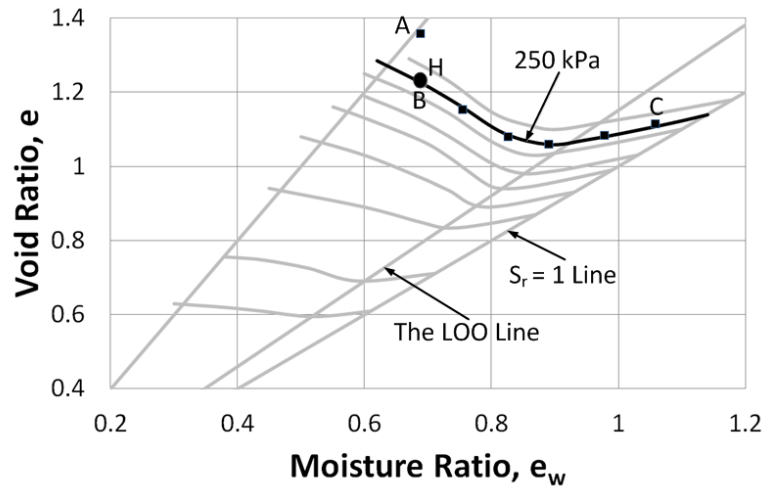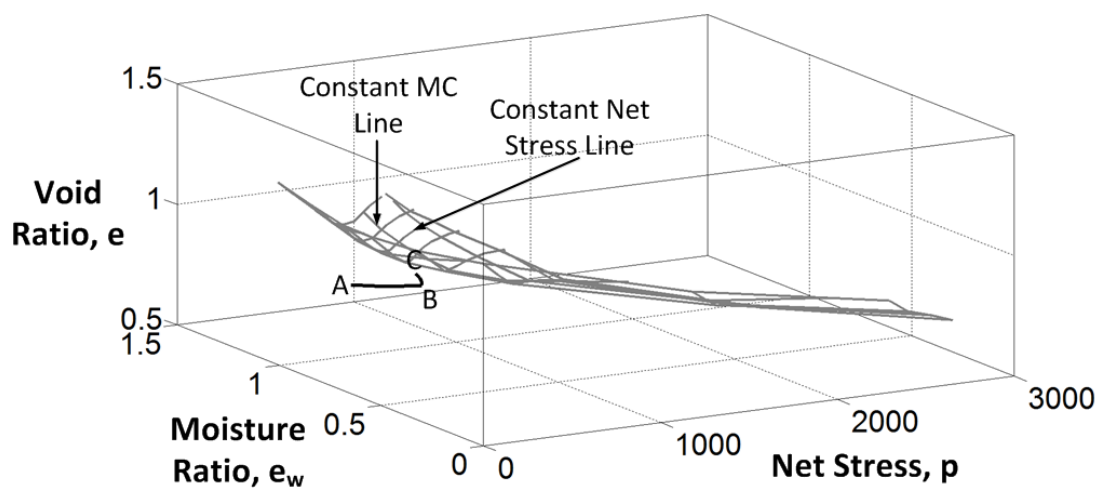

(h) 3-D view of state path test (g)
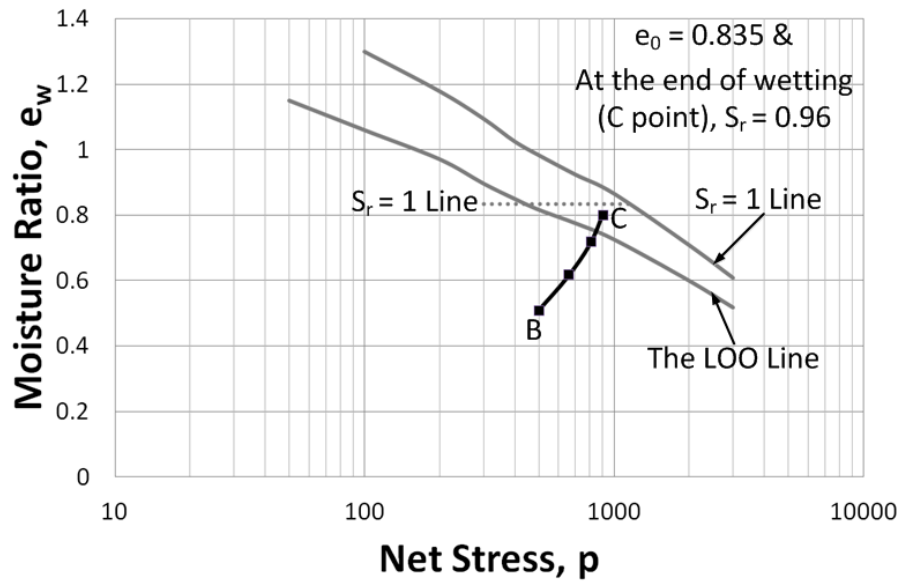
(i) High compaction, 19.27% moisture content ($e_w = 0.511$) soil specimen loaded to 500 kPa and then wetted to 30.20% moisture content ($e_w = 0.800$) ($S_r = 0.96$ and $e_0 = 0.835$) at constant volume [Test Identity => DC – EK – SPT – 5]
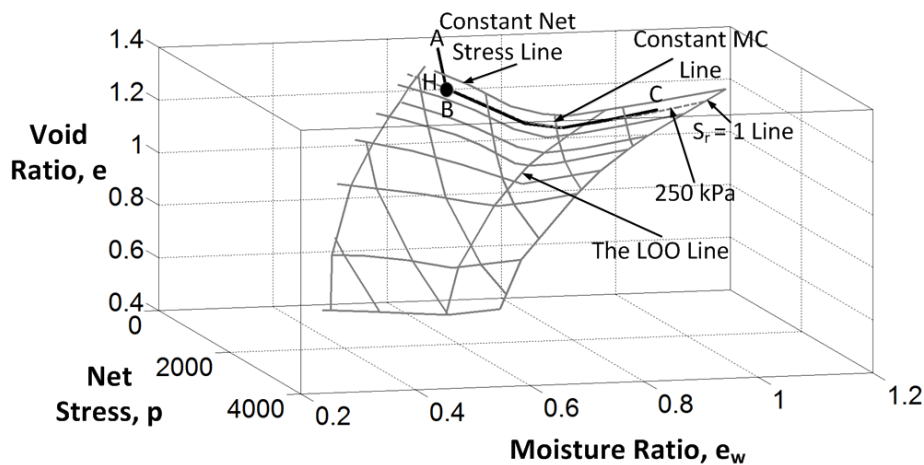

(j) 3-D view of state path test (i)

(k) High compaction, 23.54% moisture content ($e_w = 0.624$) soil specimen loaded to 1000 kPa and then wetted to 29.40% moisture content ($e_w = 0.779$) ($S_r = 0.975$ and $e_0 = 0.8$) at constant volume [Test Identity => DC – EK – SPT – 6]

(l) 3-D view of state path test (k)

Figure 5-14: Constant volume wetting state path tests for the kaolin soil

(a) High compaction, 15.70% moisture content ($e_w = 0.411$) soil specimen loaded to 1000 kPa and then wetted to 22.33% moisture content ($e_w = 0.585$) [Test Identity => DC – MC – LW – 1]
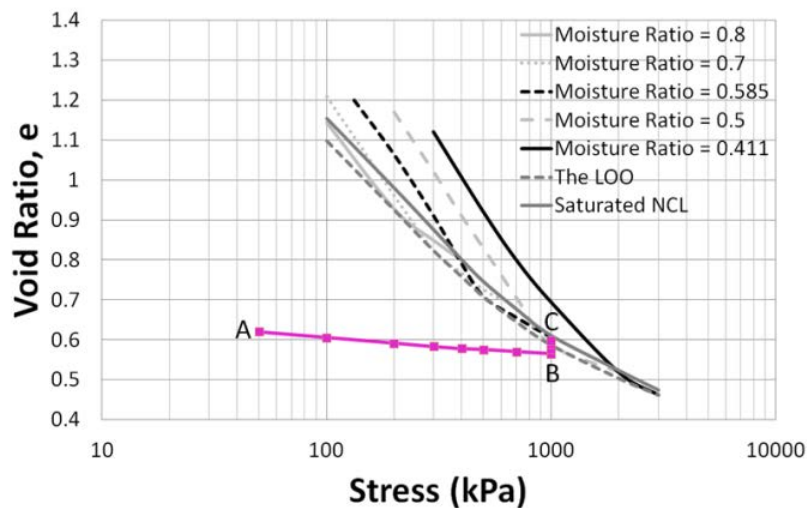
(b) $e - \log p$ relationship of state path test (a)
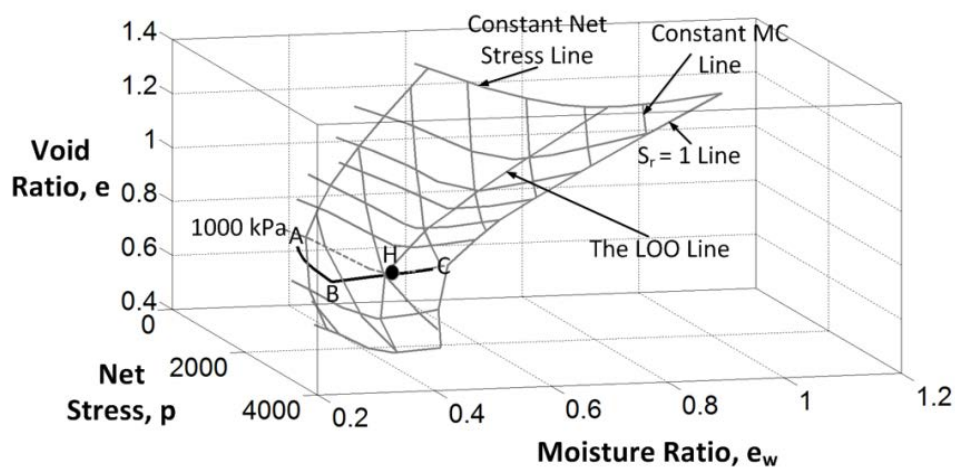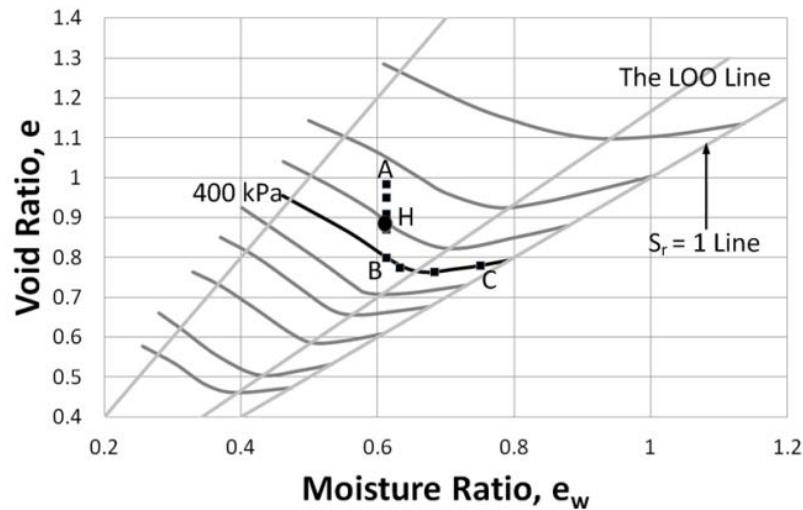
(c) 3-D view of state path test (a)

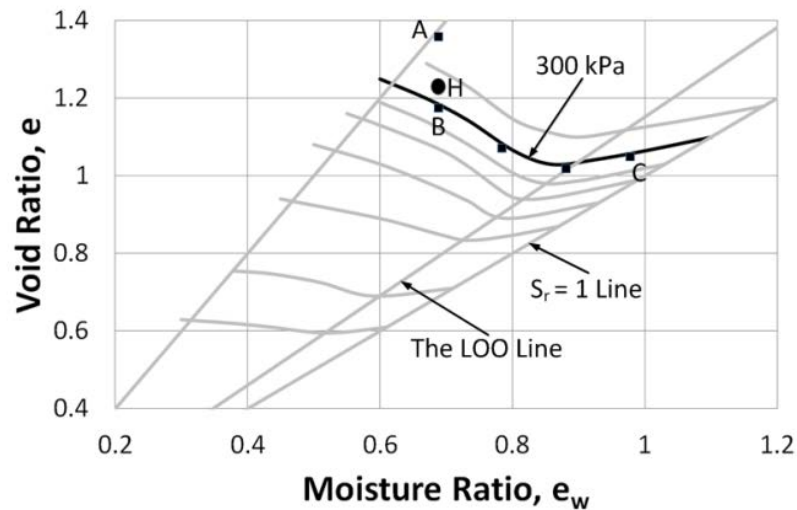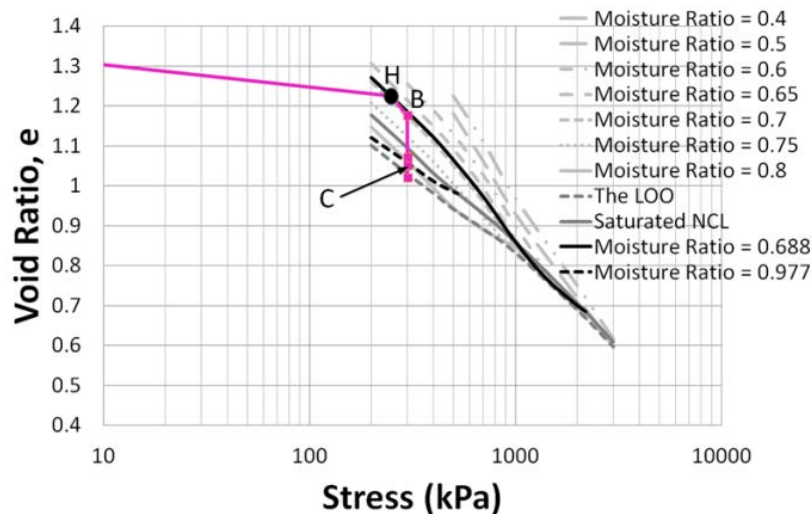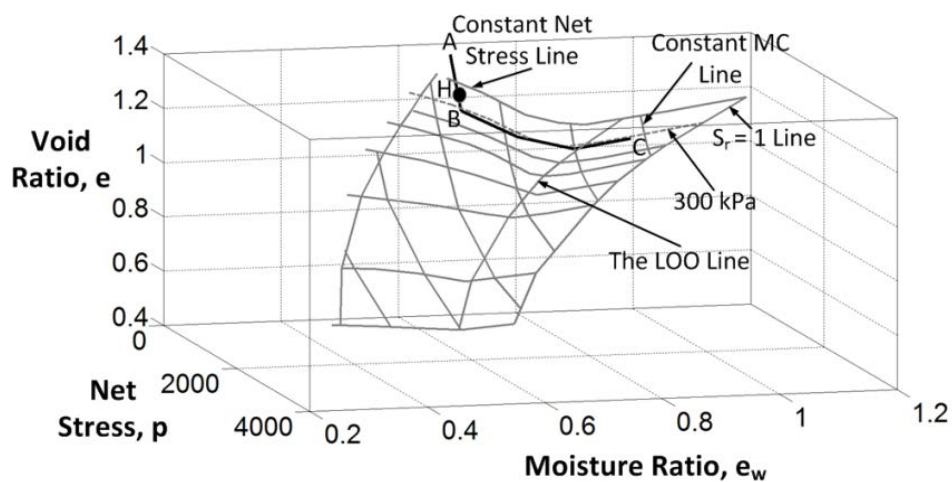**(d)** Low compaction, 23.38% moisture content ($e_w = 0.613$) soil specimen loaded to 400 kPa and then wetted to 28.62% moisture content ($e_w = 0.750$) [Test Identity => DC – MC – LW – 2]

(e) $e - \log p$ relationship of state path test (d)
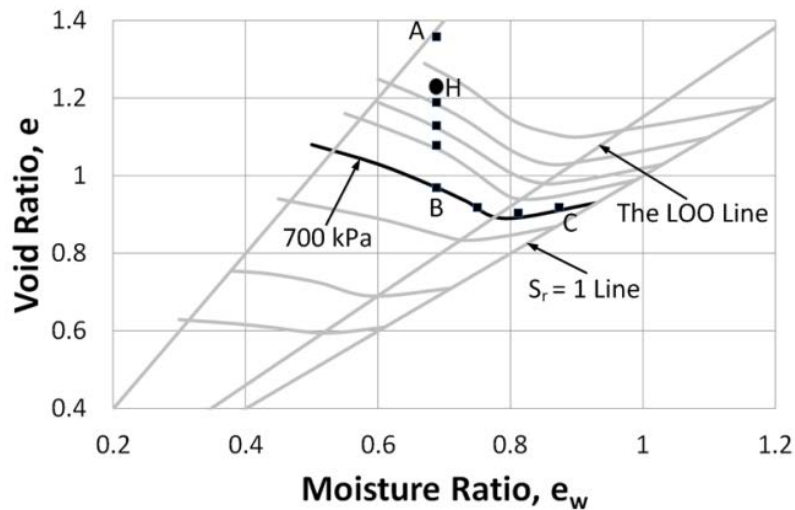

(f) 3-D view of state path test (d)

(g) High compaction, 15.93% moisture content ($e_w = 0.417$) soil specimen loaded to 2000 kPa and then wetted to 17.27% moisture content ($e_w = 0.452$) and then loaded to 3000 kPa [Test Identity => DC – MC – LWL – 1]
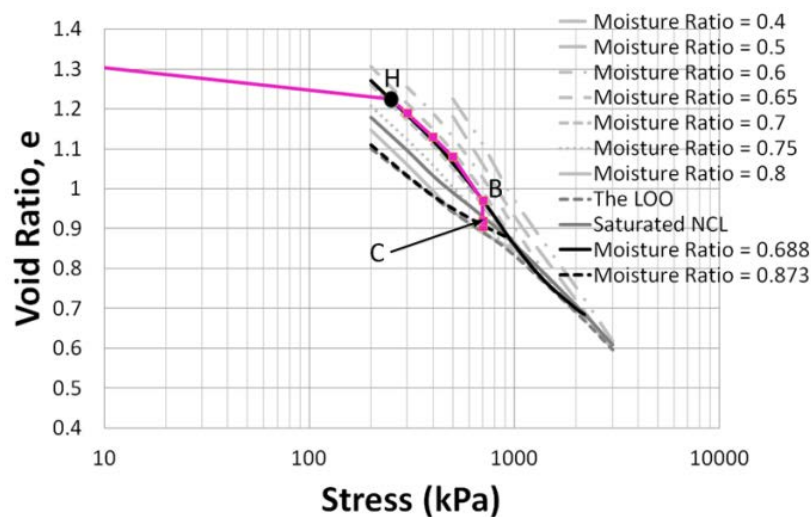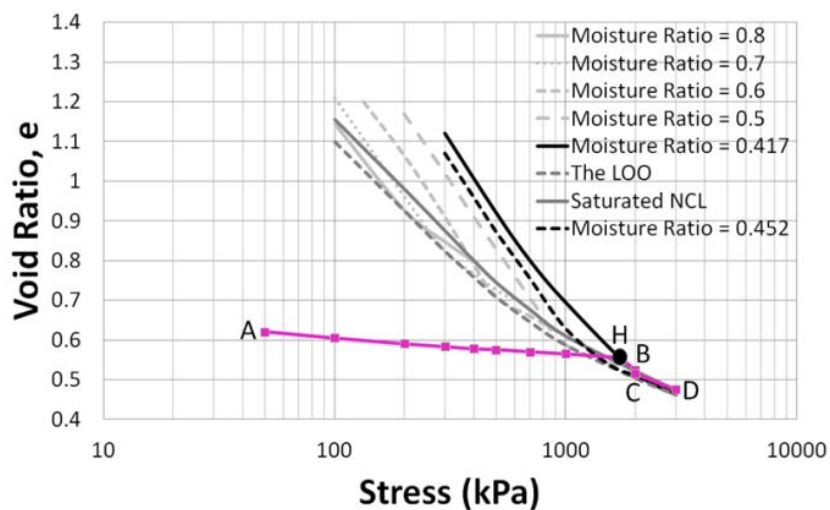

(h) $e – \log p$ relationship of state path test (g)
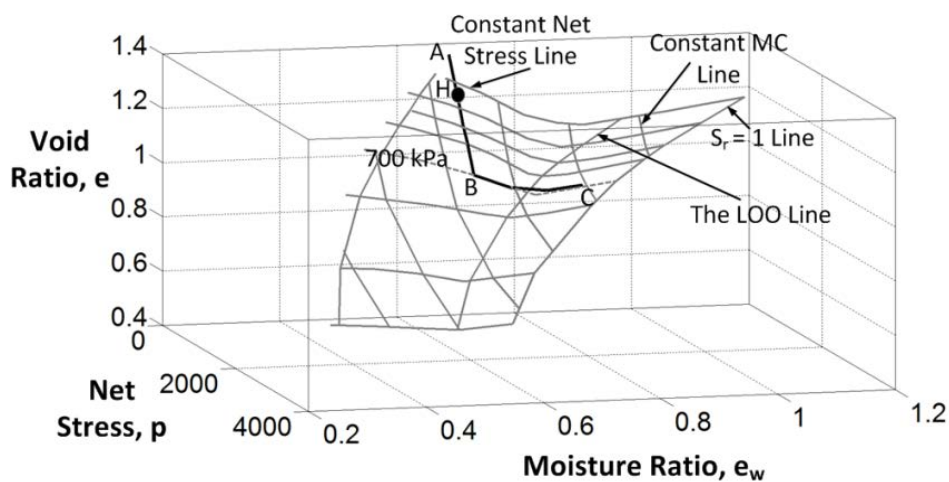

(i) 3-D view of state path test (g)

**(j)** Moderate compaction, 20.52% moisture content ($e_w = 0.538$) soil specimen loaded to 700 kPa and then wetted to 22.76% moisture content ($e_w = 0.596$) and then loaded to 1000 kPa [Test Identity => DC – MC – LWL – 2]
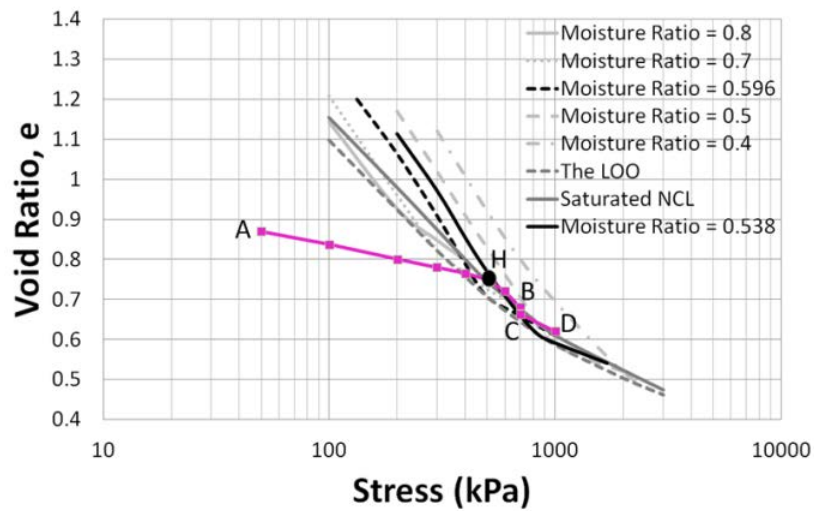
(k) e – log p relationship of state path test (j)

(l) 3-D view of state path test (j)

Figure 5-15: Loading/wetting state path tests for the Merri Creek soil
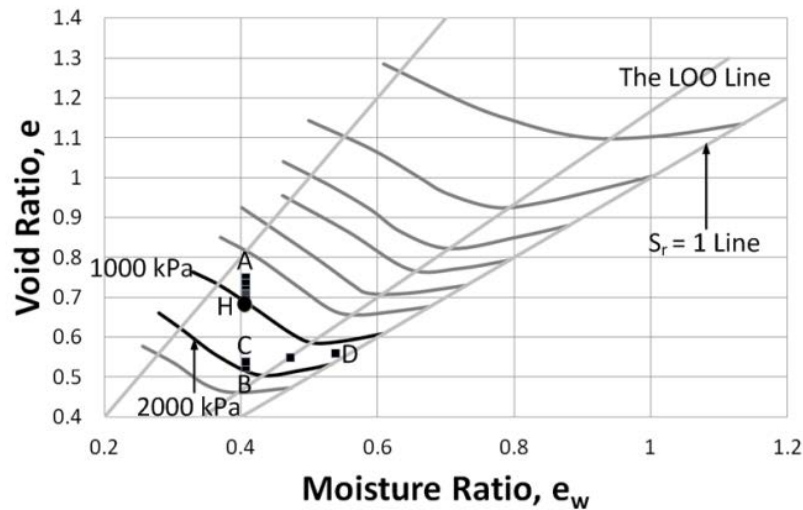
(a) Intermediate compaction, 15.52% moisture content ($e_w = 0.407$) soil specimen loaded to 2000 kPa and then unloaded to 1000 kPa and then wetted to 20.52% moisture content ($e_w = 0.538$) [Test Identity => DC – MC – LUW – 1]
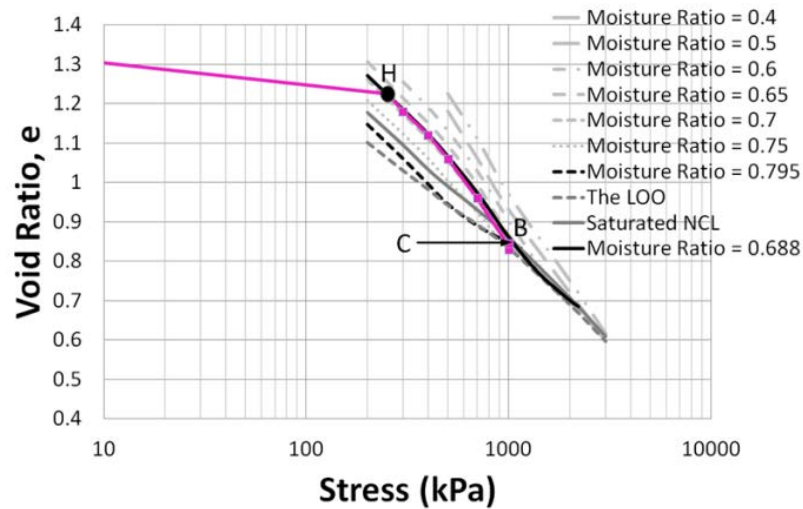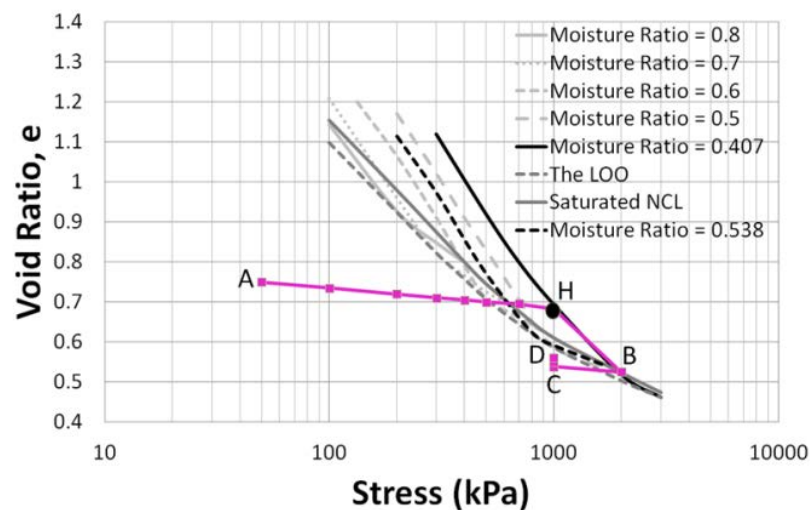

(b) $e – \log p$ relationship of state path test (a)
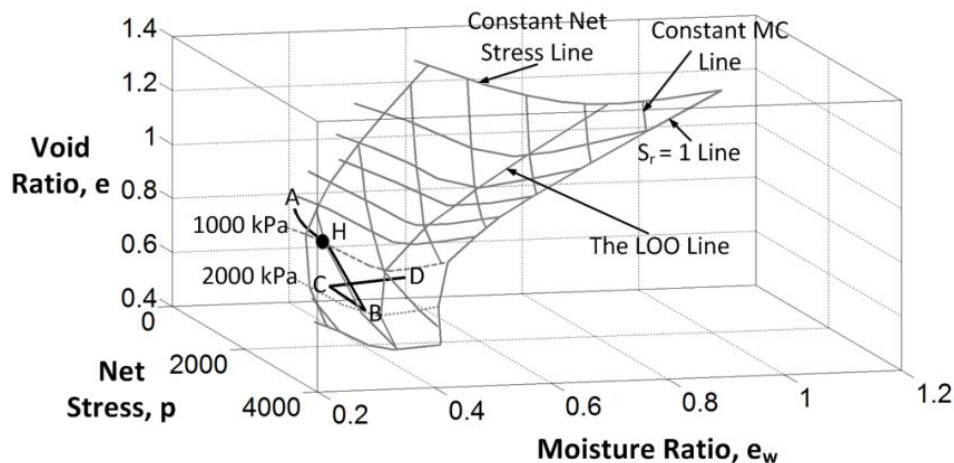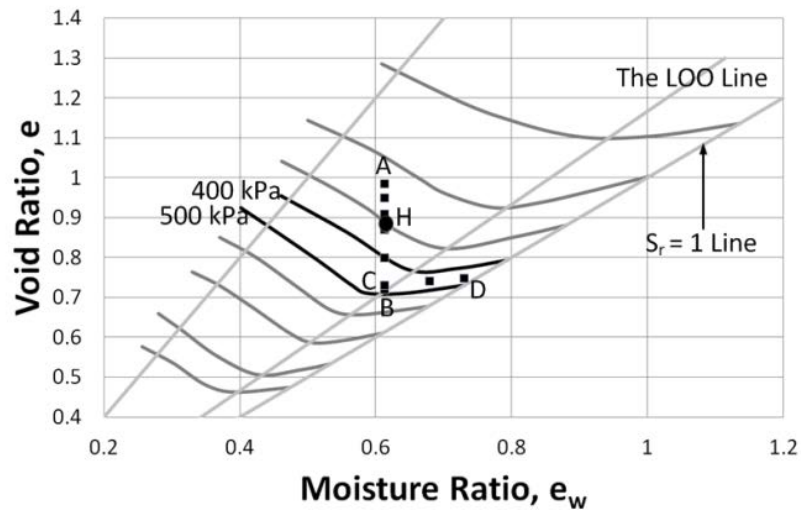
(c) 3-D view of state path test (a)

(d) Low compaction, 23.38% moisture content ($e_w = 0.613$) soil specimen loaded to 500 kPa and then unloaded to 400 kPa and then wetted to 27.86% moisture content ($e_w = 0.730$) [Test Identity => DC – MC – LUW – 2]
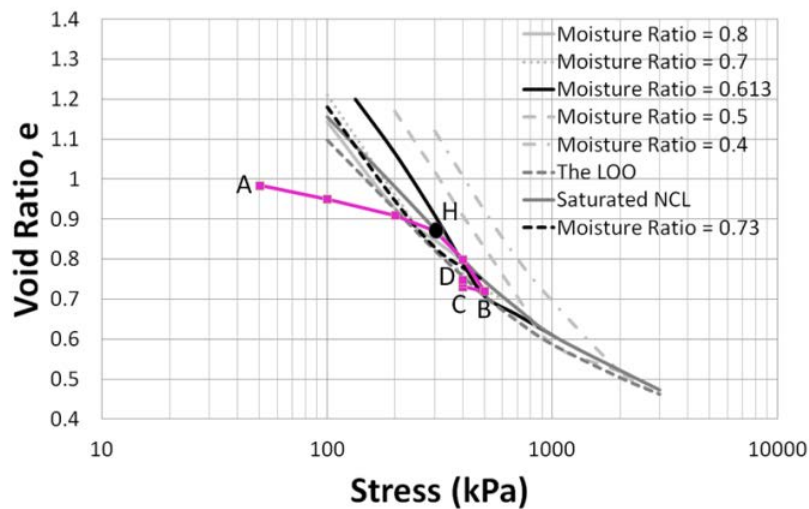
(e) $e – \log p$ relationship of state path test (d)
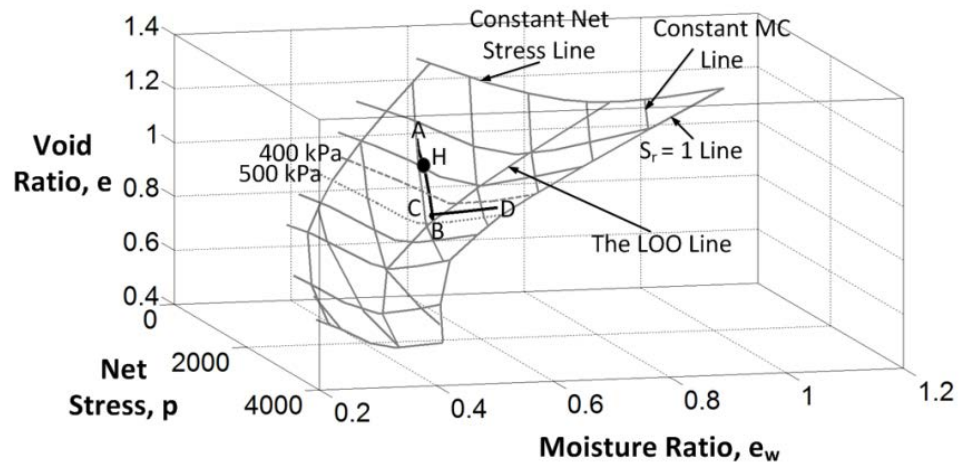
(f) 3-D view of state path test (d)

Figure 5-16: Loading/unloading/wetting state path tests for the Merri Creek soil
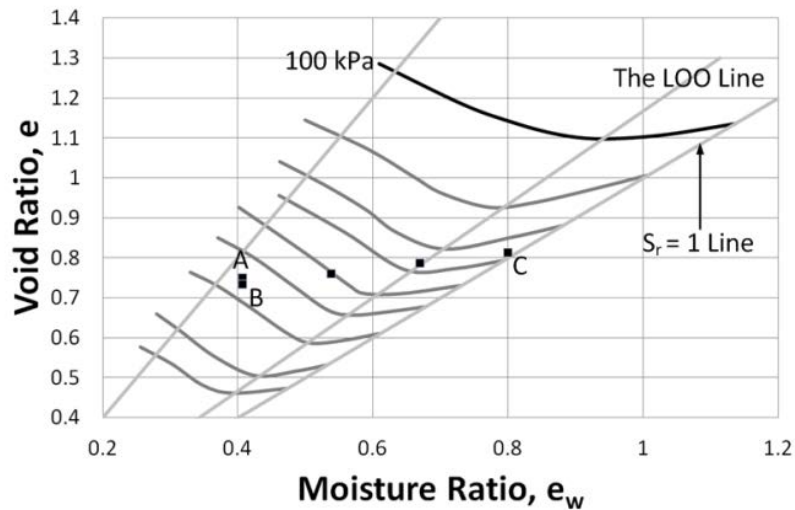
(a) Intermediate compaction, 15.52% moisture content ($e_w = 0.407$) soil specimen loaded to 100 kPa and then wetted to 30.52% moisture content ($e_w = 0.800$) [Test Identity => DC – MC – CPT – 1 or DC – MC – LW – 3]
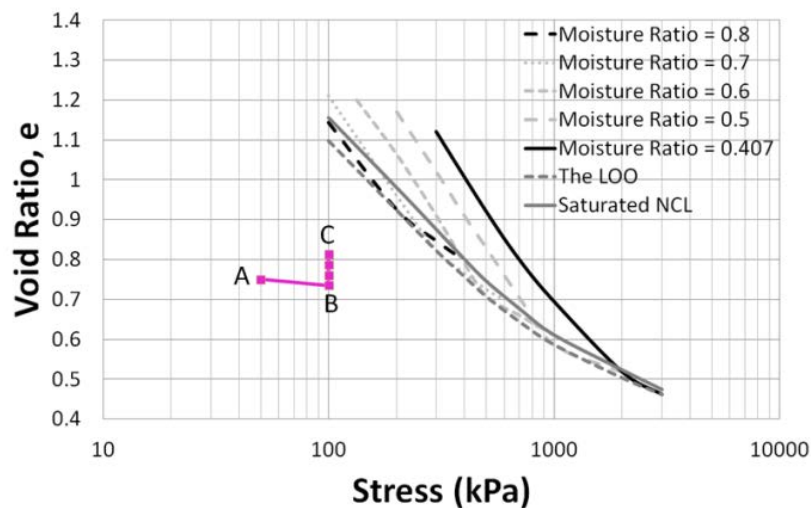
**(b)** e – log p relationship of state path test (a)
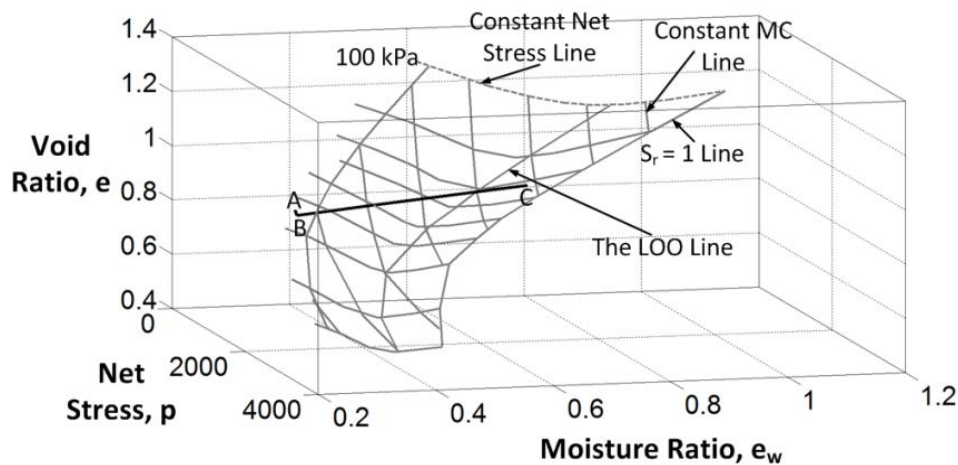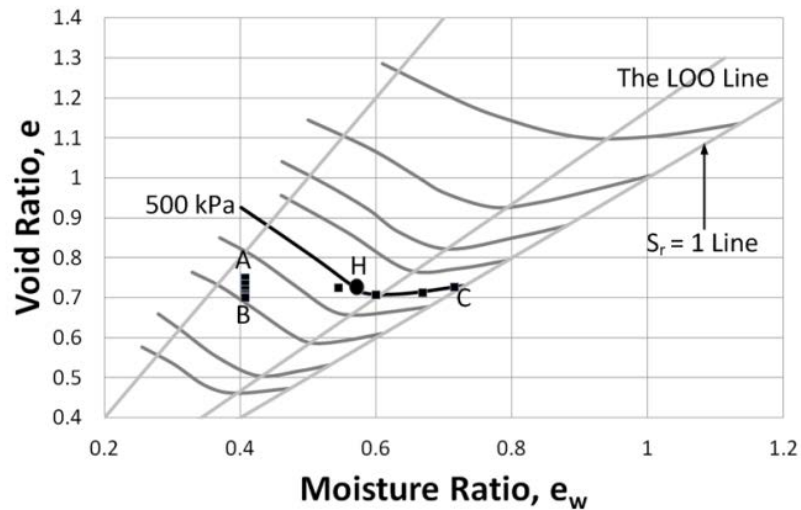
(c) 3-D view of state path test (a)

(d) Intermediate compaction, 15.52% moisture content ($e_w = 0.407$) soil specimen loaded to 500 kPa and then wetted to 27.30% moisture content ($e_w = 0.715$) [Test Identity => DC – MC – CPT – 2 or DC – MC – LW – 4]
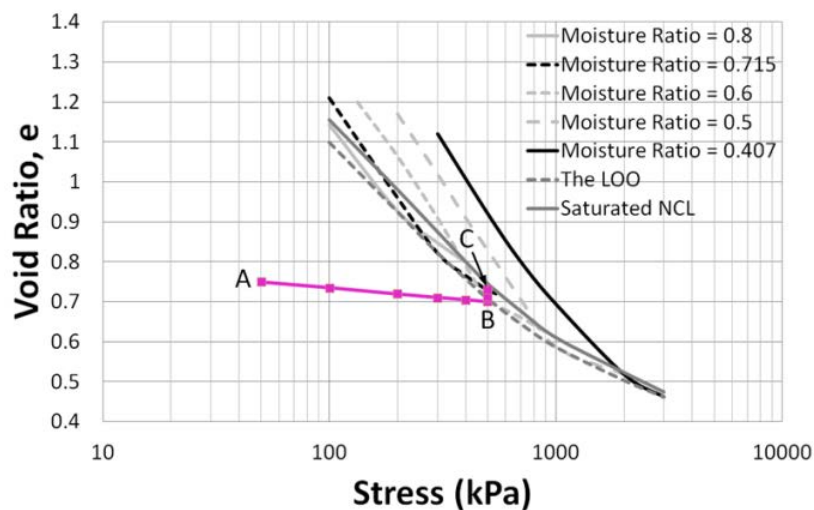
(e) $e – \log p$ relationship of state path test (d)
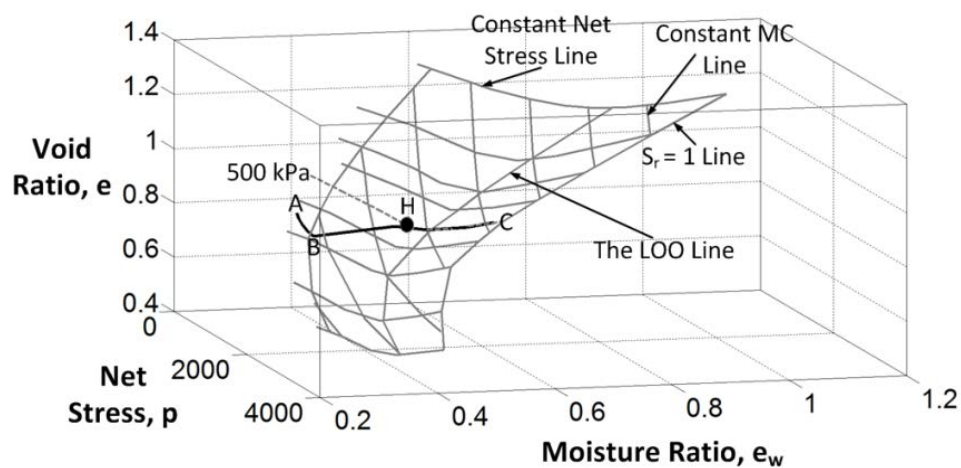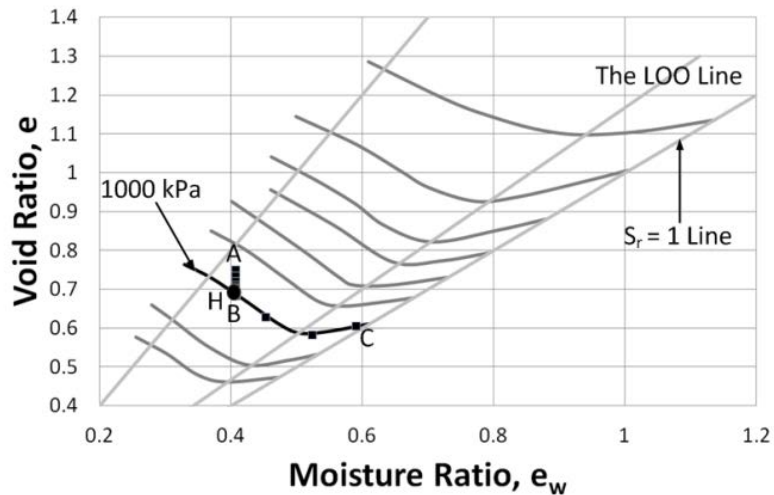
(f) 3-D view of state path test (d)

(g) Intermediate compaction, 15.52% moisture content ($e_w = 0.407$) soil specimen loaded to 1000 kPa and then wetted to 22.52% moisture content ($e_w = 0.590$) [Test Identity => DC – MC – CPT – 3 or DC – MC – LW – 5]
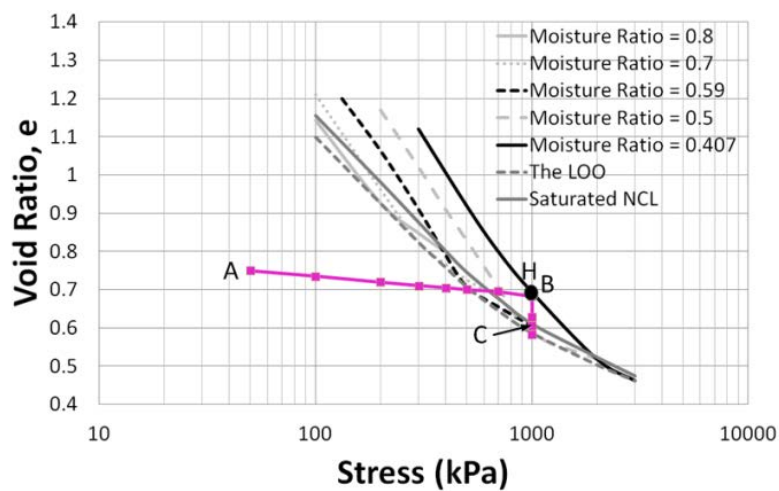
(h) $e – \log p$ relationship of state path test (g)
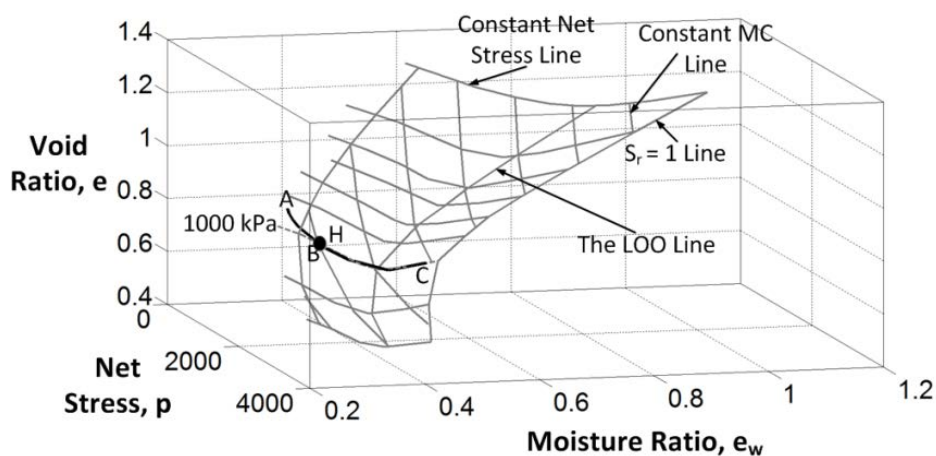
(i) 3-D view of state path test (g)
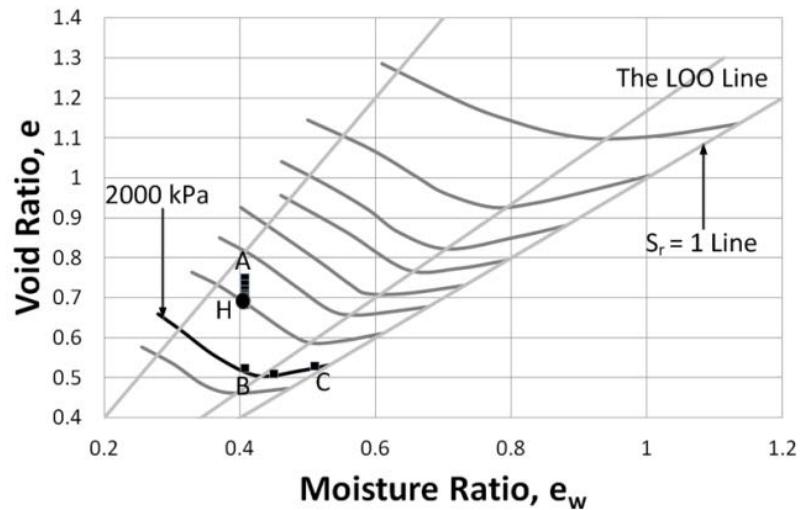
(j) Intermediate Compaction, 15.52% moisture content ($e_w = 0.407$) soil specimen loaded to 2000 kPa and then wetted to 19.46% moisture content ($e_w = 0.510$) [Test Identity => DC – MC – CPT – 4 or DC – MC – LW – 6]
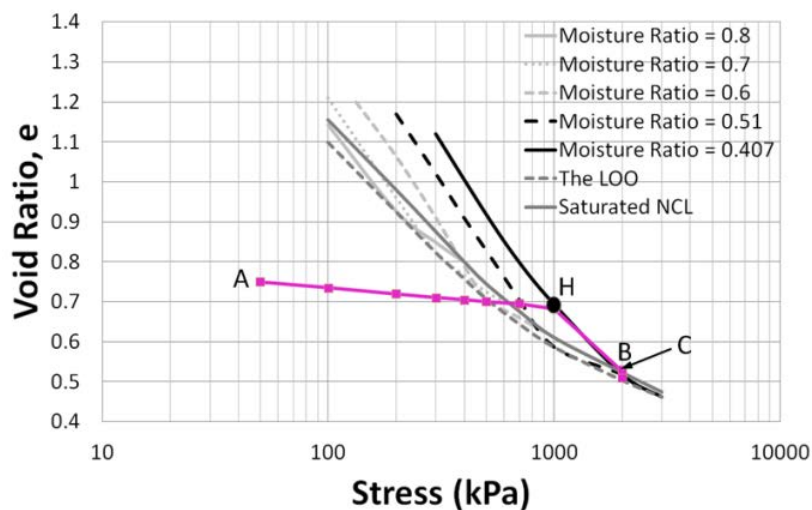
(k) e – log p relationship of state path test (j)
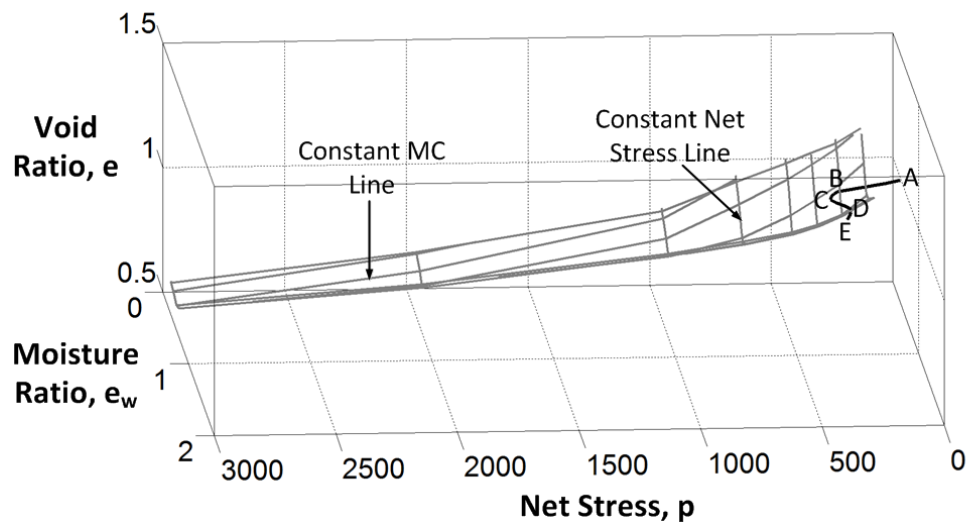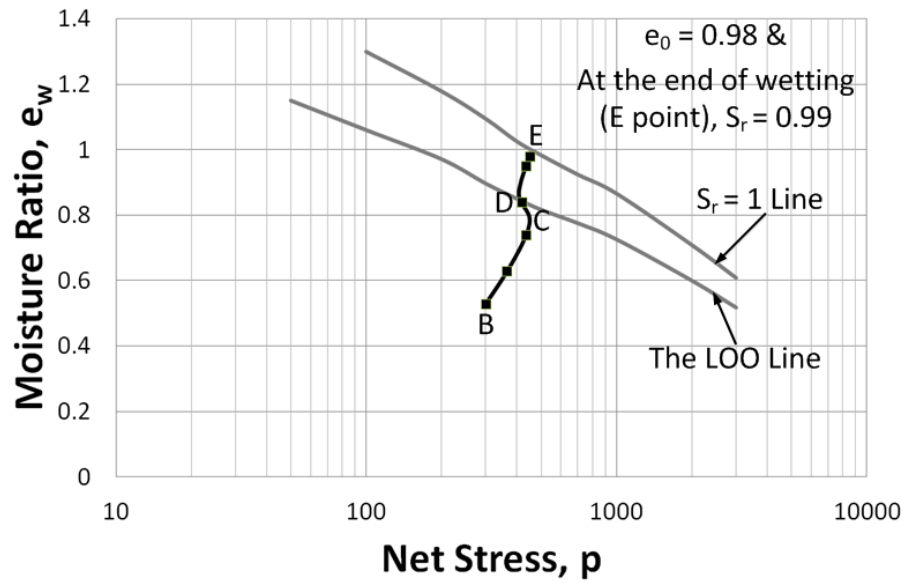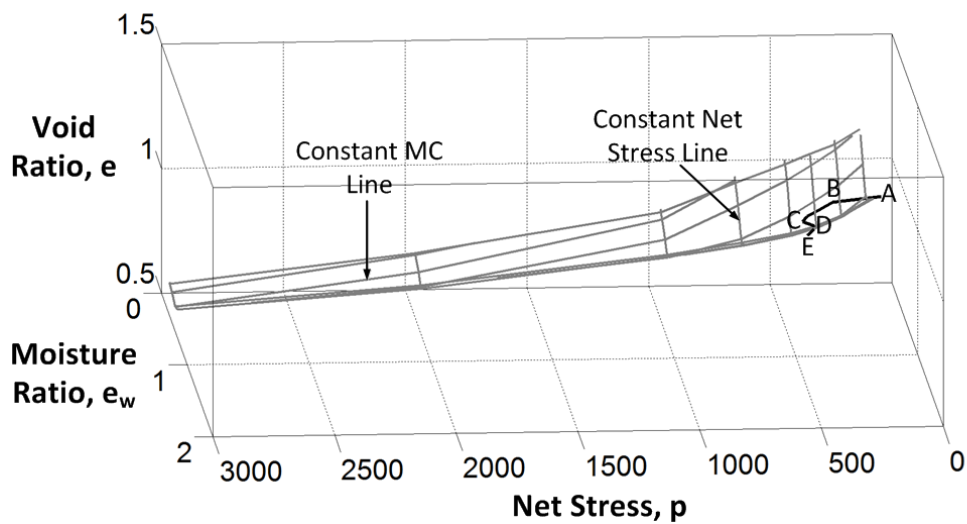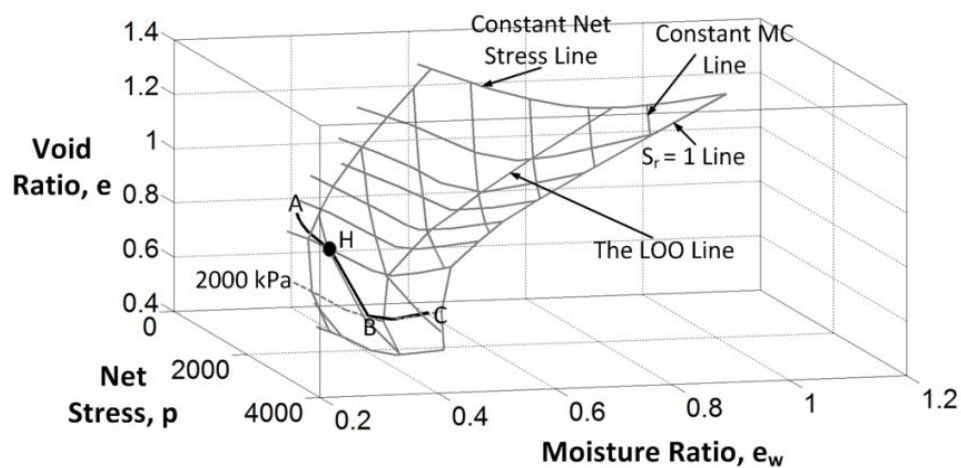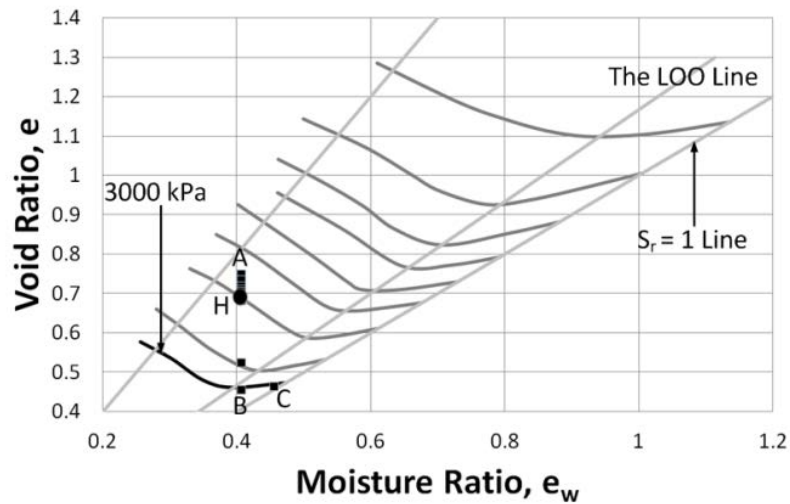

(l) 3-D view of state path test (j)

(m) Intermediate compaction, 15.52% moisture content ($e_w = 0.407$) soil specimen loaded to 3000 kPa and then wetted to 17.37% moisture content ($e_w = 0.455$) [Test Identity => DC – MC – CPT – 5 or DC – MC – LW – 7]
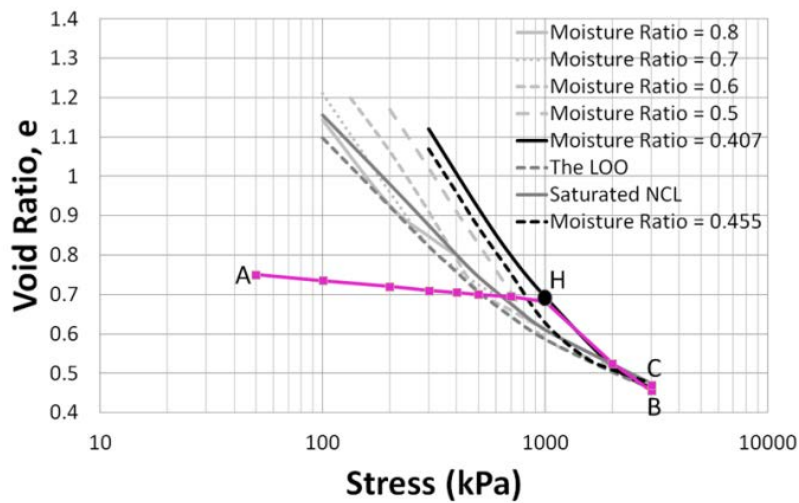
(n) e – log p relationship of state path test (m)
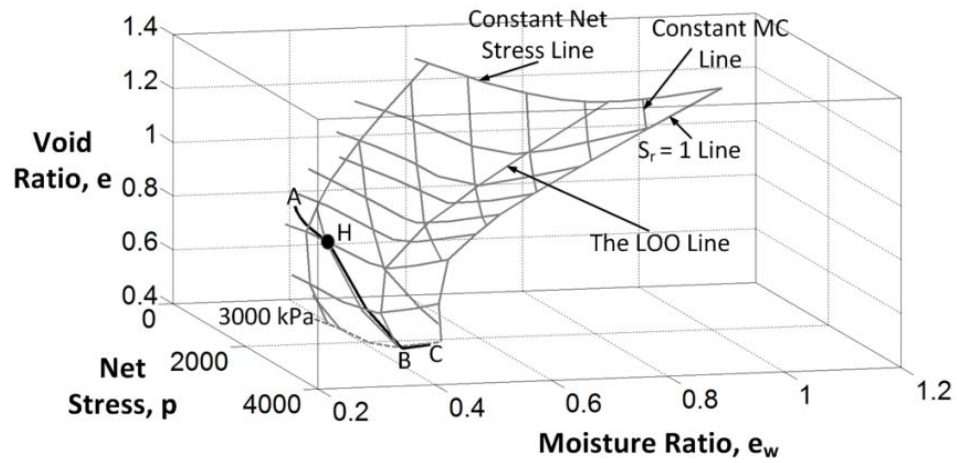
(o) 3-D view of state path test (m)

Figure 5-17: Loading/wetting state path tests on 15.52% moisture content ($e_w = 0.407$), Intermediate compaction Merri Creek soil specimens at different stress levels
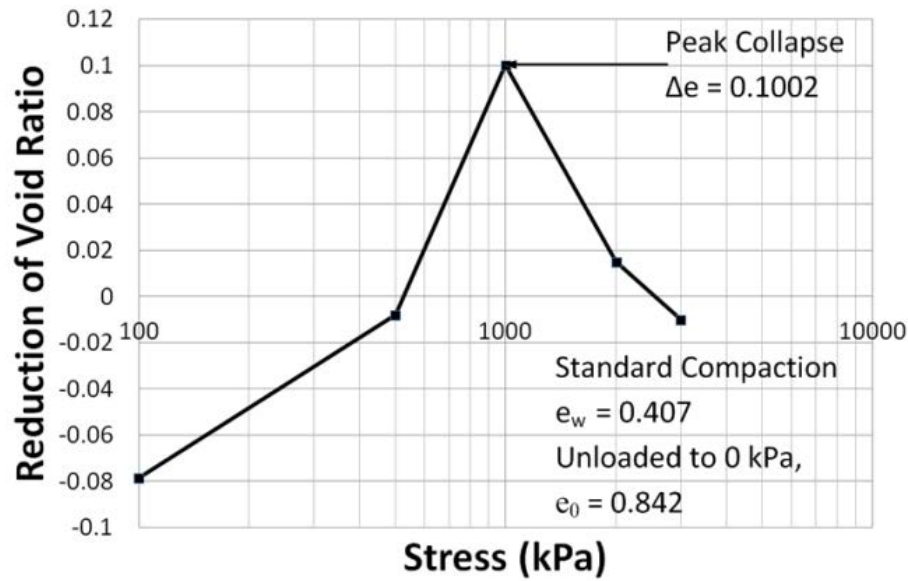
(a) Reduction of void ratio versus Operational Stress
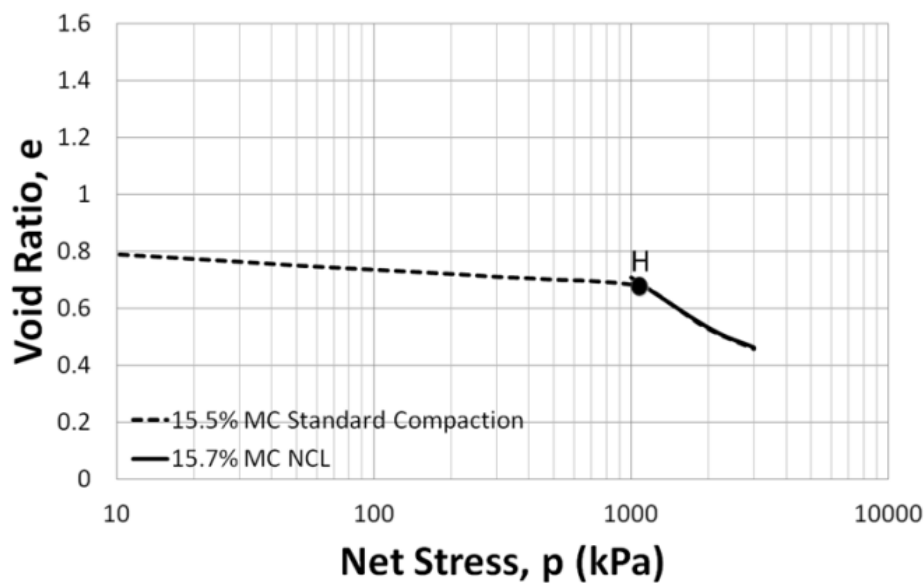
(b) Void Ratio versus Net Stress compression for Intermediate compaction Merri Creek soil specimen with initial $e_{wo} = 0.407$

Figure 5-18: Collapse potential given as a reduction of void ratio with Operational Stress for Intermediate compaction (pre-compaction stress $\approx$ 1000 kPa) Merri Creek soil specimen with initial $e_{wo} = 0.407$ and unloaded to zero stress $e_o = 0.842$ [Test Identity => Combination of DC – MC – CPT – 1 to 5]
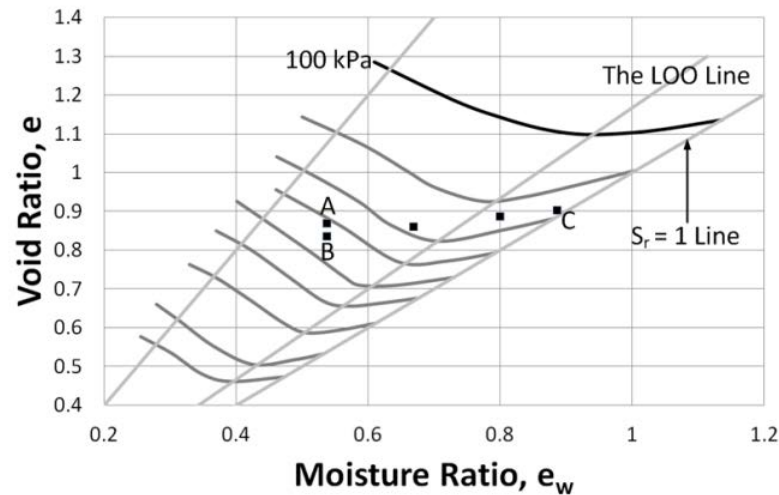
(a) Moderate compaction, 20.52% moisture content ($e_w = 0.538$) soil specimen loaded to 100 kPa and then wetted to 33.80% moisture content ($e_w = 0.886$) [Test Identity => DC – MC – CPT – 6 or DC – MC – LW – 8]
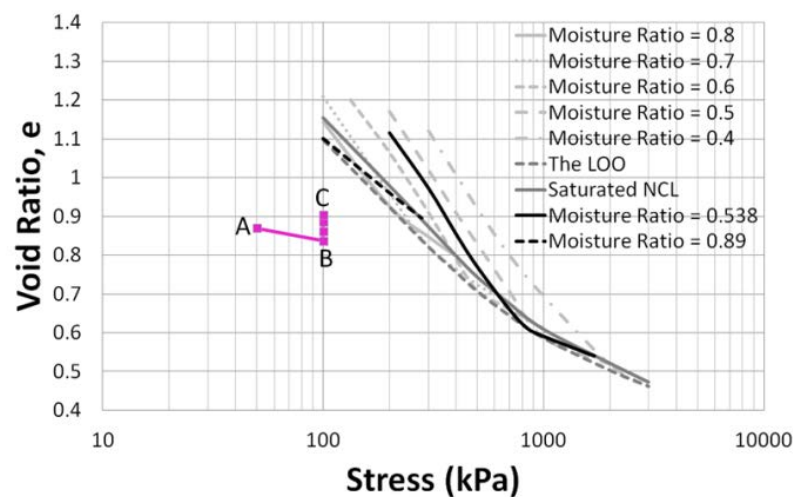
**(b)** $e - \log p$ relationship of state path test (a)
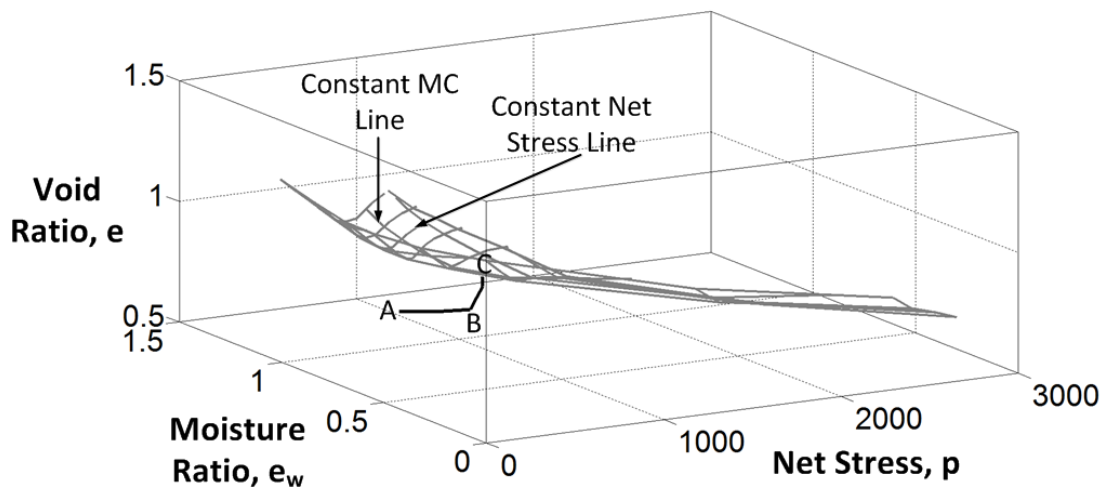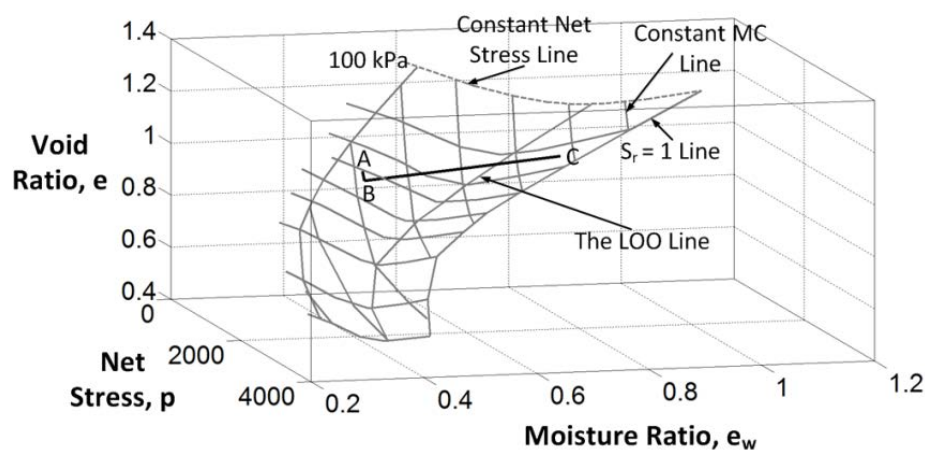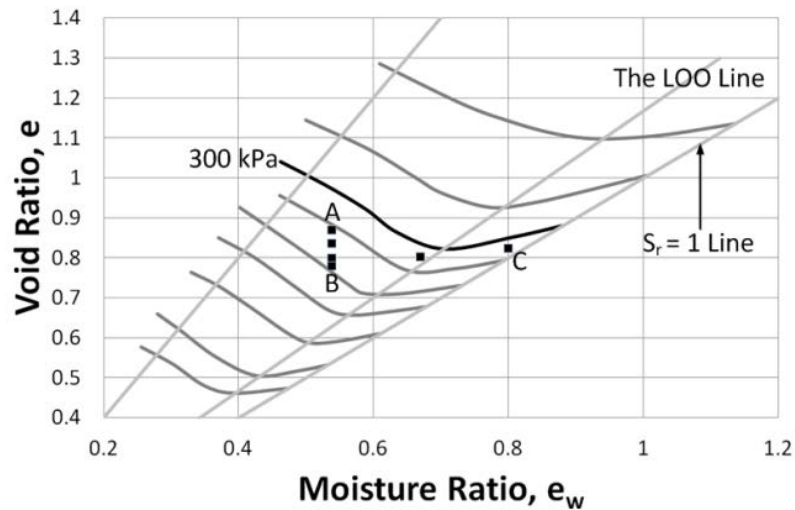

(c) 3-D view of state path test (a)

(d) Moderate compaction, 20.52% moisture content ($e_w = 0.538$) soil specimen loaded to 300 kPa and then wetted to 30.52% moisture content ($e_w = 0.800$) [Test Identity => DC – MC – CPT – 7 or DC – MC – LW – 9]
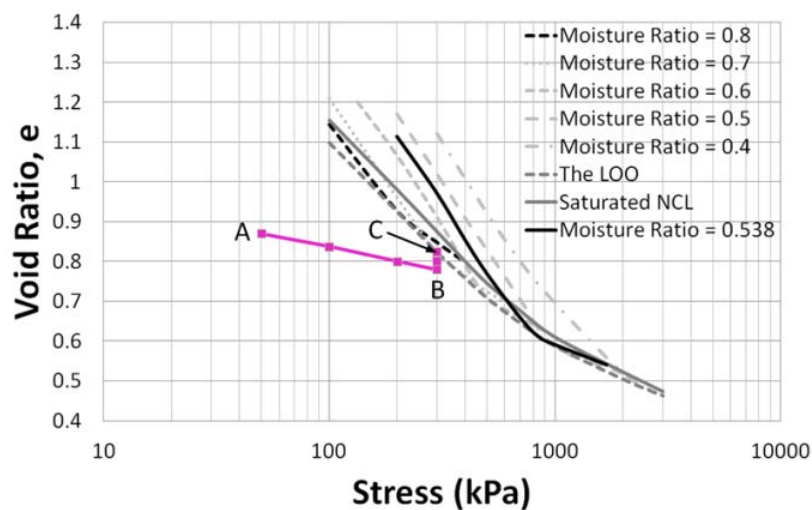
(e) e – log p relationship of state path test (d)
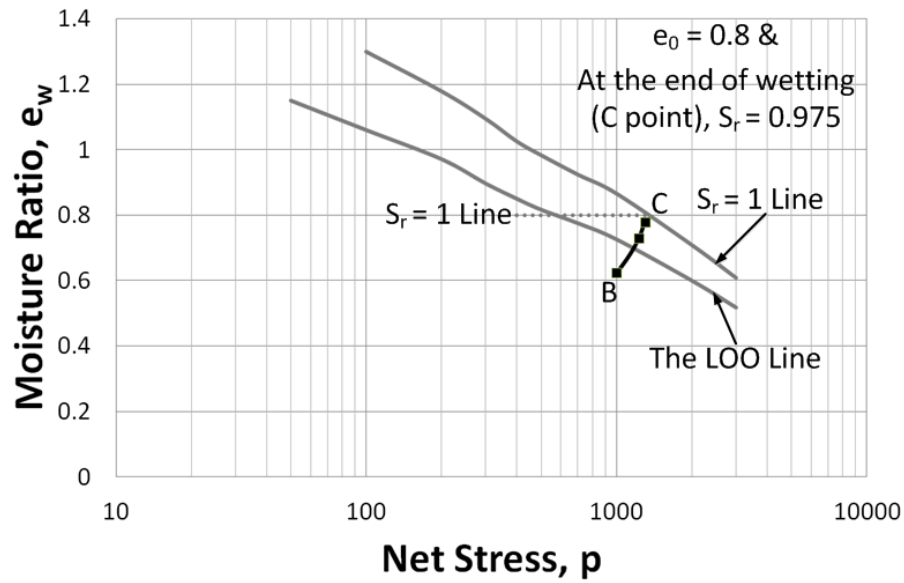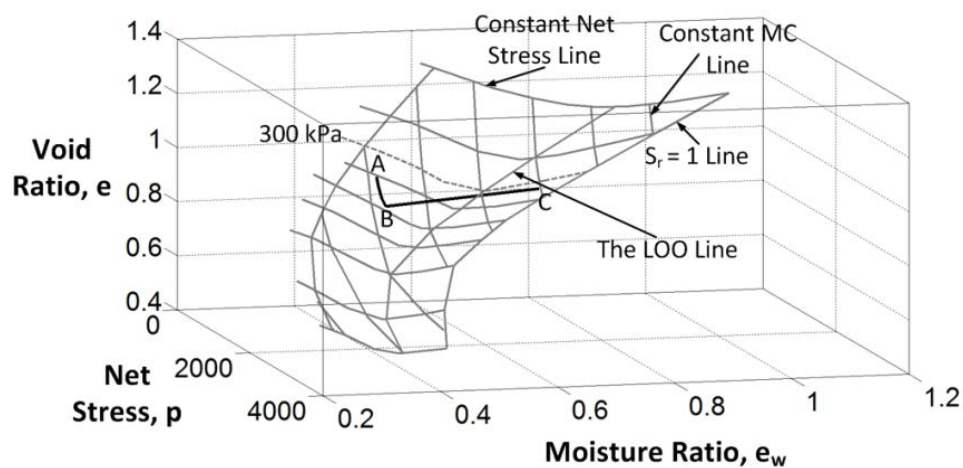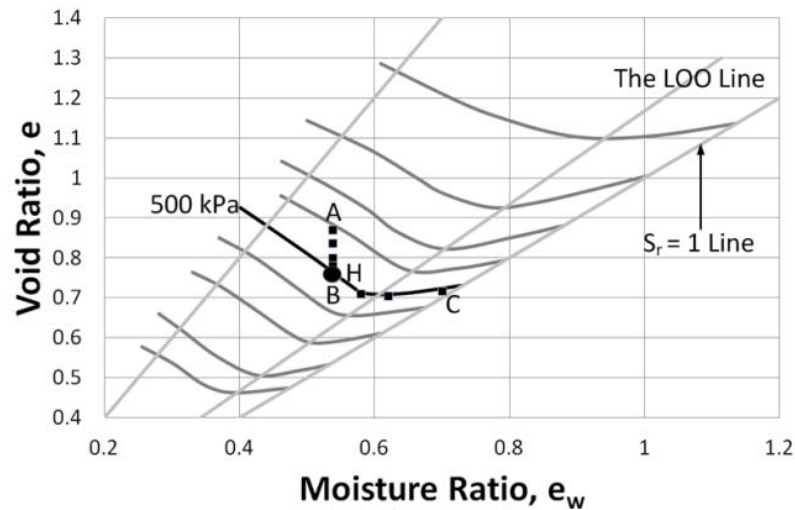

(f) 3-D view of state path test (d)

(g) Moderate Compaction, 20.52% moisture content ($e_w = 0.538$) soil specimen loaded to 500 kPa and then wetted to 26.72% moisture content ($e_w = 0.700$) [Test Identity => DC – MC – CPT – 8 or DC – MC – LW – 10]
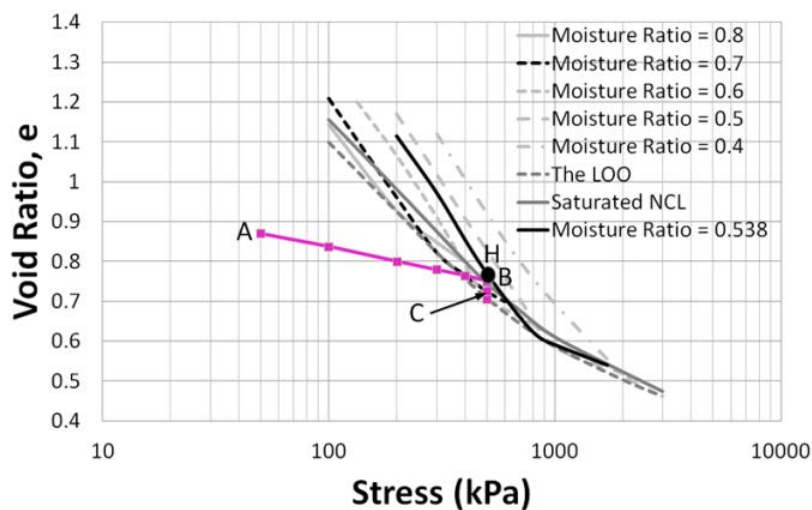
(h) $e – \log p$ relationship of state path test (g)
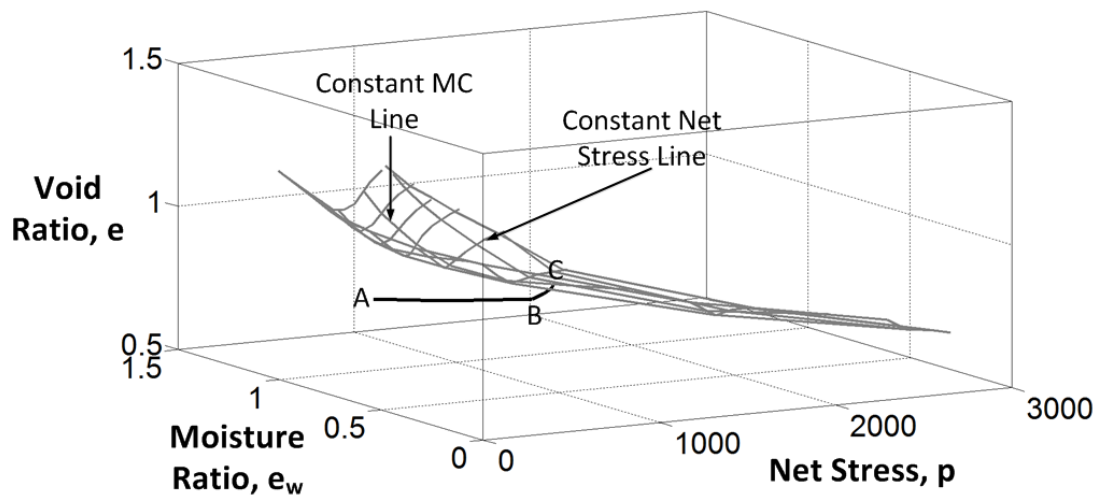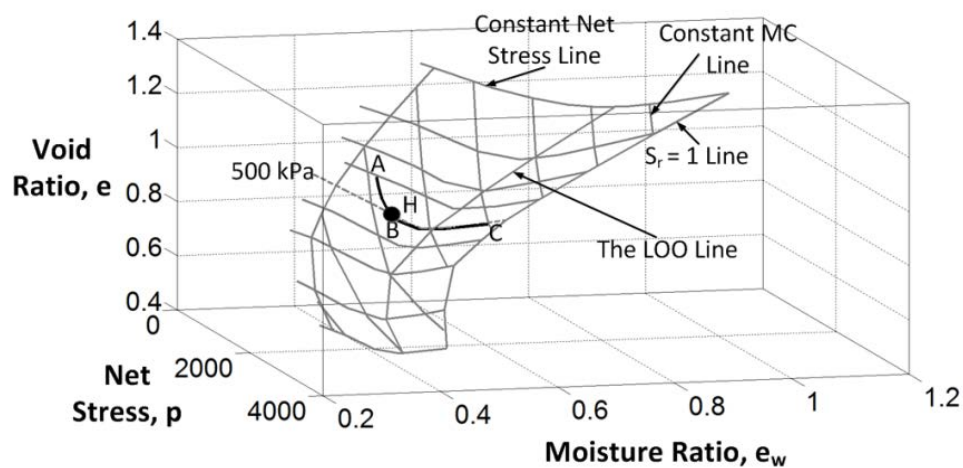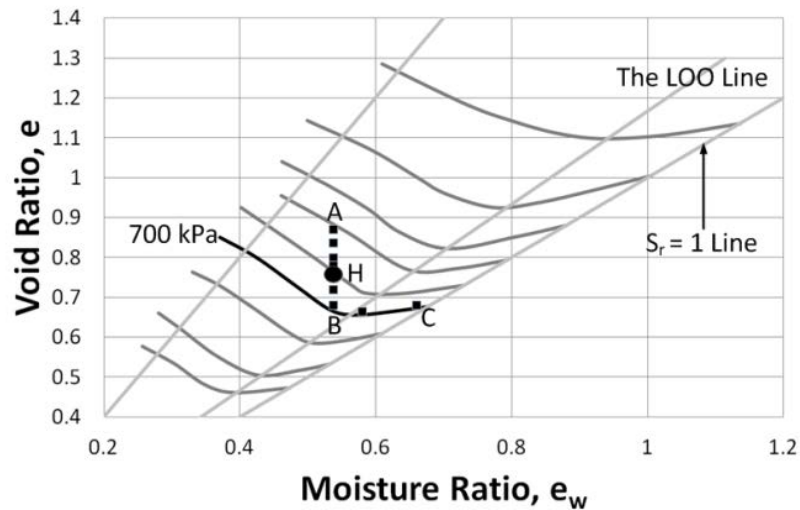

(i) 3-D view of state path test (g)

(j) Moderate compaction, 20.52% moisture content ($e_w = 0.538$) soil specimen loaded to 700 kPa and then wetted to 25.20% moisture content ($e_w = 0.660$) [Test Identity => DC – MC – CPT – 9 or DC – MC – LW – 11]
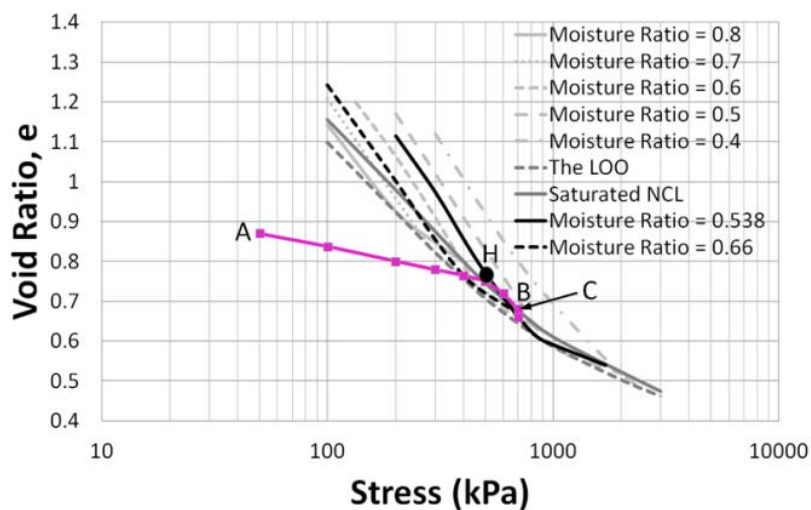
(k) $e - \log p$ relationship of state path test (j)
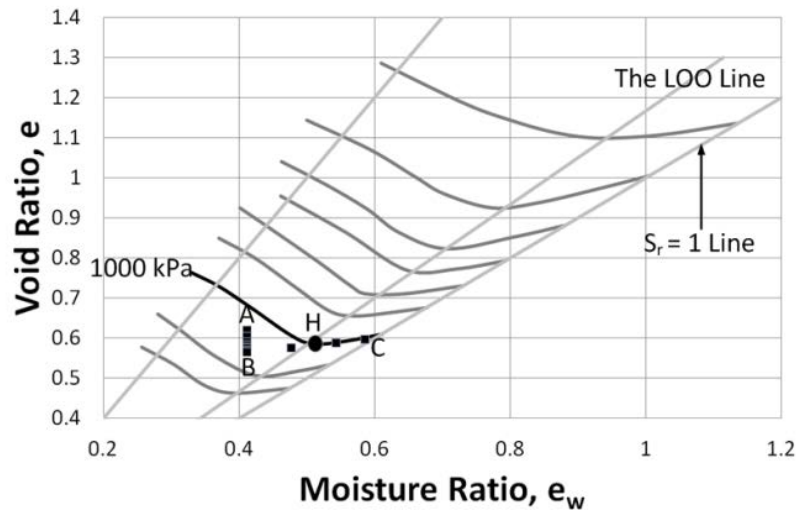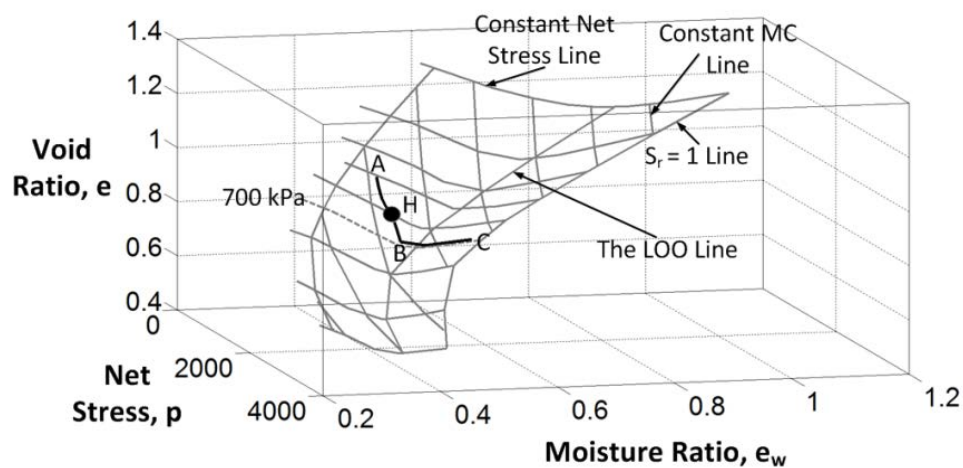

(l) 3-D view of state path test (j)
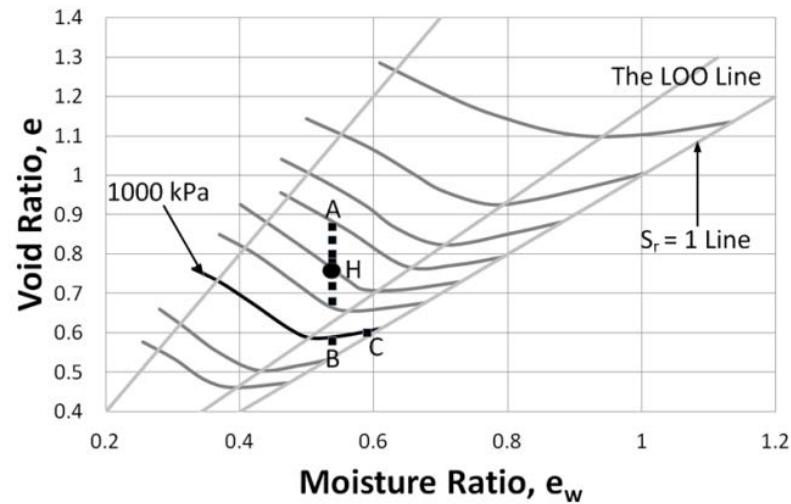
(m) Moderate compaction, 20.52% moisture content ($e_w = 0.538$) soil specimen loaded to 1000 kPa and then wetted to 22.52% moisture content ($e_w = 0.590$) [Test Identity => DC – MC – CPT – 10 or DC – MC – LW – 12]
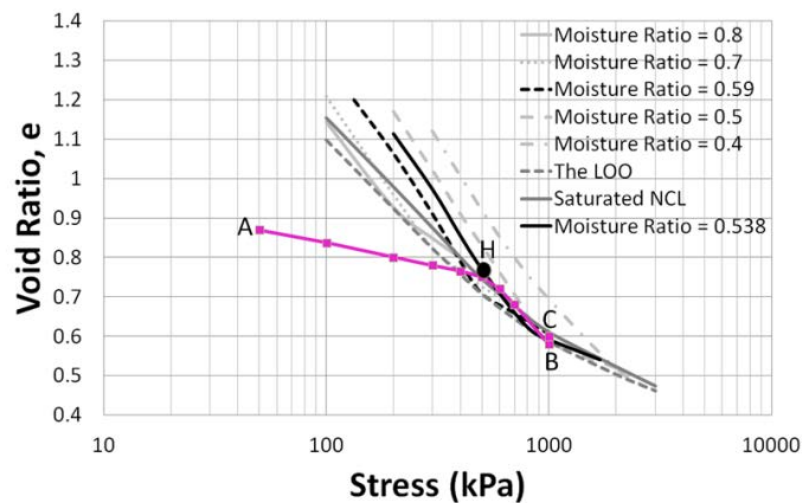
(n) e – log p relationship of state path test (m)
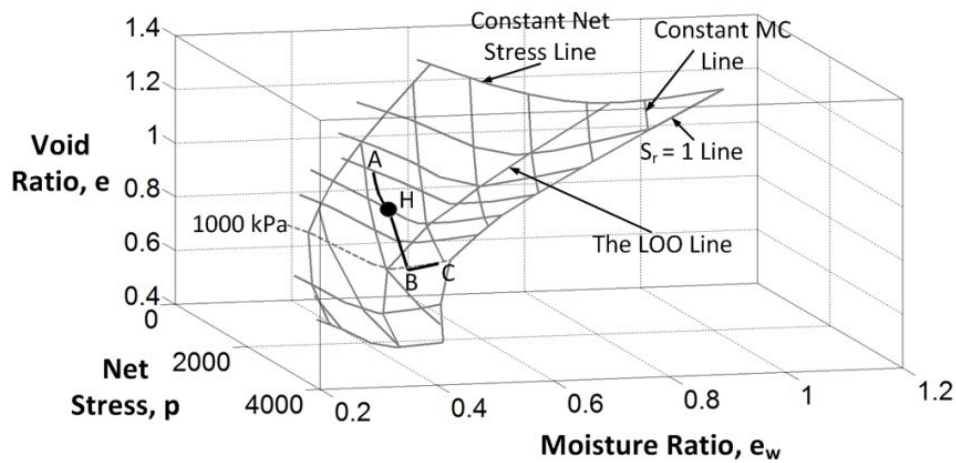
(o) 3-D view of state path test (m)

**Figure 5-19:** Loading/wetting state path tests on 20.52% moisture content ($e_w = 0.538$), Moderate compaction Merri Creek soil specimens at different stress levels
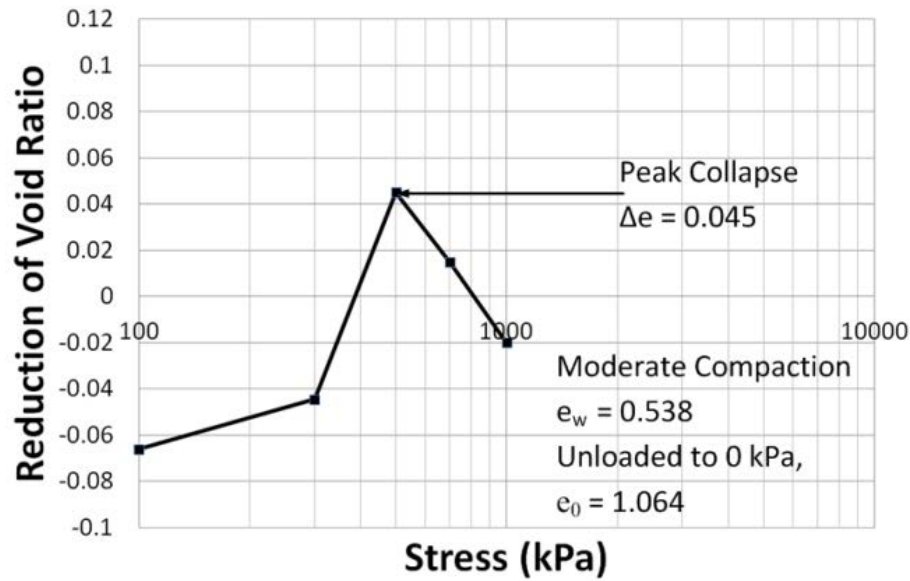
(a) Reduction of void ratio versus Operational Stress
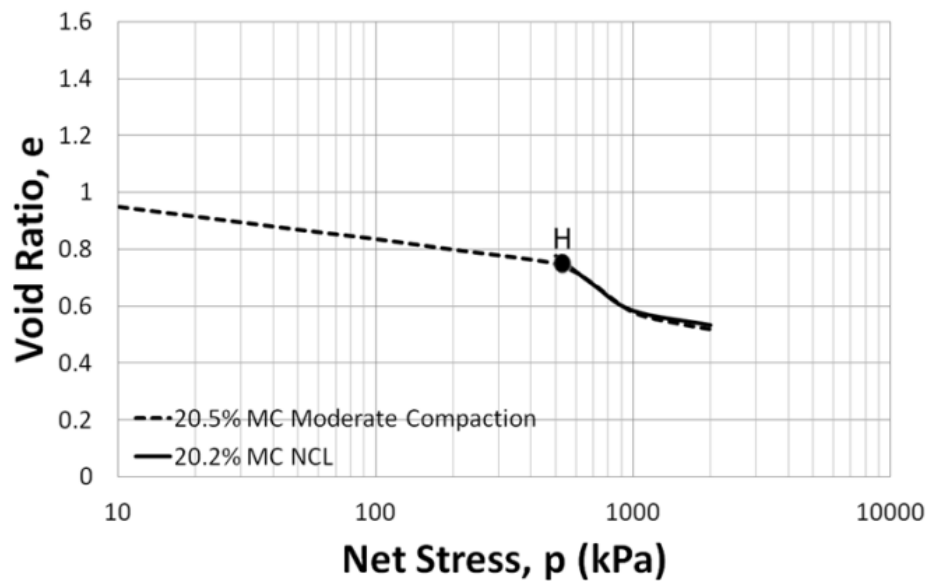
(b) Void Ratio versus Net Stress compression for Moderate compaction Merri Creek soil specimen with initial $e_{wo} = 0.538$

Figure 5-20: Collapse potential given as a reduction of void ratio with Operational Stress for Moderate compaction (pre-compaction stress ≈ 500 kPa) Merri Creek soil specimen with initial $e_{wo} = 0.538$ and unloaded to zero stress $e_o = 1.064$ [Test Identity => Combination of DC – MC – CPT – 6 to 10]
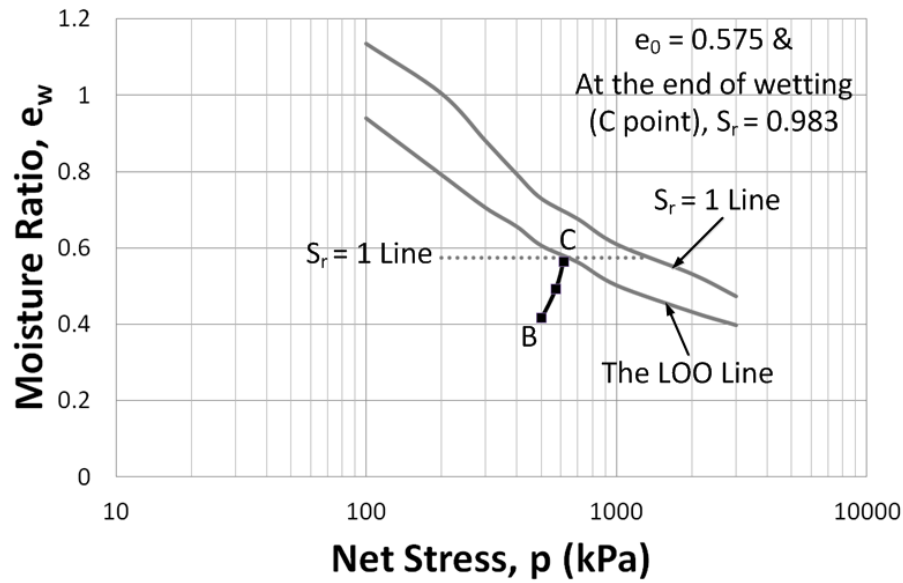
(a) High compaction 15.93% moisture content ($e_w = 0.417$) soil specimen loaded to 500 kPa and then wetted to 21.56% moisture content ($e_w = 0.565$) ($S_r = 0.983$ and $e_0 = 0.575$) at constant volume [Test Identity => DC – MC – SPT – 1]
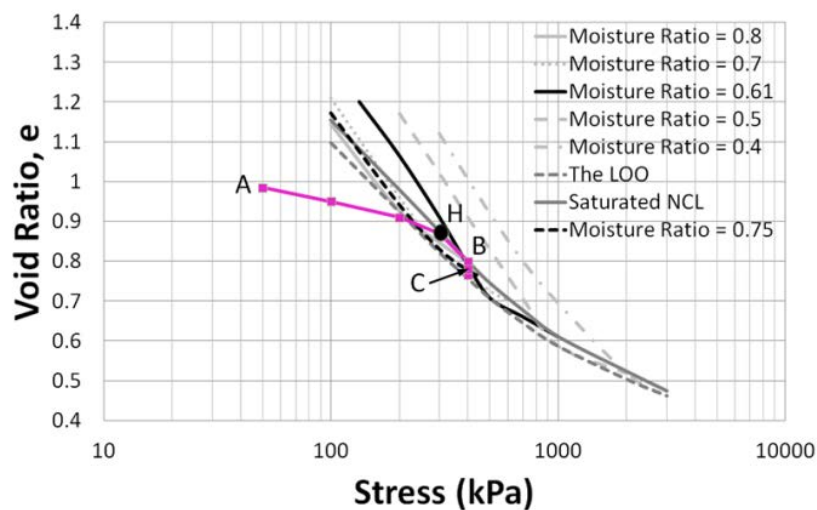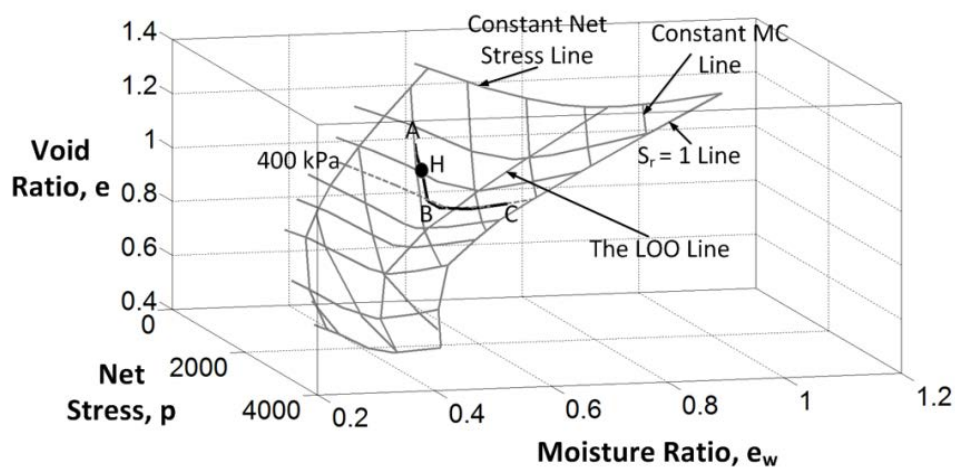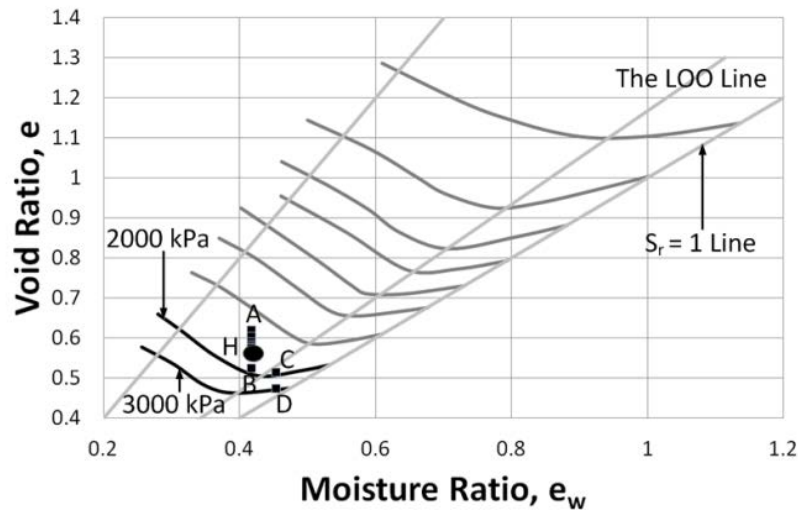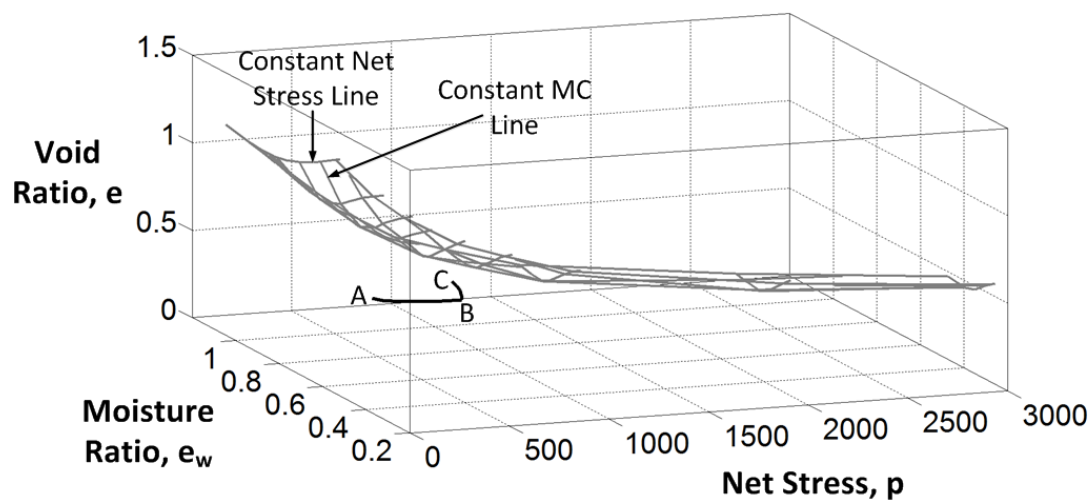

(b) 3-D view of state path test (a)
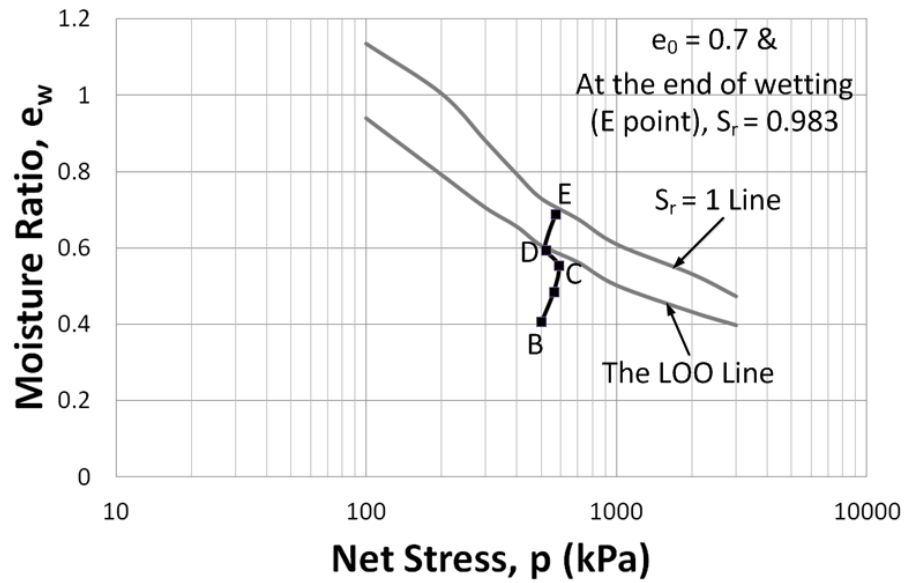
(c) Intermediate compaction 15.52% moisture content ($e_w = 0.407$) soil specimen loaded to 500 kPa and then wetted to 26.27% moisture content ($e_w = 0.688$) ($S_r = 0.983$ and $e_0 = 0.7$) at constant volume [Test Identity => DC – MC – SPT – 2]
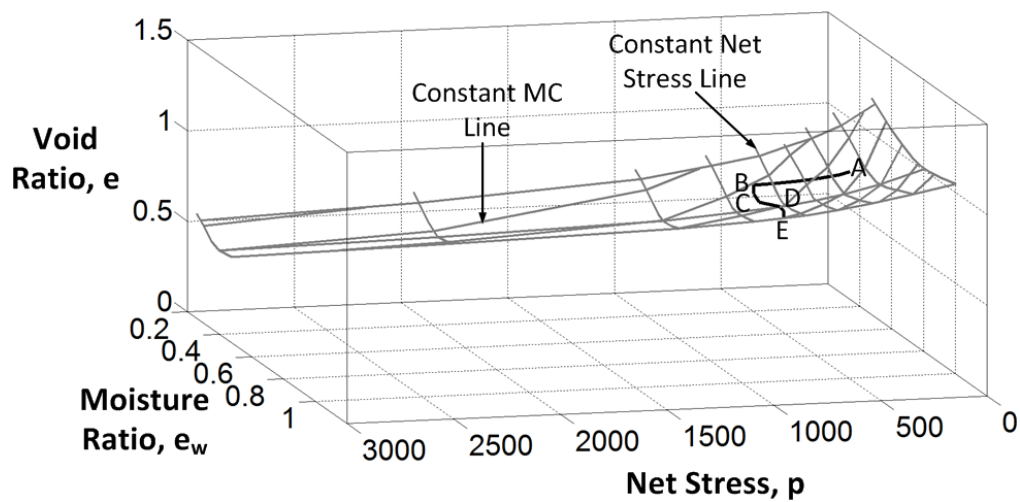
(d) 3-D view of state path test (c)
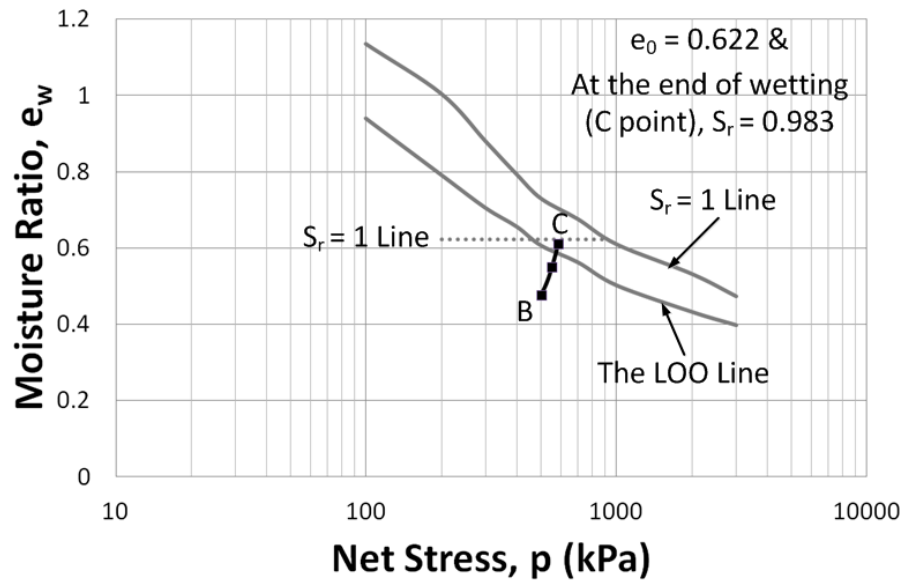
(e) Intermediate compaction 18.16% moisture content ($e_w = 0.476$) soil specimen loaded to 500 kPa and then wetted to 23.33% moisture content ($e_w = 0.611$) ($S_r = 0.983$ and $e_0 = 0.622$) at constant volume [Test Identity => DC – MC – SPT – 3]
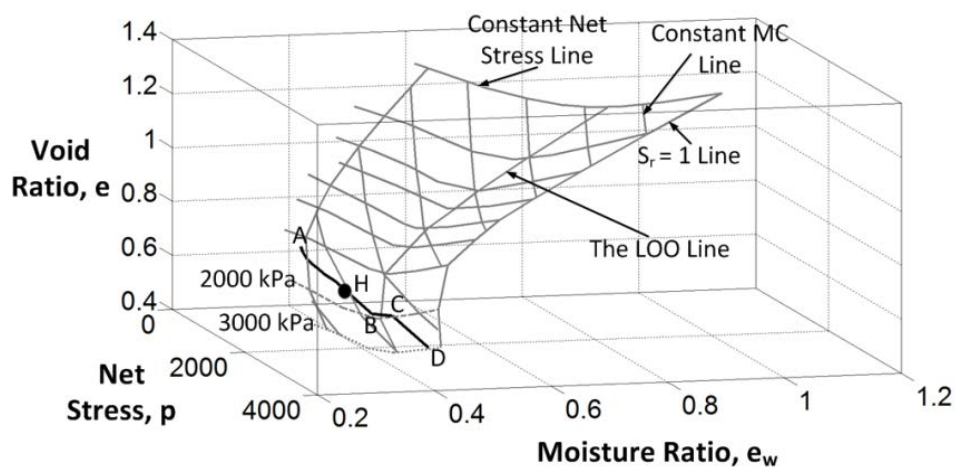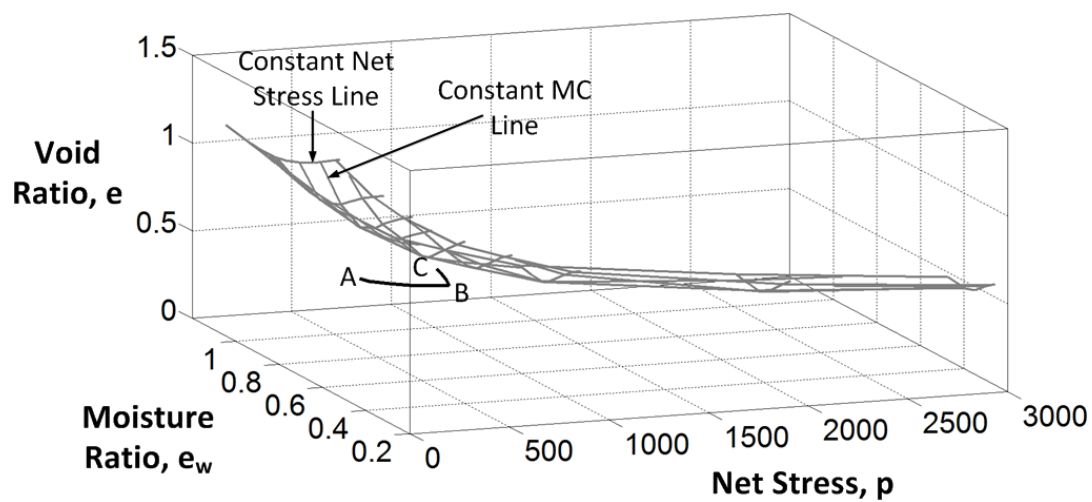

(f) 3-D view of state path test (e)
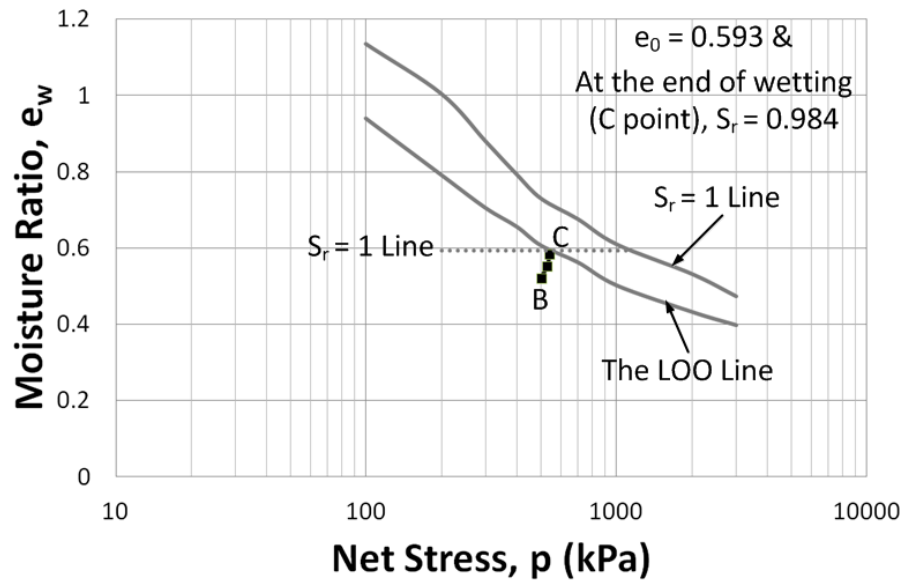
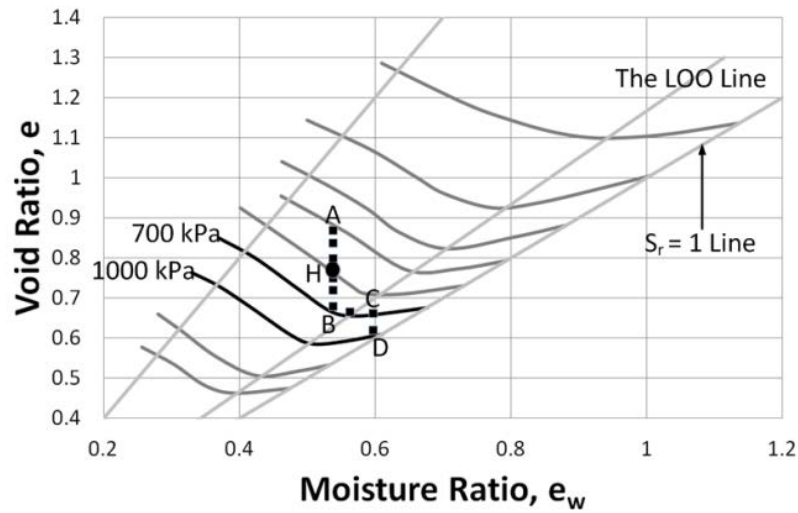**(g)** Intermediate compaction 19.89% moisture content ($e_w = 0.521$) soil specimen loaded to 500 kPa and then wetted to 22.26% moisture content ($e_w = 0.583$) ($S_r = 0.984$ and $e_0 = 0.593$) at constant volume [Test Identity => DC – MC – SPT – 4]
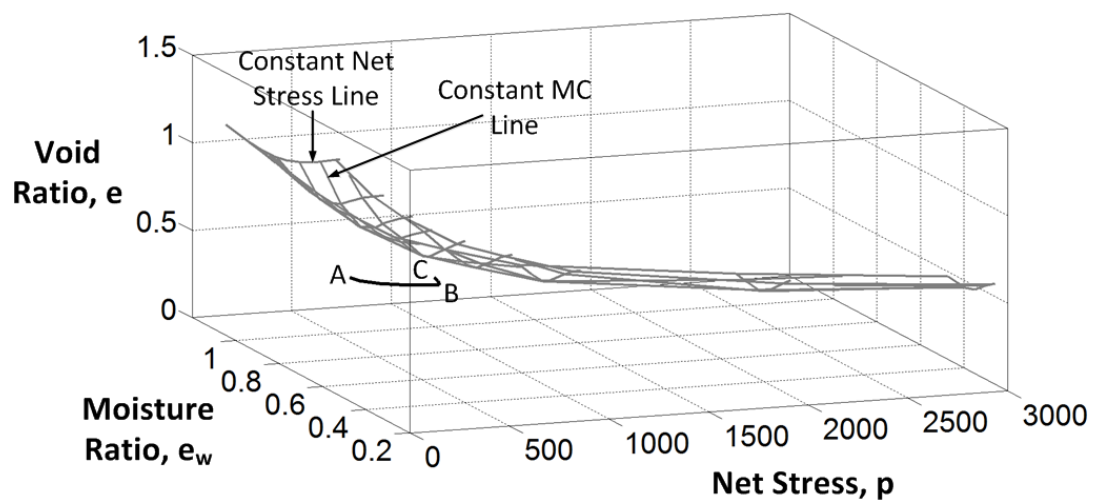
(h) 3-D view of state path test (g)
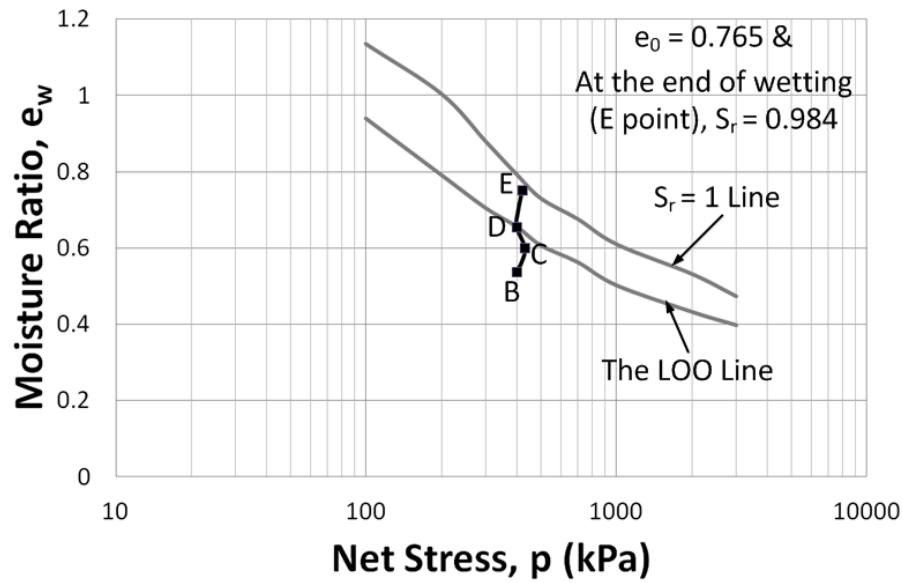
(i) Moderate compaction 20.52% moisture content ($e_w = 0.538$) soil specimen loaded to 400 kPa and then wetted to 28.73% moisture content ($e_w = 0.753$) ($S_r = 0.984$ and $e_0 = 0.765$) at constant volume [Test Identity => DC – MC – SPT – 5]

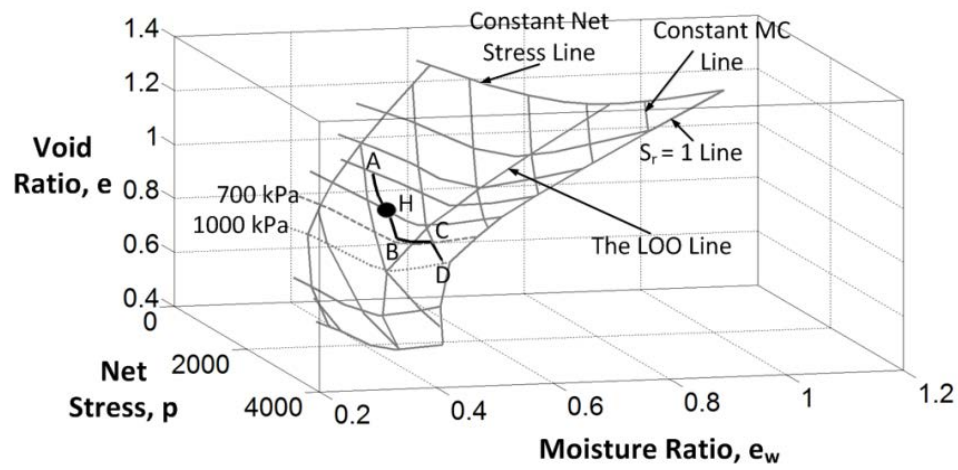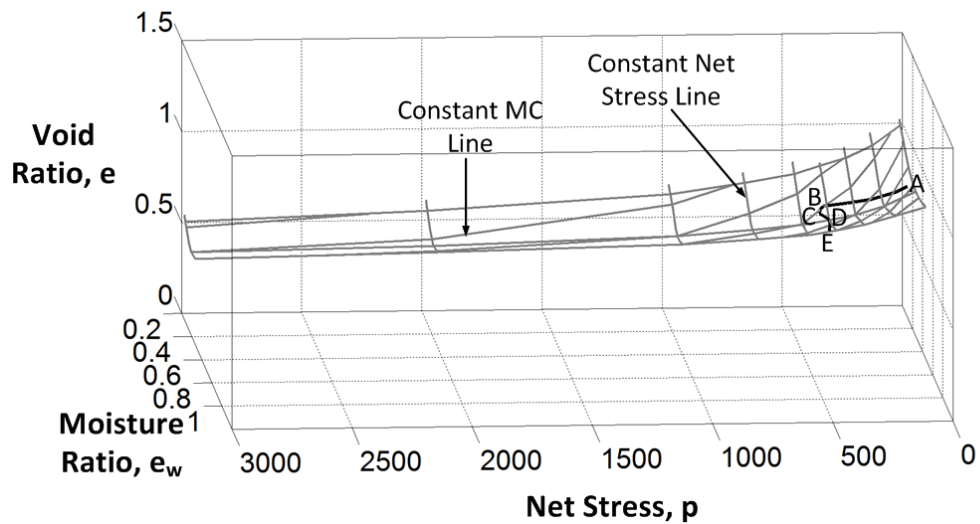**(j)** 3-D view of state path test (i)
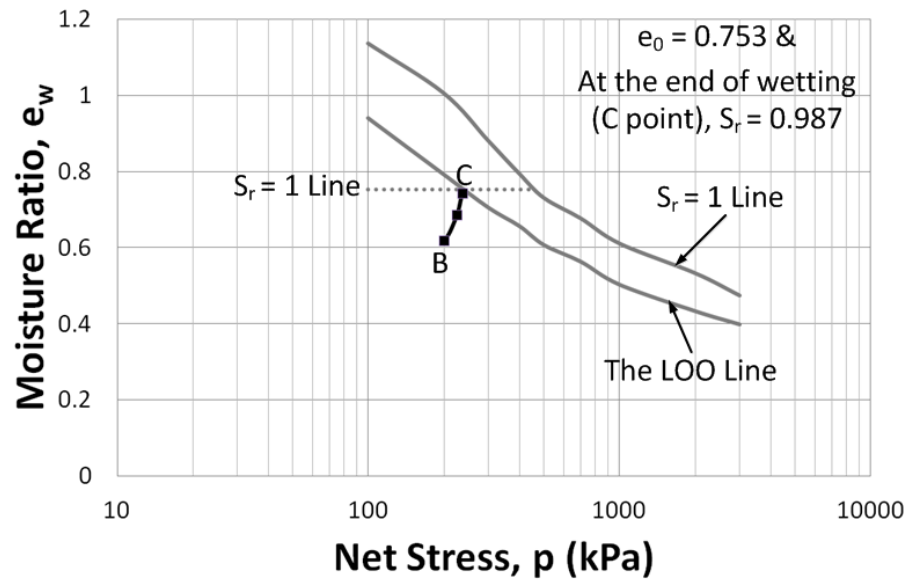
(k) Moderate compaction 23.62% moisture content ($e_w = 0.619$) soil specimen loaded to 200 kPa and then wetted to 28.33% moisture content ($e_w = 0.742$) ($S_r = 0.987$ and $e_0 = 0.7525$) at constant volume [Test Identity => DC – MC – SPT – 6]
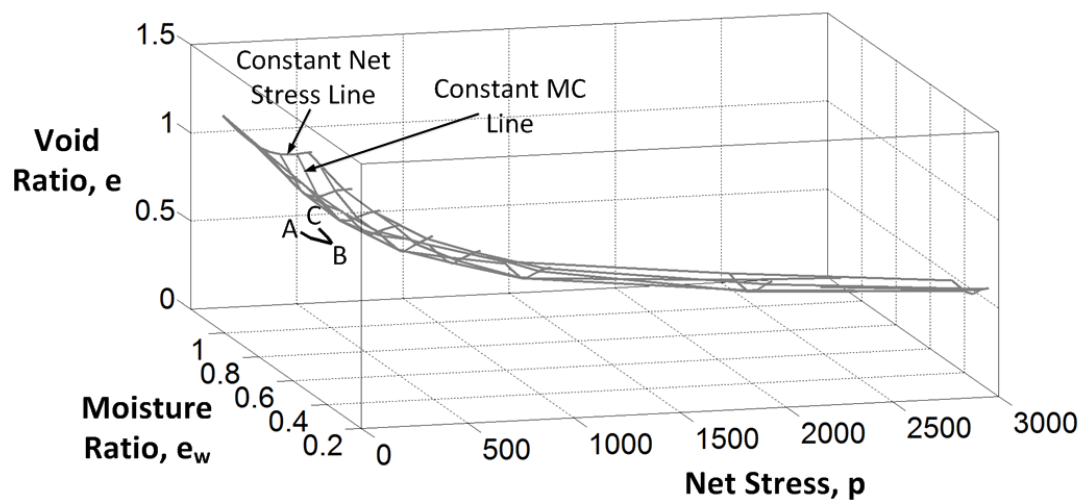
(l) 3-D view of state path test (k)
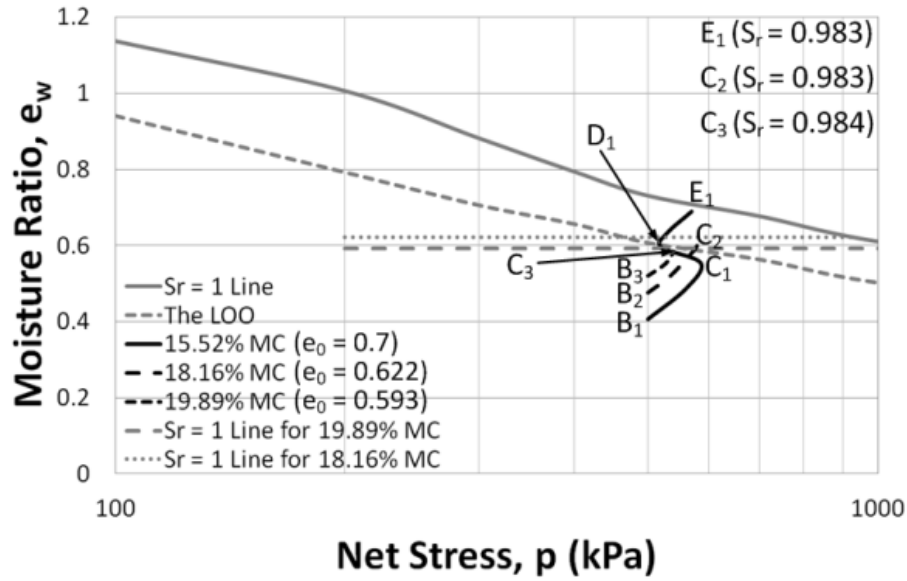
(m) Intermediate compaction 15.52% moisture content ($e_w = 0.407$), 18.16% moisture content ($e_w = 0.476$) and 19.89% moisture content ($e_w = 0.521$) soil specimens loaded to 500 kPa and then wetted to 26.27% moisture content ($e_w = 0.688$) ($S_r = 0.983$ and $e_0 = 0.7$), 23.33% moisture content ($e_w = 0.611$) ($S_r = 0.983$ and $e_0 = 0.622$) and 22.26% moisture content ($e_w = 0.583$) ($S_r = 0.984$ and $e_0 = 0.593$) respectively at constant volume [Test Identity => DC – MC – SPT – 2, 3 & 4]
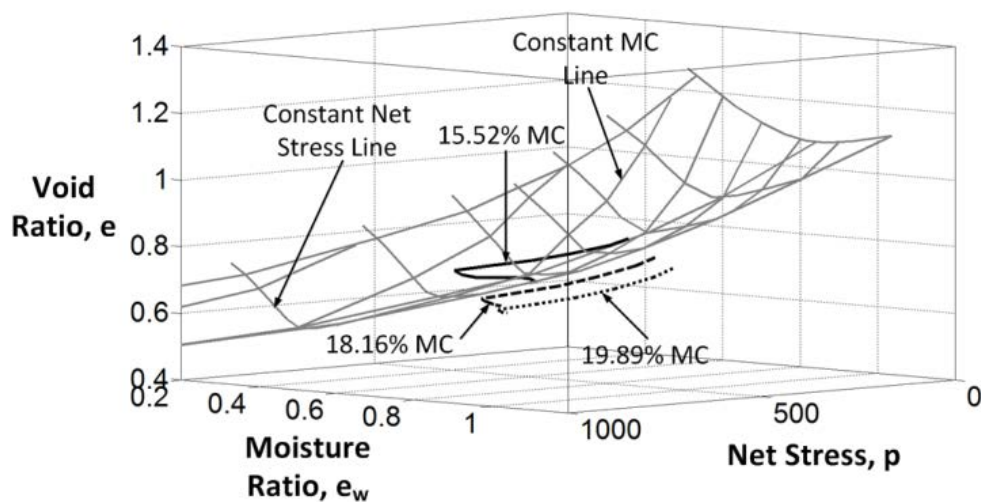
(n) 3-D view of state path test (m)
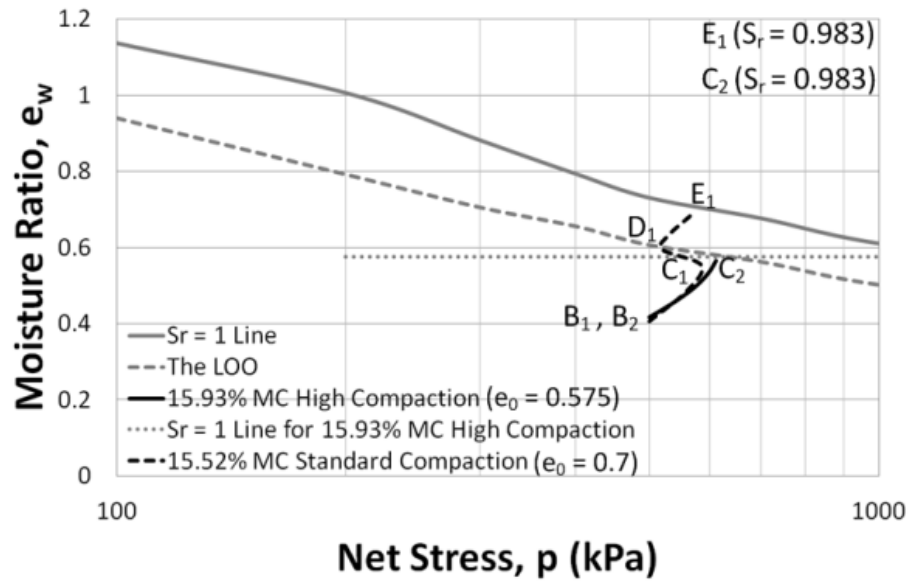
(o) High compaction 15.93% moisture content ($e_w = 0.417$) and Intermediate compaction 15.52% moisture content ($e_w = 0.407$) soil specimens loaded to 500 kPa and then wetted to 21.56% moisture content ($e_w = 0.565$) ($S_r = 0.983$ and $e_0 = 0.575$) and 26.27% moisture content ($e_w = 0.688$) ($S_r = 0.983$ and $e_0 = 0.7$) respectively at constant volume [Test Identity => DC – MC – SPT – 1 & 2]
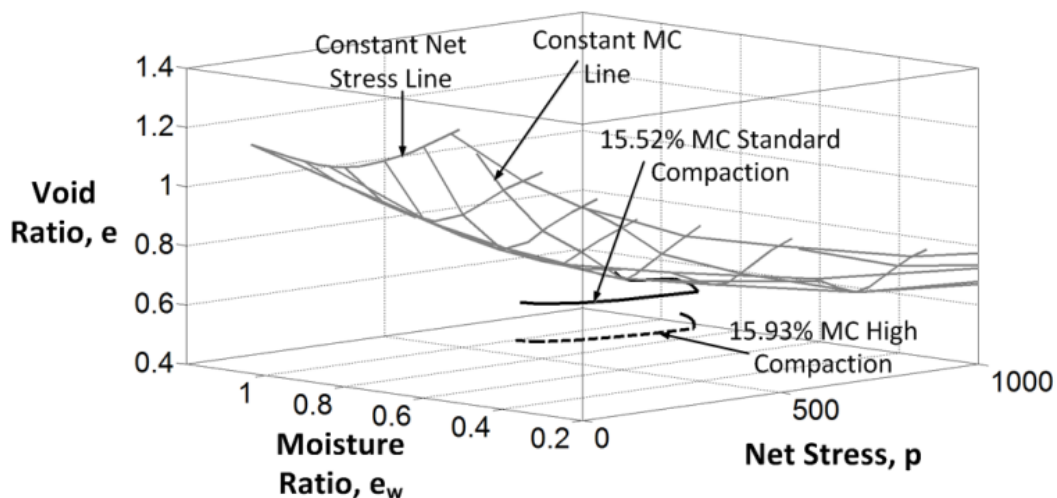
(p) 3-D view of state path test (o)

Figure 5-21: Constant volume wetting state path tests for the Merri Creek soil
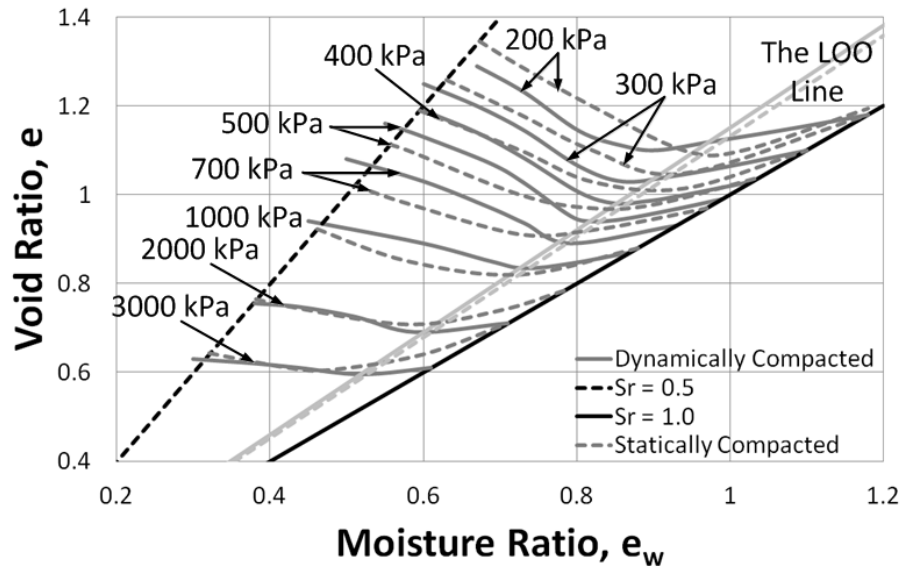
(a) The LWSBSs for the kaolin soil in $e - e_w$ plane
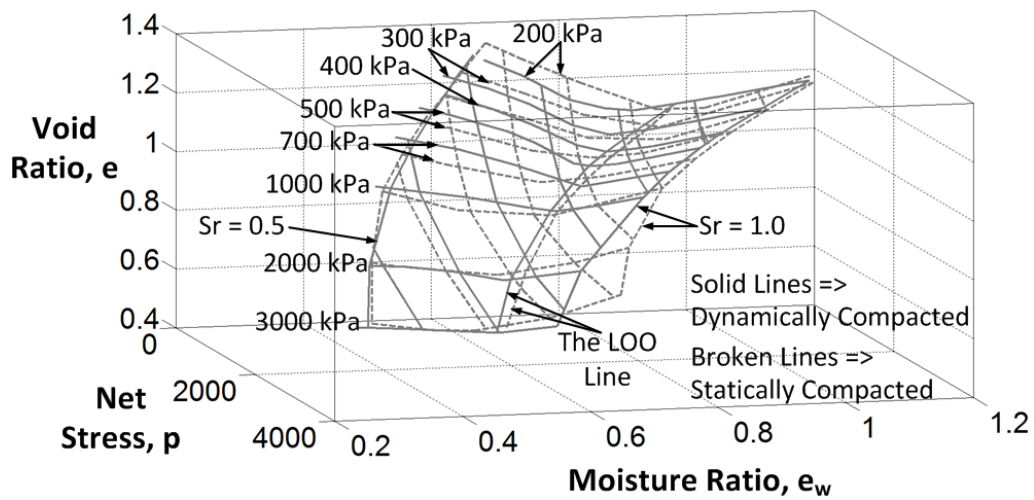
(b) The LWSBSs for the kaolin soil in $e - e_w - p$ space
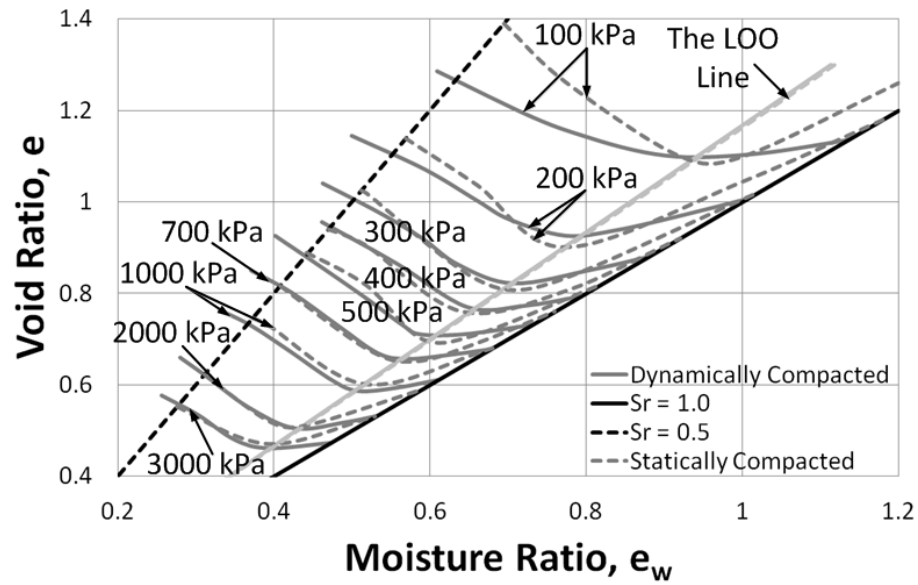
(c) The LWSBSs for the Merri Creek soil in $e - e_w$ plane
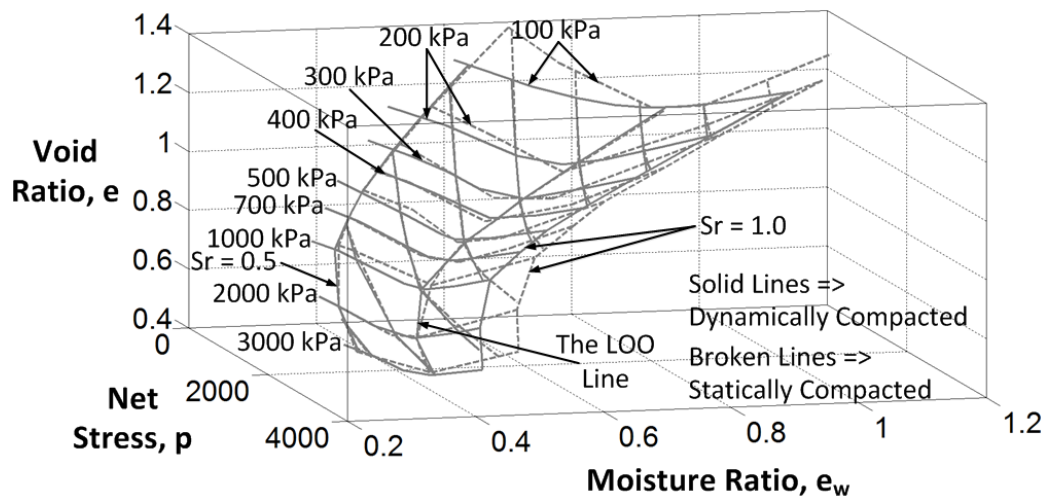
(d) The LWSBSs for the Merri Creek soil in $e - e_w - p$ space

Figure 5-22: Comparisons of the LWSBSs for the statically and dynamically compacted kaolin and Merri Creek soils
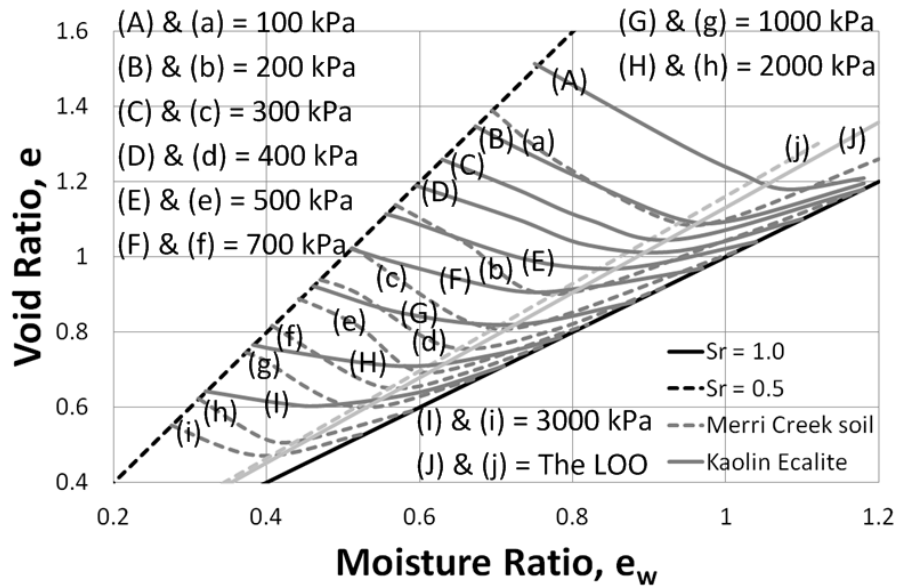
(a) The LWSBSs for the statically compacted kaolin and Merri Creek soils
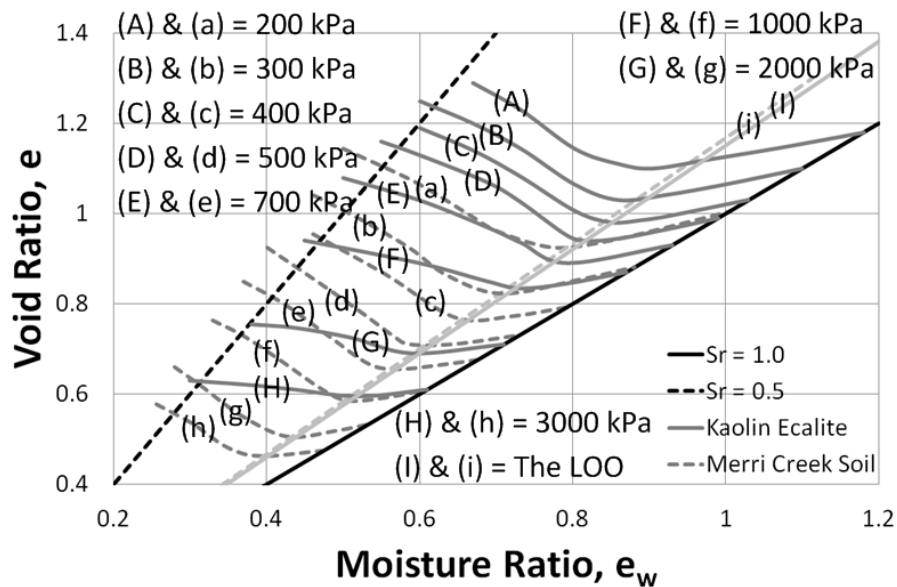
(b) The LWSBSs for the dynamically compacted kaolin and Merri Creek soils

Figure 5-23: Comparisons of the LWSBSs for the statically and dynamically compacted kaolin and Merri Creek soils
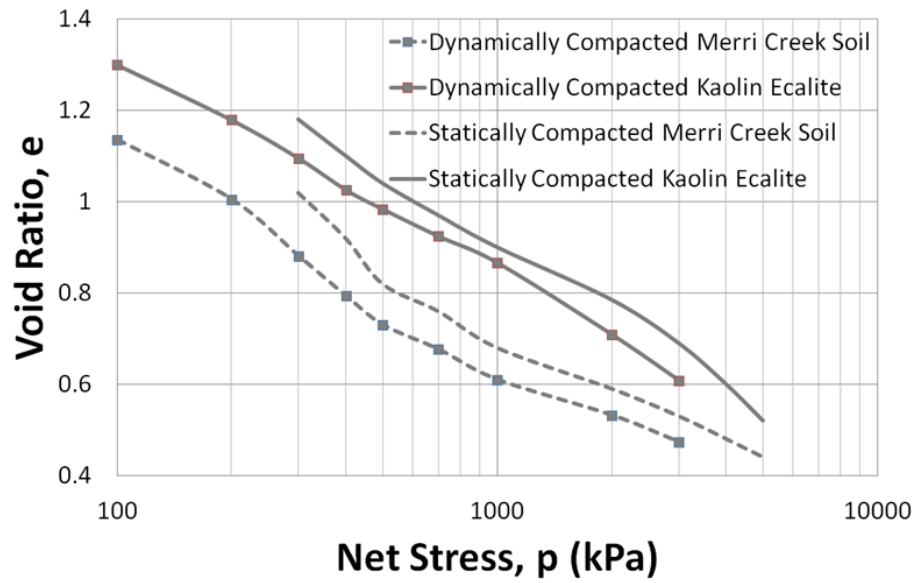
Figure 5-24: Consolidation curves (saturated *e vs log p*) of the statically and dynamically compacted kaolin and Merri Creek soils

INCORPORATION OF SUCTION WITHIN THE MPK FRAMEWORK

6.1 Introduction

This chapter deals with the incorporation of suction for wetting and loading state paths within the Monash-Peradeniya-Kodikara (MPK) framework. The MPK framework recognizes suction as a conjugate to the moisture ratio; therefore, it plays a role in compacted soil behaviour. However, as demonstrated in this thesis, many state paths as applicable to the field can be explained without suction. However, knowing the suction profile within $e - e_w - p$ space can be helpful to complete the hydro-mechanical picture in the volumetric space. Therefore, in future, research can be directed to explain the suction according to the extended framework incorporating suction within the MPK framework. The first part of this chapter presents the shape of these suction contours on and inside the Loading Wetting State Boundary Surface (LWSBS) in $e - e_w - p$ space on the basis of data from the research literature, while a mathematical representation of suction contours is presented in the later part of this chapter. Different datasets, those of Tarantino and De Col (2008), Jotisankasa (2005), Romero (1999) and Sharma (1998), are used to develop the suction profiles on and inside the LWSBS. In the mathematical representation, suction planes within $e - e_w - p$ space are divided into three segments for developmental purposes: suction contours at the wet side of the Line of Optimum (LOO) on the LWSBS, suction contours at the dry side of the LOO on the LWSBS, and suction contours inside the LWSBS. Since the air phase is discontinuous at the wet side of the optimum, during mathematical analysis, the suction contours at the wet side of the LOO on the LWSBS are developed by considering the effective stress principle. In contrast, the suction contours at the dry side of the LOO on the LWSBS are established from Soil Water Characteristics Curves (SWCCs), which are developed by considering cubic Bézier curves. Finally, the suction contours inside the LWSBS are developed using fifth order Bézier curves in void ratio versus moisture ratio graphs at the constant net stress planes.

6.2 Suction contours within $e - e_w - p$ space from the research literature

As stated earlier, the datasets of Tarantino and De Col (2008), Jotisankasa (2005), Romero (1999) and Sharma (1998) were used to examine the shape of the suction contours on and inside the LWSBS. Before starting the presentation of the suction profiles within $e - e_w - p$ space, it is important to demonstrate what actually happens to the suction during loading and unloading. When a constant moisture content soil specimen is loaded from nominal stress to a certain high stress, the value of suction decreases with the increase of net stress on the LWSBS. Subsequently, during unloading, suction increases. This can be explained by the fact that soil suction is mainly controlled by the micro voids in the soil aggregates. During loading on the LWSBS on the dry side of the LOO, macro voids between the soil particles compress permanently (or undergo plastic deformation), while micro voids in the soil aggregates predominantly compress elastically. On the wet side of the LOO, predominantly plastic deformations take place, imposing reductions in suction. As a result, overall soil suction decreases with the increase of net stress on the LWSBS. On the other hand, during unloading, as the micro voids behave elastically, they rebound like springs. Consequently, soil suction increases during unloading. At the dry side of the LOO, micro voids rebound completely. Therefore, the values of soil suction on and inside the LWSBS are equal for a certain moisture content and net stress. In contrast, at the wet side of the LOO, some of the micro voids compress plastically during loading. For this reason, during unloading, the increase of the value of suction becomes smaller than the decrease of suction during loading. This is the reason why, for a certain moisture content and net stress, the value of soil suctions on and inside the LWSBS is not equal at the wet side of the LOO. In the following section, the shapes of the suction contours on and inside the LWSBS are presented in $e - e_w - p$ space using data obtained from the research literature.

6.2.1 Suction contours on the LWSBS

Based on the previous discussion, it can be stated that during constant moisture content loading, the value of suction decreases with the increase of net stress on the LWSBS. Similar behaviour can also noticed for the suction contours on the LWSBS obtained from the research literature. Figure 6-1 and Figure 6-2 show the suction contours on the LWSBS from the data of Tarantino and De Col (2008) and Jotisankasa (2005)

respectively. It is apparent that in both cases, with the increase of net stress, the suction contours move towards the LOO with some decrease in moisture content. The data were extrapolated to cross the LOO in the case of Tarantino and De Col's (2008) data, and they move towards $(e, e_w) = (0,0)$ by creating an almost similar slope to the $S_r = 1.0$ line without bisecting each other. It is also considered that on the LOO, the soil suction increases with the increase of net stress. It should be noted that all the suction contours presented here are wetting suction contours. Between the LOO and $S_r = 1.0$ line, the suction contours travel towards $(e, e_w) = (0,0)$ by remaining very close to each other. However, they are never expected to intersect $S_r = 1.0$ line before reaching the $(e, e_w) = (0,0)$ point, which can be considered as a singular point mathematically.

6.2.2 Suction contours inside the LWSBS

As discussed earlier, when a constant moisture content soil specimen is loaded from nominal stress to a certain high stress, the suction decreases with the increase of net stress on the LWSBS. Subsequently, during unloading, soil suction increases. At the dry side of the LOO, micro voids of the soil aggregates can be expected to rebound completely during unloading. As a result, the values of soil suction on and inside the LWSBS are almost equal at a certain moisture content and net stress. Similar behaviour is found for the suction contours inside the LWSBS obtained from the research literature. Figure 6-3(a-l) show soil suction contours inside the LWSBS at constant net stress planes of 15 to 1100 kPa from Tarantino and De Col (2008). It is apparent that the suction contours at the dry side of the LOO are straight lines in the constant net stress plane, while at the wet side of the LOO, the suction contours start to curve towards the $(e, e_w) = (0,0)$ point. Figure 6-3m presents constant suction planes in 3-D inside the LWSBS in $e - e_w - p$ space using the same data. It is evident that after crossing the LOO plane, the 400 and 500 kPa constant suction planes start to curve towards the $(e, e_w) = (0,0)$ line, while other constant suction planes are straight because they had not yet crossed or come close to the LOO plane. Figure 6-3n shows a complete inferred picture of constant suction planes within $e - e_w - p$ space using the data of Tarantino and De Col (2008). After crossing the LOO, how the constant suction planes start to curve towards the $(e, e_w) = (0,0)$ line is presented in this figure. Figure 6-4 and Figure 6-5 show the suction contours inside the LWSBS at the nominal stress plane from Romero (1999) and Sharma (1998) respectively. Also shown in Figure 6-4 using dashed

lines are the inferred extrapolations of the constant suction curves. Similar to the data of Tarantino and De Col (2008), it is clear that in both cases, constant suction contours at the dry side of the LOO are approximately vertical straight lines, while at the wet side of the LOO, suction contours start to curve towards the $(e, e_w) = (0,0)$ point.

6.3 Mathematical representation of suction contours within $e - e_w - p$ space for kaolin soil

In this section, a mathematical representation of suction contours on and inside the LWSBS is presented. Suction profiles within $e - e_w - p$ space can be divided into three segments for developmental purposes: the suction contours at the wet side of the LOO on the LWSBS, the suction contours at the dry side of the LOO on the LWSBS, and the suction contours inside the LWSBS. As the air phase becomes discontinuous at the wet side of the optimum, during mathematical analysis, the suction contours at the wet side of the LOO on the LWSBS are developed by considering the effective stress principle. In contrast, there are several options available to develop the suction contours at the dry side of the LOO on the LWSBS. However, they are established from the SWCCs, which are developed completely by considering cubic Bézier curve representations at the dry side of the LOO. In addition, the suction contours inside the LWSBS are developed using a fifth order Bézier curve representation in an $e - e_w$ graph at constant net stress planes.

6.3.1 Suction contours on the LWSBS

As discussed earlier, suction contours on the LWSBS in $e - e_w - p$ space can be divided into two parts for developmental purposes: the suction contours at the wet side of the LOO on the LWSBS and the suction contours at the dry side of the LOO on the LWSBS. Mathematical representations of both are presented in the following sections.

6.3.1.1 Suction contours at the wet side of the LOO on the LWSBS

First, void ratio vs. log net stress $(e - \log p)$ graphs are plotted for different degrees of saturation (S_r) between the LOO and $S_r = 1.0$ line from the LWSBS. These lines can be fitted with straight lines. These graphs are presented in Figure 6-6. The linear equations are found to be:

For $S_r = 1.0$ line, $e = 2.3771 - 0.214\ln(p)$ ....**Equation 6-1**

And, for the LOO line, $e = 2.0742 - 0.183\ln(p)$ ....**Equation 6-2**

When different net stress values are used in Equation 6-1, the state paths move along the $S_r = 1.0$ line on the LWSBS. In Figure 6-8, all the points on $S_r = 1.0$ line, such as A, C, E and so on, are found by putting different p values in Equation 6-1. It was reported in Chapter 4 that when the soil specimens are loaded at the wet side of the LOO in drained conditions, they lose moisture to reach the $S_r = 1.0$ line. Figure 6-7 shows a qualitative representation of this phenomenon. An analysis of the data presented in Figure 4-4 indicates that for kaolin soil, the average angle with vertical is 2.5º. Once the values of e and e_w are found for the $S_r = 1.0$ line on the LWSBS using Equation 6-1, this concept is used to find the e and e_w value on the LOO line on the LWSBS. It was also presented in Chapter 4 that the gradient of normal compression line (NCL) (λ) varies linearly with moisture ratio (e_w). From Figure 4-17a the following equation is found for this linear relationship:

$\lambda = 0.42 - 0.226 e_w$ ....**Equation 6-3**

When e and e_w values are found for Point B in Figure 6-7, using Equation 6-3, the λ value is calculated for $e_{wB} (= e_{wA})$. As the value of λ does not change during loading, the same λ value is applicable all over line ABC. The effective stress principle is applicable between point C and B. Therefore, the equation can be written as:

$e_B - e_C = \lambda_{ABC}\ln(\frac{p_C}{p_B - s_B S_{r_B}})$ ....**Equation 6-4**

where, e_B and e_C are the void ratios of Point B and C; λ_{ABC} is the gradient of the NCL at $e_{wA} (= e_{wB})$ moisture ratio; p_B and p_C are the net stresses at Point B and C; S_{r_B} is the degree of saturation at Point B, here Point B is on the LOO line, so, $S_{r_B} = S_{r_{LOO}}$ and s_B is the suction at Point B. The suction and degree of saturation at Point C is zero and 1.0 respectively. In Equation 6-4, all the terms except suction at Point B are known. Therefore, Equation 6-4 can be rewritten as:

$$s_B = \frac{exp^{\left(\frac{p_C}{e_B - e_C}\right)} - p_B}{S_{r_B}}$$ ....**Equation 6-5**

Using Equation 6-5, the suction (s_B) can be calculated everywhere on the LOO on the LWSBS. Figure 6-8 shows the calculated suctions on the LOO on the LWSBS for kaolin soil. It is apparent that e_w decreases with the increase of net stress on the LOO line on the LWSBS. As a result, suction values increase with the increase of net stress.

An attempt was made to develop the suction contours between the LOO and $S_r = 1.0$ line on the LWSBS. As the equations for the AB, CD, EF and so on lines are known in Figure 6-8, it is possible to calculate the values of e and e_w for any degree of saturation on these lines. Consequently, net stress can be calculated for that void ratio using the linear relationship between e and $\ln(p)$ for that specific S_r. When these values are put in Equation 6-5, the values of suction can be found anywhere on the AB, CD, EF and so on lines. This is how all the suction values are calculated between the LOO and $S_r = 1.0$ line on the LWSBS. Suction contours are then drawn at the wet side of the LOO on the LWSBS using these results. Figure 6-9 shows the suction contours between the LOO and $S_r = 1.0$ line on the LWSBS. It is clear that the suction contours move towards $(e, e_w) = (0,0)$ without crossing each other. Figure 6-10 presents the SWCCs between the LOO and the $S_r = 1.0$ line for kaolin soil. It is apparent that the value of suction increases with the increase of net stress on the LOO. It is also evident that the slope of the SWCC near the wet side of the LOO on the LWSBS decreases with the increase of the net stress.

6.3.1.2 Suction contours at the dry side of the LOO on the LWSBS

Four possible ways were considered to develop the suction contours at the dry side of the LOO on the LWSBS. The suction contours at the dry side of the LOO can be developed mathematically from the suction contours at the wet side of the LOO on the LWSBS. This is the first option, while second option is that the suction contours at the dry side of the LOO can be developed mathematically from the nominal net stress line to the LOO on the LWSBS. On the other hand, in the third option, the suction contours at the dry side of the LOO on the LWSBS can be developed by the combination of experimental and mathematical analysis. The values of suction on the nominal stress line on the LWSBS are determined from experiments and then the suction contours at the dry side

of the LOO on the LWSBS can be developed using cubic Bézier curves. Finally, the fourth option is that the suction contours at the dry side of the LOO on the LWSBS can also be developed from the SWCC which is established completely between the LOO and dry condition by considering cubic Bézier curves. In the following section, procedures for the development of suction contours at the dry side of the LOO on the LWSBS using these four possible options are described. A mathematical representation of the suction contours at the dry side of the LOO on the LWSBS using the fourth option is also presented.

6.3.1.2.1 Option 1: Development from the suction contours at the wet side of the LOO on the LWSBS mathematically

The first option for the development of suction contours at the dry side of the LOO is through the development of the suction contours at the wet side of the LOO on the LWSBS mathematically. Figure 6-11 shows the development procedure for the suction contours using the first option. State path ABCE (A is at the nominal stress) on the LWSBS presents the constant moisture content (up to B) and drained loading (B to E) of a soil specimen from nominal stress to a certain high stress. During undrained unloading, all the points on BE line have projections on the LOO plane, depending on the unloading/reloading gradient (κ). If the value of κ is small, some of the points near the saturation line on the BE may never reach the LOO plane because they may reach the nominal net stress plane before then. In Figure 6-11a and 6-11c, two points are considered on the ABCE state path between the LOO and $S_r = 1.0$: C and E. As these two points are between the LOO and $S_r = 1.0$ on the LWSBS, all the parameters related to the effective stress principle, such as void ratio, moisture ratio, net stress, degree of saturation and suction, are known for points C and E. During unloading, say, point C reaches the LOO plane, while point B reaches the nominal net stress plane. Therefore, point C has a projection on the LOO plane, which is point D. On the other hand, point B does not have any projection on the LOO plane since the unloading path does not intersect the LOO plane. The effective stress principle is applicable between point C and D. As a result, it can be written as:

$$\kappa = \frac{e_D - e_C}{\ln\left(\frac{p_C + S_{rC}s_C}{p_D + S_{rD}s_D}\right)} \quad \text{...Equation 6-6}$$

All terms are known in Equation 6-6, except the net stress and suction at point D. The degree of saturation at point D is equal to the S_{rLOO}. As there are two unknowns in Equation 6-6, another equation is needed to solve it. During unloading from point C to D, the total void ratio change is the summation of air void change and water void change. Therefore, the equation can be written as:

$$\Delta e = \Delta e_a + \Delta e_w \dots\dots\dots\dots\dots\dots\dots\dots\dots\dots\dots\dots\dots\dots\dots\dots\dots\text{\textbf{Equation 6-7}}$$

As no moisture is added or subtracted (constant moisture unloading or undrained loading) between point C and D, $\Delta e_w = 0$. Therefore, Equation 6-7 becomes:

$$\Delta e = \Delta e_a = k_a \Delta p \dots\dots\dots\dots\dots\dots\dots\dots\dots\dots\dots\dots\dots\dots\dots\text{\textbf{Equation 6-8}}$$

where, k_a is the coefficient of air compressibility. The definition and expression of k_a can be found in the research literature. According to Fredlund and Rahardjo (1993), k_a is expressed as:

$$k_a = D_a{}^* g \dots\dots\dots\dots\dots\dots\dots\dots\dots\dots\dots\dots\dots\dots\dots\dots\dots\dots\text{\textbf{Equation 6-9}}$$

where, $D_a{}^*$ is the coefficient of transmission and is a function of the volume-mass properties of the soil and the air density. Using the above equations, net stress and suction at point D can be calculated. Figure 6-11b shows that Points D and G share same net stress, moisture ratio and suction. Therefore, once the value of suction is known at Point D, the suction value at Point G which is located at the dry side of the LOO on the LWSBS can also be known. Finally, following the same procedure, suction values can be calculated all over the dry side of the LOO on the LWSBS.

6.3.1.2.2 Option 2: Development from nominal stress line to the LOO on the LWSBS mathematically

As stated earlier, this option is opposite of the first option, which means that the suction contours at the dry side of the LOO can be developed mathematically from the nominal net stress line to the LOO on the LWSBS. Figure 6-12 presents the development procedure of the suction contours using the second option. Point A is located on the

nominal stress line on the LWSBS. All the parameters, such as void ratio, moisture ratio, net stress and degree of saturation, of point A are known except the suction. State path AB is positioned inside the LWSBS on the nominal stress plane. Point B is located on the LOO plane and all the parameters of point B are known (i.e., $p_A = p_B$, $e_{wA} = e_{wB}$ and e_B from the LWSBS) except the value of suction. From the previous explanation of the suction contours inside the LWSBS, it can be stated that the values of suction at points A and B are equal. Therefore, if the value of suction at Point B is known, the suction value of Point A which is located at the dry side of the LOO on the LWSBS is also known. State path BC, which is presented in Figure 6-12a and 6-12b, is the reloading path and point C is the point on the LWSBS where interception with the saturated NCL has taken place. The reloading state path may sometimes move to the $S_r = 1.0$ plane without intercepting the LWSBS. These reloading state paths are not useful for the calculation of the suction contours at the dry side of the LOO on the LWSBS. As points B and C are located between the LOO and $S_r = 1.0$ in Figure 6-12a and 6-12b, the effective stress principle is applicable between points B and C. Therefore, the equation can be written as:

$$\kappa = \frac{e_B - e_C}{\ln(\frac{p_C + S_{rC}s_C}{p_B + S_{rB}s_B})} \quad \text{...}\textbf{Equation 6-10}$$

In Equation 6-10, all the parameters at point C and the suction at point B are unknown. The degree of saturation at point B is equal to the S_{rLOO}. As there are five unknowns in Equation 6-10, another four equations are needed to solve for these parameters. As the moisture ratio remains unchanged between points B and C, the degree of saturation at point C can provide another equation:

$$S_{rC} = \frac{e_{wc}}{e_c} \quad \text{...}\textbf{Equation 6-11}$$

The LWSBS can provide two more equations. One is similar to the equation for the BC line in Figure 6-7 and another one is the linear relationship between $e - \ln(p)$ for different degrees of saturation between the LOO and $S_r = 1.0$. The last equation is that for the coefficient of air compressibility, which is similar to Equation 6-8. Using all of the above equations, all the parameters at point C and suction at point B can be

calculated. As noted earlier, once the value of suction is known at Point B, the suction value of Point A which is located at the dry side of the LOO on the LWSBS can also be known. Finally, following the same procedure, the suction values can be calculated all over the dry side of the LOO on the LWSBS.

6.3.1.2.3 Option 3: Development by the combination of experimental and mathematical analysis

As stated earlier, in this option, suction contours at the dry side of the LOO on the LWSBS are developed by a combination of experimental and mathematical analysis. The values of suction on the nominal stress line on the LWSBS are determined from experiments and then the suction contours at the dry side of the LOO on the LWSBS can be developed mathematically. Figure 6-13 shows the developmental procedure for the suction contours using the third option. All the suction values on the nominal stress line on the LWSBS can be known from experimental data. The high capacity tensiometer developed in the University of Newcastle (see Mendes and Buzzi, 2014) can be used for this purpose. It is clear from Figure 6-13a that the tangent of constant suction contours from the nominal stress line on the LWSBS creates a π/2 angle with the horizontal axis when the degree of saturation is zero, while on the saturation line, a π/4 angle is created by the tangent with the horizontal axis. For any other degree of saturation between these, the angle made by the tangent with the horizontal axis lies between π/2 and π/4. Figure 6-13b presents the relationship between the degree of saturation and the angle made by the constant suction contours from the nominal stress line on the LWSBS with the horizontal axis. It is assumed that the relationship follows the following equation:

$$S_r{}^2 + a^2 = 1.0 \ \dots\dots\dots\dots\dots\dots\dots\dots\dots\dots\dots\dots\dots\dots\dots\dots\text{.\textbf{Equation 6-12}}$$

For any given degree of saturation, the value of parameter "a" can be calculated by Equation 6-12. Subsequently, the angle made by the constant suction contours for that degree of saturation from the nominal stress line on the LWSBS with the horizontal axis can be found from the following equation:

$$\theta = \frac{\pi}{4} + a * \frac{\pi}{4} \ \dots\dots\dots\dots\dots\dots\dots\dots\dots\dots\dots\dots\dots\dots\text{...\textbf{Equation 6-13}}$$

Once the tangent angles with the horizontal axis are known, the suction contour at the dry side of the LOO on the LWSBS from the nominal stress line can be developed using a cubic Bézier curve, as shown in Figure 6-13c. Four points are needed to develop a cubic Bézier curve, the general form of which can be expressed by the following equation:

$$B(t) = (1-t)^3 P_0 + 3(1-t)^2 t P_1 + 3(1-t)t^2 P_2 + t^3 P_3 \; ; \; t \in [0,1] ..... \textbf{Equation 6-14}$$

where, $B(t)$ is the function using which the path of a cubic Bézier curve is traced, P_0, P_1, P_2 and P_3 are the given points which control the curve and t is a dummy variable which varies between 0 and 1. For this case, in Figure 6-13c, different values for void ratio and moisture ratio are needed to draw the curve depicted by AC. The values of void ratio and moisture ratio on the AC curve can be calculated using the following cubic Bézier curve equations:

$$e_w(t) = (1-t)^3 e_{w0} + 3(1-t)^2 t e_{w1} + 3(1-t)t^2 e_{w2} + t^3 e_{w3} \; ; \; t \in [0,1]$$
$$...............\,.....\,..\,..\textbf{Equation 6-15}$$

$$e(t) = (1-t)^3 e_0 + 3(1-t)^2 t e_1 + 3(1-t)t^2 e_2 + t^3 e_3 \; ; \; t \in [0,1] ..... \textbf{Equation 6-16}$$

where, Points A and C in Figure 6-13c are considered as zero and the third point respectively, while Point B is considered as the first and second point. This means that $e_{w0} = e_{wA}$, $e_{w1} = e_{wB}$, $e_{w2} = e_{wB}$ and $e_{w3} = e_{wC}$; $e_0 = e_A$, $e_1 = e_B$, $e_2 = e_B$ and $e_3 = e_c$. Finally, following the same procedure, all the suction contours can be developed at the dry side of the LOO on the LWSBS.

6.3.1.2.4 Option 4: Development from Soil Water Characteristics Curve (SWCC)

In this option, the suction contours at the dry side of the LOO on the LWSBS are developed from the SWCC, which is established completely between the LOO and dry condition by considering cubic Bézier curves. In this thesis, a mathematical representation of the suction contours at the dry side of the LOO on the LWSBS for both kaolin and Merri Creek soil is developed using this option. Although four options were

outlined above, only option four is used in this thesis for the mathematical representation of the suction contours, while the other three options are left for future research purposes. The parts of the SWCCs at different net stresses between the LOO and $S_r = 1.0$ have already been developed for kaolin soil in the earlier part of this chapter. Figure 6-10 shows the SWCCs at the wet side of the LOO for kaolin. During the development of the SWCCs at the dry side of the LOO on the LWSBS, these wet SWCCs are extended using cubic Bézier curves. Figure 6-14 presents the development of the SWCCs at different net stresses between the LOO and the dry condition. In the case of kaolin soil, SWCCs were not extended directly from the LOO because the gradients of the SWCCs on the LOO were not sufficiently steep to produce curves, giving realistic transition to the residual and zero water content states. After some trialling, it was determined that the SWCCs developed from the effective stress principle would be used to up to $S_r = 0.675$. If Bézier curves were used directly from the LOO, there would not be a smooth transition between the effective stress component and the Bézier component of the SWCC curve. Therefore, cubic Bézier curve equations are applied to develop the SWCCs between $S_r = 0.675$ and the fully dry condition. Figure 6-14a shows the effective stress equation extended SWCCs between the LOO and $S_r = 0.675$ for kaolin soil, while Figure 6-14b presents the development of the SWCC for 1000 kPa net stress between $S_r = 0.675$ and $S_r = 0$ using the cubic Bézier curve. As stated earlier, four points are needed to develop a cubic Bézier curve. To apply Bézier curve equations, both axes need to be in linear scale. In this case, it can be seen from Figure 6-14b that the net stress axis is in logarithmic scale. It can be converted into linear scale by the following equation:

$$p = 10^n => n = \log(p) \dots\dots\dots\dots\dots\dots\dots\dots\dots\dots\dots\dots\dots\dots\dots\dots\text{.....}\textbf{Equation 6-17}$$

where, power "n" is the linear function along the *x*-axis and once power "n" is known, net stress can also be calculated using the same equation. To draw the AC curve in Figure 6-14b, different values of moisture ratio and power "n" which can later be converted into net stress are needed. The values of moisture ratio and power "n" on the AC curve can be calculated using the following cubic Bézier curve equations:

$$n(t) = (1-t)^3 n_0 + 3(1-t)^2 t n_1 + 3(1-t)t^2 n_2 + t^3 n_3 \; ; \; t \in [0,1] \dots\textbf{Equation 6-18}$$

$$e_w(t) = (1-t)^3 e_{w0} + 3(1-t)^2 t e_{w1} + 3(1-t)t^2 e_{w2} + t^3 e_{w3} \; ; \; t \in [0,1]$$

……………..…………………………………………………...……..**Equation 6-19**

In Figure 6-14b, Point A is on the $S_r = 0.675$ line, Point B is the residual water content point and Point C is the zero moisture content and ultimate suction point (i.e., $(s, e_w) = (1,000,000 \text{ kPa}, 0)$ Point). In the cubic Bézier curve equations, Point A and Point C are considered as zero and the third point respectively, while Point B is considered as the first and second points. This means that $e_{w0} = e_{wA}$, $e_{w1} = e_{wB}$, $e_{w2} = e_{wB}$ and $e_{w3} = e_{wc}$; $n_0 = n_A$, $n_1 = n_B$, $n_2 = n_B$ and $n_3 = n_c$. Then, following the same procedure, all other SWCCs at different net stresses are developed between $S_r = 0.675$ and $S_r = 0$. Figure 6-14c shows the complete SWCCs corresponding to different net stresses for kaolin soil.

The developed SWCCs are then used to expand the constant suction contours at the dry side of the LOO on the LWSBS. Figure 6-15 shows the complete suction contours on the LWSBS for kaolin soil. It is clear that during constant moisture content loading, the value of suction decreases with the increase of net stress at constant moisture ratio on the LWSBS. This statement was made at the beginning of this chapter on the premise that the soil suction is mainly controlled by micro voids in the soil aggregates and during loading on the LWSBS, the macro voids between the soil particles compress permanently, while the micro voids of the soil aggregates compress predominantly elastically. Therefore, soil suction decreases with the increase of net stress on the LWSBS. Mathematically developed suction contours on the LWSBS for kaolin soil also capture this behaviour. This behaviour follows the pattern of behaviour inferred from the datasets of Tarantino and De Col (2008) and Jotisankasa (2005). It is also evident that on the LOO line, soil suction increases with the increase of net stress. Figure 6-15 also shows that between the LOO and $S_r = 1.0$ line, suction contours travel towards $(e, e_w) = (0,0)$ by remaining very close to each other. However, they never intersect the $S_r = 1.0$ line before reaching the $(e, e_w) = (0,0)$ point.

6.3.2 Suction contours inside the LWSBS

As discussed earlier, suction contours inside the LWSBS are developed using fifth order Bézier curves in void ratio versus moisture ratio graphs on the constant net stress planes.

Figure 6-16(a-d) present the development of the constant suction contours inside the LWSBS on the constant net stress planes, while constant suction planes inside the LWSBS in $e - e_w - p$ space are shown in Figure 6-16(e-g) for kaolin soil. The general form of a fifth order Bézier curve can be expressed by the following equation:

$$B(t) = (1-t)^5 P_0 + 5(1-t)^4 t P_1 + 10(1-t)^3 t^2 P_2 + 10(1-t)^2 t^3 P_3 +$$
$$5(1-t)t^4 P_4 + t^5 P_5 \; ; \; t \in [0,1] \dots\dots\dots\dots\dots\dots\dots\dots\dots\dots\dots\dots\dots\dots\text{Equation 6-20}$$

where, $B(t)$ is the function using which the path of a fifth order Bézier curve is traced, P_0, P_1, P_2, P_3, P_4 and P_5 are the given points which control the curve and t is a dummy variable which varies between 0 and 1. For this case, in Figure 6-16a, different values of void ratio and moisture ratio are needed to draw the AC curve. The values of void ratio and moisture ratio on the C curve can be calculated using the following fifth order Bézier curve equations:

$$e_w(t) = (1-t)^5 e_{w0} + 5(1-t)^4 t e_{w1} + 10(1-t)^3 t^2 e_{w2} + 10(1-t)^2 t^3 e_{w3} +$$
$$5(1-t)t^4 e_{w4} + t^5 e_{w5} \; ; \; t \in [0,1] \dots\dots\dots\dots\dots\dots\dots\dots\dots\dots\dots\dots\text{Equation 6-21}$$

$$e(t) = (1-t)^5 e_0 + 5(1-t)^4 t e_1 + 10(1-t)^3 t^2 e_2 + 10(1-t)^2 t^3 e_3 +$$
$$5(1-t)t^4 e_4 + t^5 e_5 \; ; \; t \in [0,1] \dots\dots\dots\dots\dots\dots\dots\dots\dots\dots\dots\dots\dots\text{Equation 6-22}$$

Six points are needed to develop a fifth order Bézier curve. Points A and C in Figure 6-16a are considered as zero and the fifth point respectively, while Point B is repeated as the first, second, third and fourth points. This means that $e_{w0} = e_{wA}$, $e_{w1} = e_{wB}$, $e_{w2} = e_{wB}$, $e_{w3} = e_{wB}$, $e_{w4} = e_{wB}$ and $e_{w5} = e_{wC}$; $e_0 = e_A$, $e_1 = e_B$, $e_2 = e_B$, $e_3 = e_B$, $e_4 = e_B$ and $e_5 = e_C$. As Point A is on the LWSBS, the value of suction at Point A is known from the suction contours on the LWSBS, while Point B is on the $S_r = 1.0$ line with the same moisture ratio as Point A. The repetition of point B is carried out to make a sharp curvature of the curve AC. Then, following the same procedure, all the suction contours can be developed inside the LWSBS on all net stress planes.

Figure 6-16b, 6-16c and 6-16d present the constant suction contours inside the LWSBS on the nominal, 100 kPa and 1000 kPa net stress planes respectively. If Figure 6-16b, 6-16c and 6-16d are compared it can be seen that as the initial point A comes from the suction contours on the LWSBS, for the same suction value, the void ratio and moisture ratio decrease from nominal to 1000 kPa net stress on the LWSBS. This occurs due to the decrease of moisture ratio on the constant suction contours on the LWSBS. It is also clear from Figure 6-16b, 6-16c and 6-16d that inside the LWSBS on a constant net stress plane, the constant suction contours are straight down at the dry side of the LOO, while at the wet side of the LOO, the suction contours curve towards the left to move to the $(e, e_w) = (0,0)$ point. This behaviour follows the pattern of behaviour identified at the beginning of this chapter on the basis of behaviour inferred from the experimental evidence. Figure 6-16e, 6-16f and 6-16g show 892 kPa, 5000 kPa and 30000 kPa constant suction planes inside the LWSBS in the $e - e_w - p$ space, respectively. These figures show the complete picture of the constant suction planes in 3-D on and inside the LWSBS within the $e - e_w - p$ space.

6.4 Mathematical representation of suction contours within $e - e_w - p$ space for Merri Creek soil

Similar to kaolin soil, the developmental process of the suction contours on and inside the LWSBS in $e - e_w - p$ space for Merri Creek soil can also be divided into three steps: suction contours at the wet side of the LOO on the LWSBS, suction contours at the dry side of the LOO on the LWSBS, and suction contours inside the LWSBS. The theoretical basis and the method of development are same as for kaolin soil.

6.4.1 Suction contours on the LWSBS

As discussed earlier, suction contours on the LWSBS in the $e - e_w - p$ space can be divided into two parts for developmental purposes: suction contours at the wet side of the LOO on the LWSBS, and suction contours at the dry side of the LOO on the LWSBS. Mathematical representations of both are presented in the following sections.

6.4.1.1 Suction contours at the wet side of the LOO on the LWSBS

Similarly to kaolin soil, void ratio vs log net stress ($e - \log p$) graphs were plotted for different degrees of saturation (S_r) between the LOO and $S_r = 1.0$ line, and these lines can be represented by semi logarithmic lines. These graphs are presented in Figure 6-17. The linear equations were found to be:

For $S_r = 1.0$ line, $e = 2.1834 - 0.209\ln(p)$ ....**Equation 6-23**

For the LOO line, $e = 1.7633 - 0.164\ln(p)$ ....**Equation 6-24**

Following the same approach as that used for kaolin soil, different values of net stress are used in Equation 6-23 to move the state paths along $S_r = 1.0$ line on the LWSBS. Figure 6-18 shows the movement of the state paths along the $S_r = 1.0$ line on the LWSBS. All the points on $S_r = 1.0$ line, such as A, C, E and so on, are found by using different p values in Equation 6-23. It was presented in Chapter 4 that during constant moisture content loading, the state paths create an angle with verticals rather than being constant at the wet side of the LOO. By analysing the data presented in Figure 4-9, it was found that for Merri Creek soil, the average angle with vertical is about 4.0°. When the values of e and e_w are found for different net stresses along $S_r = 1.0$ line on the LWSBS, this concept can be used to find the e and e_w values on the LOO line on the LWSBS. It was also stated in Chapter 4 that the gradient of the NCL (λ) varies linearly with moisture ratio (e_w). From Figure 4-28a the following equation is found for this linear relationship:

$\lambda = 0.202025 - 0.4677e_w$ ....**Equation 6-25**

When e and e_w values are found on the LOO line on the LWSBS, λ values are calculated for different moisture ratios using Equation 6-25. In Figure 6-18, the λ value remains constant on any specific line, such as AB, CD, EF and so on. The effective stress principle is applicable between the LOO and $S_r = 1.0$ line. Therefore, Equation 6-5 can be used to calculate the suction values on the LOO on the LWSBS. The net stress at B (p_B) parameter in Equation 6-5 is calculated using Equation 6-24. Figure 6-18 presents these calculated suctions on the LOO line on the LWSBS for Merri Creek soil. It is clear

that e_w decreases with the increase of net stress on the LOO on the LWSBS. As a result, suction values increase with the increase of net stress.

An attempt was made to develop the suction contours between the LOO and $S_r = 1.0$ line on the LWSBS. As the equations for lines AB, CD, EF and so on are known in Figure 6-18, it is possible to calculate the values of e and e_w for any degree of saturation on these lines. Consequently, the value of net stress can be calculated for that void ratio using the linear relationship between e and $\ln p$ for that specific S_r. Then, these values can be substituted in Equation 6-5 to determine the corresponding suction values anywhere on lines AB, CD, EF and so on. In this manner, all the suction values are calculated between the LOO and $S_r = 1.0$ line on the LWSBS. Subsequently, suction contours are drawn at the wet side of the LOO on the LWSBS using these results. Figure 6-19 shows the suction contours between the LOO and $S_r = 1.0$ line on the LWSBS for Merri Creek soil. It is apparent that the suction contours move towards $(e, e_w) = (0,0)$ without crossing each other. Figure 6-20 presents the SWCCs between the LOO and the $S_r = 1.0$ line for Merri Creek soil. It is clear that the value of suction increases with the increase of net stress on the LOO line. It is also evident that the slope of the SWCC near the wet side of the LOO on the LWSBS decreases with the increase of net stress.

6.4.1.2 Suction contours at the dry side of the LOO on the LWSBS

Similarly to the kaolin soil, the suction contours of the Merri Creek soil at the dry side of the LOO on the LWSBS were also developed from the SWCC, which is established completely between the LOO and dry condition by considering cubic Bézier curves. The SWCCs at different net stresses between the LOO and $S_r = 1.0$ were already developed for the Merri Creek soil in the previous section. Figure 6-20 shows the SWCCs at the wet side of the LOO for the Merri Creek soil. During the development of the SWCCs at the dry side of the LOO on the LWSBS, these wet SWCCs are extended using cubic Bézier curves. Figure 6-21 presents the development of the SWCCs at different net stresses between the LOO and the dry condition. Unlike for the kaolin soil, SWCCs were directly extended from the LOO to the fully dry condition for the Merri Creek soil. Figure 6-21a shows the development of the SWCC for 1000 kPa net stress between the LOO and $S_r = 0$ using a cubic Bézier curve. As stated earlier, four points are needed to develop a

cubic Bézier curve. Similar to the kaolin soil, the x axis was transformed to linear scale taking $n = \log(p)$. To draw the curve AC in Figure 6-21a, different values of moisture ratio and power "n" are needed. The values of moisture ratio and power "n" on AC curve are calculated using Equation 6-19 and Equation 6-18 respectively. In both equations, Point A, which is on the LOO and Point C, which is the zero moisture content and the ultimate suction point (i.e., $(s, e_w) = (1{,}000{,}000$ kPa, 0) Point) in Figure 6-21a are considered as zero and the third point respectively, while Point B, which is the residual water content point, is considered as the first and second points. Then, following the same procedure, all other SWCCs at different net stresses are developed between the LOO and $S_r = 0$. Figure 6-21b shows the complete SWCCs for the Merri Creek soil corresponding to different net stresses.

The developed SWCCs are then used to expand the constant suction contours at the dry side of the LOO on the LWSBS. Figure 6-22 shows the complete suction contours on the LWSBS for the Merri Creek soil. The pattern of the behaviour depicted by these theoretical curves follows the observed behaviour, as discussed earlier.

6.4.2 Suction contours inside the LWSBS

Similarly to the kaolin soil, the suction contours of the Merri Creek soil inside the LWSBS were developed using fifth order Bézier curves in void ratio versus moisture ratio graphs on the constant net stress planes. Figure 6-23(a-d) present the development of the constant suction contours inside the LWSBS on the constant net stress planes, while the constant suction planes inside the LWSBS in $e - e_w - p$ space are shown in Figure 6-23(e-g) for the Merri Creek soil. In Figure 6-23a, different values of void ratio and moisture ratio are needed to draw the AC curve. The values of void ratio and moisture ratio on the AC curve are calculated using Equation 6-22 and Equation 6-21 respectively. As stated earlier, six points are needed to develop a fifth order Bézier curve. Points A and C in Figure 6-23a are considered as the zero and fifth point respectively, while Point B is repeated as the first, second, third and fourth points. As Point A is on the LWSBS, the value of suction at Point A can be known from the suction contours on the LWSBS, while Point B is on the $S_r = 1.0$ line with the same moisture ratio as Point A. Then, following the same procedure as for the kaolin soil, all the suction contours can be developed inside the LWSBS on all the net stress planes.

Figure 6-23b, 6-23c and 6-23d present the constant suction contours inside the LWSBS at the nominal, 100 kPa and 1000 kPa net stress planes respectively. It is clear that inside the LWSBS at a constant net stress plane, the constant suction contours are straight down at the dry side of the LOO, while at the wet side of the LOO, the suction contours start to curve towards the left to move to the $(e, e_w) = (0,0)$ point. This behaviour is consistent with the explanation provided at the beginning of this chapter regarding the rebound property of the micro voids during unloading at the dry side of the LOO inside the LWSBS. Similar behaviour is also found for the constant suction contours inside the LWSBS developed from the datasets of Tarantino and De Col (2008), Romero (1999) and Sharma (1998). Figure 6-23e, 6-23f and 6-23g show 897 kPa, 3000 kPa and 10000 kPa constant suction planes inside the LWSBS in the $e - e_w - p$ space respectively. These figures show the complete picture of the constant suction planes on and inside the LWSBS within the $e - e_w - p$ space.

6.5 Summary of the development of a constant suction plane within $e - e_w - p$ space

The steps involved in the development of a constant suction plane within $e - e_w - p$ space are summarized below:

Step 1: Development of the constant suction contours at the wet side of the LOO on the LWSBS: First, different net stress values can be substituted in the linear $e - \ln(p)$ equation (e.g., Equation 6-1 for the kaolin soil and Equation 6-23 for the Merri Creek soil) to move the state path along $S_r = 1.0$ line on the LWSBS. Figure 6-24a shows the development of the constant suction contours at the wet side of the LOO on the LWSBS. Path AB represents this movement along $S_r = 1.0$ line on the LWSBS. Then, path BC is found from the virgin/normal compression of the soil specimen. Path BC usually makes a small angle with the constant moisture ratio line (e.g., this angle is 2.5° for the kaolin soil and 4° for the Merri Creek soil). When point C is found on the LOO on the LWSBS, λ value which is constant on the line BCD can be calculated from the relationship between λ and e_w for any particular soil (e.g., Equation 6-3 for the kaolin soil and Equation 6-25 for the Merri Creek soil). As the equations for the line BC is known, it is possible to calculate the value of e and e_w for any degree of saturation on this line. Subsequently, net stress can be calculated for that void ratio using the linear relationship

between e and $\ln(p)$ for that specific S_r. As the effective stress principle is applicable at the wet side of the LOO, an equation like Equation 6-5 is used to determine the values of suction on the line BC. Similarly, suction values can be calculated on the other lines parallel to the line BC. After that, suction contours are developed between the LOO and $S_r = 1.0$ line on the LWSBS using the calculated suction values (e.g., EF in Figure 6-24a).

Step 2: Development of the constant suction contours at the dry side of the LOO on the LWSBS: After developing the suction contour at the wet side of the LOO on the LWSBS, the SWCC for a certain net stress can be plotted from the developed suction contours (see Figure 6-10 for the kaolin soil and Figure 6-20 for the Merri Creek soil). Subsequently, the SWCC is needed to expand in the dry side of the LOO by cubic Bézier curves using the similar equations as Equation 6-18 and Equation 6-19. Figure 6-24b and 6-24c present the development of the constant suction contour at the dry side of the LOO on the LWSBS. While four points are needed to develop a cubic Bézier curve, it is apparent that the coordinate on the LOO is used as zeroth point, the residual water content is used as first and second points and the suction at 1,000,000 kPa with zero moisture ratio is used as third point. This procedure may be modified if more experimental data are available. For example, the SWCCs of the kaolin soil cannot be extended from the LOO as the gradients of the SWCCs on the LOO were not sufficiently steep to produce curves, giving realistic transition to the residual and zero water content states (see Figure 6-14). In that case, it is needed to determine the closest smaller degree of saturation to the LOO where smooth transition between the effective stress component and the Bézier component can be performed (e.g., for the kaolin soil this $S_r = 0.675$). After that, the suction contours are developed at the dry side of the LOO on the LWSBS using the extended SWCCs (e.g., FG in Figure 6-24c).

Step 3: Development of the constant suction contours inside the LWSBS: Once the suction contour on the LWSBS is found, constant suction plane can be developed by expanding the contour by fifth order Bézier curve inside the LWSBS at different constant net stress $e - e_w$ planes using the similar equations as Equation 6-21 and Equation 6-22. Figure 6-24d and 6-24e show the development of the constant suction contours inside the LWSBS. Here in the case of kaolin and Merri Creek soil, the fifth order Bézier curves

were used to satisfy the hypothesis obtained from the research literature. However, in reality it is possible for suction contours to curve prior to reaching the LOO. In that case, lower order (such as the fourth order, cubic or quadratic) Bézier curves may be used, as the experimental data dictate. While six points are needed to develop a fifth order Bézier curve, it is evident from Figure 6-24d that the coordinate on the LWSBS (e.g., point G in Figure 6-24e) is used as zeroth point, the point with similar moisture ratio on the saturation line used as first, second, third and fourth points and zero moisture content and ultimate suction point (i.e., $(s, e_w) = (1,000,000$ kPa, 0) Point) is used as fifth point. Figure 6-24e presents the developed constant suction contour inside the LWSBS (suction contour GH) from point G on the LWSBS at the nominal stress plane. Similarly, the parallel suction contours can be developed inside the LWSBS from different points on EFG line on the LWSBS. All of these lines together will form a constant suction plane (e.g., plane EGHI in Figure 6-24f).

6.6 Discussion

Full theoretical profiles of the soil suction during wetting and loading within the $e - e_w - p$ space for kaolin and Merri Creek soil have been presented mathematically in this chapter. Two hypotheses were developed by analysing the datasets of Tarantino and De Col (2008), Jotisankasa (2005), Romero (1999) and Sharma (1998). The theoretical shapes of the constant suction contours on and inside the LWSBS in the $e - e_w - p$ space have been identified from this analysis. It was also found that the identified profile of the soil suction is valid from a soil mechanics point of view. Mathematical representation of the suction contours was also performed on the basis of the identified shape of the suction profile.

For the mathematical representation, suction planes within $e - e_w - p$ space are divided into three parts. Different parts are developed differently and then attached together to obtain the full suction profile. Suction contours at the wet side of the LOO on the LWSBS are established by considering the effective stress principle between the optimum and the saturated plane. As the equations of the LWSBS between the LOO and $S_r = 1.0$ are known, it is possible to find the value of suction anywhere at the wet side of the LOO on the LWSBS. Subsequently, the suction contours at the dry side of the LOO on the LWSBS were developed considering cubic Bézier curves in the SWCC between

the LOO and the dry condition. It was found that for kaolin soil, the SWCCs are not ready on the LOO for the application of cubic Bézier curve equations. Nevertheless, it was found to be appropriate for the Merri Creek soil to apply cubic Bézier curve equations from the LOO to establish the SWCCs at the dry side of the LOO. The other three options for the development of suction contours at the dry side of the LOO on the LWSBS are left for future research. One of the options, the development of the suction contours at the dry side of the LOO on the LWSBS by the combination of experimental and mathematical analysis, can be used to validate the other options in future. According to the research literature, at the dry side of the LOO, the values of soil suction on and inside the LWSBS are equal for a certain moisture content and net stress. In order to satisfy this, it was necessary to employ fifth order Bézier curves to approximate the suction contours inside the LWSBS at the constant net stress planes. However, in reality it is possible for suction contours to curve prior to reaching the LOO. In this case, lower order (such as the fourth order, cubic or quadratic) Bézier curves may be used, as the experimental data dictate.

As the MPK framework is not dependant on the suction parameter, any volumetric behaviour related to the loading or/and wetting of the compacted or virgin unsaturated soil can be explained by the LWSBS in the $e - e_w - p$ space for any type of soil, irrespective of the degree of reactivity. However, knowing the suction profile within $e - e_w - p$ space can be helpful to complete the hydro-mechanical picture in the volumetric space. Therefore, in future, research can be directed to explain the suction according to the extended framework incorporating suction within the MPK framework.

6.7 Conclusion

The aim of this chapter was to develop a full profile of soil suction for wetting and loading within the $e - e_w - p$ space. First, data from the research literature were analysed and two hypotheses were proposed to present the suction contours on and inside the LWSBS. The explanation of the shape of the suction contours was provided from a soil mechanics point of view. Finally, a mathematical representation was provided to establish full suction profiles within $e - e_w - p$ space for kaolin and Merri Creek soils. During the mathematical representation, the suction profile within $e - e_w - p$ space has been divided into three segments. Suction contours at the wet side of the LOO on the

LWSBS were developed by considering the effective stress principle between the optimum and saturated plane, while several options were proposed to develop the suction contours at the dry side of the LOO on the LWSBS. However, they were established from the SWCCs which were developed completely by considering cubic Bézier curves between the LOO and the fully dry condition. Finally suction contours inside the LWSBS on the constant net stress planes were developed using fifth order Bézier curves in void ratio versus moisture ratio planes. These mathematical representations within and on the LWSBS generate the entire space of suction within the LWSBS under wetting and loading state paths. Further research is needed to examine these developments through direct measurement of suction, possibly by the high capacity tensiometers, such as those developed recently at the University of Newcastle (see Mendes and Buzzi, 2014), for compacted clay soils.
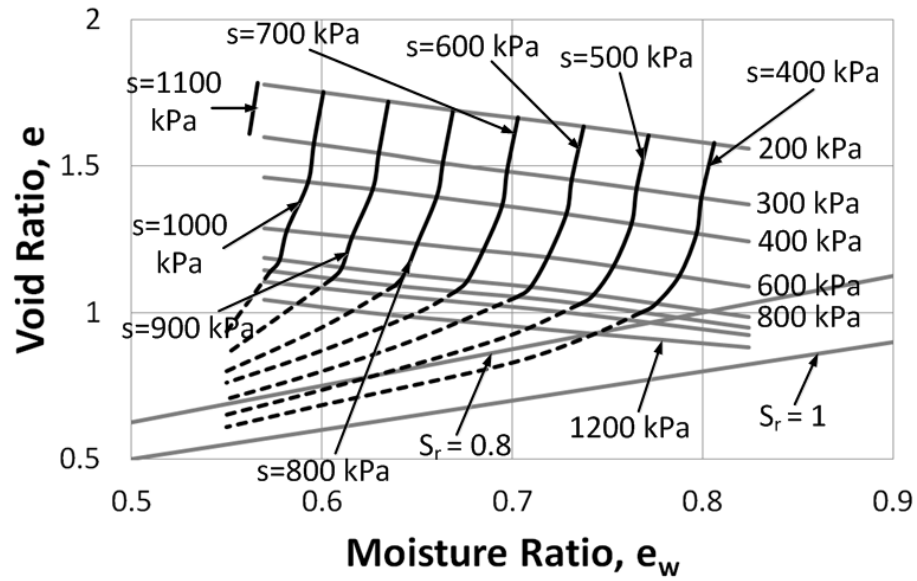
(a) In $e - e_w$ plane
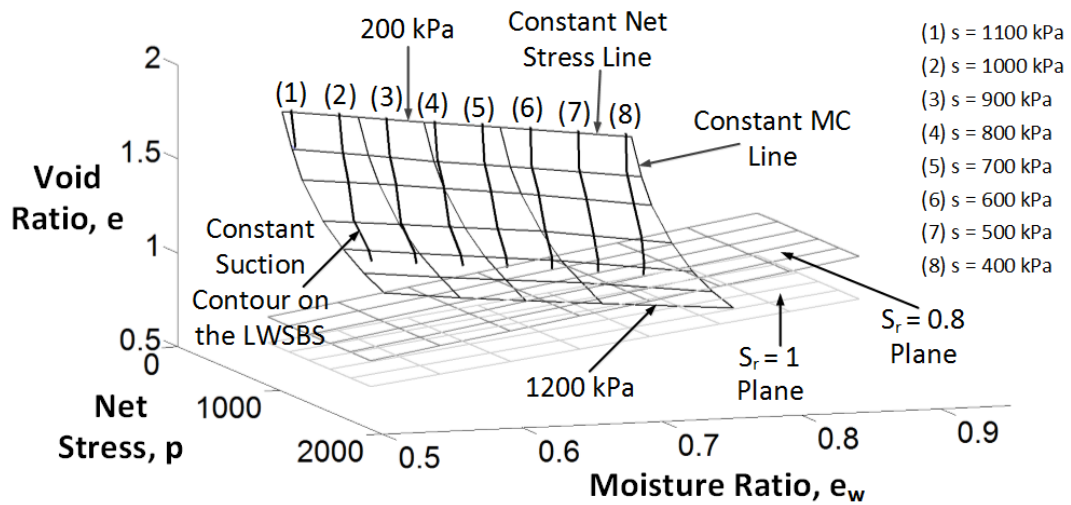
(b) In $e - e_w - p$ space

Figure 6-1: Suction contours on the LWSBS from Tarantino and De Col (2008)
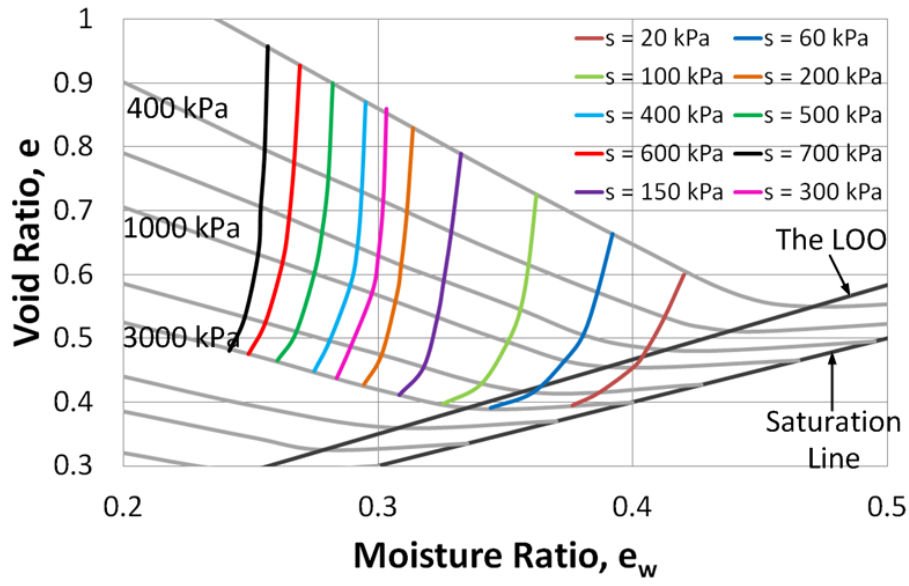
(a) In $e - e_w$ plane
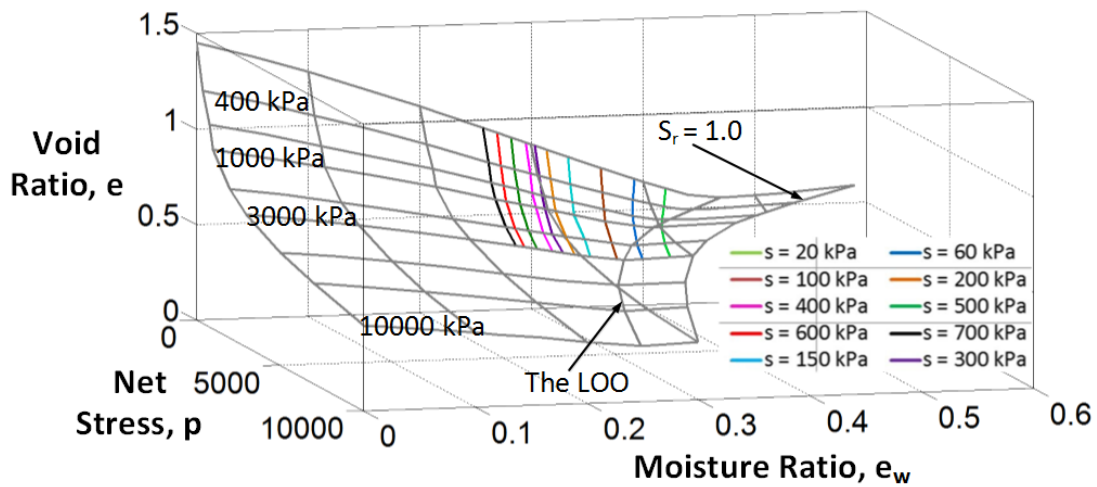
(b) In $e - e_w - p$ space

Figure 6-2: Suction contours on the LWSBS from Jotisankasa (2005)
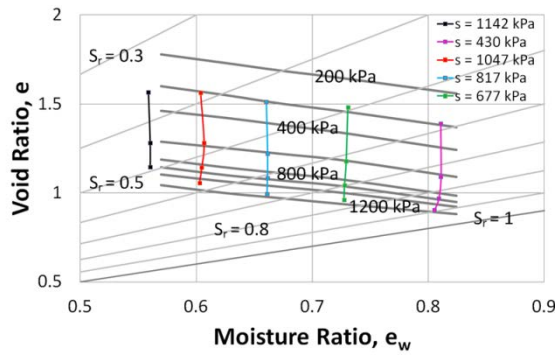
(a) 15 kPa constant net stress plane
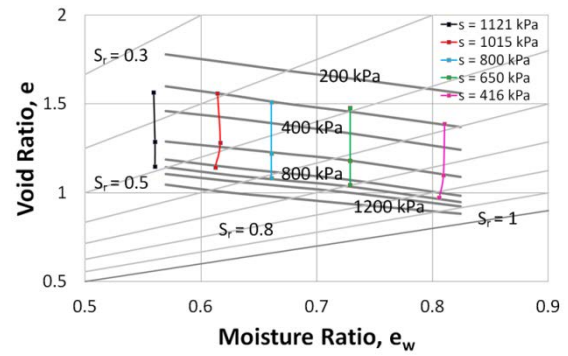
(b) 100 kPa constant net stress plane
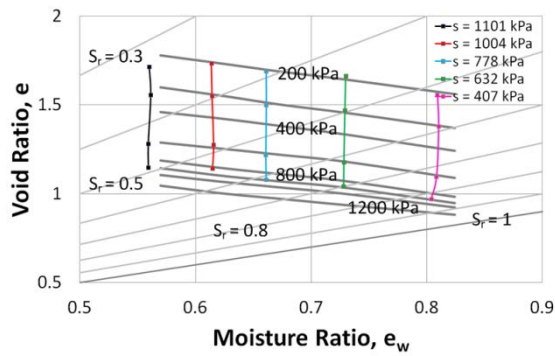
(c) 200 kPa constant net stress plane
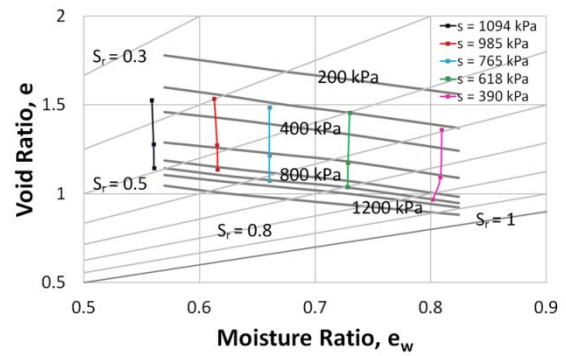
(d) 300 kPa constant net stress plane
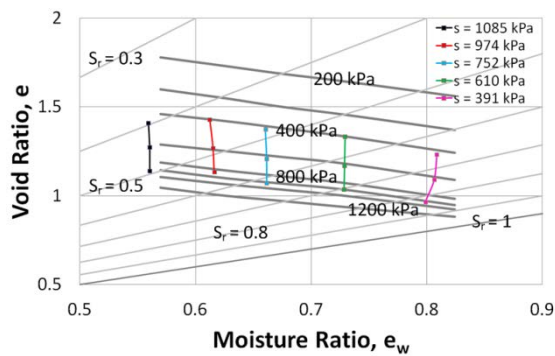
(e) 400 kPa constant net stress plane
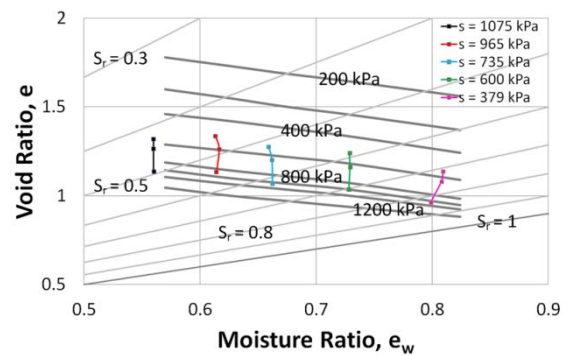
(f) 500 kPa constant net stress plane
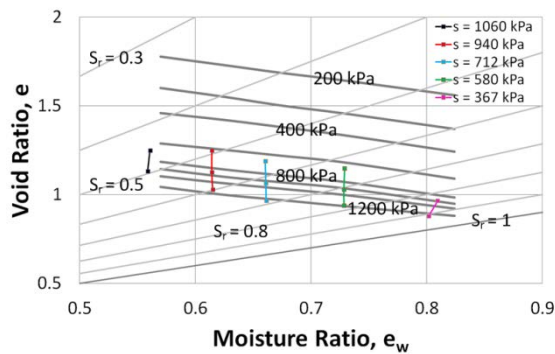
(g) 600 kPa constant net stress plane
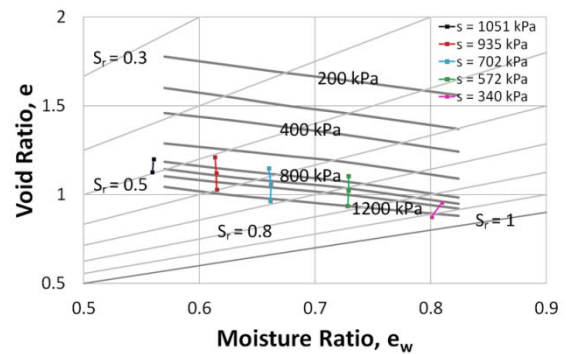
(h) 700 kPa constant net stress plane
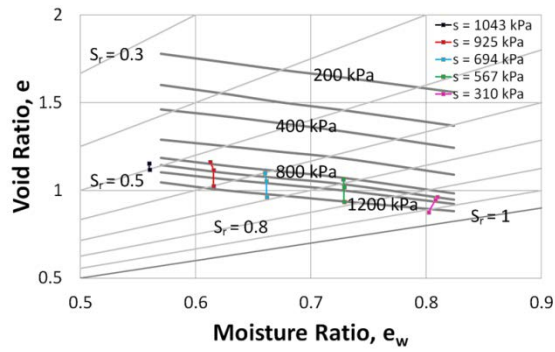
(i) 800 kPa constant net stress plane
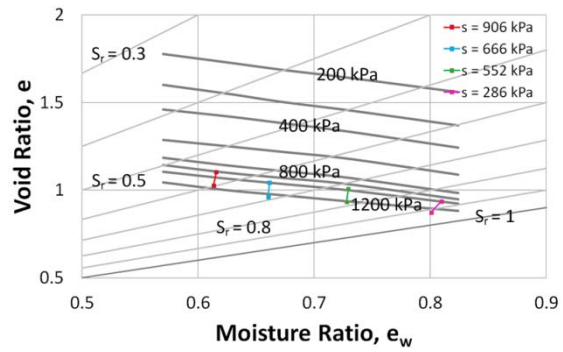
(j) 900 kPa constant net stress plane
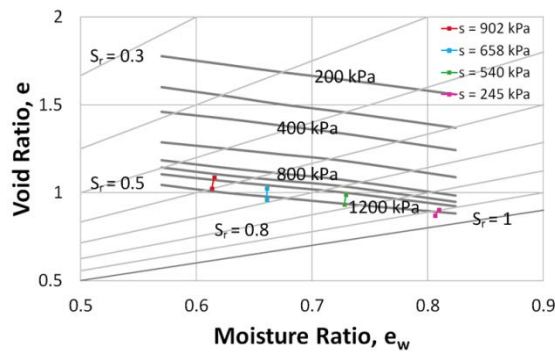
(k) 1000 kPa constant net stress plane
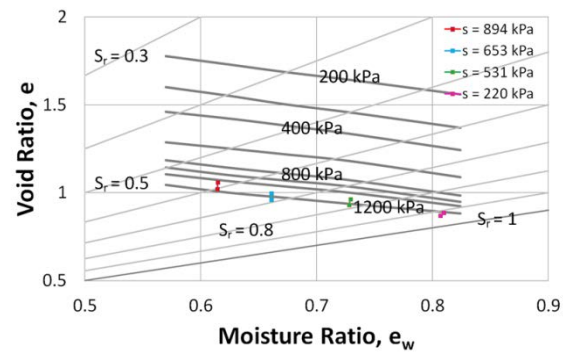
(l) 1100 kPa constant net stress plane
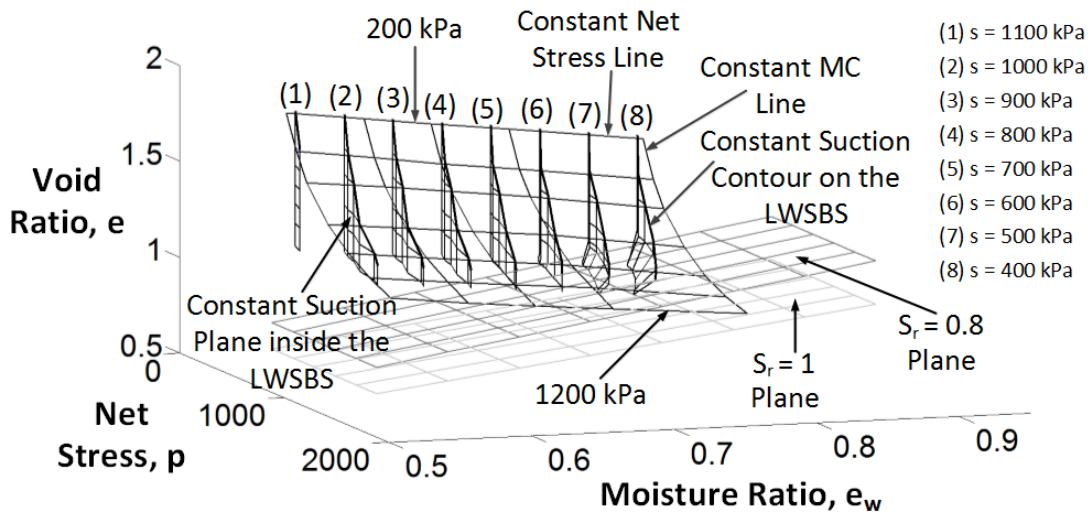
(m) Suction contours inside the LWSBS (using actual data)
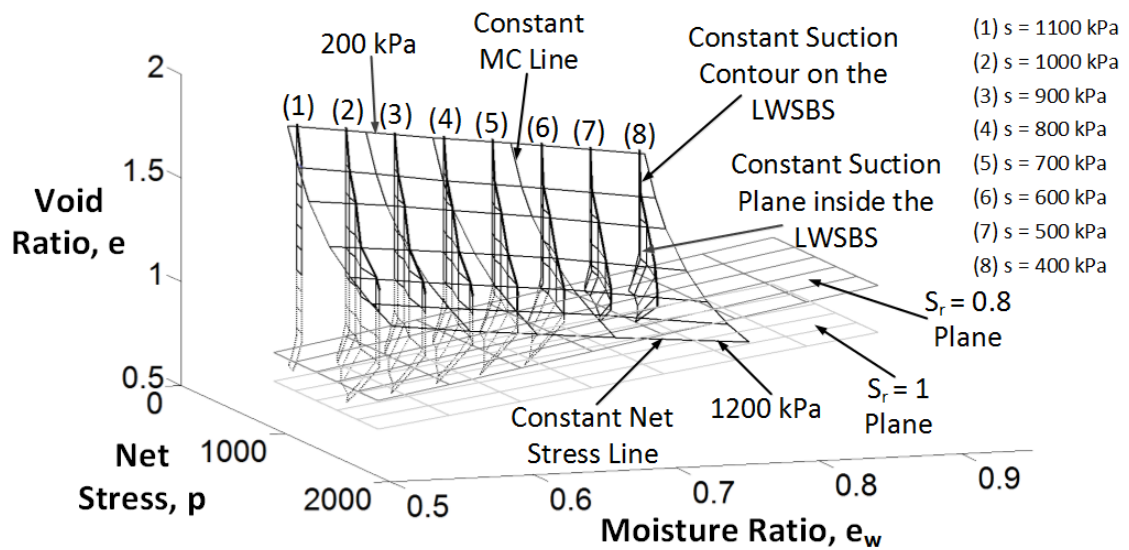
(n) Suction contours inside the LWSBS (complete picture)

Figure 6-3: Suction contours inside the LWSBS from Tarantino and De Col (2008)
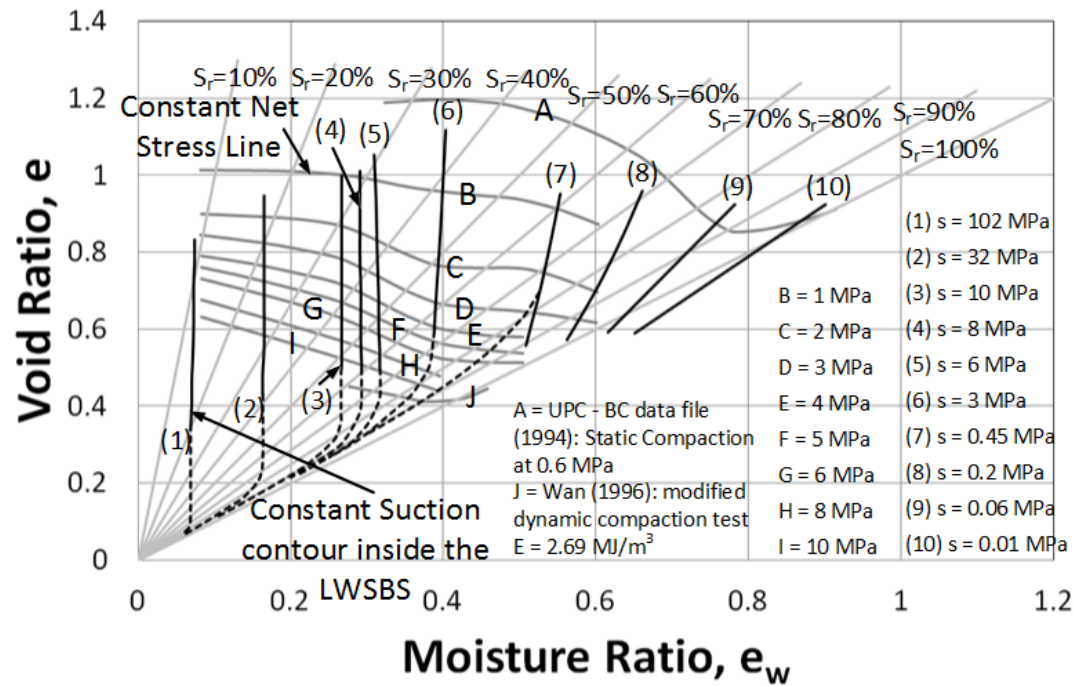
Figure 6-4: Suction contours inside the LWSBS at the nominal stress plane from Romero (1999)
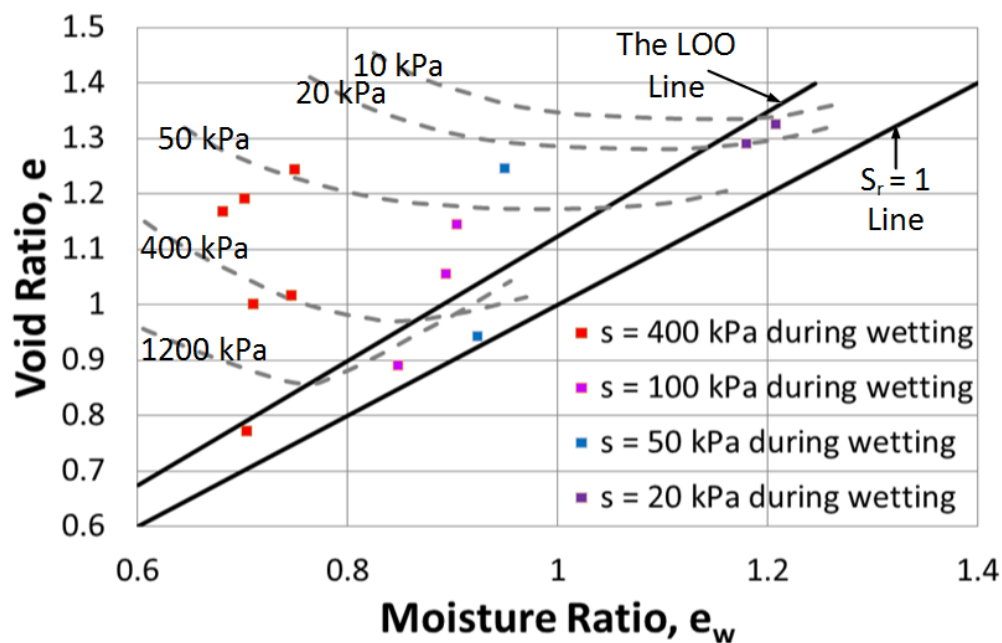
Figure 6-5: Suction contours inside the LWSBS at the nominal stress plane from Sharma (1998)
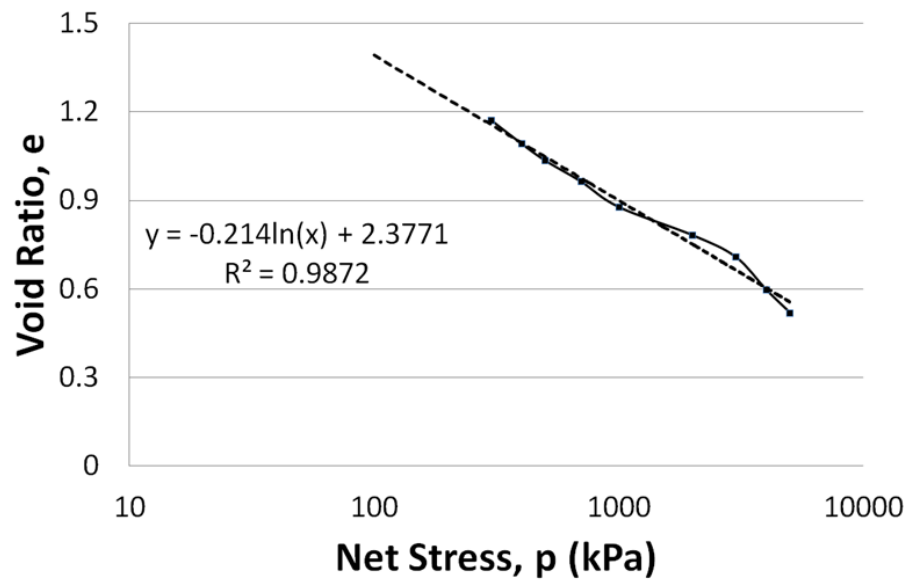
(a) For 100% saturation ($S_r = 1.0$) line
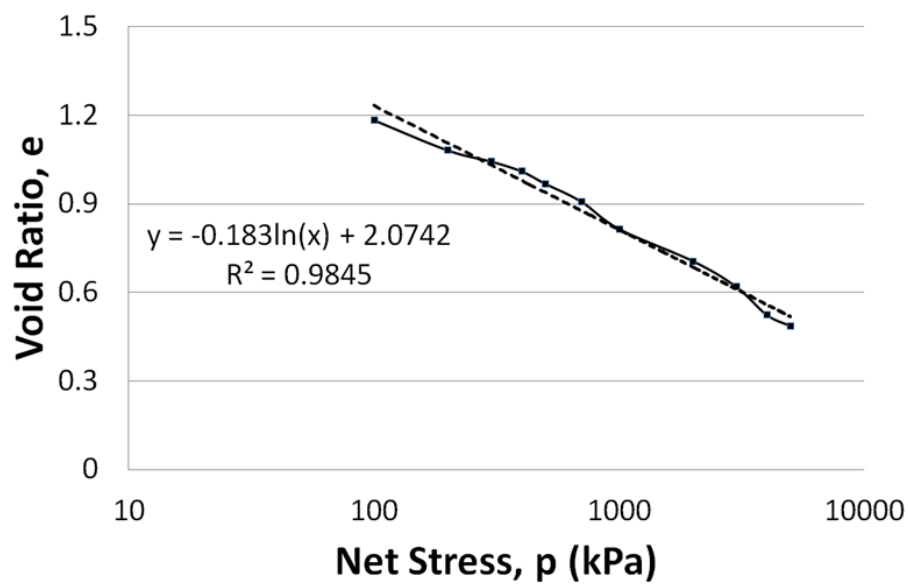
(b) For the LOO ($S_r = 0.8833$) line

Figure 6-6: $e - \log p$ relationship at different degree of saturations for kaolin soil
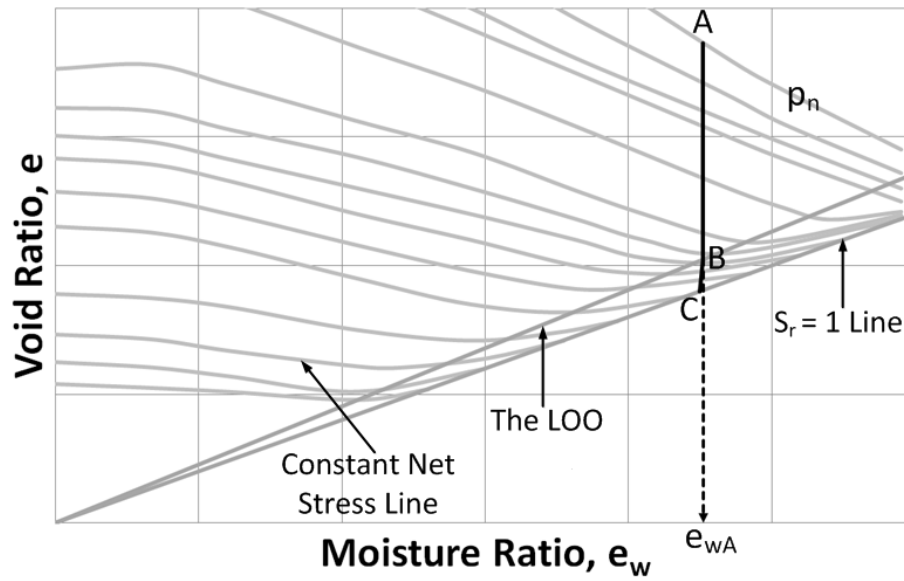
Figure 6-7: A qualitative presentation of the reduction of moisture content during loading at the wet side of the LOO on the LWSBS
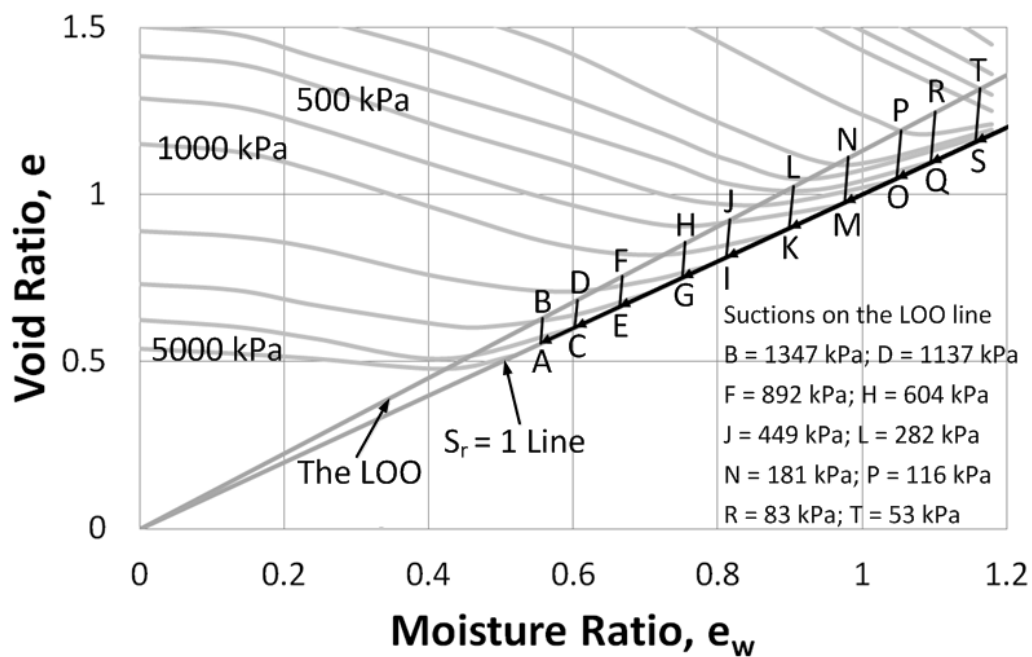
Figure 6-8: Suction values on the LOO on the LWSBS for kaolin soil
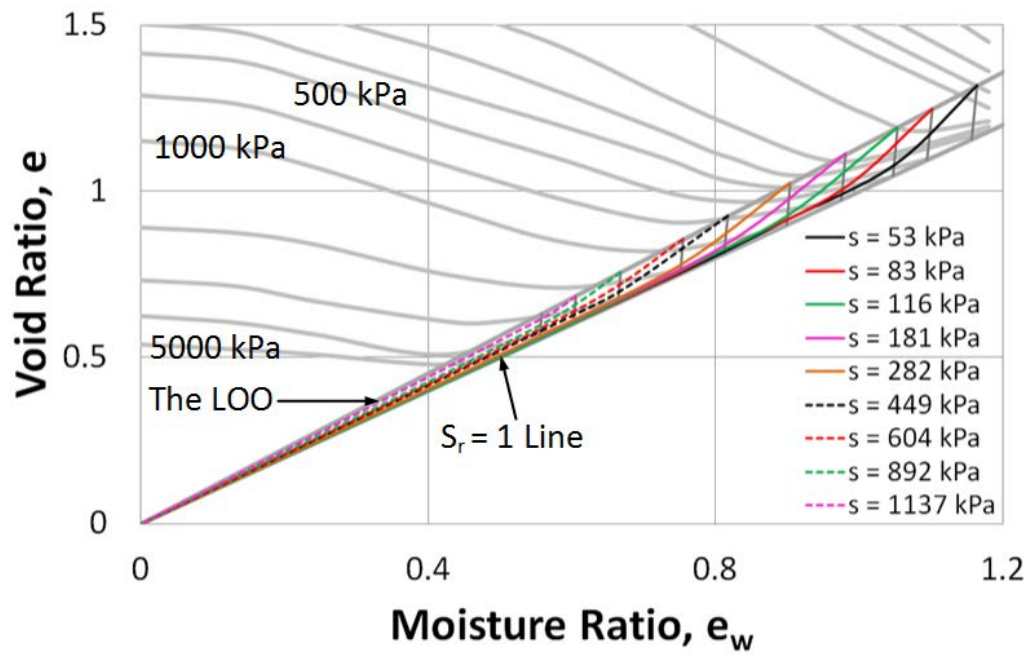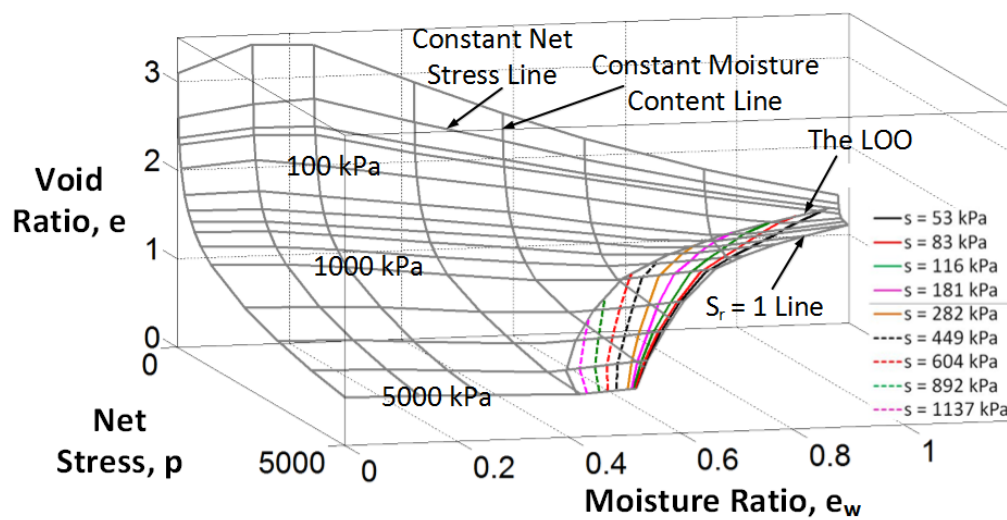
(a) In $e - e_w$ plane

(b) In $e - e_w - p$ space

Figure 6-9: Suction contours at the wet side of the LOO on the LWSBS for kaolin soil
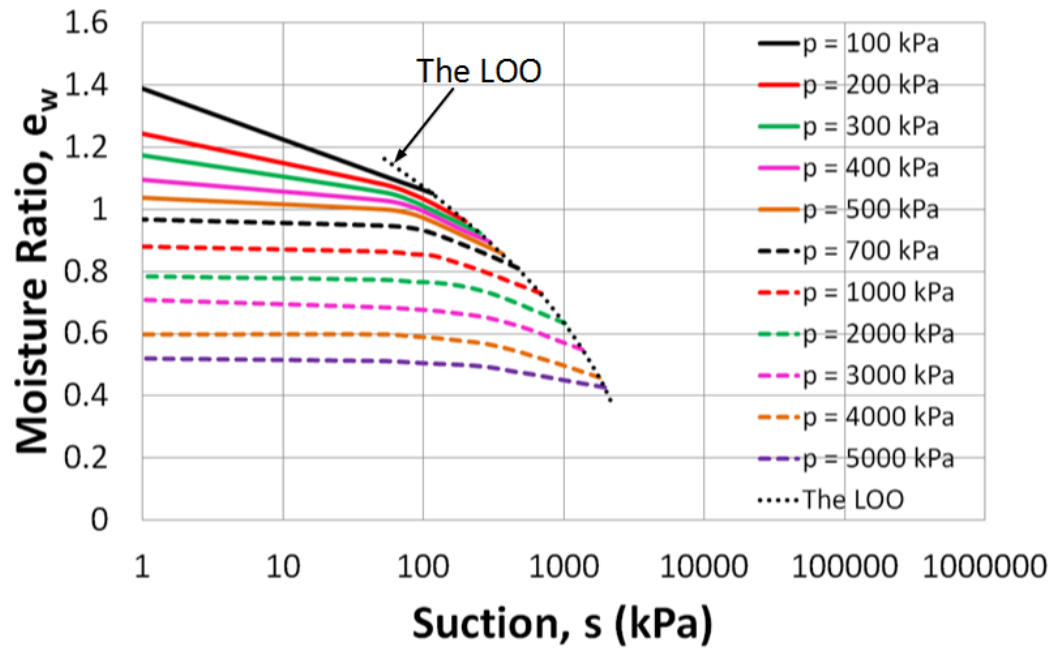
Figure 6-10: SWCCs at different net stresses at the wet side of the LOO for kaolin soil
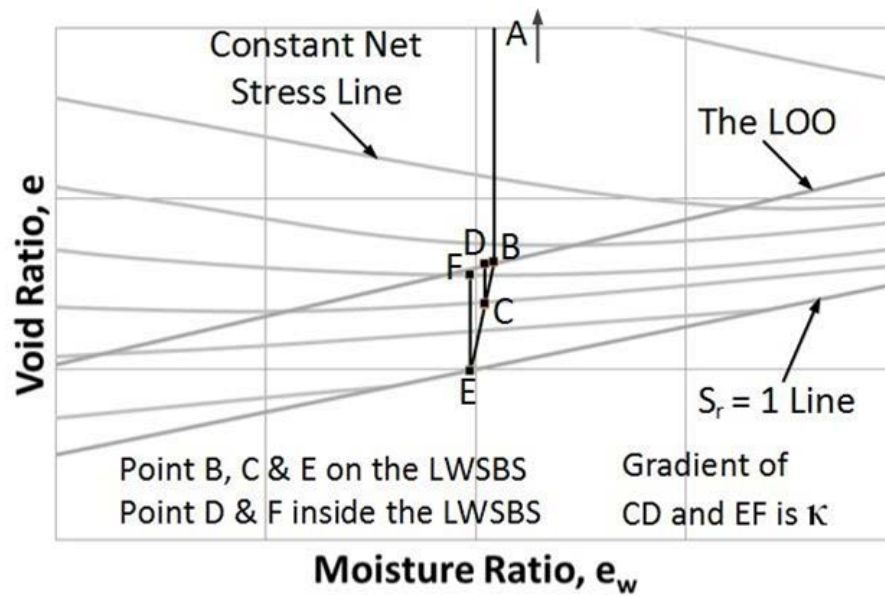
(a) In $e - e_w$ plane on the LWSBS
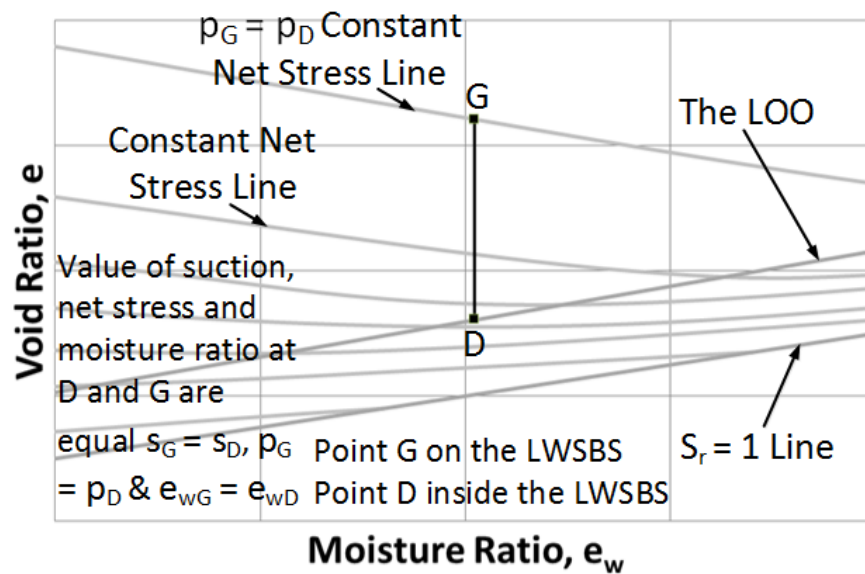
(b) In $e - e_w$ plane inside the LWSBS at $p_D = p_G$ net stress plane
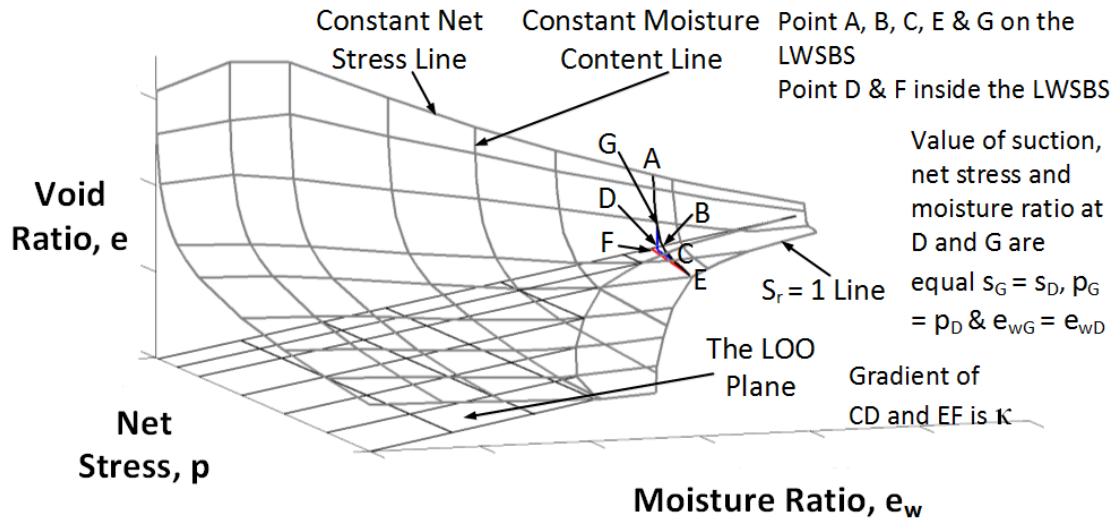
(c) In $e - e_w - p$ space

Figure 6-11: Development of the suction contours at the dry side of the LOO from the suction contours at the wet side of the LOO on the LWSBS mathematically (Option 1)
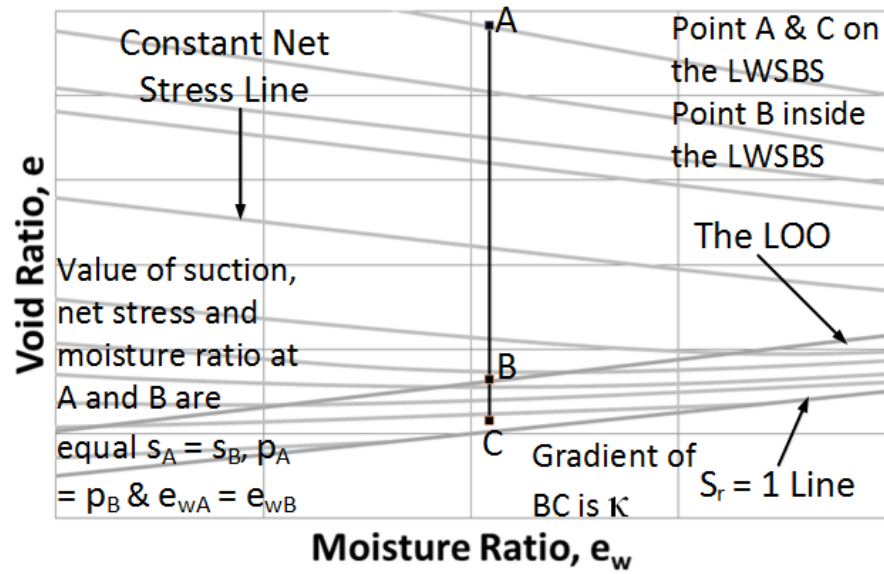
(a) In $e - e_w$ plane
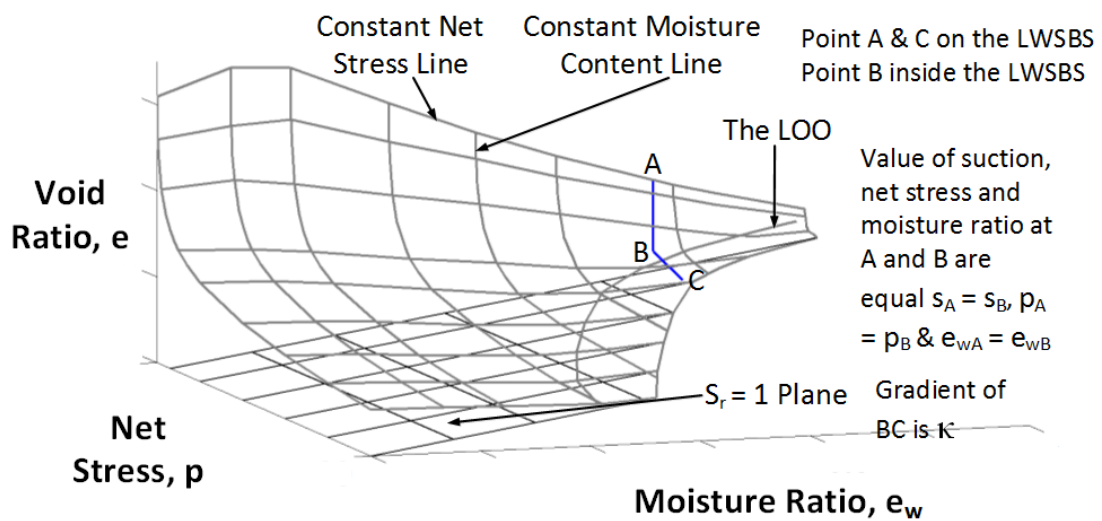
(b) In $e - e_w - p$ space

Figure 6-12: Mathematical development of the suction contours from nominal stress line to the LOO at the dry side of the LOO on the LWSBS (Option 2)
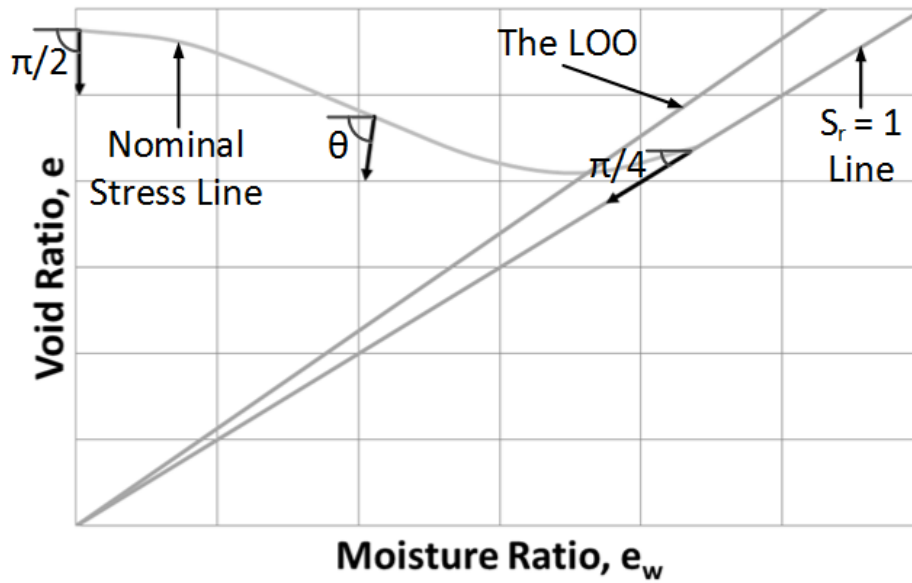
(a) Presentation of the angle with horizontal axis made by the tangent of the constant suction contours from the nominal stress line on the LWSBS
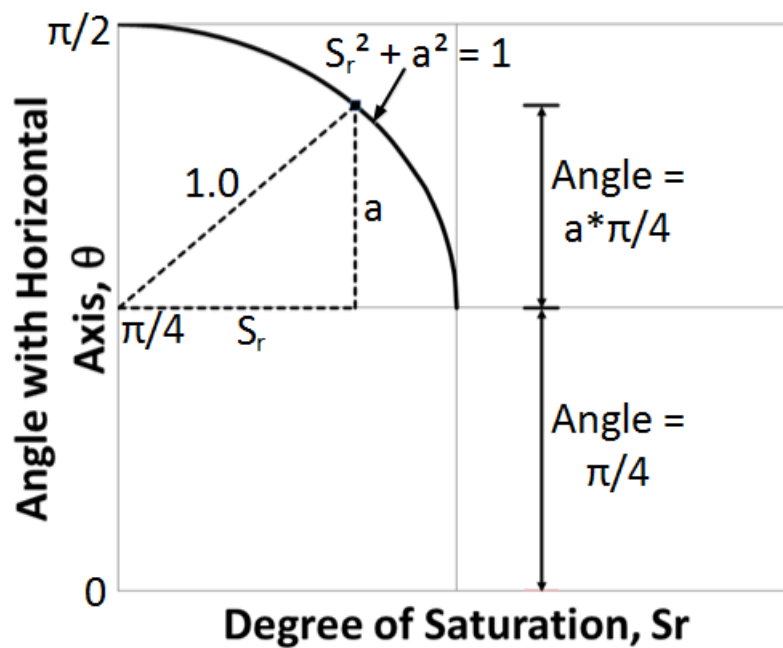
(b) Relationship between the degree of saturation and the angle made by the constant suction contours from the nominal stress line on the LWSBS with the horizontal axis
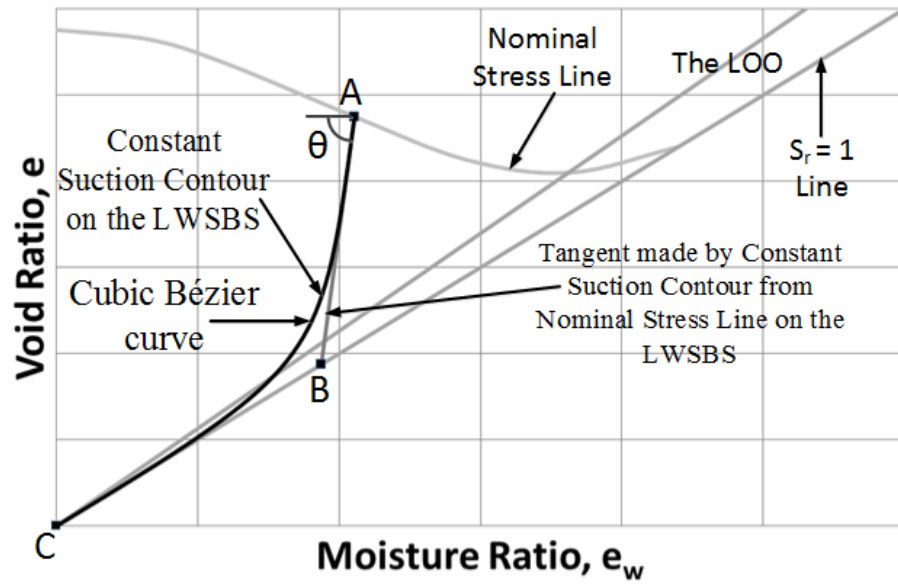
(c) Development of the suction contour at the dry side of the LOO on the LWSBS from the nominal stress line using cubic Bézier curve

Figure 6-13: Development of the suction contours at the dry side of the LOO on the LWSBS by the combination of experimental and mathematical analysis (Option 3)
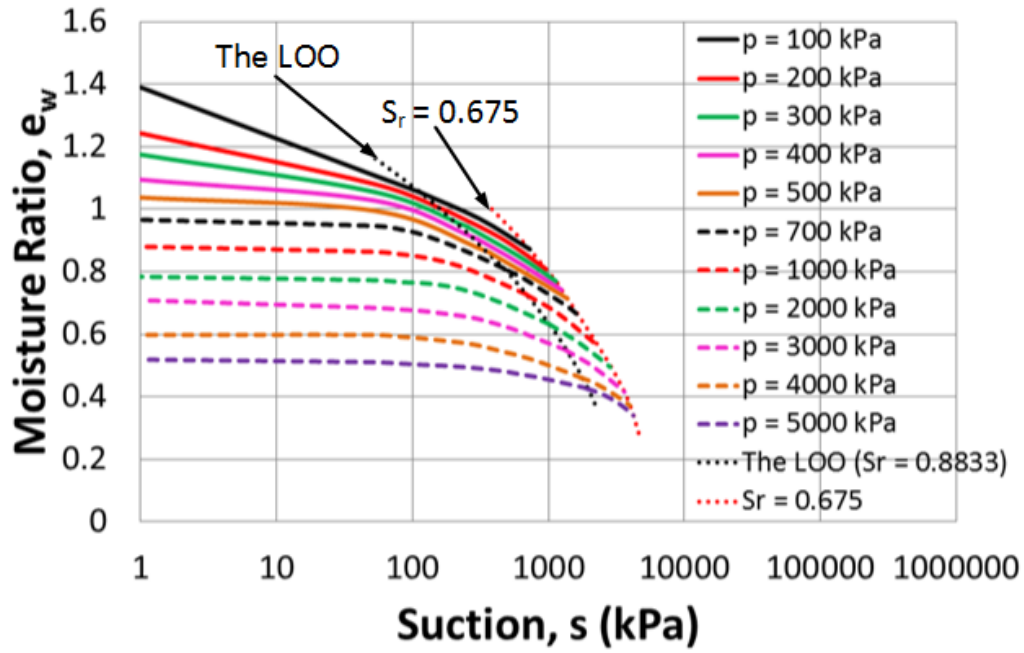
(a) Development of the SWCCs at different net stresses between the LOO and $S_r = 0.675$ by the extension of effective stress equation
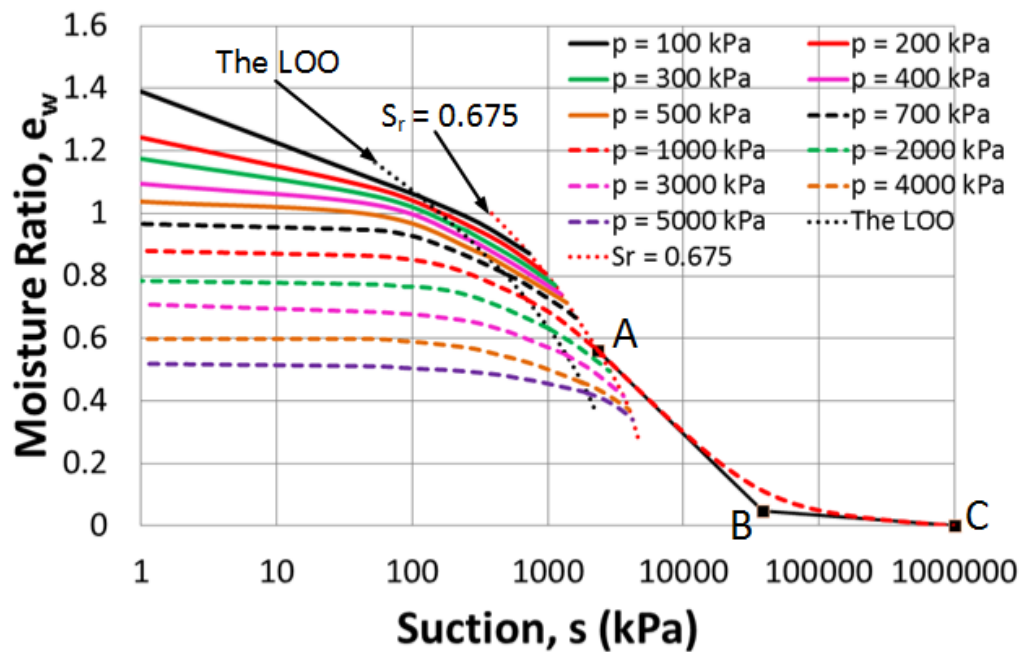
(b) Development of the SWCC between $S_r = 0.675$ and $S_r = 0$ using cubic Bézier curve
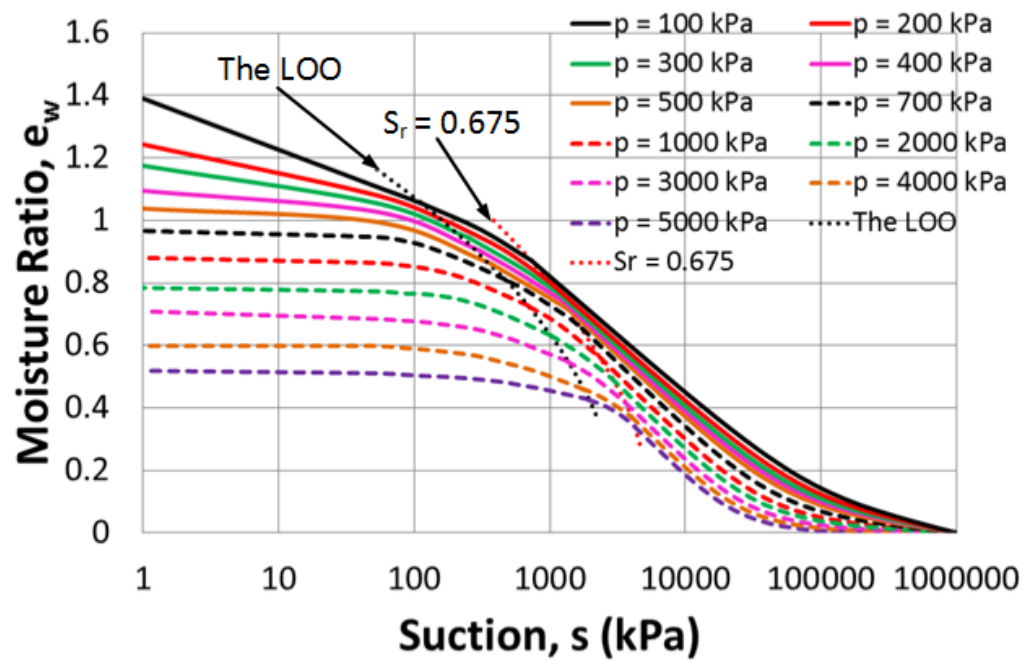
(c) The complete SWCCs at different net stresses

Figure 6-14: Development of the SWCCs at different net stresses at the dry side of the LOO for kaolin soil
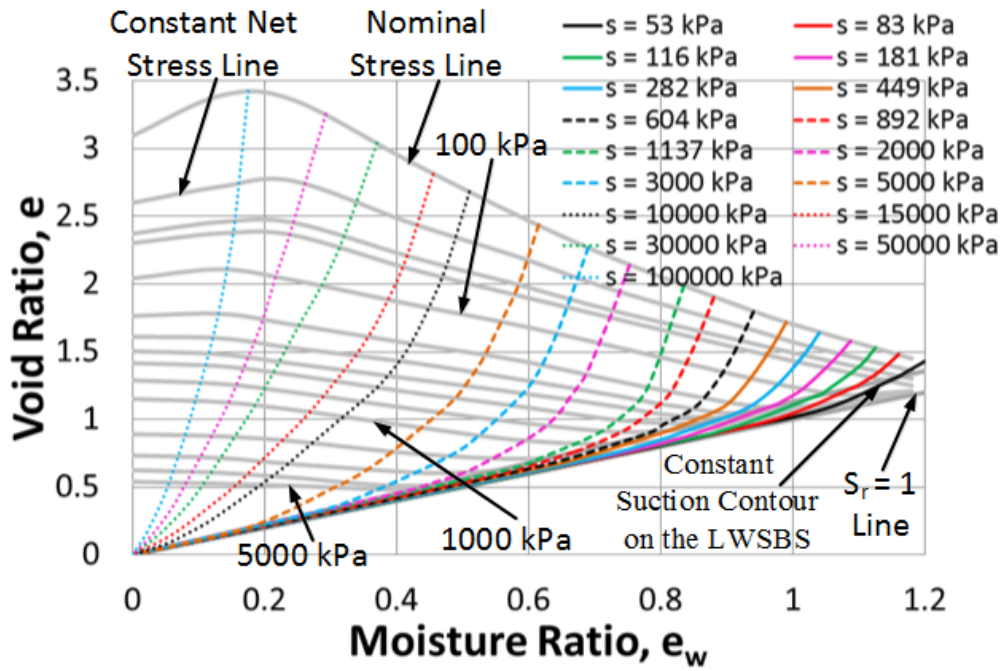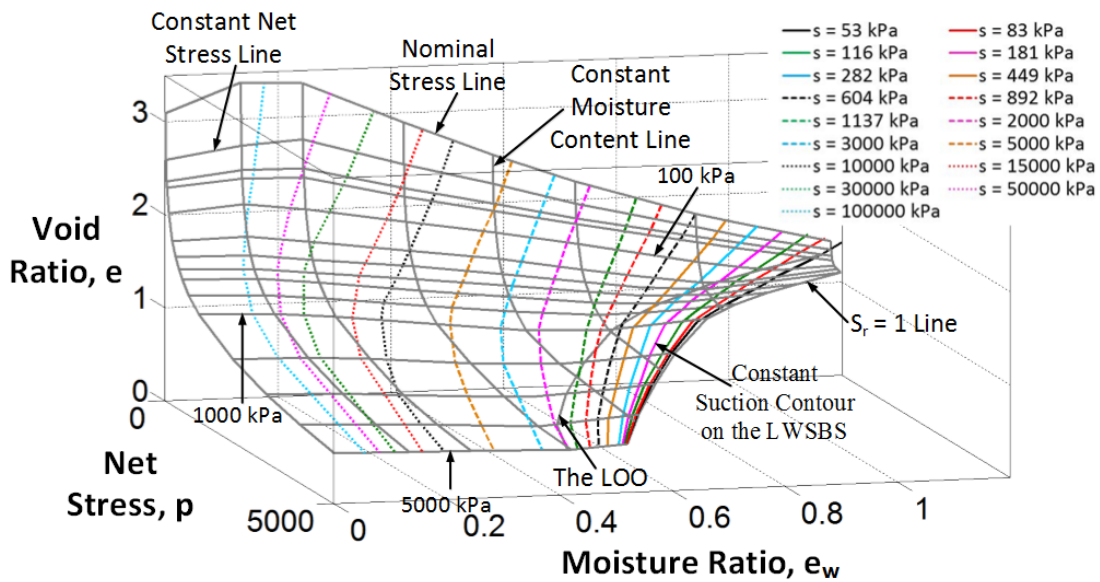
(a) In $e - e_w$ plane

(b) In $e - e_w - p$ space

Figure 6-15: The complete suction contours on the LWSBS for kaolin soil
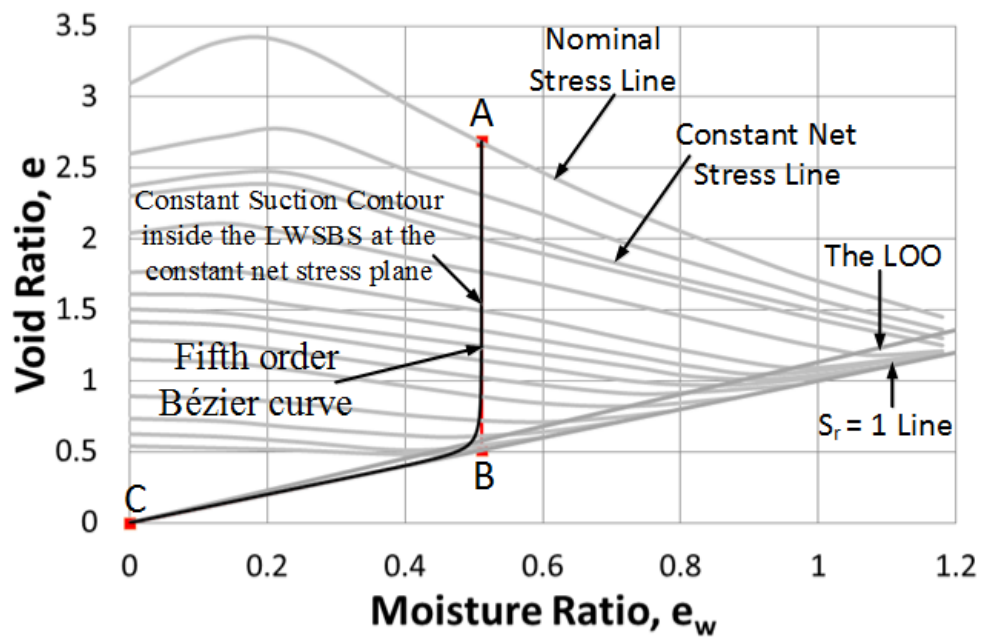
(a) Development of the constant suction contour inside the LWSBS on the constant net stress plane using fifth order Bézier curve
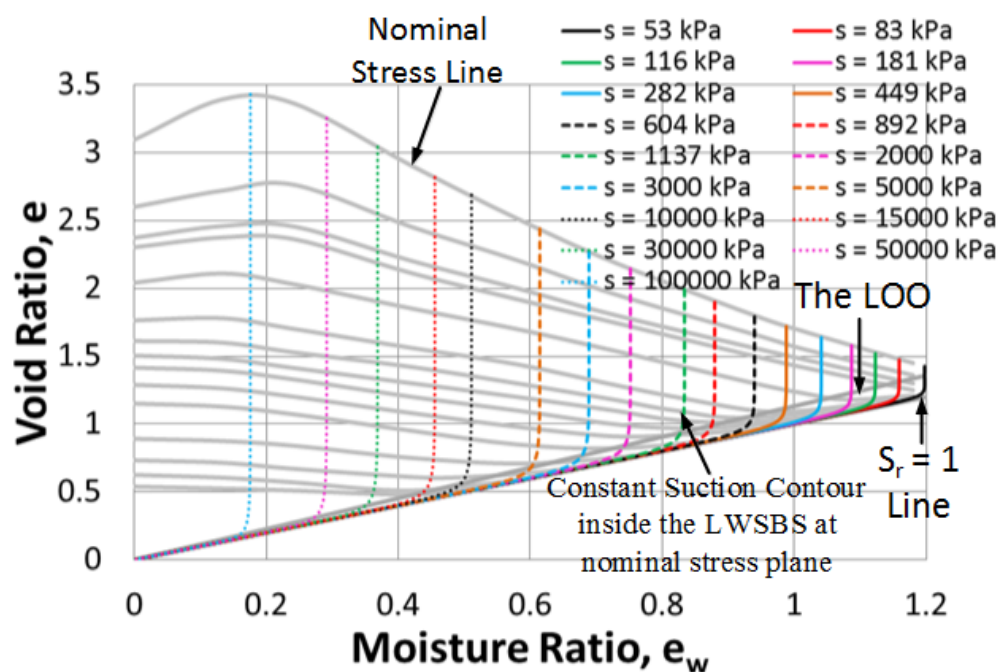
(b) Constant suction contours inside the LWSBS on the nominal stress plane
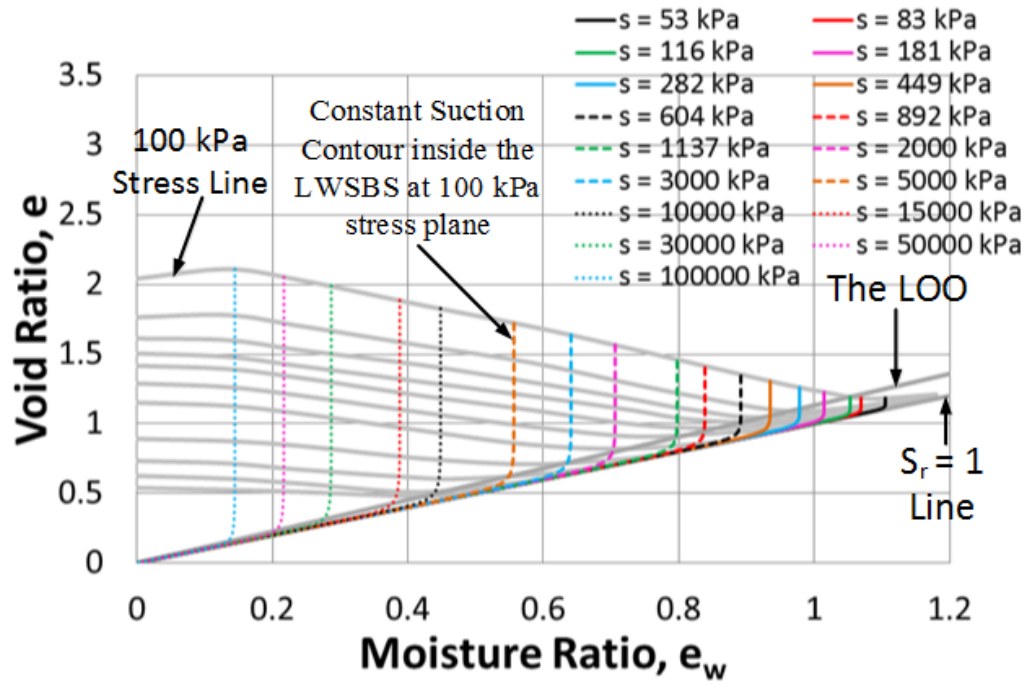
(c) Constant suction contours inside the LWSBS on the 100 kPa stress plane
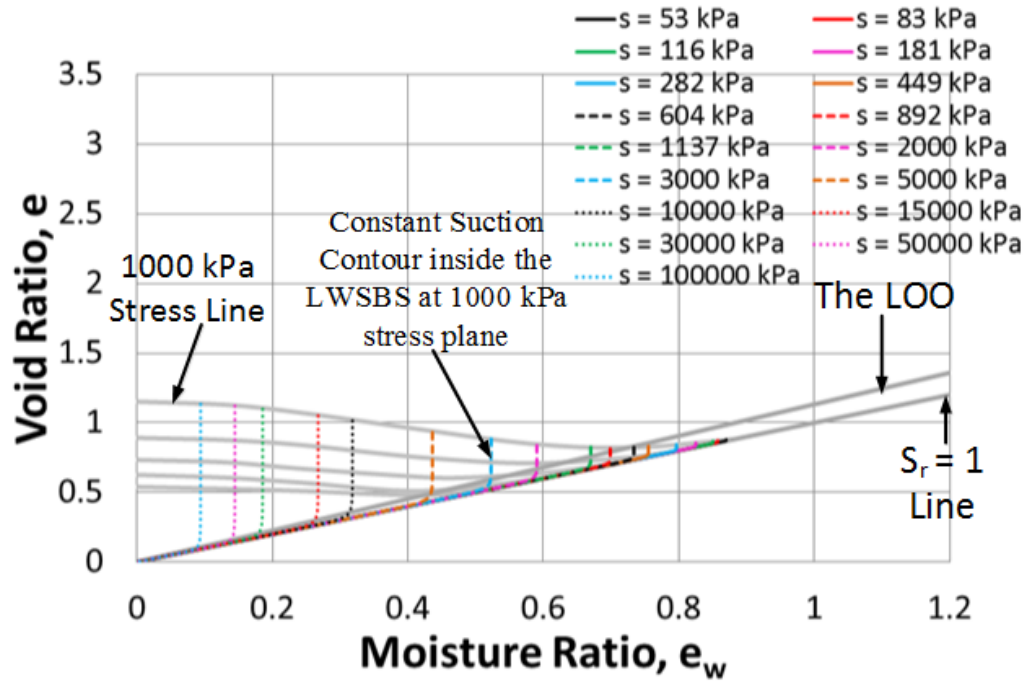
(d) Constant suction contours inside the LWSBS on the 1000 kPa stress plane
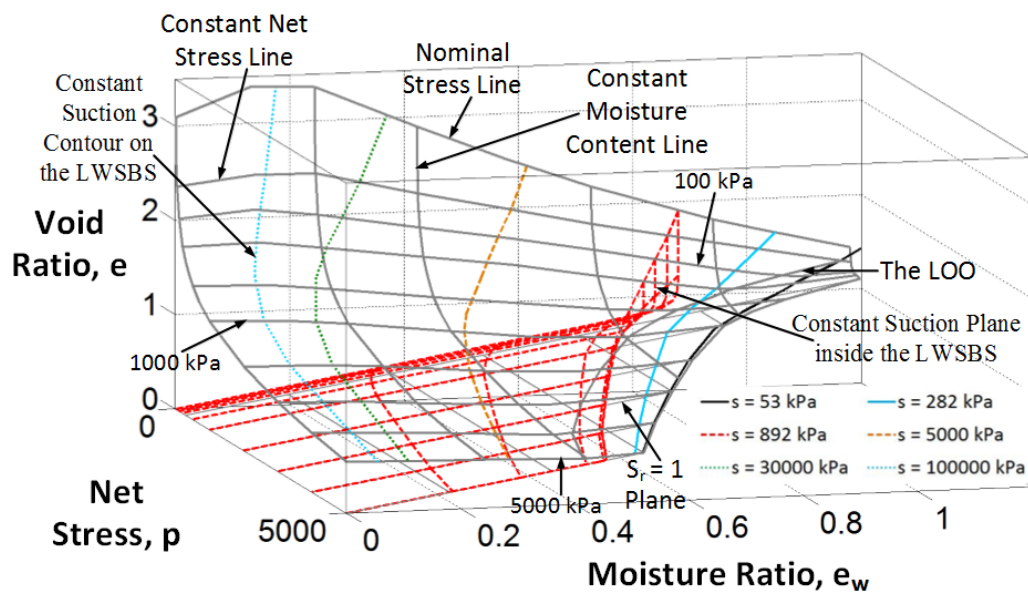
(e) 892 kPa constant suction plane inside the LWSBS in the $e - e_w - p$ space
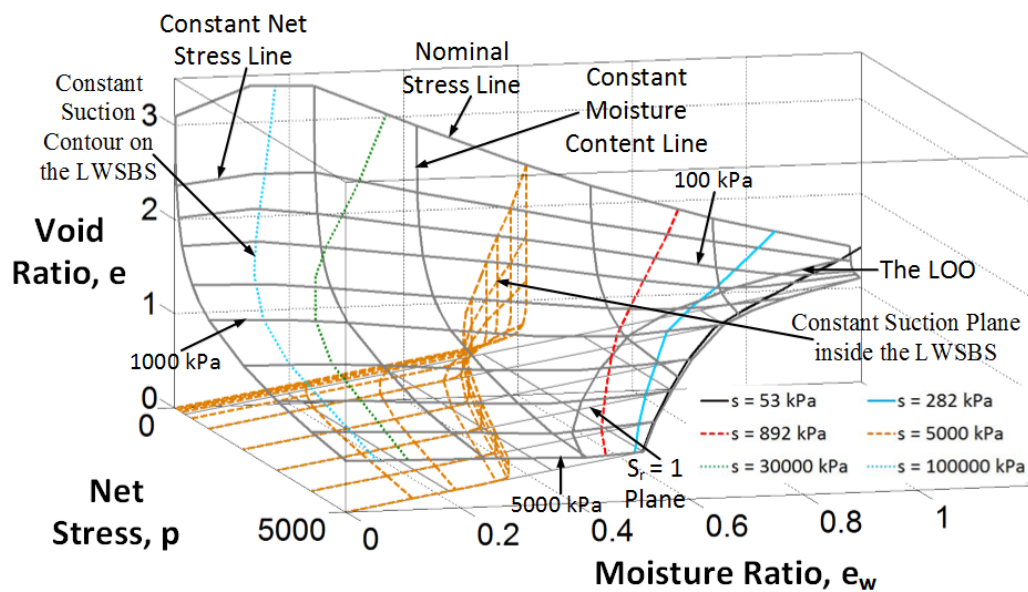
(f) 5000 kPa constant suction plane inside the LWSBS in the $e - e_w - p$ space
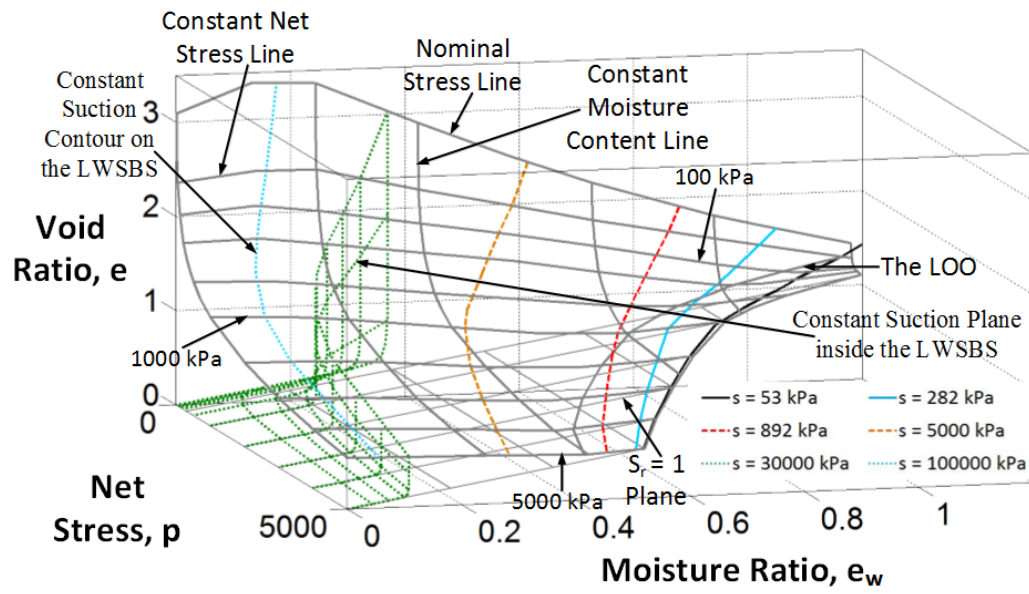
(g) 30000 kPa constant suction plane inside the LWSBS in the $e - e_w - p$ space

Figure 6-16: Constant suction contours inside the LWSBS for kaolin soil
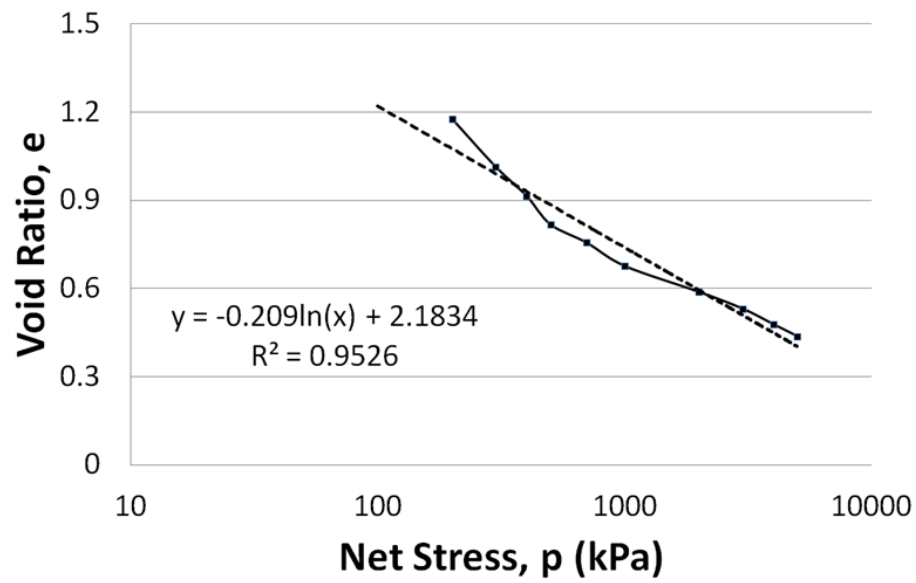
(a) For 100% saturation ($S_r = 1.0$) line
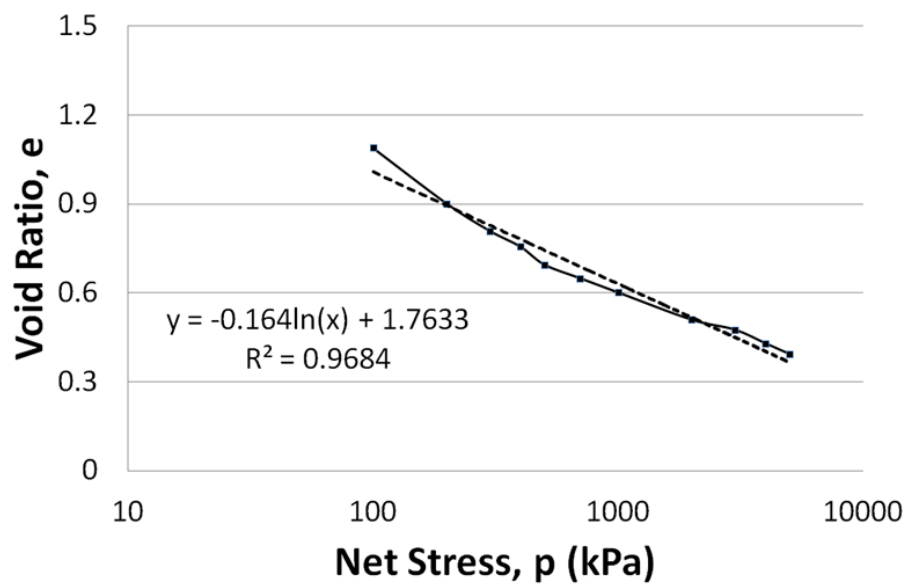
(b) For the LOO ($S_r = 0.86$) line

Figure 6-17: $e - \log p$ relationship at different degrees of saturation for Merri Creek soil
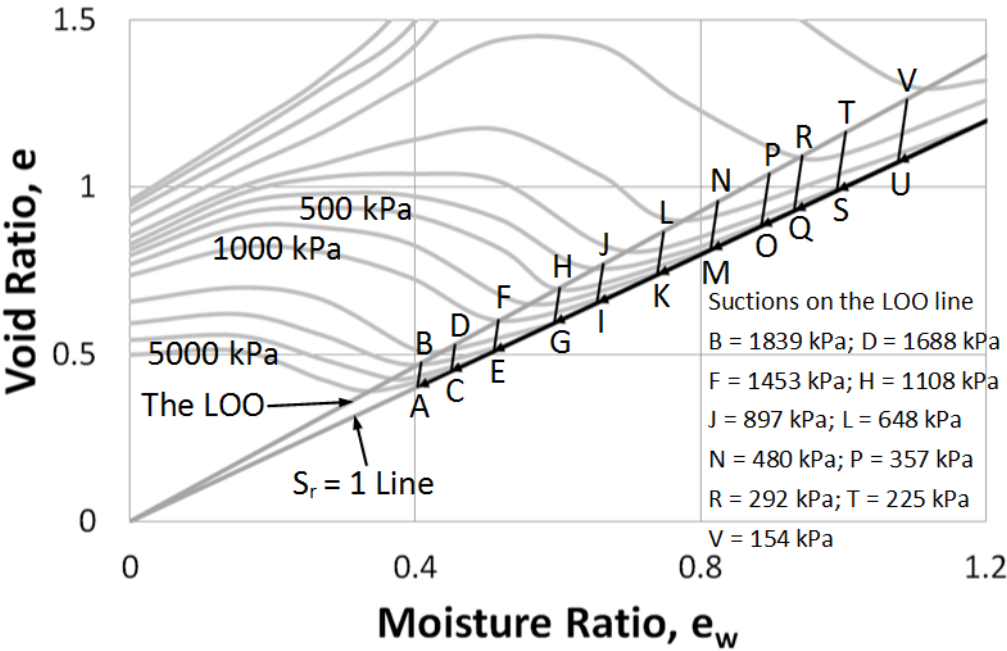
Figure 6-18: Suction values on the LOO line on the LWSBS for Merri Creek soil
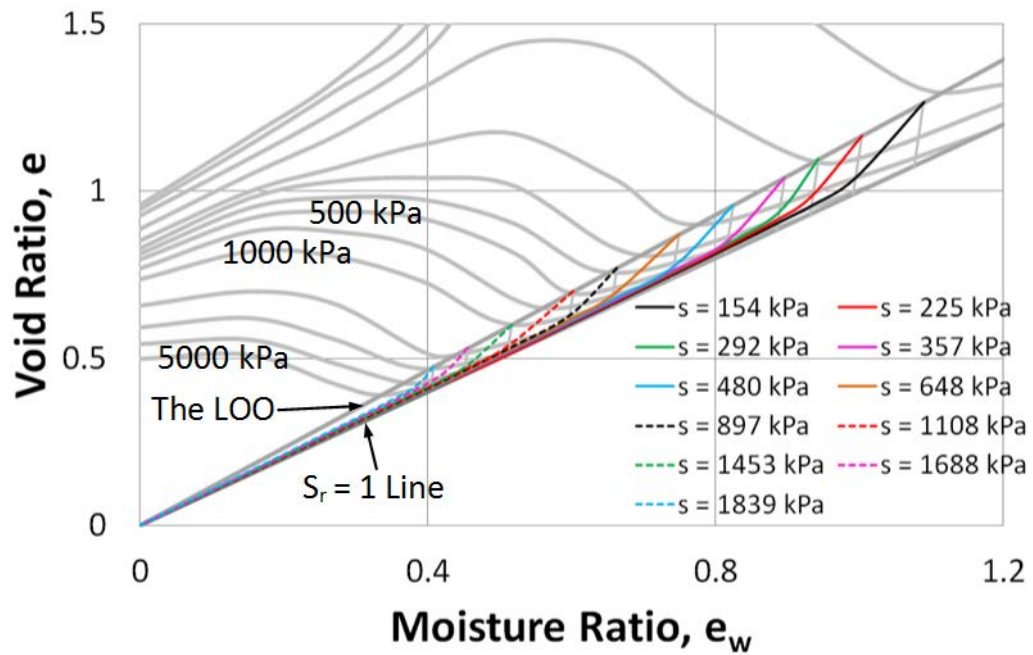
(a) In $e - e_w$ plane
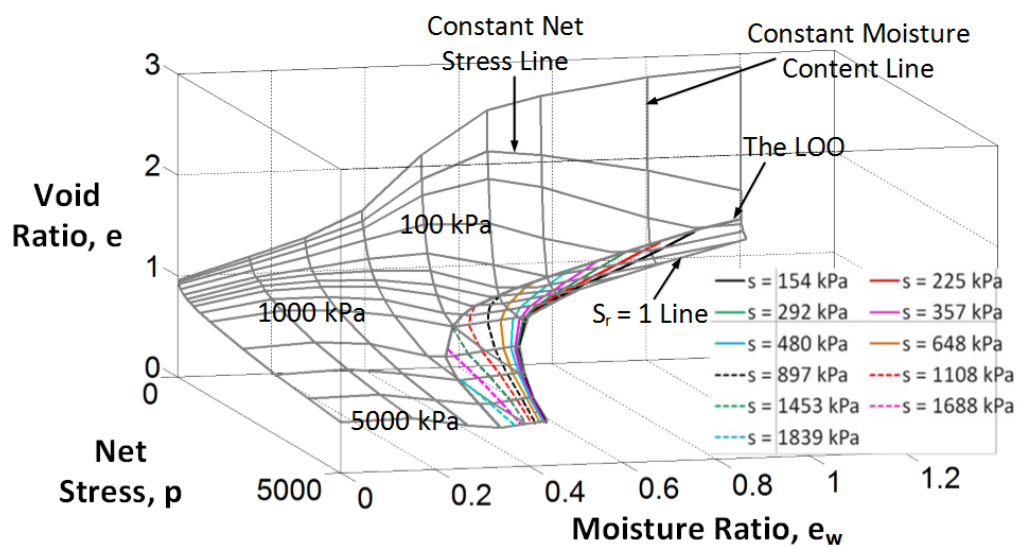
(b) In $e - e_w - p$ space

Figure 6-19: Suction contours at the wet side of the LOO on the LWSBS for Merri Creek soil
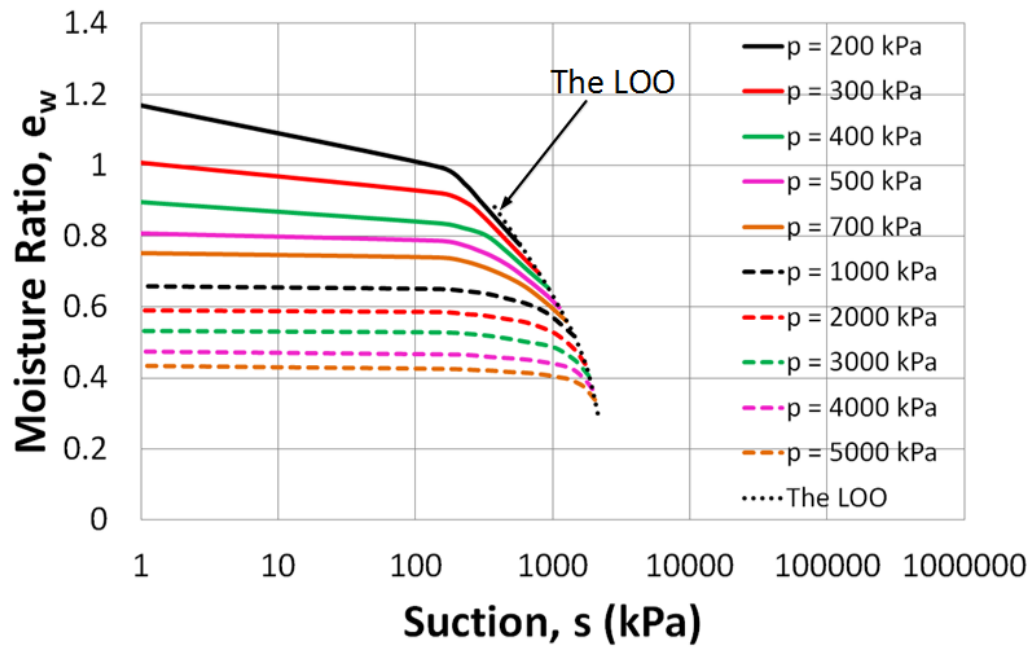
Figure 6-20: SWCCs at different net stresses at the wet side of the LOO for Merri Creek soil
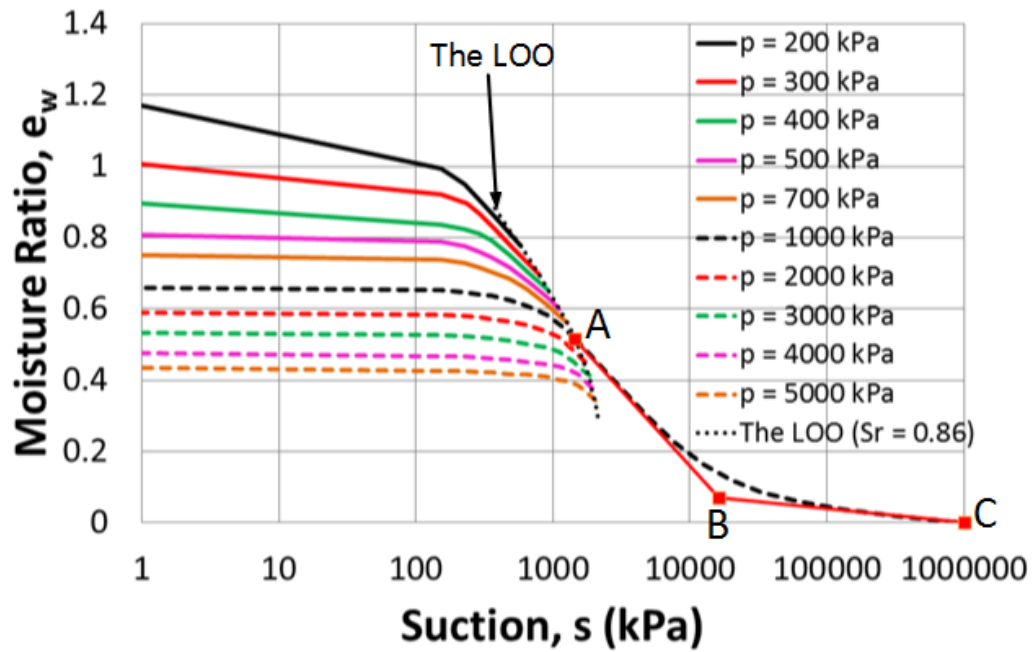
(a) Development of the SWCC between the LOO and $S_r = 0$ using a cubic Bézier curve
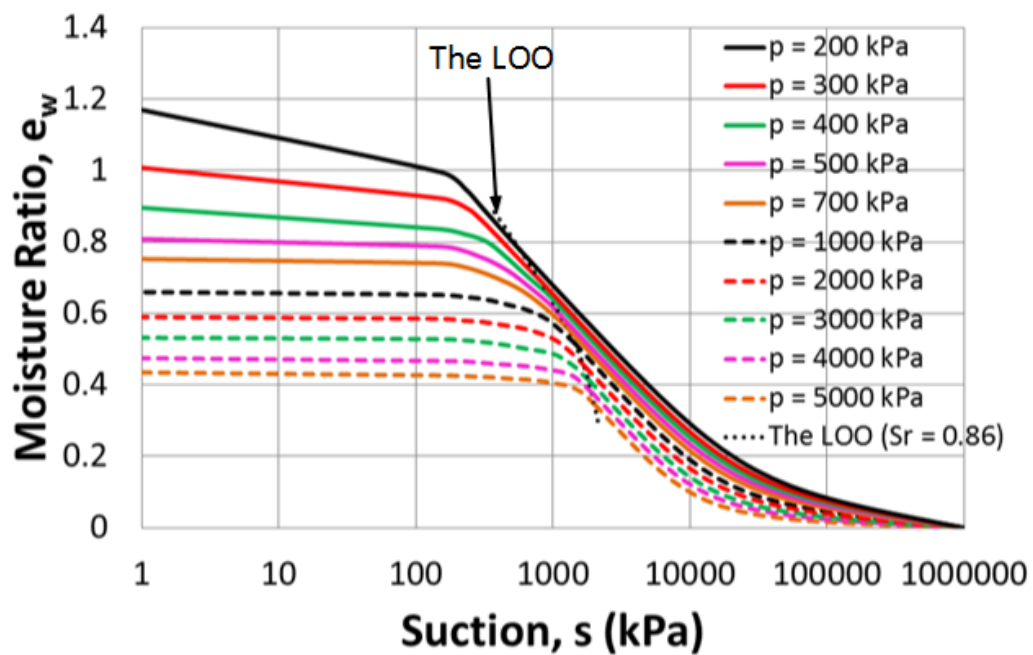
(b) The complete SWCCs at different net stresses

Figure 6-21: Development of the SWCCs at different net stresses at the dry side of the LOO for the Merri Creek soil
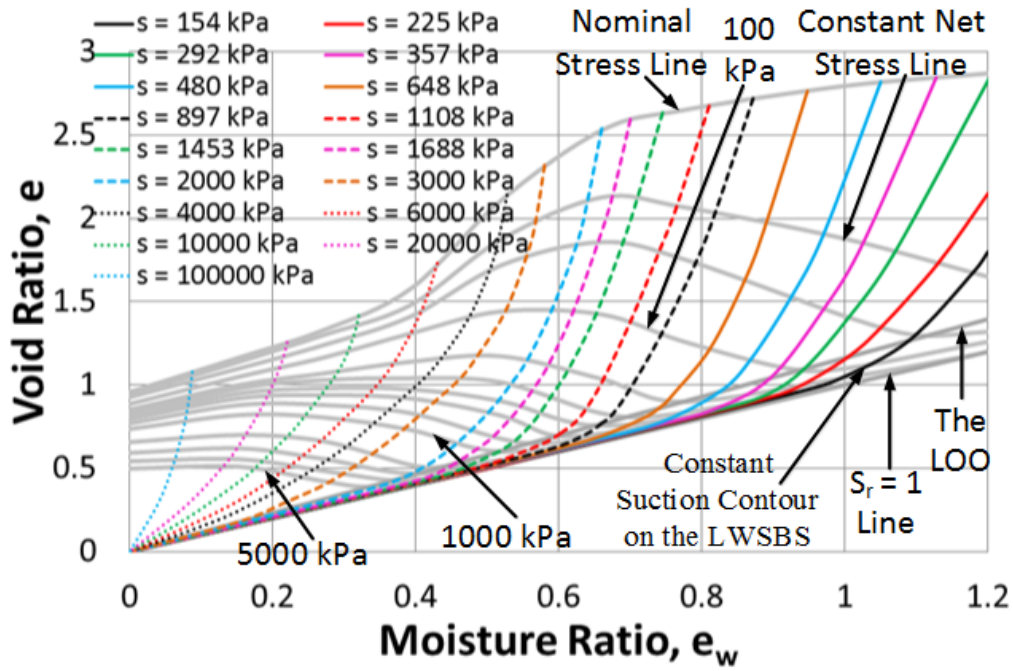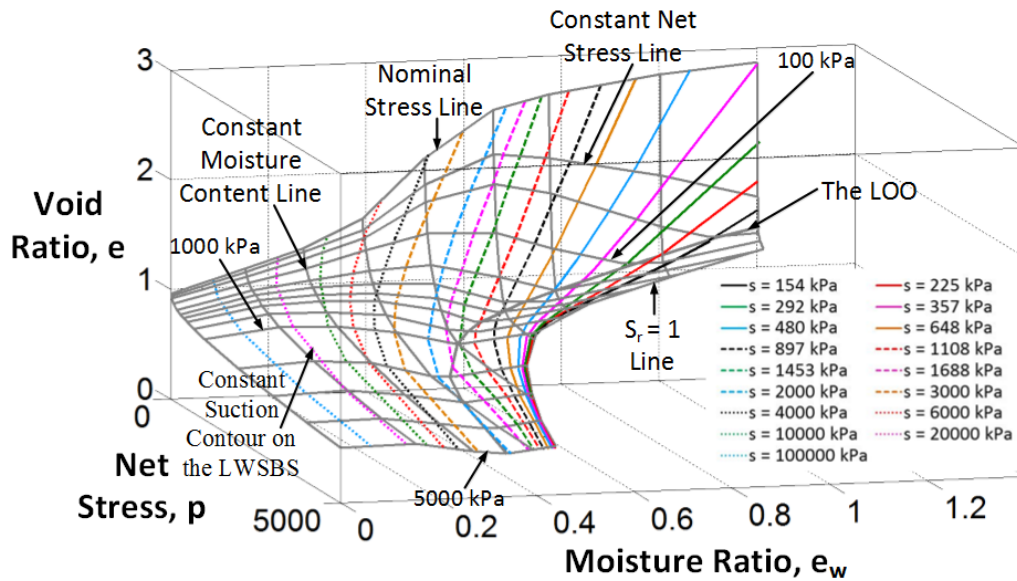
(a) In $e - e_w$ plane

(b) In $e - e_w - p$ space

Figure 6-22: The complete suction contours on the LWSBS for the Merri Creek soil
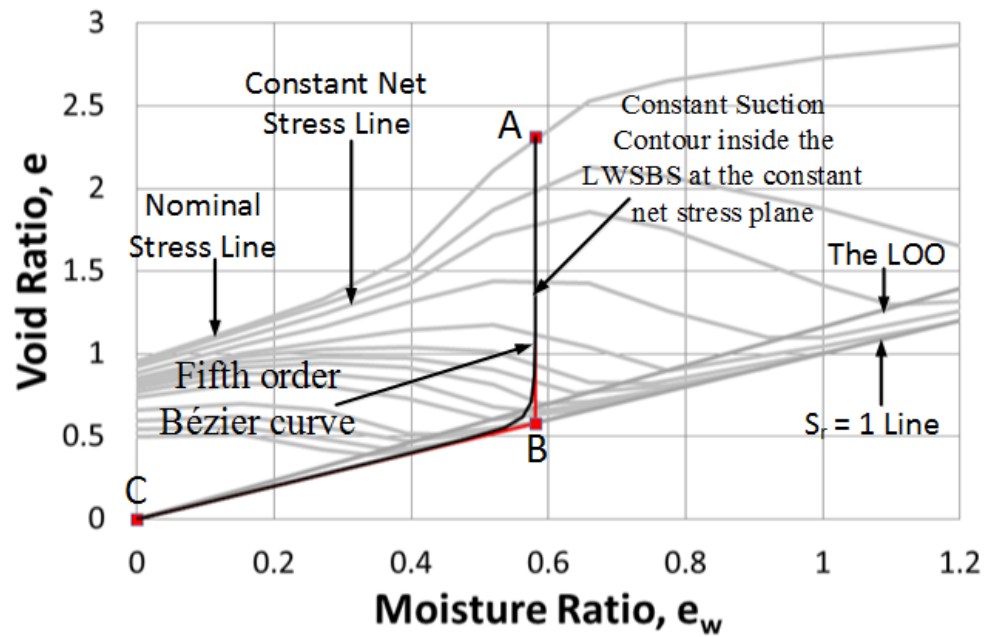
(a) Development of the constant suction contour inside the LWSBS at the constant net stress plane using fifth order Bézier curve
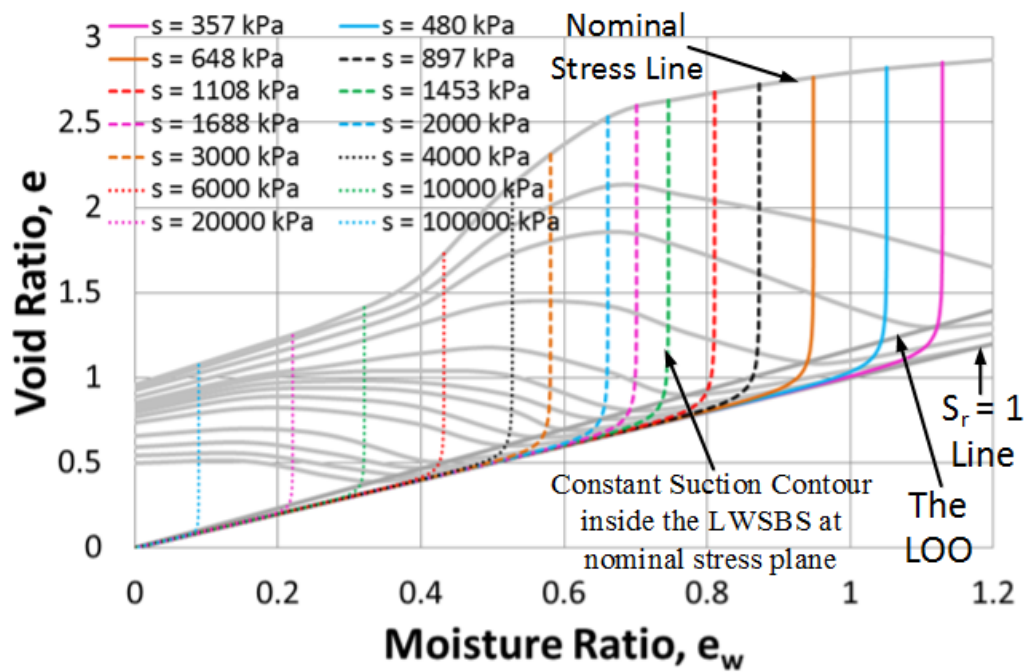
(b) Constant suction contours inside the LWSBS at the nominal stress plane
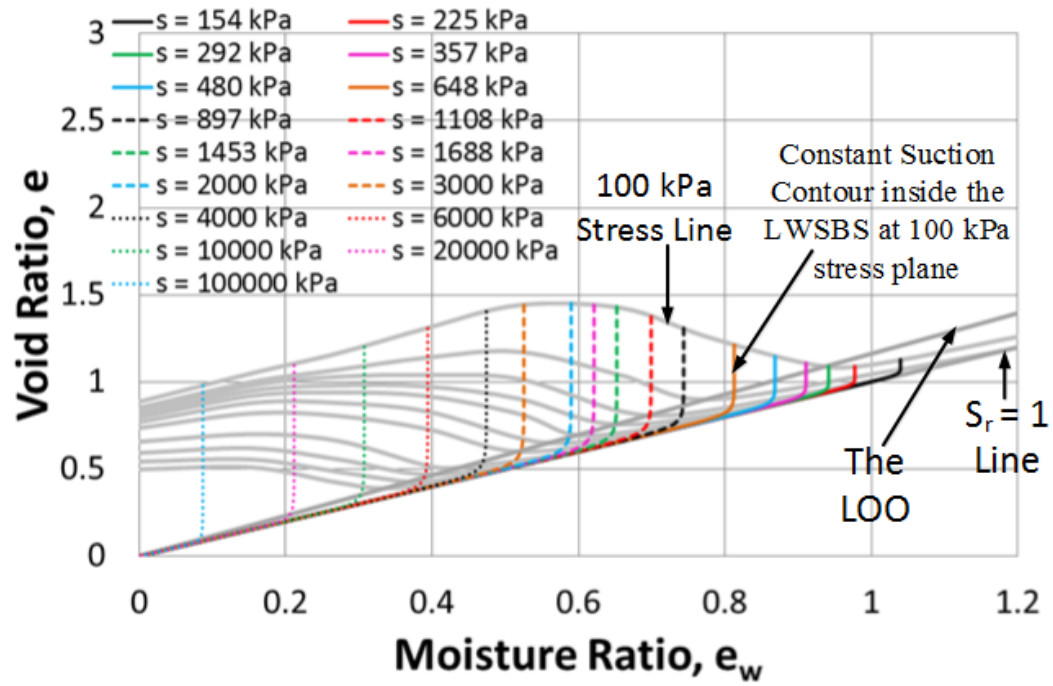
(c) Constant suction contours inside the LWSBS at the 100 kPa stress plane
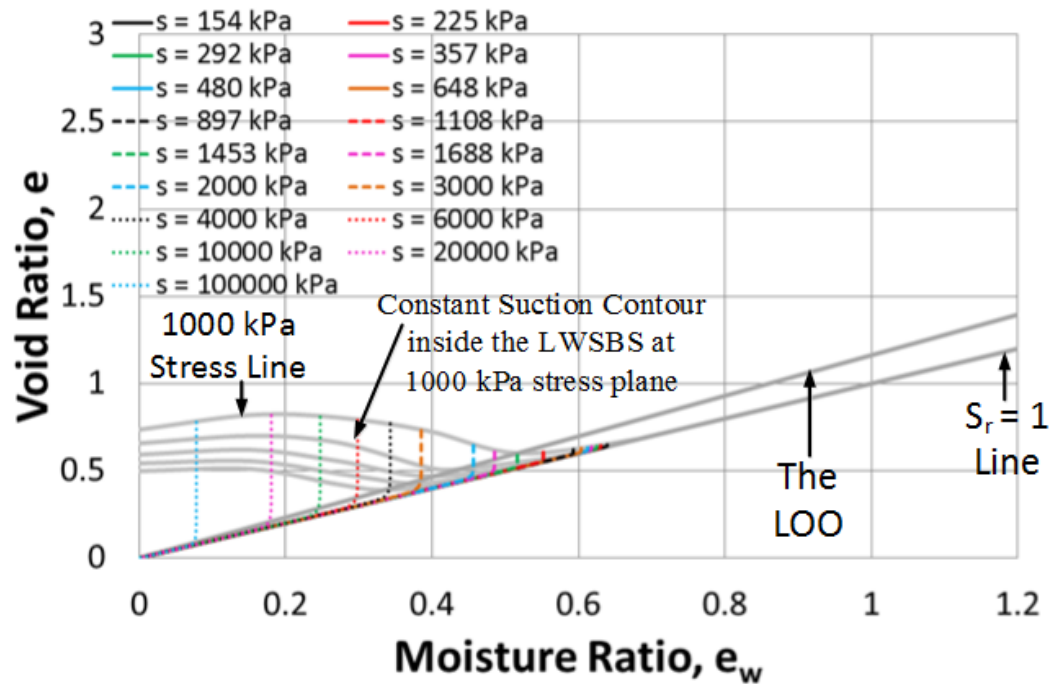
(d) Constant suction contours inside the LWSBS at the 1000 kPa stress plane
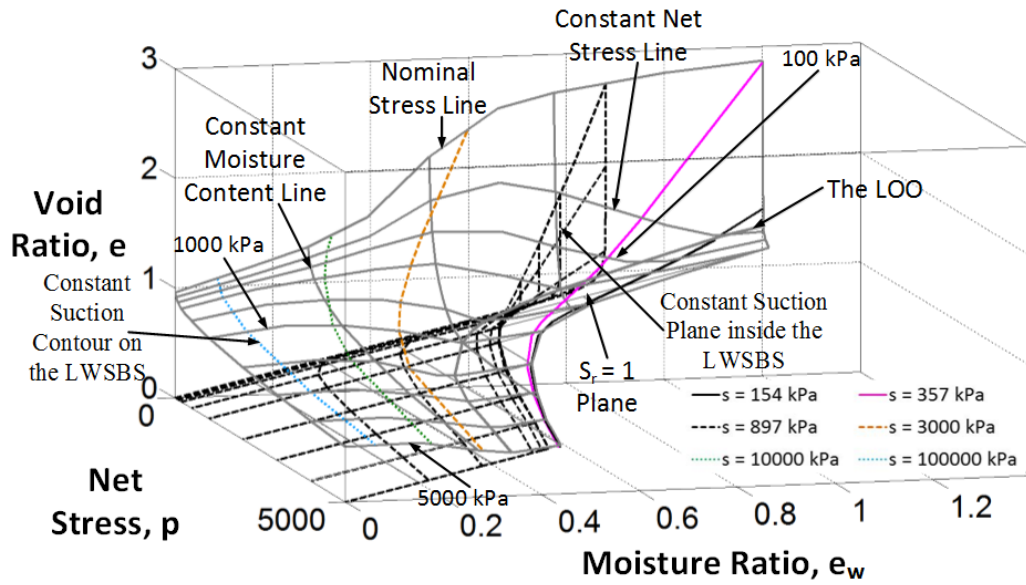
(e) 897 kPa constant suction plane inside the LWSBS in the $e - e_w - p$ space
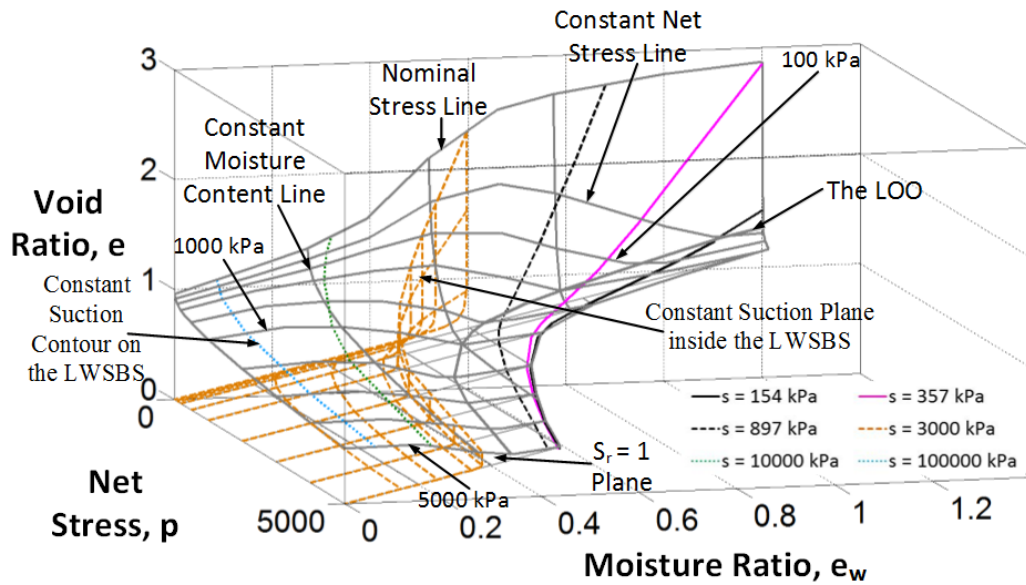
(f) 3000 kPa constant suction plane inside the LWSBS in the $e - e_w - p$ space
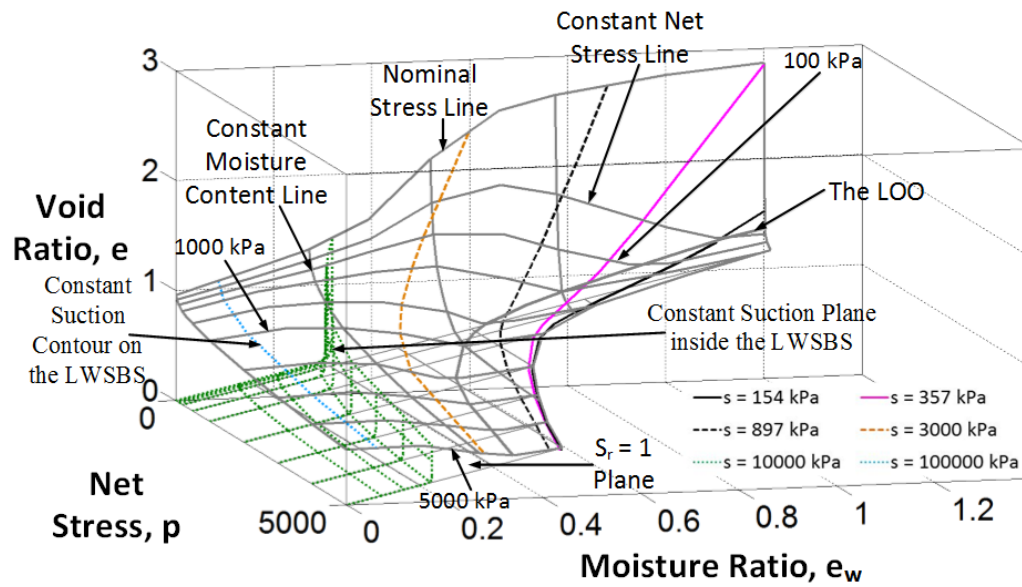
(g) 10000 kPa constant suction plane inside the LWSBS in the $e - e_w - p$ space

Figure 6-23: Constant suction contours inside the LWSBS for Merri Creek soil
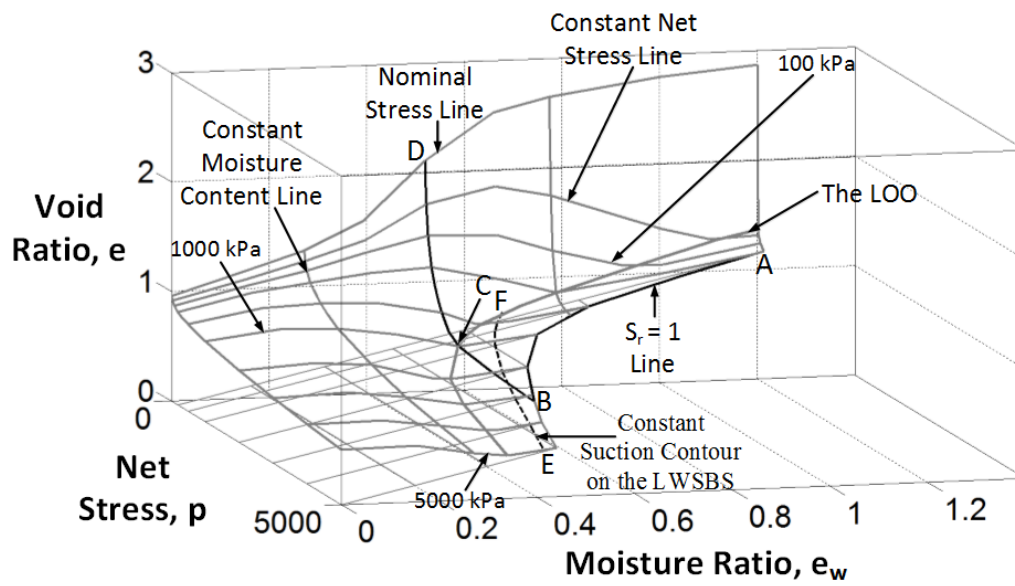
(a) Development of the constant suction contour at the wet side of the LOO on the LWSBS
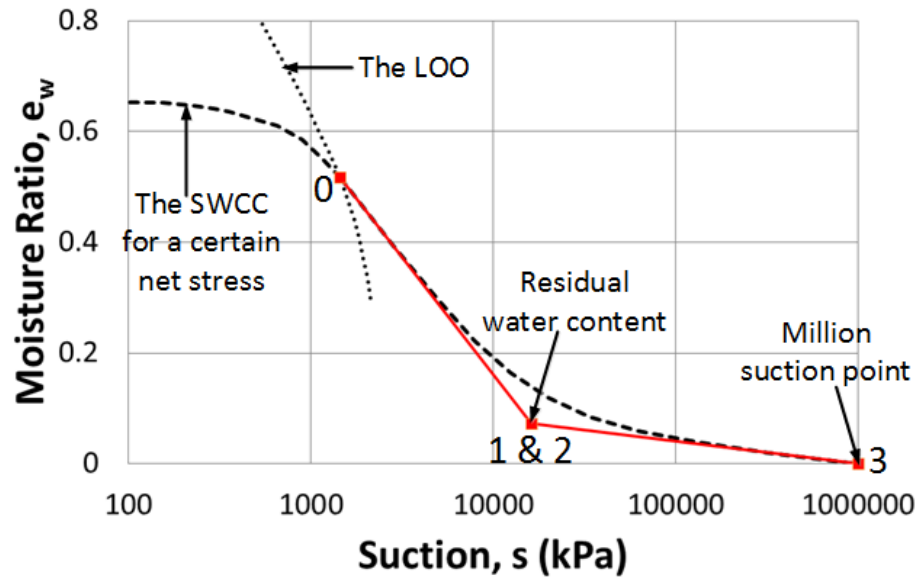
(b)
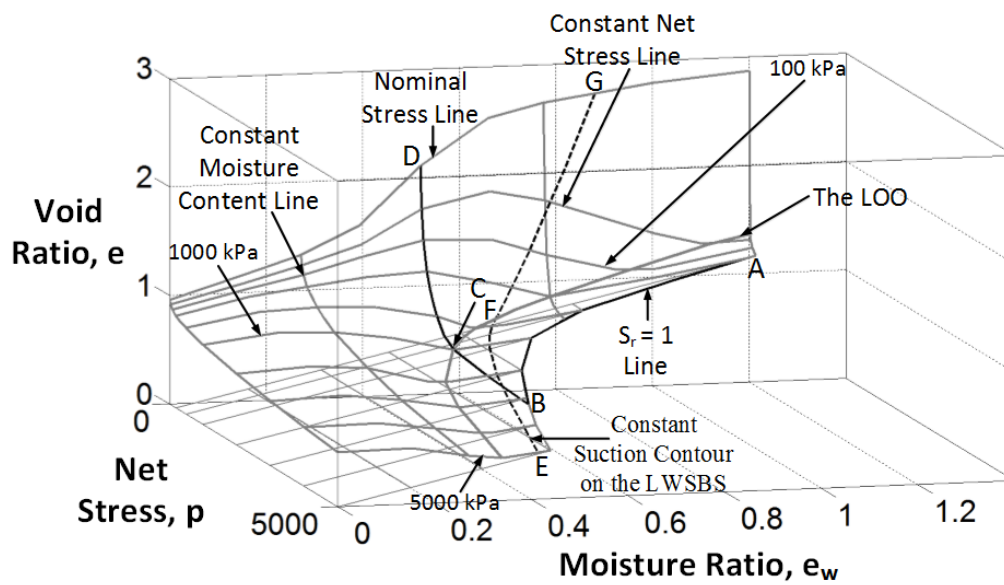
(c)

(b) & (c) Development of the constant suction contour at the dry side of the LOO on the LWSBS
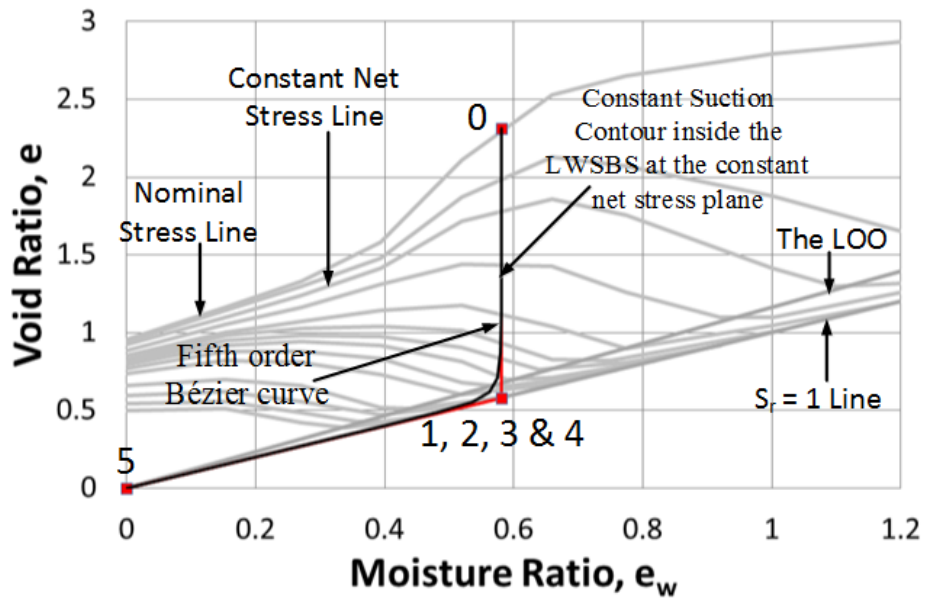
(d)
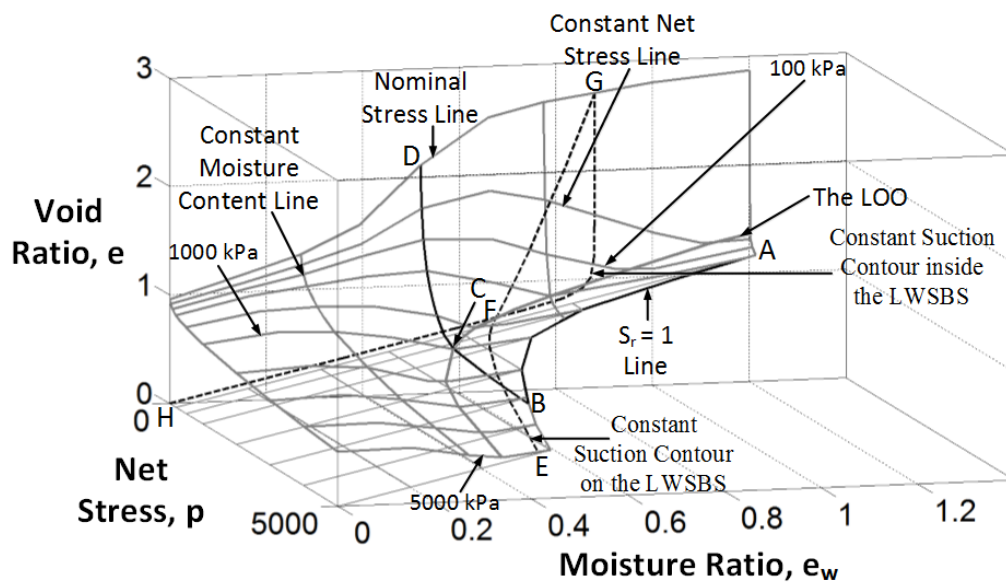
(e)

(d) & (e) Development of the constant suction contours inside the LWSBS at a constant net stress plane
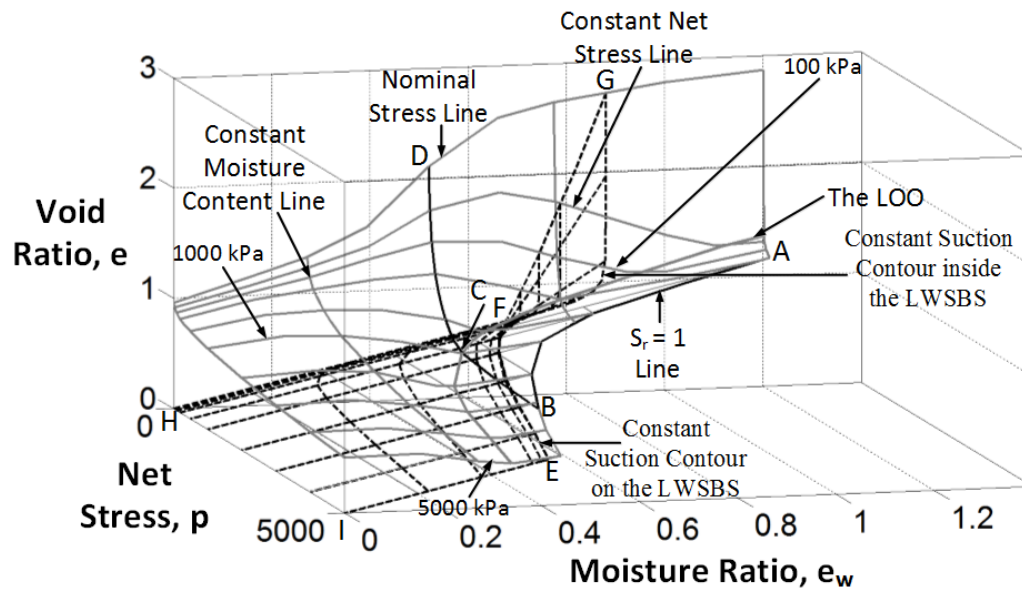
(f) Development of a constant suction plane within $e - e_w - p$ space

Figure 6-24: Summary of the development of a constant suction plane within $e - e_w - p$ space

FIELD APPLICATION OF THE MPK

FRAMEWORK

7.1 Introduction

This chapter demonstrates a conceptual field application of the Monash-Peradeniya-Kodikara (MPK) framework. In this chapter, the volumetric behaviour of a hypothetical 30 metre high embankment with different initial conditions, such as degree of saturation (i.e., $S_r = 0.7 \,\&\, 0.8$) and compaction level (high, intermediate, and moderate compaction and Standard Proctor) are modelled for major wetting events using the concept of the MPK framework for both kaolin and Merri Creek soils. Soil sample preparation techniques and other important information relevant to different compaction levels, such as compaction mould size, hammer weight, hammer fallen height, number of layers, number of blows per layer, total energy input during compaction and yield stress, were presented in Chapter 5. The LWSBSs which were developed in Chapter 5 for the kaolin and Merri Creek soils are used for modelling purpose in this chapter. Before starting the modelling of embankment problems, it is important to validate whether the MPK framework is capable of correctly predicting volumetric behaviour for major wetting events. To do this, different initial conditions (i.e. moisture content, dry density/void ratio and operational stress) for kaolin and Merri Creek soil specimens are modelled for major wetting events using the MPK framework. Subsequently, qualitative comparisons are made between the results and the experimental results of Noorany and Stanley (1994), who performed similar types of tests on soil samples collected from Villa Trinidad, San Diego, California. When major wetting events are considered for compacted unloaded unsaturated soils, it is important to quantify the hydric coefficient (α) correctly. This plays a vital role in strain calculation during major wetting events. For this reason, in the first part of this chapter, the hydric coefficient (α) is incorporated in the MPK framework. Next qualitative validation of the MPK framework for major wetting events is presented, followed by the modelling of an embankment for different initial conditions.

7.2 Hydric Coefficient

According to the MPK framework, if a compacted unsaturated clayey soil specimen is wetted under a certain constant stress to which the soil has been unloaded from a compaction stress, the state path initially experiences swelling until the interception of the LWSBS, and subsequently compression to follow the LWSBS. After compaction of the soil, wetting usually takes place, subject to a certain operational stress level less than the compaction (yield) stress. As a result, all the movements of the state paths take place in the void ratio (e) – moisture ratio (e_w) plane corresponding to operational stress. The hydric coefficient (α) can be defined as the gradient of the swelling line in ($e - e_w$) plane, here $\left(\alpha = (\frac{\partial e}{\partial e_w})_p \right)$. Researchers who have worked with the swelling behaviour of compacted unloaded soils and hydric coefficient (α) have found that the swelling line is not a straight line and the value of α is not normally a constant (c.f., Wijesooriya, 2012; Wijesooriya and Kodikara, 2012; Kodikara et al., 2014). However, for practical modelling purposes in this chapter, the swelling line is considered as a straight line on average and the value of α is considered to be a constant for simplicity. This constant hydric coefficient (α) is named the average hydric coefficient (α_{av}) for the rest of this chapter. α_{av} is calculated considering a straight line approximation between the unloaded stress point where the wetting begins and the final wetted point, which is usually very close to saturation.

7.2.1 Dependence of average hydric coefficient on state parameters

As average hydric coefficient (α_{av}) is the gradient of the swelling line of compacted unloaded soil during wetting, swelling and α_{av} should depend on the same state parameters. A number of researchers have demonstrated the influential factors of the complex soil swelling phenomenon (e.g., Holtz and Gibbs, 1956; Seed et al., 1962; Yevnin and Zaslavsky, 1970; Brackley, 1973; Morgenstern and Balasubramonian, 1980; Delage et al., 1998; Alonso et al., 2005; Monroy et al., 2007; Buzzi, 2010; Buzzi et al., 2010). They emphasize the initial water content, initial dry unit weight or void ratio, confining pressure and previous mechanical history of the soil (e.g. soil preconsolidation pressure, drying–wetting history). For modelling of major wetting events in this chapter, it is considered that α_{av} depends on the following state parameters: the initial compaction, nominal stress and operational stress conditions. Figure 7-1 shows a

possible functional relationship of the dependence of (α_{av}) on state parameters. If a soil specimen of initial moisture ratio (e_{wo}) is loaded from nominal stress (p_n) (Point A) to a certain compaction stress of p_c (Point B), and subsequently unloaded to a lower operational stress (p_o) (Point C), and if the void ratios at the compaction and operation stresses are e_c and e_o respectively, α_{av} will be a function of compaction stress (p_c), nominal stress (p_n), operational stress (p_o), compaction void ratio (e_c), operational void ratio (e_o) and initial moisture ratio (e_{wo}) when wetting proceeds from Point C, as shown in Figure 7-1. These parameters are generally required to uniquely define the current Position C within the LWSBS. Therefore, α_{av} can be written as:

$$\alpha_{av} = f(p_c, p_n, p_o, e_c, e_o, e_{wo}) \quad \dots\dots\text{Equation 7-1}$$

The compaction void ratio (e_c) and the unloading/reloading gradient (κ) are related to each other by the following equation:

$$e_o - e_c = \kappa \ln\frac{p_c}{p_o} \quad \dots\dots\text{Equation 7-2}$$

As a result, the unloading/reloading gradient (κ) can replace the compaction void ratio (e_c) and Equation 7-1 becomes:

$$\alpha_{av} = f(p_c, p_n, p_o, \kappa, e_o, e_{wo}) \quad \dots\dots\text{Equation 7-3}$$

Now, using Buckingham's π theorem, Equation 7-3 can be rewritten as:

$$\alpha_{av} = \phi\left(\frac{p_o}{p_c}, \frac{p_c}{p_n}, \kappa, e_o, e_{wo}\right) \quad \dots\dots\text{Equation 7-4}$$

Operational void ratio (e_o) and initial moisture ratio (e_{wo}) can be replaced by operational degree of saturation (S_{ro}) because $S_{ro} = \frac{e_{wo}}{e_o}$ and as a result, Equation 7-4 becomes:

$$\alpha_{av} = \phi\left(\frac{p_o}{p_c}, \frac{p_c}{p_n}, \kappa, S_{ro}\right) \quad \dots\dots\text{Equation 7-5}$$

Equation 7-5 can be rewritten as:

$$\alpha_{av} = \phi\left(\frac{p_o}{p_n}, \frac{p_c}{p_n}, \kappa, S_{ro}\right)$$ ....**Equation 7-6**

Therefore, from Equation 7-6, it can be seen that the average hydric coefficient (α_{av}) depends on the ratio of operational stress (p_o) and nominal stress (p_n), the ratio of compaction stress (p_c) and nominal stress (p_n), the gradient of unloading/reloading (κ) and the operational degree of saturation (S_{ro}). To examine the dependence of α_{av} on these state parameters, different datasets available in the literature (Sharma, 1998; Romero, 1999; Tripathy, 2000; Jotisankasa, 2005; Wijesooriya, 2012) were analysed. Unfortunately, none of these datasets was able to produce sufficient evidence, since the relevant experiments were not performed specifically for this purpose. Fortunately, a dataset by Noorany and Stanley (1994) was found in the literature which provided sufficient evidence to establish correct assumptions in relation to the relationships between α_{av} and the state parameters. The soil considered in the research by Noorany and Stanley (1994) was obtained from a construction site at Villa Trinidad, in San Diego, California. This dataset is used the following analyses.

Figure 7-2a shows the dependence of the average hydric coefficient (α_{av}) on the state parameters. Figure 7-2a presents the variation of α_{av} with operational degree of saturation (S_{ro}). It is clear that at a constant $\frac{p_c}{p_n}$, which is represented by the black line in the figure, α_{av} increases with the increase of S_{ro}. At the loose state, when water is mixed with the dry soil, soil aggregates are formed. These soil aggregates stay nearly in saturated (i.e., $S_r \approx 1.0$) state, even if on the dry side of the Line of Optimum (LOO). During compaction, these aggregates remain saturated while macro pores between the aggregates shrink, which results in reduction of the void ratio (e). On a constant $\frac{p_c}{p_n}$ line, with the increase of S_{ro}, the void ratio (e) decreases, which also means the reduction of macro pores. The change of void ratio during wetting of a compacted unloaded soil specimen is the summation of the change of void ratio due to soil aggregate expansion, and collapse due to slippage between aggregates (i.e., $\Delta e = \Delta e_{aggregare} + \Delta e_{slippage}$). As the aggregates are nearly saturated, irrespective of the operational degree of saturation, during wetting, $\frac{de_{aggregate}}{de_w} \approx 1.0$. This means that the swelling rate of

aggregates does not change much with S_{ro}. On the other hand, aggregate slippage reduces with the reduction of macro voids between the aggregates with the increase of S_{ro}. This means that $\Delta e_{slippage}$ reduces with the increase of S_{ro}. This translates to high α_{av} with the increase of S_{ro}.

Figure 7-2b shows the variation of average hydric coefficient (α_{av}) with the ratio of compaction stress and nominal stress ($\frac{p_c}{p_n}$). It is apparent that, at a constant S_{ro}, α_{av} increases with the increase of $\frac{p_c}{p_n}$. When a soil specimen is compressed from nominal stress to a certain high stress, soil aggregates compress, and then expand elastically during unloading. Subsequently, during wetting, dense soil specimens expand more than loose specimens. Furthermore, the amount of slipping at the contacts between the aggregates is less at higher $\frac{p_c}{p_n}$ values. As a result, they expand more during wetting. This translates to high α_{av} with the increase of $\frac{p_c}{p_n}$. However, when the position of the state path comes close to the LOO, plastic deformation of aggregates increases, and on the wet side of the LOO, the aggregates becomes predominantly plastic. This may lead to deviation from this pattern of behaviour.

Figure 7-2c presents the variation of α_{av} at constant operational void ratio (e_o). It is evident that for a certain e_o, α_{av} remains constant without depending on the operational degree of saturation (S_{ro}). If e_o remains constant, $\frac{p_c}{p_n}$ decreases with the increase of S_{ro}. This means that the increment of α_{av} due to the increase of S_{ro} is negated by a reduction of α_{av} due to the decrease of $\frac{p_c}{p_n}$ (i.e., $(\Delta\alpha_{av})_{S_{ro}} = -(\Delta\alpha_{av})_{\frac{p_c}{p_n}}$). Hence, this is inferred as the reason for the average hydric coefficient (α_{av}) remaining constant at a unique operational void ratio (e_o).

Based on this evidence, S_{ro} and $\frac{p_c}{p_n}$ can be replaced by e_o in Equation 7-6 and as a result, the equation becomes:

$$\alpha_{av} = \phi\left(\frac{p_o}{p_n}, e_o, \kappa\right)$$ ....**Equation 7-7**

For a specific type of soil, the unloading/reloading gradient (κ) can be considered as constant over moisture contents and stress levels, as presented in Chapter 4 for kaolin and Merri Creek soil. Alonso et al. (1990) and Wheeler and Sivakumar (1995) showed similar behaviour for κ. As a result, it is simpler to remove κ from the functional relationship of α_{av}. In addition, if nominal stress (p_n) is considered as 1 kPa, Equation 7-7 can be rewritten as:

$$\alpha_{av} = \phi(p_o, e_o)$$ ………………………………………………………..**Equation 7-8**

Therefore, based on Equation 7-8, the average hydric coefficient (α_{av}) depends primarily on the operational stress (p_o) and operational void ratio (e_o). Figure 7-2d shows the variation of α_{av} with e_o for different operational stresses (p_o) for the Noorany and Stanley (1994) dataset. It is clear that at a certain p_o, α_{av} decreases almost exponentially with the increase of e_o. It is also apparent that at a constant e_o, α_{av} decreases with the increase of p_o. Similar types of relationship are found for α_{av} with e_o and p_o based on the experimental results of the kaolin and Merri Creek soils and are presented later in this chapter.

7.2.2 Average hydric coefficient for kaolin soil

First, the average hydric coefficients (α_{av}) are calculated from the unloading/wetting state paths for the kaolin soil, as presented in Figure 7-3. Figure 7-4a shows the variation of these average hydric coefficients (α_{av}) with operational void ratio (e_o) for different operational stresses (p_o). As for the Noorany and Stanley (1994) dataset, an exponential relationship is found between α_{av} and e_o:

$$\alpha_{av} = Ae^{-ce_o}$$ ....**Equation 7-9**

In Equation 7-9, Parameter "A" varies with p_o, while c is considered to remain constant. Figure 7-4b shows the variation of Parameter "A" with p_o. Another exponential relationship is found between Parameter "A" and p_o:

$$A = ae^{-bp_o}$$ ....**Equation 7-10**

Finally, Parameter "A" is substituted in Equation 7-9, giving:

$$\alpha_{av} = ae^{-(bp_o+ce_o)}$$ ....**Equation 7-11**

In addition, from Figure 7-4a and 7-4b, the values of the constants are found to be $a = 13.774$, $b = 1.4$ and $c = 4.55$ for kaolin soil. Figure 7-4c shows the validation of Equation 7-11 using experimental data. The solid lines are drawn using the empirical equation (Equation 7-11) of α_{av}, while the points depicted by square symbols are plotted using the experimental data. It is clear that most of the data points fall on the lines developed by the empirical equation. Therefore, the developed empirical equation for α_{av} captures the pattern of behaviour and may be used for modelling purposes later in this chapter.

7.2.3 Average hydric coefficients of Merri Creek soil

Similar to the kaolin soil, the average hydric coefficients (α_{av}) of the Merri Creek soil are calculated from unloading/wetting state paths, as presented in Figure 7-5. Subsequently, these average hydric coefficients (α_{av}) are plotted against operational void ratio (e_o). Figure 7-6a shows the variation of α_{av} with e_o for different operational stresses (p_o). Similar to the kaolin soil, an exponential relationship is found between α_{av} and e_o (i.e., $\alpha_{av} = Ae^{-ce_o}$). In this case also, Parameter "A" varies with p_o, while c remains constant. Figure 7-6b presents the variation of Parameter "A" with p_o. Similar to the kaolin soil, another exponential relationship is found between Parameter "A" and p_o (i.e., $A = ae^{-bp_o}$). Finally, the final equation for α_{av} becomes, $\alpha_{av} = ae^{-(bp_o+ce_o)}$. The values of the constants are found to be $a = 29.376$, $b = 2.303$ and $c = 5.53$ from Figure 7-6a and 7-6b. Figure 7-6c shows the validation of the empirical equation of α_{av} using experimental data. The solid lines are drawn using the empirical equation of α_{av}, while the points depicted by the square symbols are plotted using the experimental data. It is evident that most of the data points fall on the empirical lines. As a result, it can be concluded that the developed empirical equation for α_{av} may be used for the modelling of Merri Creek soil, as presented later in this chapter.

7.3 Major wetting tests: Experimental versus modelling results

In this section, an analysis of strain (i.e., swelling or compression) during major wetting/flooding events is presented. First, experimental results of major wetting events are shown from Noorany and Stanley (1994), and later, modelling of major wetting tests using the MPK framework for the kaolin and Merri Creek soils is presented. In addition, the experimental results of major wetting events are explained in the light of the MPK framework, and, comparisons are made between the experimental and the modelling results.

7.3.1 Experimental results of major wetting events from Noorany and Stanley (1994)

Noorany and Stanley (1994) performed 32 flooding tests on soil collected from a construction site at Villa Trinidad in San Diego, California. Soil specimens were prepared with eight different combinations of moisture contents and unloaded dry densities. Four specimens were prepared for each moisture content and unloaded dry density and were subjected to different operational stresses before flooding. Table 7-1 presents a summary of the flooding tests performed by Noorany and Stanley (1994). The researchers found that, even if the soil specimens were flooded, the final positions of the state paths were around the LOO. This indicates that it is generally difficult for the soil specimens to absorb more water wetter than the LOO since air becomes trapped. Figure 7-7 shows the effect of dry density on swelling/compression during flooding. It is apparent that, for a certain initial moisture content, higher density soil specimens swell more and compress less, while lower density soil specimens swell less and compress more. Increased swelling of the high density soil specimens can be explained by the fact that the operational degree of saturation (S_{ro}) and the ratio of compaction stress and operational stress ($\frac{p_c}{p_o}$) are both high for high density soil specimens. As a result, the average hydric coefficient (α_{av}) and strain are also high. On the other hand, the state paths of the low density soil specimens have to wet more to reach the LOO because of the shape of the LWSBS. Consequently, they compress more during flooding. Figure 7-8 presents the effect of initial water content on swelling/compression during flooding. The initial unloaded dry density is the same for all three soil specimens. It is

clear that the soil specimens with low moisture content swell more as well as compress more. Based on the MPK framework, the state paths of the low moisture content soil specimens need to wet more to reach the LOO. Consequently, they swell and compress more than others. Figure 7-9 shows the contours of equal swell and equal compression for Villa Trinidad fill soil. It is evident that the low operational stress soil specimens swell more, while the soil specimens with high operational stress compress more.

7.3.2 Modelling of major wetting tests using the MPK framework for validation

Similar types of major wetting tests to those reported in Noorany and Stanley (1994) were analysed for kaolin and Merri Creek soils using work developed in this chapter. As explained earlier, even if the soil specimens were flooded, it is very difficult for them to absorb more water well beyond the LOO. For this reason, during modelling of major wetting tests, it is considered that the soil specimens are wetted up to the LOO. In the following section, modelling results of major wetting tests for kaolin and Merri Creek soil are presented.

7.3.2.1 Modelling of major wetting tests for the kaolin soil

Following the Noorany and Stanley (1994) experiments, a total of 60 major wetting tests were modelled for the kaolin soil. In this section it is assumed that the soil specimens were prepared with twelve different combinations of moisture contents and unloaded dry densities. It is also assumed that five specimens were prepared for each type of moisture content and unloaded dry density and subjected to different operational stresses prior to major wetting events. Table 7-2 presents a summary of major wetting tests modelled for the kaolin soil. Basic rules of the MPK framework were followed during the modelling. As all the soil specimens were considered compacted at the beginning, the state paths started from inside the LWSBS. Subsequently, during the application of operational stress, the state paths move elastically inside the LWSBS and then follow the LWSBS after intercepting it. Depending on the operational stress (p_o) and the initial dry density that is related to the compaction stress (p_c), the final position of the state path at the end of the operational stress application may be on $(p_o \geq p_c)$ or inside $(p_o < p_c)$ the LWSBS. Usually, if the operational stress is low, the state path may end up inside the LWSBS, while a high operational stress may bring the state path on the LWSBS.

However, if the initial unloaded dry density of a soil specimen is high, after the application of a high operational stress, the position of the state path may still be inside the LWSBS. During a major wetting event, if the position of the state path is on the LWSBS at the end of the operational stress application stage, compression has taken place to follow the LWSBS up to the LOO.

On the other hand, if the position of the state path is inside the LWSBS at the end of the operational stress application stage, swelling has taken place, with the gradient defined by the average hydric coefficient (α_{av}), where $\alpha_{av} = ae^{-(bp_o + ce_o)}$. Once it intercepts the LWSBS, the state path follows the LWSBS up to the LOO. In this case, the soil specimen swells when the state path is inside the LWSBS and compresses when the state path follows the LWSBS. The final strain of the soil specimen can be calculated by the summation of the swelling and compression. Nevertheless, if the operational stress is low, the state path may reach the LOO without intercepting the LWSBS. At this time, the total strain is only the swelling. This phenomenon is also possible for a high operational stress if the initial dry density of the soil specimen is also high.

Figure 7-10 shows graphs depicting the modelling of major wetting tests using the MPK framework for the kaolin soil. Figure 7-10a and 7-10b present the modelling graphs for soil specimens with 13.5 % initial moisture content ($e_{wo} = 0.358$) and 1.31 and 1.21 gm/cc unloaded dry densities respectively, subjected to major wetting at 25, 100, 250, 500 and 1000 kPa operational stresses. It is clear that all the state paths of 1.31 gm/cc unloaded dry density soil specimens swell up to the LOO during major wetting without intercepting the LWSBS, while the state paths of soil specimens with 500 and 1000 kPa operational stresses and 1.21 gm/cc unloaded dry density swell initially and then compress after intercepting the LWSBS during major wetting. Figure 7-10c shows the modelling graph for soil specimens with 13.5 % initial moisture content ($e_{wo} = 0.358$) and 1.09 gm/cc unloaded dry density, subjected to major wetting at 25, 100, 250, 500 and 1000 kPa operation stresses. It is apparent that the state path of 25 kPa operational stress swells up to the LOO during major wetting, while the state paths of the soil specimens of 100, 250 and 500 kPa operational stresses swell initially and then compress after intercepting the LWSBS during major wetting. On the other hand, the state path of 1000 kPa operational stress shows compression from the beginning of the major wetting,

because the location of the state path at the end of the operational stress application is already on the LWSBS.

Figure 7-10d, 7-10g and 7-10j present the modelling graphs for the soil specimens with 1.31 gm/cc unloaded dry density and 18.5 % (e_{wo} = 0.490), 21.0 % (e_{wo} = 0.557) and 23.5 % (e_{wo} = 0.623) initial moisture contents respectively. The specimens were subjected to major wetting at 25, 100, 250, 500 and 1000 kPa operational stresses. It is clear that all the state paths of the soil specimens swell up to the LOO during major wetting without intercepting the LWSBS. This phenomenon is consistent with the statement made earlier, that if the initial dry density of the soil specimen is high, the state path may never intercept the LWSBS during major wetting. Figure 7-10e, 7-10h and 7-10k show the modelling graphs for the soil specimens with 1.21 gm/cc unloaded dry density and 18.5 % (e_{wo} = 0.490), 21.0 % (e_{wo} = 0.557) and 23.5 % (e_{wo} = 0.623) initial moisture contents accordingly. The specimens were subjected to major wetting at 25, 100, 250, 500 and 1000 kPa operational stresses. It is apparent that the state paths of 25, 100 and 250 kPa operational stress swell up to the LOO during major wetting, while the state paths of the soil specimens with 500 kPa operational stress initially show swelling and then compression after intercepting the LWSBS during major wetting. In addition, the state paths of 1000 kPa operational stress show compression from the beginning of the major wetting because, at the end of the operational stress application, the locations of the state paths are entirely on the LWSBS.

Figure 7-10f, 7-10i and 7-10l present the modelling graphs for the soil specimens with 1.09 gm/cc unloaded dry density and 18.5 % (e_{wo} = 0.490), 21.0 % (e_{wo} = 0.557) and 23.5 % (e_{wo} = 0.623) initial moisture contents, respectively. The specimens were subjected to major wetting at 25, 100, 250, 500 and 1000 kPa operational stresses. It is evident that the state paths of 25 kPa operational stress show swelling up to the LOO during major wetting, while the state paths of the soil specimens with 100 and 250 kPa operational stresses initially show swelling and then compression after intercepting the LWSBS during major wetting. On the other hand, the state paths with 500 and 1000 kPa operational stresses show compression from the beginning of the major wetting, because the locations of the state paths at the end of the operational stress application are on the LWSBS.

7.3.2.2 Modelling of major wetting tests for the Merri Creek soil

Similar to the kaolin soil test program, a total 45 major wetting tests were modelled for Merri Creek soil. It was assumed that the soil specimens were prepared with nine different combinations of moisture contents and unloaded dry densities. It was also assumed that five specimens were prepared for each moisture content and unloaded dry density, and subjected to different operational stresses prior to major wetting events. Table 7-3 shows a summary of the major wetting tests modelled on the Merri Creek soil. Following the same approach as for the kaolin soil, basic rules of the MPK framework were applied during the modelling. First, the state paths of the soil specimens start from inside the LWSBS. Subsequently, during the application of operational stress, the state paths move elastically inside the LWSBS and then follow the LWSBS after its interception. Depending on the operational stress (p_o) and initial dry density, which is related to the compaction stress (p_c), the final position of the state path at the end of the operational stress application may be on ($p_o \geq p_c$) or inside ($p_o < p_c$) the LWSBS. During major wetting events, if the position of the state path is inside the LWSBS at the end of the operational stress application stage, swelling takes place with the gradient defined by the average hydric coefficient (α_{av}), where $\alpha_{av} = ae^{-(bp_o+ce_o)}$, and then the state path follows the LWSBS after intercepting it up to the LOO. In this case, the soil specimen swells when the state path is inside the LWSBS and compresses when the state path follows the LWSBS. The final strain of the soil specimen can be calculated by the summation of the swelling and the compression.

On the other hand, if the position of the state path is on the LWSBS at the end of the operational stress application stage, compression takes place during major wetting because the state path follows the LWSBS up to the LOO. Finally, if the amount of operational stress applied is low, the state path may reach the LOO without intercepting the LWSBS. In that case, the total strain is only due to swelling. This can also happen for high operational stresses if the initial dry density of the soil specimen is also high.

Figure 7-11 shows the modelling graphs for major wetting tests using the MPK framework for the Merri Creek soil. Figure 7-11a and 7-11d present the modelling graphs for the soil specimens of 1.28 gm/cc unloaded dry density and 11.0 % ($e_{wo} = 0.288$) and 15.0 % ($e_{wo} = 0.393$) initial moisture contents respectively. The specimens

were subjected to major wetting at 25, 100, 200, 300 and 500 kPa operational stresses. It is clear that the state paths of 25, 100 and 200 kPa operational stresses swell up to the LOO during major wetting, while the state paths for the soil specimens of 300 and 500 kPa operational stresses swell initially and then compress after intercepting the LWSBS during major wetting. Figure 7-11g shows the modelling graph of 19.0 % ($e_{wo} = 0.498$) initial moisture content and 1.28 gm/cc unloaded dry density soil specimens subjected to major wetting at 25, 100, 200, 300 and 500 kPa operational stresses. It is apparent that the state paths of 25, 100, 200 and 300 kPa operational stresses swell up to the LOO during major wetting, while the state path for the soil specimen of 500 kPa operational stress swells initially and then compresses after intercepting the LWSBS during major wetting.

Figure 7-11 b, 7-11e and 7-11h present the modelling graphs for the soil specimens of 1.16 gm/cc unloaded dry density and 11.0 % ($e_{wo} = 0.288$), 15.0 % ($e_{wo} = 0.393$) and 19.0 % ($e_{wo} = 0.498$) initial moisture contents respectively. The specimens were subjected to major wetting at 25, 100, 200, 300 and 500 kPa operational stresses. It is evident that the state paths of 25 and 100 kPa operational stress show swelling up to the LOO during major wetting, while the state paths for the soil specimens of 200 and 300 kPa operational stresses initially show swelling and then compression after intercepting the LWSBS during major wetting. On the other hand, the state paths for soil specimens with 500 kPa operational stresses and 15.0% and 19.0% moisture content show compression from the beginning of the major wetting, because at the end of the operational stress application, the locations of the state are on the LWSBS.

Figure 7-11c, 7-11f and 7-11i show the modelling graphs for soil specimens with 1.10 gm/cc unloaded dry density and 11.0 % ($e_{wo} = 0.288$), 15.0 % ($e_{wo} = 0.393$) and 19.0 % ($e_{wo} = 0.498$) initial moisture contents respectively, subjected to major wetting at 25, 100, 200, 300 and 500 kPa operational stresses. It is clear that the state paths of 25 kPa operational stress show swelling up to the LOO during major wetting, while the state paths for the soil specimens of 100 and 200 kPa operational stresses initially show swelling and then compression after intercepting the LWSBS during major wetting. In addition, the state paths for soil specimens with 300 and 500 kPa operational stresses and 15.0% and 19.0% moisture content show compression from the beginning of the major

wetting, because the locations of the states at the end of the operational stress application are on the LWSBS.

7.3.3 Comparison of the modelling results with experimental results from the research literature

Using the modelling results, graphs similar to those presented by Noorany and Stanley (1994) showing the effect of moisture content and dry density on swelling/compression during major wetting events and the contours of equal swell and equal compression were generated for the kaolin and Merri Creek soils. Subsequently, comparisons were made between the experimental and modelling results to show the effectiveness of the MPK framework for predicting the volumetric behaviour of compacted unsaturated soils.

7.3.3.1 Comparison using kaolin soil modelling results

Graphs similar to those presented by Noorany and Stanley (1994) were generated using the modelling results of kaolin soil. Figure 7-12 shows the effect of dry density on swelling/compression during major wetting. It is clear that for a certain moisture content, high density soil specimens swell more and compress less, while low density soil specimens swell less and compress more. This behaviour is qualitatively similar to the experimental results presented by Noorany and Stanley (1994) in Figure 7-7. One quantitative difference is that in Noorany and Stanley's (1994) results, swelling is observed at relatively low operational stresses (substantially lower than 100 kPa), whereas for the modelled results, much less swelling may be expected at such low stress levels. This can be explained with the aid of the empirical equation of the average hydric coefficient (α_{av}), where $\alpha_{av} = ae^{-(bp_o+ce_o)}$. The difference in swelling strain increases lower than 100 kPa operational stresses occurs due to the rate of increase of α_{av} as the operational stress is reduced. If a compacted soil specimen is loaded from nominal stress (p_n) to a certain operational stress (p_o), the void ratio starts to decrease in the elastic space by the unloading/reloading gradient (κ). In the α_{av} equation, if p_o increases and e_o decreases, the value of α_{av} may increase or decrease, depending on the relative values of the a and b parameters. If, however, the value of κ of a particular type of soil is high, the change of e_o becomes significantly higher than the change of p_o at low stress levels. Therefore, higher α_{av} can be expected at low operational stress. However, with

the increase of the operational stress, the change of p_o dominates over the change of e_o and as a result, both α_{av} and, in turn, swelling strain decrease.

Figure 7-13 presents the effect of initial moisture content on swelling/compression during major wetting. It is clear that the soil specimens with low moisture content swell more at low operational stresses (see Figure 7-13a and 7-13b), and compress more at high operational stresses (see Figure 7-13b). This behaviour is also similar to the experimental results obtained by Noorany and Stanley (1994) shown in Figure 7-8. It can be explained from the MPK framework that the state paths with low moisture content soil specimens need to wet more to reach the LOO. This is the reason why they both swell and compress more than others. Figure 7-14 shows the contours of equal swell or equal compression for kaolin soil for different vertical stresses on the dry density-moisture content and void ratio-moisture ratio planes. It is apparent that at low operational stresses, soil swells more, while soils with high operational stresses undergo more compression. This behaviour is qualitatively identical to the experimental results presented by Noorany and Stanley (1994), as shown in Figure 7-9.

7.3.3.2 Comparison using Merri Creek soil modelling results

Similar graphs as for the kaolin soil above were generated using the modelling results for the Merri Creek soil. Figure 7-15 shows the effect of dry density on swelling/compression during major wetting. It is apparent that for certain moisture contents, low density soil swells less at low operational stresses and compresses more at high operational stresses, whereas the opposite is true for high density soils. This behaviour is qualitatively identical to the experimental results obtained by Noorany and Stanley (1994).

Figure 7-16 presents the effect of initial moisture content on swelling/compression during major wetting. It is clear that, similar to kaolin soil, soil with low moisture content swells more as well as compresses more. This behaviour is also similar to the experimental results obtained by Noorany and Stanley (1994).

7.4 Modelling of an embankment problem for major wetting events using the MPK framework

The volumetric behaviour of a 30 metre high embankment was conceptually modelled and subjected to major wetting events using the concept of the MPK framework for different initial conditions. Both kaolin and Merri Creek soil were considered in the modelling. Eight different initial conditions were assumed, based on the compacted degrees of saturation ($S_r = 0.7 \& 0.8$) and compaction levels (high, intermediate and moderate compaction, and Standard Proctor) for each soil type. The preparation of these dynamically compacted soil samples and other relevant information on different compaction levels (compaction mould size, hammer weight, hammer fallen height, number of layers, number of blows per layer, total energy input during compaction, yield stress) have been presented in Chapter 5. The LWSBSs developed in Chapter 5 for dynamically compacted kaolin and Merri Creek soils were used for modelling. The results of Noorany and Stanley's (1994) experiments revealed that, even if the soil specimens were flooded, it was very difficult for them to absorb more water beyond the LOO. For this reason, for the modelling of major wetting events, it was considered that the soil was wetted up to the LOO. For the analysis, the 30 metre high embankment was divided into ten equal sub-layers, each 3 metres in depth. Figure 7-18 shows the schematic drawing of the 30 embankment. During modelling, all the relevant parameters, such as operational stress, operational void ratio and strain were calculated at the centre of each sub-layer. In the following section, modelling of major wetting events on the embankment is presented using the MPK framework for the kaolin and Merri Creek soils.

7.4.1 The embankment made of kaolin soil

A total of eight different initial conditions were considered on the basis of the compacted degrees of saturation ($S_r = 0.7 \& 0.8$) and compaction levels (high, intermediate and moderate compaction and Standard Proctor) for the kaolin soil. Figure 7-19 shows the graphs depicting modelling of the major wetting events for the embankment using the MPK framework for kaolin soil. Point C presents the compaction state which is on the LWSBS, while Point U shows unloading to the nominal stress point, which is inside the LWSBS. On the UC line, other points represent the states corresponding to increasing operational stresses for different sub-layers from top to bottom. Figure 7-19a presents the

modelling for major wetting of the embankment prepared using high compaction and compacted to $S_r = 0.7$. It is clear that the state paths of all sub-layers swell up to the LOO during wetting. None of the state paths intercepts the LWSBS under this condition. Table 7-4 shows the swelling deformations for different sub-layers of the embankment during major wetting events.

Figure 7-19b presents the modelling graph for major wetting of the embankment constructed using intermediate compaction and compacted to $S_r = 0.7$. It is evident that in this case also the state paths of the entire sub-layers swell up to the LOO during wetting. Figure 7-19c and 7-19d present the modelling for major wetting of the embankments constructed by Standard Proctor and moderate compaction respectively and compacted to $S_r = 0.7$. It is apparent that the bottom two sub-layers of the Standard Proctor embankment and the bottom four sub-layers of the moderate compaction embankment intercept the LWSBS during wetting. The state paths of these sub-layers compress or undergo collapse after the interception of the LWSBS. It is evident from Table 7-4 that the overall deformation is in compression for the bottom sub-layer of the embankment with Standard Proctor compaction, while for the embankment with moderate compaction, the bottom three sub-layers experience overall compression.

Figure 7-19e, 7-19f and 7-19g present the modelling for major wetting of the embankments constructed using high and intermediate compaction and Standard Proctor respectively and compacted to $S_r = 0.8$. It is clear that in all cases, the state paths of the entire sub-layers show swelling up to the LOO during wetting. It is also apparent from Table 7-4 that all the sub-layers of these embankments swell during major wetting and the total deformations are also swelling. Figure 7-19h presents the modelling for major wetting of the embankment constructed using moderate compaction and compacted to $S_r = 0.8$. It is evident that only the bottom sub-layer intercepts the LWSBS during wetting. It is also apparent from Table 7-4 that the overall deformation of this sub-layer is in compression.

The effect of the compaction levels and the degree of saturation on the swelling/compression of different sub-layers and the total deformation of the embankments during major wetting events were analysed for kaolin soil. Figure 7-20

shows the effect of compaction levels on swelling/compression with the depth of the embankment during major wetting events. It is clear that for a certain compacted degree of saturation, swelling of the top sub-layers increases with increasing compaction. This can be explained by the fact that if the ratio of compaction stress and operational stress ($\frac{p_c}{p_o}$) increases, both the average hydric coefficient (α_{av}) and the strain increase. It is also apparent that for all compaction levels, swelling decreases with depth. This happens because $\frac{p_c}{p_o}$, α_{av} and strain decrease with the increase of operational stress as a result of the increase of the depth within the embankment. It is also evident that compression takes place in a few of the bottom layers of the embankments with Standard Proctor and moderate compaction, while for embankments with high and intermediate compaction, no compression is found in any of the sub-layers. As the compaction energy is relatively low embankments with Standard Proctor and moderate compactions, the state paths of different sub-layers for these embankments are closer to the LWSBS than the other two compaction embankments. Therefore, interception of the LWSBS takes place for some of the bottom layers of embankments with Standard Proctor and moderate compaction, which, in turn, translates to the compression of these layers.

Figure 7-21 presents the effect of degree of saturation on swelling/compression with the depth of the embankment during major wetting events. It is clear that for a certain compaction level, an embankment with lower degree of saturation, meaning generally lower moisture, content swells more at low stresses, and compresses more at high stresses. This can be explained using the MPK framework. The state paths of the sub-layers of the embankment with low saturation need to travel more to reach the LOO. As a result, they swell and compress more than others. Figure 7-22 shows the effect of compaction level and the degree of saturation on the total deformation of the embankment during major wetting events for kaolin soil. It is apparent that for a certain compaction level, total deformation decreases with the increase of the degree of saturation. This can be explained by the fact that the state paths of the sub-layers of embankments with high saturation need to travel less to reach the LOO. As a result, total deformation is less for embankments with high degrees of saturation. It is also evident that the rate of reduction of total deformation over compaction level is high for embankments with low degrees of saturation. As explained earlier, the state paths of the sub-layers of an embankment with a low degree of saturation need to travel more to

reach the LOO. Therefore, when the bottom layers of the moderately compacted embankment intercept the LWSBS, they can compress more due to the shape of the LWSBS to reach the LOO. This translates to a low total deformation for an embankment with moderate compaction and a low degree of saturation. It is also clear that for a certain degree of saturation, total heave of the embankment increases with increasing compaction effort. This behaviour matches with the results from the literature (see Alonso et al., 1990; Wheeler and Sivakumar, 1995; Thom et al., 2007; Sivakumar et al., 2010; Boyd and Sivakumar, 2011).

7.4.2 The embankment made of Merri Creek soil

Similar to the kaolin testing program, eight different initial conditions were considered on the basis of the compacted degrees of saturation ($S_r = 0.7$ & 0.8) and compaction levels (high, intermediate and moderate compaction and Standard Proctor) for the Merri Creek soil. Figure 7-23 presents the modelling for major wetting events of the embankment using the MPK framework for the Merri Creek soil. On the UC line, Points C and U show the compaction point which is on the LWSBS and unloading to the nominal stress point, which is inside the LWSBS respectively, while other points present operational stresses at different sub-layers, increasing from top to bottom. Figure 7-23a and 7-23b present the modelling for major wetting of embankments constructed using high and intermediate compaction levels respectively and compacted to $S_r = 0.7$. It is clear that in both cases, the state paths of all the sub-layers show swelling up to the LOO during wetting. Table 7-5 shows the deformations for different sub-layers of the embankment during major wetting events for the Merri Creek soil. It is also apparent that all the sub-layers of both embankments swell during major wetting and the total deformations are also swelling. Figure 7-23c and 7-23d present the modelling for major wetting of the embankments constructed with Standard Proctor and moderate compaction levels respectively and compacted to $S_r = 0.7$. It is evident that the bottom two sub-layers of the embankment with Standard Proctor compaction and the bottom four sub-layers of the embankment with moderate compaction intercept the LWSBS during wetting. The state paths of these sub-layers show compression after the interception of the LWSBS. It is apparent from Table 7-5 that the overall deformation is in compression for the bottom sub-layer of the embankment with Standard Proctor

compaction, while for the embankment with moderate compaction, the bottom two sub-layers experience overall compression.

Figure 7-23e, 7-23f and 7-23g show the modelling for major wetting of the embankments constructed using high, intermediate and Standard Proctor compaction levels respectively and compacted to $S_r = 0.8$. It is clear that in all cases, the state paths of all the sub-layers swell up to the LOO during wetting. It is also evident from Table 7-5 that all the sub-layers of these embankments swell during major wetting and the total deformations are also swelling. Figure 7-23h presents the modelling graph for major wetting of the embankment constructed using moderate compaction and compacted to $S_r = 0.8$. It is apparent that only the bottom sub-layer intercepts the LWSBS during wetting. It is also evident from Table 7-5 that the overall deformation of this sub-layer is in compression.

Similar to kaolin soil, the effect of compaction level and degree of saturation on the swelling/compression of different sub-layers and the total deformation of the embankments during major wetting events were analysed for Merri Creek soil. Figure 7-24 presents the effect of compaction levels on swelling/compression with the depth of the embankment during major wetting events. It is apparent that for a certain compacted degree of saturation, swelling of the top sub-layers increases with increased compaction. This can be explained by the fact that if the ratio of compaction stress and operational stress $(\frac{p_c}{p_o})$ increases, both the average hydric coefficient (α_{av}) and strain increase. It is also evident that for all compaction levels, swelling decreases with depth. This happens because $\frac{p_c}{p_o}$, α_{av} and strain decrease with the increase of operational stress as a result of the increase of the depth within the embankment. However, if the compaction of the embankment is high, swelling strain increases with depth in the shallow depth zone. This can be explained by the empirical equation of the average hydric coefficient (α_{av}), where $\alpha_{av} = ae^{-(bp_o+ce_o)}$. Because of the value of the unloading/reloading gradient (κ) is high for Merri Creek soil, in the $\alpha_{av} = ae^{-(bp_o+ce_o)}$ equation, the change of e_o becomes significantly higher than the change of p_o in the shallow depth zone where the level of the operational stress is low. Therefore, the value of α_{av} and swelling strain increases with depth in the shallow depth zone. Nevertheless, with the increase of depth, the operational stress level also increases, giving rise to the

reduction of both α_{av} and the swelling strain. It is also apparent that compression takes place in a few of the bottom layers of embankments with Standard Proctor and moderate compactions, while no compression is found in any of the sub-layers of embankments with high and intermediate compactions. As the compaction efforts are less for embankments with Standard Proctor and moderate compactions, the state paths of different sub-layers of these embankments are closer to the LWSBS than for the other two compaction embankments. Therefore, the interception of the LWSBS takes place for a few of the bottom layers of embankments with Standard Proctor and moderate compactions, which results in compressive deformation.

Figure 7-25 shows the effect of degree of saturation on swelling/compression with the depth of the embankment during major wetting events. It is apparent that for a certain compaction level, an embankment with lower degree of saturation swells more at lower stresses, and compresses more at higher stresses. The explanation for this behaviour is similar to the explanation given earlier for embankments with kaolin soil. Figure 7-26 shows the effect of compaction level and degree of saturation on the total deformation of the embankment during major wetting events for Merri Creek soil. It is evident that for a certain compaction level, total deformation decreases with the increase of degree of saturation. This can be explained by the fact that the state paths of the sub-layers of an embankment with a high degree of saturation need to travel less to reach the LOO. As a result, the total deformation is less for an embankment with a higher degree of saturation. It is also apparent that the rate of reduction of total deformation over compaction level is high for embankments with low degrees of saturation. This translates to the low total deformation of moderate compaction embankments for low degrees of saturation. It is also clear that for a certain degree of saturation, total heave of the embankment increases with increasing compaction effort. This behaviour matches with the results from the literature (see Alonso et al., 1990; Wheeler and Sivakumar, 1995; Thom et al., 2007; Sivakumar et al., 2010; Boyd and Sivakumar, 2011).

7.5 Discussion

In this chapter, a large number of tests and field scenarios were modelled using the MPK framework on compacted unsaturated kaolin and Merri Creek soil for major wetting events. The obtained results were then compared with the experimental results from

Noorany and Stanley (1994). The results show that with the extensions developed in this chapter, the performance of the MPK framework in predicting the volumetric behaviour of compacted unsaturated soil is very encouraging. The complex experimental results of the volumetric behaviour due to major wetting events are easily explainable with the help of the MPK framework. Although it is important to know the compaction stress of a compacted fill, operational stress is the most important parameter on which most of the volumetric behaviour of compacted unsaturated soil depends. Some other important factors which control the strain during major wetting events are the position of the LWSBS and the gradient (as depicted by the hydric coefficient) of the swelling during wetting. The gradient of swelling during wetting of compacted unsaturated soil depends on various parameters, as established in this chapter. On the basis of the observed behaviour and using the principles of the MPK framework, a simplified equation was developed which has only two parameters, operational stress (p_o) and operational void ratio (e_o). Based on the findings of this chapter, it now appears possible to predict volumetric behaviour during major wetting events by knowing the position of the LWSBS and the equation of the gradient of swelling during wetting, which can be found by conducting fairly simple laboratory tests.

7.6 Conclusion

This chapter was dedicated to the field applicability of the MPK framework. A significant number of tests and field scenarios were modelled using the MPK framework on compacted unsaturated kaolin and Merri Creek soils for major wetting events. Data from the research literature were used to validate the modelling results. A simplified equation was developed to compute the gradient of swelling during wetting of compacted unsaturated soil. Since major wetting is one scenario that needs to be evaluated in field conditions, a practically useful approach was established to predict volumetric behaviour during major wetting events in field-scale problems.

Table 7-1: A summary of major wetting/flooding tests performed by Noorany and Stanley (1994)

Initial Moisture Content	Unloaded Dry Density (pcf, kN/m³)	Operational Stress (ksf, kPa)	Comment on Wetting
8%	113.1, 17.77	0.506, 24	Flooding
		2.055, 98	
		5.086, 243	
		10.244, 490	
	106.7, 16.76	0.507, 24	
		2.042, 98	
		4.126, 197	
		8.184, 392	
11%	119.4, 18.76	0.517, 25	
		2.052, 98	
		5.098, 244	
		9.195, 440	
	113.1, 17.77	0.425, 20	
		2.051, 98	
		5.081, 243	
		9.194, 440	
	106.7, 16.76	0.499, 24	
		2.065, 99	
		5.093, 244	
		9.233, 442	
13.6%	119.4, 18.76	0.495, 24	
		2.066, 99	
		5.111, 245	
		8.141, 390	
	112.9, 17.74	0.480, 23	
		2.065, 99	
		5.094, 244	
		8.153, 390	
	106.7, 16.76	0.524, 25	
		2.093, 100	
		5.087, 244	
		8.186, 392	

Table 7-2: A summary of major wetting tests modelled on kaolin soil

Initial Moisture Content	Unloaded Dry Density (gm/cc, kN/m^3)	Operational Stress (kPa)	Comment on Wetting
13.5%	1.31, 12.85	25	Up to the LOO
		100	
		250	
		500	
		1000	
	1.21, 11.87	25	
		100	
		250	
		500	
		1000	
	1.09, 10.69	25	
		100	
		250	
		500	
		1000	
18.5%	1.31, 12.85	25	
		100	
		250	
		500	
		1000	
	1.21, 11.87	25	
		100	
		250	
		500	
		1000	
	1.09, 10.69	25	
		100	
		250	
		500	
		1000	
21.0%	1.31, 12.85	25	
		100	
		250	
		500	
		1000	
	1.21, 11.87	25	

		100	
		250	
		500	
		1000	
	1.09, 10.69	25	
		100	
		250	
		500	
		1000	
23.5%	1.31, 12.85	25	
		100	
		250	
		500	
		1000	
	1.21, 11.87	25	
		100	
		250	
		500	
		1000	
	1.09, 10.69	25	
		100	
		250	
		500	
		1000	

Table 7-3: A summary of major wetting tests modelled on Merri Creek soil

Initial Moisture Content	Unloaded Dry Density (gm/cc, kN/m^3)	Operational Stress (kPa)	Comment on Wetting
11.0%	1.28, 12.56	25	Up to the LOO
		100	
		200	
		300	
		500	
	1.16, 11.38	25	
		100	
		200	
		300	
		500	
	1.10, 10.79	25	
		100	
		200	
		300	
		500	
15.0%	1.28, 12.56	25	
		100	
		200	
		300	
		500	
	1.16, 11.38	25	
		100	
		200	
		300	
		500	
	1.10, 10.79	25	
		100	
		200	
		300	
		500	
19.0%	1.28, 12.56	25	
		100	
		200	
		300	
		500	
	1.16, 11.38	25	

		100	
		200	
		300	
		500	
	1.10, 10.79	25	
		100	
		200	
		300	
		500	

Table 7-4: Deformations at different layers of the embankment made of kaolin soil for different initial conditions during major wetting events

S_r	0.7				0.8			
Compaction Level	HC	IC	SP	MC	HC	IC	SP	MC
Layer 1 Deformation (mm)	86	56	40	32	71	45	33	27
Layer 2 Deformation (mm)	88	58	41	33	67	42	31	25
Layer 3 Deformation (mm)	84	55	39	32	62	38	28	22
Layer 4 Deformation (mm)	80	52	37	30	56	35	25	20
Layer 5 Deformation (mm)	75	49	35	28	50	31	22	18
Layer 6 Deformation (mm)	69	46	33	26	46	28	20	16
Layer 7 Deformation (mm)	64	42	31	13	42	26	18	15
Layer 8 Deformation (mm)	59	40	29	-26	37	23	16	13
Layer 9 Deformation (mm)	55	37	2	-52	34	21	15	12
Layer 10 Deformation (mm)	52	34	-19	-79	31	19	14	-3
Total Deformation (mm)	712	469	267	38	495	307	222	165

Table 7-5: Deformations at different layers of the embankment made of Merri Creek soil for different initial conditions during major wetting events

S_r	0.7				0.8			
Compaction Level	HC	IC	SP	MC	HC	IC	SP	MC
Layer 1 Deformation (mm)	256	163	107	79	264	166	105	76
Layer 2 Deformation (mm)	291	179	114	83	288	171	103	71
Layer 3 Deformation (mm)	276	168	107	78	264	151	90	61
Layer 4 Deformation (mm)	248	152	97	71	227	129	76	51
Layer 5 Deformation (mm)	216	134	86	63	186	106	62	42
Layer 6 Deformation (mm)	188	117	76	56	156	89	52	34
Layer 7 Deformation (mm)	162	102	67	42	128	73	43	28
Layer 8 Deformation (mm)	139	89	59	13	106	60	35	23
Layer 9 Deformation (mm)	119	77	37	-25	88	51	30	18
Layer 10 Deformation (mm)	102	67	-7	-68	73	42	25	-3
Total Deformation (mm)	1995	1247	744	393	1779	1038	621	403

For Table 7-4 and Table 7-5, HC => High Compaction, IC => Intermediate Compaction, SP => Standard Proctor, MC => Moderate Compaction, Positive and Negative Deformation means Swelling and Compression respectively.
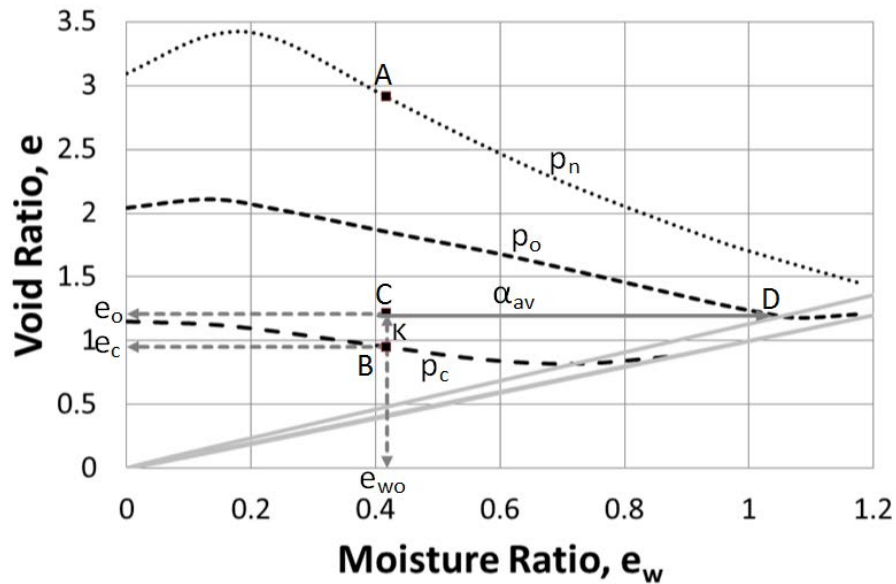
Figure 7-1: Theoretical development of the dependence of average hydric coefficient (α_{av}) with the state parameters
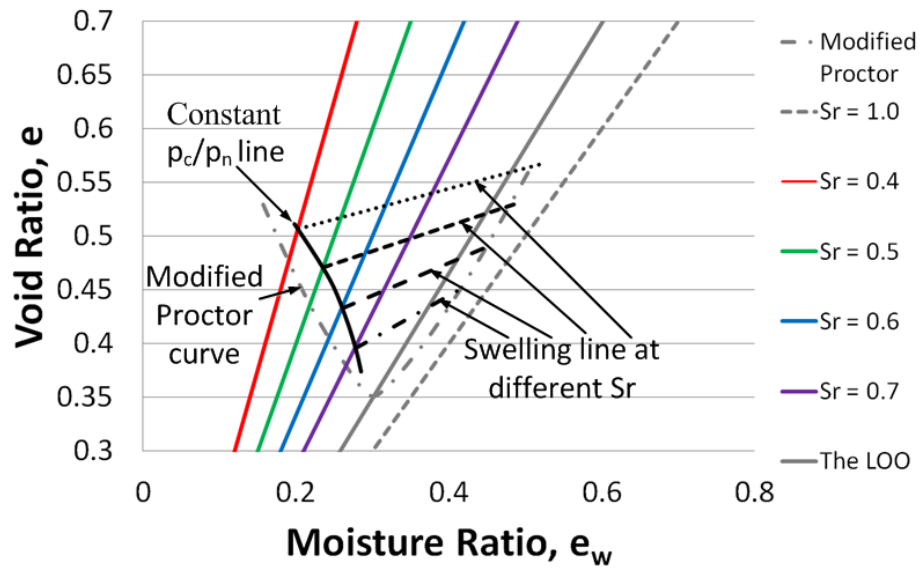
(a) Variation of average hydric coefficient (α_{av}) with operational degree of saturation (S_{ro})
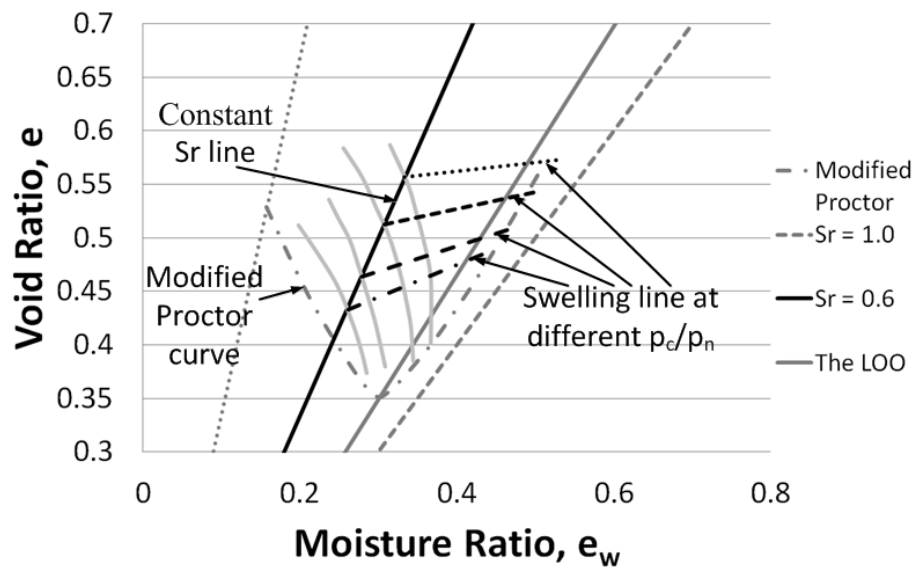
(b) Variation of average hydric coefficient (α_{av}) with the ratio of compaction stress (p_c) and nominal stress (p_n)
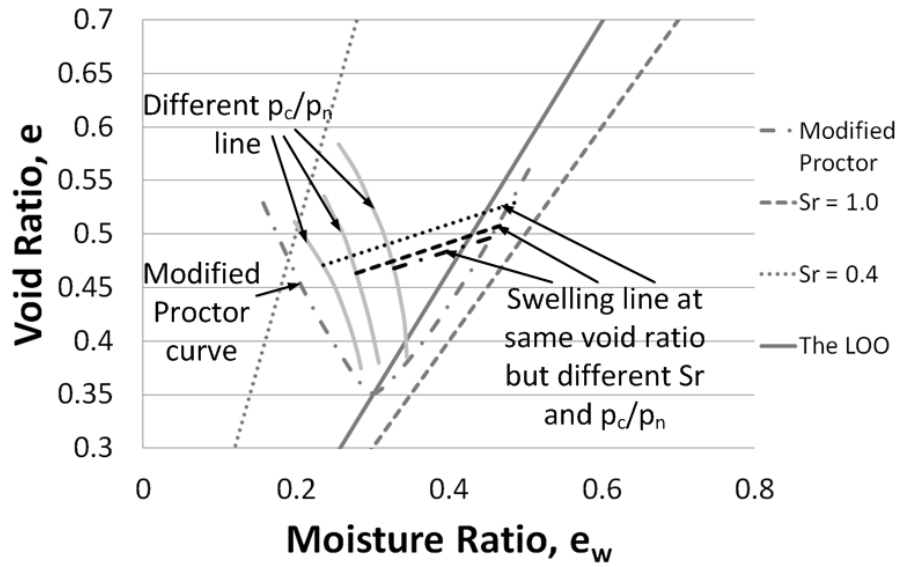
(c) Variation of average hydric coefficient (α_{av}) at operational void ratio (e_o)
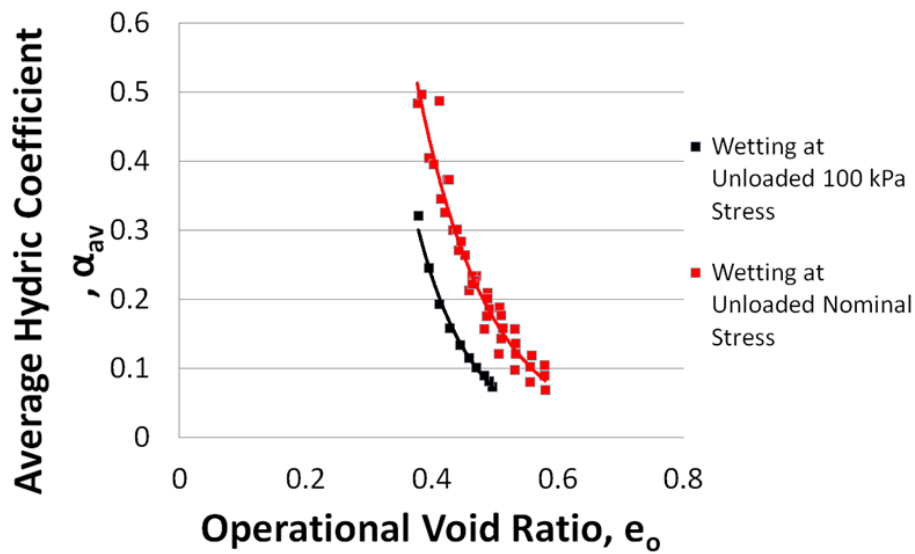
(d) Variation of average hydric coefficient (α_{av}) with operational void ratio (e_o)

Figure 7-2: Dependence of average hydric coefficient (α_{av}) with state parameters from Noorany and Stanley (1994)

(a)

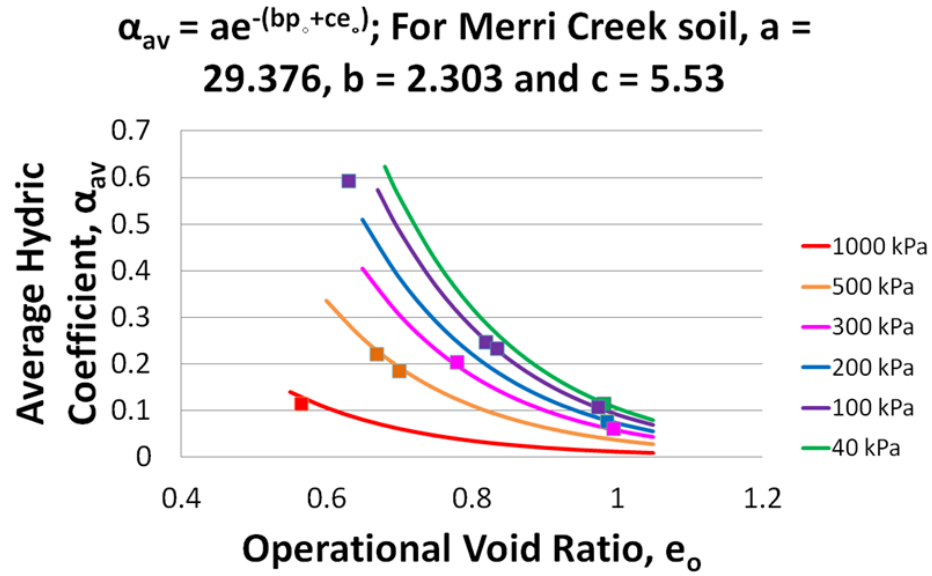**(b)**

(c)

(d)

(e)

(f)

(g)

(h)
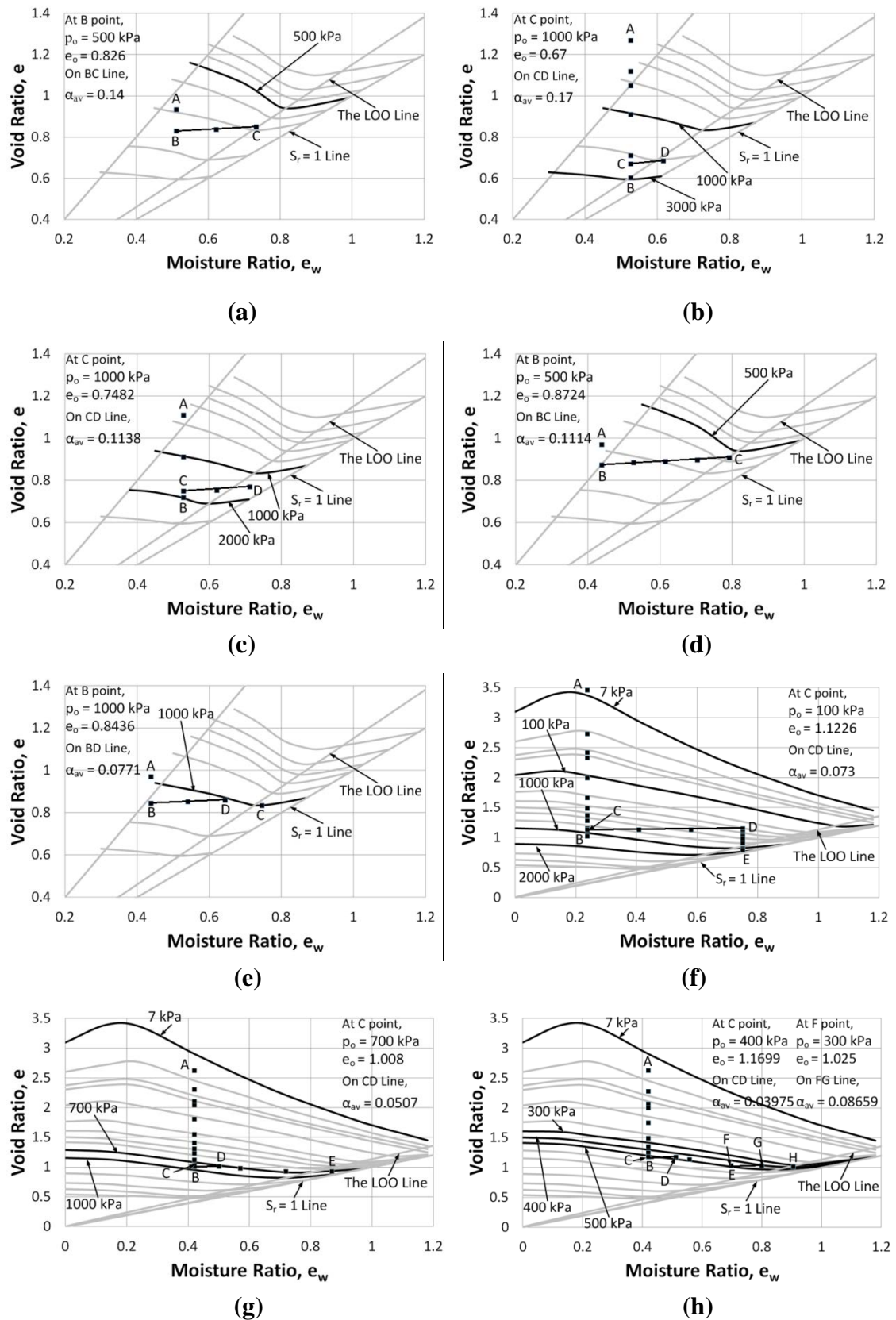
Figure 7-3: Average hydric coefficient (α_{av}) calculation from experimental data for kaolin soil
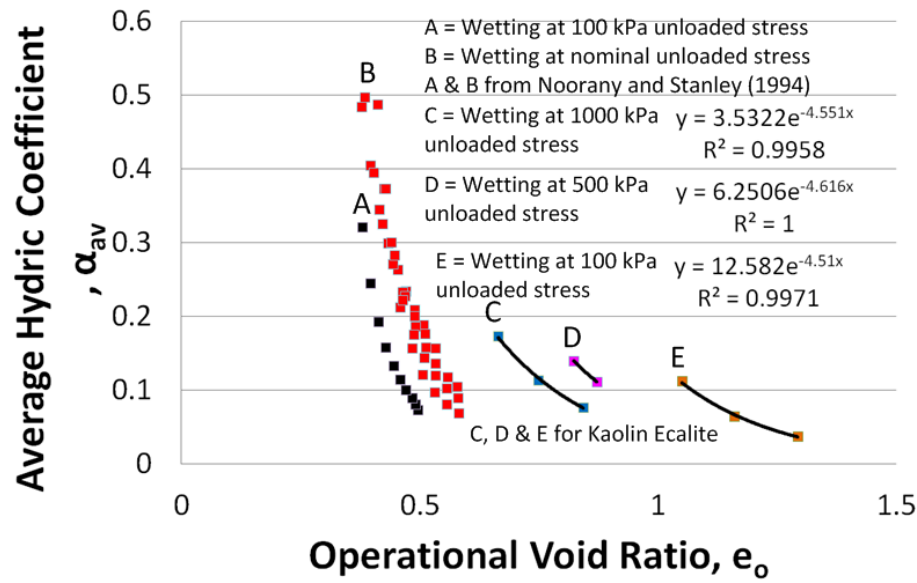
(a) Variation of average hydric coefficient (α_{av}) with operational void ratio (e_o) for kaolin soil
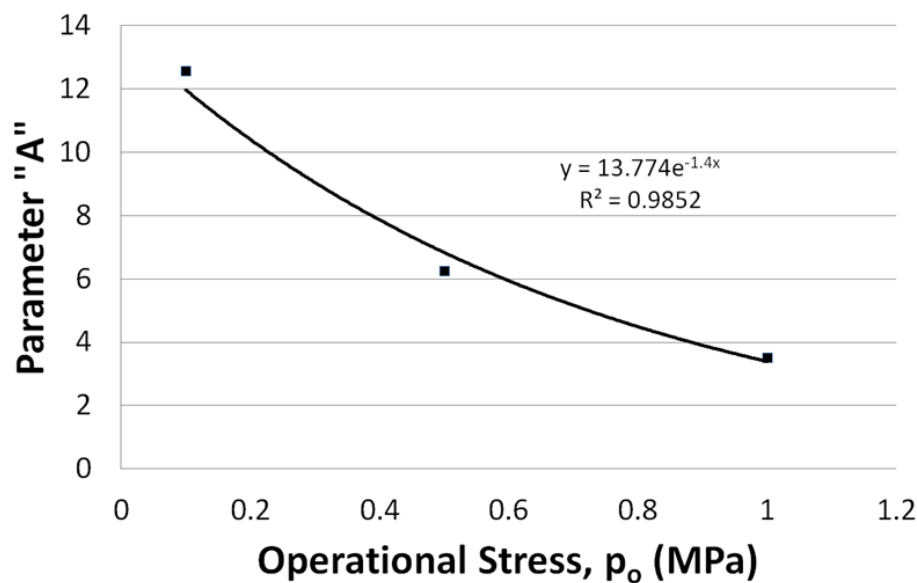
(b) Variation of parameter "A" with operational stress (p_o) for kaolin soil
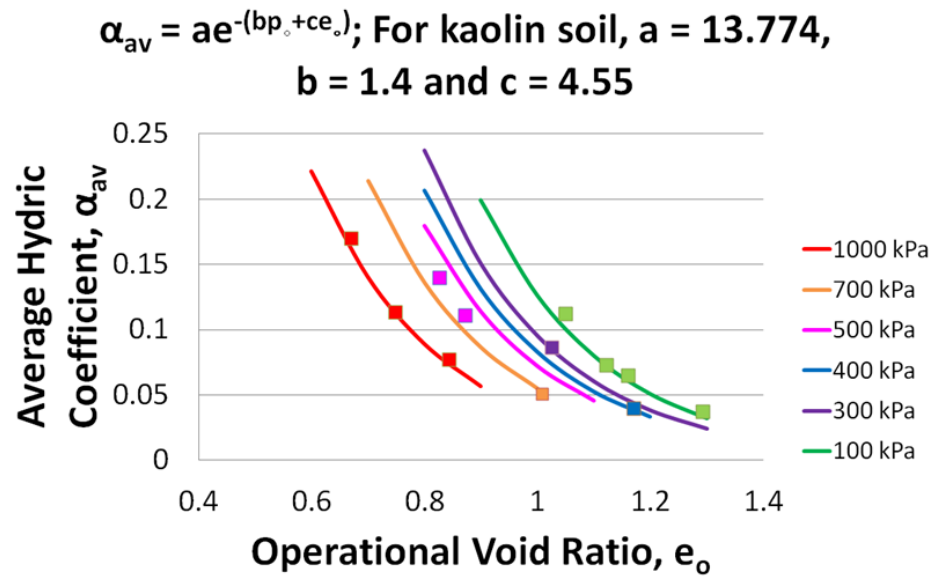
$$\alpha_{av} = ae^{-(bp_\circ + ce_\circ)}; \text{ For kaolin soil, a = 13.774,}$$
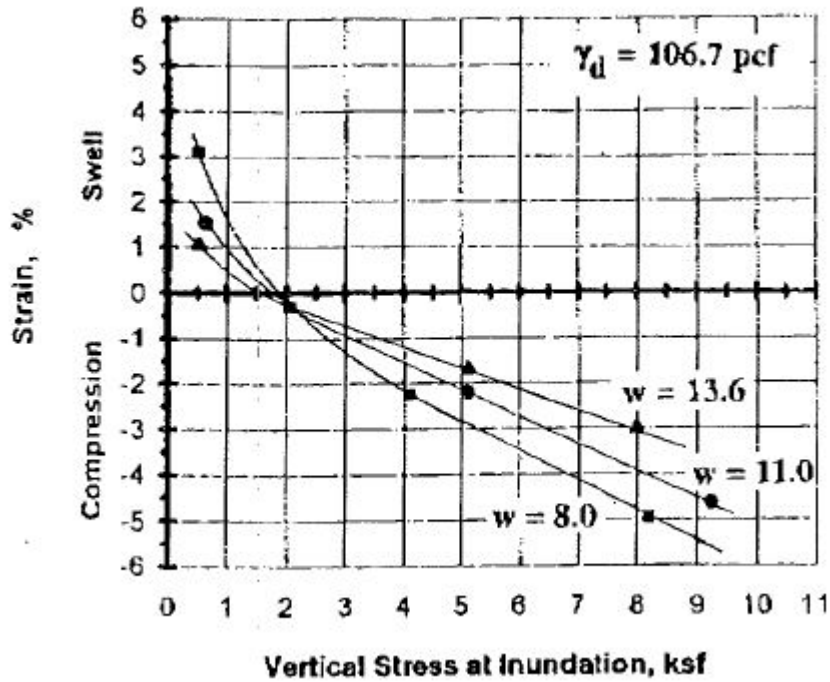$$b = 1.4 \text{ and c = 4.55}$$

(c) Validation of average hydric coefficient (α_{av}) equation using experimental data for kaolin soil

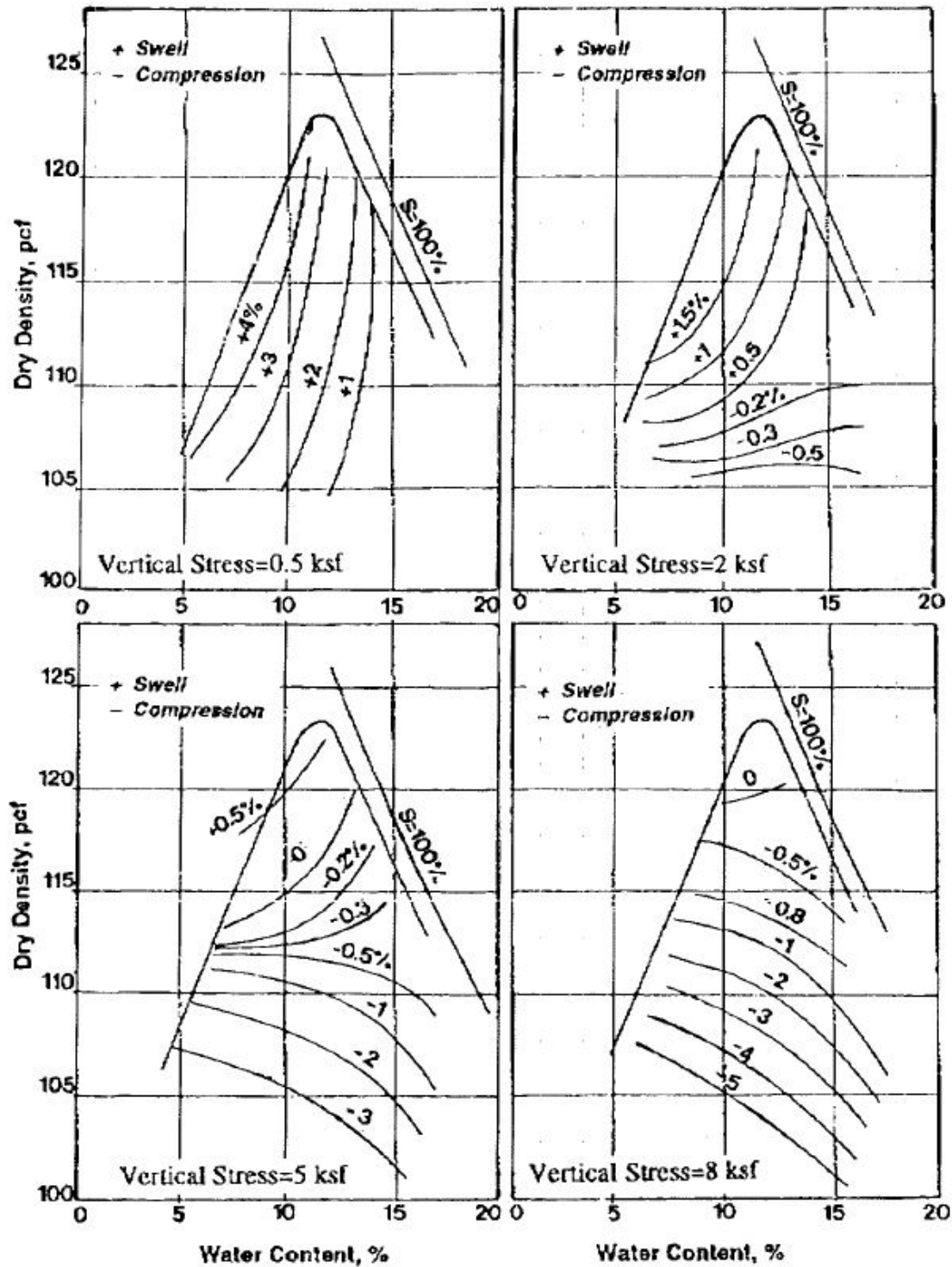**Figure 7-4:** Development of average hydric coefficient (α_{av}) equation for kaolin soil
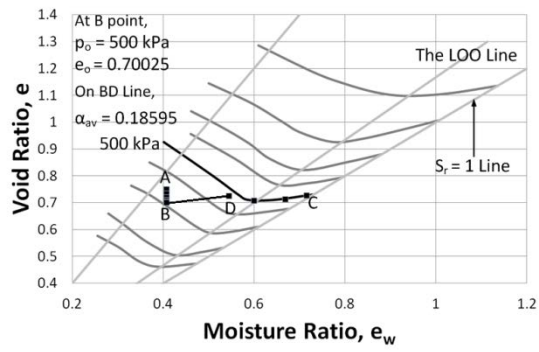
(a)
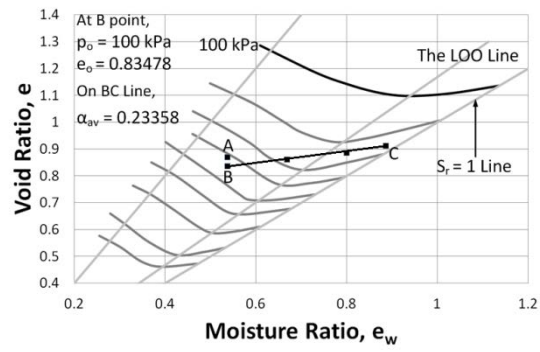
(b)
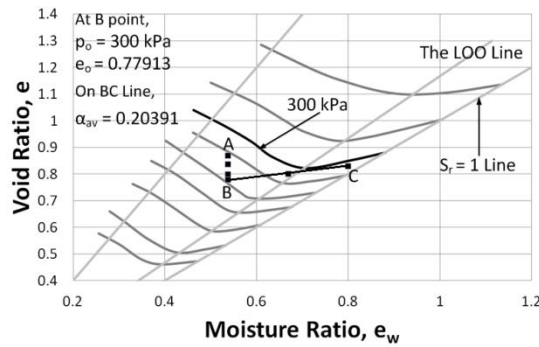
(c)
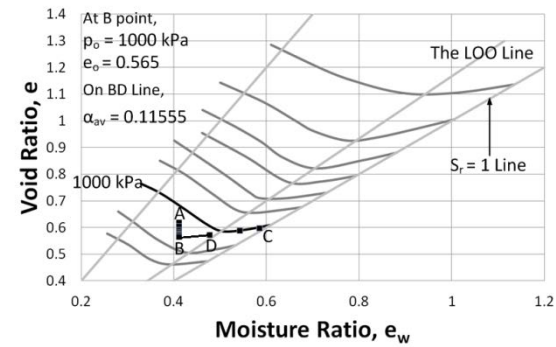
(d)
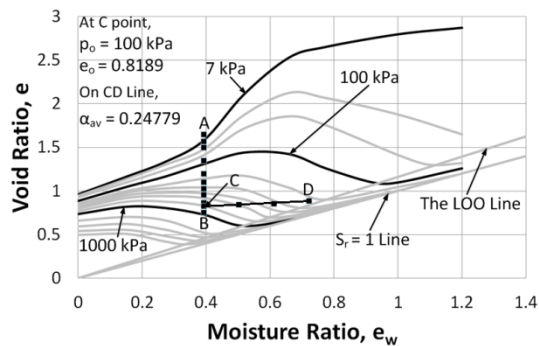
(e)
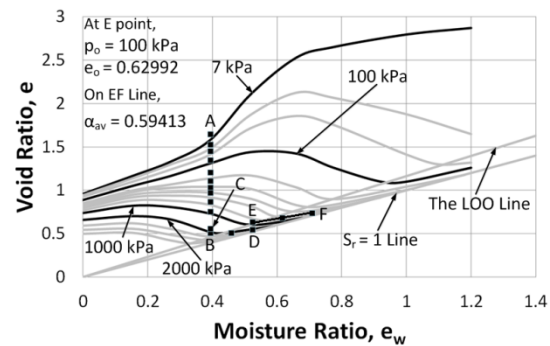
(f)
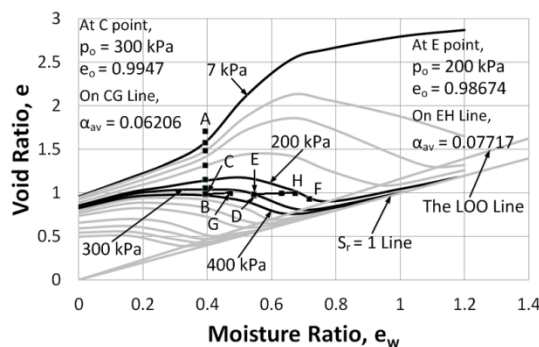
(g)
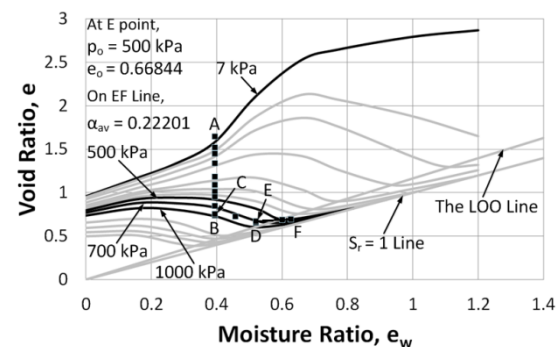
(h)
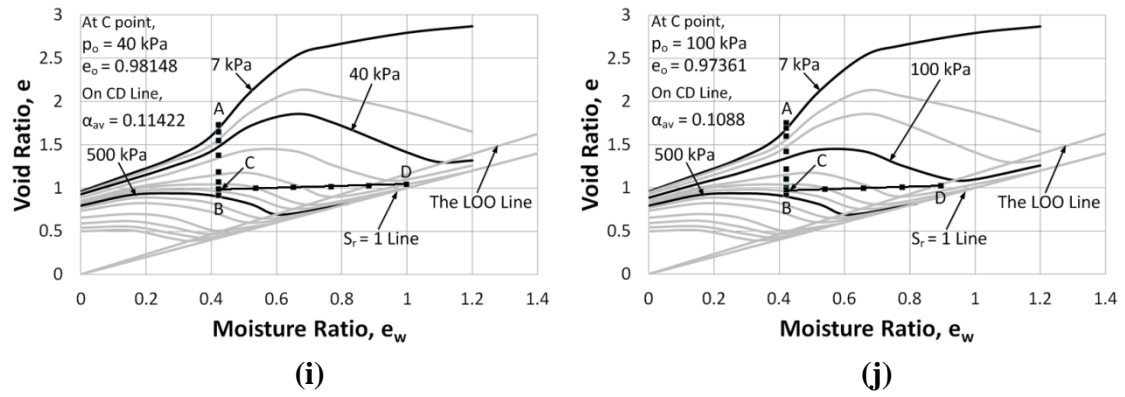
Figure 7-5: Average hydric coefficient (α_{av}) calculation from experimental data for Merri Creek soil
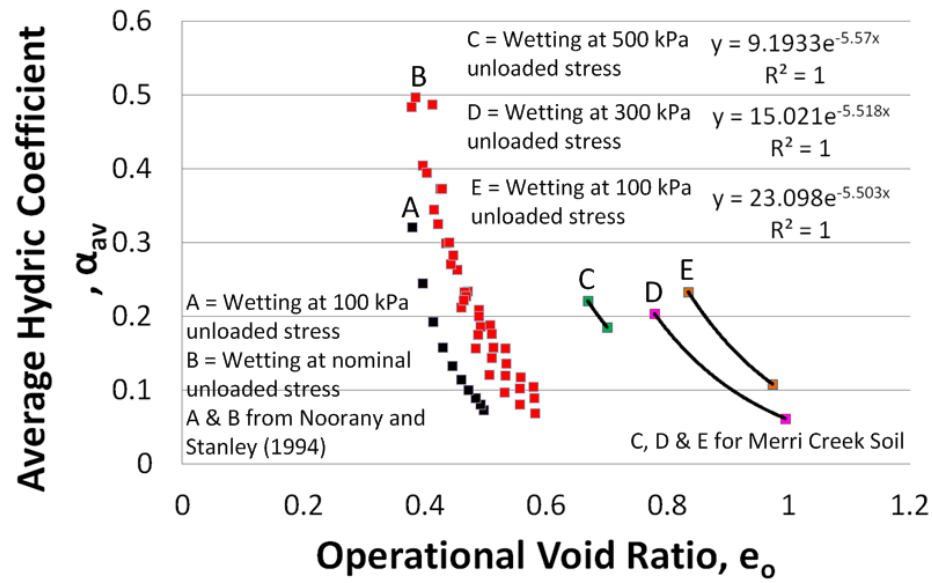
(a) Variation of average hydric coefficient (α_{av}) with operational void ratio (e_o) for Merri Creek soil

(b) Variation of parameter "A" with operational stress (p_o) for Merri Creek soil

$$\alpha_{av} = ae^{-(bp_\circ + ce_\circ)}; \text{ For Merri Creek soil, } a = 29.376, b = 2.303 \text{ and } c = 5.53$$

(c) Validation of average hydric coefficient (α_{av}) equation using experimental data for Merri Creek soil

Figure 7-6: Development of average hydric coefficient (α_{av}) equation for Merri Creek soil

Figure 7-7: Effect of water content and dry density on swelling/compression during flooding for Villa Trinidad fill (obtained from Noorany and Stanley (1994) with permission from ASCE)

Figure 7-8: Effect of water content on swell/compression during flooding for Villa Trinidad fill (obtained from Noorany and Stanley (1994) with permission from ASCE)

Figure 7-9: Contours of equal swell and equal compression for Villa Trinidad fill (obtained from Noorany and Stanley (1994) with permission from ASCE)
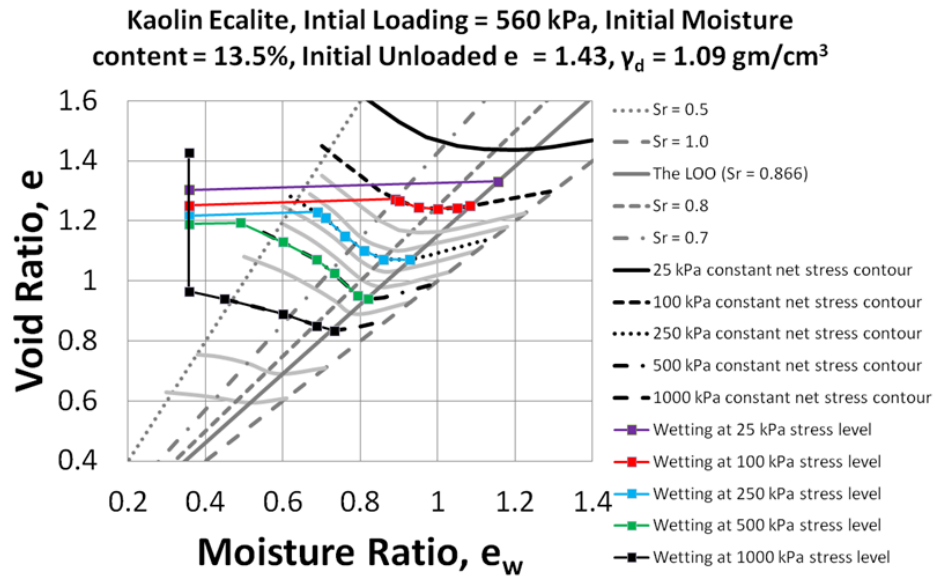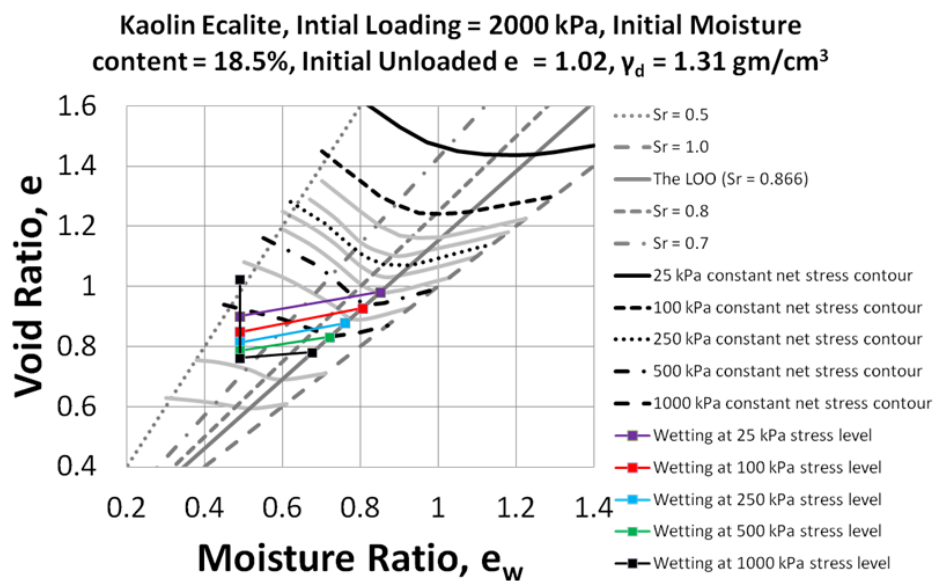
(a) 13.5 % initial moisture content, 1.31 gm/cc unloaded dry density and major wetting at 25, 100, 250, 500 and 1000 kPa operational stresses

(b) 13.5 % initial moisture content, 1.21 gm/cc unloaded dry density and major wetting at 25, 100, 250, 500 and 1000 kPa operational stresses
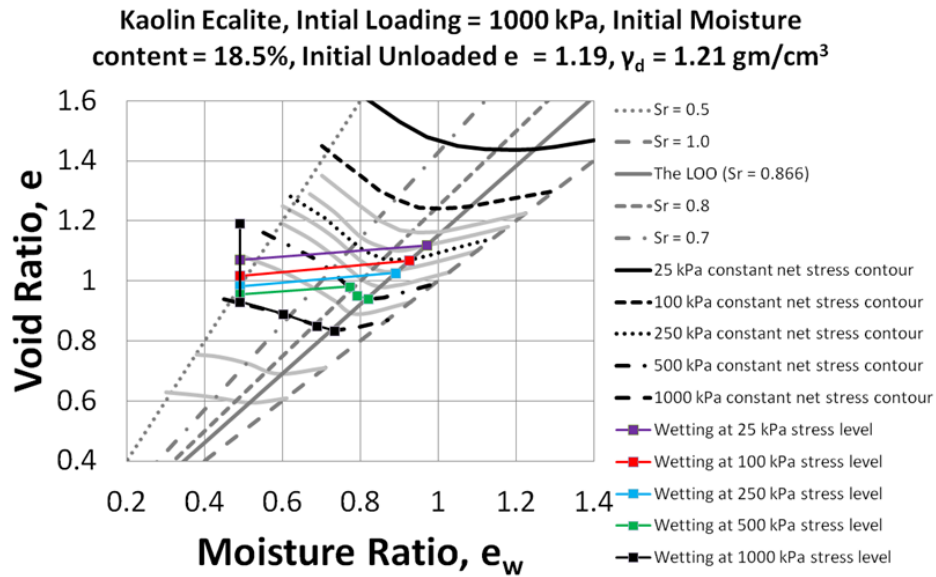
(c) 13.5 % initial moisture content, 1.09 gm/cc unloaded dry density and major wetting at 25, 100, 250, 500 and 1000 kPa operational stresses
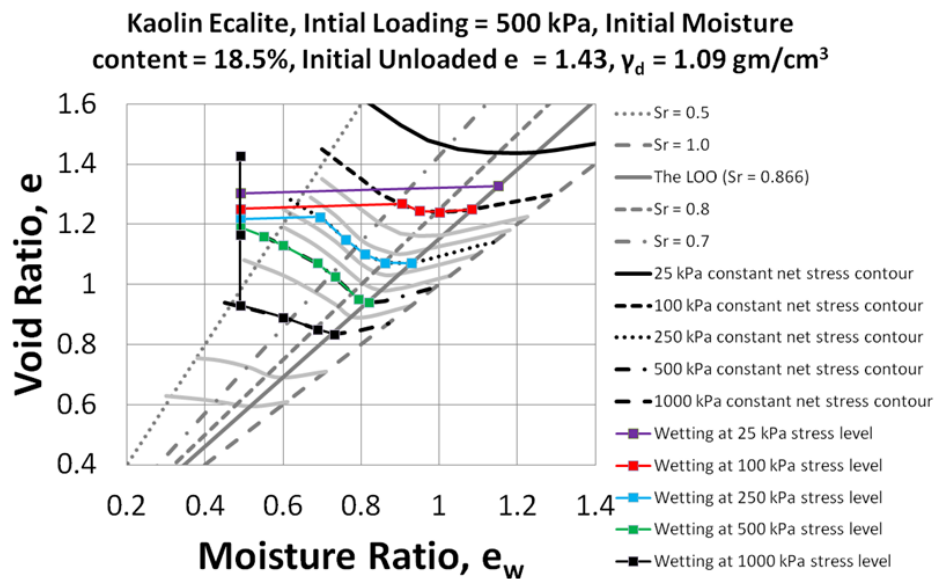

(d) 18.5 % initial moisture content, 1.31 gm/cc unloaded dry density and major wetting at 25, 100, 250, 500 and 1000 kPa operational stresses
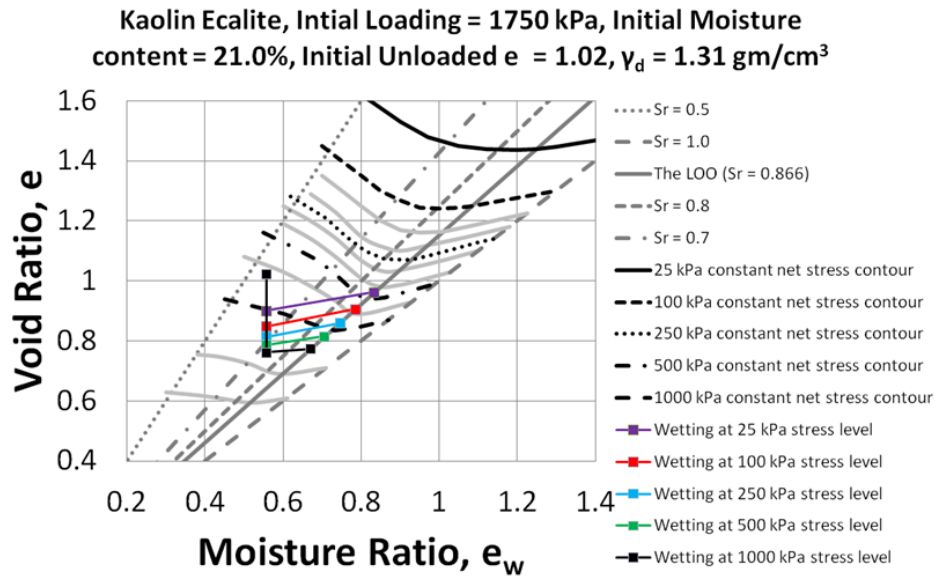
(e) 18.5 % initial moisture content, 1.21 gm/cc unloaded dry density and major wetting at 25, 100, 250, 500 and 1000 kPa operational stresses

(f) 18.5 % initial moisture content, 1.09 gm/cc unloaded dry density and major wetting at 25, 100, 250, 500 and 1000 kPa operational stresses

(g) 21.0 % initial moisture content, 1.31 gm/cc unloaded dry density and major wetting at 25, 100, 250, 500 and 1000 kPa operational stresses
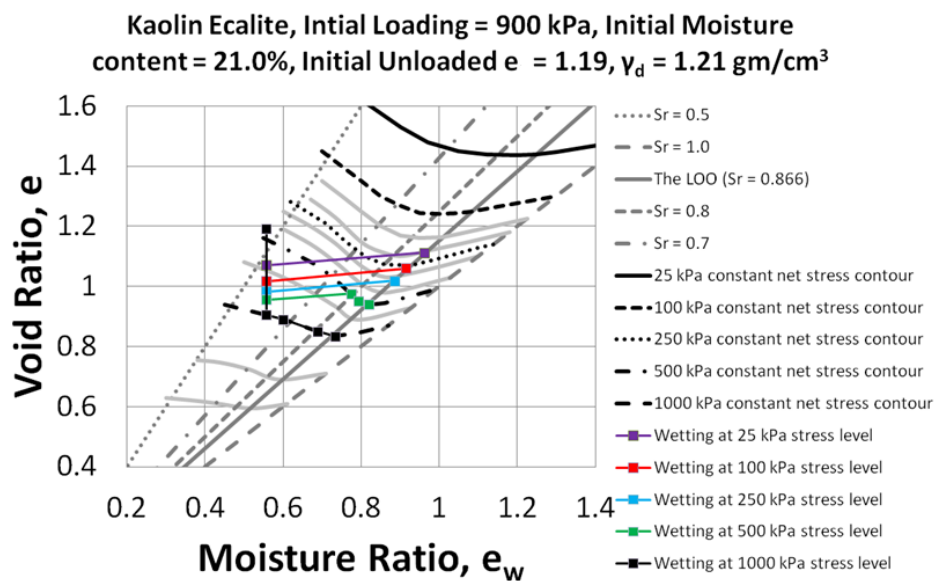

(h) 21.0 % initial moisture content, 1.21 gm/cc unloaded dry density and major wetting at 25, 100, 250, 500 and 1000 kPa operational stresses
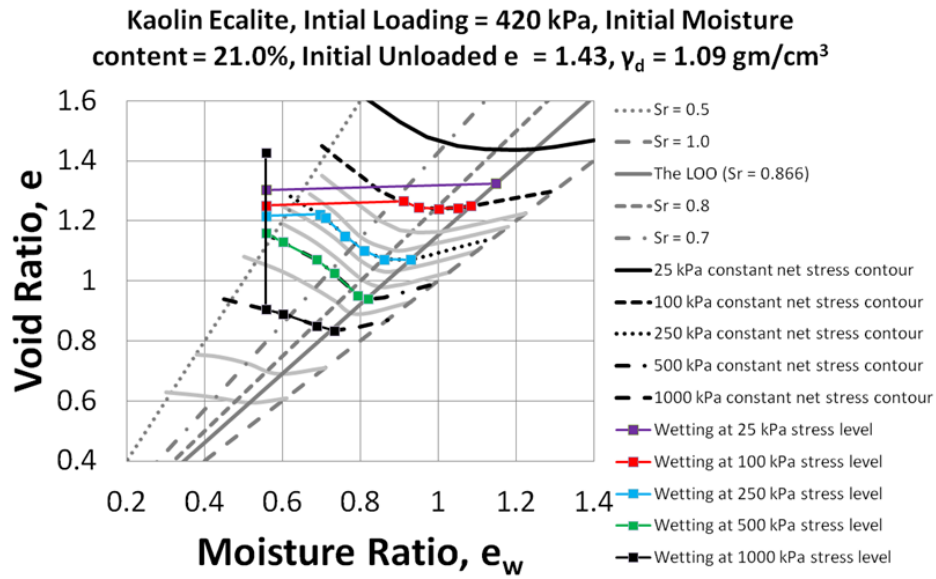
(i) 21.0 % initial moisture content, 1.09 gm/cc unloaded dry density and major wetting at 25, 100, 250, 500 and 1000 kPa operational stresses
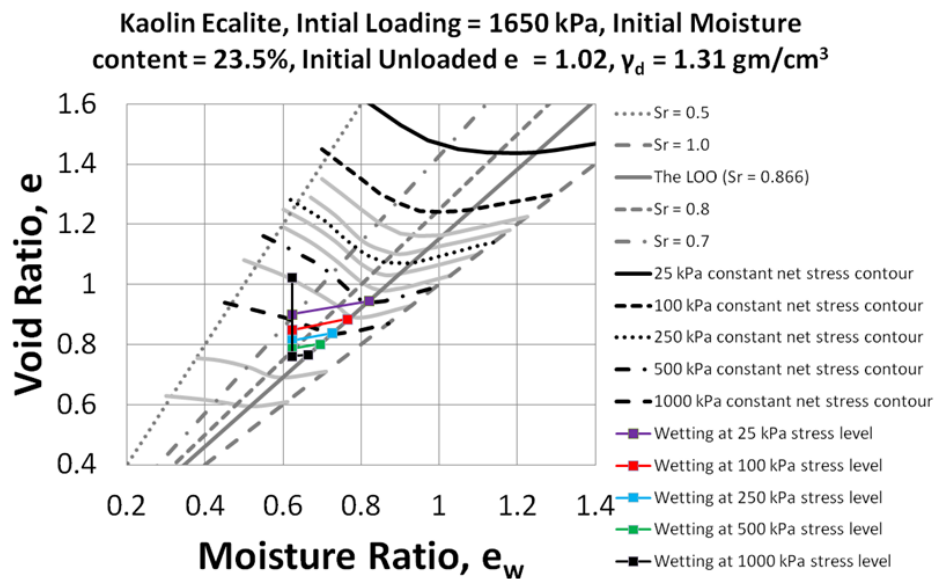

(j) 23.5 % initial moisture content, 1.31 gm/cc unloaded dry density and major wetting at 25, 100, 250, 500 and 1000 kPa operational stresses
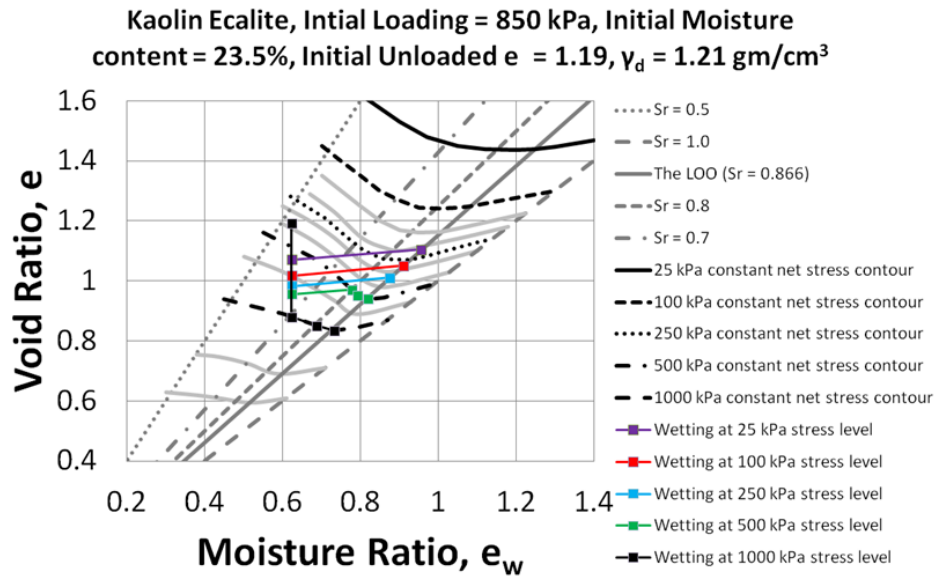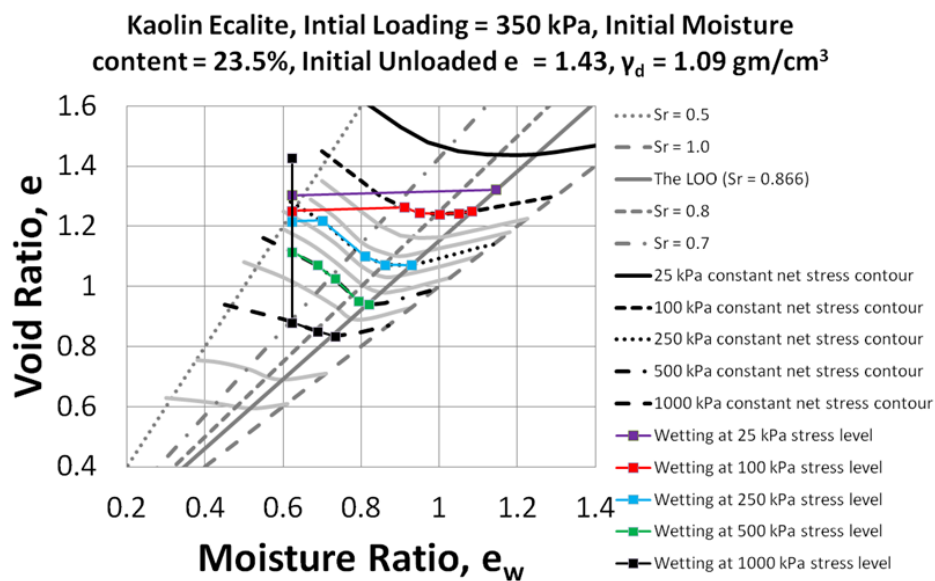
(k) 23.5 % initial moisture content, 1.21 gm/cc unloaded dry density and major wetting at 25, 100, 250, 500 and 1000 kPa operational stresses

(l) 23.5 % initial moisture content, 1.09 gm/cc unloaded dry density and major wetting at 25, 100, 250, 500 and 1000 kPa operational stresses

Figure 7-10: Modelling of major wetting tests using the MPK framework for kaolin soil

(a) 11.0 % initial moisture content, 1.28 gm/cc unloaded dry density and major wetting at 25, 100, 200, 300 and 500 kPa operational stresses

(b) 11.0 % initial moisture content, 1.16 gm/cc unloaded dry density and major wetting at 25, 100, 200, 300 and 500 kPa operational stresses

(c) 11.0 % initial moisture content, 1.10 gm/cc unloaded dry density and major wetting at 25, 100, 200, 300 and 500 kPa operational stresses

(d) 15.0 % initial moisture content, 1.28 gm/cc unloaded dry density and major wetting at 25, 100, 200, 300 and 500 kPa operational stresses

(e) 15.0 % initial moisture content, 1.16 gm/cc unloaded dry density and major wetting at 25, 100, 200, 300 and 500 kPa operational stresses
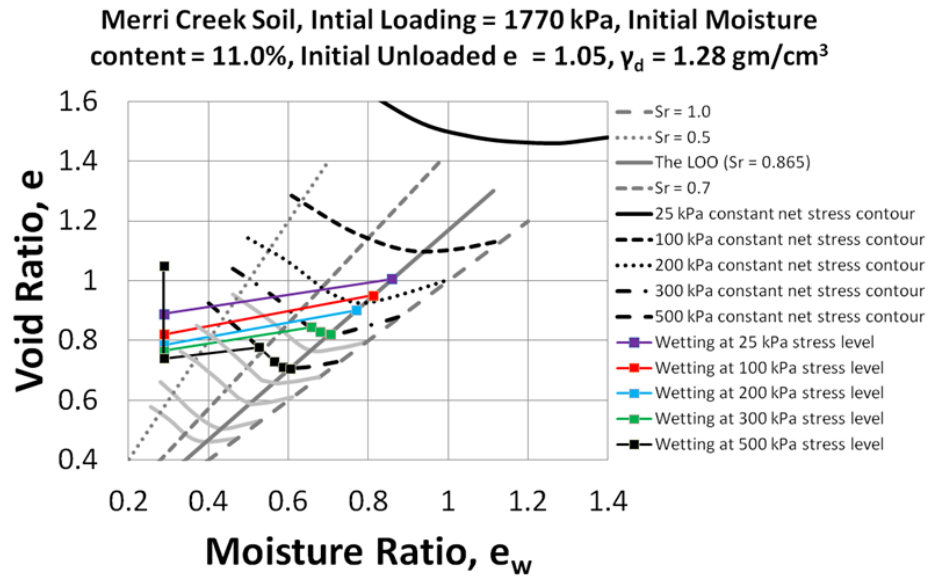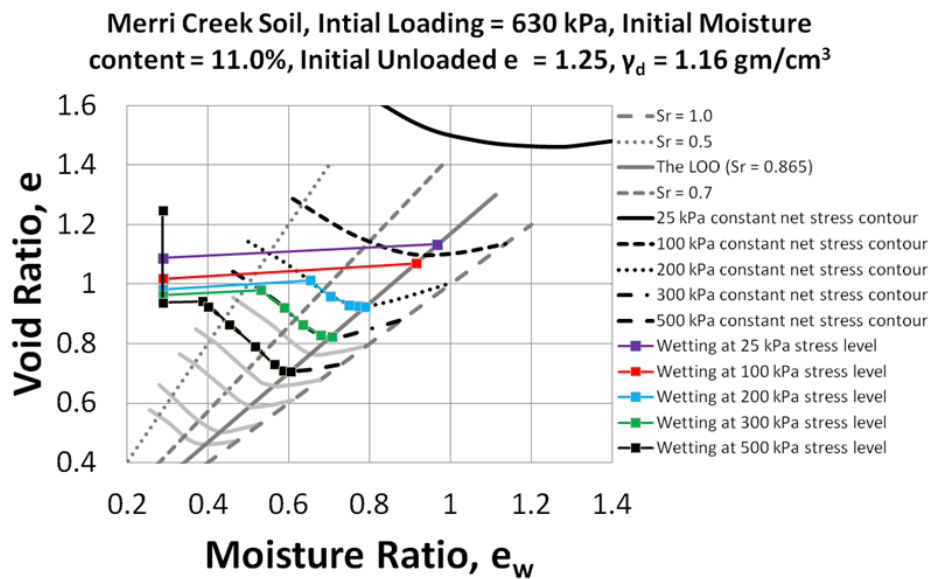

(f) 15.0 % initial moisture content, 1.10 gm/cc unloaded dry density and major wetting at 25, 100, 200, 300 and 500 kPa operational stresses
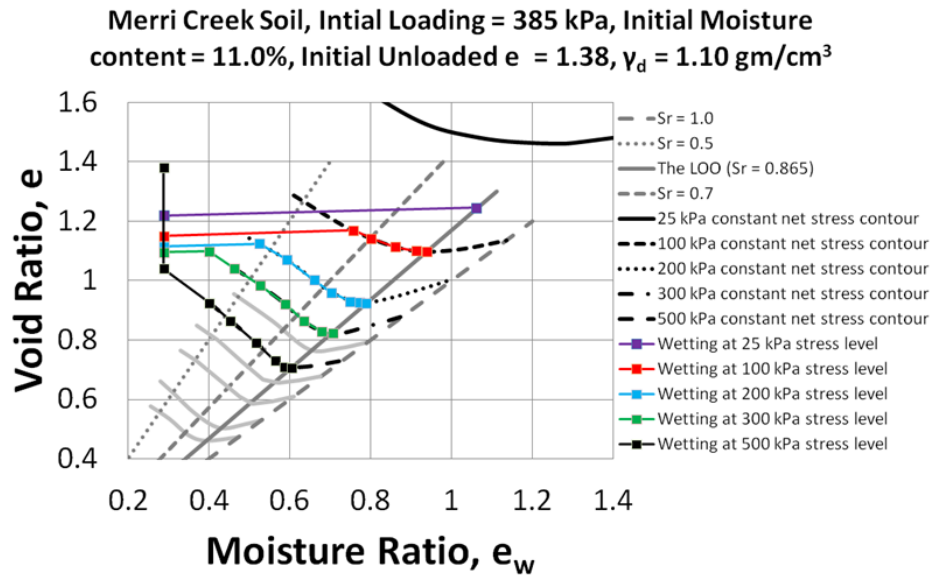
(g) 19.0 % initial moisture content, 1.28 gm/cc unloaded dry density and major wetting at 25, 100, 200, 300 and 500 kPa operational stresses

(h) 19.0 % initial moisture content, 1.16 gm/cc unloaded dry density and major wetting at 25, 100, 200, 300 and 500 kPa operational stresses
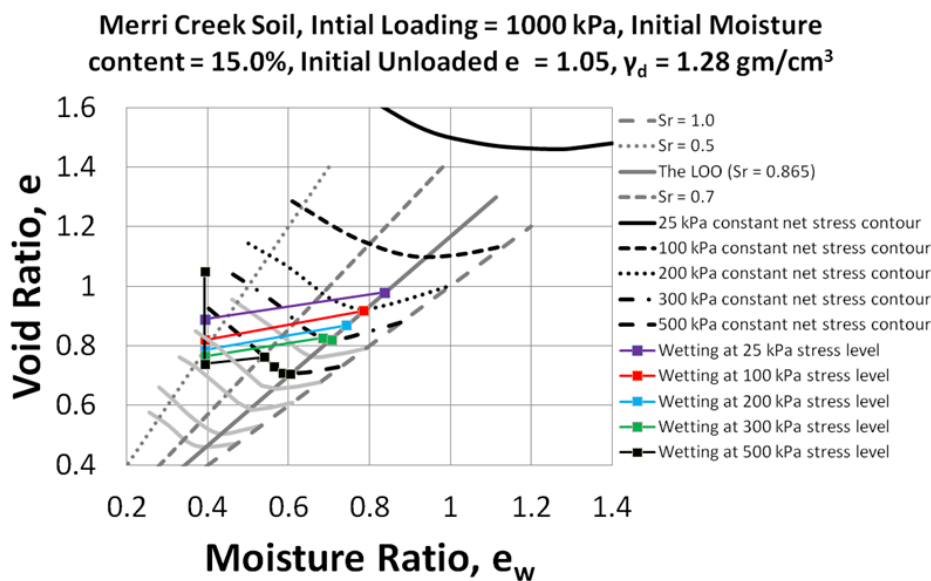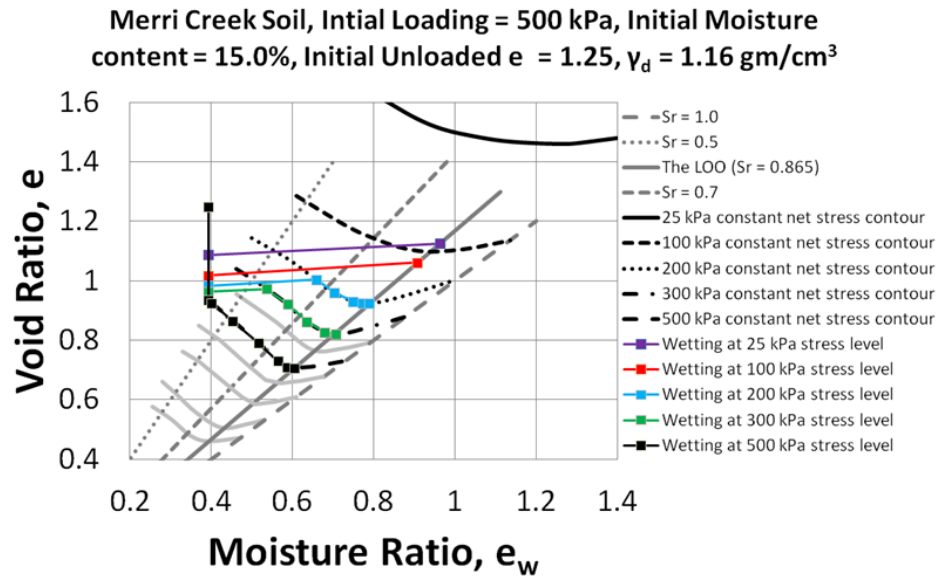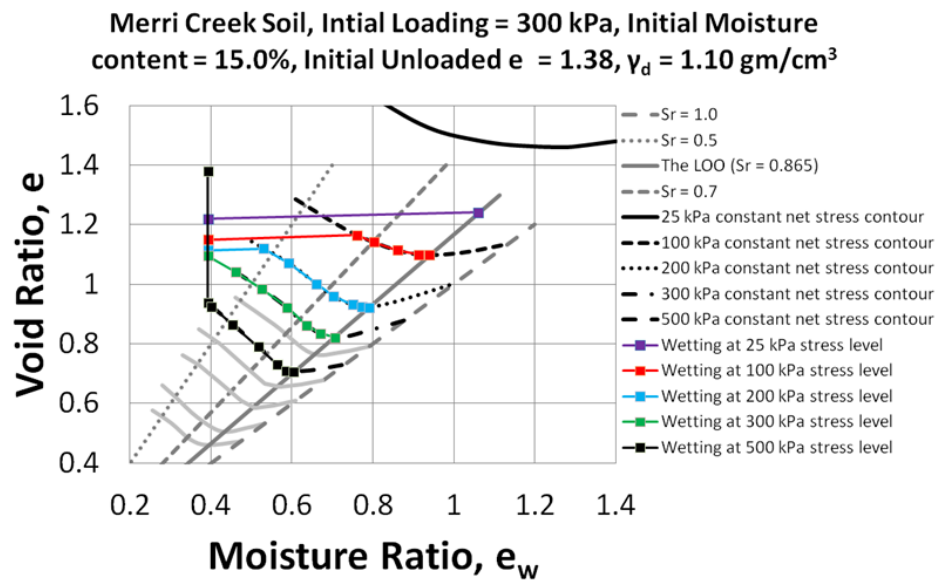
(i) 19.0 % initial moisture content, 1.10 gm/cc unloaded dry density and major wetting at 25, 100, 200, 300 and 500 kPa operational stresses
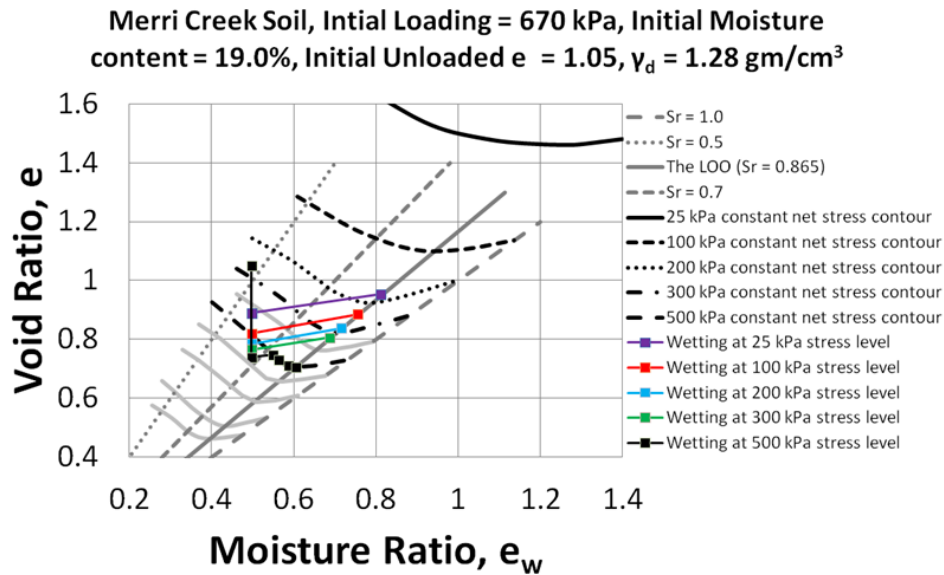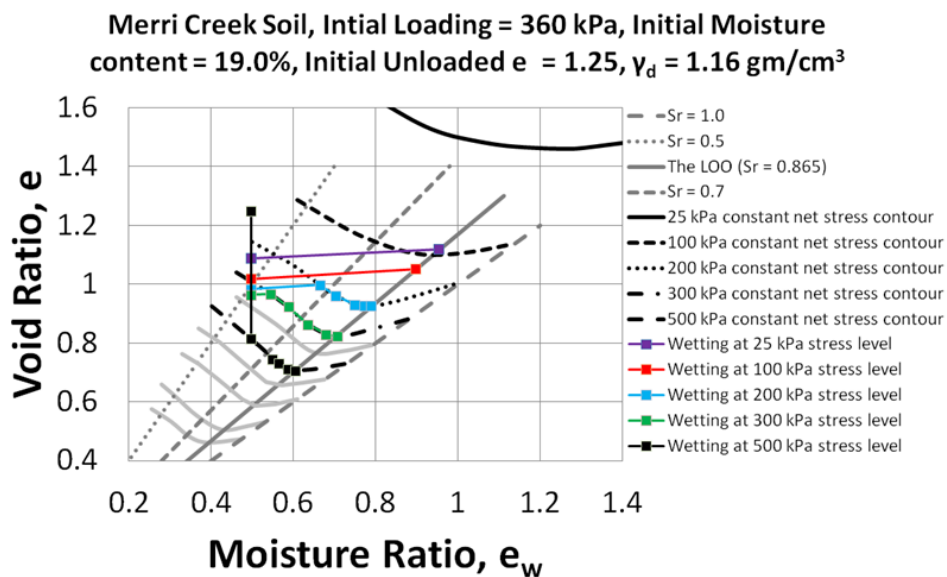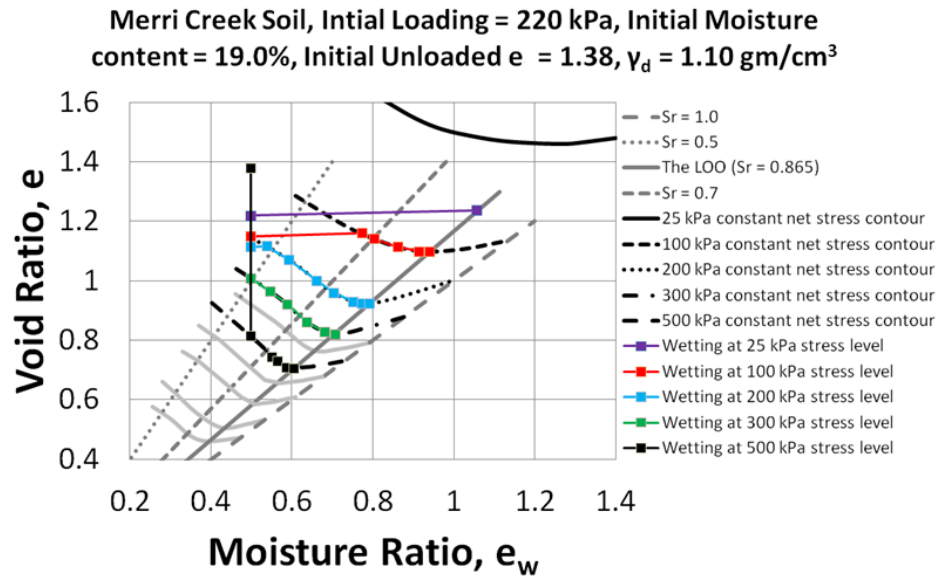
Figure 7-11: Modelling of major wetting tests using the MPK framework for Merri Creek soil
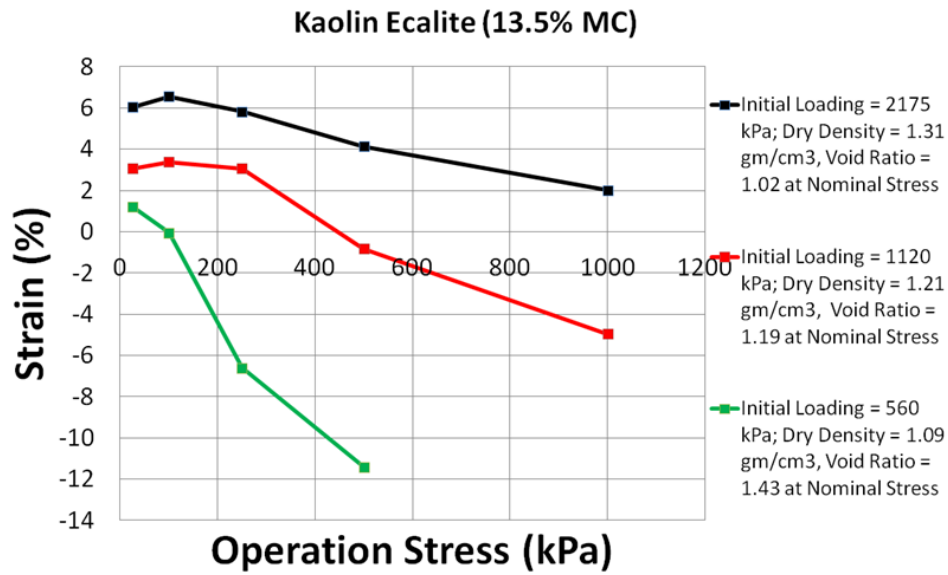
(a) For 13.5% initial moisture content or $e_{wo} = 0.358$

(b) For 18.5% initial moisture content or $e_{wo} = 0.490$

Kaolin Ecalite (21% MC)

Initial Loading = 1750 kPa; Dry Density = 1.31 gm/cm3, Void Ratio = 1.02 at Nominal Stress

Initial Loading = 900 kPa; Dry Density = 1.21 gm/cm3, Void Ratio = 1.19 at Nominal Stress

Initial Loading = 420 kPa; Dry Density = 1.09 gm/cm3, Void Ratio = 1.43 at Nominal Stress
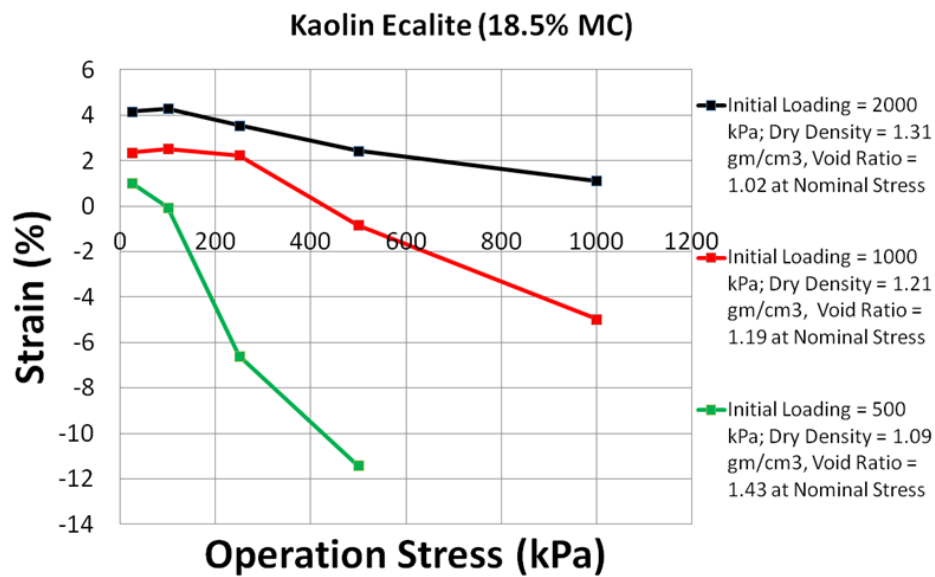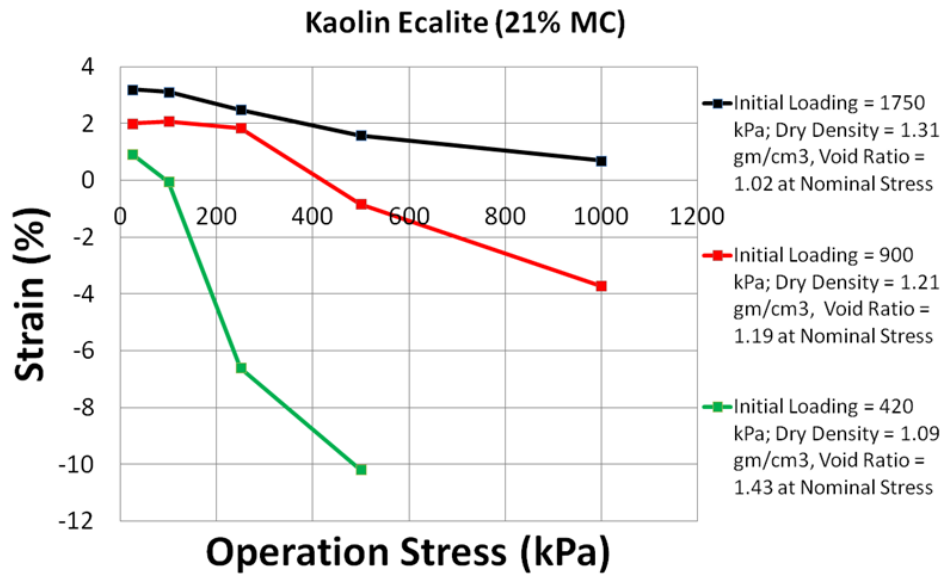
(c) For 21.0% initial moisture content or $e_{wo} = 0.557$

Kaolin Ecalite (23.5% MC)

Initial Loading = 1650 kPa; Dry Density = 1.31 gm/cm3, Void Ratio = 1.02 at Nominal Stress

Initial Loading = 850 kPa; Dry Density = 1.21 gm/cm3, Void Ratio = 1.19 at Nominal Stress

Initial Loading = 350 kPa; Dry Density = 1.09 gm/cm3, Void Ratio = 1.43 at Nominal Stress

(d) For 23.5% initial moisture content or $e_{wo} = 0.623$

Figure 7-12: Effect of moisture content and dry density on swelling/compression during major wetting for kaolin soil
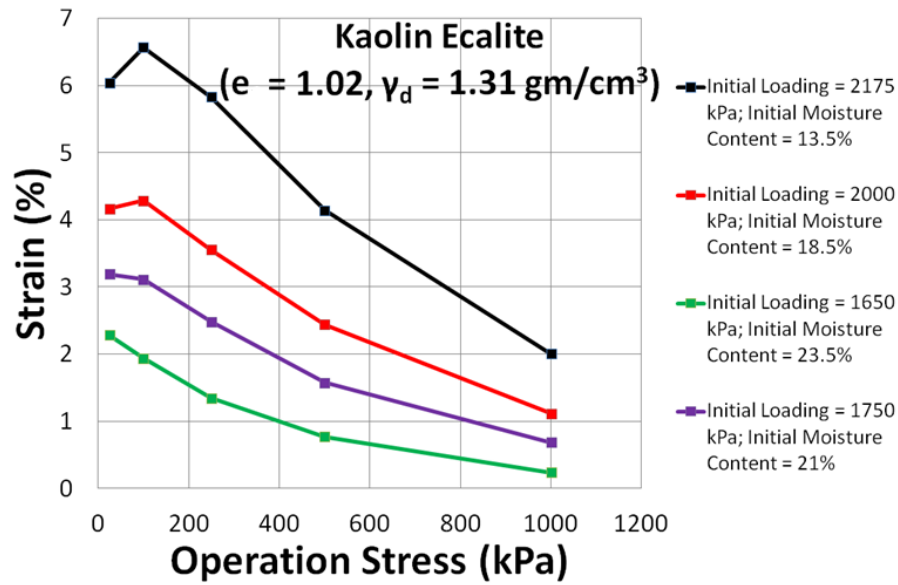
(a) For 1.31 gm/cc or 12.85 kN/m^3 unloaded dry density
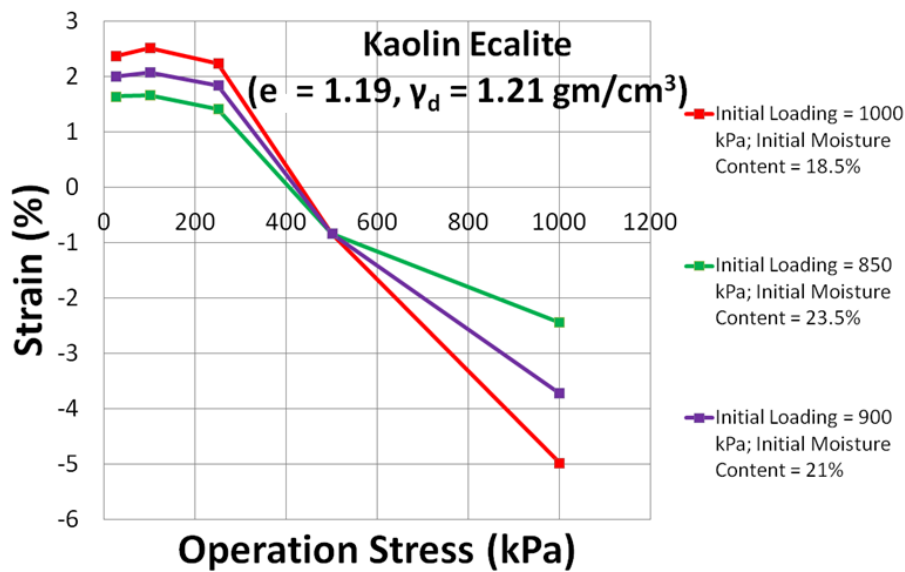
(b) For 1.21 gm/cc or 11.87 kN/m^3 unloaded dry density

Figure 7-13: Effect of moisture content on swelling/compression during major wetting for kaolin soil
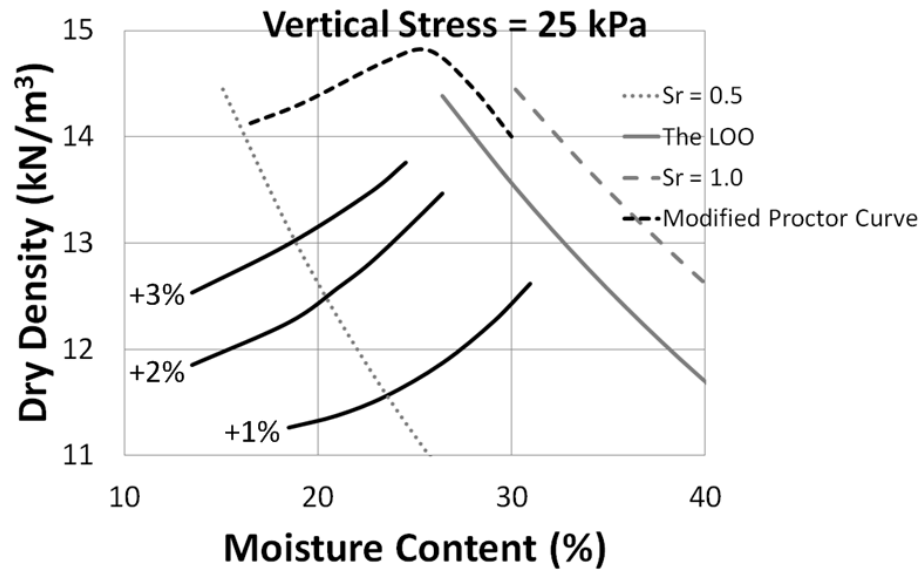
(a) On dry density – moisture content plane for 25 kPa vertical stress
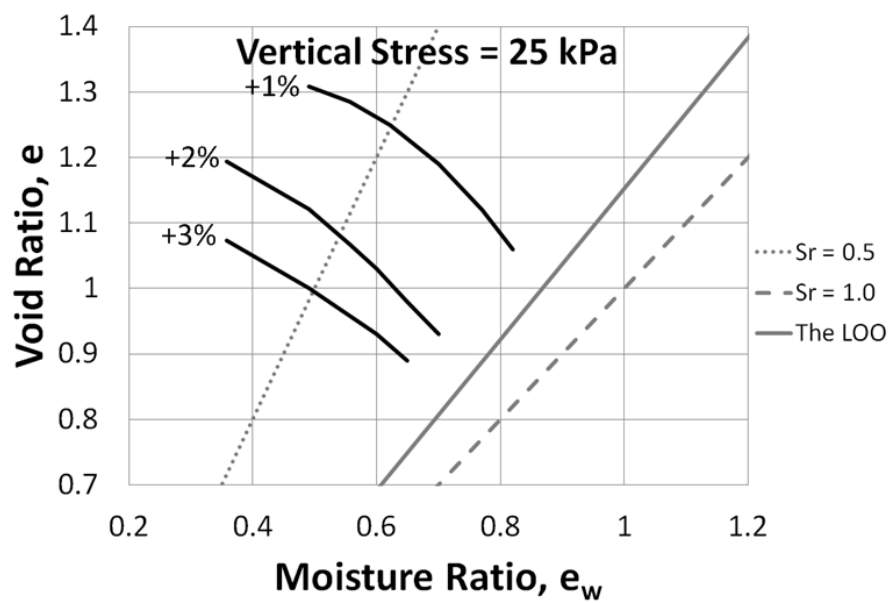
(b) On void ratio – moisture ratio plane for 25 kPa vertical stress
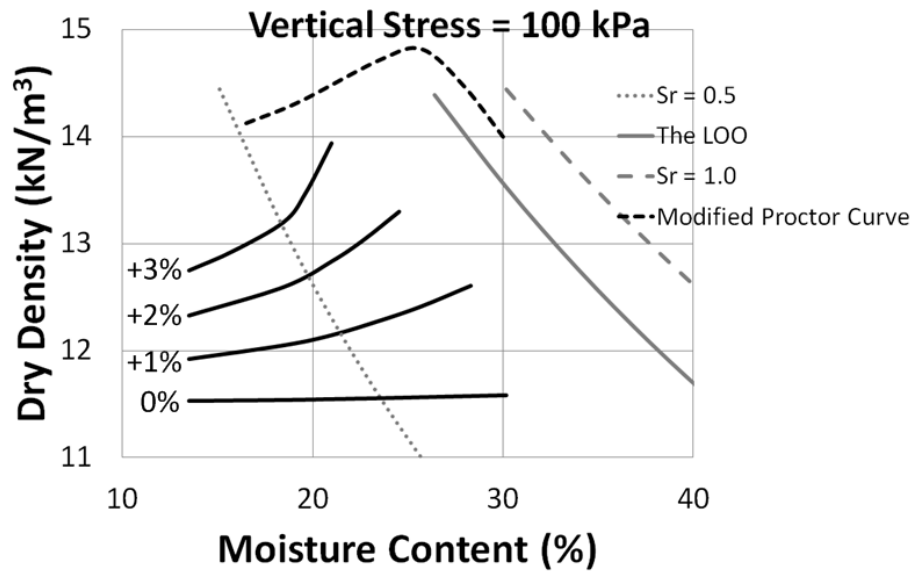
(c) On dry density – moisture content plane for 100 kPa vertical stress
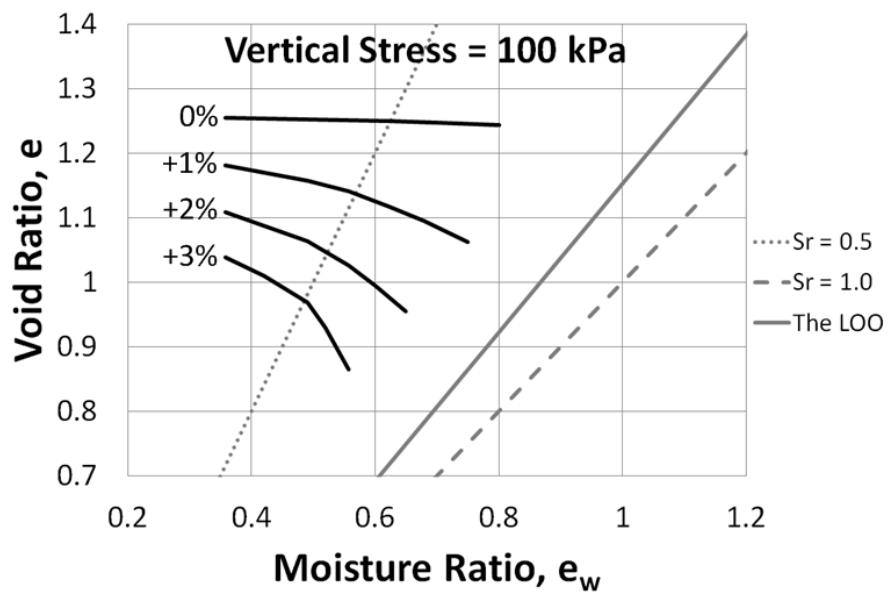
(d) On void ratio – moisture ratio plane for 100 kPa vertical stress
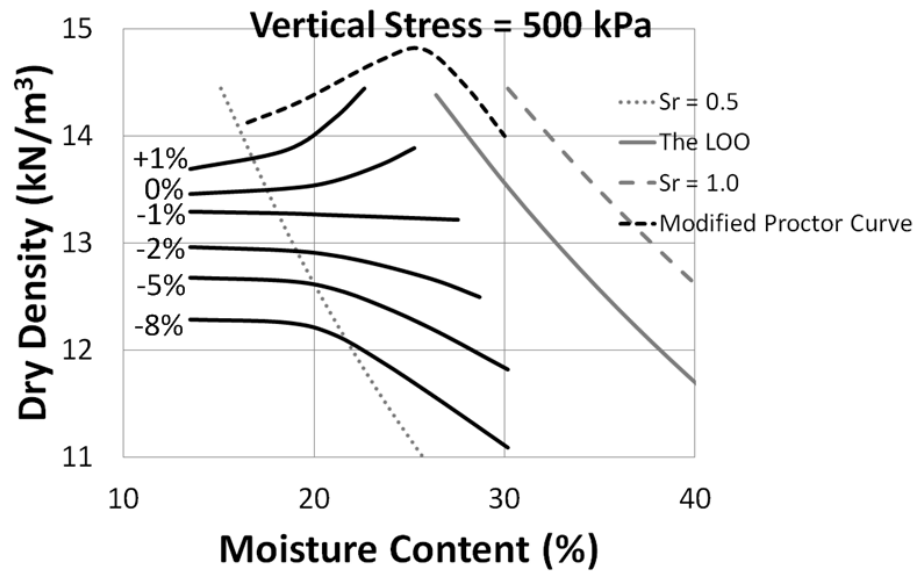
(e) On dry density – moisture content plane for 500 kPa vertical stress
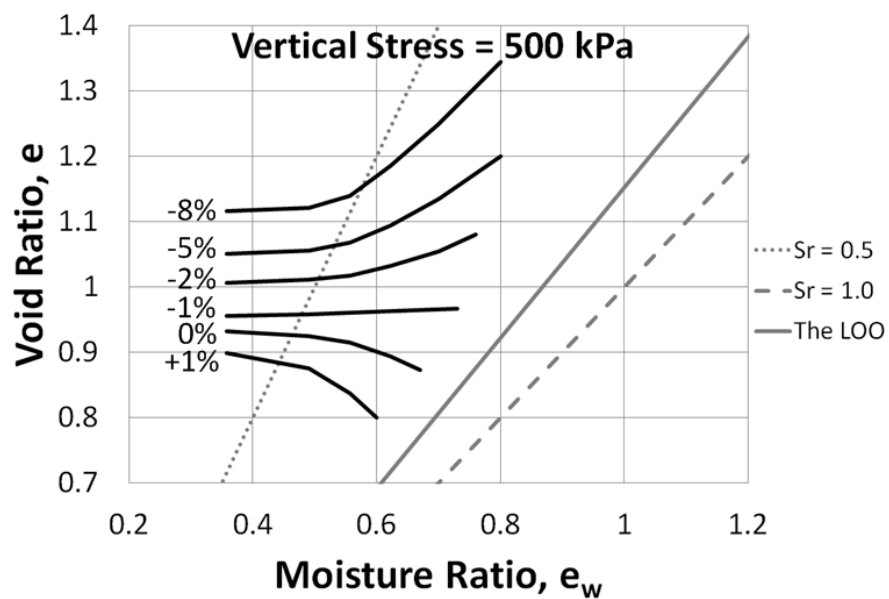
(f) On void ratio – moisture ratio plane for 500 kPa vertical stress

Figure 7-14: Contours of equal swell and equal compression for kaolin soil
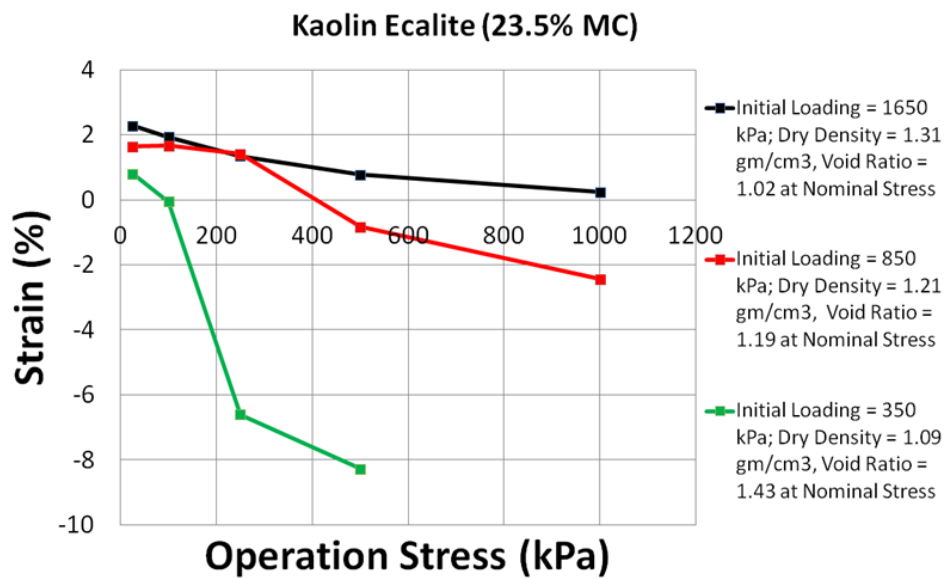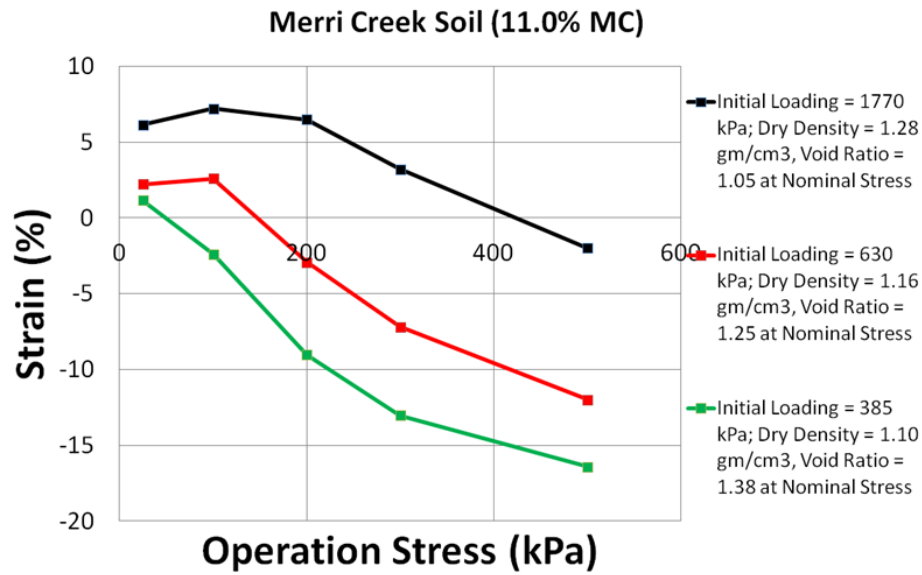
(a) For 11.0% initial moisture content or $e_{wo} = 0.288$
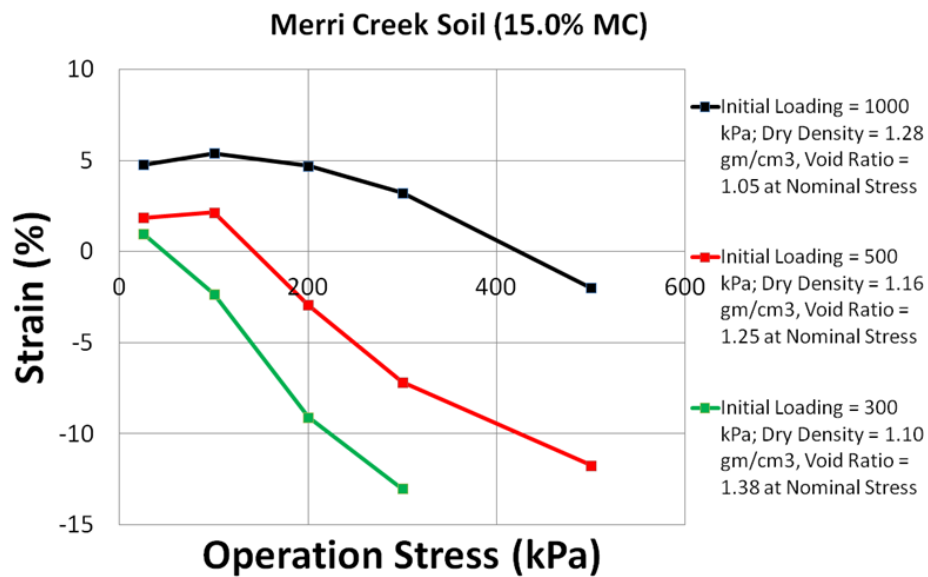

(b) For 15.0% initial moisture content or $e_{wo} = 0.393$
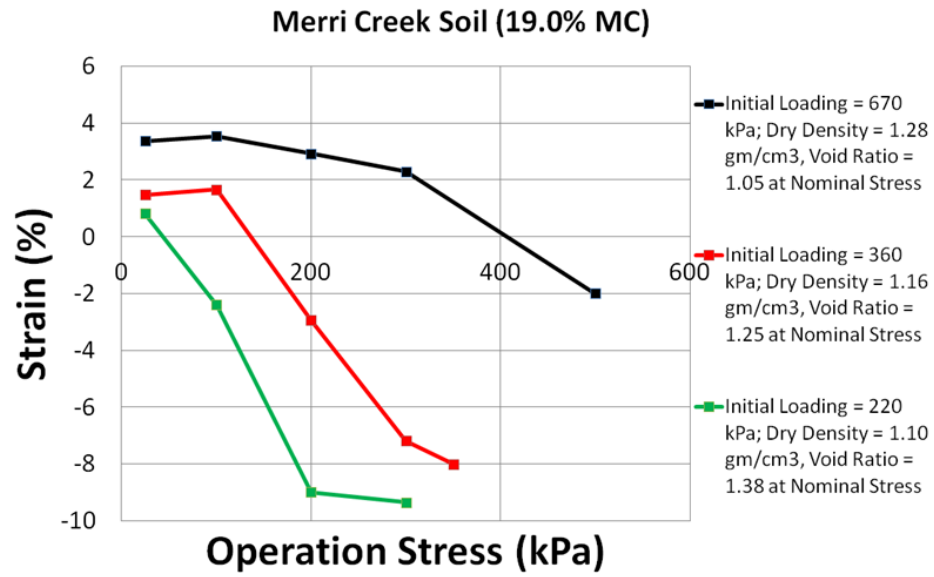
**(c)** For 19.0% initial moisture content or $e_{wo} = 0.498$

Figure 7-15: Effect of moisture content and dry density on swelling/compression during major wetting for Merri Creek soil
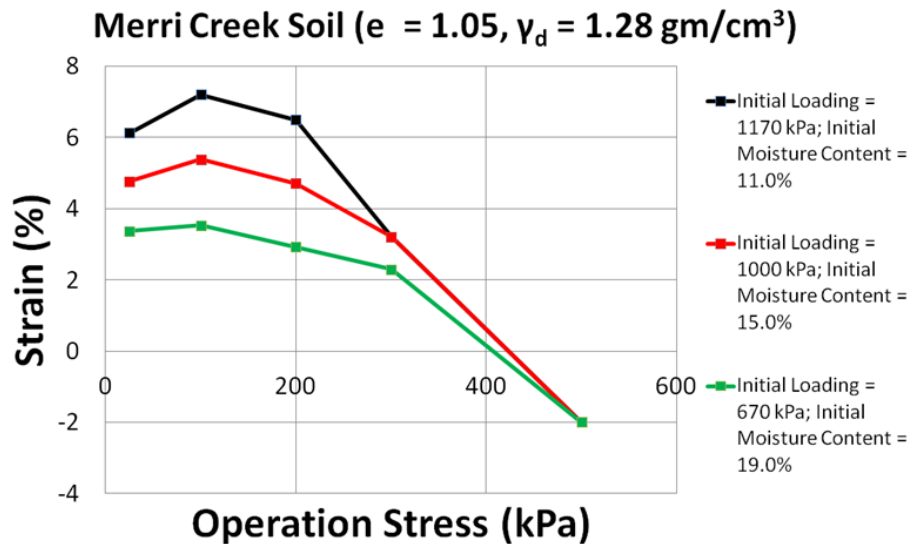
(a) For 1.28 gm/cc or 12.56 kN/m^3 unloaded dry density
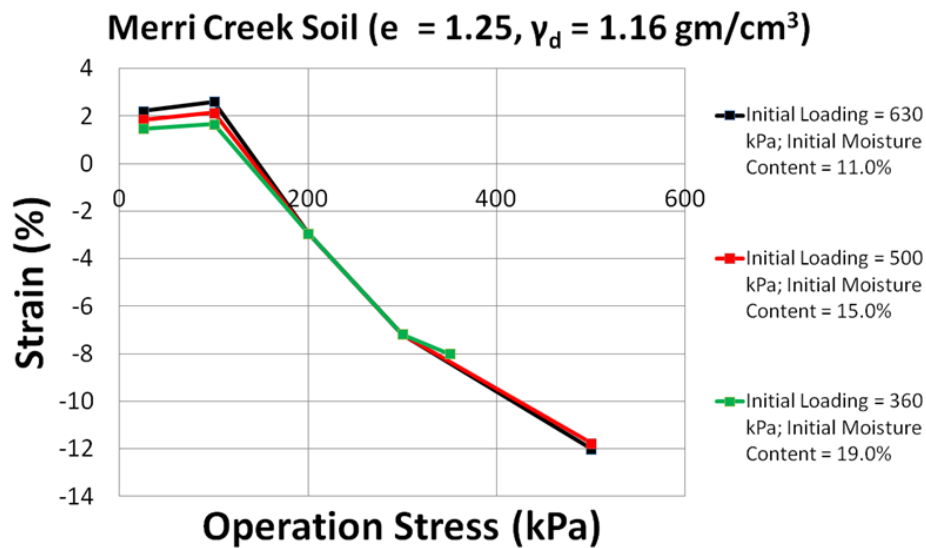
(b) For 1.16 gm/cc or 11.38 kN/m^3 unloaded dry density

Figure 7-16: Effect of moisture content on swelling/compression during major wetting for Merri Creek soil
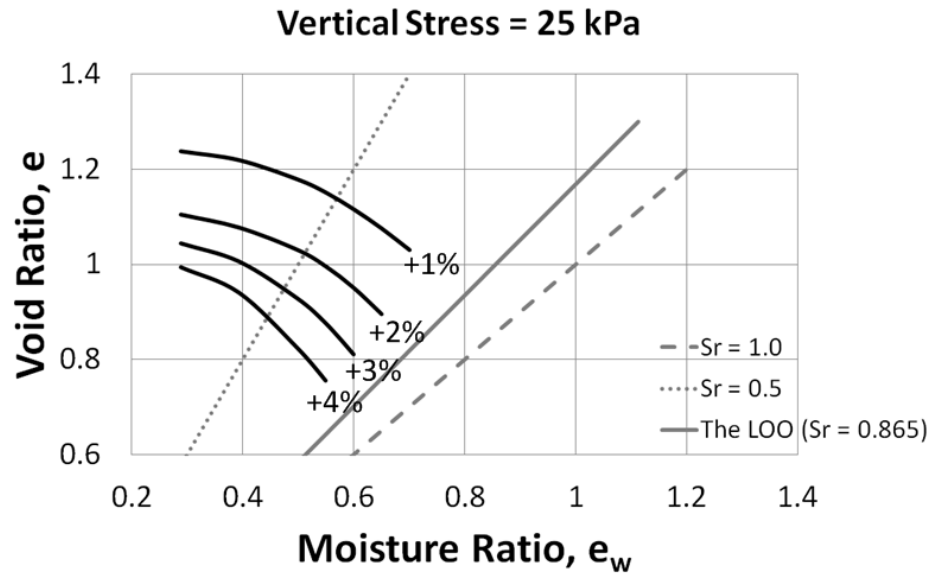
(a) On void ratio – moisture ratio plane for 25 kPa vertical stress
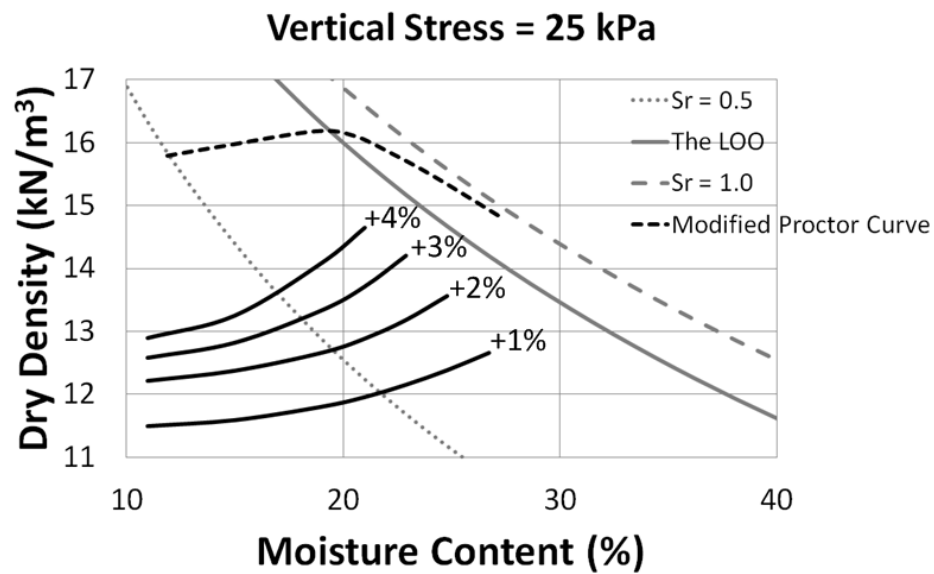
(b) On dry density – moisture content plane for 25 kPa vertical stress
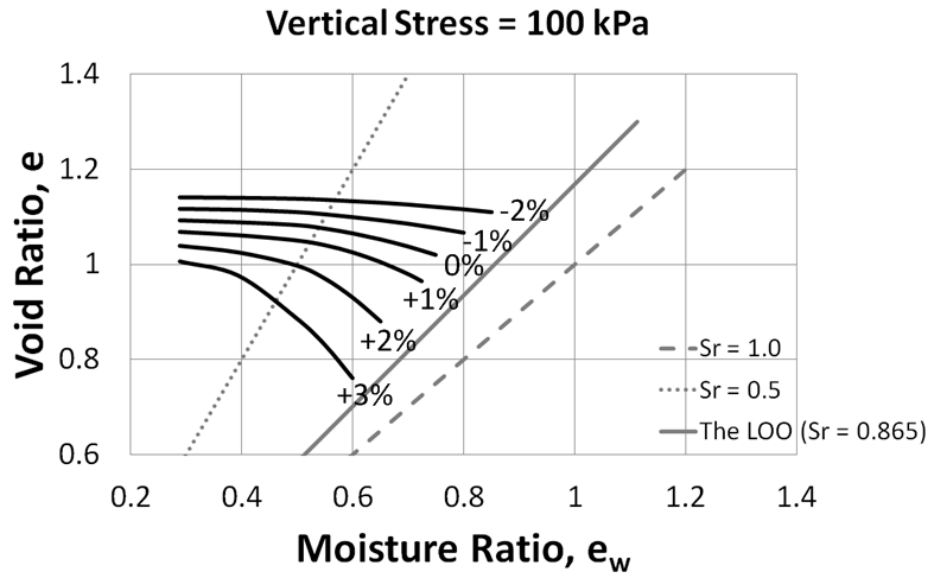
(c) On void ratio – moisture ratio plane for 100 kPa vertical stress
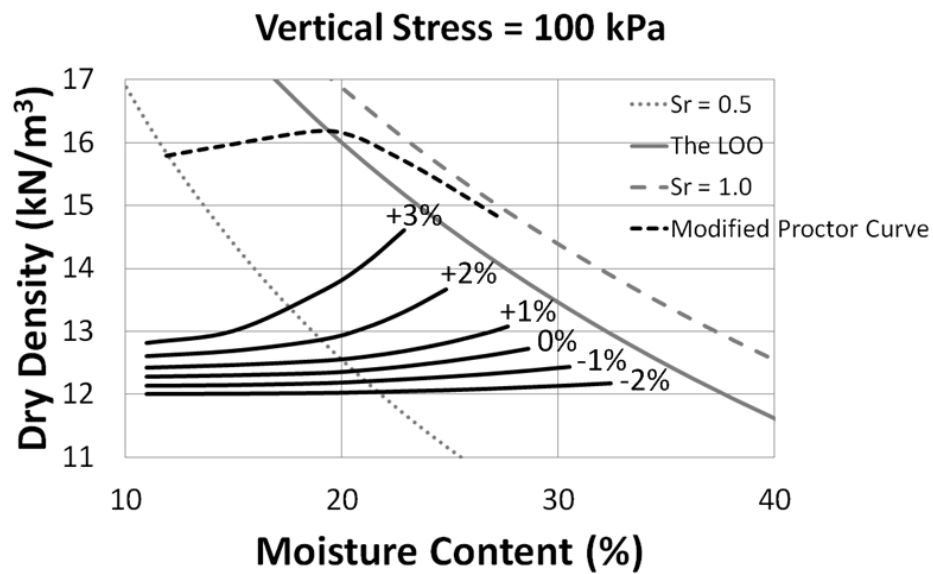
(d) On dry density – moisture content plane for 100 kPa vertical stress
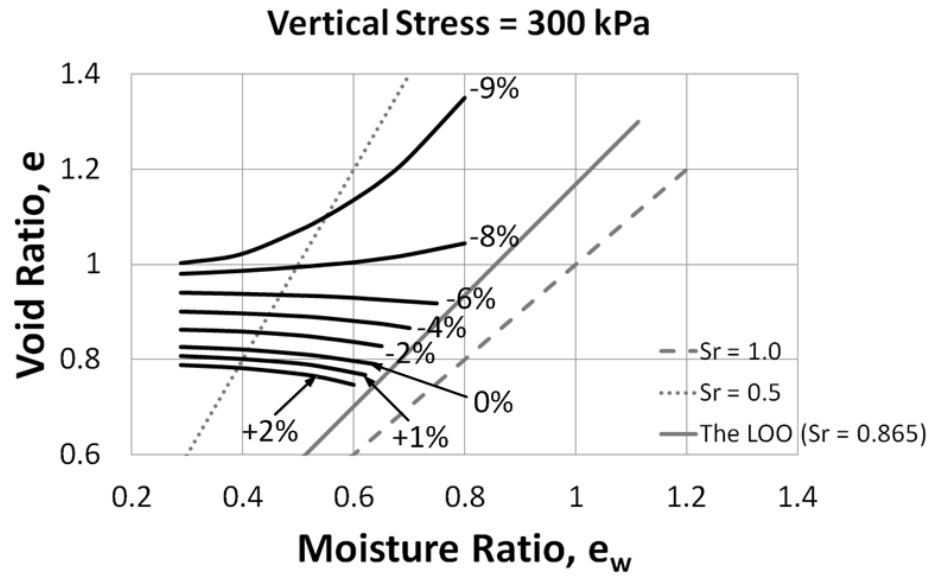
(e) On void ratio – moisture ratio plane for 300 kPa vertical stress
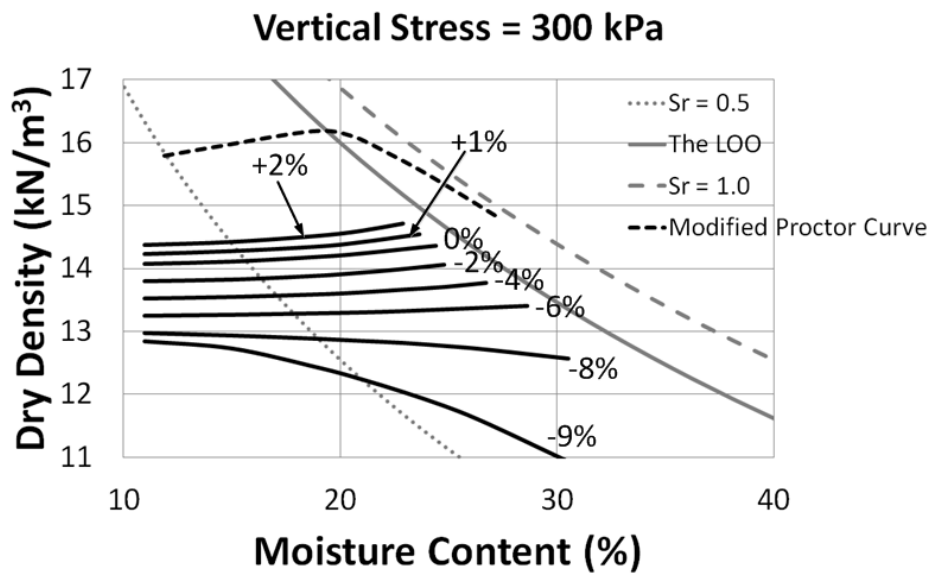
(f) On dry density – moisture content plane for 300 kPa vertical stress

Figure 7-17: Contours of equal swell and equal compression for Merri Creek soil
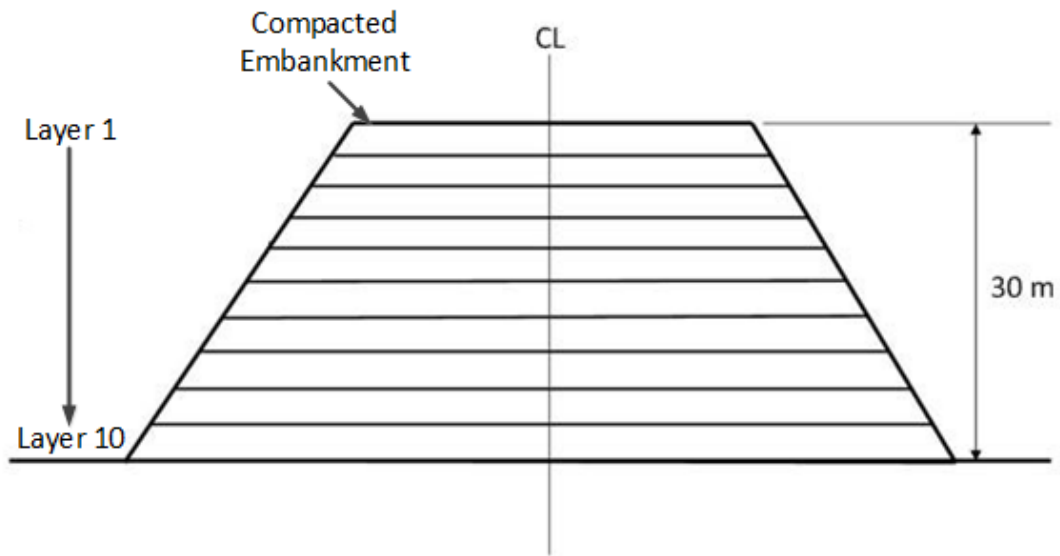
Figure 7-18: The 30 metre high embankment
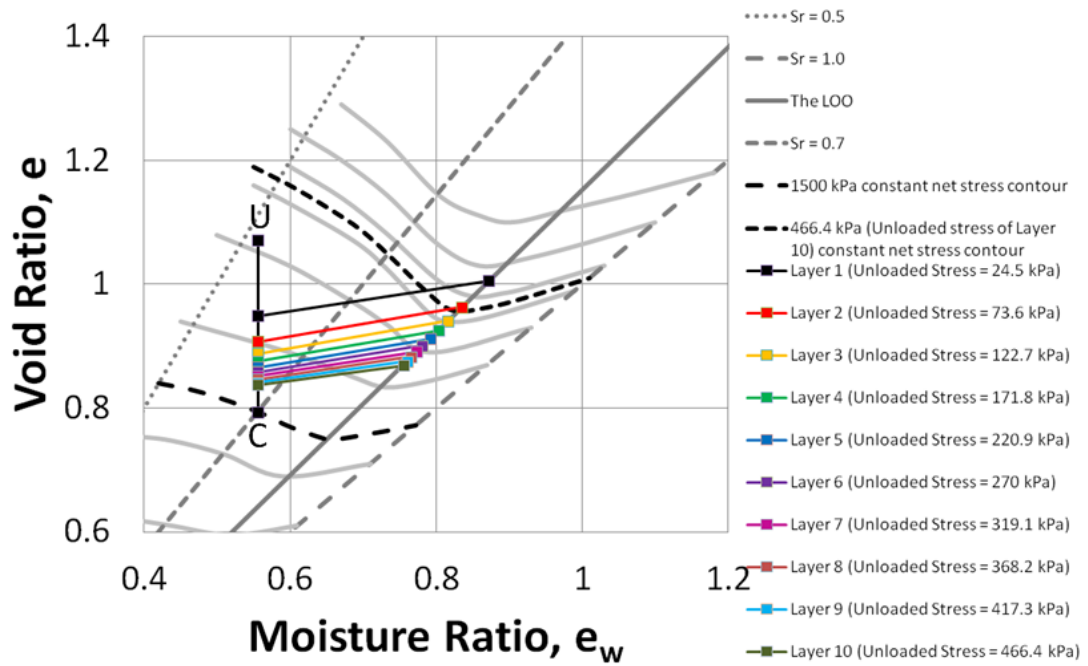
(a) Initial Condition: High Compaction and Compacted to $S_r = 0.7$
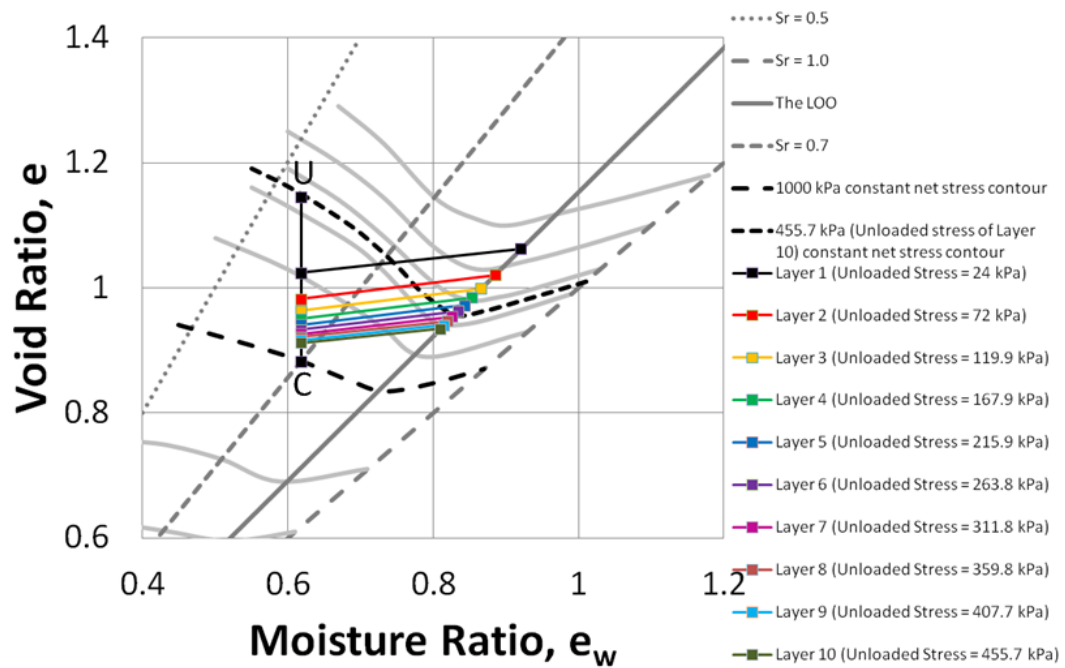
(b) Initial Condition: Intermediate Compaction and Compacted to $S_r = 0.7$

(c) Initial Condition: Standard Proctor and Compacted to $S_r = 0.7$
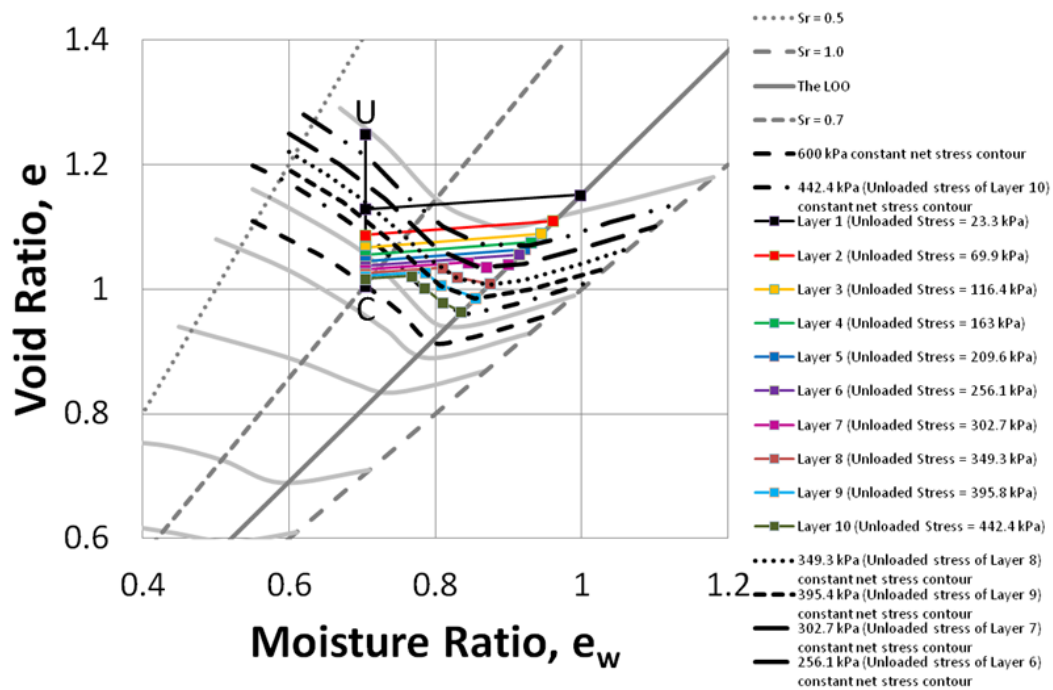
(d) Initial Condition: Moderate Compaction and Compacted to $S_r = 0.7$
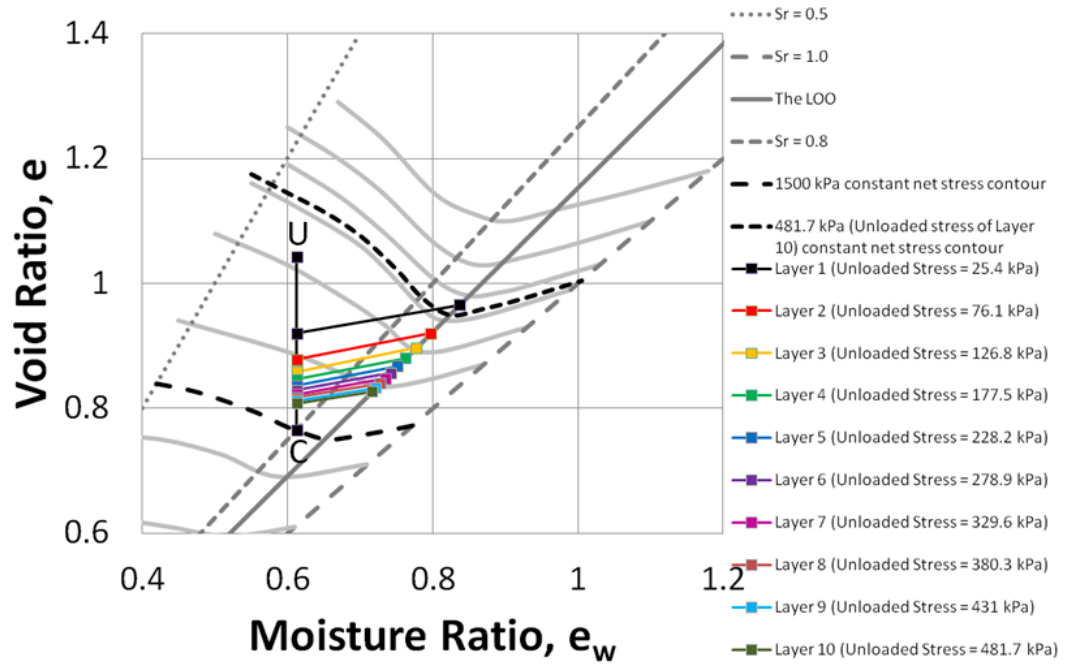
(e) Initial Condition: High Compaction and Compacted to $S_r = 0.8$
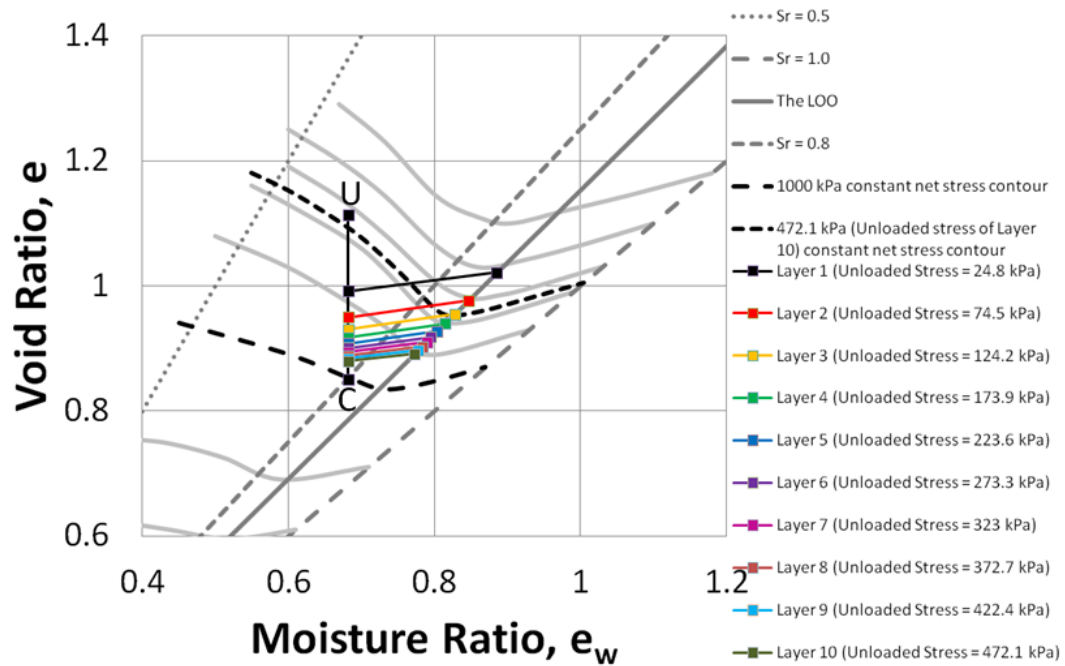
(f) Initial Condition: Intermediate Compaction and Compacted to $S_r = 0.8$
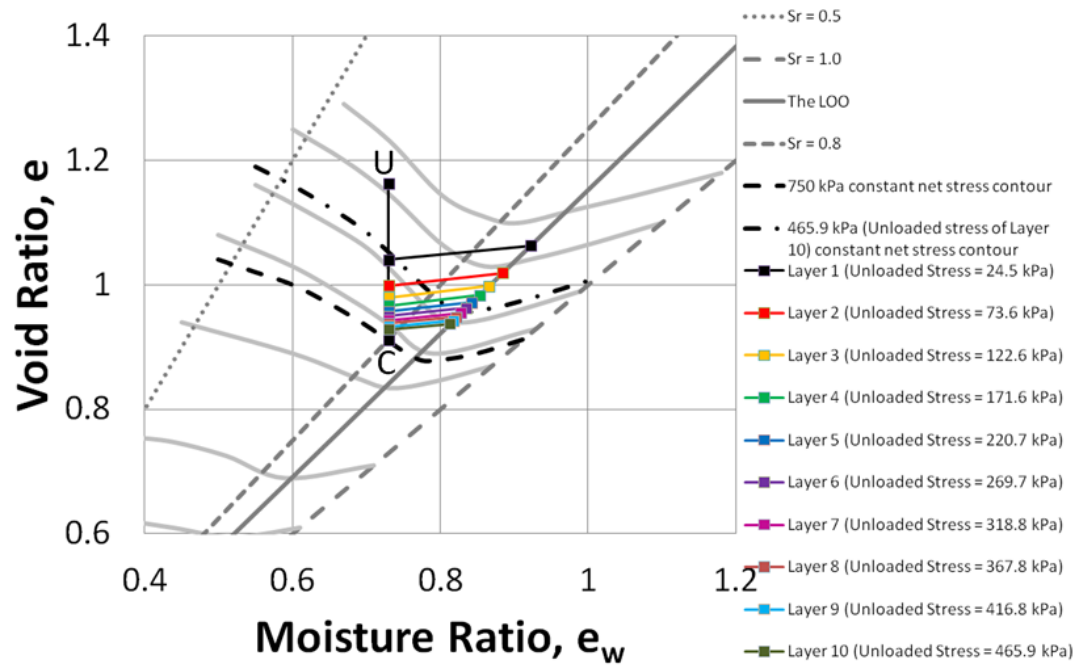
(g) Initial Condition: Standard Proctor and Compacted to $S_r = 0.8$
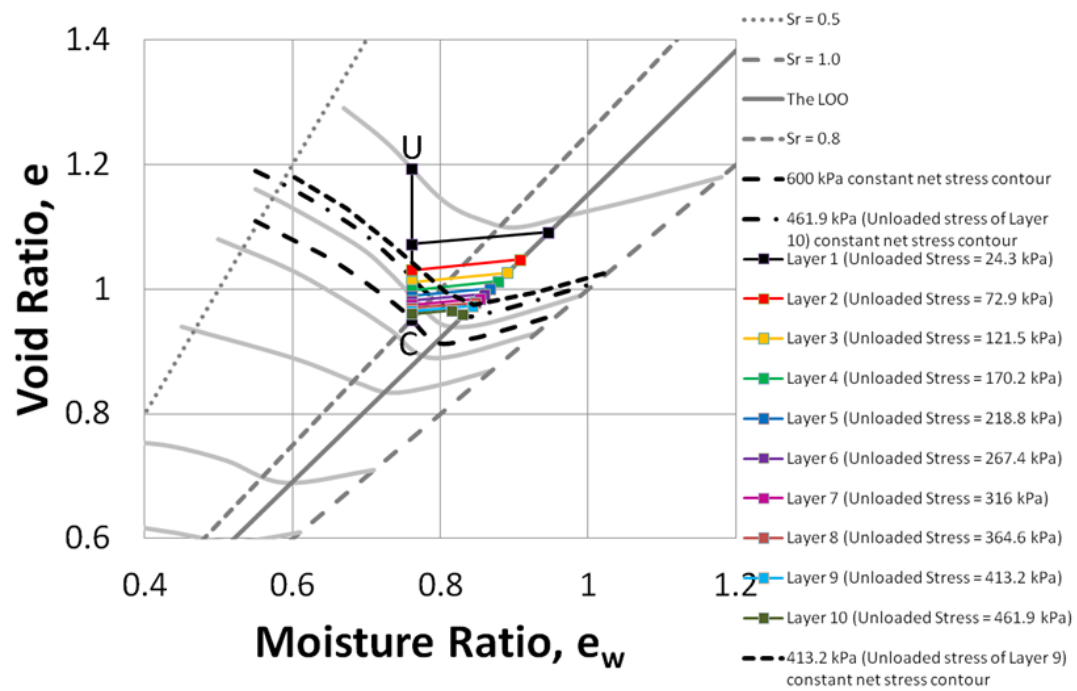
(h) Initial Condition: Moderate Compaction and Compacted to $S_r = 0.8$

Figure 7-19: Modelling of major wetting events on an embankment made of kaolin soil using the MPK framework for different initial conditions
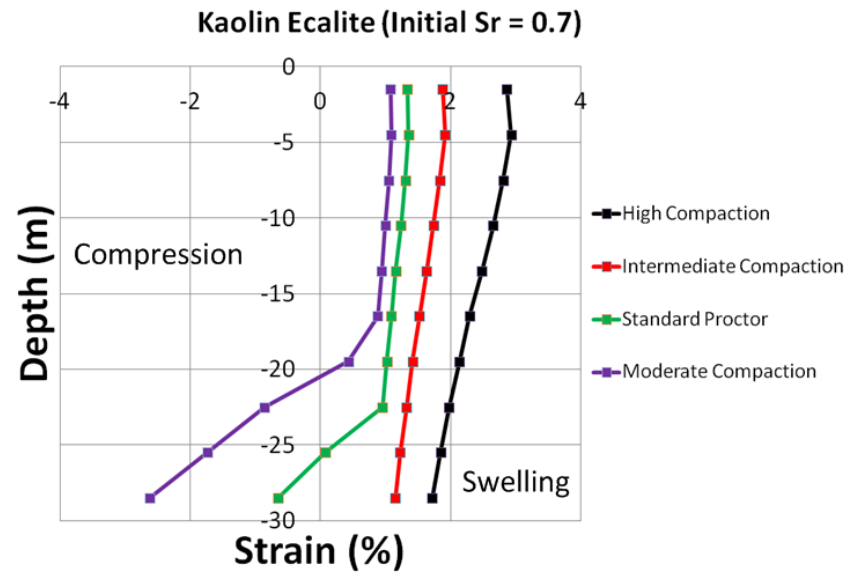
(a) Initial Compacted $S_r = 0.7$
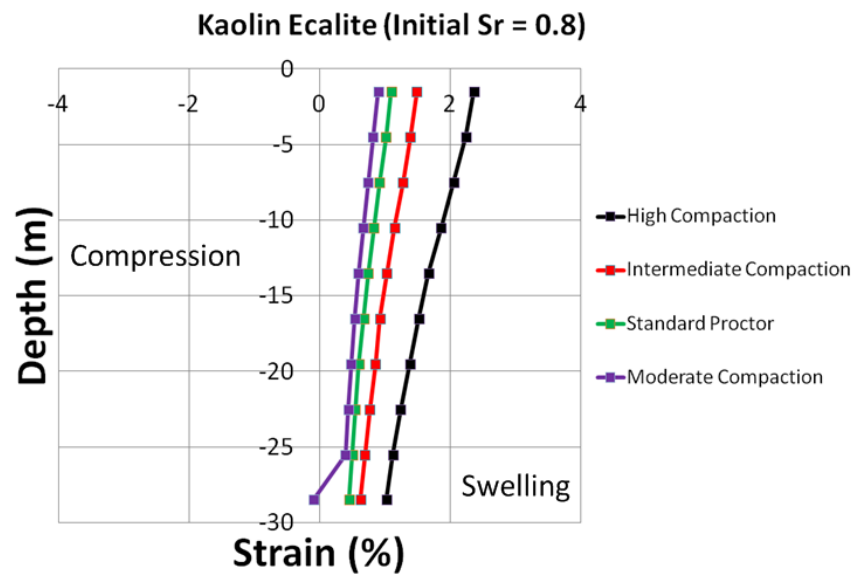
(b) Initial Compacted $S_r = 0.8$

Figure 7-20: Effect of compaction levels on swelling/compression with the depth of the embankment during major wetting events for kaolin soil

Kaolin Ecalite (High Compaction)

(a) Initial level of compaction: High Compaction

Kaolin Ecalite (Intermediate Compaction)
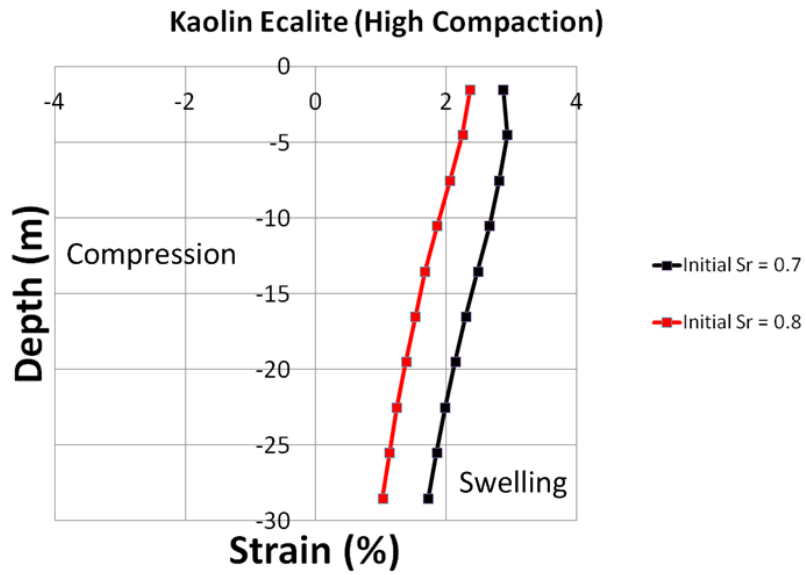
(b) Initial level of compaction: Intermediate Compaction

(c) Initial level of compaction: Standard Proctor

(d) Initial level of compaction: Moderate Compaction

Figure 7-21: Effect of degree of saturation on swelling/compression with the depth of the embankment during major wetting events for kaolin soil
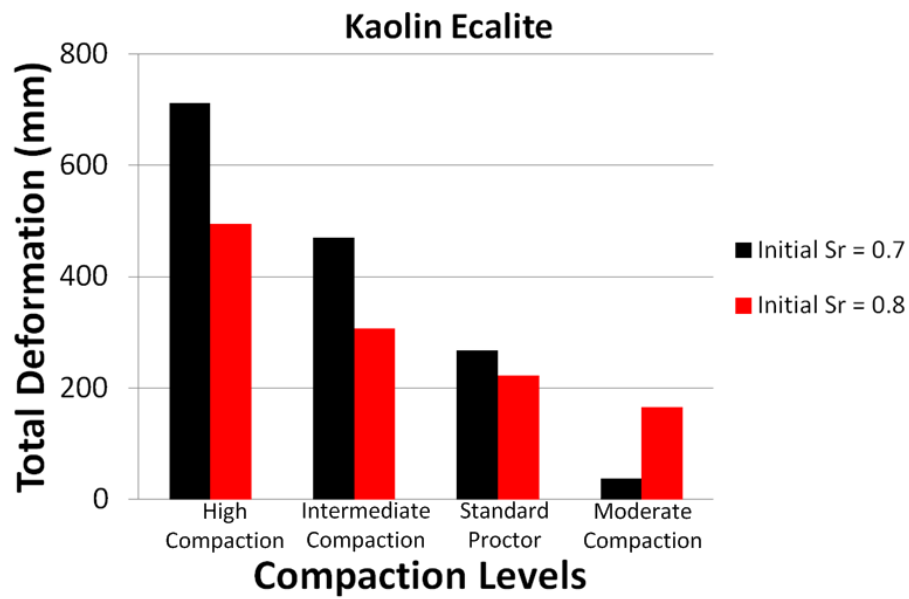
Figure 7-22: Effect of compaction levels and degree of saturation on the total deformation (swelling) of the embankment during major wetting events for kaolin soil

(a) Initial Condition: High Compaction and Compacted to $S_r = 0.7$
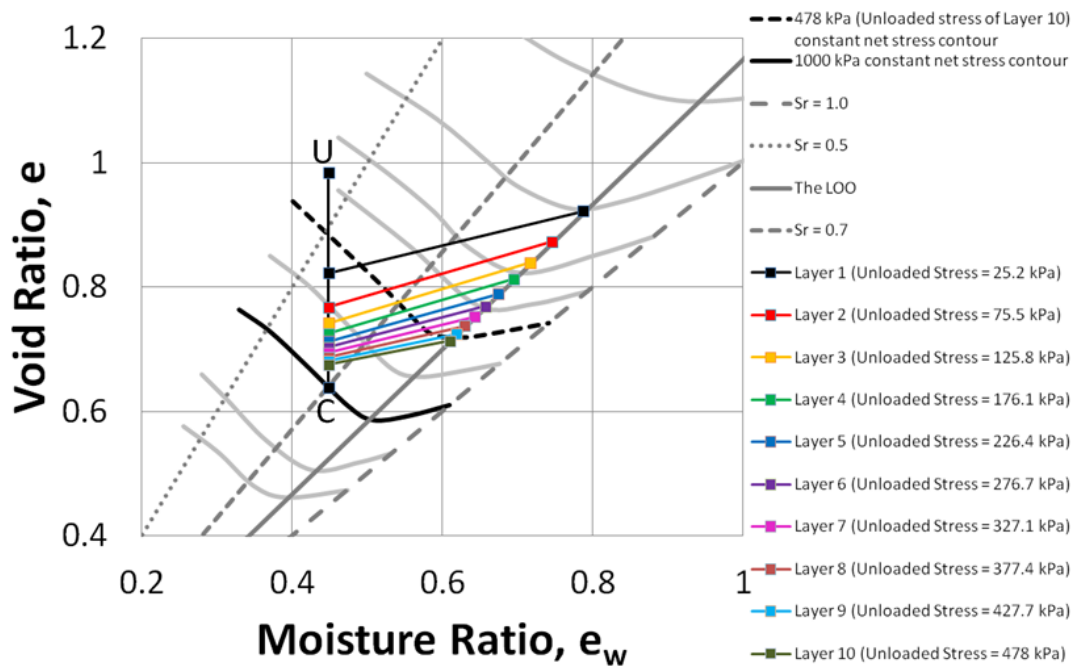
(b) Initial Condition: Intermediate Compaction and Compacted to $S_r = 0.7$

(c) Initial Condition: Standard Proctor and Compacted to $S_r = 0.7$
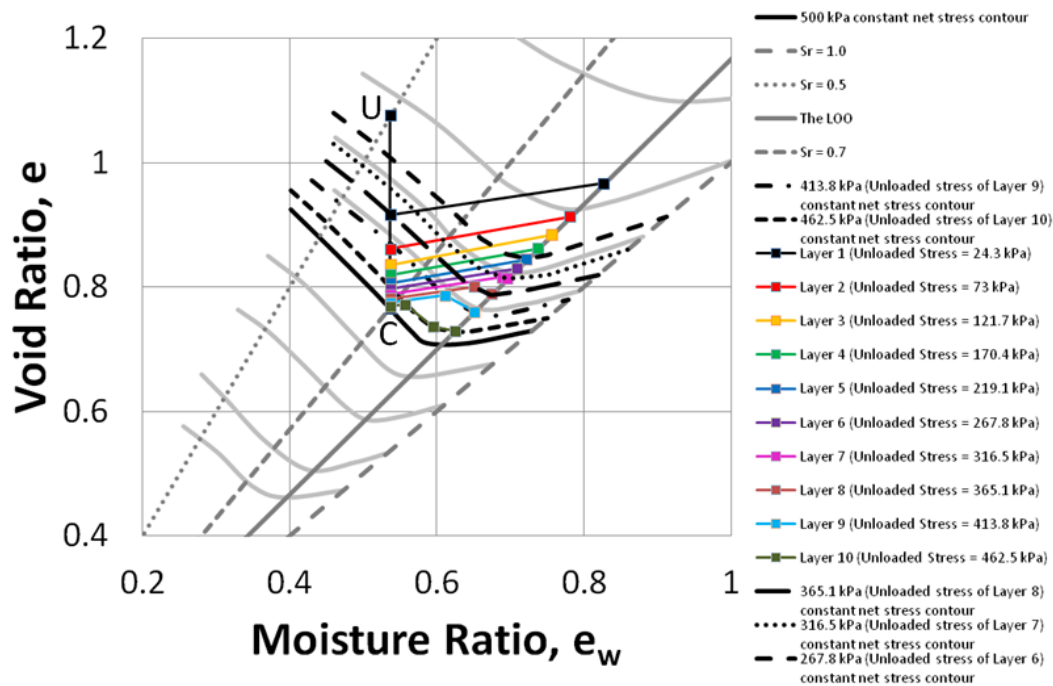
(d) Initial Condition: Moderate Compaction and Compacted to $S_r = 0.7$
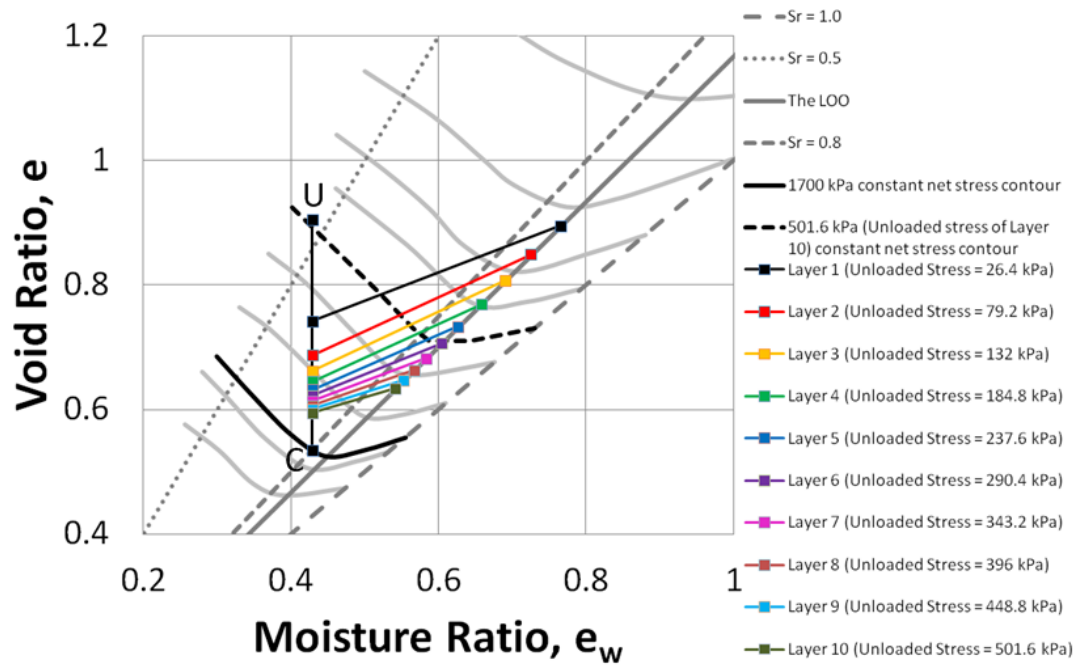
(e) Initial Condition: High Compaction and Compacted to $S_r = 0.8$
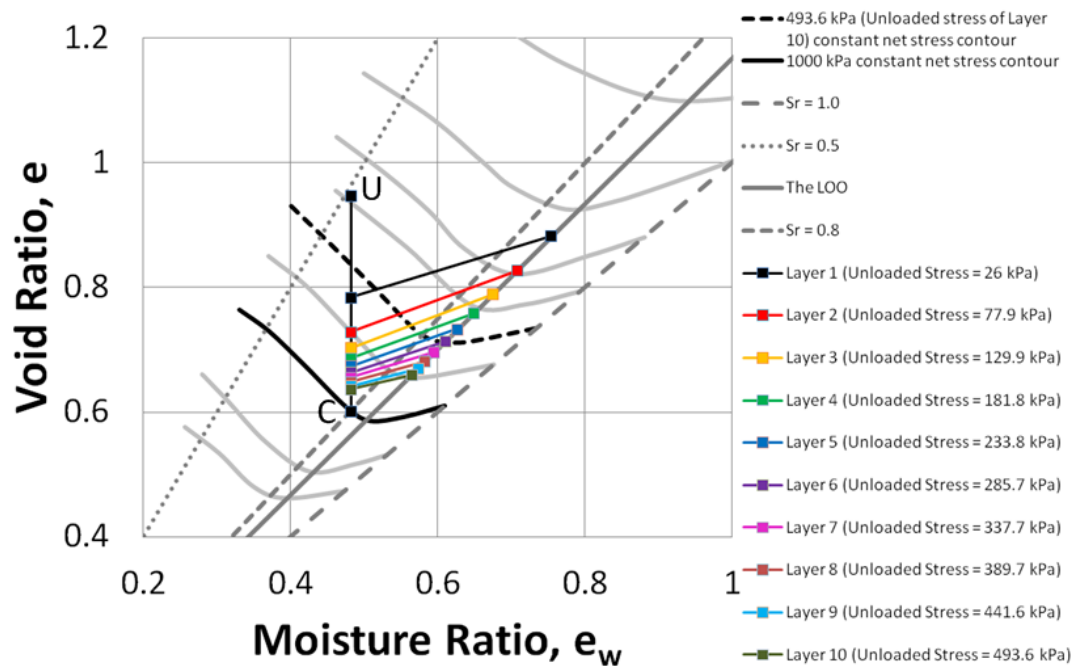
(f) Initial Condition: Intermediate Compaction and Compacted to $S_r = 0.8$
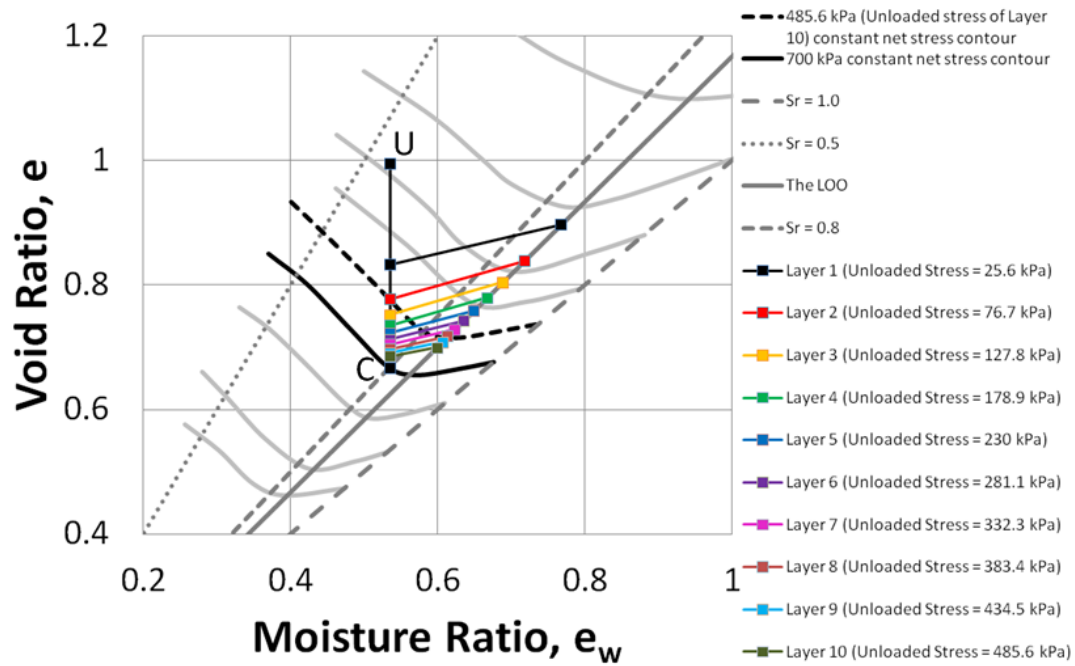
(g) Initial Condition: Standard Proctor and Compacted to $S_r = 0.8$
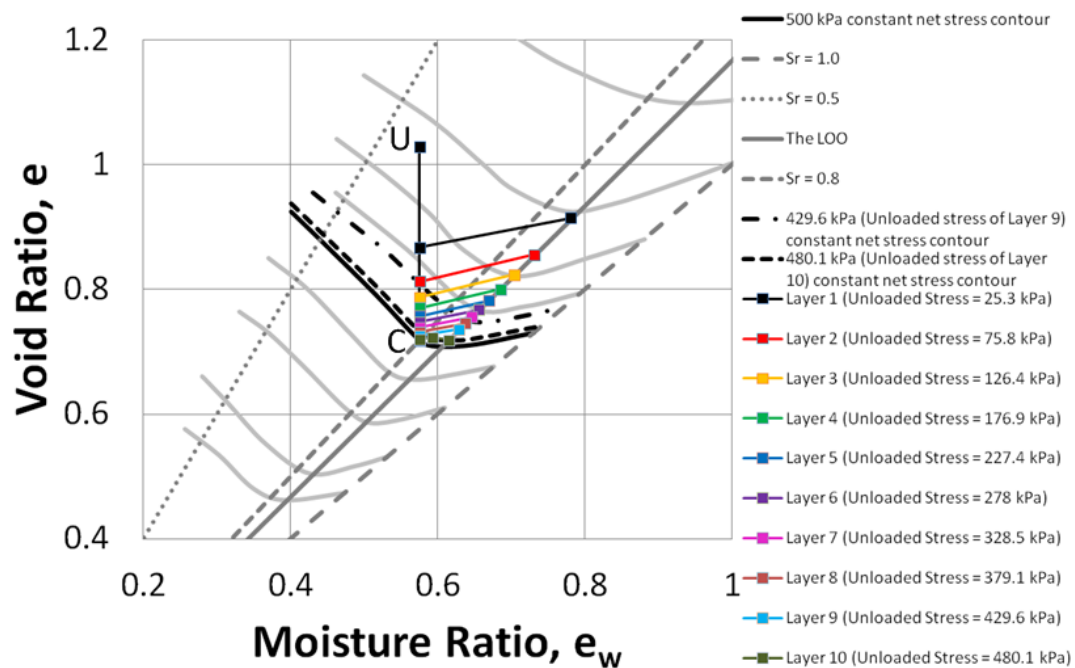
(h) Initial Condition: Moderate Compaction and Compacted to $S_r = 0.8$

Figure 7-23: Modelling of major wetting events on an embankment made of Merri Creek soil using the MPK framework for different initial conditions
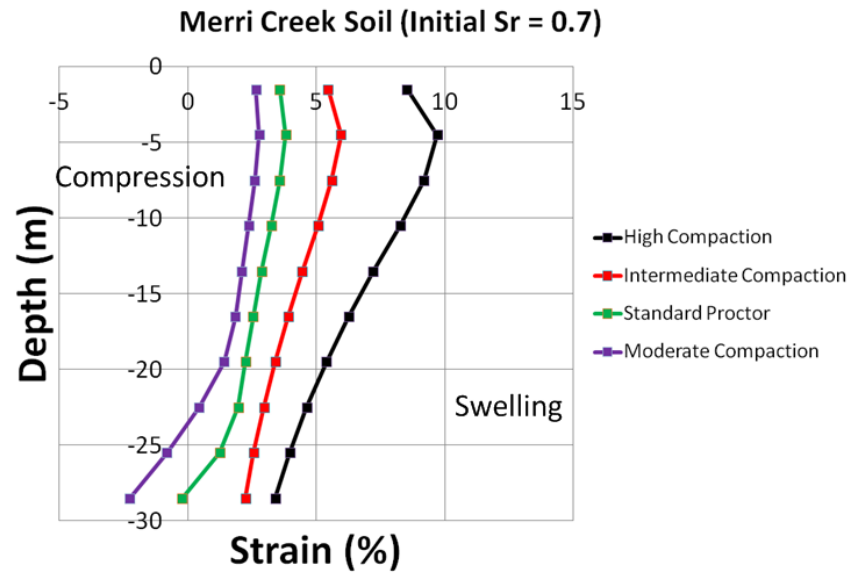
(a) Initial Compacted $S_r = 0.7$
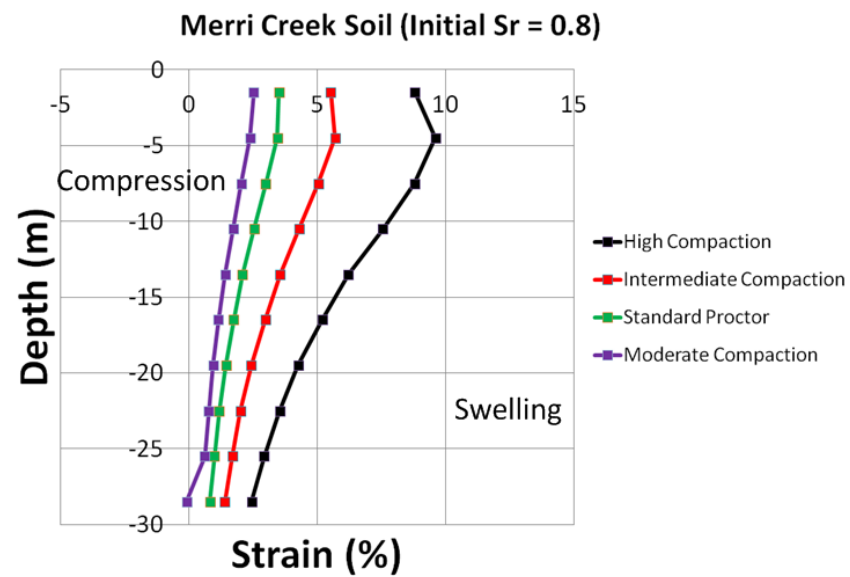
(b) Initial Compacted $S_r = 0.8$

Figure 7-24: Effect of compaction levels on swelling/compression with the depth of the embankment during major wetting events for Merri Creek soil
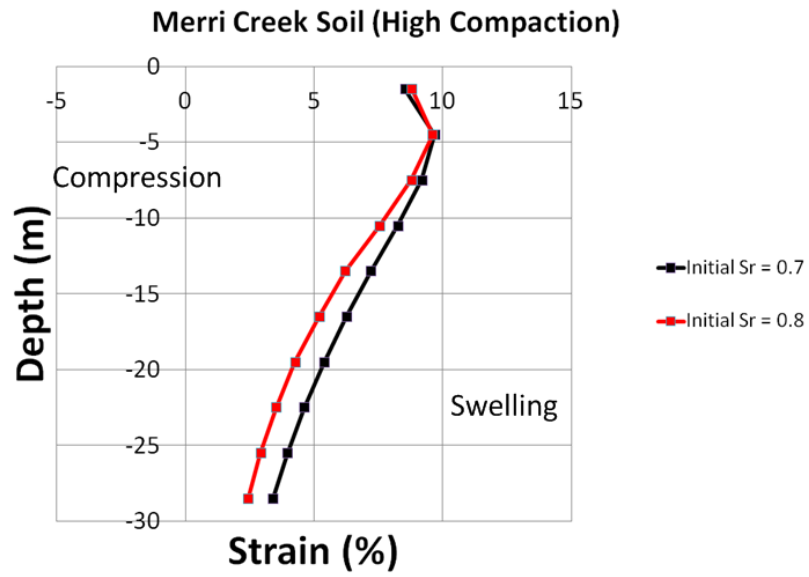
(a) Initial level of compaction: High Compaction
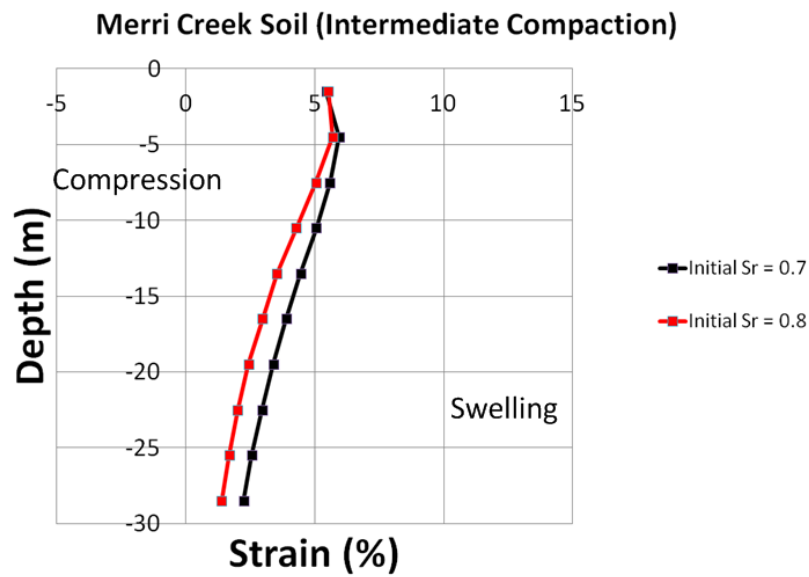
(b) Initial level of compaction: Intermediate Compaction
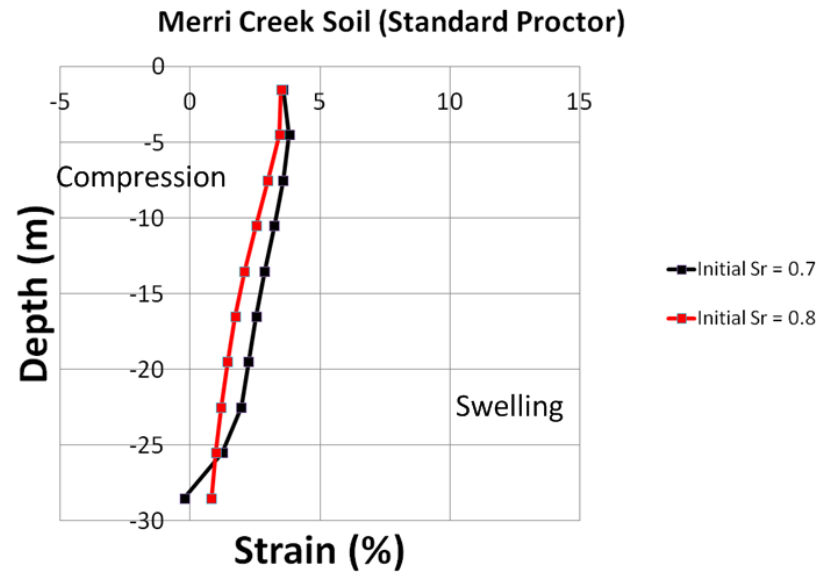
(c) Initial level of compaction: Standard Proctor
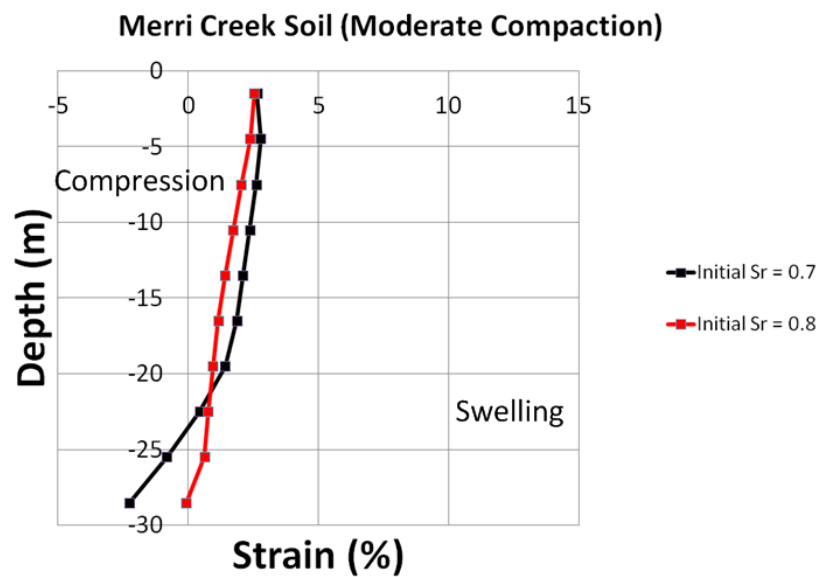
(d) Initial level of compaction: Moderate Compaction

Figure 7-25: Effect of degree of saturation on swelling/compression with the depth of the embankment during major wetting events for Merri Creek soil
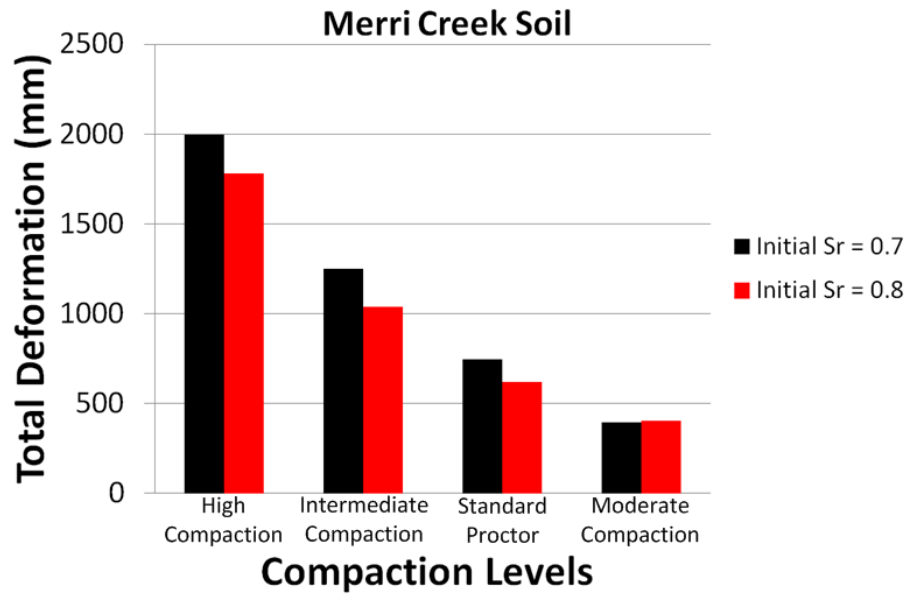
Figure 7-26: Effect of compaction levels and degree of saturation on the total deformation (swelling) of the embankment during major wetting events for Merri Creek soil

CONCLUSIONS AND DIRECTIONS FOR

FUTURE RESEARCH

8.1 Conclusions

The primary objectives of this research project were the comprehensive validation and the extension of the Monash-Peradeniya-Kodikara (MPK) framework proposed by Kodikara (2012). The research was concentrated on the following areas: the provision of a complete set of experimental evidence in support of the MPK framework; an extension of the MPK framework to dynamically compacted soils; the incorporation of suction and average hydric coefficient within $e - e_w - p$ space; and a qualitative comparison between the MPK framework predicted heave/settlement results and the experimental results obtained from the literature for field-scale compacted fills. The conclusions gained from the study are presented in this chapter.

8.1.1 Validation of the MPK framework using statically compacted soils

A large number of experiments were performed for statically compacted lightly reactive kaolin soil and reactive Merri Creek soil under combinations of loading, wetting and unloading state paths subjected to different boundary and initial conditions. Despite the difference in their degrees of reactivity, both soils closely followed the concepts of the MPK framework proposed by Kodikara (2012). Some tests undertaken by Jotisankasa (2005), Jotisankasa et al. (2007a), Sharma (1998) and Romero (1999) were also successfully interpreted within the framework. The results indicate that the void ratio-moisture ratio-net stress space, along with the loading wetting state boundary surface (LWSBS), can be used to explain/predict the behaviour of statically compacted soil under hydro-mechanical state paths of non-decreasing degrees of saturation.

In relation to the LWSBS for both soils, the void ratio increases with decreasing moisture ratio due to the macroscopic structure build-up, but at very low moisture contents, the void ratio can decrease again. This feature is more prominent for Merri Creek soil.

However, this effect appears to decrease and eventually vanish at higher net stress levels. The occurrence of this feature is similar to having compaction curves with multiple peaks, and appears to be related to the weakening of the effect of suction to form stronger contacts among aggregates that give larger macro void space. Another important feature is the cross-validity and the uniqueness of the compression curves at constant moisture ratio to represent the LWSBS across moisture ratios, as incorporated in the MPK framework. This is highlighted by the validated ability for the LWSBS to predict the behaviour of soil state paths during wetting and loading (or a combination of both) when the LWSBS is intercepted.

Another important feature of the MPK framework is the introduction of the influence of the Line of Optimum (LOO) on the soil behaviour, which demarcates the boundary between dry and wet of optimum. The LOO can be defined as the boundary where the air phase moves from a continuous phase in the dry side to a discontinuous phase in the wet side. Along with this, the all-round influence of suction becomes prominent in the wet side and this gives rise to the increase of void ratio with increasing moisture ratio (or vice versa). This behaviour gives the canyon-like feature in the LWSBS with the LOO at its bottom associated with the minimum void ratio (or maximum dry density). The wetting tests that followed the LWSBS showed the existence of this feature. Similarly, constrained swelling tests also clearly demonstrated the influence of the LOO on the LWSBS. For instance, the swelling pressure increased to a peak until the state path intercepted the LWSBS and then followed it, the swelling pressure then decreased to the LOO and then increased again towards full saturation. Another important validation is the confirmation of the characteristic behaviour of collapse potential, where the peak collapse occurred at the compaction stress.

The LWSBS, which is the basic building block of the MPK framework, can be established by constant moisture content compression tests and assuming cross-validity in the increasing direction of moisture content. Since constant moisture content tests do not require the specialised test equipment necessary for suction control tests, this approach remarkably simplifies the test method and reduces testing time. No suction was measured when the validation experiments were performed, as it was not essential to explain most volumetric behaviour as per the MPK framework.

8.1.2 Volume change behaviour of dynamically compacted unsaturated soils within the MPK framework

A large number of experiments were performed on the dynamically compacted lightly reactive kaolin and reactive Merri Creek soils with constant moisture content. Since the compaction stress was unknown for dynamic compaction, recompression of soil specimens from compacted soil was used to establish the LWSBS. Independent tests showed that the MPK framework could predict well the behaviour of compacted soils under loading/unloading and yielding, collapse during wetting, change of loading yield stress after wetting, and swelling pressure development during constrained wetting.

Similar to statically compacted soils, the influence of the LOO is clearly evident from the experimental results. The cross-validity and the uniqueness of the LWSBS have been established by a large number of state paths involving a combination of loading, unloading and wetting. The capability for the LWSBS to predict the change in yield point for state paths that undergo wetting at constant stress has also been verified. Similarly, constrained swelling tests also clearly demonstrate the influence of the LOO on the LWSBS. For instance, similar to statically compacted soils, the swelling pressure increases to a peak until the state path intercepts the LWSBS and then follows it, the swelling pressure subsequently decreasing to the LOO and then increasing again towards full saturation. Another important validation is the confirmation of the characteristic behaviour of collapse potential, where the peak collapse occurs at the compaction (yield) stress, similar to the behaviour displayed for the statically compacted soils.

The most significant application of these findings to practice is that, with the proposed MPK framework, it now appears possible to directly evaluate compacted clay performance at the field scale. For instance, it is possible to obtain cores from field pads, where compaction is conducted using rollers to be used in the field. These cores can then be used to establish the LWSBS for compacted soils and then analyses can be undertaken to predict the performance under the expected field environmental and external loadings. As noted previously, constant moisture content testing is very straightforward and, furthermore, it is only necessary to develop the relevant section of the LWSBS that is considered operative for a given field application.

8.1.3 Incorporation of suction within the MPK framework

The aim was to mathematically develop the full profile of the soil suction for wetting and loading within the $e - e_w - p$ space for the kaolin and Merri Creek soils. Two hypotheses were proposed to present the suction contours on and inside the LWSBS by analysing several datasets (Tarantino and De Col (2008); Jotisankasa (2005); Romero (1999); Sharma (1998)) from the research literature. Subsequently, a mathematical representation was provided to establish the full suction profile within the $e - e_w - p$ space for both kaolin and Merri Creek soil.

During mathematical representation, suction planes within the $e - e_w - p$ space were divided into three parts. Different parts were developed differently and then attached together to obtain the full suction profile. The suction contours at the wet side of the LOO on the LWSBS were established by considering the effective stress principle between the optimum and the saturated plane. As the equations of the LWSBS between the LOO and $S_r = 1.0$ are known, it is possible to determine the value of suction anywhere at the wet side of the LOO on the LWSBS. Subsequently, the suction contours at the dry side of the LOO on the LWSBS were developed considering cubic Bézier curves in the Soil Water Characteristics Curve (SWCC) between the LOO and the dry condition. The other three options for the development of suction contours at the dry side of the LOO on the LWSBS were left for future research. According to the research literature (c.f., Sharma, 1998; Romero, 1999; Tarantino and De Col, 2008), at the dry side of the LOO, the values of soil suction on and inside the LWSBS are equal for a certain moisture content and net stress. In order to satisfy this, it was necessary to employ fifth-order Bézier curves to approximate the suction contours inside the LWSBS at the constant net stress planes. However, in reality it is possible for suction contours to curve prior to reaching the LOO. In this case, lower order (such as fourth-order, cubic or quadratic) Bézier curves may be used, as the experimental data dictate.

As the MPK framework is not dependant on the suction parameter, any volumetric behaviour related to the loading and/or wetting of compacted or virgin unsaturated soil can be explained by the LWSBS in the $e - e_w - p$ space for any type of soil, irrespective of the degree of reactivity. However, knowledge of the suction profile within the $e - e_w - p$ space can be helpful to complete the hydro-mechanical picture in the

volumetric space. Therefore, in future, research can be directed to explain the suction according to the extended framework, incorporating the suction within the MPK framework.

8.1.4 Field application of the MPK framework

A significant number of tests and field scenarios were modelled using the MPK framework on the compacted unsaturated kaolin and Merri Creek soils for major wetting events. The results were then compared with the experimental results from Noorany and Stanley (1994). It was found that with this extension, the performance of the MPK framework in predicting the volumetric behaviour of compacted unsaturated soil is very encouraging. The complex experimental results of the volumetric behaviour due to major wetting events are easily explainable with the help of the MPK framework. The operational stress is as important as the compaction stress of a compacted fill, as most of the volumetric behaviour of compacted unsaturated soil depends on these two parameters.

Another important item is the gradient (as depicted by the hydric coefficient) of the swelling during wetting, which controls the strain during major wetting events. The gradient of swelling during wetting of compacted unsaturated soil depends on the various parameters related to compaction, operational and nominal conditions. On the basis of observed behaviour and using the principles of the MPK framework, a simplified equation was developed where there are only two parameters, viz., operational stress (p_o) and operational void ratio (e_o). From these findings, it now appears possible to predict the volumetric behaviour during major wetting events by knowing the position of the LWSBS and the equation of the gradient of swelling during wetting, which can be found by performing fairly simple laboratory tests.

8.2 Directions for future research

The current research program has completed the validation and extension of the MPK framework in volumetric space. The following studies need to be undertaken in future for the complete development of the MPK model for unsaturated soils.

Extension of volumetric behaviour to drying and loading state paths including suction: The current thesis placed emphasis on the state paths involving loading and wetting. However, some evaluations involving drying and loading state paths were performed on the basis of some available data. These results were encouraging to explain the change in yield stress due to drying using the LWSBS. However, these evaluations were preliminary, and further research needs to be undertaken to fully address this area.

Extension to model shear behaviour: From the previous discussion, as the volumetric space of e, e_w, p and s is now established, the next requirement is to be able to model shear behaviour. This basically means incorporation of the deviatoric stress q. In the Barcelona Basic Model (BBM), this behaviour is based on the loading/wetting collapse (LC) curve, which actually corresponds to the constant plastic part of volume change in q, p and s space in combination with the volumetric space given by $v(= 1 + e)$, p and s. A similar approach may be followed to incorporate shear behaviour using either q, p, v and v_w or q, p, v and s as constitutive variables. The loading/wetting collapse curves could be developed from the LWSBS which represents the boundary yield surface for loading/wetting states.

Development of basic numerical models to simulate volumetric and shear models: The constitutive models for volumetric and shear behaviour can be used to implement the numerical models, which could considered as basic models for use in routine applications.

Targeted experimentation to refine validate constitutive models for shear behaviour and numerical simulation: A targeted test program can be undertaken to examine some of the hypotheses used in the numerical model derivations and to provide data for refinement and validation of the constitutive modelling approaches. Experiments may be undertaken in unsaturated stress path triaxial under both triaxial loading and K_0 loading.

Enhancement of the developed model to capture volumetric environmental stabilization: There is significant evidence that compacted clayey soils undergo changes when subjected to environmental loadings in the form of wet/dry cycles. Following the BBM approach, Gens and Alonso (1992) have developed models to cater for these

conditions. However, these models are very complicated with many parameters that are difficult to calibrate. Kodikara (2012) outlined that compacted clayey soils, when subjected to wet/dry cycles, will undergo changes and will eventually reach an "environmentally stabilised" state. At this stage, soils will shrink and swell reversibly without much plastic energy dissipation. A hypothesis for this behaviour was further explained in Kodikara et al. (2014). A series of targeted experiments (isotropic and K_0) can be undertaken to examine the hypothesis. Subsequently, in the light of the experimental results, the numerical model can be extended to cater for wet/dry cycling.

Model application to selected field problems: A centrifuge test can be undertaken to validate the numerical model for a field-scale problem. The beam centrifuge set-up in the University of Western Australia can be used for this purpose. Finally, it is possible to undertake field test pads to directly validate and demonstrate the use of the MPK framework for field-compacted fills.

Ahmed, S., Lovell, C.W., and Diamond, S., (1974). Pore sizes and strength of compacted clay. Journal of the Geotechnical Engineering Division, **100**(4): 407-425.

Alonso, E., Romero, E., Hoffmann, C., and García-Escudero, E., (2005). Expansive bentonite–sand mixtures in cyclic controlled-suction drying and wetting. Engineering geology, **81**(3): 213-226.

Alonso, E.E., Gens, A., and Hight, D.W., (1987). Special Problem soils. General Report. 9th European Conference of Soil Mechanics and Foundation Engineering. Dublin. pp. 1087-1146.

Alonso, E.E., Gens, A., and Josa, A., (1990). A constitutive model for partially saturated soils. Ge´otechnique, **40**(3): 405-430.

Alonso, E.E., Vaunat, J., and Gens, A., (1999). Modelling the mechanical behaviour of expansive clays. Engineering Geology, **54**(1–2): 173-183.

AS1289.3.1.1, (2009). Determination of the liquid limit of a soil – Four-point Casagrande method. Standards Australia, Sydney, Australia.

AS1289.3.2.1, (2009). Determination of the plastic limit of a soil – Standard method. Standards Australia, Sydney, Australia.

AS1289.3.4.1, (2008). Determination of the linear shrinkage of a soil – Standard method. Standards Australia, Sydney, Australia.

AS1289.3.6.3, (2003). Standard method of fine analysis using hydrometer. Standards Australia, Sydney, Australia.

AS1289.5.1.1, (2003). Determination of the dry density/moisture content relation of a soil using standard compactive effort. Standards Australia, Sydney, Australia.

AS1289.5.2.1, (2003). Determination of the dry density or moisture content relation of a soil using modified compactive effort. Standards Australia, Sydney, Australia.

References

AS1726, (1993). Geotechnical site investigations. Standards Australia, Sydney, Australia.

Barden, L., and Sides, G.R., (1970). Engineering behavior and structure of compacted clay. Journal of Soil Mechanics & Foundations Div, **96**(4): 1171-1200.

Bishop, A., Alpan, I., Blight, G., and Donald, I., (1960). Factors controlling the strength of partly saturated cohesive soils. ASCE Conference on Shear Strength of Cohesive Soils. Boulder, Colorado, USA.

Bishop, A.W., (1959). The principle of effective stress. Tecknisk Ukebald **106**(39): 859-863.

Blanchfield, R., and Anderson, W., (2000). Wetting collapse in opencast coalmine backfill. Proceedings of the ICE-Geotechnical Engineering, **143**(3): 139-149.

Bolzon, G., Schrefler, B., and Zienkiewicz, O., (1996). Elastoplastic soil constitutive laws generalized to partially saturated states. Géotechnique, **46**(2): 279-289.

Boyd, J., and Sivakumar, V., (2011). Experimental observations of the stress regime in unsaturated compacted clay when laterally confined. Géotechnique, **61**(4): 345-363.

Brackley, I.J., (1973). Swell pressure and free swell in a compacted clay. 3rd International Conference on Expansive Soils. Haifa, Israel. pp. 169–176.

BS1377-4, (1990). Methods of test for soils for civil engineering purposes. Compaction-related tests. British Standards, London, United Kingdom.

Buzzi, O., (2010). On the use of dimensional analysis to predict swelling strain. Engineering Geology, **116**(1): 149-156.

Buzzi, O., Giacomini, A., and Fityus, S., (2010). Towards a dimensionless description of soil swelling behaviour. Géotechnique, **61**(3): 271-277.

Charles, J., Burford, D., and Hughes, D., (1993). Settlement of opencast coal mining backfill at Horsley 1973-1992. Engineering Fills'93. Newcastle.

Chiu, C., and Ng, C., (2003). A state-dependent elasto-plastic model for saturated and unsaturated soils. Ge´otechnique, **53**(9): 809-830.

Costa, W.D.S.M., (2009). Study of desiccation cracking and fracture properties of clay soils. Ph.D. Thesis, Monash University, Australia.

Daniel, D., and Benson, C., (1990). Water Content Density Criteria for Compacted Soil Liners. Journal of Geotechnical Engineering, ASCE, **116**(12): 1811 - 1830.

Day, R.W., (1995). Discussion: California housing damage related to expansive soils. Performance of Constructed Facilities, **9**(3): 243-247.

Delage, P., Howat, M., and Cui, Y., (1998). The relationship between suction and swelling properties in a heavily compacted unsaturated clay. Engineering geology, **50**(1): 31-48.

DiMillio, A., (1982). Performance of Highway Bridge Abutments Supported by Spread Footings on Compacted Fill. Federal Highway Administration, U.S. Department of Transportation, Washington, D.C., United States.

Dineen, K., Colmenares, J.E., Ridley, A.M., and Burland, J.B., (1999). Suction and volume changes of a bentonite-enriched sand. Geotechnical Engineering, **137**: 197–201.

Ferber, V., Auriol, J.-C., Cui, Y.-J., and Magnan, J.-P., (2008). Wetting-induced volume changes in compacted silty clays and high-plasticity clays. Canadian Geotechnical Journal, **45**(2): 252-265.

Fityus, S., and Buzzi, O., (2009). The place of expansive clays in the framework of unsaturated soil mechanics. Applied Clay Science, **43**(2): 150-155.

Fleureau, J.-M., Verbrugge, J.-C., Huergo, P.J., Correia, A.G., and Kheirbek-Saoud, S., (2002). Aspects of the behaviour of compacted clayey soils on drying and wetting paths. Canadian Geotechnical Journal, **39**(6): 1341-1357.

Fredlund, D., and Morgenstern, N., (1976). Constitutive relations for volume change in unsaturated soils. Canadian Geotechnical Journal, **13**(3): 261-276.

References

Fredlund, D.G., and Rahardjo, H., (1993). Soil mechanics for unsaturated soils. John Wiley & Sons, New York.

Fredlund, D.G., and Xing, A., (1994). Equations for the soil-water characteristic curve. Canadian Geotechnical Journal, **31**(3): 521-532.

Gallipoli, D., Gens, A., Sharma, R., and Vaunat, J., (2003a). An elasto-plastic model for unsaturated soil incorporating the effects of suction and degree of saturation on mechanical behaviour. Géotechnique., **53**(1): 123-136.

Gallipoli, D., Wheeler, S.J., and Karstunen, M., (2003b). Modelling the variation of degree of saturation in a deformable unsaturated soil. Géotechnique., **53**(1): 105-112.

Gens, A., and Alonso, E., (1992). A framework for the behaviour of unsaturated expansive clays. Canadian Geotechnical Journal, **29**(6): 1013-1032.

Gens, A., Alonso, E.E., Suriol, J., and Lloret, A., (1995). Effect of structure on the volumetric behavior of a compacted soil. 1st International Conference on Unsaturated Soils. Paris, France. pp. 83–88.

Gilbert, O.H., (1959). The influence of negative pore water pressures on the strength of compacted clays. Master's Thesis, Massachusetts Institute of Technology, Cambridge, United States.

Gould, S.J.F., (2011). A Study of the Failure of Buried Reticulation Pipes in Reactive Soils. PhD Thesis, Monash University, Melbourne, Australia.

Gould, S.J.F., Kodikara, J., Rajeev, P., Zhao, X.-L., and Burn, S., (2011). A void ratio – water content – net stress model for environmentally stabilized expansive soils. Canadian Geotechnical Journal, **48**(6): 867-877.

Groenevelt, P.H., and Bolt, G.H., (1972). Water retention in soil. Soil Science, **113**(4): 238-245.

Hilf, J., (1975). Foundation Engineering Handbook, chapter Compacted fill. Chapman & Hall Ltd., London. pp. 249-316.

Hilf, J.W., (1956). An investigation of pore water pressure in compacted cohesive soils. Bureau of Reclamation.

Hogentogler, C., (1936). Essentials of soil compaction. Highway Research Board: pages 309-316.

Holtz, W.G., and Gibbs, H.J., (1956). Engineering properties of expansive clays: Transactions. ASCE, **121**: 641-677.

Horn, H.M., (1960). An investigation of the frictional characteristics of minerals. PhD Thesis, University of Illinois, Urbana-Champaign, Illinois, United States.

Houlsby, G.T., (1997). The work input to an unsaturated granular material. Géotechnique **47**: 193-196.

Houston, W.N., and Houston, S.L., (1995). Infiltration Studies for Unsaturated Soils. 1st Int. Conf. on Unsaturated Soils (UNSAT 95). *Edited by* E.E. Alonzo and P. Delage. Rotterdam: Balkema, Paris, France pp. 869-875.

Imbert, C., and Villar, M.V., (2006). Hydro-mechanical response of a bentonite pellets/powder mixture upon infiltration. Applied Clay Science, **32**(3 – 4): 197–209.

Islam, T., and Kodikara, J., (2015*). Interpretation of the loading/wetting behaviour of compacted soils within the MPK framework: Part I Static compaction. Canadian Geotechnical Journal, **under review**.

Jones, D.E.J., and Holtz, W.G., (1973). Expansive Soils –The hidden Disaster. Civil Engineering, **43**: 49–51.

Jotisankasa, A., (2005). Collapse Behaviour of a Compacted Silty Clay. PhD Thesis, Imperial College London, London, United Kingdom.

Jotisankasa, A., Coop, M. and Ridley, A., (2009). The mechanical behaviour of an unsaturated compacted silty clay. Ge´otechnique, **59**(5): 415 –428.

Jotisankasa, A., Ridley, A., and Coop, M., (2007a). Collapse Behavior of Compacted Silty Clay in Suction-Monitored Oedometer Apparatus. Journal of Geotechnical and Geoenvironmental Engineering, **133**(7): 867-877.

Joyce, E.B., (1992b). Geomorphology of the Melbourne region. *In* Engineering Geology of Melbourne. *Edited by* W.A. Peck and J.L. Neilson and R.J. Olds and K.D. Seddon. A. A. Balkema, Rotterdam. pp. 21–25.

Justo, J.L., Delgado, A., and Ruiz, J., (1984). The influence of stress path in the collapse-swelling of soils in the laboratory. Fifth International Conference on Expansive Soils. National Conference Publication, Adelaide, South Australia. pp. 67–71.

Kassiff, G., and Shalom, A.B., (1971). Experimental Relationship between Swell Pressure and Suction. Ge´otechnique, **21**(3): 245 - 255.

Khalili, N., Khabbaz, M.H., and Valliappan, S., (2000). An effective stress based numerical model for hydro-mechanical analysis in unsaturated porous media. Computational Mechanics, **26**(2): 174-184.

Kodikara, J., (2012). New framework for volumetric constitutive behaviour of compacted unsaturated soils. Canadian Geotechnical Journal, **49**(11): 1227-1243.

Kodikara, J., and Choi, X., (2006). A simplified analytical model for desiccation cracking of clay layers in laboratory tests. Proceedings of the Fourth International Conference on Unsaturated Soils. *Edited by* G.A. Miller and C.E. Zapata and S.L. Houston and D.G. Fredlund. ASCE Geotechnical Special Publication 147. American Society of Civil Engineers. pp. 2558–2567.

Kodikara, J., Islam, T., Wijesooriya, S., Bui, H., and Burman, B.C., (2014). On controlling influence of the line of optimums on the compacted clayey soil behavior. Proceedings of the Sixth International Conference on Unsaturated Soils, UNSAT2014. *Edited by* N. Khalili and A.R. Russell and A. Khoshghalb, Sydney, Australia. pp. 219-225.

Krohn, J.P., and Slosson, J.E., (1980). Assessment of expansive soils in the United States. 4th International Conference on Expansive Soils. Denver. pp. 596-608.

Kurucuk, N., (2011). Compaction behaviour of soils. PhD Thesis, Monash University, Melbourne.

Lambe, T., (1958). The structure of compacted clay. Journal of the Soil Mechanics and Foundations Division, ASCE, **84**: 1-34.

Langfelder, L.J., Chen, C., and Justice, J.A., (1968). Air permeability of compacted cohesive soils. Journal of Soil Mechanics & Foundations Div, **92**.

Lawton, E.C., Fragaszy, R.J., and Hetherington, M.D., (1992). Review of wetting-induced collapse in compacted soil. Journal of geotechnical engineering, **118**(9): 1376-1394.

Lee, J.O., Chao, W.J., and Chun, K.S., (1999). Swelling pressures of a potential buffer material for high-level waste repository. Journal of the Korean Nuclear Society, **31**(2): 139-150.

Lloret, A., and Alonso, E.E., (1985). State surfaces for partially saturated soils. 11th International Conference on Soil Mechanics and Foundation Engineering. San Francisco, California. pp. 557–562.

Lloret, A., Villar, M.V., Sánchez, M., Gens, A., Pintado, X., and Alonso, E.E., (2003). Mechanical behaviour of heavily compacted bentonite under high suction changes. Géotechnique **53**: 27-40.

Loret, B., and Khalili, N., (2002). An effective stress elastic–plastic model for unsaturated porous media. Mechanics of Materials, **34**(2): 97-116.

Mancuso, C., Jommi, C., and D'Onza, F., (2012). Unsaturated Soils: Research and Applications: Volume 2. Springer, Berlin, Heidelberg, Germany.

Matyas, E.L., and Radhakrishna, H., (1968). Volume change characteristics of partially saturated soils. Géotechnique, **18**(4): 432-448.

Meehan, R.L., and Karp, L.B., (1994). California housing damage related to expansive soils. Performance of Constructed Facilities, **8**(2): 139-157.

Mendes, J., and Buzzi, O., (2014). Performance of the University of Newcastle high capacity tensiometers. *In* Unsaturated Soils: Research & Applications. *Edited by* N. Khalili and A. Russell and A. Khoshghalb. Taylor and Francis Group, London. pp. 1611-1616.

Monroy, R., Zdravkovic, L., and Ridley, A., (2007). Fabric changes in compacted London clay due to variations in applied stress and suction. *In* Experimental Unsaturated Soil Mechanics. Springer, Berlin, Heidelberg, Germany. pp. 41-48.

Montanez, J.E.C., (2002). Suction and volume changes of compacted sand-bentonite mixtures. PhD Thesis, Imperial College London, London, United Kingdom.

Morgenstern, N.M., and Balasubramonian, B.I., (1980). Effects of pore fluid on the swelling of clay-shale. 4th International Conference on Expansive Soils. Denver, Canada. pp. 190–205.

Noorany, I., (1987). Precision and accuracy of field density tests in compacted soils. Department of Civil Engineering, San Diago State University, San Diago, California, United States.

Noorany, I., and Stanley, J.V., (1990). Swell and hydrocompression behaviour of compacted soils: Test data. Department of Civil Engineering, San Diago State University, San Diago, California, United States.

Noorany, I., and Stanley, J.V., (1994). Settlement of Compacted Fills Caused by Wetting. Vertical and Horizontal Deformations of Foundations and Embankments. ASCE, College Station, Texas. pp. 1516-1530.

Olson, R.E., (1963). Effective stress theory of soil compaction. Journal of the Soil Mechanics and Foundations Division, ASCE, **89**(SM2): 27-45.

Pham, H., Fredlund, D., and Barbour, S., (2003). A practical hysteresis model for the soil-water characteristic curve for soils with negligible volume change. Ge´otechnique, **53**(2): 293-298.

Pham, H.Q., Fredlund, D.G., and Barbour, S.L., (2005). A study of hysteresis models for soil-water characteristic curves. Canadian Geotechnical Journal, **42**(6): 1548-1568.

Proctor, R., (1933). Fundamental principles of soil compaction. Engineering News Record, **111**(9): 245-248.

Rajeev, P., and Kodikara, J., (2011). Numerical analysis of an experimental pipe buried in swelling soil. Computers and Geotechnics, **38**(7): 897-904.

Ridley, A.M., and Perez-Romero, J., (1998). Suction–water content relationships for a range of compacted clays. 2nd International Conference on Unsaturated Soils. International Academic Publishers, Beijing, China. pp. 114–118.

Romero, E., (1999). Characterization and thermo-hydro-mechanical behavoiur of unsaturated Boom clay: an experimental study. PhD Thesis, Technical University of Catalonia, Barcelona, Spain.

Santagiuliana, R., and Schreer, B.A., (2006). Enhancing the Bolzon-Schreer-Zienkiewicz constitutive model for partially saturated soil. Transport in Porous Media, **65**: 1-30.

Seed, H.B., and Chan, C.K., (1959). Structure and strength characteristics of compacted clays. J. Soil Mech. Foundation. Div., ASCE, **85**(SM5): 87-128.

Seed, H.B., Mitchell, J.K., and Chan, C.K., (1962). Studies of swell and swell pressure characteristics of compacted clays. Highway Research Board, Washington, D.C., United States.

Sharma, R.S., (1998). Mechanical Behaviour of Unsaturated Highly Expansive Clays. PhD Thesis, University of Oxford, Oxford, United Kingdom.

Sheng, D., (2010). Constitutive modelling of unsaturated soils: Discussion of fundamental principles. Proceedings of the 5th International Conference on Unsaturated Soils. *Edited by* E.E. Alonso and A. Gens. Taylor & Francis Group CRC Press. pp. 91-112.

References

Sheng, D., Fredlund, D.G., and Gens, A., (2008). A new modelling approach for unsaturated soils using independent stress variables. Canadian Geotechnical Journal, **45**(4): 511-534.

Sheng, D., and Zhou, A., (2011). Coupling hydraulic with mechanical models for unsaturated soils. Canadian Geotechnical Journal, **48**: 826-840.

Sitharam, T., Sivapullaiah, P., and Subba Rao, K., (1995). Shrinkage behaviour of compacted unsaturated soils. The first international conference on unsaturated soils (UNSAT'95). Paris, France.

Sivakumar, V., Sivakumar, R., Murray, E., MacKinnon, P., and Boyd, J., (2010). Mechanical behaviour of unsaturated kaolin (with isotropic and anisotropic stress history). Part 1: wetting and compression behaviour. Géotechnique, **60**(8): 581-594.

Sivakumar, V., Tan, W., Murray, E., and McKinley, J., (2006). Wetting, drying and compression characteristics of compacted clay. Géotechnique, **56**(1): 57-62.

Sivakumar, V., and Wheeler, S.J., (2000). Influence of compaction procedure on the mechanical behaviour of an unsaturated compacted clay. Part 1: Wetting and isotropic compression. Géotechnique **50**: 359-368.

Skinner, H., (2001). Construction on fill. Problematic Soils: Proceedings of the Symposium Held at the Nottingham Trent University, School of Property and Construction on 8 November 2001. Thomas Telford. p. 127.

Skinner, H., Charles, J., and Watts, K., (1999). Ground deformations and stress redistribution due to a reduction in volume of zones of soil at depth. Géotechnique, **49**(1): 111-126.

Sun, D.A., Matsuoka, H., and Xu, Y., (2004). Collapse behaviour of compacted clays by suction-controlled triaxial tests. Geotechnical Testing Journal, **27**(4): 362-370.

Tarantino, A., and De Col, E., (2008). Compaction behaviour of clay. Géotechnique **58**: 199-213.

Tarantino, A., and Tombolato, S., (2005). Coupling of hydraulic and mechanical behaviour in unsaturated compacted clay. Géotechnique, **55**(4): 307 - 317.

Taylor, D.W., (1948). Fundamentals of Soil Mechanics. Wiley, New York.

Thom, R., Sivakumar, V., Sivakumar, R., Murray, E.J., and Mackinnon, P., (2007). Technical Note: Pore size distribution of unsaturated compacted kaolin: the initial states and final states following saturation. Ge´otechnique, **57**(7): 469–474.

Thu, T.M., Rahardjo, H., and Leong, E.C., (2007). Elastoplastic model for unsaturated soil with incorporation of the soil-water characteristic curve. Canadian Geotechnical Journal, **44**(1): 67-77.

Tripathy, S., (2000). Behaviour of compacted expansive soils under swell–shrink cycles. PhD Thesis, Indian Institute of Science, Bengaluru, Karnataka, India.

Vaunat, J., Romero, E., and Jommi, C., (2000). An elasto-plastic hydromechanical model for unsaturated soils. Experimental evidence and theoretical approaches in unsaturated soils. *Edited by* A. Tarantino and C. Mancuso, Rotterdam, the Netherlands. pp. 121–138.

Wheeler, S., Sharma, R., and Buisson, M., (2003a). Coupling of hydraulic hysteresis and stress–strain behaviour in unsaturated soils. Géotechnique, **53**(1): 41-54.

Wheeler, S.J., Gallipoli, D., and Karstunen, M., (2002). Comments on use of the Barcelona Basic Model for unsaturated soils. International Journal for Numerical and Analytical Methods in Geomechanics, **26**(15): 1561-1571.

Wheeler, S.J., Sharma, R.S., and Buisson, M.S.R., (2003b). Coupling of hydraulic hysteresis and stress & strain behaviour in unsaturated soils. Géotechnique **53**: 41-54.

Wheeler, S.J., and Sivakumar, V., (1995). An elasto-plastic critical state framework for unsaturated soil. Géotechnique **45**: 35-53.

Wijesooriya, R.M.S.D., (2012). Modelling of Desiccation Crack Depths in Clay Soils. PhD Thesis, Monash University, Clayton.

References

Wijesooriya, S.D., and Kodikara, J., (2012). Experimental study of shrinkage and swelling behaviour of a compacted expansive clay soil. 11th Australia New Zealand Conference on Geomechanics (ANZ 2012). Melbourne, Australia.

Yevnin, A., and Zaslavsky, D., (1970). Some factors affecting compacted clay swelling. Canadian Geotechnical Journal, **7**(1): 79-91.

Zhang, X., and Lytton, R.L., (2008). Discussion of " A new modelling approach for unsaturated soils using independent stress variables by Sheng et al., 2008". Canadian Geotechnical Journal, **45**: 1784-1787.

Zhang, X., and Lytton, R.L., (2009). Modified state-surface approach to the study of unsaturated soil behavior. Part I: Basic concept. Canadian Geotechnical Journal, **46**(5): 536-552.